UNIVERSITAT POLITÈCNICA DE VALÈNCIA

DOCTORADO EN INGENIERÍA Y PRODUCCIÓN INDUSTRIAL

TESIS DOCTORAL

Fabricación y caracterización de materiales compuestos de alto rendimiento medioambiental derivados de resinas ecológicas y refuerzos de fibras naturales y estructuras híbridas

Autor

Diego Sebastián Lascano Aimacaña

Dirigida por

Dr. Teodomiro Boronat Vitoria

Dr. Néstor Montañés Muñoz

Alcoy, Julio 2022

UNIVERSITAT POLITÈCNICA DE VALÈNCIA

DOCTORADO EN INGENIERÍA Y PRODUCCIÓN INDUSTRIAL

TESIS DOCTORAL

Fabricación y caracterización de materiales compuestos de alto rendimiento medioambiental derivados de resinas ecológicas y refuerzos de fibras naturales y estructuras híbridas

Diego Sebastián Lascano Aimacaña

El Dr. Teodomiro Boronat Vitoria y el Dr. Néstor Montañés Muñoz, Profersores Titulares de Universidad del Departamento de Ingeniería Mecánica y de Materiales de la Universitat Politècnica de València en calidad de directores de la Tesis Doctoral (modalidad Doctorado Internacional) presentada por D. Diego Sebastián Lascano Aimacaña, con el título **"Fabricación y caracterización de materiales compuestos de alto rendimiento medioambiental derivados de resinas ecológicas y refuerzos de fibras naturales y estructuras híbridas".**

CERTIFICAN

Que la presente memoria, **"Fabricación y caracterización de materiales compuestos de alto rendimiento medioambiental derivados de resinas ecológicas y refuerzos de fibras naturales y estructuras híbridas"**, para aspirar al grado de Doctor por la Universitat Politècnica de València reúne las condiciones adecuadas para constituir la tesis doctoral de D. Diego Sebastián Lascano Aimacaña (modalidad Doctorado Internacional).

Asimismo, certifican que la citada tesis doctoral se ha realizado en el Instituto de Tecnología de Materiales de la Universitat Politècnica de València y en el Dipartimento di Ingegneria Civile ed Ambientale de la Universidad of Perugia (Italia).

Y para que conste a los efectos oportunos, firman la presente en Alcoy a 16 de mayo de 2022

Fdo. Dr. Teodomiro Boronat Vitoria Dr. Néstor Montañés Muñoz

A *Gladys y Josefina*

"*Discovery consits of seeing what everybody has seen,*
and thinking what nodody has tought"

-Albert Szent-Gyori

AGRADECIMIENTOS

En primer lugar, quiero agradecer de la manera más atenta a mis directores de tesis, los profesores Teodomiro Boronat Vitoria y Néstor Montañés Muñoz. Gracias por todo el tiempo que le han dedicado al desarrollo de este trabajo, por el soporte científico y más que nada por apoyo personal que me han brindado. Muchas gracias por todo.

Al Instituto de Tecnología de Materiales (ITM), de la Universitat Politècnica de València, por el apoyo financiero a través de la ayuda otorgada en la beca FPI, además por acogerme durante todo el desarrollo de la tesis doctoral.

A los catedráticos Rafael Balart Guimeno, Juan López Martínez, Lourdes Sanchez Nácher, David García Sanoguera. Gracias Lourdes por ayudarme en mi formación docente. Y un agradecimiento especial a Rafa por haber confiado en mi desde el principio de mi formación en el máster y por haberme dado la oportunidad de desarrollar mi trabajo de doctorado en este grupo de investigación, al cual le tengo mucho aprecio.

A los profesores Octavio Fenollar, Santiago Ferrándiz, Vicent Fombuena y Sergio Torres, gracias por el aporte de sus conocimientos a lo largo de estos años.

A los técnicos de laboratorio Javi, Matías por el apoyo en la parte técnica del laboratorio, en especial a Javi por las divertidas charlas de tecnología.

A mis compañeros de despacho Cris, Sandra, Miguel por haber compartido tanto y hacer del despacho un rinconcito de Ecuador, en especial a Cris por esas charlas en las que siempre aprendo algo nuevo.

A mis compañeros de laboratorio Dani, Luis, Pelayo, Mado, Ramón, Jaume, Juan, Iván, Paco el polaco, Harrison, con quienes he compartido muchos gratos momentos y he aprendido mucho.

Al profesor Luigi Torre de la Università degli Studi di Perugia, por permitirme realizar mi estancia de investigación en su centro, y en especial a Franco Dominicci por el apoyo, ayuda y los consejos brindados a lo largo de la estancia.

A todos mis amig@s, Saray, Judith, Christian, María José, Thelma, gracias por apoyarme durante todo el desarrollo de este trabajo. Especialmente Saray y Judith, amigas que, desde el máster han sabido sacarme una sonrisa y han hecho que todos estos años sean inolvidables.

A mis “panas” Ángel y René, personas que la vida ha puesto en mi camino y han llegado a ser como mi familia. Les agradezco todo el tiempo que hemos compartido. Y tengo la seguridad que vienen cosas más grandes. Muchas Gracias.

No puedo dejar de agradecer a Nuria, una de las mejores personas que he conocido en mi vida, gracias por abrir las puertas de tu casa durante todo este tiempo y lograr que me sienta como en la mía. Siempre te estaré agradecido a ti y tu familia.

A toda mi familia, a mis tíos Rodrigo, Fanny, Aida y Nancy, a mis primos que siempre han confiado en mí. Especialmente a Nancy, por el aliento y consejos que me has dado durante toda mi vida.

Y, por último, a mi madre Gladys, y mi abuela Josefina, las personas más importantes en mi vida. Ustedes siempre me han demostrado que trabajando duro las cosas llegan. Gracias por su apoyo incondicional y por soportar todo el tiempo que he estado fuera de casa. A pesar de estar tan lejos siempre he sentido su apoyo como que estuvieran a mi lado. No me alcanzará la vida para agradecerles.

RESUMEN

“Fabricación y caracterización de materiales compuestos de alto rendimiento medioambiental derivados de resinas ecológicas y refuerzos de fibras naturales y estructuras híbridas”

Es evidente cómo el aumento de la concienciación medioambiental respecto al uso de materiales poliméricos de origen petroquímico o plásticos de un único uso ha cambiado por completo el panorama de los materiales poliméricos, desde el punto de vista de su concepción o de su uso. Durante el desarrollo de esta tesis doctoral se ha abarcado varias alternativas con el fin de obtener materiales nuevos, que no tengan solo un bajo impacto ambiental, sino también que posean propiedades competitivas al compararlos con materiales convencionales, además de que su elaboración no conlleve un cambio drástico con respecto a las tecnologías existentes en la actualidad. Es por eso por lo que el objetivo principal de esta tesis doctoral se centra en el desarrollo y caracterización de nuevos materiales con un alto rendimiento medioambiental a partir de matrices termoplásticas como el poli(ácido láctico) (PLA) y matrices termoestables como resinas epoxi con un contenido parcial o total de origen natural. Además del uso de rellenos y fibras de origen natural.

El PLA es un polímero de origen natural que ha ganado popularidad en los últimos años. Se debe principalmente a su biodegradabilidad, biocompatibilidad y a sus interesantes propiedades, como la memoria de forma. Sin embargo, el PLA tiene varias limitaciones, entre ellas, su elevada fragilidad. Es por ello, que en el presente trabajo se han realizado diferentes modificaciones con el propósito de suplir esta carencia. Se empezó con la formulación a través de una mezcla física con otro polímero flexible y con capacidad de biodegradación como el poli(butilén succionato-*co*-adiapato) (PBSA), donde para sobrellevar la baja miscibilidad entre estos dos polímeros se utilizó un oligómero epoxi estireno-acrílico (ESAO). Se observó el claro impacto que tuvo el PBSA en el aumento de las propiedades dúctiles y de tenacidad del PLA, siendo más notorio este efecto con la incorporación del ESAO, lamentablemente disminuyendo su capacidad de memoria de forma. Otra estrategia utilizada para la modificación de las propiedades del PLA fue la incorporación de agentes plastificantes como el oligómero de ácido láctico (OLA), donde se obtuvo una mejora considerable tanto en las propiedades de resistencia al impacto como de memoria forma, así también como un

ligero efecto plastificante, obteniendo resultados alentadores para su uso en envases compostables.

Teniendo en cuenta las capacidades del PLA a ser modificado y moldeado por técnicas convencionales, se aprovechó esto en la elaboración de diferentes tipos de materiales compuestos. Se comenzó con la fabricación de una estructura ligera de tipo sándwich. Esta estructura estaba formada por un núcleo en forma de panal y unas caras exteriores; donde el núcleo en forma de panal estaba hecho completamente de PLA, y las caras exteriores estaban constituidas por una matriz de PLA y reforzadas por fibras de lino, estos componentes fueron unidos por una capa de PLA no tejido impregnadas con una resina epoxi con un contenido parcial de origen renovable. Las estructuras resultantes presentaron excelentes propiedades a flexión y compresión, además de contener un alto porcentaje de componentes de origen natural. Posteriormente, se fabricó una segunda estructura, cuyo compuesto se basó en una matriz de PLA reforzada con fibras de yute, fabricada por termoconformado. Se logró conseguir materiales compuestos con hasta el 50 % de fibras de refuerzo. Los materiales obtenidos presentaron buenas propiedades a tracción cuando se reforzaron con fibras direccionadas (tejidas) y buenas propiedades de flexión al utilizar tanto fibras tejidas como no tejidas.

Internándonos en el mundo de las matrices termoestables. Es bien conocido que uno de sus mayores inconvenientes es su origen petroquímico. Para intentar solventarlo, en este trabajo se estudió en primer lugar una resina epoxi con un contenido parcial de origen natural, y una resina epoxi derivada de aceite epoxidado de lino (ELO). A través de un análisis cinético del curado de estas resinas, se determinó que el contenido parcial de la resina epoxi, y la diferente ubicación de los grupos epoxi en la resina epoxi basada en ELO no influye en su proceso de curado, comportándose de forma similar a una resina epoxi convencional. Estos interesantes resultados posibilitan su aplicación en la industria sin afectar en gran medida a los procesos de producción. Además de dar luz verde a la optimización del proceso de curado a través de medios convencionales como es el control de la temperatura de curado y de poscurado. Los estudios determinaron que las temperaturas de curado moderadas y las altas temperaturas de poscurado producían piezas con un grado de reticulación óptimo, lo que se traduce en buenas propiedades mecánicas.

Aprovechando la gran versatilidad que tiene las resinas epoxi como matriz de materiales compuestos, se fabricaron tres tipos de estructuras con diferentes rellenos y fibras de refuerzo de origen natural. Un primer material se elaboró incorporando hasta

un 40 % partículas derivadas de la semilla de lino con diferentes tamaños de grano, obteniendo materiales con propiedades mecánicas balanceadas y una apariencia similar a la madera, que puede ser interesante en sectores como el mobiliario. El segundo material fue un laminado, formado por telas de fibras de lino y de basalto, donde para obtener una mejor interacción superficial entre la matriz y las fibras de refuerzo, estas fueron tratadas con agentes de acoplamiento basado en silanos. Como resultado se obtuvieron materiales con buenas propiedades a flexión. El último material fue una estructura sándwich ligera con un núcleo permeable cuyo núcleo garantizó una buena distribución de la resina por toda la estructura y aportaba ligereza al sistema. Los buenos resultados obtenidos con el tratamiento de las fibras de lino y basalto mostraron una excelente interacción fibra/núcleo/resina, dando lugar a materiales con una buena capacidad de absorción de impactos.

RESUM

“Fabricació i caracterització de materials compostos d'alt rendiment mediambiental derivats de resines ecològiques i reforços de fibres naturals i estructures híbrides”

És evident com l'augment de la conscienciació mediambiental respecte a l'ús de materials polimèrics d'origen petroquímic o plàstics d'un únic ús ha canviat per complet el panorama dels materials polimèrics, des del punt de vista de la seua concepció o del seu ús. Durant el desenvolupament d'aquesta tesi doctoral s'han tingut en compte diverses alternatives amb la finalitat d'obtindre materials nous, que no tinguen només un baix impacte ambiental, sinó també que posseïsquen propietats competitives en comparar-los amb materials convencionals, a més de que la seua elaboració no comporte un canvi dràstic respecte a les tecnologies existents en l'actualitat. És per això, per la qual cosa l'objectiu principal d'aquesta tesi doctoral se centra en el desenvolupament i caracterització de nous materials amb un alt rendiment mediambiental a partir de matrius termoplàstiques com el àcid polilàctic (PLA) i matrius termoestables com a resines epoxi amb un contingut parcial o total d'origen natural. A més de l'ús de reforços i fibres d'origen natural.

El PLA és un polímer d'origen natural que ha guanyat popularitat en els últims anys. Es deu principalment a la seua biodegradabilitat, biocompatibilitat i a les seues interessants propietats, com la memòria de forma. No obstant això, el PLA té diverses limitacions, entre elles, la seua elevada fragilitat. És per això, que en el present treball s'han realitzat diferents modificacions amb el propòsit de suplir aquesta limitació. Es va començar amb la formulació a través d'una mescla física amb un altre polímer flexible i amb capacitat de biodegradació com el poli(butilen succionate-co-adiapate) (PBSA), on per a suportar la baixa miscibilitat entre aquests dos polímers es va utilitzar un oligòmer epoxi estiré-acrílic (ESAO). Es va observar el clar impacte que va tindre el PBSA en l'augment de les propietats dúctils i de tenacitat del PLA, sent més notori aquest efecte amb la incorporació del ESAO, lamentablement disminuint la seua capacitat de memòria de forma. Una altra estratègia utilitzada per a la modificació de les propietats del PLA va ser la incorporació d'agents plastificants com el oligòmero d'àcid làctic (ONA), on es va obtindre una millora considerable tant en les propietats de resistència a l'impacte com de memòria forma, així també com un lleuger efecte plastificant, obtenint resultats encoratjadors per al seu ús en envasos compostables.

Tenint en compte les capacitats del PLA a ser modificat i modelat per tècniques convencionals, es va aprofitar això en l'elaboració de diferents tipus de materials compostos. Es va començar amb la fabricació d'una estructura lleugera de tipus sàndwitx. Aquesta estructura estava formada per un nucli en forma de bresca i unes cares exteriors; on el nucli en forma de bresca estava fet completament de PLA, i les cares exteriors estaven constituïdes per una matriu de PLA i reforçades per fibres de lli, aquests components van ser units per una capa de PLA no teixit impregnades amb una resina epoxi amb un contingut parcial d'origen renovable. Les estructures resultants van presentar excel·lents propietats a flexió i compressió, a més de contindre un alt percentatge de components d'origen natural. Posteriorment, es va fabricar una segona estructura, el compost de la qual es va basar en una matriu de PLA reforçada amb fibres de jute, fabricada per termoconformat. Es va aconseguir materials compostos amb fins al 50 % de fibres de reforç. Els materials obtinguts van presentar bones propietats a tracció quan es van reforçar amb fibres adreçades (teixides) i bones propietats de flexió en utilitzar tant fibres teixides com no teixides.

Aprofundint en el món de les matrius termoestables. És ben conegut que un dels seus majors inconvenients és l'origen petroquímic. Per a intentar solucionar-ho, en aquest treball es va estudiar en primer lloc una resina epoxi amb un contingut parcial d'origen natural, i una resina epoxi derivada d'oli epoxidat de lli (ELO). A través d'una anàlisi cinètica del curat d'aquestes resines, es va determinar que el contingut parcial de la resina epoxi, i la diferent ubicació dels grups epoxi en la resina epoxi basada en ELO no influeix en el seu procés de curat, comportant-se de manera similar a una resina epoxi convencional. Aquests interessants resultats possibiliten la seua aplicació en la indústria sense afectar en gran manera als processos de producció. A més de donar llum verda a l'optimització del procés de curat a través de mitjans convencionals com és el control de la temperatura de curat i de postcurat. Els estudis van determinar que les temperatures de curat moderades i les altes temperatures de postcurat produïen peces amb un grau de reticulació òptim, la qual cosa es tradueix en bones propietats mecàniques.

Aprofitant la gran versatilitat que tenen les resines epoxi com a matriu de materials compostos, es van fabricar tres tipus d'estructures i fibres de reforç d'origen natural. Un primer material es va elaborar incorporant fins a un 40 % partícules derivades de la llavor de lli amb diferents grandàries de gra, obtenint materials amb propietats mecàniques balancejades i una aparença similar a la fusta, que pot ser interessant en sectors com el mobiliari. El segon material va ser un laminatge, format per teles de fibres de lli i de basalt, on per a obtindre una millor interacció superficial entre la matriu i les

fibres de reforç, aquestes van ser tractades amb agents d'acoblament basat en silans. Com a resultat es van obtindre materials amb bones propietats a flexió. L'últim material va ser una estructura sàndwitx lleugera amb un nucli permeable el nucli del qual va garantir una bona distribució de la resina per tota l'estructura i aportava lleugeresa al sistema. Els bons resultats obtinguts amb el tractament de les fibres de lli i basalt van mostrar una excel·lent interacció fibra/nucli/resina, donant lloc a materials amb una bona capacitat d'absorció d'impactes.

ABSTRACT

“Manufacturing and characterization of high environmental performance composites based on environmentally friendly resins and natural fiber reinforcements, and hybrid structures”

It is remarkable how the increase in environmental awareness regarding the use of polymeric materials of petrochemical origin or single-use plastics has completely changed the scenario of polymeric materials development and use. This doctoral thesis has proposed several alternatives in order to obtain new materials with low environmental impact and competitive properties to conventional materials. In addition to the fact that their elaboration does not entail a drastic change respect to existing technologies. Therefore, the main objective of this doctoral thesis focuses on developing and characterizing new materials with a high environmental performance from thermoplastic matrices such as poly(lactic acid) (PLA) and thermosetting matrices such as epoxy resins with a partial or total content of natural origin. In addition to the use of fillers and fibers of natural origin.

PLA is a naturally occurring polymer that has gained popularity in recent years. It is mainly due to its biodegradability, biocompatibility, and exciting properties such as shape memory. However, PLA has several limitations, among which is its high brittleness. For this reason, in the present work, different modifications have been made to make up for this deficiency. This methodology started with the formulation through a physical blend with another flexible and biodegradable polymer such as poly(butylene succinate-*co*-adipate) (PBSA). This blend incorporated a coupling agent such as epoxy styrene-acrylic oligomer (ESAO) to overcome the low miscibility between these two polymers. The PBSA cleared increased the ductile and toughness properties of PLA; this effect was more noticeable with the incorporation of ESAO, unfortunately decreasing its shape memory capacity. The second strategy applied to modify PLA properties was incorporating plasticizing agents such as oligomeric lactic acid (OLA). This agent considerably improved impact resistance and shape memory properties, and it also provided a slightly plasticizing effect, obtaining encouraging results for its use in compostable packaging.

Considering the potential of PLA to be modified and molded by conventional techniques, PLA was used to develop different types of composite materials. It started

with the fabrication of a lightweight sandwich-type structure. This structure consisted of a honeycomb core and some outer faces; the honeycomb core was made entirely of PLA, and the outer faces were made of a PLA matrix and reinforced with flax fibers. Finally, the bonded method to join both components consisted of a nonwoven PLA impregnated with an epoxy resin with a partial content of renewable origin. The obtained results can be used in industrial applications. The second structure built was a composite based on a PLA matrix reinforced with jute fibers produced by thermoforming. The manufacturing process enabled composites with up to 50 % fiber content. The materials obtained showed good tensile properties when reinforced with directional (woven) fibers. Moreover, both woven and nonwoven fibers offered good flexural properties.

In the world of thermosetting matrices, it is well-known that one of their major drawbacks is their petrochemical origin. In order to try to solve that, this work studied an epoxy resin with a partial content of a natural source, continuing with an epoxy resin derived from epoxidized linseed oil (ELO). The results obtained through the kinetic study of these resins determined that the partial content of the epoxy resin and the different location of the epoxy groups in the ELO-based epoxy resin did not influence its curing process, behaving similarly to a conventional epoxy resin. These exciting results make it possible to apply them in the industry without significantly affecting the production processes. In addition to giving the green light to the optimization of the curing process through conventional means such as curing and post-curing temperature control. The studies determined that moderate curing temperatures and high post-curing temperatures produced pieces with an optimum crosslinking degree, which results in good mechanical properties.

The last phase of the work took advantage of the incredible versatility of epoxy resins as a matrix for composite materials. In this phase, three structures were fabricated with different fillers and reinforcing fibers of natural origin. The first material incorporated up to 40 % particles derived from flax seed with different grain sizes, obtaining materials with balanced mechanical properties and a wood-like appearance, which can be interesting in sectors such as furniture. The second material was a laminate formed by flax and basalt fiber mats. In order to increase the surface interaction between the matrix and the reinforcement fibers, these fibers were treated with silane-based coupling agents, obtaining materials with good flexural properties. The last material was a lightweight sandwich structure with a permeable core. This core ensured a good distribution of the resin throughout the structure and provided lightness to the system. The good results obtained with the treatment of flax and basalt fibers showed an

excellent fiber/core/resin interaction, resulting in materials with a good impact absorption capacity.

LISTADO DE ARTÍCULOS

La presente tesis doctoral consta de un compendio de los siguientes artículos y manuscritos:

I. Toughened poly (lactic acid)-PLA formulations by binary blends with poly(butylene succinate-*co*-Adipate)-PBSA and shape memory behavior.

II. Development of injection-molded polylactide pieces with high toughness by the addition of lactic acid oligomer and characterization of their shape memory behavior.

III. Manufacturing and characterization of highly environmentally friendly sandwich composites from polylactide cores and flax-polylactide faces.

IV. A comparative study of mechanical properties of polylactide bio-composites with woven and non-woven jute reinforcements.

V. Kinetic analysis of the curing of a partially biobased epoxy resin using dynamic differential scanning calorimetry.

VI. Kinetic analysis of the curing process of biobased epoxy resin from epoxidized linseed oil by dynamic differential scanning calorimetry.

VII. Optimization of the curing and post-curing conditions for the manufacturing of partially bio-based epoxy resins with improved toughness.

VIII. Manufacturing and characterization of green composites with partially biobased epoxy resin and flaxseed flour wastes.

IX. Manufacturing and characterization of hybrid composites with basalt and flax fabrics and a partially bio-based epoxy resin.

X. Manufacturing of composite materials with high environmental efficiency using epoxy resin of renewable origin and permeable light cores for vacuum-assisted infusion molding.

ECUACIONES

$\alpha = \frac{\Delta H_t}{\Delta H_T}$	α= grado de conversión ΔH_t= entalpia liberada a un tiempo particular ΔH_T= entalpia total liberada durante la reacción
$\frac{d\alpha}{dt} = k(T)f(\alpha)$	$\frac{d\alpha}{dt}$= velocidad de conversión $k(T)$= constante de rapidez de reacción $f(\alpha)$= modelo de reacción
$k(T) = A\, e^{\left(-\frac{E_a}{R\,T}\right)}$	$k(T)$= constante de rapidez de reacción A= factor pre exponencial E_a= energía de activación aparente R= constante universal de los gases T= temperatura absoluta
$\beta = \frac{dT}{dt}$	β= tasa de calentamiento $\frac{d\alpha}{dT}$= conversión con respecto a la temperatura
$ln\left(\beta\ \frac{d\alpha}{dT}\right) = \ln A\ \ f(\alpha) - \frac{E_a}{R\,T}$	β= tasa de calentamiento $\frac{d\alpha}{dT}$= conversión con respecto a la temperatura A= factor pre exponencial $f(\alpha)$= modelo de reacción E_a= energía de activación aparente R= constante universal de los gases T= temperatura absoluta
$ln\left(\frac{\beta}{T^B}\right) = constante - C\ \frac{E_a}{R\,T}$	β= tasa de calentamiento A= factor pre exponencial E_a= energía de activación aparente R= constante universal de los gases T= temperatura absoluta

	B, C= valores correspondientes a una aproximación particular: FWO: B=0, C=1,052 KAS: B=2, C=1 Starink: B=1,92, C=1,008
$ln\left(\frac{\beta}{T_p^2}\right) = ln\left(\frac{A\,R}{E_a}\right) + ln\left(-\frac{d\,f(\alpha)}{d\alpha}\right) - \frac{E_a}{R\,T_p}$	β = tasa de calentamiento A= factor pre exponencial E_a= energía de activación aparente R= constante universal de los gases T_p= temperatura en la máxima tasa de reacción
$ln(\Delta t_{FWHM}) = \frac{E_a}{R\,T_p} + ln\frac{\Delta t'_{FWHM}}{A}$	Δt_{FWHM}= amplitud total a la altura del máximo A= factor pre exponencial E_a= energía de activación aparente R= constante universal de los gases T_p= temperatura en la máxima tasa de reacción
$f(\alpha) = \alpha^m\,(1-\alpha)^n$	$f(\alpha)$= modelo de reacción α= grado de conversión m= efecto auto catalítico n= modelo de reacción de enésimo orden
$y(\alpha) = \left(\frac{d\alpha}{dt}\right)\,e^x$	$\frac{d\alpha}{dt}$= velocidad de conversión x= temperatura reducida $\left(\frac{\mathrm{E_a}}{\mathrm{R\,T}}\right)$
$\alpha_M = \frac{m}{m+n}$	α_M= pico de la función $y(\alpha)$ m= efecto auto catalítico n= modelo de reacción de enésimo orden
$z(\alpha) = \left(\frac{d\alpha}{dt}\right)\,\pi(x)\,\frac{T}{\beta}$	$\frac{d\alpha}{dt}$= velocidad de conversión $\pi(x)$= forma racional de aproximaciones de la integral de Arrhenius

	β= tasa de calentamiento T= temperatura absoluta
$\pi(x) = \frac{x^3 + 18x^2 + 86x + 96}{x^4 + 20x^3 + 120x^2 + 240x + 120}$	$\pi(x)$= forma racional de aproximaciones de la integral de Arrhenius x = temperatura reducida $\left(\frac{\mathrm{E_a}}{\mathrm{R\,T}}\right)$
$\chi_c(\%) = \left[\frac{\Delta H_m - \Delta H_{cc}}{\Delta H_m^0\, w}\right] 100$	χ_c= grado de cristalinidad ΔH_m= entalpia de fusión ΔH_{cc}= entalpia de cristalización en frio ΔH_m^0= entalpia de fusión para un polímero 100 % cristalino w= fracción en peso del polímero
$\%R_f = \frac{(\pi - \theta_t)}{(\pi - \theta_f)}$	R_f= índice de fijación de forma θ_t= ángulo temporal de deformación θ_f= ángulo de fijación
$\%R_r = \frac{(\pi - \theta_f)/(\pi - \theta_r)}{(\pi - \theta_f)}$	R_r= índice de recuperación de forma θ_f= ángulo de fijación θ_r= ángulo de recuperación
$\tau = \frac{P}{(d + c) \cdot b}$	τ= tensión de cizallamiento del núcleo P= carga máxima d= espesor de la estructura sándwich b= ancho de la estructura sándwich c= espesor del panal de abeja
$\sigma_b = \frac{P \cdot L}{2 \cdot t \cdot (d + c) \cdot b}$	σ_b= esfuerzo de flexión de las caras P= carga máxima L= longitud de luz t= espesor de las caras exteriores d= espesor de la estructura sándwich c= espesor del panal de abeja b= ancho de la estructura sándwich
$t_{gel} = C\frac{1}{k(T)}$	t_{gel}= tiempo de gel C= constante

	$k(T)$= constante de rapidez de reacción
$Water\ uptake\ (\%) = \left[\frac{(W_t - W_0)}{W_0}\right] 100$	W_t= peso seco de la muestra a un tiempo particular W_0= peso seco inicial de la muestra
$D = \pi \left[\frac{m\ h}{4}\right]^2$	D= coeficiente de difusión m= valor de la pendiente de la curva ($W_t/W_s\ vs\ t^{1/2}$) h= espesor inicial de la muestra
$D_c = D\left[1 + \frac{h}{L} + \frac{h}{w}\right]^{-2}$	D_c= coeficiente de difusión corregido h= espesor inicial de la muestra L= longitud de la muestra w= ancho de la muestra
$\Delta E = \sqrt{(\Delta L^*)^2 + (\Delta a^*)^2 + (\Delta b^*)^2}$	ΔE= diferencia total de color ΔL^*= diferencia de luminosidad entre dos muestras Δa^*= diferencia de coordenadas de a^* Δb^*= diferencia de coordenadas de b^*

ABREVIATURAS Y NOMENCLATURA

α_M	Máximo de la función $y(\alpha)$
α_p^{∞}	Máximo de la función $z(\alpha)$
α_p	Conversión a la máxima velocidad de reacción
ε_b	Elongación a la rotura
θ_f	Ángulo de fijación
θ_r	Ángulo de recuperación
θ_t	Ángulo temporal de deformación
σ_b	Resistencia a la rotura por tracción, esfuerzo de flexión de las caras
σ_{f}, FS	Resistencia a la flexión
σ_T	Resistencia a la tracción
χ_c	Grado de cristalinidad
χ_{cmax}	Cristalinidad máxima
τ	Factor de escala de tiempo, tensión de cizallamiento del núcleo
α	Grado de conversión
ΔE	Diferencia de color
|η*|	Viscosidad compleja
A	Factor pre exponencial
a*	Coordenada de color de rojo a verde
ABS	Acrilonitrilo butadieno estireno
AESO	Aceite acritlatado epoxidado de soja
AEW	Peso equivalente de anhídrido
AF	Fibra de aramida
AFA	Ácido graso aminado
ALA	Ácido linolenico-α
ASF	Harina de cascara de almendra
b	Ancho de la estructura sándwich
B, C	Constantes de la temperatura integral
b*	Coordenada de color de amarillo a azul

Bio-PA	Bio-poliamida
Bio-PE	Bio-polietileno
Bio-PET	Bio-polietilén tereftalato
Bio-PP	Bio-polipropileno
BioEP	Resina epoxi de origen natural
BMI	N, N-(1,3-fenileno dimaleimida)
BPA	Bisfenol A
c	Espesor del panal de abeja
CF	Fibra de carbono
CFF	Harina grano grueso
CLTE	Coeficiente de dilatación lineal
CNF	Nano fibras de carbono
CNSL	Líquido de la cascara del anacardo
CNT	Nano tubos de carbono
CRP	Polimerización radical controlada
D	Coeficiente de difusión
d	Espesor de la estructura sándwich
DBMI	1,1-(metilendi-4,1-fenileno) bismaleimida
D_c	Coeficiente de difusión corregido
DCP	Peróxido de dicumíl
DDSA	Anhídrido dodecenilsuccínico
DGEBA	Diglicidil éter de bisfenol A
DGEBF	Diglicidil éter de bisfenol F
DGT	Primera derivada del porcentaje de masa con respecto a la temperatura
DMTA	Análisis termomecánico dinámico
DSC	Calorimetría diferencial de barrido
E', G'	Módulo de almacenamiento
E'', G''	Módulo de perdida
E_a	Energía de activación aparente
EAO	Aceite de alga epoxidado
ECO	Aceite epoxidado de ricino

ECSO	Aceite de algodón epoxidado
EEW	Peso equivalente de epoxi
E_f	Módulo de flexión
ELO	Aceite epoxidado de lino
EP	Resina epoxi
ESAO	Oligómero epoxi estireno-acrílico
ESBO	Aceite epoxidado de soja
ESO	Aceite epoxidado de girasol, aceite epoxidado de soja
E_T	Módulo de elástico
EVA	Polietilén viníl acetato
EVO	Aceite vegetal epoxidado
FESEM	Microscopía electrónica de barrido de emisión de campo
FFF	Harina grano fino
FR	Método de Friedman
FRC	Compuesto reforzado por fibras
FRP	Polímero reforzado con fibra, polimerización radical libre
FS	Semilla de lino
FTIR	Infrarojo por transformada de Fourier
FWHM	Amplitud total a la altura del máximo
FWO	Método Flynn-Wall-Ozawa
G'_{max}	Módulo de almacenamiento máximo
GA	Anhídrido glutárico
GF	Fibra de vidrio
h	Espesor inicial de la muestra
HA	Hidroxiapatita
HCN	Cianuro de hidrógeno
HDPE	Polietileno de alta densidad
HMDIC	Diisocianato de hexametileno
HSF	Harina de cáscara de avellana
KAS	Método Kissnger-Akahira-Sunose
L	Longitud de luz, longitud de lamuestra
L*	Coordenada de luminosidad

LDPE	Polietileno de baja densidad
m	Efecto auto catalítico
m	Valor de la pendiente de la curva ($W_t/W_s \ vs \ t^{1/2}$)
MAESO	Aceite de soja epoxidado con anhídrido metacrilico
MAH	Anhídrido maleico
MAH-*g*-PLA	Ácido poliláctico injertado con anhídrido maléico
MDIC	Diisocianato de metilendifenilo
MFI	Índice de fluidez
MFK	Métodos isoconversionales libres de modelo
MI	Isosorbida metacrilada
MLO	Aceite de lino maleinizado
MNA	Anhídrido metílico nádico
MVA	Alcohol vanílico metacrilado
MVO	Aceites vegetales modificados
M_w	Peso molecular
n	Modelo de reacción de enésimo orden
NFRP	Plásticos reforzados con fibras naturales
OLA	Oligómero de ácido láctico
P	Presión, carga máxima
P3HO	Poli(3-hidroxioctanoato)
P4HB	Poli(4-hidroxibutirato)
PA	Poliamida
PB	Tableros de partículas
PBA	Poli(butilén adipato)
PBAT	Poli(butilén adipato-*co*-tereftalato)
PBS	Poli(butilén succionato)
PBSA	Poli(butilén succionato-*co*-adiapato)
PBT	Poli(butilén terftalato)(PBT)
PBT	Polibutilén tereftalato
PC	Policarbonato, poscurado
PCL	Poli(ε-caprolactona)
PDLA	Poli(D-ácido láctico)

PDLLA	Poli(DL-ácido láctico)
PE	Polietileno
PEA	Poliéster amida
PEEK	Poli(éter-éter-cetona)
PEG	Poli(etilén glicol)
PEI	Poliéter imida
PET	Polietilén tereftalato
PF	Resinas fenólicas
PGA	Poli(ácido glicólico)
PHA	Polihidroxialcanoato
PHB	Poli(3-hidroxibutirato)
phr	Partes por cada 100 de resina
PHV	Poli(3-hidroxivalerato)
PLA	Poli(ácido láctico)
PLLA	Poli(L-ácido láctico)
PLLA-*b*-PBS-*b*-PLLA	Poli(*L*-lactida-*b*-butileno succinato-*b*-*L*-lactida)
PMPPIC	Polimetileno polifenil isocianato
PP	Polipropileno
PPC	Poli(propileno carbonato)
PPG	Poli(propileno glicol)
PS	Poliestireno
PVA	Alcohol polivinilico
PVA	Poli(vinil alcohol)
PVC	Policloruro de vinilo
R	Constante universal de los gases
RD	Diluyente reactivo
Rf	Índice de fijación de forma
ROP	Apertura de anillo
Rr	Índice de recuperación de forma
RTM	Moldeo de transferencia de resina
SC	Curado estándar
SEM	Microscopía electrónica de barrido

t	Espesor de las caras exteriores
T	Temperatura
T_{α}	Temperatura para una conversión particular
$T_{5\%}$, T_0	Temperatura cuando se pierde el 5 % de masa inicial
TA	Ácido tánico
Tan δ	Factor de amortiguamiento
T_{cc}	Temperatura de cristalización en frio
T_{curing}	Temperatura de curado
t_{curing}	Tiempo de curado
TDIC	Tolueno 2,4-diisocianato
T_g	Temperatura de transición vítrea
TGA	Análisis termogravimétrico
t_{gel}	Tiempo de gel
TGMDA	Tetra glicidil metileno dianilina
T_m	Temperatura de fusión
TMA	Análisis termomecánico
T_{max}, T_{deg}	Temperatura de degradación máxima
T_p	Temperatura del pico
TPS	Amidon termoplástico
UP	Resinas de poliéster insaturado
VA	Método de Vyazovkin
VARIM	Moldeo por infusión de resina asistida por vacío
VARTM	Moldeo por transmisión de resina asistido por vacío
VE	Resinas de viniléster
VO	Aceites vegetales
w	Fracción en peso del polímero, ancho de la muestra
W_0	Peso seco inicial de la muestra
WPC	Wood plastic composites
W_s	Porcentaje de saturación de agua
W_t	Peso seco de la muestra a un tiempo particular
Wt %	Porcentaje por peso
x	Temperatura reducida

β	Tasa de calentamiento
γ	Tensión de cizalladura máxima
δ	Ángulo de desfase
ΔH_m^0	Entalpia de fusión para un polímero 100 % cristalino
ΔH_t	Entalpia liberada a un tiempo particular
ΔH_T	Entalpia total liberada durante la reacción
ΔH_{cc}	Entalpia de cristalización en frio
ΔH_m	Entalpia de fusión
σ	Esfuerzo aplicado

TABLA DE CONTENIDOS

LISTADO DE FIGURAS

LISTADO DE TABLAS

I. INTRODUCCIÓN

I.1. Polímeros de alto rendimiento medioambiental.

I.1.1. Polímeros termoplásticos

Desde su invención en el siglo XIX [1], los materiales poliméricos han tenido una presencia crucial en nuestro día a día, los comúnmente llamados plásticos se encuentran en productos cotidianos como envolturas de golosinas o patatas, envases de alimentos, botellas de agua, juguetes, en la fabricación de almohadas, colchones, sabanas, o como partes en sectores como el automotriz, construcción, eléctrico, entre otros.

El aumento de la población, así como de sus necesidades han provocado un aumento de la producción de polímeros, llegando a ser la increíble cantidad de 368 millones de toneladas en el 2019. Donde el mercado europeo ocupa la tercera posición con un 16 % superado solamente por América del Norte (19 %) y Asia (51 %) [2]. La gran versatilidad que tienen los polímeros a ser modificados y adaptados en áreas con requerimientos específicos ha llamado la atención en sectores industriales como el envase y embalaje, o la construcción, viéndose reflejado en su demanda en el mercando con un 39,6 % y 20,4 %, respectivamente, sumándose a estos el sector de la ingeniería con un 16,7 %. A pesar de que, en estos dos últimos sectores, se suelen utilizar en el desarrollo y fabricación de elementos con una vida útil prolongada. El sector del envase y embalaje lo suele destinar a productos de consumo diarios o una vida útil muy corta y/o de un solo uso.

Por desgracia desde sus inicios hasta el día de hoy la gran mayoría de los materiales poliméricos son de origen sintético, es decir provenientes de fuentes de origen fósil. Según la Asociación de fabricantes de plásticos (PlasticsEurope) en el 2018 se recolectaron 29,1 millones de toneladas de plásticos posconsumo en toda Europa, de los cuales 2,5 millones de toneladas fueron recolectadas en España. Por su naturaleza, la mayoría de los polímeros sintéticos presentan una alta resistencia a la degradación, ya sean estos por medios físicos o químicos, dificultando así su tratamiento. Esto ha provocado una excesiva cantidad de desechos que terminan sus días en vertederos, convirtiéndolo en uno de los mayores contaminantes ambientales. Todo esto ha desencadenado un incremento en la conciencia medioambiental, lo que en general ha permitido que se promueva un uso inteligente de materiales poliméricos, resultando indirectamente en una disminución en la enorme huella de carbono y emisión de dióxido de carbono (CO_2) que se genera en su producción. Además, esto ha ayudado

a implantar una cultura del reciclado, facilitando el tratamiento de estos desechos. Esto se ve reflejado en las estadísticas de estos últimos años, ya que el tratamiento de desechos poliméricos ha mejorado. En el 2018 en España se ha llegado a reciclar el 41,9 % de los desechos poliméricos generados y se ha logrado disminuir la cantidad de vertederos de 1686 (2006) a 996 (2018) [2].

A pesar de que el interés global acerca del tratamiento de polímeros posconsumo va en aumento, la sociedad requiere el desarrollo de nuevos materiales con un bajo impacto ambiental. Como se mencionó anteriormente, la mayoría de estos materiales son derivados de productos petroquímicos, y presentan una dificultad en degradarse. Varias investigaciones se han dedicado al desarrollo de biomateriales que por diseño correspondan a un modelo sostenible, generalmente relacionados a materiales termoplásticos ya que son los que más problemas medioambientales causan.

El concepto de bio-materiales se puede relacionar a dos factores, el primero de estos factores es su origen, es decir la materia prima de donde se obtienen. La industria petrolífera que brinda esta materia prima para la producción de la mayoría de los polímeros, aparte de producir grandes cantidades de dióxido de carbono (CO_2), es una fuente no renovable por lo cual se busca reducir su dependencia. Con este fin, en los últimos años varios investigadores se han dedicado a buscar una fuente renovable de materia prima para la obtención de materiales termoplásticos con propiedades comparables con los convencionales. El segundo de estos factores se puede englobar en el término “biodegradabilidad”, refiriéndose a la capacidad que tienen los materiales a degradarse bajo condiciones controladas de compost, esta degradación implica actividad biológica, es decir el material sufre una descomposición (metano, CO_2, agua, etc.) por la acción de microorganismos como los hongos, bacterias y algas. [3,4]. Por lo tanto, teniendo en cuenta lo planteado, se puede considerar biomaterial a aquel material que cumpla con uno de estos factores o los dos.

La figura I.1. presenta una vista global de la clasificación de los polímeros termoplásticos basados en su origen (renovable o no renovable) y en su capacidad de biodegradabilidad (biodegradable o no biodegradable).

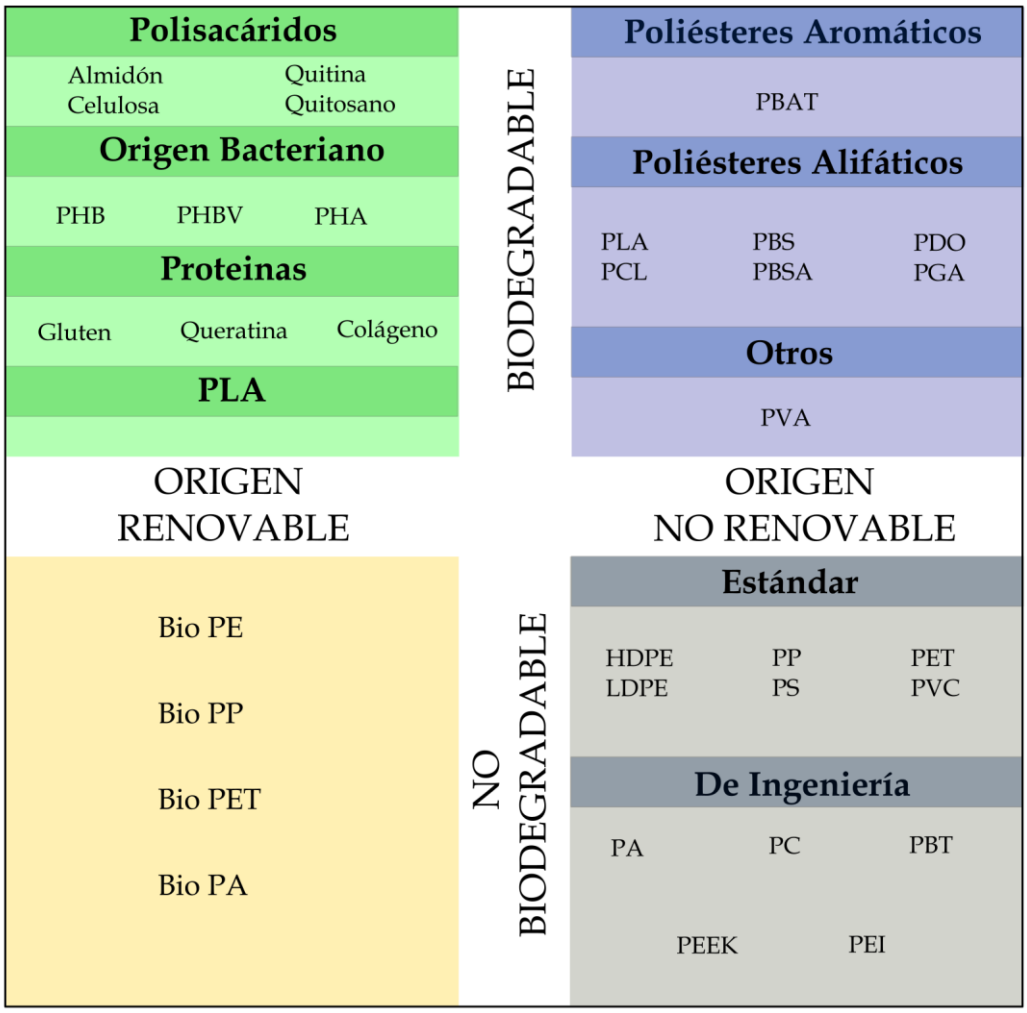

Figura I.1. Clasificación de los polímeros termoplásticos basados en su origen y en su capacidad de biodegradabilidad.

Se pude observar que los biomateriales o en su término más estricto, los biopolímeros se pueden englobar en tres grupos. El primer grupo corresponde a los polímeros que se obtienen de fuentes renovables y que presentan la capacidad de biodegradarse. El segundo grupo está conformado por los polímeros derivados de compuestos petroquímicos, pero que presentan la capacidad de biodegradarse. El último grupo engloba a los polímeros que se obtienen de fuentes renovables pero que carecen de la capacidad de biodegradarse en condiciones de compost controlados. Para completar el panorama de los polímeros se presenta un cuarto grupo, en este se encuentran los polímeros que provienen de fuentes no renovables y que no presentan la capacidad de biodegradarse.

I.1.1.1. Polímeros de origen no renovable no biodegradable

El desarrollo y auge de estos polímeros empezó desde mediados del siglo XIX, ganando popularidad debido al amplio abanico de composiciones químicas que se

pudieron obtener, además de su bajo coste de producción. Las buenas propiedades mecánicas, químicas, de barrera, su rigidez, y la facilidad de moldeo han provocado que su popularidad aumente. En este grupo se encuentran polímeros comúnmente denominados *"commodities"*, término que hace referencia al gran volumen de su producción y a su bajo precio [5]. En esta categoría se encuentra el polipropileno (PP), el polietileno de alta y de baja densidad (HDPE, LDPE), el poliestireno (PS), el policloruro de vinilo (PVC) y el polietilén tereftalato (PET) [6]. El PP, LDPE, y el HDPE encabezan la lista de los termoplásticos más utilizados en Europa en el 2019 con una presencia en el mercado del 19,4 %, 17,4 % y 12,4 %, respectivamente. La facilidad que tiene este grupo a ser moldeados por moldeo por inyección, moldeo por soplado, termoconformado, extrusión, entre otras [7], hacen que estén presentes en sectores como el del envasado de alimentos (envolturas de alimentos, botellas de agua, botellas de champú…), sectores de construcción (tuberías, marcos de ventanas, perfiles, aislamiento eléctrico…), sector de automoción (partes de automóvil), sector de esparcimiento y deportes (juguetes, equipamiento deportivo), agricultura, entre otros. En la figura I.2. se puede observar la estructura química de estos materiales poliméricos.

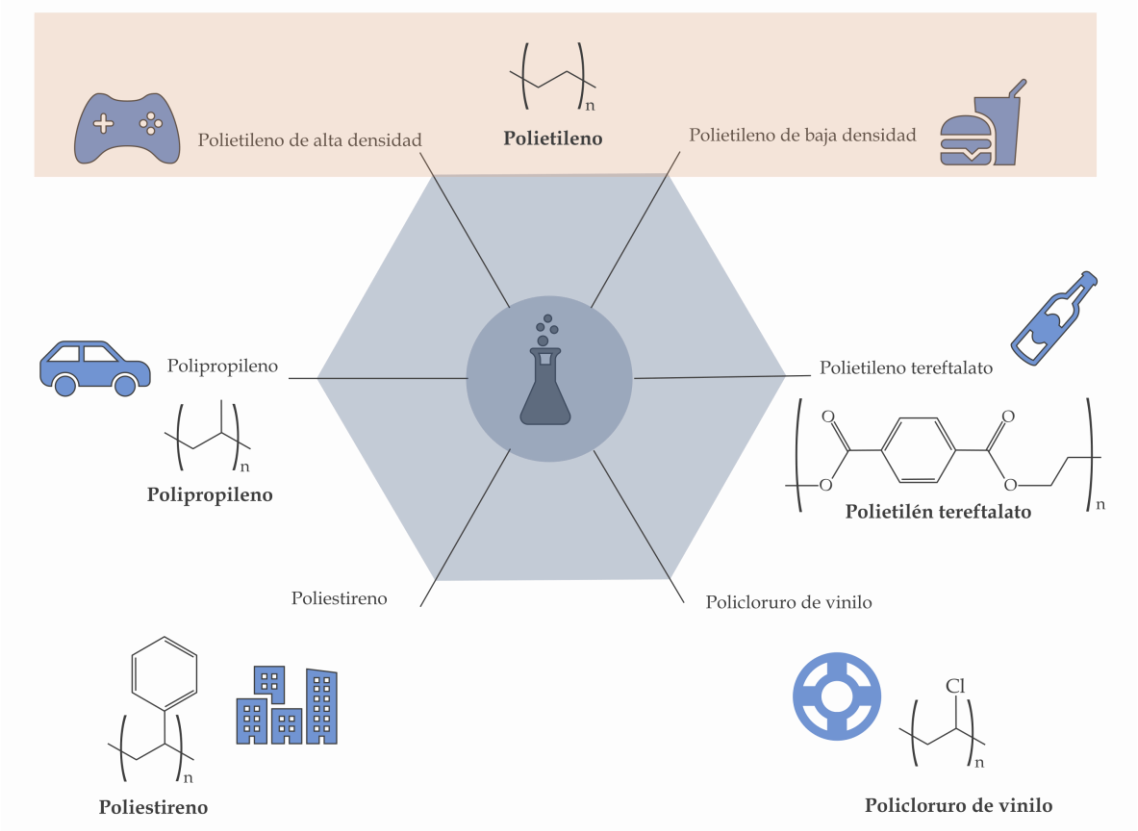

Figura I.2. Estructura química de polímeros *"commodities"*.

En general la composición de estos polímeros son cadenas de carbono, hidrógeno, oxígeno, nitrógeno y cloro, dando como resultado un material inerte incapaz de degradarse y/o descomponerse en el medioambiente, por ende, resultan en materiales resistentes a la biodegradación. Como se mencionó anteriormente esto provoca una acumulación incontrolable de desechos, derivados principalmente de la industria del envase y embalaje.

A diferencia de los ya mencionados polímeros *"commodities"* que su empleo se suele hacer en aplicaciones que tengan bajos requerimientos mecánicos. Sectores como el de ingeniería e industrial son necesarios una nueva gama de materiales poliméricos de alto rendimiento, conocidos comúnmente como "polímeros de ingeniería" en general se buscan materiales con propiedades superiores, pudiendo ser una alta resistencia mecánica o térmica, o con propiedades de aislamiento térmico o eléctrico.

Dentro de esta subcategoría se encuentra las poliamidas (PA), las poliamidas aromáticas se destacan por su sobresaliente resistencia térmica y propiedades mecánicas [8]. Teniendo su aplicación en la industria de armamento en la fabricación de chalecos antibalas, o en productos textiles resistentes al fuego, además de su aplicación en ingeniera en productos con alta resistencia a la corrosión química o la abrasión [9,10]. El policarbonato (PC) es otro polímero que se encuentra en esta subcategoría, el PC es un polímero amorfo utilizado en ingeniería debido a su buena estabilidad térmica y dimensional, además de su alta transparencia y buenas propiedades mecánicas que mantienen las piezas después del moldeo. Dando como nicho de aplicación el sector de la construcción, transporte, en aplicaciones de iluminación o como reemplazo al vidrio [11]. También se encuentra el polibutilén tereftalato (PBT); el PBT es un poliéster que posee buenas propiedades mecánicas, elevadas velocidades de cristalización y facilidad de moldeo, resistencia a la intemperie y a productos químicos. Esto ha hecho que gane terreno en la fabricación de fibras, en el sector automotriz con la fabricación de piezas, en el sector de ingeniería electrónica con la fabricación de componentes [12,13]. En la figura I.3. se puede observar la estructura química de estos polímeros de ingeniería.

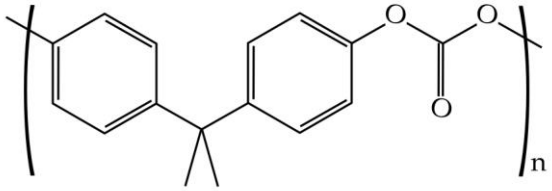

Policarbonato

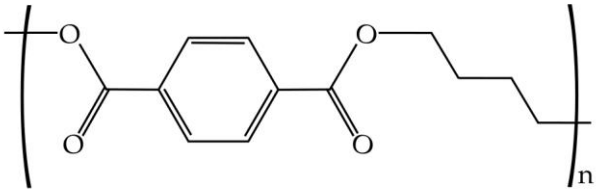

Polibutilén tereftalato

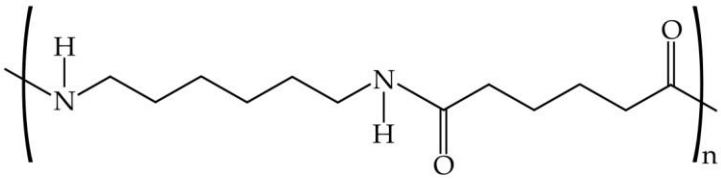

Poliamida

Figura I.3. Estructura química de polímeros de ingeniería.

Sectores especiales como el aeroespacial, microelectrónico, medicina, energético, o aviación de alta velocidad donde se necesitan requerimientos específicos como alta resistencia, buena estabilidad térmica, excelsa estabilidad dimensional y retención de propiedades mecánicas a altas temperaturas y a condiciones externas adversas. Existe un pequeño grupo de polímeros, los denominados polímeros de alto rendimiento, donde materiales como el poli(éter-éter-cetona) (PEEK), o poliéter imida (PEI) son requeridos [14,15]. La estructura de estos polímeros de alto rendimiento se puede observar en la figura I.4.

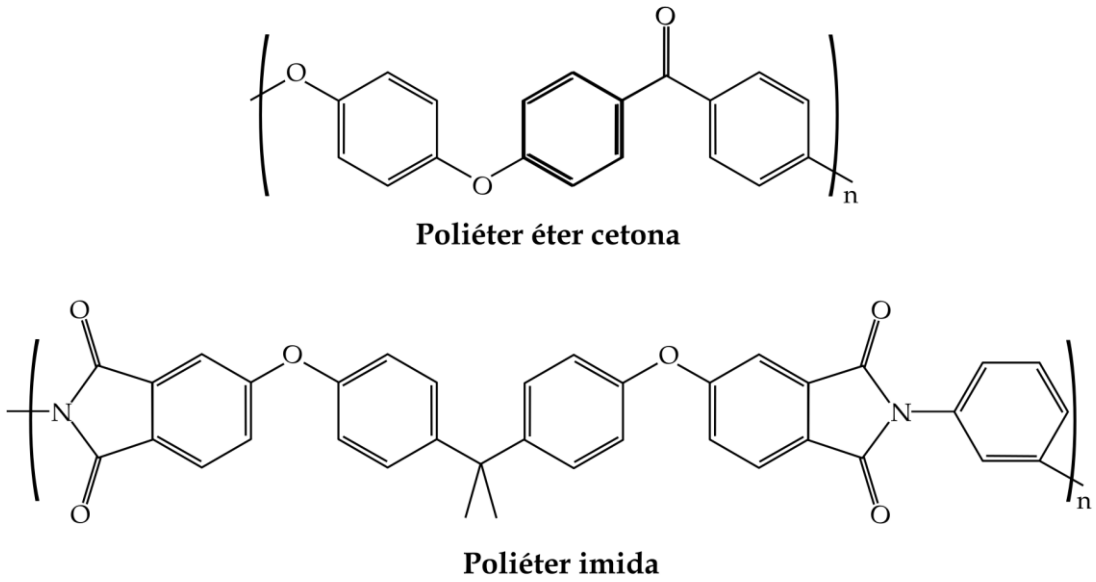

Figura I.4. Estructura química de polímeros de alto rendimiento.

I.1.1.2. Polímeros de origen renovable no biodegradables

Como se citó en la sección anterior, parte del aumento en la huella de carbono generada por el uso de materiales poliméricos deriva en las emisiones de CO_2 resultante de la producción de estos polímeros cuya materia prima es de origen fósil. La búsqueda de reducir y/o eliminar la dependencia que se tiene del uso del petróleo como materia prima ha provocado que el desarrollo de materiales poliméricos provenientes total o parcialmente de materias primas renovables sea inminente.

Polímeros termoplásticos como el bio-polipropileno (bio-PP), bio-polietileno (bio-PE), bio-polietilén tereftalato (bio PET), o bio-poliamida (bio-PA), entran en este grupo de biopolímeros [16]. Estos biopolímeros tienen la ventaja de presentar las mismas propiedades que sus homólogos de origen petroquímicos, característica que los hacen una opción llamativa desde el punto de vista industrial y ambiental, ya que, son una alternativa viable a polímeros de uso común, con un evidente menor impacto medioambiental. A pesar de esto, dentro las características que heredan de sus homólogos petroquímicos esta la incapacidad de biodegradarse en condiciones controladas de compost. Esto se debe a que los monómeros que se utilizan para su síntesis son los mismos, como es el caso del bio-PE, donde se utiliza un monómero derivado del etileno, el cual se puede obtener por deshidratación del bio-etanol que se obtiene de la glucosa de productos como la caña de azúcar o rábanos, en lugar de la destilación de productos petroquímicos [17]. Caso similar ocurre con el bio-PP el cual se puede sintetizar de la deshidratación del butileno del bio-isobutanol que se obtiene de la glucosa [16].

El aumento de interés por parte de la sociedad en el uso de estos biomateriales se refleja en el crecimiento de su industria y producción, donde se observa una mejora constante en la tecnología de síntesis, ayudando a que su disponibilidad en el mercado aumente. Esto les coloca en una situación muy competitiva con sus homólogos de origen petroquímico, donde el precio volátil que tiene su precursor los coloca en una ligera desventaja.

I.1.1.3. Polímeros de origen no renovable biodegradables

La incorporación de materiales poliméricos biodegradables en la vida cotidiana se ha convertido en una opción factible para controlar los residuos sólidos generados por el consumo de plásticos de origen petroquímico, ya que muchos de estos residuos terminan sus días en vertederos, ya sean estos controlados o no. En esta categoría se pueden encontrar varios tipos de materiales como poliésteres con estructuras alifáticas o aromáticas.

En general, los poliésteres alifáticos están compuestos por monómeros unidos por grupos éster, estos grupos se pueden hidrolizar con facilidad, además, las enzimas que degradan a estos polímeros se encuentran en casi cualquier organismo. Esto es de gran utilidad ya que se puede biodegradar en cualquier ambiente biótico [18].

Dentro de los poliésteres alifáticos existen varios materiales que han ganado relevancia como es el caso de la poli(ε-caprolactona) (PCL) y el poli(ácido glicólico) (PGA), los dos materiales son termoplásticos semicristalinos con una alta cristalinidad de aproximadamente un 50% que aparte de ser biodegradable, son biocompatibles con el cuerpo humano, propiedad que les abre un gran abanico de oportunidades en aplicaciones en sectores de la medicina y la biomedicina. El PCL y PGA se suelen emplear en la fabricación de dispositivos para el suministro contralado de medicamentos, y al ser compatible con los tejidos se suele utilizar en suturas reabsorbibles o en la fabricación de soportes para la regeneración de huesos o ligamentos [19,20]. El envase y embalaje es otras de las áreas de mayor empleabilidad del PCL y el PGA como sustitutos a termoplásticos convencionales [21]. Ventajas como la rápida degradación y buenas propiedades barrera colocan al PGA como una buena opción para aplicaciones de vida útil corta o de un solo uso, como el envasado de alimentos [22]. La estructura de estos materiales se puede observar en la figura I.5.

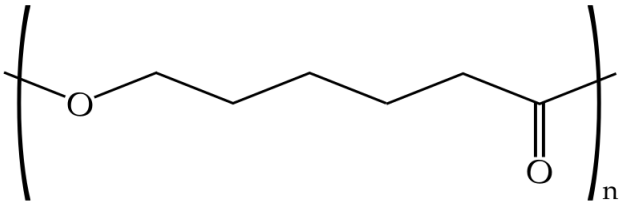

Policaprolactona

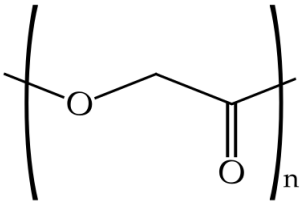

Ácido poliglicólico

Figura I.5. Estructura química de poliésteres alifáticos de origen no renovable biodegradables con alta cristalinidad.

El poli(butilén succionato) (PBS) y el poli(butilén succionato-*co*-adiapato) (PBSA) cuyas estructuras se pueden observar en la figura I.6., son biopolímeros que se han comercializado desde hace varios años, el PBS es un poliéster semicristalinos que presenta buenas propiedades mecánicas y una buena procesabilidad muy similares al polipropileno, lo que lo hace muy llamativo del punto de vista industrial, para aplicaciones como el envase y embalaje o productos de usos cotidianos. Tradicionalmente sus monómeros se obtienen del butanediol y ácido succínico; en la actualidad estos monómeros se pueden obtener de la fermentación de productos agroindustirales [23,24]. El PBSA es un poliéster que se sintetiza por la policondensación de butanediol, ácido succínico y ácido adípico. Este biopolímero llama la atención debido a su baja cristalinidad que le concede una alta biodegradabiliad por procesos enzimáticos al compararlos con otros polímeros, además de su alta ductilidad y buena resistencia química, propiedades que lo hacen apropiados para fabricación de bolsas compostables, productos de agricultura, *"films"*, entre otros [25].

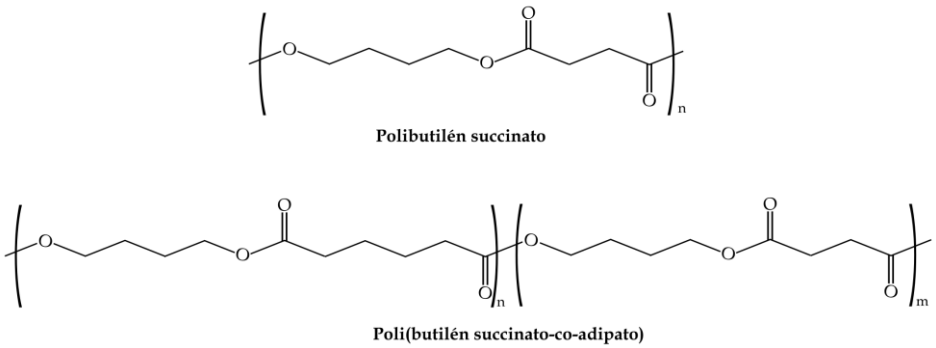

Figura I.6. Estructura química de poliésteres alifáticos de origen no renovable biodegradables con baja cristalinidad.

Adicional a los poliésteres alifáticos citados anteriormente, se encuentra el poli(butilén adipato-*co*-tereftalato) (PBAT) que es el resultado de la copolimerización entre monómeros alifáticos (poli(butilén adipato) (PBA)) y monómeros aromáticos (poli(butilén terftalato)(PBT)) (figura I.7.). Este biopolímero tiene una baja cristalinidad y buena procesabilidad lo que lo hace candidato a sustituir materiales como el polietileno, ya que posee propiedades mecánicas (elevada ductilidad) y térmicas similares, además de un alto carácter hidrófilo lo que lo hace adecuado para el sector del envasado de alimentos (*"films"*) y en el sector agrícola [26].

Es verdad que la capacidad que tienen estos biopolímeros de biodegradarse en condiciones de compost ayuda enormemente con el control de desechos generados, no obstante, no podemos olvidar el origen de su materia prima (origen fósil) y por lo tanto el impacto medioambiental que esto genera. Actualmente esto se está tratando de mitigar con la posibilidad de obtener los mismos materiales a partir de recursos renovables.

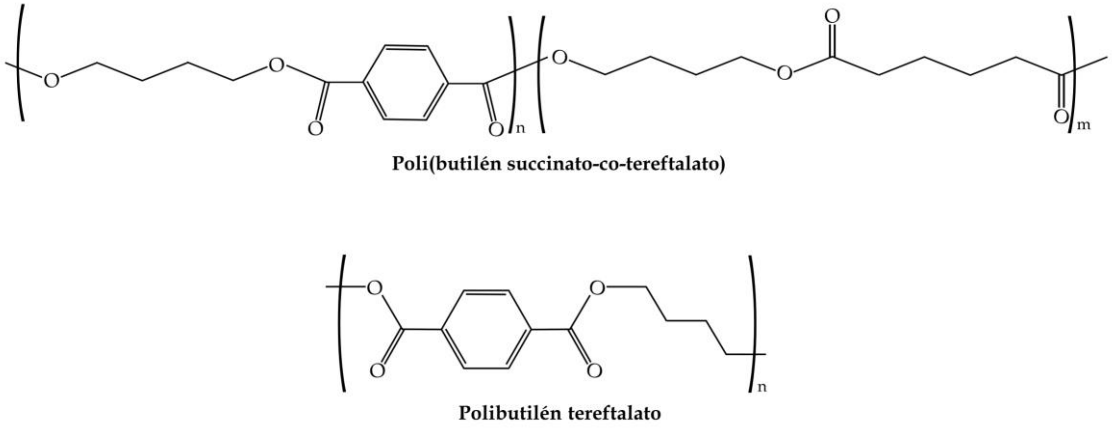

Figura I.7. Estructura química de poliésteres aromáticos de origen no renovable biodegradables.

I.1.1.4. Polímeros de origen renovable biodegradable

De los grupos de biopolímeros mencionados anteriormente podemos concluir, que a pesar de que su uso disminuye en algún porcentaje el impacto medioambiental, ya sea cambiando el origen de su materia prima, es decir de productos derivados del petróleo a productos derivados de recursos renovables, o debido a su capacidad de biodegradarse; no podemos eliminar completamente la huella de carbono que se deriva del uso de materiales poliméricos.

Para solventar estas carencias, se plantea un interesante grupo de biopolímeros que presentan estas dos características, es decir, su materia prima es de origen renovable y tienen la capacidad de biodegradarse en condiciones de compost.

Dentro de estos polímeros naturales se encuentran los polisacáridos y proteínas, polímeros derivados de la biomasa. Los polisacáridos más abundantes son la celulosa, el almidón, y la quitina o quitosano. Estos presentan una gran importancia en la industria ya que contienen grupos funcionales polares, que pueden formar puentes de hidrógeno al mezclarlo con otros polímeros (poliésteres, poliamidas, entre otros). Generalmente son utilizados para la fabricación de *"films"*, membranas e hidrogeles [27]. El almidón es un polisacárido que se pude obtener de una gran variedad de fuentes como la caña de azúcar, las patatas, remolacha, entre otras, razón por la cual genera una gran abundancia de materia prima y por ende bajo costo. El almidón es el precursor de los conocidos como almidones termoplásticos (TPS) y del poli(ácido láctico) o ácido poliláctico (PLA), uno de los polímeros con mayor presencia en diferentes áreas industriales, debido a su gran potencial.

Por otro lado, están las proteínas que pueden ser de origen vegetal y animal. La soja y el gluten son de las proteínas vegetales con mayor popularidad, debido en gran manera a su bajo costo. La soja industrialmente se suele utilizar tanto en la fabricación de materiales termoestables o de polioles de soja, dándole una gran versatilidad en el mundo de los materiales compuestos, o en sectores industriales en forma de adhesivos, *"films"* y recubrimientos, aplicaciones que no requieren altas prestaciones [28]. El gluten de trigo o gluten como se le conoce comúnmente se obtiene de la planta del trigo y es uno de los subproductos más baratos y abundantes. Esta proteína presenta alta viscosidad, elasticidad y capacidad de absorción de agua la cual hace que sus propiedades a largo tiempo dependan de su contenido de humedad, lo que limita su uso en ingeniería [29].

Proteínas de origen animal como la gelatina y el colágeno presentan una alta biocompatibilidad, biodegradabilidad y muy baja antigenicidad. En sí, el colágeno constituye la mayor parte de la estructura de tejidos como tendones, cartílagos o piel, razón por la cual uno de sus mayores campos de aplicación es la biomedicina. La gelatina se obtiene de la hidrolisis parcial del colágeno y tiene una gran presencia en el sector alimentario, cosmético, farmacéutico y envasado biodegradable debido a su biocompatibilidad, biodegradabilidad, propiedades viscoelásticas y presentar características como la transparencia o la carencia de olor y sabor [30].

Finalmente, se tiene un grupo denominado polímeros bacterianos, aquí se encuentran los polihidroxialcanoatos (PHAs) y se refirieren a aquellos biopolímeros sintetizados completamente por microrganismos en condiciones específicas (exceso de carbono y bajas concentraciones de otros minerales) [31]. Propiedades como biocompatibilidad, biodegradabilidad, buena resistencia a la luz ultravioleta, y su fácil procesado lo están colocando como posible sustituto al PLA. A pesar de esto sus propiedades dependen mucho de la longitud de su cadena, la distancia entre el grupo R y el enlace éster. Dentro de los más utilizados podemos nombrar al poli(3-hidroxibutirato) (P3HB) o (PHB) como se le conoce comúnmente, el poli(3-hidroxivalerato) (PHV), o el poli(4-hidroxibutirato) (P4HB), estos PHAs presentan cadenas cortas (3-5 carbonos) (figura I.8.) que los dotan de una alta rigidez y fragilidad, factor que limita su uso en aplicaciones de alto rendimiento. PHAs con cadenas medias (6-14 carbonos) como el poli(3-hidroxioctanoato) (P3HO) son elastómeros que presentan una baja resistencia mecánica, o PHAs con cadenas largas (> 15 carbonos) como el poli(3-hidroxipentadecanoato) [32].

Por desgracia, aunque estos materiales medioambientalmente son prácticamente perfectos, existen varios problemas relacionados a sus propiedades químicas, físicas y mecánicas, además de su coste de producción. Estas carencias han abierto puertas para que grupos de investigación dediquen sus esfuerzos a la mejora de estas propiedades sin sacrificar su biodegradabilidad, con ansias de obtener materiales que puedan competir y sustituir a los convencionales.

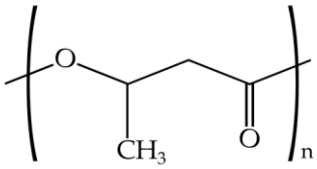

Poli(3-hidroxibutirato)

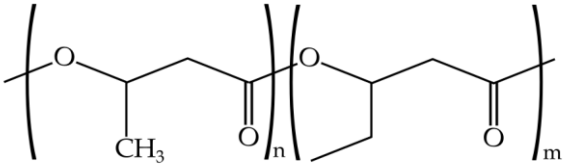

Poli(3-hidroxibutirato-co-3-hidroxivalerato)

Figura I.8. Estructura química de algunos polímeros de origen renovable biodegradables.

I.1.2. Polímeros termoestables

Los polímeros termoestables son otro de los grandes grupos que forma parte de esta familia de los materiales poliméricos. Estos materiales a diferencia de los materiales termoplásticos sufren un cambio químico (polimerización o curado), es decir, pasan de un estado líquido a un estado sólido rígido al sufrir un proceso de entrecruzamiento. El proceso de curado hace referencia a la formación de estructuras tridimensionales por la unión química de sus moléculas. El proceso químico que se genera es irreversible, es decir una vez formado la interconexión de las moléculas no se puede deshacer térmicamente, provocando una descomposición química y/o alteraciones en su estructura al incrementar su temperatura, lo que por consecuencia hace imposible su refundido y su posible reconformado (reciclado) [33].

Por desgracia, la gran mayoría de polímeros termoestables son derivados de productos petroquímicos, lo que sumado a su incapacidad de reciclaje implica un notable impacto ambiental. Esto conlleva un gran problema, tomando en cuenta que cada vez se está expandiendo su uso a ya no solo aplicaciones industriales, sino a artículos cotidianos. A pesar de que en las últimas décadas se ha logrado un avance en el desarrollo de materiales termoestables de origen renovable, todavía no se alcanza a el punto de ser comercialmente viable, debido al elevado coste y las limitadas prestaciones que estos materiales ofrecen.

Dentro de los polímeros termoestables más utilizados en la industria se encuentran las resinas epoxi, resinas de poliéster insaturado, poliuretanos, fenol-formaldehido, viniliésteres, entre otros.

I.1.2.1. Resinas epoxi

Las resinas epoxi (EP) acuñan su nombre debido a la presencia de grupos oxirianos (al menos uno) en su estructura (figura I.9**)**, este grupo suele ubicarse generalmente en los terminales de cadena, factor por el cual lo hacen altamente reactivo [34]. Propiedades como alta resistencia química, buena estabilidad dimensional, alta resistencia de adhesión, excelentes propiedades mecánicas y térmicas han marcado su gran presencia en aplicaciones industriales como adhesivos, recubrimientos, electrónica y materiales compuestos. No hay que olvidar una de las grandes desventajas que presenta este tipo de resinas, su fragilidad debido a su alto grado de entrecruzamiento.

Figura I.9. Representación esquemática de la estructura de un anillo oxiriano.

Dentro las resinas epoxi más utilizadas actualmente se encuentran las basadas en diglicidil éter de bisfenol A (DGEBA) (figura I.10.), diglicidil éter de bisfenol F (DGEBF) y tetra glicidil metileno dianilina (TGMDA). En términos generales las propiedades del sistema dependen de su peso molecular, donde resinas con bajo peso molecular suelen ser liquidas y resinas con un peso molecular mayor suelen ser viscosas o sólidas. El sistema epoxi se completa con la incorporación de algún agente de entrecruzado o endurecedor, este agente es el que en su mayoría influencia a las propiedades finales del sistema, lamentablemente al igual que la resina, los agentes de entrecruzado con mayor presencia en el mercado provienen de productos petroquímicos y presentan una alta toxicidad previo a su curado, pudiendo causar daño en la piel, ojos y pulmones. La elección del agente de entrecruzamiento en general depende de los requerimientos de procesado, con eso se tiene que los más utilizados son de tipo amina, anhídridos, ácidos, por nombrar los principales [35].

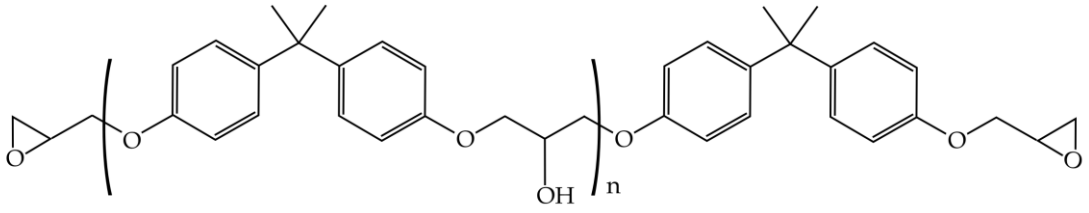

Figura I.10. Representación esquemática de la estructura química de una resina epoxi DGEBPA.

Resinas epoxi de alto rendimiento medioambiental

Con ansias de disminuir el uso de resinas epoxi de origen petroquímico, varios avances se han conseguido en la formulación de resinas epoxi derivada total o parcial de orígenes renovables, el uso de aceites vegetales (VOs) es de los recursos con mayor auge para la formulación de resinas termoestables, debido a su estructura, que presenta insaturaciones (C=C) las cuales pueden ser modificadas y dotadas de grupos funcionales específicos, siendo la epoxidación una de las más utilizadas, donde dichas insaturaciones son convertidas en grupos oxirianos. Entre los aceites más utilizados se encuentran los de canola, palma, soja, ricino, lino, entre otros. Industrial y comercialmente el aceite epoxidado de soja (ESBO), aceite epoxidado de ricino (ECO) y el aceite epoxidado de lino (ELO) son los que tienen mayor presencia [36,37]. En la figura I.11. se puede observar las estructuras de estos aceites vegetales epoxidados. El bajo precio y la abundancia de la materia prima es lo que los hace muy atractivos, pero en muchos casos presentan propiedades mecánicas que todavía no pueden rivalizar con resinas epoxi sintéticas.

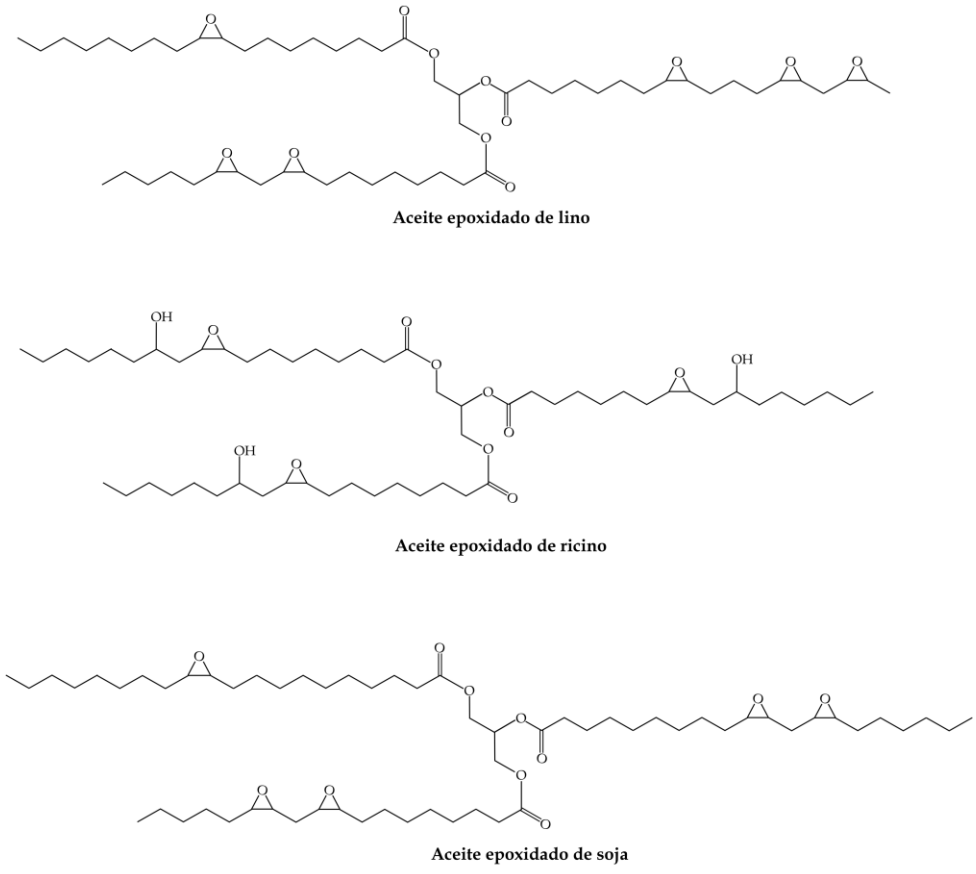

Figura I.11. Representación esquemática de la estructura química de algunos aceites epoxidados.

A pesar de esto, el uso de estas resinas epoxidadas han encontrado un nicho muy valioso como plastificantes, estabilizantes o como diluyentes reactivos [38,39]. Varias resinas epoxi sintéticas disponibles comercialmente tienen ya un contenido parcial de origen renovable sin que este comprometa sus propiedades. Con esto se ha logrado mitigar en cierto nivel la huella de carbono que causa el uso de estos materiales.

I.1.2.2. Resinas de poliéster insaturado

Las resinas de poliéster insaturado o resinas de poliéster (UP) como se le conoce comúnmente, se obtiene a través de la condensación de ácidos o anhídridos insaturados y un dialcohol [40]. El bajo coste, la buena procesabilidad y las relativamente buenas propiedades mecánicas y químicas, son características que la han ubicado dentro de las resinas comerciales con mayor uso en aplicaciones de uso común como en la fabricación de piscinas, tanques de agua, sillas, o en aplicaciones de ingeniería en el sector automotriz, naval y de aviación. El balance que se tiene entre el coste y rendimiento es quizá la mayor ventaja que se tiene con este tipo de resinas. Como en las resinas epoxi, las propiedades finales van a depender del tipo de agente entrecruzador (diácido o diol), catalizadores y aceleradores. En general el uso de anhídrido maleico suele ser mayor, debido a su bajo costo, aunque las resinas de fumarato y maleato suelen ofrecer una mayor densidad de entrecruzamiento [41], entre los dialcoholes suelen estar el etileno glicol y polipropileno glicol. En la figura I.12. se puede observar la estructura química de una resina de poliéster insaturado.

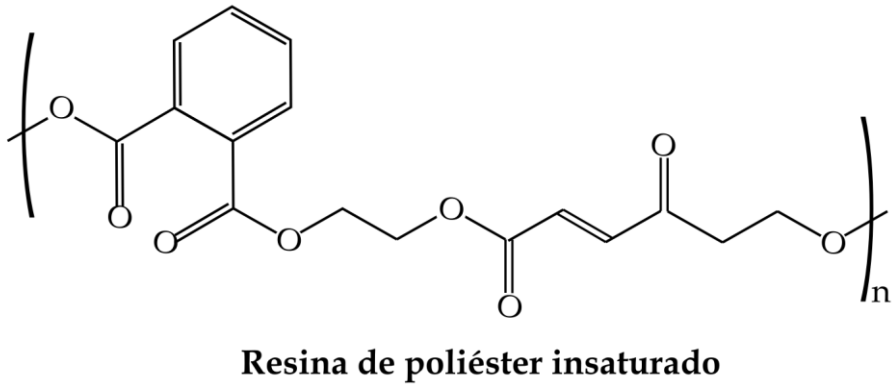

Figura I.12. Representación esquemática de la estructura química de una resina de poliéster insaturado.

Resinas de poliéster insaturado de alto rendimiento medioambiental

En la actualidad el uso de compuestos de origen natural, como los carbohidratos o aceites vegetales se han utilizado como reemplazo a los reactivos sintéticos de las actuales resinas de poliéster insaturado.

Como se mencionó las resinas UP dependen del tipo de diácido que forma su estructura principal, los diácidos de origen natural más desarrollados son el ácido itacónico, ácido succínico y el butaneidiol [42]. Otra estructura con gran potencial es la de base isosorbida ya que posee una estructura de anillo bicíclico y dioles quirales, teniendo como ventaja que se puede obtener ya sea del almidón (hidrolisis enzimática) o del sorbitol (deshidratación catalítica), [43].

De los problemas que desde el punto de vista industrial se tiene, es encontrar un diluyente reactivo (RD) capaz de sustituir al estireno, ya que debería poseer características como: baja viscosidad, buena compatibilidad con el prepolímero, además de una capacidad suficiente para copolimerizar con las insaturaciones de los prepolímeros. En este sentido, varios avances se han realizado, logrando con éxito utilizar monómero derivados de ácidos grasos acrilados y metacrilados, monómeros aromáticos, levulinato de vinilo, entre otros. La limitante que se encuentra al sustituir al estireno con alguno de estos compuestos es una baja temperatura de transición vítrea y bajas propiedades mecánicas [44,45].

I.1.2.3. Resinas de viniléster

Las resinas de viniléster (VE) son resinas que se encuentran formados por una estructura principal y por dos terminales que pueden ser un acrilato o un metacrilato, donde, para controlar su procesabiliad se suele utilizar diluyentes reactivos durante el proceso de copolimerzación. A pesar de ser consideradas como parte de las resinas poliéster insaturado debido a que presentan un proceso de entrecruzamiento muy similar, la verdad es que, su estructura principal se puede obtener a partir de resinas epoxi, resinas de poliéster, por nombrar las principales, siendo las derivadas de resinas epoxi la que tiene una presencia mayor en el mercado.

La resina derivada en diglicidil éter de bisfenol A y esterificada con ácido de metacrilato son de las más utilizadas. Este tipo de resinas presentan excelente resistencia química, razón por la cual se suele utilizar en la fabricación de tuberías, conductos, depuradores, entre otros. Además, presenta una relativamente buena estabilidad dimensional, ligeramente menor a las resinas epoxi, pero superior a las

resinas de poliéster insaturado, así como una buena resistencia eléctrica [46,47]. Como diluyente reactivo se suele utilizar el estireno debido a la facilidad y rapidez que reacciona con endurecedores con funcionalidad acrilato o metacrilato. En la figura I.13. se puede observar la estructura de una resina derivada del bisfenol A y el epicloroidrin.

Resina vinil éster derivada del bisfenol A y el epicloroidrin

Figura I.13. Representación esquemática de la estructura química de una resina vinil éster obtenida del bisfenol A y el epicloroidrin.

Resinas de viniléster de alto rendimiento medioambiental

Haciendo símil con las resinas presentadas anteriormente, las resinas de viniléster también presenta una variante de origen ecológico, la ventaja que tiene este tipo de resinas es que sus precursores son similares a los utilizados tanto en las resinas epoxi, así como en las resinas de poliéster. Dentro de los principales precursores se encuentran productos lignocelulósicos y aceites vegetales [48].

Los aceites vegetales han sido un punto clave en el desarrollo de resinas termostables debido a la facilidad que tienen en ser modificados y dotados de grupos funcionales específicos, en el caso de las resinas de viniléster el más utilizado es el aceite de soja, el cual debe ser funcionalizado por medio de la inserción de grupos acrilatos o metacrilatos, este proceso se debe realizar subsecuente a un proceso de epoxidación. Otros de los aceites utilizados es el aceite de cardanol, este puede ser modificado para obtener un entrecruzador o un diluyente reactivo. Además, se puede utilizar la sacarosa, materiales lignocelulósicos (furanos, isosorbida, lignina) [49,50].

Como se mencionó anteriormente, se han presentado varias alternativas al estireno como diluyente reactivo, entre estos se encuentra monómero de ácidos grasos acrilados y metacrilados siendo los principales los derivados de aceite de soja, cardanol, furanos, así como los derivados de la lignina [51].

I.1.2.4. Resinas fenólicas

Las resinas fenólicas (PF) son aquellas que se obtienen por la policondensación de compuestos fenólicos (m- cresoles, p-fenifenol, xilenol) con el formaldehido en un

ambiente ácido o básico como se puede observar en la figura I.14. Las PFs desde su descubrimiento se han utilizado en el sector automotriz, aeroespacial en la fabricación de elementos de alto rendimiento, en la fabricación de adhesivos, en el sector de procesamiento de madera, material eléctrico y computación, debido a que presenta alta resistencia mecánica, química y térmica, infusibilidad, e inflamabilidad, excelentes características de aislamiento y fácil procesamiento. Sin embargo, estas resinas presentan varias desventajas siendo una de las principales su alta fragilidad, así como la emanación de fuertes olores durante el proceso de curado.

De la reacción del fenol con el formaldehido se puede obtener dos clases de PF, que puede ser de tipo resol o de tipo novolaca formándose cuando la relación molar fenol: formaldehido es mayor que 1 en condiciones básicas o cuando la relación molar fenol: formaldehido es menor que 1 en condiciones acidas, respectivamente [52,53].

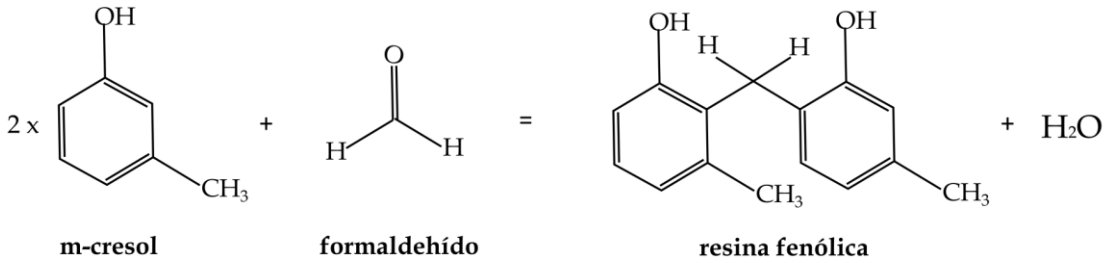

Figura I.14. Reacción química de condensación para la obtención de una resina fenólica a través de un cresol y formaldehido.

Resinas fenólicas de alto rendimiento medioambiental

El esfuerzo de disminuir el uso de productos sintéticos, han hecho que se genere innovación en la síntesis de resinas fenólicas de origen natural, dentro de los compuestos utilizados están los derivados de la biomasa, encabezados por la lignina (figura I.15.), o el cardanol que es un subproducto del líquido de la cascara del anacardo (CNSL), donde se suelen utilizar como sustitutos del fenol.

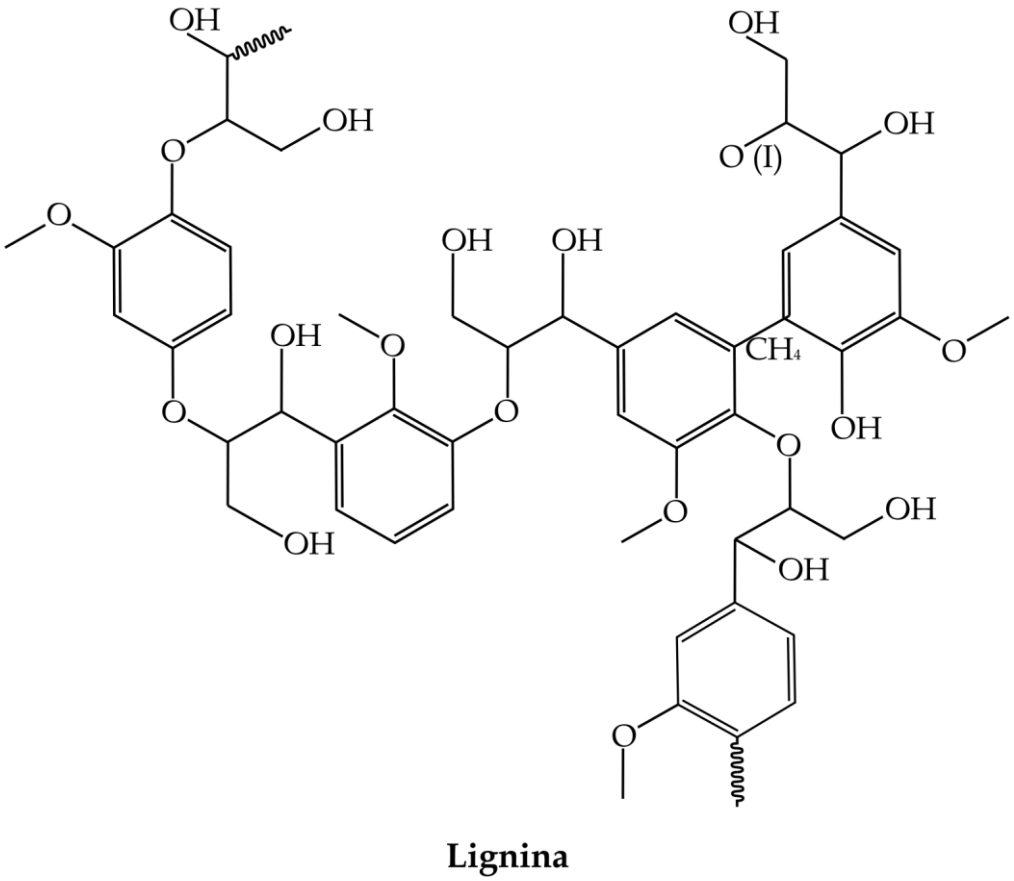

Figura I.15. Estructura de la lignina.

En la literatura se presentan varias investigaciones donde se aprovecha la lignina como sustituto del fenol en la preparación de resinas fenólicas de curado rápido, esto se debe a que la su estructura (alcohol *p*-cumárico, alcohol coniférilico, y alcohol sinapílico) es muy similar. Para que la lignina pueda ser utilizada se suele modificar con el propósito de aumentar su reactividad. Varias técnicas suelen ser utilizadas como la metilación, fenolación y desmetilación, donde la desmetilación es una de las más efectivas para obtener grupos hidroxilos fenólicos y disminuir el contenido de grupos metóxilos [54,55].

La utilización del cardanol para la preparación de resinas fenólicas es de gran relevancia debido a que gracias a la presencia de grupos fenólicos en su estructura se pueden sintetizar resinas novolacas o resoles, al reaccionarlas con formaldehido. Con esto se puede obtener resinas con buenas propiedades mecánicas, con alta dureza y transparencia, o incluso una mejor estabilidad térmica. Estas propiedades pueden ser similar o incluso mejores que las resinas fenólicas convencionales [56,57].

La disminución en el uso de formaldehido debido a los problemas de salud y el efecto ambiental que este acarrea [58], han hecho que varias alternativas de origen orgánico sean propuestos, entre estos está el hidroximetilfurfural, el furfural, y la vainillina. Estos compuestos se pueden obtener de productos ricos en carbohidratos y celulosa [59].

I.2. Tecnología del poli(ácido láctico)

El poli(ácido láctico) (PLA) o ácido poliláctico es un polímero termoplástico perteneciente a la familia de los poliésteres alifáticos, este bioplástico es de los más relevantes y con mayor presencia a nivel comercial, debido en gran manera a que presenta una buena procesabilidad semejante a los *"commodities polymers"*, buenas propiedades mecánicas, además a que gracias a su estructura es biocompatible y biodegradable.

Su monómero iniciador es el ácido láctico, este se puede obtener por medio de síntesis química de productos derivados del petróleo, o de fuentes completamente renovables [22]. El PLA se puede obtener naturalmente de la fermentación bacteriana de productos ricos en almidón como la batata, maíz, patatas, caña de azúcar, remolacha, por nombrar algunos [60,61], dando como resultado una molécula de estructura quiral presente en dos estereoisómeros nombrados L(+)-ácido láctico y D(-)-ácido láctico (figura I.16) [62].

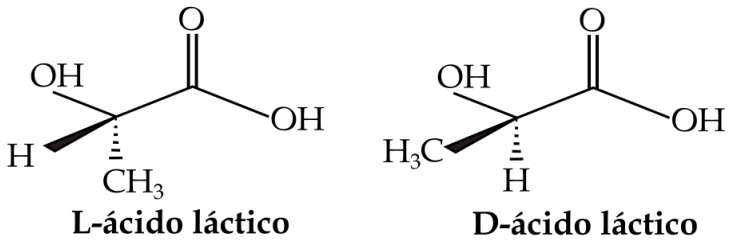

Figura I.16. Estructura química de los isómeros del ácido láctico.

La presencia de estos dos isómeros le da la capacidad al PLA a que su estructura pueda ser fácilmente modificada al controlar la mezcla de estos, pudiendo obtener polímeros amorfos de alto peso molecular o polímeros cristalinos.

En general el PLA presenta tres formas isoméricas típicas que dependen del monómero utilizado. El primero es el poli(L-ácido láctico)(PLLA), el poli(D-ácido

láctico)(PDLA) y el poli(DL-ácido láctico)(PDLLA), siendo los dos primeros ópticamente activos y cristalizables, y el ultimo ópticamente inactivo y no cristalizable [61].

I.2.1. Obtención del poli(ácido láctico)

La síntesis del PLA se pude realizar por tres vías las cuales determinaran las propiedades finales del mismo, la primera es a través de la policondensación del ácido láctico, la segunda a través de la polimerización por apertura de anillo (ROP, *"ring opening polymerization"*) de la lactida y la última es a través de la condensación por deshidratación azeotrópica. En la figura I.17. se puede observar un esquema representando las diferentes vías de obtención del PLA.

La policondensación del ácido láctico es el método más barato para la producción de PLA, el material resultante es un PLA de bajo peso molecular, frágil y prácticamente inútil en aplicaciones industriales. El bajo peso molecular es el resultado del agua que se genera en el proceso y la dificultad en eliminarla debido a que la difusión de la humedad en el polímero fundido es muy lenta, razón por la cual se debe utilizar diferentes tipos de solventes, altas temperaturas y alto vacío para la eliminación de esta. La remoción de solventes en el sistema hace prácticamente imposible la obtención de polímeros de alto peso molecular, factor por el cual es necesario la incorporación de agentes de acoplamiento y/o aditivos que ayuden a la esterificación. Haciendo que se encarezca y se complique el proceso de producción, provocando que la práctica de esta ruta vaya disminuyendo [63,64].

Por otro lado, se tiene la síntesis atreves de la apertura de anillo de la lactida. Este proceso es el más utilizado industrialmente, ya permite obtener grados de PLA con alto peso molecular (M_w>100000 g/mol). La clave de este método es el uso de lactida (dímero cíclico) de un alto grado de pureza, la cual puede ser obtenida por medio de la despolimerización catalítica del polímero (bajo peso molecular) producido por la condensación que posteriormente es purificado por un proceso de destilación. Así finalmente, el PLA puede ser obtenido por la reacción de apertura de anillo de ésta lactida purificada a temperaturas por encima del punto de fusión de la lactida e inferiores a la temperatura de degradación del PLA [22,65]. Gracias a que el proceso de síntesis tiene un mayor grado de control, es posible controlar de igual manera las propiedades finales del polímero, pudiendo modificarlas y generar diferentes grados para aplicaciones específicas.

El último método de obtención del PLA es por medio de la deshidratación azeotrópica, método en donde el ácido láctico y un catalizador se deshidratan

azeotropicamente en un disolvente aprótico de alto punto de ebullición a reflujo, bajo presiones reducidas. Por medio de este método se pueden obtener PLA de un peso molecular superior a 300000 g/mol [66].

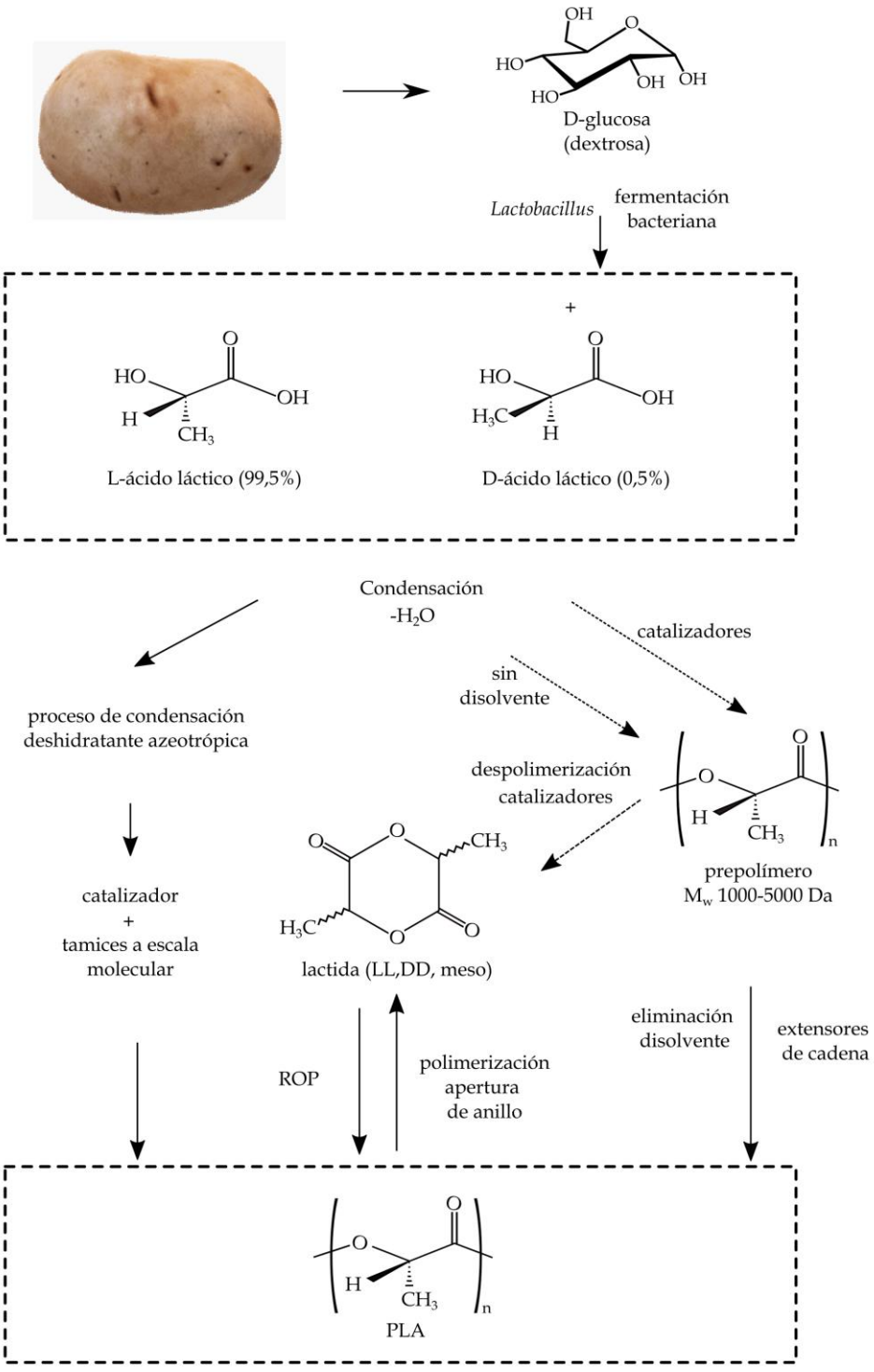

Figura I.17. Representación esquemática de las vías de obtención del PLA.

I.2.2. Propiedades generales del poli(ácido láctico)

Las propiedades del PLA dependen de varios factores como el peso molecular, la estereoquímica del monómero, la cristalinidad, etc. Donde la estereoquímica se puede controlar a través de la polimerización de los isómeros L-ácido láctico, D-ácido láctico, o D, L-ácido láctico para formar estructuras aleatorias, y el peso molecular se controla a través de la adición de compuestos hidróxilos, y de la pureza de la lactida.

El grado de cristalinidad en el PLA aumenta con el aumento de porcentaje del isómero (L-), así, un PLA con un porcentaje mayor al 93 % del isómero (L-) son semicristalinos. Un PLA completamente amorfo se obtiene cuando el porcentaje del isómero (L-) está entre un 50 y 93 % o cuando el porcentaje del isómero (D-) es mayor al 15 % [67,68].

I.2.2.1. Propiedades mecánicas

Como se comentó anteriormente las propiedades mecánicas dependen en gran manera de la estereoquímica del PLA, así como de su grado de cristalinidad. Esta última depende de la concentración del isómero (L-) así como de la presencia de agentes nucleantes, el tiempo y temperatura de procesado.

Un material con un mayor grado de cristalinidad presenta una mayor rigidez y resistencia, por ende, un PLA semicristalino tiene una mayor resistencia, que está caracterizada por un elevado módulo de Young, una elevada resistencia a la tracción, además de una baja capacidad de deformación. Por otro lado, se tiene que un PLA amorfo suele tener un comportamiento más dúctil representados por valores de módulo menores pero un mayor alargamiento a la rotura.

En general, el PLA es un material muy rígido con un comportamiento frágil, una baja resistencia al impacto, baja ductilidad y escasa capacidad de deformación. En este aspecto, varias investigaciones se están llevando a cabo para superar estas carencias, por medio de varias técnicas de modificación.

I.2.2.2. Procesabilidad

El PLA presenta propiedades muy similares a materiales termoplásticos clásicos o *"comodities"* como el poliestireno (PS), polipropileno (PP), o el polietilén tereftalato (PET), factor por el cual facilita su procesado por diferentes métodos convencionales como el moldeo por inyección, extrusión, soplado, laminado, termoconformado, entre otros. Esta característica lo coloca en una posición muy competitiva a nivel industrial.

Al igual que los polímeros derivados de productos petroquímicos, este biopolímero tiene limitaciones al procesarlo, como la degradación que sufre al calentarlo a altas temperaturas o a la cizalla. Además de que, es un material sensible al agua y puede sufrir degradación por hidrólisis, factor que hay que tener en cuenta antes de procesarlo.

El tipo de PLA va a dictar la temperatura de procesabilidad, teniendo que para un PLA amorfo la temperatura de trabajo tienen que ser superior a la temperatura de transición vítrea (T_g) y en el caso de un PLA semicristalino la temperatura tiene que ser superior a su temperatura de fusión (T_m), con el propósito de asegurar que los dominios cristalinos sean fundidos [69]. Hay que tener en cuenta que antes de cualquier tipo de procesado, el PLA debe secarse para eliminar o minimizar la humedad absorbida al máximo, así evitar la degradación hidrolítica que puede sufrir durante la etapa de fundido.

I.2.2.3. Propiedades térmicas

Al tener la capacidad de modificar su estructura (amorfo o semicristalino), se tiene que parámetros como la transición vítrea (T_g) o la temperatura de fusión (T_m) tienen mayor relevancia dependiendo el tipo de PLA. Donde para un PLA completamente amorfo la T_g tiene más importancia, ya a que grandes cambios con respecto a la movilidad de sus cadenas ocurren por encima de este valor. Pasando de un estado definido por un comportamiento frágil (< T_g) a un comportamiento dúctil, hasta llegar a la transición de un estado caucho a viscoso, hasta finalmente llegar a su descomposición (>300 ºC).

Por otro lado, para un PLA semicristalino se tiene que tanto la transición vítrea (T_g) como la temperatura de fusión (T_m) son parámetros que definen cambios físicos importante [70]. La T_g define la transición de un comportamiento frágil a uno dúctil. Y la T_m identifica el cambio desde un estado cristalino a un estado viscoso líquido, hasta finalmente llegar a la temperatura de degradación.

Generalmente un PLA presenta una T_g en el rango de los 50 a los 80 ºC, una T_m entre el rango de 130 a los 180 ºC y una temperatura de inicio de degradación por encima de los 190 ºC [4,71].

I.2.2.4. Propiedades barreras

Actualmente uno de los principales usos del PLA es en aplicaciones de envase-embalaje de alimentos, por lo que se hace necesario denotar las propiedades de barrera

que este material posee. En general los polímeros biodegradables suelen tener propiedades de barrera media- baja a los gases o vapores [72]. A pesar de esto, se tiene que a temperatura ambiente el PLA presenta una mayor permeabilidad de CO_2 que un PET, pero menores que un poliestireno cristalino, siendo más notorio para PLAs con alto grado de cristalinidad.

Otro factor que es determinante en la industria del envase-embalaje de alimentos es la capacidad de permeabilidad que tiene el oxígeno a trevés del material, ya que este es el causante de la oxidación de los alimentos. En este aspecto se tiene que menor es la capacidad de difusión del oxígeno cuanto mayor es el porcentaje de cristalinidad del PLA, debido a que el ordenamiento de las cadenas dificulta el movimiento de las moléculas de oxígeno. También tiene buenas propiedades barrera contra compuestos orgánicos como el acetato de etilo y el D-limoneno [70].

Además, se tiene que al ser un material hidrofóbico absorbe bajos porcentajes de agua y presenta buena resistencia al contacto con la grasa, incluso mejor que el polietileno de alta densidad.

I.2.2.5. Biodegradabilidad

De lo citado anteriormente tenemos que la biodegradación de un material implica la descomposición de estos en CO_2, metano, agua y biomasa. Este proceso ocurre por medio de diferentes mecanismos como la hidrólisis, oxidación, o degradación catalizada por encimas. En el caso del PLA la biodegradación ocurre en dos etapas, siendo la predominante la descomposición por hidrólisis, donde se produce una ruptura de los grupos éster de las cadenas, produciendo una disminución en el peso molecular del polímero y obteniendo oligómeros de bajo peso molecular capaces de disolverse y ser asimilados por microorganismos, para transformarlos en CO_2 y agua, como se puede observar en la figura I.18. [73].

Así como las propiedades mencionadas anteriormente, la biodegradabilidad depende de la composición estereoquímica, en especial del grado de cristalinidad. Teniendo que la degradación hidrolítica que sufre un PLA con alta cristalinidad suele ocurrir en grandes periodos de tiempo (varios meses o años), y un PLA amorfo se suele degradar en semanas.

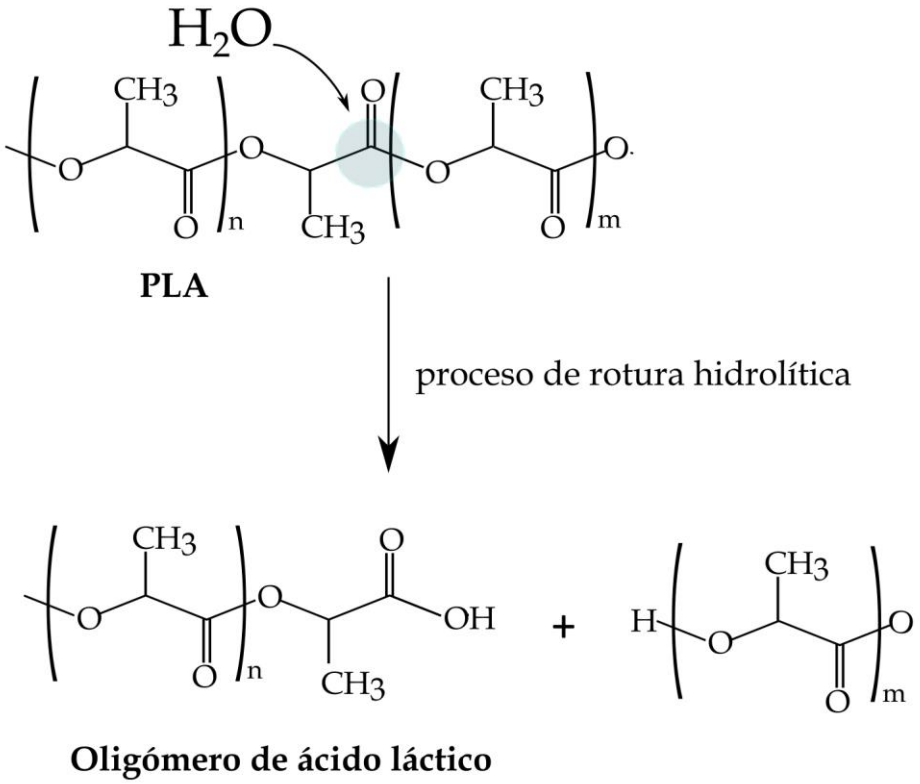

Figura I.18. Representación del proceso de hidrólisis auto catalítico del PLA.

I.2.3. Tecnologías de modificaciones del poli(ácido láctico)

La alta fragilidad, baja ductilidad, baja capacidad de alargamiento a la rotura, entre otras, son carencias que han limitado el uso del PLA en varias aplicaciones. Esta es la razón por la que en los últimos años se han realizado varios trabajos centrados en mejorar las propiedades del PLA. A continuación, se va a detallar algunas de las tecnologías de modificación más utilizadas actualmente a nivel industrial.

I.2.3.1. Mezclas físicas *"blend"*

La modificación de un polímero a través del mezclado físico es uno de los métodos más sencillos y económicos que se utiliza en la industria con el objetivo de obtener un material con nuevas propiedades. Estas propiedades pueden ser modificadas mediante la selección de los polímeros constituyentes y/o dependiendo del uso final que se le vaya a dar al material [74].

Las propiedades del nuevo material van a depender en gran medida de la miscibilidad (homogeneidad) o inmiscibilidad (heterogeneidad) que tienen los polímeros constituyentes. Teniendo en cuenta esto, las mezclas pueden llegar a ser

completamente miscibles, parcialmente miscibles o inmiscibles. Las interacciones más comunes que se generan en la fabricación de las mezclas son los puentes de hidrógeno, dipolo-dipolo, y las iónicas [75]. Por practicidad se suele realizar mezclas binarias o ternarias con el objetivo de llevar un mejor control de las propiedades y por no complicar la procesabilidad del material, factor que encarecería el producto final.

Una de las carencias que presenta el PLA es su baja tenacidad, con ansias de mejorar esta propiedad se suele utilizar polímeros flexibles o blandos para la realización de los *"blends"*. En un principio se utilizaban polímeros de origen petroquímico como el polietileno (PE) [76], el acrilonitrilo-butadieno-estireno (ABS) [77], o el poliuretano (PU) [78]. Pero debido a la concienciación medioambiental con respecto al uso indiscriminado de productos derivados del petróleo, se ha buscado utilizar biopolímeros, ya sean estos de origen renovable o biodegradables. En este sentido, autores como Matta, *et al*. [79], prepararon y caracterizaron mezclas con una matriz de PLA y poli(ε-caprolactona) (PCL) (un polímero biodegradable) a porcentajes variables (10, 20 y 30 %), donde se observaron una inmiscicbilidad entre el PLA y PCL, caracterizados por la formación de esferulitas de la fase dispersa (PCL) en la matriz de PLA, a pesar de esto se pudo observar un aumento de la elasticidad y viscosidad de la mezcla con el aumento del porcentaje de PCL, además de acelerar la cristalización del PLA. Supthanyakul, *et al*. [80], utilizaron poli(butilén succionato) (PBS) junto con PLA para la fabricación de *"films"* en presencia de un copolímero tribloque poli(*L*-lactida-*b*-butileno succinato-*b*-*L*-lactida)(PLLA-*b*-PBS-*b*-PLLA) para mejorar la miscibilidad entre el PLA y PBS. De los resultados se pudo observar que la presencia de (PLLA-*b*-PBS-*b*-PLLA) mejoró la miscibilidad, viéndose reflejado en el aumento de uniformidad de las superficies como se observaron en las imágenes de AFM. Además, se observó que para una mezcla de (80/20 %) (PLA/PBS) con un porcentaje de 3 phr de (PLLA-*b*-PBS-*b*-PLLA) disminuyó su T_g a valores inferiores que el PLA (55 ºC) y en términos de las propiedades mecánicas se observó una disminución del módulo de Young y un incremento en el alargamiento a la rotura. Przybytek, *et al.* [81] prepararon formulaciones de polímeros completamente biodegradables basados en PLA y en almidón termoplástico de patata (TPS) con aceite epoxidado de soja (ESBO) como aditivo reactivo con el propósito de mejorar la ductilidad. Acorde con los resultados presentados, se pudo concluir que la incorporación de ESBO provocó un efecto plastificante en la mezcla (PLA/TPS) siendo este mayor con el aumento de porcentaje de ESBO. Esto provocó un aumento en la flexibilidad de las mezclas, en el alargamiento a la rotura y en la resistencia al impacto, así como una ligera disminución de la resistencia a la tracción.

Para poder aprovechar de todo el potencial que tiene la mezcla de polímeros se debe superar en muchos casos la baja o falta de miscibilidad que se tiene en el sistema, esto se debe generalmente a la diferencia de polaridades (polar o no polar) de los polímeros constituyentes. Para ello es muy común el uso de agentes de acoplamiento que suelen ser copolímeros injertados o en bloque cuya función es interactuar químicamente con los polímeros del sistema. En general la doble funcionalidad que tienen este tipo de aditivos suelen interaccionar entre los dos polímeros inmiscibles y generar un puente entre los dos, así incrementar su interacción [17].

Ferri, *et al.* [82] realizaron un estudio con el fin de observar el efecto que tienen diferentes agentes compatibilizantes en la miscibilidad de una mezcla binaria entre una matriz de ácido poliláctico (PLA) y de polietileno de alta densidad biobasado (Bio-HDPE), los compatibilzantes utilizados fueron el polietilén viníl acetato (EVA), alcohol polivinílico (PVA) incorporados por medio de extrusión no reactiva y peróxido de dicumíl (DPC) incorporado por extrusión reactiva. La incorporación de los diferentes agentes compatibilizantes es fácilmente perceptibles ya que se puede observar una mejora en las propiedades dúctiles (alargamiento a la rotura) y la tenacidad (resistencia al impacto) de la mezcla (PLA/BioHDPE), al compararlo con las propiedades de la mezcla sin compatibilizantes. Este efecto es más notorio con el EVA, donde mejora la de interacción entre los dos polímeros es mayor, y se pudo evidenciar en el aumento de un 86 % y 63 % en el alargamiento a la rotura y resistencia al impacto, respectivamente. Debido a que el EVA presenta una mayor afinidad ya que posee dos co-monómeros (etileno y acetato de polivinilo) que por un lado interaccionan de mejor manera con las cadenas del polietileno y por el otro reaccionan con los grupos polares del PLA. Además, se pudo diferenciar una disminución entre la formación de la fase dispersa de BioP-HDPE en la matriz, lo que es indicativo de una mejora en la interacción PLA/BioHDPE.

Continuando por línea de investigación de mezclas binarias de origen renovable se tiene que Ferri, *et al.* [83] utilizaron aceite maleinizado de lino (MLO) en una mezcla de PLA y almidón termoplástico (TPS) que posee un contenido de poliéster alifático/aromático. En un inicio se observó que la mezcla a pesar de que presenta una baja miscibilidad tiene un incremento de alargamiento a la rotura y una mejora en la resistencia al impacto al compararlo con el PLA. La incorporación de bajos porcentajes de MLO (6 %) muestran una increíble mejora en estas propiedades llegando a ser hasta de un 500 % mayor en el caso de la resistencia al impacto, al compararlo con el PLA virgen. Este efecto que se relaciona directamente con el aumento de interacción entre los dos polímeros, adicional al efecto compatibilizante se puede observar un ligero efecto plastificante, marcado por la disminución de la temperatura de transición vítrea,

debido a que el MLO reacciona con relativa facilidad con los grupos (-OH) presentes en los terminales del PLA y en el TPS.

I.2.3.2. Plastificación

La plastificación es entre otras, una de las vías que se tiene para mejorar el rendimiento del PLA de una manera económica. El objetivo de la incorporación de un agente plastificante dentro del sistema es ayudar a la movilidad de las cadenas, con esto se busca mejorar la flexibilidad y la ductilidad del polímero, así como facilitar su procesamiento, debido a la disminución de la viscosidad y su índice de fluidez. Esto es posible ya que la función del plastificante es interrumpir la formación de enlaces entre las cadenas del polímero produciendo que estas se separen y se facilite su movimiento, a la vez que las moléculas del plastificante generen enlaces con la matriz. Varios agentes plastificantes como el poli(etilén glicol) (PEG), glicerol triacetato, ésteres de ácidos grasos, aceites vegetales epoxidados, oligómeros de ácido láctico, entre otros, han sido utilizados con el fin de disminuir la fragilidad que tiene el PLA.

Wang, *et al.* [84] formularon mezclas de PLA con PEG como agente plastificador con una relación (PLA/PEG) (100/0, hasta 50/50). En base a los resultados obtenidos para muestras con un porcentaje superior al 10 % de PEG se puede diferenciar dos fases cristalinas, denotando la poca miscibilidad entre estos dos elementos. A pesar de esto, se aprecia una mejora en las propiedades dúctiles del material, confirmando la actuación del PEG como plastificante del PLA. Esto se expone de mejor manera en el claro aumento de la capacidad de deformación y la disminución del módulo de Young que se observaron en las muestras. Burgos, *et al.* [85] estudiaron el uso de un oligómero de ácido láctico (OLA) en porcentajes que van del 5 % al 20 %. Donde se reportó el efecto que tiene un OLA en películas obtenidos a través de mezcla por fundido y posteriormente por moldeo por compresión. Se pudo apreciar el efecto plastificante que tiene el oligómero en la matriz de PLA, se identificó por un lado la disminución de los valores de módulo elástico y la resistencia a la tracción, y, por otro lado, se pudo observar un notorio aumento en el alargamiento a la rotura pasando de un 4 % del PLA virgen hasta un 200 % aproximado con un 15 % de OLA. Así también, se tuvo que los valores de T_g paso de 63 ºC del PLA virgen a 50 ºC de la mezcla con un 15 % de OLA. Además, de que con esta formulación se obtuvo un aumento increíble en la tenacidad (resistencia al impacto) donde aumento casi un 200 % en comparación con el PLA virgen.

Dentro de otra línea de plastificantes se encuentran los basados en aceites vegetales (VOs), estos han llamado la atención debido a que su materia prima se encuentran en abundancia y a que generalmente suelen ser extraídos de desechos agroalimentarios (biomasa), además de que no afectan propiedades como biodegradabilidad y biocompatibilidad que tiene el PLA. En este contexto se encuentran varios trabajos interesantes, como es el caso del presentado por Bouti, *et al.* [86] que comparo el efecto que tiene el aceite epoxidado de girasol (ESO) y el aceite epoxidado de soja (ESBO) como plastificante del PLA, para esto se varió el porcentaje constitutivo de estos dos plastificantes de 10 al 40 %. En general se pudo observar una marcada tendencia de incremento de la ductilidad de los dos materiales, disminuyendo a su vez su fragilidad. Esto se ve reflejado en la disminución de los valores de módulo, así como el aumento en el alargamiento a la rotura. Este efecto es más notorio en las mezclas plastificadas con un 20 % ESBO, que llega a ser hasta un 570 % mayor que el PLA virgen. Este efecto se debe a que el plastificante provoca una disminución de los enlaces intermoleculares entre las cadenas de la matriz y sustituyéndolos por puentes de hidrógeno que se forman entre el ESBO y el PLA como se pudo observar por los ensayos FTIR. A pesar del efecto positivo que se tiene en las propiedades mecánicas, no se puede decir lo mismo de la temperatura de transición vítrea, siendo el caso que solo se observó una ligera disminución al compararlas con el PLA virgen.

Hay que tener en cuenta que la eficacia del plastificante deriva de la estructura molecular del mismo, así como la compatibilidad que tenga con el polímero base, es decir la capacidad de solubilidad en este. Si la compatibilidad entre el plastificante y polímero base es baja o la cantidad utilizada sobrepasa la capacidad que puede admitir este, se puede producir un efecto anti-plastificante que va a producir la aparición de una fase dispersa resultado de la ausencia de la formación de enlaces, provocando así un efecto concentrador de tensiones lo que es contraproducente para las propiedades finales del polímero.

I.2.4. Compuestos con base de poli(ácido láctico)

Los materiales compuestos o *"composites"* son una de las piedras angulares en el desarrollo de la industria de polímeros. Su aplicación en productos convencionales es casi tan habitual como el uso de materiales puros. El concepto básico de un material compuesto es la unión de un material base o matriz que dota de una fase continua y un relleno que va a formar una fase dispersa, todo esto con la finalidad de obtener un nuevo material con propiedades diferentes a sus partes constitutivas.

En la industria de los polímeros el enfoque por el cual la incorporación de cargas o rellenos en una matriz polimérica es empleado son muy variadas, empezando por la modificación de propiedades: mecánicas, térmicas, barrera, para que actúen como agentes nucleantes y así aumentar su cristalinidad o como en la mayoría de los casos para abaratar costes. Las propiedades finales del material compuesto van a depender de varios factores como la naturaleza del relleno (orgánico o inorgánico), dimensiones (partícula o fibra), el volumen en peso incorporada, la distribución de la carga en la matriz, el direccionamiento de la carga, y la calidad de cohesión entre el relleno y la matriz.

Se han presentado estudios donde se utiliza partículas inorgánicas como relleno como es el caso de $Mg_3Si_4O_{10}(OH)_2$ o talco como se le conoce comúnmente para la fabricación de materiales compuestos con una matriz de PLA. La incorporación de este tipo de rellenos ayuda a sobrellevar la baja velocidad de cristalización que tiene el PLA [87]. El incorporar partículas inorgánicas en la estructura en cantidades relativamente bajas actúan como agentes nucleantes, incrementado la cristalinidad lo que dota de una mayor estabilidad térmica si se compara con el PLA virgen. Este resultado es de gran valía ya que una de las desventajas del PLA es su poca estabilidad térmica. A pesar de la mejora en la estabilidad térmica, la incorporación del talco suele perjudicar a sus propiedades mecánicas disminuyendo su resistencia a la tracción y elongación a la rotura, debido al efecto de concentración de tensiones que genera la poca interacción que tiene estas partículas con la matriz [88]. Un efecto similar sucede al incorporar carbonato de calcio, donde se observa que la presencia del relleno intensifica la cristalización en frio, reflejándose en la disminución la temperatura de cristalización en frio, disminuyéndola aún más cuando se incrementa su contenido. El efecto nucleante que genera estas partículas está relacionado a la cantidad de carga incorporada y a su dispersión, ya que se ha observado una disminución en la cristalización en grandes cantidades de cargas o por la formación de aglomerados. Para evitar esto y mejorar su dispersión se suelen realizar tratamientos superficiales, como por ejemplo el uso de ácido esteárico [89].

Tomando en cuenta que una de las principales aplicaciones que tiene el PLA es el envase- embalaje de alimentos, se han realizado estudios donde se incorpora nano partículas de dióxido de titanio (TiO_2), debido a que este compuesto presenta buena resistencia ante la radiación UV, buenas propiedades antibacterianas, baja toxicidad y buena biocompatibilidad. Se ha observado que la adición del TiO_2 a pesar de no producir grandes cambios en las propiedades del PLA dota de un ligero aumento en la degradación térmica. Sin embargo se pudo observar que la presencia del dióxido de

titanio disminuye considerablemente la cantidad de sustancia polimérica extracelular, influenciando esto en el tamaño de las bacterias [90]. Cabe mencionar que el efecto antibacterial que proporciona el dióxido de titanio aumenta con el aumento de la carga de este compuesto, además de que depende del tamaño, forma y área superficial de las nano partículas; teniendo que nano partículas con grandes áreas superficiales presentan mayores propiedades antibacterianas [91].

Debido a la gran relevancia que ha tenido el PLA en el área de la biomedicina, varios tipos de relleno con base de calcio se han utilizado, como es el caso hidroxiapatita (HA). Estas partículas inorgánicas llaman mucho la atención ya que presentan buena compatibilidad con estructuras óseas, debido a que poseen características similares a los huesos, y suelen ser utilizadas para tratamientos de regeneración de huesos. La buena afinidad que se genera resultante de la reacción química de sus grupos polares (PLA-HA) y a la buena interacción física debido a la alta porosidad de la HA, da origen a un material altamente rígido, además de una reducida capacidad de absorción de energía en condiciones de impacto. Siendo este efecto más intenso cuando el porcentaje de carga es mayor [92].

I.2.4.1. Compuestos con refuerzos lignocelulósicos

La alta demanda de materiales amigables con el medioambiente ha provocado que se busque una alternativa a los refuerzos sintéticos utilizados en la industria de los polímeros. Los materiales lignocelulósicos son atractivos para su uso industrial debido a que presentan varias ventajas empezando por que su origen es totalmente natural y su fuente es renovable, lo que derivaba en un costo menor y alta disponibilidad, además de presentar alta resistencia especifica. Este tipo de relleno se suele utilizar en forma de harina o en forma de fibra. En general un compuesto lignocelulósico está constituido principalmente de celulosa, hemicelulosa y lignina.

La celulosa (figura I.19**.**) suele ser el mayor constituyente de la estructura, y es un polímero de condenación lineal que consta de tres grupos hidroxilos (-OH) de los cuales dos forman enlaces (puentes de hidrógeno) dentro de la molécula y la otra forma enlaces con otras moléculas de celulosa. Las propiedades mecánicas van a depender del tipo de celulosa que lo constituyen (tipo I o tipo II) ya que cada una tiene su propia geometría, siendo su principal función dar resistencia, rigidez y estabilidad a la carga, [93,94]. La hemicelulosa comprende un grupo de polisacáridos que se asocia a la celulosa después de la eliminación de la lignina, en este grupo se excluye a la pectina. Este compuesto contiene diferentes unidades de azúcares, su cadena presenta un alto

grado de ramificaciones, y presenta un grado de polimerización mucho menor que la celulosa [95]. La lignina es un polímero complejo que consta de hidrocarburos complejos con componentes alifáticos y aromáticos, está constituido por tres unidades de repetición fenilpropanos llamados guayacil-propano, siringil-propano y p-hidroxi-fenil-propano. Este compuesto tiene una gran variedad de grupos funcionales hidroxilos y carboxilos [96]. Generalmente la lignina suele dotar de un incremento de propiedades mecánicas térmicas y suele retrasar la oxidación.

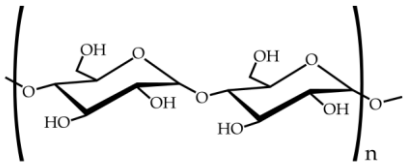

Celulosa

Figura I.19. Representación de la estructura de la celulosa.

Los rellenos lignocelulósicos además de reducir la huella de carbono presentan varias ventajas como buenas propiedades térmicas y biodegradabilidad. Del punto de vista de producción reduce el desgaste de las herramientas, así como de reducir problemas respiratorios a operarios.

El uso de rellenos lignocelulósicos o *"biofillers"* ha llevado al desarrollo de los llamados "*Wood plastic composites* (WPC)", este término hace referencia a la fabricación de elementos que combinan una matriz polimérica (termoplástica o termoestable) con una carga derivada de la madera, generalmente en forma de partícula. El objetivo de este tipo de materiales es la obtención de productos con apariencia de madera con propiedades balanceadas y con un alto contenido de origen orgánico [97]. En las últimas décadas su producción ha ganado el interés de varios investigadores, debido en gran manera al extenso desarrollo de los biopolímeros, ya que es factible combinar una matriz polimérica de origen orgánico como es el caso del PLA con alguna carga natural y así obtener compuestos altamente respetuosos con el medioambiente y con propiedades comparables a materiales convencionales. Como sucede con los rellenos sintéticos, uno de los objetivos de su incorporación es mejorar propiedades de la matriz (generalmente propiedades mecánicas y térmicas), y a su vez abaratar el precio del producto final que visto del punto de vista industrial es beneficioso. Como se mencionó anteriormente, las similitudes que tiene el PLA a materiales termoplásticos convencionales hacen posible que la fabricación de los WPC con base

de PLA sea más sencilla, las principales técnicas de fabricación son el moldeo por extrusión, inyección, moldeo por compresión o termoconformado.

Teniendo esto en cuenta Borysiuk, *et al.* [98] estudiaron el efecto que tiene el tamaño de un relleno de corteza de árbol en altas cantidades concentración (40, 50 y 60 %) en una matriz de PLA en la conformación de un material compuesto, Este material fue fabricado por medio de extrusión seguido de termoconformado, obteniendo muestras con dimensiones uniformes. En general se pudo determinar que el tamaño de partícula tiene un efecto importante en las propiedades mecánicas, siendo el caso de los compuestos cargados con partículas grandes presentan un mejor comportamiento mecánico. Se pudo determinar también que el compuesto tiene propiedades mecánicas balanceados con un 40 % porcentaje de cargas indistintamente del tamaño de la partícula. El incremento en el porcentaje de carga hasta los 60 % llevan a una disminución en las propiedades resistente acentuadas con partículas de un tamaño menor.

En un principio las cargas lignocelulósicas se limitaban al uso de desechos provenientes únicamente de la industria maderera como es el caso del serrín o corteza de madera, hoy en día esta área ha aumentado su aplicabilidad a residuos o desechos provenientes de la industria agroalimentaria. En este sentido investigadores como Balart, *et al*. [99] desarrollaron un biocompuesto con base de ácido poliláctico (PLA) con un relleno de harina de cáscara de avellana (HSF) a través de moldeo por inyección. Acorde con los resultados presentados se puede observar que la incorporación de la HSF provoca discontinuidades en la matriz de PLA, debido a la poca interacción que tiene el PLA con la carga. Esto repercute directamente en las propiedades mecánicas, ya que la usencia de interacción evita la correcta transmisión de esfuerzo lo que termina produciendo un efecto de concentración de tensiones, a pesar de esto se observa que la HSF promueve la cristalización del PLA debido a un efecto nucleante lo que ayuda a la estabilidad dimensional de los compuestos, así también aumentando su rigidez siendo más acentuado este efecto cerca de los 100 ºC. Quiles-Carrillo, *et al.* [100] fabricaron compuestos con base de PLA y harina de cascara de almendra (ASF) donde se añadió aceite maleinizado de lino (MLO) como plastificante por medio de extrusión reactiva. Se pudo observar que al incorporar elevadas cantidades de ASF en la matriz de PLA incrementa la dureza de los compuestos, a su vez reduce la ductilidad y la estabilidad térmica. Al añadir pequeñas cantidades de MLO (<5 phr) aumenta las propiedades dúctiles, térmicas y termomecánicas de los materiales, debido a un doble efecto (plastificante-compatibilizante) que produce el MLO, lo que ayudó a que se mejora la interacción entre las partículas de ASF y la matriz de PLA.

A pesar de que los *"biofillers"* abren una puerta al desarrollo de compuestos amigables con el medioambiente, presentan varias desventajas como es su alta hidrofilidad, que suele ser la causante de la poca compatibilidad con la mayoría de las matrices termoplástica. Como se observó anteriormente, a pesar de que la conformación de WPC es factible, el decaimiento de sus propiedades es el resultado de la baja compatibilidad entre el relleno y la matriz.

Compatibilización

Se demostró que el mayor problema que tienen los *"Wood plastic composite"* es la poca interacción que se genera entre los compuestos lignocelulósicos y la matriz termoplástica. Por un lado, se tiene que la mayoría de los termoplásticos utilizados entre estos el PLA tienen carácter hidrofóbico. Por otro lado, se tiene que las cargas lignocelulósicas poseen una naturaleza altamente hidrófila debido a la gran cantidad de grupos hidroxilos (-OH) presentes en la celulosa y en la hemicelulosa. Esto además facilita la formación de aglomerados debido a los puentes de hidrógeno que se generan durante su procesado, dificultando su dispersión en la matriz produciendo que las propiedades mecánicas sean menores [95].

Varios enfoques se han propuestos con el fin de aumentar la afinidad entre los *"biofillers"* y matrices poliméricas. Industrialmente se suelen realizar modificaciones químicas a la carga con el propósito de reducir el carácter hidrófilo que tienen estos compuestos naturales. Las modificaciones son de carácter permanente y además de reducir la capacidad de absorción de agua, los tratamientos proveen de una mayor estabilidad dimensional a la carga. Es bien conocido que componentes como la hemicelulosa es de los constituyentes con un marcado carácter amorfo, inestable e hidrófilo, así que varios de estos tratamientos se basan en la remoción de este compuesto [101].

Dentro de las modificaciones más comunes está el mercerizado y el acetilado. El mercerizado es un tratamiento que consiste en sumergir los compuestos lignocelulósicos en una solución de hidróxido de sodio (NaOH) como se observa en la figura I.20. A través de esta modificación se logra eliminar algunos componentes no-celulósicos como la hemicelulosa, la lignina, e impurezas, que cubren a la celulosa. Así, tenemos que al eliminar estos compuestos resulta en un aumento de los grupos hidroxilos (-OH) de la celulosa lo que produce un aumento de la rugosidad, que desemboca en un aumento del área superficial y por consecuencia aumenta la capacidad de un entrelazamiento mecánico de la carga con el PLA [102,103].

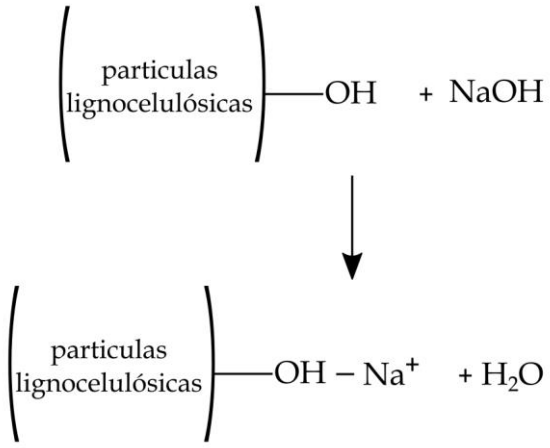

Figura I.20. Representación del proceso de mercerizado de refuerzos lignocelulósicos.

La acetilación es otro de los procesos por el cual se logra disminuir la hidrofilicidad de las cargas ligonocelulósicas. Este tratamiento se basa en la introducción de un grupo funcional acetilo en la estructura en lugar de los grupos hidroxilos través de un proceso de esterificación, como se puede observar en la figura I.21. Al igual que el proceso de mercerización, este proceso aumenta la rugosidad de la superficie de la carga lo que facilita el anclamiento con la matriz. El tratamiento consiste en sumergir la carga en una concentración de anhídrido acético, donde se produce ácido acético como subproducto de la reacción. Debido a que tanto el ácido acético como el anhídrido acético presentan una baja reactividad con las cargas naturales, se suele realizar un pretratamiento con ácido acético, seguido del tratamiento con anhídrido acético, para finalmente ser lavadas con agua destilada [104].

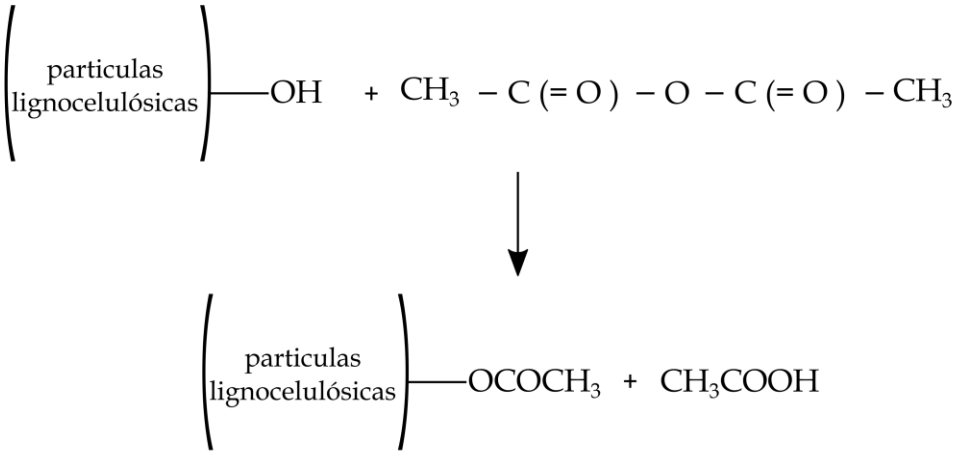

Figura I.21. Representación del proceso de acetilado de refuerzos lignocelulósicos.

Otra vía de modificación es la incorporación de agentes de acoplamiento, estos agentes de acoplamiento suelen tener dos funcionalidades. La primera es reaccionar con los grupos hidroxilos presentes en la celulosa de la carga y la segunda es reaccionar con los grupos funcionales de la matriz. Existen varios tipos de agentes de acoplamiento entre estos están los derivados de silanos.

La silanización es un tratamiento que se basa en la incorporación de una molécula multifuncional con estructura R-Si-X, donde "R" corresponde al grupo alkoxi (grupo silicofuncional), y "X" es el grupo organofuncional. La efectividad de la silanizacion radica en que las moléculas de silanos tienen una doble funcionalidad. El grupo organofuncional reacciona con la matriz y el grupo silicofuncional que reacciona con la superficie de la carga. Para esto, el grupo alcoxi silanos (grupos silicofuncional) de la molécula deben ser previamente hidrolizados para la formación de silanoles. Estos silanoles interaccionan fuertemente con los grupos hidroxilos de la superficie de la carga a través de puentes de hidrógeno. Esta interacción produce que se disminuyan el número de grupos hidroxilos presentes en la superficie de la carga, lo que a su vez disminuye su capacidad de interactuar con el agua, desembocando en una mejora en la adhesión con la matriz. Finalmente se produce una reacción de condensación entre la superficie de la carga y los grupos silanoles por medio de la formación de enlaces covalentes, obteniendo una capa de polixiloxano anclada a la superficie de la carga lignocelulósica [105]. En la figura I.22. se puede apreciar un esquema donde se detalla el proceso de silanización de un refuerzo lignocelulósico.

La elección del grupo organofuncional de silanos dependerá del tipo de matriz que se utilice, ya que de esto dependerá de que sea químicamente compatible y así poder establecer un enlace estable entre la carga y la matriz. Los grupos organofuncionales de silanos suelen ser de tipo amino, mercapto, glicidoxi, vinil o metacriloxi [106]. En la tabla I.1 se puede observar alguno de los grupos organofuncionales más utilizados, con sus respectivas matrices.

Tabla I.1.Silanos: grupos organofuncinales con sus respectivas matrices poliméricas. Adaptado de Xie*, et al.* [106].

Organofuncionalidad	**Matriz**
Amino	Epoxi
	Polietileno
	Poliacrilato
	PVC
	Caucho butílico

Vinil	Polietileno
	Polipropileno
	Poliacrilato
Metacril	Polietileno
	Poliéster
Mercapto	Caucho natural
	PVC
Glicidoxi	Epoxy
	Caucho butílico
	Polisulfuro
Clorino	Polietileno
	PVC
Alkil	Polietileno
	Caucho natural

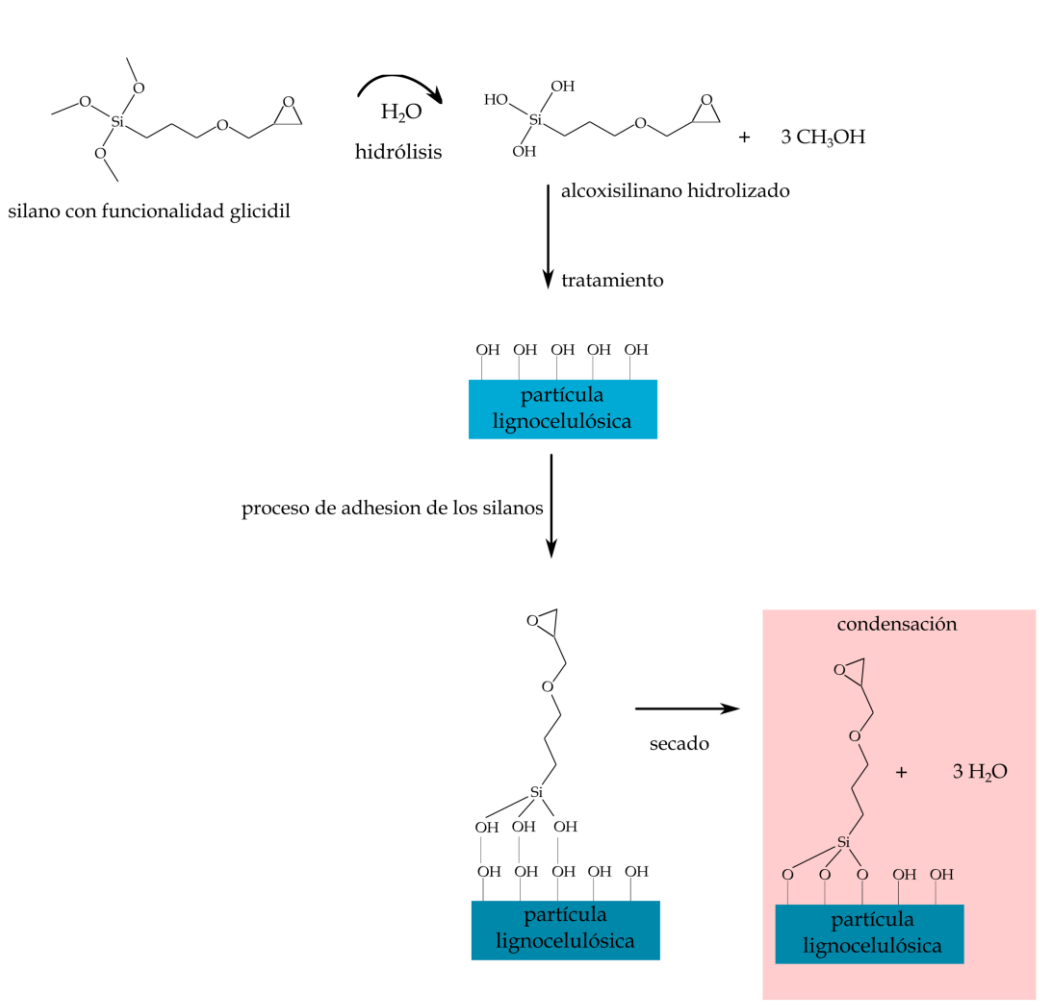

Figura I.22. Esquema del proceso de silanización de refuerzos lignocelulósicas.

La eficacia de este tipo de agentes de acoplamiento se ha observado en trabajos como el presentado por Qian, *et al.* [107] donde estudiaron el efecto que tiene diferentes concentraciones de trietoxivinilsilanos en las propiedades finales de biocompuestos basados en PLA y reforzados con *"nanowhiskers"* de bambú, donde para obtener mejores resultados en el tratamiento con silanos todas las partículas fueron previamente sometidos a un tratamiento de mercerizado y de blanqueado. Los resultados de FTIR demuestran la correcta condensación de los silanos con la superficie de las partículas de bambú, lo que mejoró la compatibilidad entre estas y la matriz de PLA. Esto se ve reflejado en varias de sus propiedades, empezando por las propiedades mecánicas donde se observó que los compuestos presentan un aumento de resistencia además de un aumento considerable en el alargamiento a la rotura de aproximadamente un 100 %, debido al efectivo trabajo que realizaron los silanos como agentes de acoplamientos lo que permite la correcta transmisión de esfuerzo. O como el presentado por Lee, *et al*. [108] que estudiaron el efecto que tienen los silanos con funcionalidad amina en el tratamiento de partículas de madera y talco en la fabricación de compuestos con PLA, para esto se varió el porcentaje de de silanos en 1 wt % y 3 wt %. Se pudo observar que el tratamiento con silanos condujo a una mejora en la resistencia térmica, llevando su temperatura de degradación a temperaturas más altas para el caso donde se utilizó una concentración de 1 wt % que los que contenían una concentración de 3 wt % de silanos. Se observó también que la incorporación de 1wt % en compuestos mixtos con harina de madera y talco disminuyó su cristalinidad, además de mejorar el módulo y la resistencia a la tracción.

Otra de las rutas de mejorar la interacción entre compuestos lignocelulósicos y la matriz de PLA es la preparación y el uso de PLA modificado como por ejemplo con anhídrido maleico (MAH) (MAPLA) como agente compatibilizante. Esta modificación se suele realizar a través de extrusión reactiva y se ha reportado que el número de grupos AM enlazados con el PLA aumenta con la cantidad de AM, así como su efectividad. Una representación de este proceso se puede observar en la figura I.23. Resultando en un aumento en la resistencia y en la calidad del refuerzo que proporciona la carga en la matriz, debido a la mejora en la interacción entre relleno y matriz lo que permite una correcta transmisión de esfuerzos, por la reacción entre los grupos AM con los grupos hidroxilos de la carga lignocelulósica [109].

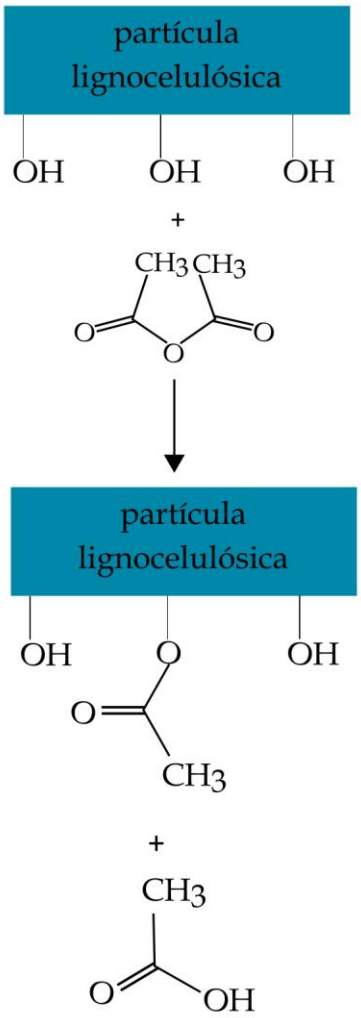

Figura I.23. Esquema del proceso de reacción entre un refuerzo lignocelulósico y un PLA modificado con anhídrido maléico (MAgPLA).

Los isocianatos se han establecido como buenos agentes compatibilizantes, donde producen una mejora en las propiedades mecánicas, así como una disminución en la capacidad de absorción de agua de los compuestos. Con estos agentes compatibilizantes los grupos [-N=C=O] reaccionan con los grupos hidroxilos de la celulosa y forma enlaces covalentes. En compuestos basados en PLA, los isocianatos reaccionan con los grupos hidroxilos o carbonilos del PLA, así como con los grupos hidroxilos del almidón de maíz para formar enlaces de uretano. A pesar de esto, estos agentes compatiblizantes tienden a hidrolizar en presencia de humedad, por lo que se limita su aplicación. Los compuestos más utilizados (tabla I.2.) son el diisocianato de metilendifenilo (MDIC), polimetileno polifenil isocianato (PMPPIC), tolueno 2,4-diisocianato (TDIC) y diisocianato de hexametileno (HMDIC) [110].

Tabla I.2. Agentes de acoplamiento isocianatos para biopolímeros. Adaptada de Ghaffar, *et al.* [110].

Compuesto	Estructura
Diisocianato de metilendifenilo (MDIC)	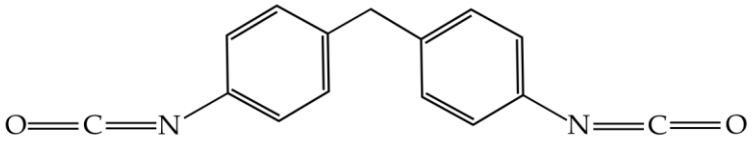
Polimetileno polifenil isocianato (PMPPIC)	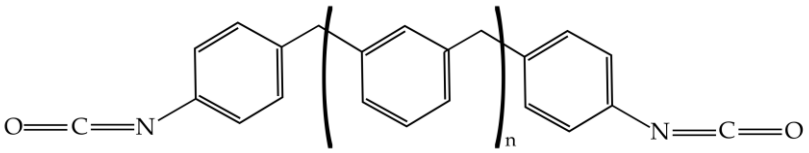
Tolueno 2,4-diisocianato (TDIC)	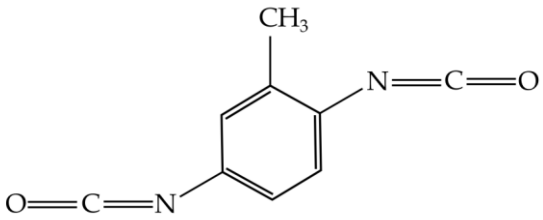
Diisocianato de hexametileno (HMDIC)	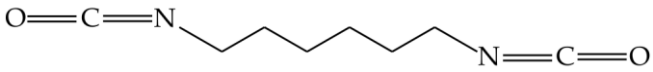

También se ha observado que agentes de acoplamiento reactivos como el N, N-(1,3-fenileno dimaleimida) (BMI) o el 1,1-(metilendi-4,1-fenileno)bismaleimida (DBMI) aumentan la interacción entre compuestos lignocelulósicos y matrices de PLA, mostrando una fuerte adherencia de las partículas a la matriz y por consecuencia se observa un aumento en la rigidez, resistencia y capacidad de deformación [111].

I.2.4.2. Compuestos con fibras de refuerzo.

La incorporación de fibras en matrices de PLA es otra de las alternativas que industrialmente se utiliza para sobrellevar las carencias que presenta este material. De manera similar como ocurre con partículas se puede mejorar propiedades mecánicas, térmicas o sobrellevar la pobre capacidad de cristalización. Las fibras presentan algunas ventajas a comparación de los rellenos en forma de partícula, ya que no solo pueden promover eficazmente propiedades como la cristalización, sino también mejorar significativamente la matriz del polímero, lo que se denomina refuerzo. En general para este propósito se suele utilizar dos tipos de fibras como son: fibras sintéticas y fibras naturales.

Durante varias décadas las fibras sintéticas como las de carbono, aramida o de vidrio han dominado el mercado, debido a sus excelentes propiedades mecánicas y a su relativo bajo costo. Estas fibras además presentan propiedades como alta resistencia mecánica, peso ligero, buena resistencia al agua y a productos químicos, entre otras. Razones por las cuales han sido empleados en sectores con altos requerimientos como el automotriz, aeronáutica, o construcción [112].

En los últimos años la creciente concienciación medioambiental y la búsqueda de la sostenibilidad, han provocado un gran cambio en la industria donde se busca reemplazar el uso de materiales sintéticos por materiales sostenibles y así dejar de depender de productos no renovables como el petróleo. En este contexto el uso de fibras naturales en lugar de fibras sintéticas en la fabricación de materiales compuestos es más frecuente. Las fibras naturales presentan varias ventajas sobre las fibras sintéticas, desde el punto de vista medioambiental el uso de fibras naturales reduce la dependencia de recursos no renovables, disminuye la emisión de productos contaminantes y de gases de tipo invernadero derivados de su producción, además de ser biodegradables lo que reduce significativamente su impacto ambiental. Del punto de vista industrial, las fibras naturales presentan un menor costo de producción, una densidad menor, unas propiedades de resistencia especifica aceptables y facilidad de procesado [113].

Las fibras naturales se caracterizan dependiendo su origen, pudiendo ser este de origen animal, vegetal o mineral, una vista global de su clasificación se pude observar en la figura I.24.

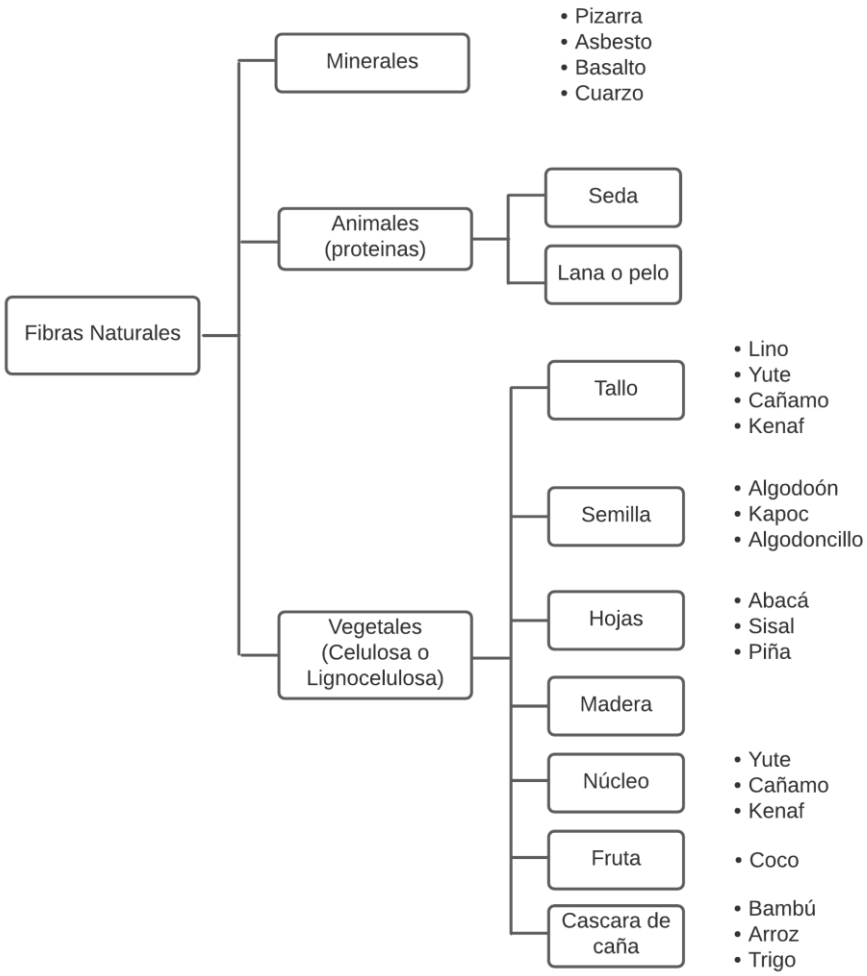

Figura I.24. Clasificación de fibras naturales según su origen. Adaptada de Anbupalani*, et al.* [114].

Las fibras animales se componen generalmente de proteínas y suelen ser extraídas del pelaje de animales o plumas de aves, así también pueden ser producidas por insectos como es el caso de la seda [115]. Históricamente este tipo de fibras se han utilizado en el sector textil, en la fabricación de vestimenta. Pero en los últimos años han ganado presencia en el sector de los polímeros, donde se han desarrollado compuestos con lana o plumas de pollo con matrices termoplásticas sintéticas u de origen biológico [116-118]. Por otro lado, tenemos las fibras minerales, estas fibras son obtenidas a partir de recursos minerales o rocas y han ganado relevancia en sectores como la construcción o en el sector ingeniería de polímeros, debido a su baja o nula toxicidad, su origen ecológico, su facilidad de procesamiento y su relativo bajo costo. Este tipo de fibra han surgido como una alternativa a la fibra de vidrio, y las más utilizadas son las fibras de pizarra, cuarzo y basalto. Esta relevancia se ve reflejado en varias investigaciones donde desataca el uso de fibras como las de basalto como fibra de

refuerzo en matrices de PLA en la fabricación de materiales compuestos o en la fabricación de filamentos para impresión 3D, así también como en la fabricación de materiales compuestos con matrices termoestables de origen sintético u orgánico [119-121], este apartado se detallará en el desarrollo de este documento. Se tiene también que la fibra de pizarra se ha utilizado en la fabricación de materiales compuestos con matrices termostables de origen orgánico o en el desarrollo de compuestos con matrices termoplásticas [122].

Como se pude observar en la figura I.24., debido a la gran diversidad de fibras vegetales, éstas se han convertido en una de las fibras naturales más utilizadas como refuerzo en materiales compuestos de origen orgánico. Las fibras vegetales se pueden catalogar como primarias y secundarias tomando en cuenta su aplicación. Teniendo esto en cuenta, fibras extraídas de plantas como el yute, lino, sisal, cáñamo, el kenaf, o el bambú son consideradas como primarias, ya que estas especies son cultivadas exclusivamente para la extracción de fibras, mientras plantas que se cultivan por el fruto como el coco, plátanos, o piñas, donde las fibras son un subproducto son consideras secundarias.

Dentro del mundo de los materiales compuesto, fibras como las de yute, lino, cáñamo, kenaf, sisal, algodón, entre otras son las más utilizadas, debido en gran medida al bajo coste de producción, así como la baja densidad que presentan al compararlas con fibras convencionales, además de una alta resistencia especifica y rigidez. La estructura y composición química de este tipo de fibras dependen de varios factores como pueden ser la especie y la parte de la planta donde son extraídas. En general las fibras vegetales están compuestas por tres componentes principales que son la celulosa, hemicelulosa y lignina. La celulosa es un polímero natural que brinda estabilidad estructural a la fibra, el puente de hidrógeno que unen sus unidades constitutivas (glucosa) regula su cristalinidad que es la causante de propiedades físicas de la fibra como la resistencia, estabilidad y rigidez. Además, tenemos la hemicelulosa que está conformada por cadenas cortas y ancladas a la celulosa, este constituyente influenciara directamente las propiedades térmicas y la capacidad de biodegradabilidad. Finalmente tenemos a la lignina que es un hidrocarburo aromático que aporta parte de la rigidez a la fibra. Debido a la constitución de la celulosa y la lignina son los constituyentes que controlan la capacidad de absorción de humedad de las fibras [123]. En la tabla I.3**.** se puede observar la composición de las fibras vegetales más utilizadas.

Tabla I.3. Composición química de fibras vegetales. Adaptada de Awais, *et al.* [123],Gholampour and Ozbakkaloglu [124].

Fibra	Celulosa (wt%)	Lignina (wt%)	Hemicelulosa (wt%)	Cera (wt%)	Ángulo microfibrilar (º)	Contenido de humedad (wt%)
Abacá	56 - 63	20 - 25	7 - 9	3		15
Algodón	85 - 90	0,15 – 0,25	40 - 45	-	20 - 30	
Lino	71	18,6-20,6	2,2	0,6	5 - 10	7
Yute	61 - 71	14 - 20	12 - 13	0,5	8	12
Kenaf	72	20,3	9	-		-
Kapok	64	23	-	-		-
Cáñamo	68	15	10	0,8	6	9
Bambú	26 - 43	30	21 - 31	-		8,9
Sisal	65	12	9,9	2	10 - 22	11

Su estructura se basa en una pared principal la cual se encuentra en la parte exterior de la fibra que está constituida por redes de microfibras y de celulosa cristalina desordenada y de tres paredes secundarias que se encuentran en el interior y en el lumen constituidas por microfibrillas cristalinas de celulosa con dirección helicoidal alineada con la dirección de la fibra principal, como se puede observar en la figura I.25. [125].

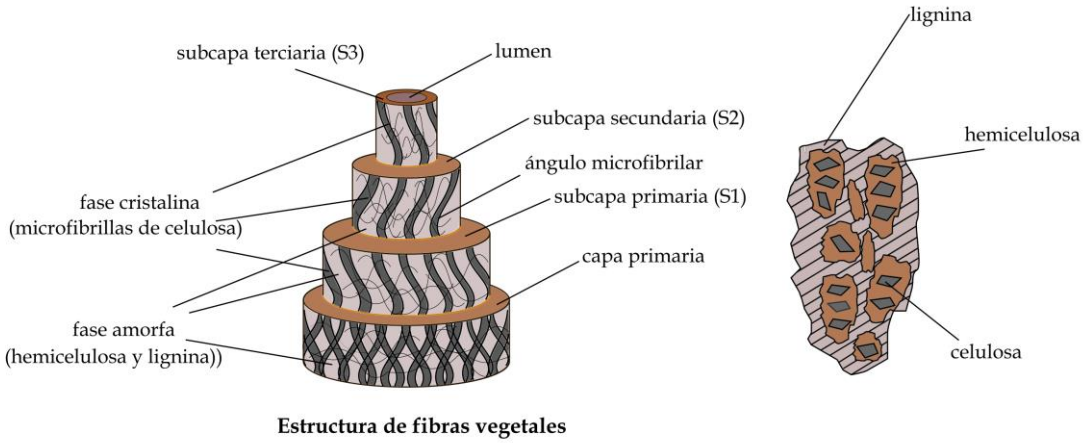

Figura I.25. Estructura general de fibras vegetales y organización microestructural de sus principales constituyentes.

Las fibras vegetales que presentan propiedades mecánicas interesantes se pueden observar en la tabla I.4. Estas propiedades las hacen candidatos para sustituir

a fibras sintéticas como la fibra de vidrio, ya que presentan alrededor de la mitad de su densidad, son biodegradables, además de que la relación costo-rendimiento, es muy superior a las presentadas por fibras sintéticas.

Tabla I.4. Composición química de fibras vegetales. Adaptada de Li*, et al.* [105].

Fibra	Alargamiento (%)	Resistencia a la tracción (MPa)	Módulo Elástico (GPa)	Densidad (g cm^{-3})
Algodón	3 - 10	287 - 597	5,5 - 12,6	1,5 - 1,6
Yute	1,5 - 1,8	393 - 800	10 - 30	1,3 - 1,46
Lino	1,2 - 3,2	345 - 1500	27,6 - 80	1,4 - 1,5
Cáñamo	1,6	550 - 900	70	1,48
Sisal	2 - 3,8	400 - 700	9 - 38	1,33 - 1,5
Vidrio-E	2,5 - 3	2000 - 3500	70	2,5

Debido a que el mayor constituyente de las fibras vegetales es la celulosa, presentan las mismas carencias que las partículas lignocelulósicas, anteriormente presentadas. Es decir, presentan un alto carácter hidrófilo, debido a la gran cantidad de grupos hidroxilos presente en este compuesto. Esta hidrofilicidad produce dificultades en la adhesión con matrices termoplásticas hidrofóbicas, limitando su interacción, lo que repercute en el efecto de refuerzo que se busca con la incorporación de estas fibras. Con relación a compuestos basados en PLA, el PLA posee átomos polares de oxígeno que podrían formar puentes de hidrógeno con los grupos hidroxilos presentes en las fibras naturales, a pesar de estos enlaces formados tienen poca influencia en la interacción fibra matriz, por lo que la modificación química es una de las opciones más viables y necesarias para aumentar esta interacción.

Al tener una constitución similar a las cargas lignocelulósicas las modificaciones químicas suelen ser similares, como por ejemplo el mercerizado y el acetilado. Verma and Goh [126] describieron como un tratamiento de mercerizado con álcalis aumento el comportamiento hidrófobo de fibras naturales debido a la interacción que tuvo el NaOH con los grupos (-OH) de la celulosa y además se produjo una remoción parcialmente de compuestos como lignina, pectina, hemicelulosa y cera de la superficie de la fibra, lo que ayudo a la mejor interacción con matrices hidrófobicas. Esto se tradujo en una mejora en la unión intersuperficial entre la fibra y la matriz. Esta buena interrelación tuvo una repercusión directa aumentando sus propiedades mecánicas, el cual es la finalidad de la fabricación de compuestos de origen orgánico.

De la misma manera se tiene que la incorporación de agentes de acoplamiento (silanos) o monómeros injertados de anhídrido maleico (MAH) ayudan a mejorar la interacción fibra/matriz. Autores como Agüero, *et al.* [127], comprobaron como el proceso de mercerización combinado con agentes de acoplamiento como el glicidil silano mejoraron la interacción entre fibras cortas de lino en una matriz de PLA, viéndose reflejado en la mejora del rendimiento mecánico y térmico. Así también Zhang, *et al.* [128] que utilizó ácido poliláctico injertado con anhídrido maleico (MAH-*g*-PLA) como agente compatibilizador en la fabricación de compuestos de PLA reforzados con fibras de madera. Donde el buen trabajo efectuado por MAH-*g*-PLA como agente compatibilizador se observó en el efecto de refuerzo que proporcionaron las fibras aumentando la resistencia a la tracción y a la flexión, así como su cristalinidad.

Como se mencionó anteriormente uno de los propósitos de incorporar fibras en una matriz termoplástica es reforzarla. Las fibras pueden ser catalogadas como cortas o largas, siendo así que su efecto de refuerzo puede ser de manera continua o discontinua. Este efecto dependerá de la direccionalidad o arquitectura de las fibras. La tecnología de textiles cataloga a estas telas como tejidas, tejida de punto, no tejidas y trenzadas, de las cuales las telas no tejidas son las únicas que pueden estar fabricadas por fibras cortas o largas, las demás estructuras están conformadas por fibras largas.

Las telas de fibras no tejidas se caracterizan porque las fibras no pasan por un previo proceso de hilado y se suelen fabricar enredando fibras y posteriormente unidas por medios mecánicos, térmicos o químicos. Estas fibras suelen tener una distribución aleatoria y esto les da un carácter anisótropo a las mantas y a los materiales compuestos. En cambio, en las estructuras tejidas, las fibras deben pasar por un previo proceso de hilado, y una vez conformados los hilos estos se entrelazan en una estructura perpendicular, lo que comúnmente se le conoce como urdimbre (sentido longitudinal) y trama (sentido transversal). Este direccionamiento de 0º y 90 º le dota de una buena resistencia mecánica en estas dos direcciones. Existe una infinidad de formas de entrelazar los hilos de la urdimbre y la trama, este entrelazado, así como el número de hilos utilizados (densidad de tejido) y la cantidad de fibra, van a determinar las propiedades finales del tejido. Los tejidos más comunes son el plano, la sarga y el satén. Otra de las técnicas de fabricación de tejidos es el tejido de punto. En este método un hilo va haciendo bucles y pueden ser en sentido de la trama o de la urdimbre. Esta estructura presenta algunas ventajas sobre las mantas tejidas como una mayor elasticidad, su procesamiento es más barato, además de una gran versatilidad en sus diseños. Como desventaja se tiene que presenta una menor estabilidad dimensional, al compararlo con las mantas tejidas. Finalmente, se tiene los tejidos trenzados, estos se

fabrican entrelazando tres o más hilos en una misma dirección. Estos hilos suelen formar ángulos entre 30 y 80º con respecto a su eje principal, y generalmente se utilizan en estructuras con sección constante [123,129,130].

En los materiales compuestos reforzados por fibras o "*fiber reinforced composites*, (FRC)", la arquitectura de los tejidos tiene una influencia directa en sus propiedades finales, así como que determinará el método de fabricación de los mismos.

Comúnmente estructuras basadas en fibras largas suelen ser fabricadas por técnicas como el moldeo por compresión, donde lo que se busca es que, durante el procesado, este no interfiera con la distribución de las fibras. Se ha observado que en biocompuestos formados por una matriz de PLA y reforzados por telas con fibras lignocelulosicas no tejidas y tejidas, a pesar de que este proceso de fabricación toma un tiempo considerable, se logra impregnar completamente las fibras. Esto se pude comprobar en la alta resistencia a la flexión, tracción e impacto que presentan estos compuestos, comparándolos con la matriz [131]. Además, se ha observado que al someter previamente las fibras a tratamientos químicos (NaOH, $NaClO_2$, acrilonitrilo, entre otros), se obtiene una mejora en las propiedades mecánicas, debido al aumento en la interacción mecánica y química de las fibras con la matriz. El tratamiento químico ayuda a eliminar parte de la hemicelulosa, lo que provoca que la región interfibrilar sea menos densa y rígida, lo que en el caso de las fibras no tejidas ayuda a que las fibras se puedan ordenar y alinear en dirección de la deformación y así aumentar ligeramente su resistencia [132]. También se tiene que al utilizar telas con fibras tejidas los compuestos tienen mejores prestaciones con respecto a propiedades mecánicas (tracción, flexión e impacto) comparadas con compuestos con fibras no tejidas, debido generalmente al direccionamiento de las fibras pero hay que tener en cuenta que al ser mantas compuestas por fibras perpendiculares, se suelen producir cargas transversales en las secciones de solapamiento, lo que reduce la transmisión de esfuerzo, disminuyendo a largo plazo su rendimiento [133].

Por otro lado, tenemos que el uso de fibras cortas abre un abanico más grande en técnicas de fabricación de FRC, ya que generalmente ofrecen menores tiempos de procesamiento, mejor control dimensional, una mejor distribución de la fibra en la matriz y en general una mayor facilidad en su procesamiento. Técnicas como la extrusión, moldeo por inyección, o combinadas son de las más utilizadas. Se ha observado que la ruta de procesamiento influencia en la distribución, orientación y desgaste de las fibras, lo que repercutirá en las propiedades mecánicas, termomecánicas, o en su cristalinidad. Teniendo mejores resultados con respecto a la distribución y orientación de las fibras

cuando se realiza un proceso de extrusión, seguido de un proceso de inyección, lo que se refleja en un mejor comportamiento en condiciones de tracción y compresión [127,134].

Otras estructuras basadas en PLA

Varias alternativas han surgido a los materiales compuestos convencionales, como el trabajo presentado por Luedtke, *et al.* [135], en donde fabricaron materiales compuestos tipo sándwich con *"films"* de PLA como medio de unión de dos chapa de madera. Donde el proceso de fabricación influenció directamente en la calidad de unión entre el núcleo y la matriz, obteniendo mejores resultados cuando se trabajó por encima de la temperatura de fusión del PLA, ya que al bajar su viscosidad aumento la capacidad de migrar a hacia el núcleo, resultando en una unión de alta resistencia, lo que dio paso a la obtención de materiales con buenas propiedades mecánicas.

O el presentado por Rebelo, *et al.* [136] donde fabricaron materiales tipo sándwich con placas de aluminio con un núcleo de PLA en forma de panal de abeja (honeycomb) impreso en 3D, con el propósito de estudiar el comportamiento no lineal de estos compuestos expuestos a explosiones y analizar su capacidad de absorción de energía. Se observó una buena respuesta de este tipo de núcleos ya que la capacidad de absorción de energía de estos compuestos dependió de la densidad relativa del núcleo de PLA, además ayudó a controlar de mejor manera el aplastamiento de las caras exteriores. Dichos resultaros fueron alentadores ya que presentan valores similares a materiales convencionales utilizados para este fin.

I.3. Tecnologías de compuestos de resina epoxi de origen renovable

Como se comentó anteriormente la presencia de resinas epoxi de origen orgánico ha ido aumentando, esto se debe en gran manera al aumento en el interés de dejar de depender de resinas termoestables provenientes de fuentes no renovables y que además presentan problemas para la salud humana. Una de las fuentes preferentes para el desarrollo de resinas termoestables de origen renovable son los aceites vegetales (VOs), estos han ganado el interés de la industria gracias a su enorme disponibilidad, facilidad de obtención, bajos costes, además de ser biodegradables y presentar una baja o nula toxicidad. La mayoría de los VOs son extraídos de granos y semillas, a través de prensado. Dentro de los aceites vegetales más utilizados para la

formulación de resinas termoestables están el aceite de soja, aceite de lino, aceite de algodón, aceite de canola, aceite de ricino, y aceite de cáñamo nombrar los principales.

I.3.1. Triglicéridos y aceites vegetales

Una de las principales razones por la cual los aceites vegetales han ganado interés en la industria es debido a su estructura que le brinda una gran versatilidad. Dicha estructura se basa principalmente en triglicéridos, estos están caracterizados por tener columna vertebral de tres carbonos con una larga cadena de hidrocarburos unida a cada uno de los carbonos [137]. De esta estructura se ha dado paso a la producción de una gran variedad de configuraciones poliméricas, pasando por polímeros lineales hasta llegar a polímeros reticulares. En la figura I.26. se puede observar la estructura genérica de una molécula triglicéridos. [138].

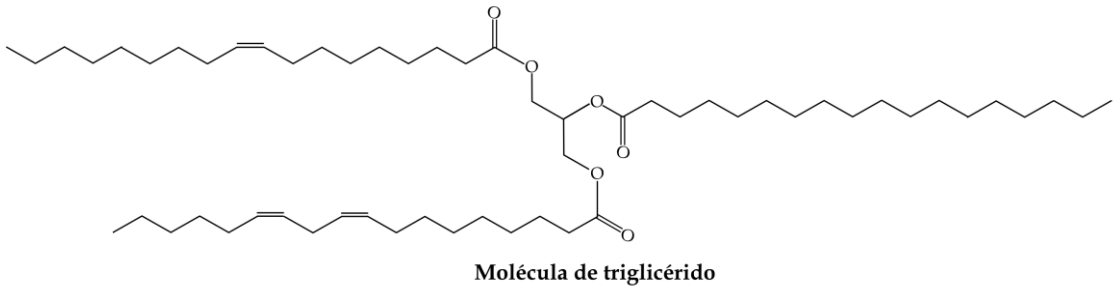

Figura I.26. Representación esquemática de la estructura de una molécula de triglicéridos genérica.

En general los aceites vegetales están formados por una molécula de glicerol a la cual están ligados tres ácidos grasos, estos pueden ser ácidos grasos saturados o insaturados, y suelen tener una longitud entre 14 y 22 átomos de carbono. Los ácidos grasos saturados contienen un enlace simple entre dos átomos de carbono, y los ácidos grasos insaturados contienen varios dobles y triples enlaces entre los átomos de carbono. El origen y el tipo de aceite va a determinar la composición de ácidos grasos que lo constituyen, esto determinará el grado de instauraciones presentes, lo que posteriormente dictará la facilidad de ser modificados. Los ácidos grasos más comunes se pueden observar en la tabla I.5.

Tabla I.5. Estructura de ácidos grasos presentes en aceites vegetales.

Ácido Graso	CT:C=C	Estructura
Laurítico	12:0	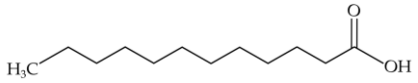
Mirístico	14:0	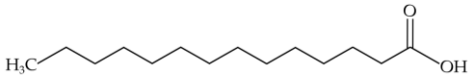
Palmítico	16:0	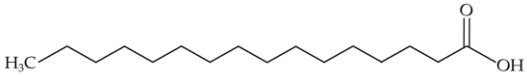
Esteárico	18:0	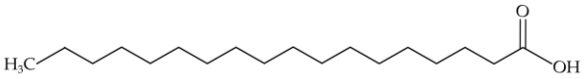
Oléico	18:1	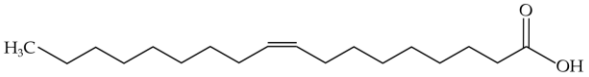
Linoléico	18:2	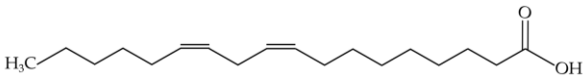
Linolénico	18:3	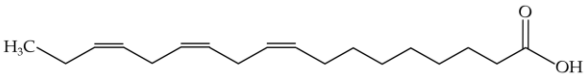
Araquídico	20:0	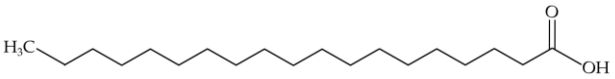
Behénico	22:0	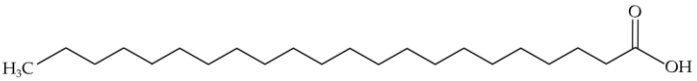

Esta marcada distribución de ácidos grasos permite conocer cuál de los diferentes aceites vegetales pueden cumplir con requerimientos específicos en aplicaciones industriales. Teniendo que aceites vegetales con un alto contenido de ésteres de ácidos grasos con fracción insaturada, como el ácido linolénico, presentan mejores propiedades que aceites vegetales con un menor grado de insaturaciones como el ácido linoleico u oleico. La composición de los diferentes ácidos grasos presentes en los principales aceites vegetales utilizados en la industria se puede observar en la **t**abla I.6.

Tabla I.6. Porcentaje en peso de ácidos grasos de los aceites vegetales principales. Adaptada de Giakoumis [137]

Aceite Vegetal	Ácidos grasos (wt%)								
	14:0	16:0	18:0	18:1	18:2	18:3	20:0	22:0	24:0
Maíz	-	11,88	2,1	27,23	57,74	0,64	0,32	-	0,14
Semilla de algodón	0,72	25,19	1,79	16,47	54,83	0,19	0,22	0,11	-

Lino	0,04	5,18	3,26	19,04	16,12	54,59	0,09	0,1	0,03
Palma	1,13	42,31	4,27	40,90	10,07	0,28	0,31	0,04	0,05
Canola	-	4,52	1,99	60,43	21,19	9,42	0,57	0,35	0,16
Soja	0,12	11,50	4,11	23,50	53,33	6,76	0,32	0,27	0,13
Colza	0,04	4,06	1,54	62,29	20,65	8,71	0,87	0,27	0,04
Girasol	0,04	6,35	3,92	20,91	67,58	0,17	0,22	0,66	0,26

I.3.2. Modificación de aceites vegetales

A pesar de que los aceites vegetales presentan una gran cantidad de instauraciones por molécula de triglicéridos, estas instauraciones presentan una baja reacción durante el proceso de polimerización, además carecen de estructuras aromáticas o cicloalifáticas, lo que resulta en una falta de rigidez y de resistencia en el compuesto. Para aumentar la reactivad de los aceites vegetales es necesario un proceso de funcionalización de estas instauraciones (dobles enlaces) previo a su polimerización por medio de una modificación química.

Hay que tener en cuenta que los triglicéridos presentan varias posiciones reactivas como son los grupos éster, los dobles enlaces carbono-carbono (C=C), posiciones alílicas y la posición α de los grupos éster, que facilitan la modificación química [139]. Entre las modificaciones más comunes están la epoxidación, la acrilación, maleinización, entre otros, donde se introducen grupos funcionales oxirianos, acrilatos, anhídridos, respectivamente.

I.3.2.1. Epoxidación

El proceso de epoxidación de los dobles enlaces de los ácidos grasos es una de las modificaciones más utilizadas en los aceites vegetales, de este proceso resultan los comúnmente llamados aceites vegetales epoxidados (EVO). Estos EVOs tienen una presencia importante en la industria de los materiales termoestables como iniciadores de resinas epoxi, debido a que son económicos y que provienen de fuentes renovables.

La epoxidación consiste básicamente en la conversión de las insaturaciones (C=C) presentes en los ácidos grasos en un anillo oxirano, lo que dota la funcionalidad epoxi al VO, eso ocurre por medio de la incorporación de un átomo de oxígeno activo, como se puede observar en la figura I.27.

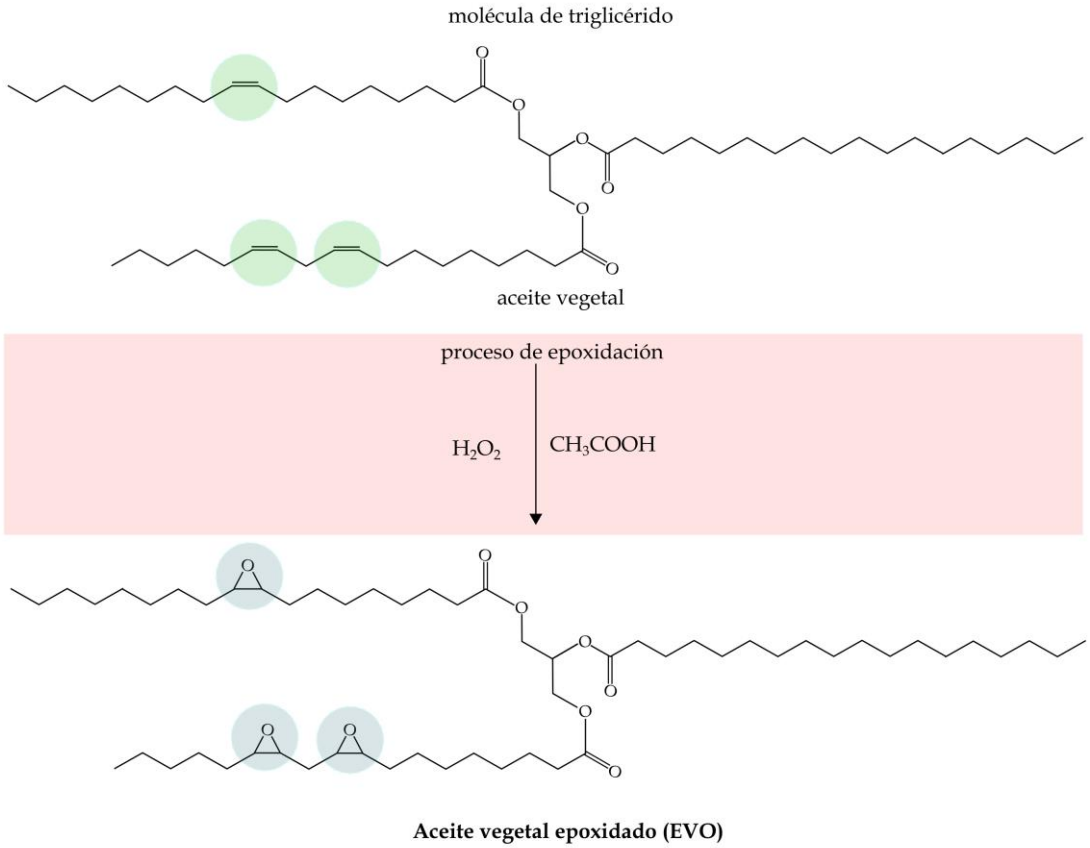

Figura I.27. Esquema del proceso de epoxidación de un aceite vegetal.

La epoxidación de los dobles enlaces de los aceites vegetales se puede realizar por medio de diferentes rutas, donde se destacan:

- Epoxidación con ácidos percarboxílicos catalizados por ácidos o encimas.
- Epoxidación con peróxidos catalizados por una transición metálica.
- Epoxidación con halohidrinas (como ácidos hipohalógenos) y sus sales.
- Epoxidación con oxígeno molecular.

A nivel industrial el proceso de epoxidación a través de perácidos orgánicos es de las rutas más aceptadas, donde gran variedad de ácidos orgánicos son utilizados, aquí la reactividad de cada ácido afecta de diferente manera en el proceso de epoxidación. De los ácidos más utilizados son el ácido acético y ácido fórmico, donde se suele preferir el ácido acético, debido a la facilidad de obtención en estado líquido y su bajo costo. En la reacción, el ácido acético actúa como catalizador proporcionando el oxígeno requerido de la fase acuosa a la fase oleosa para producir la formación de un anillo oxiriano [140]. Además se ha observado el uso de ácido sulfúrico y ácido fosfórico como catalizadores, donde se han obtenido un mayor grado de conversión en

aceites con alto número de insaturaciones, como el aceite de lino, de soja o el de ricino [141,142].

A pesar de que comercialmente las resinas epoxi obtenidas de aceites vegetales no pueden competir directamente con sus contrapartes de origen petroquímico en términos de resistencia, se han presentado varias investigaciones que han demostrado resultados alentadores en este campo. Carbonell-Verdu, *et al.* [143] desarrollaron una resina termoestable basada en aceite epoxidado de algodón (ECSO) entrecruzado con anhídridos cíclicos como el anhídrido metílico nádico (MNA) y anhídrido dodecenilsuccínico (DDSA). Los resultados demostraron la versatilidad que tienen los OVE, donde estableciendo una adecuada mezcla con el endurecedor, se pueden obtener materiales termoestables flexibles (entrecruzados con anhídrido dodecenilsuccínico, DDSA) o materiales rígidos (entrecruzado con anhídrido metílico nádico, MNA) con unas propiedades interesante. De igual manera Samper, *et al.* [144] formularon una resina termoestable utilizando como base aceite epoxidado de lino (ELO) y una mezcla dos entrecruzadores, el primero de origen petroquímico (anhídrido metílico nádico, MNA) el segundo de origen de orgánico (aceite maleinizado de lino, MLO). Al aumentar la cantidad de MLO en el sistema se obtuvo resinas con una mayor flexibilidad. La incorporación del MLO es favorable del punto de vista medioambiental. Al combinar un 10 % de MLO y un 40 % de MNA como sistema entrecruzador, se obtuvo un material termoestable con propiedades balanceadas con un alto contenido de origen orgánico. A pesar de que la mayoría de los sistemas termoestables nombrados están basados en aceites vegetales epoxidados, infortunadamente para obtener buenas propiedades mecánicas y térmicas, es necesario utilizar productos de origen petroquímico, ya sean estos agentes acelerantes o endurecedores. En los últimos años varios autores han apostado por el desarrollo de un sistema epoxi (resina:endurecedor) derivados completamente de origen natural. En este sentido Ding, *et al.* [145] desarrollaron un sistema termoestable basado en una resina basada en aceite epoxidado de soja, y un endurecedor de tipo polifenol, quercitina. A pesar de que el gran porcentaje del sistema es de origen natural, se utilizaron diferentes aceleradores de tipo imidazol de origen petroquímico, y uno de origen natural. Se obtuvo materiales con excelentes propiedades a tracción y flexión sobresaliendo, los que tuvieron componentes de origen petroquímico, aunque el material formulado con el imidazol natural presento valores a impacto incluso mayores a los de resinas convencionales. Continuando con el esfuerzo de obtener materiales completamente de origen renovable Qi, *et al.* [146] formularon un sistema epoxi utilizando aceite epoxidado de soja (ESBO) en donde para superar la típica flexibilidad que presentan los aceites vegetales debido

a su estructura, aprovecharon la estructura aromática del ácido tánico (TA) como agente de curado, y utilizaron histidina, un imidazol natural para acelerar la reacción. Los resultados fueron alentadores, ya que el material resultante presento buenas propiedades térmicas y mecánicas, debido en gran manera a la alta densidad de entrecruzado y los segmentos rígidos formados, además se observó el excelente trabajo que la histidina realizó como agente acelerador ya que se obtuvo una baja energía de activación.

Estos estudios son una muestra alentadora para materiales termoestables completamente de origen natural y abre la puerta para su futuro uso en aplicación con mayores requerimientos como sectores de la construcción e industriales.

I.3.2.2. Acrilación

A diferencia del proceso de epoxidación donde las insaturaciones que contienen los ácidos grasos pueden ser funcionalizados directamente en grupos epoxi, el proceso de incorporar funcionalidades acrilatos en la estructura se suele realizar con triglicéridos ya epoxidados. Estos triglicéridos epoxidados pueden ser de origen natural como los que se encuentran o en el aceite de veronia, o sintentizado de cualquier aceite vegetal, por medio del proceso de epoxidación [147].

La síntesis de funcionalidades acrilatos es a través de la reacción de ácidos carboxílicos sustituidos etilénicamente como, el ácido acrílico con triglicéridos epoxidados. En la figura I.28**.** se puede observar un esquema del proceso de acrilación de un aceite vegetal epoxidado. Esta reacción ocurre por sustitución estándar y tiene dependencia de primer orden con respecto a la concentración de grupos epoxi y de segundo orden con respecto a la concentración de ácido acrílico [148]. También se han presentado trabajos donde el proceso de acrilatado se puede realizar en un solo paso como reporta Zhang and Zhang [149], donde obtuvieron aceite de soja acrilatado al reaccionar aceite de soja con ácido acrílico directamente catalizado por $BF_3{\cdot}Et_2O$, o por medio de la reacción de Ritter [150]. Su, *et al.* [151] reportaron el proceso de síntesis para la obtención de aceite de lino acrilatado en un solo paso, donde se utilizó trifluoruro de boro éter dietílico como catalizador para introducir con éxito el ácido acrílico en el doble enlace de la cadena larga del aceite de lino.

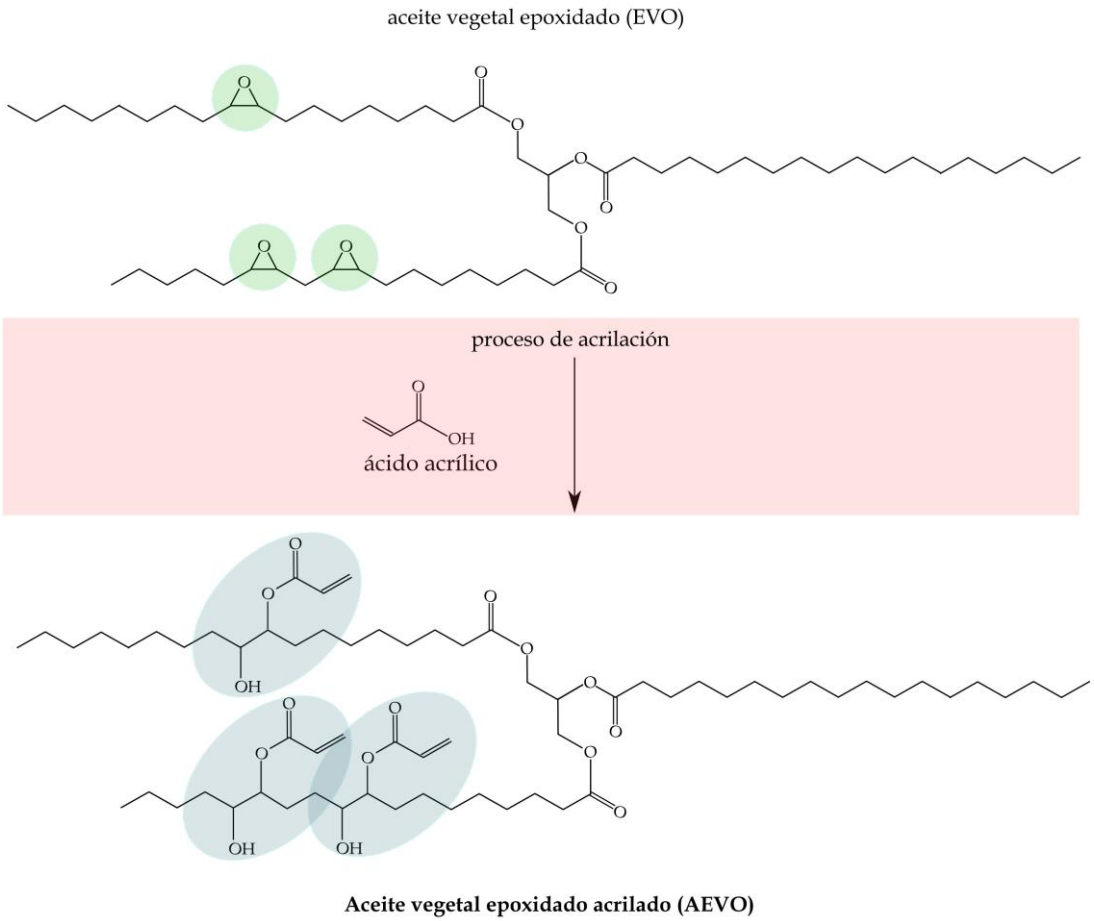

Figura I.28. Esquema del proceso de acrilación de un aceite vegetal epoxidado.

En la literatura el aceite acritlatado epoxidado de soja (AESO) es de los que más tiene relevancia en la fabricación de resinas termoestables donde generalmente se suele utilizar agentes de curado con bajo peso molecular y estructura rígida como anhídridos, isocianatos o estireno, para poder compensar la alta viscosidad y la baja capacidad de entrecruzado que inherentemente tienen los VOs [152,153], por desgracia la mayoría de estos compuestos son de origen petroquímico. Es verdad que el uso de estireno provoca un notable incremento en el rendimiento mecánico, pero la búsqueda de sistemas con alto rendimiento medioambiental ha provocado el reemplazo de este compuesto por compuestos de origen natural, como productos derivados de carbohidratos o lignina. Autores como Liu, *et al.* [154] utilizaron una matriz termoestable tomando como base AESO copolimerizado con isosorbida metacrilada (MI) (derivado de la lignina) para la fabricación de materiales compuestos reforzados por fibras naturales, donde la resina formada se modificó con anhídrido metacrilato para injertar más enlaces C=C. Se observó que la resina aparte de presentar un alto contenido biológico presentó buenas propiedades mecánicas, facilidad de procesado, lo que proporcionó un mejor rendimiento a los materiales compuestos. De igual manera Chen,

et al. [155] sintetizaron una resina termostable utilizando monómero derivados de la lignina como el alcohol vanílico metacrilado (MVA) con AESO, obteniendo materiales con excelentes propiedades a flexión y buena estabilidad térmica.

I.3.2.3. Maleinización

El proceso de maleinización se refiere a la incorporación de grupos anhídridos en la estructura de los aceites vegetales. En este proceso el compuesto anhídrido maléico reacciona con los dobles enlaces de un ácido graso insaturado. El anhídrido maléico puede reaccionar tanto con los dobles enlaces conjugados como con los dobles enlaces aislados [156]. La representación de este proceso se puede observar en la figura I.29.

Esta reacción se produce a través de una reacción “eno” con temperaturas superiores a los 200 ºC, para el caso de los ésteres de ácidos grasos monoinsaturados, donde un grupo anhídrido se adiciona a la posición alílica del ácido graso. Lo que implica el desplazamiento alílico de un doble enlace a través de la transferencia del hidrógeno alílico al enófilo y la unión de las dos moléculas. En cambio, para el caso de ácidos grasos diinsaturados no conjugados, la reacción “eno” resulta en la conjugación de dos dobles enlaces, que resulta en un isómero trans-trans, para posteriormente producirse una reacción Diels-Alder [157].

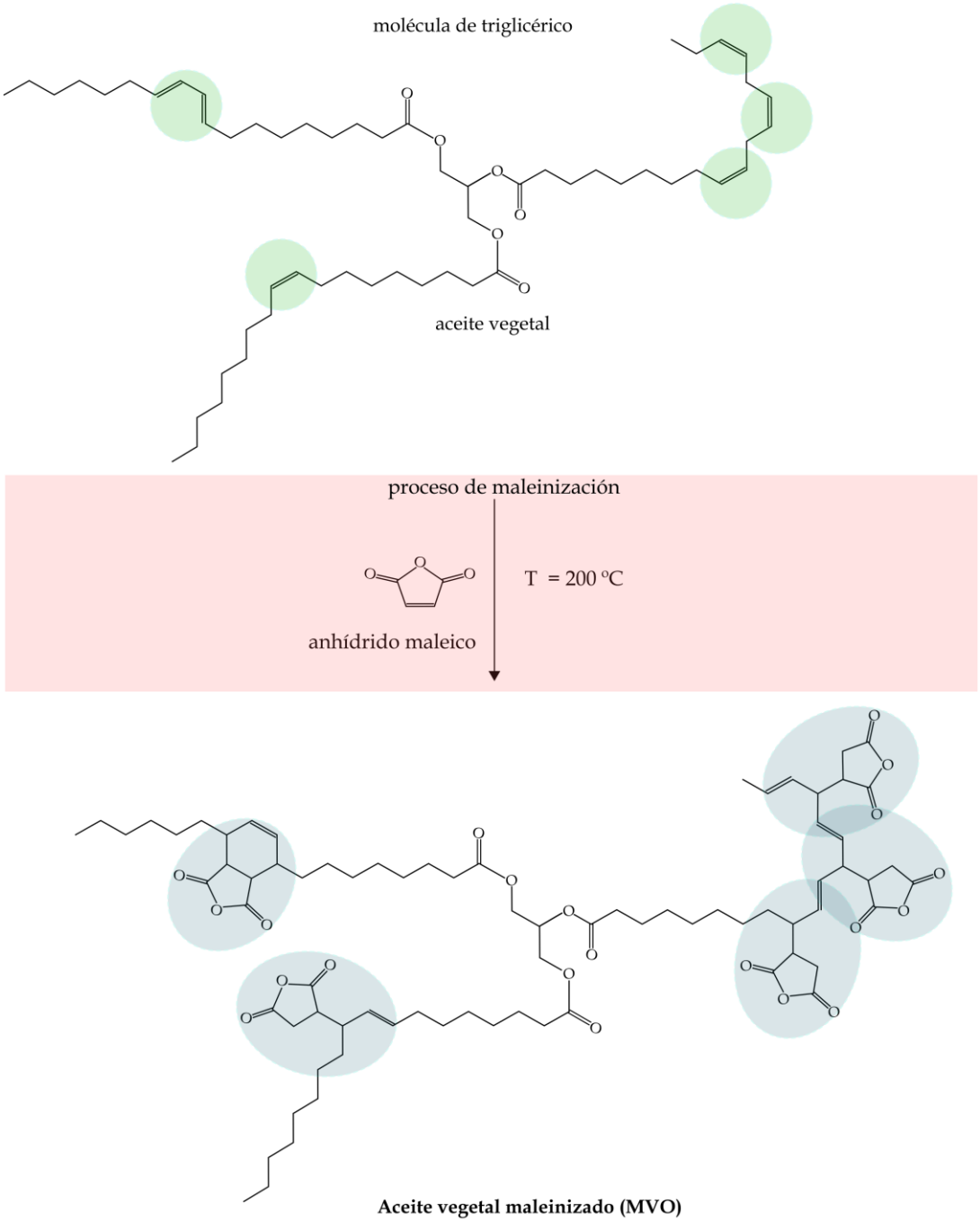

Figura I.29. Representación esquemática del proceso de maleinización de un aceite vegetal por reacción con anhídrido maléico.

Dentro de los aceites maleinizados, el aceite maleinizado de lino (MLO) ha ganado relevancia en el sector de los materiales termoestables de origen natural. Donde autores como Samper, *et al.* [144] propusieron el uso de MLO como parte del sistema endurecedor formado junto con anhídrido metílico nádico (MNA) en una resina epoxi basado en aceite de lino epoxidado (ELO), aquí se pudo aprovechar la estructura alargada que tiene el MLO para proporcionar mayor ductilidad al sistema, a la par que

incrementa el porcentaje de origen orgánico, obteniendo propiedades balanceadas al incorporar un 10 % MLO. Tomando estos prometedores resultados Fombuena, *et al*. [158] fabricaron materiales compuesto con una matriz de ELO endurecido por una mezcla de (MNA:MLO) y reforzados con fibras naturales (lino y basalto), en este estudio a diferencia del presentado por Samper, se pudo aumentar el contenido de MLO hasta un 25 % logrando obtener materiales con una buena densidad de entrecruzamiento, con buenas propiedades dúctiles (resistencia al impacto y elongación a la rotura) y con un alto porcentaje de origen orgánico, además se observó que el MLO ayudó a promover la interacción superficial entre las fibras de refuerzo y la matriz. Por otro lado, *Motoc, et al.* [159] fabricaron materiales compuestos reforzados con fibras naturales (lino y basalto), tomado como matriz una resina epoxi basada en ELO y un endurecedor producido por la mezcla de anhídrido glutárico (GA) y MLO. Los materiales obtenidos además de poseer un alto porcentaje de origen natural, los materiales tuvieron propiedades termomecánicas y térmicas interesantes, ya que el sistema resina:endurecedor se comportó como una resina epoxi convencional, derivando el rendimiento de los compuesto directamente a la distribución y apilamiento de los tejidos.

I.3.3. Cinética de entrecruzamiento

En la fabricación de materiales compuestos, conocer completamente las características y propiedades tanto de la matriz como de los materiales de refuerzo es de gran valía. Se ha comentado las diferentes características y propiedades que presentan las fibras de refuerzo, dependiendo su tipo, naturaleza, distribución, etc., y como afecta esto a las propiedades finales de los compuestos que están reforzando, de igual manera ocurre con la matriz, que en el caso de materiales compuestos es una resina termoestable. El estudio del comportamiento de una matriz termoestable o el estudio de la cinética de curado de una resina es de gran importancia desde el punto de vista industrial, ya que interviene directamente con el desarrollo de estos materiales.

Este estudio se basa en utilizar la tecnología de análisis térmico para seguir los cambios físicos (de líquido a sólido) y las reacciones químicas que ocurren, utilizando un enfoque matemático para entender el mecanismo de reacción [160]. Desarrollando e implementando el modelo cinético de curado adecuado, se puede optimizar los ciclos de curado, lo que se traduce en una mejora en la calidad del producto final, así como la disminución del tiempo de producción.

La metodología del análisis térmico se puede enfocar tanto de un punto de vista isotermo como no isotermo, debido a la fiabilidad en la obtención de datos, los métodos

no isotermos se han establecido como los principales métodos para el desarrollo del análisis térmico cinético, dentro de este método (no isotermo) se recomienda el método con programas con varias tasas de calentamiento, sobre aquellos que utilizan una sola tasa de calentamiento, además según los diferentes métodos matemáticos estos se pueden dividir en métodos diferenciales y métodos integrales [161].

El estudio de la cinética de un proceso térmicamente activado se encuentra relacionado a la velocidad de conversión ($\frac{\mathrm{d}\alpha}{\mathrm{dt}}$), la misma que puede ser parametrizada por la temperatura (*T*), el grado de conversión (α) y la presión (*P*), siguiendo la expresión I.1.1 [162]:

$$\frac{d\alpha}{dt} = k(T)f(\alpha)h(P) \tag{I.1.1}$$

Cabe recalcar que la mayoría de los análisis térmicos relacionados con el estudio cinético, la dependencia de la presión suele ser ignorada. Por lo que la expresión se ve reducida en términos más generales, donde la rapidez de reacción puede ser expresada por solo dos variables, la temperatura y el grado de conversión:

$$\frac{d\alpha}{dt} = k(T)f(\alpha) \tag{I.1.2}$$

Donde la dependencia del proceso está representada por la constante de rapidez $k(T)$ que depende de la temperatura, y el modelo de reacción $f(\alpha)$ que depende a su vez del grado de conversión α que va desde 0 a 1. La función $f(\alpha)$ se presenta en diferentes formas dependiendo del tipo de reacción que se esta produciendo, algunos de los cuales representan reacciones de estado sólido y se muestran en la tabla I.7**.**; y la función $k(T)$ se describe por medio de la ecuación de Arrhenius:

$$k(T) = A\, e^{\left(-\frac{E_a}{R\,T}\right)} \tag{I.1.3}$$

Donde *A* es el factor pre exponencial, E_a es la energía de activación aparente, R es la constante universal de los gases (8,314 J mol^{-1} K^{-1}) y *T* es la temperatura absoluta.

La expresión general que representa el estudio cinético del curado de una resina se puede apreciar en la ecuación I.1.4 y resulta combinando la ecuación I.1.2 y I.1.3.

$$\frac{d\alpha}{dt} = A\, e^{\left(-\frac{E_a}{RT}\right)} f(\alpha) \qquad \text{(I.1.4)}$$

Los parámetros *A*, E_a, y $f(\alpha)$ se conoce como el triplete cinético, y su obtención es de gran importancia para la comprensión de la cinética del proceso de entrecruzado. Como se comentó anteriormente el análisis no isotermo es de los más utilizados, en este caso la temperatura es función del tiempo ($T = T(t)$), en donde la temperatura suele variar linealmente con el tiempo, lo que se conoce como la tasa de calentamiento (β) y se representa por siguiente expresión:

$$\beta = \frac{dT}{dt} \qquad \text{(I.1.5)}$$

Introduciendo la tasa de calentamiento en la expresión I.1.4 obtenemos una ecuación general para el análisis cinético de métodos diferenciales aplicable para programas de calentamiento dinámicos.

$$\beta\, \frac{d\alpha}{dT} = A\, e^{\left(-\frac{E_a}{RT}\right)} f(\alpha) \qquad \text{(I.1.6)}$$

Esta expresión puede ser representada en su forma integral, la cual se puede observar en la ecuación I.1.7, esta expresión es la base para varios métodos integrales.

$$\int_0^{\alpha} \frac{d\alpha}{dT} = \frac{A}{\beta} \int_0^{T} e^{\left(-\frac{E_a}{RT}\right)} dT = g(\alpha) \qquad \text{(I.1.7)}$$

Donde la $g(\alpha)$ es la forma integral de los modelos de reacción, los cuales se pueden ver resumidos en tabla I.7.

Tabla I.7. Ecuaciones cinéticas utilizadas en análisis isotérmicos. Adaptada de Dickinson and Heal [163].

Modelo de reacción	**Cód**	***f*(*α*)**	***g*(*α*)**
		Potencia/exponencial	
Ley de potencia (mitad)	P2	$2\alpha^{1/2}$	$\alpha^{1/2}$

Ley de potencia (tercio)	P3	$3\alpha^{2/3}$	$\alpha^{1/3}$
Ley de potencia (cuarto)	P4	$4\alpha^{3/4}$	$\alpha^{1/4}$
Exponencial	E1	α	$\ln(\alpha)$
		Orden/interfaz	
Orden cero	F0	constante	α
Primer orden	F1	$(1-\alpha)$	$-\ln(1-\alpha)$
Segundo orden	F2	$(1-\alpha)^2$	$1/(1-\alpha)-1$
Área de contracción	R2	$2(1-\alpha)^{1/2}$	$\left[1-(1-\alpha)^{1/2}\right]$
Volumen de contracción	R3	$3(1-\alpha)^{2/3}$	$\left[1-(1-\alpha)^{1/3}\right]$
Interfaz de contracción	R4	$3/2\,(1-\alpha)^{1/3}$	$\left[1-(1-\alpha)^{2/3}\right]$
		Avrami-Erofeev (JMA) nucleación y crecimiento	
Avrami-Erofeev	A1	$4(1-\alpha)[-\ln(1-\alpha)]^{3/4}$	$[-\ln(1-\alpha)]^{1/4}$
Avrami-Erofeev	A2	$2(1-\alpha)[-\ln(1-\alpha)]^{1/2}$	$[-\ln(1-\alpha)]^{1/2}$
Avrami-Erofeev	A3	$3(1-\alpha)[-\ln(1-\alpha)]^{2/3}$	$[-\ln(1-\alpha)]^{1/3}$
Avrami-Erofeev	A4	$4/3\,(1-\alpha)[-\ln(1-\alpha)]^{1/4}$	$[-\ln(1-\alpha)]^{3/4}$
Avrami-Erofeev	A5	$1{,}5(1-\alpha)[-\ln(1-\alpha)]^{1/3}$	$[-\ln(1-\alpha)]^{2/3}$
		Ecuaciones de difusión	
Una dimensión (parabólica)	D1	$1/(2\alpha)$	α^2
Dos dimensiones (Valensi-Barrer)	D2	$-1/\ln(1-\alpha)$	$(1-\alpha)\ln(1-\alpha)+\alpha$
Tres dimensiones (Jander)	D3	$1{,}5(1-\alpha)^{2/3}/\left[1-(1-\alpha)^{1/3}\right]$	$\left[1-(1-\alpha)^{1/3}\right]^2$
(Ginstling-Brounshtein)	D4	$1{,}5/\left[(1-\alpha)^{-1/3}-1\right]$	$\left[1-2/3\alpha-(1-\alpha)^{2/3}\right]$
(Zhuravlev)	D5	$1{,}5(1-\alpha)^{4/3}/\left[1/(1-\alpha)^{1/3}-1\right]$	$\left[1/(1-\alpha)^{1/3}-1\right]^2$
(Anti-Jander)	D6	$1{,}5(1+\alpha)^{2/3}/\left[1/(1+\alpha)^{1/3}-1\right]$	$\left[(1+\alpha)^{1/3}-1\right]^2$

(Kroger-Ziegler)	D7	$\left\{1{,}5(1-\alpha)^{2/3}/\left[1-(1-\alpha)^{1/3}\right]\right\}/t$	$\left[1-(1-\alpha)^{1/3}\right]^2 = \log(t)$
Dos dimensiones (Jander)	D8	$(1-\alpha)^{1/2}/\left[1-(1-\alpha)^{1/2}\right]$	$\left[1-(1-\alpha)^{1/2}\right]^2$
Dos dimensiones (Anti-Jander)	D9	$(1+\alpha)^{1/2}/\left[(1+\alpha)^{1/2}-1\right]$	$\left[(1+\alpha)^{1/2}-1\right]^2$
Transferencia interfacial	D10	$3(1-\alpha)^{4/3}$	$\left[1/(1-\alpha)^{1/3}-1\right]$
Transmisión y difusión	D11	$3/\left[(1-\alpha)^{-4/3}-(1-\alpha)^{-1}\right]$	$1/(1-\alpha)^{-1/3}-1 + 1/3\ln(1-\alpha)$
Difusión en dos direcciones	D12	$3/\left[(1-\alpha)^{-8/3}-(1-\alpha)^{-7/3}\right]$	$1/5(1-\alpha)^{-5/3} + 1/4(1-\alpha)^{-4/3} + 1/20$

Una de las limitaciones que presenta la ecuación I.1.2**,** es que esta descrita para procesos que se producen en un solo paso (*"single-step process"*), lo que aplicarlo en procesos que ocurren en múltiples pasos, puede ocasionar procesos más complejos, a pesar de esto, el uso de este método no lo limita. Cuando se trata de procesos de reacción que se producen en múltiples pasos, es recomendable utilizar modelos computacionales que detectan y tratan procesos que envuelven múltiples pasos. En este sentido la ICTAC, propone el uso de métodos isoconversionales o como se les conoce *"model-free kinetics methods (MFK)"* para solventar estos problemas [164].

I.3.3.1. Métodos isoconversionales: "model-free kinetics methods"

Los métodos isoconversionales han sido ampliamente utilizados en el estudio del curado de resinas termoestables debido a su practicidad, ya que permite identificar si el proceso de curado se rige por la reacción o por la difusión. En términos generales nos permite determinar la energía de activación aparente (E_a) parámetro importante del triplete cinético. Esto se puede obtener ya se por métodos diferenciales (ecuación I.1.6) o integrales (ecuación I.1.7), se comentó anteriormente que estas ecuaciones son válidas para procesos en los cuales su reacción se produce en un solo paso, siendo limitante en procesos que ocurren en múltiples pasos. Aquí es donde la utilidad de los métodos isoconversionales es notoria ya que a pesar de que estos métodos se derivan de este mismo principio, es decir en lo que se conoce como el principio de isoconversión. Estos métodos se pueden aplicar también en el estudio de procesos que ocurren en múltiples pasos ya permite describir la cinética de un proceso complejo utilizando

múltiples ecuaciones cinéticas de un solo paso, donde cada una está ligada a un grado de conversión y que el rango de temperatura entre estos sea estrecho como se observa en la figura I.30 [164].

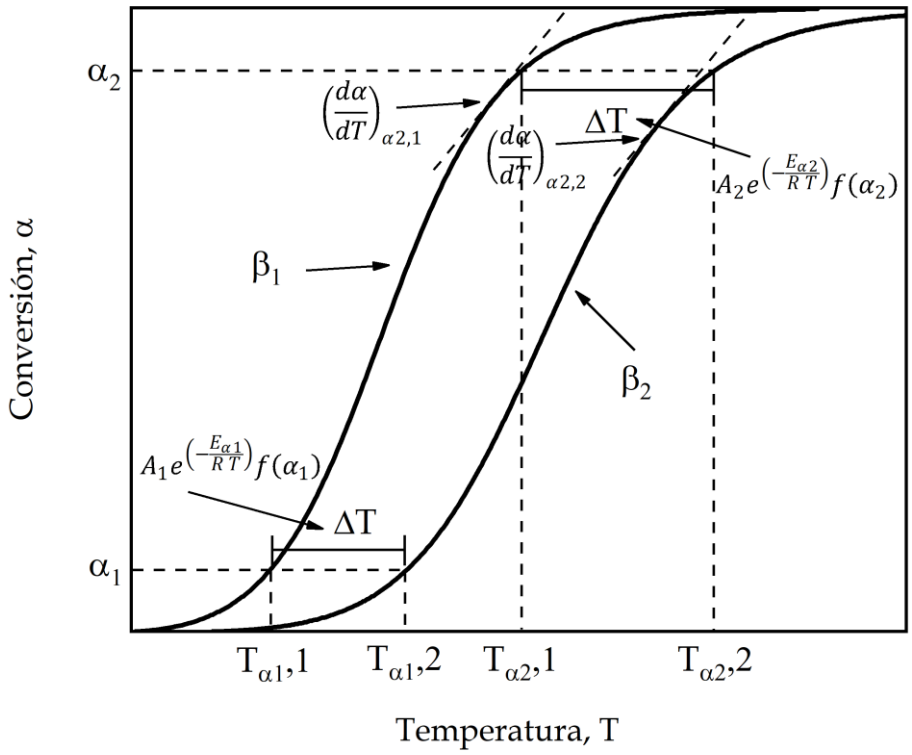

Figura I.30. Ecuación de Arrhenius aplicada a los métodos isoconversionales, asociado a un determinado grado de conversión α para una región estrecha de temperatura ΔT

Estos métodos tienen su origen en el principio de isoconversión el cual establece que la velocidad de reacción a una conversión constante (α_c) es solo función de la temperatura, es decir que es aplicable cuando ocurre en un único grado de conversión y en la región de temperatura que está relacionada con esta. Este principio se puede demostrar tomando como punto de partida la expresión de la velocidad de reacción (ecuación I.1.4) y aplicando logaritmo natural para obtener la ecuación I.1.8, seguidamente aplicando la derivada parcial con respecto al inverso de la temperatura para un α constante, obteniendo la ecuación I.1.9.

$$ln\left(\frac{d\alpha}{dt}\right) = ln\, k(T) + ln\, f(\alpha) \tag{I.1.8}$$

$$\left[\frac{\partial\, ln\left(\frac{d\alpha}{dt}\right)}{\partial\, T^{-1}}\right]_{\alpha_i} = \left[\frac{\partial\, ln\, k(T)}{\partial\, T^{-1}}\right]_{\alpha_i} + \left[\frac{\partial\, ln\, f(\alpha)}{\partial\, T^{-1}}\right]_{\alpha_i} \quad \text{(I.1.9)}$$

Aplicando el principio de isoconversión en la ecuación I.1.9, donde α es constante (α = α_i), se tiene que también la $f(\alpha)$ es constante, esto da como resultado que el segundo término de la parte derecha de la ecuación I.1.9 sea igual a 0. Substituyendo la ecuación I.1.3 en la expresión, y aplicando la derivada parcial con respecto a la inversa de la temperatura, se obtiene la ecuación I.1.10**.** Esta expresión permite estimar valores de la energía de activación aparente (para un determinado grado de reacción constante) sin la necesidad de asumir ni determinar ningún modelo de reacción, razón por la cual toman el nombre de métodos sin modelo o *"model-free* methods" [165].

$$\left[\frac{\partial\, ln\left(\frac{d\alpha}{dt}\right)}{\partial\, T^{-1}}\right]_{\alpha_i} = -\frac{E_a}{R} \quad \text{(I.1.10)}$$

Varios métodos se basan en el principio de isoconversión, en términos generales se pueden dividir en dos tipos, métodos diferenciales o métodos integrales.

Métodos isonversionales diferenciales

Método de Friedman

De los métodos isoconversionales diferenciales más utilizados para estimar la energía de activación aparente (E_a) es el planteado por Henry Friedman, el denominado método de Friedman [166]. Este método se basa en aplicar el principio de isoconversión a la ecuación I.1.5 (ecuación general para el análisis cinético de métodos diferenciales), donde al emplear logaritmo natural se obtiene la ecuación I.1.11, siendo la expresión que regirá este método. El método de Friedman asume que la función de reacción $f(\alpha)$ permanece constante para valores constantes del grado de conversión α, y puede ser utilizada para cualquier programa térmico.

$$ln\left(\beta\, \frac{d\alpha}{dT}\right) = ln\, A\;\, f(\alpha) - \frac{E_a}{R\, T} \quad \text{(I.1.11)}$$

Para programas no isotermos donde se utiliza diferentes velocidades de calentamiento (β), la energía de activación aparente se puede obtener de la pendiente del gráfico $\ln\left(\beta\ \frac{d\alpha}{dT}\right)$ en función del inverso de temperatura $\left(\frac{1}{R\ T}\right)$. Al permanecer la $f(\alpha)$ constante para un cierto valor de α, no existe la necesidad de conocer ni asumir ningún modelo de reacción, lo que resulta en valores de E_a con una alta precisión incluso puede tener mayor precisión que la obtenida por métodos integrales.

Métodos isonversionales integrales

Estos métodos se derivan de la aplicación del principio de isoconversión en la forma integral de la ecuación I.1.7. Donde el término derecho de la ecuación, es decir la integral de la constante de Arrhenius que depende de la temperatura ($\int_o^T e^{-\frac{E_a}{R\,T}}\,dT$) no tiene una solución analítica directa. Es debido a esto que varios autores han propuesto métodos numéricos, a través de aproximaciones, para resolverlo [167]. Para esto, se puede reducir la expresión $\frac{\mathrm{E_a}}{\mathrm{R\,T}}$ por *x*, y así obtener una función polinomial $p(x)$, conocida como la integral de Arrhenius. Substituyendo esto en la ecuación I.1.7 obtenemos la siguiente expresión:

$$g(\alpha) = \frac{A\ E_a}{\beta\ R}\ p(x) \tag{I.1.12}$$

La función $p(x)$ se puede resolver por métodos numéricos o por aproximaciones, las cuales están definidas por una seria de funciones asintótica. Varios autores han presentado diferentes aproximaciones a través de los años, las cuales siguen vigentes [168-170]. Sin embargo, estas aproximaciones se pueden englobar en la siguiente expresión:

$$p(x) = \frac{e^{-x}}{x}\ \pi(x) \tag{I.1.13}$$

Donde $\pi(x)$ es la forma racional de estas aproximaciones. Senum and Yang [171] sugirieron varias expresiones las cuales están enlistadas en la tabla I.8. En la presente tabla se puede observar una corrección realizada por Flynn [167] para la aproximación racional de cuarto grado. Con respecto a esto, Pérez-Maqueda and Criado [172] han realizado un magnífico trabajo validando la precisión de las aproximaciones de la integral de Arrhenius hasta expresiones polinomiales de ocho grados. En su trabajo

determinaron que con el aumento de grado aumenta la precisión. A pesar de esto, se concluyó que para el análisis cinético se obtiene una precisión suficiente con el uso de una aproximación de cuarto grado.

Tabla I.8. Aproximaciones racionales de la integral de Arrhenius expresiones desde grado 1 al 8. Adaptada de Senum and Yang [171] y Pérez-Maqueda and Criado [172].

Grado	$p(x)$
1	$\frac{e^{-x}}{x}\frac{1}{x+2}$
2	$\frac{e^{-x}}{x}\frac{x+4}{x^2+6x+6}$
3	$\frac{e^{-x}}{x}\frac{x^2+10x+18}{x^3+12x^2+368x+24}$
4	$\frac{e^{-x}}{x}\frac{x^3+18x^2+86x+96}{x^4+20x^3+120x^2+240x+120}$
5	$\frac{e^{-x}}{x}\frac{x^4+28x^3+246x^2+756x+600}{x^5+30x^4+300x^3+1200x^2+1200x+720}$
6	$\frac{e^{-x}}{x}\frac{x^5+40x^4+552x^3+3168x^2+7092x+4320}{x^6+42x^5+360x^4+4200x^3+12600x^2+15120x+5040}$
7	$\frac{e^{-x}}{x}\frac{x^6+54x^5+1070x^4+9720x^3+41112x^2+71856x+35280}{x^7+56x^6+1176x^5+11760x^4+58800x^3+141120x^2+141120x+40320}$
8	$\frac{e^{-x}}{x}\frac{x^7+70x^6+1886x^5+24920x^4+170136x^3+577584x^2+844560x+357120}{x^8+72x^7+2024x^6+28560x^5+216720x^4+880320x^3+1794240x^2+1572480x+403200}$

Partiendo de las aproximaciones de la integral de Arrhenius, Starink [173], estableció una expresión general para lo que nombró métodos isoconversionales $p(x)$, dicha ecuación se observa a continuación:

$$ln\left(\frac{\beta}{T^B}\right) = constante - C\ \frac{E_a}{R\,T} \tag{I.1.14}$$

Donde B y C son valores relacionados a una aproximación particular de la temperatura integral. En este tipo métodos la energía de activación se puede determinar de la gráfica derivada de los parámetros *T* y β, es decir de la pendiente del ajuste lineal al graficar $\ln\left(\frac{\beta}{T^B}\right)$ con respecto a $\frac{1}{T}$.

Aplicando diferentes aproximaciones en la ecuación I.1.4 se pueden obtener una gran cantidad de métodos. Está claro que, la precisión de cada método, está ligado por un lado a la fiabilidad en la parte práctica, es decir, en las posibles imprecisiones en la medición de la temperatura, y, por otro lado, la correcta aplicación de los métodos. Teniendo esto en cuenta varios métodos integrales se han desarrollado utilizando diferentes aproximaciones.

Método de Flynn-Wall-Ozawa

El método integral planteado por Flynn and Wall [174] y Ozawa [175] comúnmente conocido como el método Flynn-Wall-Ozawa (FWO). Es de los métodos isoconversionales más utilizados, se basa en la aproximación de Doyle [176] siendo esta aproximación una de las más sencillas y burdas (ecuación I.1.15), donde se proponen como valores de B y C 0 y 1,052, respectivamente. Lo que resulta la siguiente expresión (I.1.16):

$$p(x) \cong e^{(-1{,}0518x - 5{,}330)} \tag{I.1.15}$$

$$ln(\beta) = constante - 1{,}052\ \frac{E_a}{R\,T} \tag{I.1.16}$$

La energía de activación (E_a) se obtiene de la pendiente de la curva obtenida al graficar $\ln(\beta)$ con respecto a $\frac{1}{T}$. Debido a que la aproximación de la temperatura integral utilizada es muy básica los valores de E_a presentan una baja exactitud. Lo que resulta en un método con poca precisión.

Método de Kissnger-Akahira-Sunose

Otro de los métodos utilizados es el denominado Kissnger-Akahira-Sunose (KAS) [177], este parte de una aproximación más precisa para $p(x)$, la planteada por Murray and White [178], que se obtiene integrando por partes y truncando la serie para una reacción de estado sólido a la integral de Arrhenius resultando la ecuación I.1.17. En donde para una fracción constante de conversión α, el valor de B y C es 2 y 1. Resultando la expresión I.1.18:

$$p(x) \cong \frac{e^{-x}}{x^2} \tag{I.1.17}$$

$$ln\left(\frac{\beta}{T^2}\right) = constante - \frac{E_a}{R\,T} \tag{I.1.18}$$

Del gráfico resultante de la representación de $\ln\left(\frac{\beta}{T^2}\right)$ vs $\frac{1}{T}$, obtenemos líneas rectas, donde a través de su pendiente podemos estimar la energía de activación $\frac{E_a}{R}$.

Método de Starink

Se observó que la aproximación de Doyle y de Murray y White son parte de una aproximación más grande descrita por la expresión:

$$p(x) \cong \frac{e^{(-AX+B)}}{x^k} \tag{I.1.19}$$

De este grupo de aproximaciones para cada valor de *k,* A y B, se puede optimizar por medio de la disminución de la desviación entre la función de aproximación y la integral exacta. Starink [173] estableció que si A no es igual a 1 se puede obtener aproximaciones con una alta precisión, y está dada por la siguiente ecuación:

$$p(x) \cong \frac{e^{(-1{,}008X-0{,}312)}}{x^{1{,}92}} \tag{I.1.20}$$

Basándose en la ecuación I.1.20 y en la ecuación I.1.4 propone un nuevo método utilizando B=1,92 y C=1,008. Dando como resultado la ecuación I.1.21., al igual que los métodos mencionados anteriormente (FWO y KAS). La energía de activación se puede obtener a través de la pendiente del ajuste lineal al graficar $\ln\left(\frac{\beta}{T^{1{,}92}}\right)$ vs $\frac{1}{T}$.

$$ln\left(\frac{\beta}{T^{1,92}}\right) = constante - 1{,}0008\,\frac{E_a}{R\,T} \tag{I.1.21}$$

El método de Kissinger se recomienda sobre los métodos FWO y KAS ya que los valores de E_a obtenidos mediante la ecuación I.1.21, presentan mayor precisión que los obtenidos por otros métodos isoconversionales integrales.

Método de Kissinger

El método de Kissinger [179] debido a la facilidad de su aplicabilidad es otro de los métodos más utilizados para la determinación de la energía de activación a través de múltiples tasas de calentamiento. Este método asume que la tasa máxima de transformación se puede aproximar a una etapa fija y tiene su punto de partida en la ecuación I.1.4**,** bajo la condición de la tasa máxima reacción, donde $\frac{d}{dt}\left(\frac{d\alpha}{dt}\right) = 0$. Derivando la ecuación I.1.6 donde se toma cuenta la velocidad de calentamiento (β) se obtiene la siguiente expresión:

$$\frac{d}{dt}\left(\frac{d\alpha}{dt}\right) = \left(\frac{d\alpha}{dt}\right)\left[\frac{\beta\,E_a}{R\,T^2} + \left(\frac{d\,f(\alpha)}{d\alpha}\right)\,A\,e^{-\frac{E_a}{R\,T}}\right] \tag{I.1.22}$$

Aplicando la condición donde $\frac{d}{dt}\left(\frac{d\alpha}{dt}\right) = 0$, se obtiene:

$$\frac{\beta\,E_a}{R\,T_p^2} + \left(\frac{d\,f(\alpha)}{d\alpha}\right)\,A\,e^{-\frac{E_a}{R\,T_p}} = 0 \tag{I.1.23}$$

Finalmente, tomando logaritmo natural obtenemos, la ecuación que rige el método, como se observa a continuación:

$$ln\left(\frac{\beta}{T_p^2}\right) = ln\left(\frac{A\,R}{E_a}\right) + ln\left(-\frac{d\,f(\alpha)}{d\alpha}\right) - \frac{E_a}{R\,T_p} \tag{I.1.24}$$

Donde la T_p es la temperatura en la máxima tasa de reacción, temperatura del pico.

El método presenta varias limitaciones, una de las cuales es que aporta con un solo valor de la energía de activación (en α_m), lo que quiere decir que no se puede hacer

seguimiento de la evolución de E_a a través del proceso de conversión, además, de asumir que todo el proceso ocurre en un solo paso. Esta energía de activación se puede obtener de la pendiente del ajuste lineal al graficar $\ln\left(\frac{\beta}{T_p^2}\right)$ vs $\frac{1}{T_p}$, cuando el término $\left(-\frac{d\,f(\alpha)}{d\alpha}\right)$ es constante en la (ecuación I.1.14). Por otro lado, hay que tener en cuenta que el termino $\left(-\frac{d\,f(\alpha)}{d\alpha}\right)$ deber ser independiente de la velocidad de calentamiento para que los valores de E_a sean precisos.

Debido a la sensibilidad que tiene el método de Kissinger con lo que respecta a procesos cinéticos que ocurren en un solo paso, varios métodos se han propuesto para verificar esto y validar el análisis cinético. Dentro de los más interesantes está el planteado por Farjas, *et al.* [180], donde plantean el uso de la amplitud del pico de la velocidad de reacción, debido a que es un parámetro muy sensible a la aparición de transformaciones que ocurren en múltiples pasos.

Para esto hay que tener en cuenta que todas las curvas termo analíticas obtenidas a diferentes temperaturas solo varían por un factor de escala de tiempo τ, como se indica a continuación:

$$\tau \equiv \frac{1}{k(T)} \tag{I.1.25}$$

Además de que existe una relación directa entre la amplitud total a la altura del máximo (Δt_{FWHM}) y la escala de tiempo correspondiente a la temperatura del pico (τ_p).

$$\Delta t_{FWHM} = \Delta t'_{FWHM}\,\tau_p \tag{I.1.26}$$

Donde $\Delta t'_{\mathrm{FWHM}}$ es la amplitud total a la altura del máximo de la curva obtenida al normalizar el valor de $\tau_p = 1$. Donde el valor es constante y depende exclusivamente del modelo cinético. Reemplazando el valor de τ_p en la ecuación I.1.26, y aplicando logaritmo natural a los dos lados se obtiene una ecuación la cual presenta una relación lineal entre Δt_{FWHM} y la $\frac{1}{T_p}$, como se observa a continuación:

$$ln(\Delta t_{FWHM}) = \frac{E_a}{R\,T_p} + ln\frac{\Delta t'_{FWHM}}{A} \tag{I.1.27}$$

Esta relación es similar a la ecuación de Kissinger. Por lo tanto, el valor de la pendiente debe coincidir con el valor absoluto obtenida por el método de Kissinger, para que se cumpla con la premisa de que el proceso de reacción está ocurriendo en un solo paso, caso contrario el método de Kissinger no se pudiera utilizar en ese caso particular.

Determinación del modelo cinético

Los métodos descritos anteriormente permiten evaluar la energía de activación E_a con una alta precisión sin determinar ni conocer el modelo de reacción $f(\alpha)$. Pero una vez conocido el valor E_a, es necesario determinar el modelo cinético que mejor se ajusta al proceso de reacción. Como establecen Criado, *et al.* [181] y Málek [182] el modelo se puede determinar definiendo dos funciones $y(\alpha)$ y $z(\alpha)$, que se puede obtener a través de datos experimentales, como se observa a continuación:

$$y(\alpha) = \left(\frac{d\alpha}{dt}\right) e^{x} \tag{I.1.28}$$

$$z(\alpha) = \left(\frac{d\alpha}{dt}\right) \pi(x) \frac{T}{\beta} \tag{I.1.29}$$

Donde la temperatura reducida se expresa por $x = \frac{\mathrm{E_a}}{\mathrm{R\,T}}$.

Refiriéndonos a la función $y(\alpha)$, si substituimos la ecuación I.1.3, resulta en una expresión la cual es proporcional a la función $f(\alpha)$, como se observa en la ecuación I.1.30. Donde si se normaliza se puede comparar las funciones teóricas (tabla I.7.) y determinar el modelo cinético. Cabe recalcar la importancia de conocer el valor de E_a con anticipación ya que, seria prácticamente imposible obtener el mecanismo de reacción desconociéndolo.

$$y(\alpha) = \left(\frac{d\alpha}{dt}\right) e^{\frac{E_a}{R\,T}} = A\, f(\alpha) \tag{I.1.30}$$

Se puede hacer un análisis similar con respecto a la función $z(\alpha)$, la cual corresponde a un modelo de reacción diferente. Esta función hace referencia tanto a la función integral $g(\alpha)$ y la función $f(\alpha)$ como se muestra en la ecuación I.1.31. Esta expresión se obtiene sustituyendo la ecuación I.1.4, I.1.12 y I.1.13 en la función $z(\alpha)$ (ecuación I.1.29).

$$z(\alpha) = f(\alpha)\, g(\alpha) \tag{I.1.31}$$

La función $z(\alpha)$ obtenida a partir de datos experimentales no isotermos se puede comparar con las curvas teóricas para determinar el modelo cinético adecuado. La función $z(\alpha)$ experimental se puede obtener incluyendo la función $\pi(x)$ y la expresión de la temperatura reducida, obteniendo la expresión (I.1.32):

$$z(\alpha) = \left(\frac{d\alpha}{dt}\right) \frac{E_a}{\beta\, R}\, e^{\frac{E_a}{RT}}\, p(x) \tag{I.1.32}$$

Donde $p(x)$ corresponde a los diferentes modelos cinéticos de transformaciones en estado sólido representados en la tabla I.8. En la figura I.31 se puede observar algunos *"master plots"* teóricos que representan los modelos de reacción a la función $g(\alpha)$ y $z(\alpha)$.

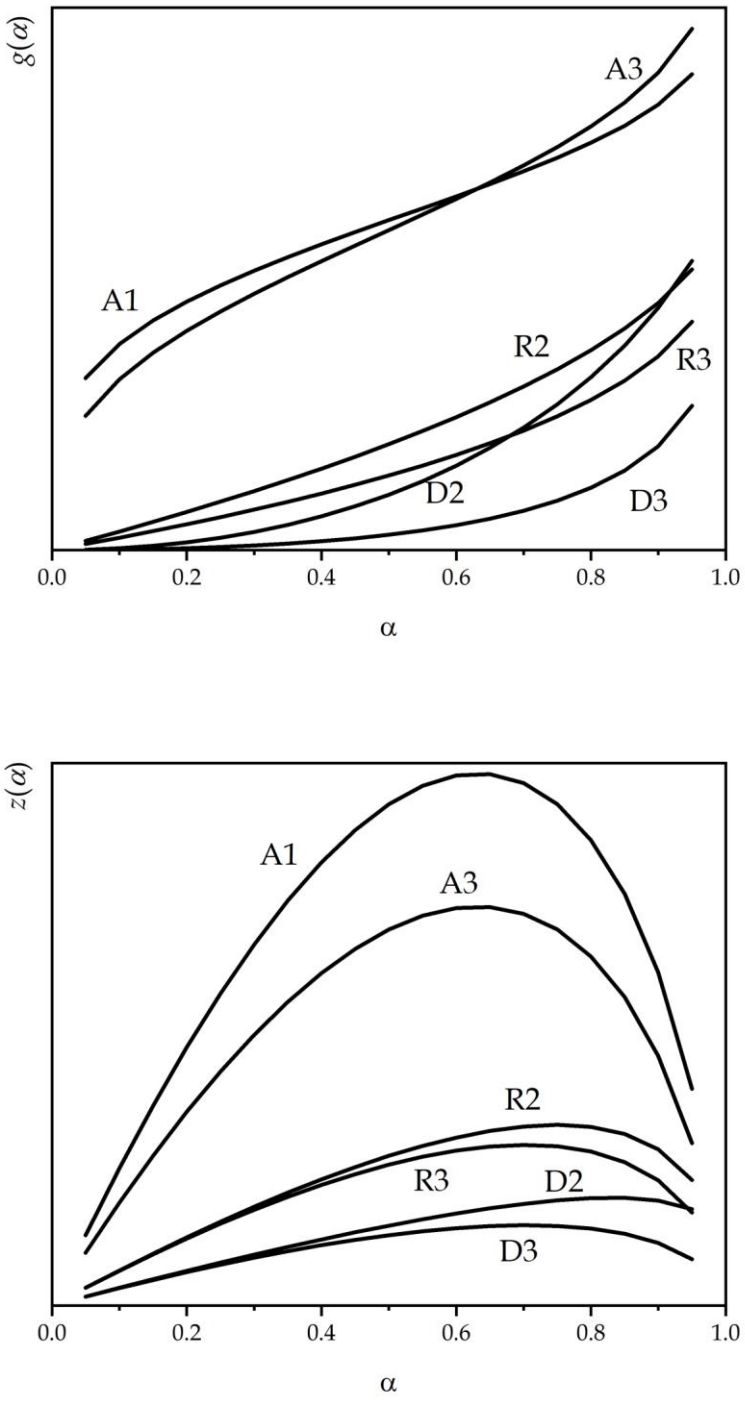

Figura I.31. *"Master plots"* teóricos de las funciones $g(\alpha)$ y $z(\alpha)$.

I.3.4. Materiales compuestos de alto rendimiento medioambiental con matrices termoestables

Durante el desarrollo del presente documento se ha mostrado el avance logrado en el estudio y aplicación de diferentes compuestos de origen natural en la constitución

de materiales compuestos. Se presentó como varios tipos de aceites vegetales se están utilizando como base para la formulación matrices termoestables, además del potencial que tienen las fibras y/o partículas de origen natural. Es verdad que el mayor avance se está realizando en el campo de los materiales termoplásticos, pero el área de los materiales compuestos termoestables con alto rendimiento medioambiental ha avanzado considerablemente.

I.3.4.1. Materiales compuestos con partículas

Se manifestó como el uso de partículas de origen orgánico como por ejemplo partículas lignocelulósicas dio paso al desarrollo de los *"Wood plastic composites"*. Este campo tiene también su área de aplicación dentro de los materiales termoestables [183], así también como los denominados *"particle boards"* (PB), aunque el uso matrices termoestables de origen petroquímico sigue siendo preferente [102,184]. Pero con el avance que se ha conseguido en los últimos años en el desarrollo de matrices termoestables de origen natural como los derivados de aceites vegetales, han servido de incentivos para que varios investigadores dediquen su tiempo en el estudio y desarrollo de materiales compuestos basados en matrices de origen natural.

Se tiene como por el ejemplo el trabajo presentado por Mandal, *et al.* [185], que utilizaron partículas de madera suave para reforzar una matriz termoestable basada en aceite epoxidado de soja (ESBO) por medio de moldeo por compresión. El ESBO fue modificado inicialmente con ácido metacrílico y después con anhídrido metacrílico, para obtener aceite epoxidado de soja con anhídrido metacrilico (MAESO). Como medio de comparación se formularon mezclas con y sin estireno. Se observó que al aumentar la fracción de anhídrido metacrílico se obtuvo un aumento en los dobles enlaces reactivos, lo que resultó en un aumento en las propiedades mecánicas, térmicas y en la resistencia al fuego, obteniendo aún mejores resultados en los sistemas mezclados con estireno, donde su presencia incremento la interacción entre la carga y la matriz. Es verdad que la incorporación de estireno en el sistema disminuye el contenido renovable de los compuestos, pero es un punto de referencia para la fabricación de materiales con buenas propiedades y con un alto contenido biológico, ya que en un futuro se puede plantear la sustitución del estireno, como por ejemplo el aumento de la cantidad de ácido metacrílico o anhídrido metacrílico. Se tiene también el trabajo de Wechsler, *et al.* [186] donde estudiaron la factibilidad de producir *"particle boards"* con materiales sostenibles, para esto partieron de desechos de cascaras de la nuez de macadamia y como reemplazo a la resina basada en formaldehido, se utilizó una resina derivada de aceite de ricino. Donde, debido a la constitución de la cascara de la nuez se generaron buenos

enlaces internos entre las partículas, generándose compuestos con alta densidad, comparado con otros compuestos basados en aceite de ricino. Así también los compuestos presentaron una alta resistencia a la humedad. Características que lo hacen atractivos para áreas de la construcción ya que se pueden utilizar en entornos húmedos como en aplicaciones de baños o cocinas.

Cabe mencionar que el problema de baja interacción entre partículas de refuerzo de origen natural y matrices termoplásticas, debido a su diferente naturaleza, también lo presentan con matrices termoestables, es decir, la mayoría de las matrices termoestables tienen un carácter hidrofóbico y las partículas de origen natural son de carácter hidrofílico. Donde para superar esta deficiencia se suele utilizar métodos de compatibilización similares a los presentados anteriormente, como por ejemplo el uso de agentes de acoplamiento, tratamientos superficiales, etc.

I.3.4.2. Materiales compuestos con fibras de refuerzo

El aumento de la concienciación medioambiental provocó el incremento del interés en el uso de fibras de origen natural como sustitutos a fibras sintéticas convencionales. Hay que recalcar que el rendimiento de las fibras naturales aún no se acerca al rendimiento que presentan fibras técnicas como las de carbono. Pero se observa un panorama alentador como reemplazo a fibras como la de vidrio; se han presentado varios candidatos dentro de las cuales están las fibras de origen vegetal y de origen mineral. En secciones anteriores se presentaron varias fibras de origen vegetal que presentan más posibilidades de uso industrial como la fibra lino, de yute o de cáñamo, debido a su constitución y estructura que se resume en la tabla I.3. Autores como Fombuena, *et al.* [158] anteriormente mencionado por formular sistemas epoxis con un alto porcentaje de origen orgánico de productos derivados del lino (aceite epoxidado de lino, ELO y aceite maleinizado de lino, MLO), fabricaron materiales compuestos utilizando esta matriz y reforzada con fibras de lino, donde utilizó diferentes tipos de agentes de acoplamiento para mejorar la interacción entre la matriz y las fibras. Se pudo observar que los agentes de acoplamiento cumplieron su trabajo mejorando la interacción intersuperficial (fibra-matriz), resultando un aceptable efecto de refuerzo por parte de las fibras, cabe mencionar que el aumento de la cantidad de MLO resulta en un aumento en la ductilidad de los materiales.

Tenemos también que fibras minerales como las de pizarra o de basalto han llamado la atención en la fabricación de materiales compuestos de matriz termoestable, debido en gran manera a que su composición basada en silicio es similar a fibras de

vidrio comerciales, incluso presentan mejores propiedades mecánicas, térmicas que algunos grados [187]. Autores como Samper, *et al.* [188] habrían fabricado materiales compuestos con un alto porcentaje de origen natural formados con una matriz basa en aceite epoxidado de lino (ELO) y reforzada con mantas de fibras de pizarra, fabricadas por moldeo de transferencia de resina (RTM). Donde con el propósito de mejorar la interacción entre la matriz y las fibras de refuerzo, estas fueron sometidas a un tratamiento basado en silanos. Los resultados obtenidos fueron alentadores ya que demostraron por un lado que la fabricación de materiales basados en productos naturales se puede realizar con procesos escalables industrialmente. Y, por otro lado, que se pueden obtener materiales con propiedades que pueden competir con compuestos basados con fibras de vidrio. Por otro lado tenemos que Motoc, *et al.* [159] fabricaron materiales híbridos con fibras de basalto y fibras de lino, utilizando una matriz similar a la formulada por Fombuena, *et al*., basada en una resina de ELO y un endurecedor basado en MLO. Donde por un lado se estudió el efecto de hibridación que se obtiene al combinar fibras de lino y basalto, y por otro lado se estudió el efecto del MLO en materiales reforzados completamente con fibras de lino. Se observó un mejor comportamiento termomecánico en los materiales híbridos debido al aumento de resistencia que aportan las fibras de basalto en el compuesto, siendo más notorio cuando las fibras de basalto se encuentran en las capas exteriores, además se tiene que la incorporación de MLO produce un efecto similar al presentado por Fombuena, *et al*., es decir, materiales con mayor ductilidad al incrementar el porcentaje de MLO.

I.4. Referencias

1. S.C. Rasmussen. Revisiting the early history of synthetic polymers: critiques and new insights. *Ambix* **2018**, *65*, 356-372.
2. PlasticsEurope. *Plastics- the Facts 2020: An analysis of European plastics production, demand and waste data*; PlasticsEurope: Belgium, Europe, 2020.
3. K. Leja, G. Lewandowicz. Polymer biodegradation and biodegradable polymers-a review. *Polish Journal of Environmental Studies* **2010**, *19*, 255-266.
4. A. Agüero, M.d.C. Morcillo, L. Quiles-Carrillo, R. Balart, T. Boronat, D. Lascano, S. Torres-Giner, O. Fenollar. Study of the influence of the reprocessing cycles on the final properties of polylactide pieces obtained by injection molding. *Polymers* **2019**, *11*, 1908.
5. L. Lebreton, A. Andrady. Future scenarios of global plastic waste generation and disposal. *Palgrave Communications* **2019**, *5*, 1-11.
6. S. Walker, R. Rothman. Life cycle assessment of bio-based and fossil-based plastic: A review. *Journal of Cleaner Production* **2020**, *261*, 121158.
7. A.L. Andrady, M.A. Neal. Applications and societal benefits of plastics. *Philosophical Transactions of the Royal Society B: Biological Sciences* **2009**, *364*, 1977-1984.
8. J.M. García, F.C. García, F. Serna, L. José. High-performance aromatic polyamides. *Progress in polymer science* **2010**, *35*, 623-686.
9. J.A. Reglero Ruiz, M. Trigo-López, F.C. García, J.M. García. Functional aromatic polyamides. *Polymers* **2017**, *9*, 414.
10. A. Ramgobin, G. Fontaine, S. Bourbigot. Investigation of the thermal stability and fire behavior of high performance polymer: A case study of polyimide. *Fire Safety Journal* **2021**, *120*, 103060.
11. T. Sai, S. Ran, Z. Guo, H. Yan, Y. Zhang, H. Wang, P. Song, Z. Fang. Transparent, highly thermostable and flame retardant polycarbonate enabled by rod-like phosphorous-containing metal complex aggregates. *Chemical Engineering Journal* **2021**, *409*, 128223.
12. B. Guo, C.M. Chan. Chain extension of poly (butylene terephthalate) by reactive extrusion. *Journal of Applied Polymer Science* **1999**, *71*, 1827-1834.

13. Z. Li, W. Li, L. Liao, J. Li, T. Wu, L. Ran, T. Zhao, B. Chen. Preparation and properties of polybutylene-terephthalate/graphene oxide in situ flame-retardant material. *Journal of Applied Polymer Science* **2020**, *137*, 49214.

14. Y. Niu, S. Zheng, P. Song, X. Zhang, C. Wang. Mechanical and thermal properties of PEEK composites by incorporating inorganic particles modified phosphates. *Composites Part B: Engineering* **2021**, *212*, 108715.

15. Z. Xu, L. Gehui, K. Cao, D. Guo, J. Serrano, A. Esker, G. Liu. Solvent-resistant self-crosslinked poly (ether imide). *Macromolecules* **2021**, *54*, 3405-3412.

16. V. Siracusa, I. Blanco. Bio-Polyethylene (Bio-PE), Bio-Polypropylene (Bio-PP) and Bio-Poly (ethylene terephthalate)(Bio-PET): recent developments in bio-based polymers analogous to petroleum-derived ones for packaging and engineering applications. *Polymers* **2020**, *12*, 1641.

17. S. Rojas-Lema, D. Lascano, J. Ivorra-Martinez, J. Gomez-Caturla, R. Balart, D. Garcia-Garcia. Manufacturing and characterization of high-density polyethylene composites with active fillers from persimmon peel flour with improved antioxidant activity and hydrophobicity. *Macromolecular Materials and Engineering* **2021**, 2100430.

18. S. Li, M. Vert. Biodegradation of aliphatic polyesters. In *Degradable polymers*, Springer: 2002; 71-131.

19. M. Abrisham, M. Noroozi, M. Panahi-Sarmad, M. Arjmand, V. Goodarzi, Y. Shakeri, H. Golbaten-Mofrad, P. Dehghan, A.S. Sahzabi, M. Sadri. The role of polycaprolactone-triol (PCL-T) in biomedical applications: A state-of-the-art review. *European Polymer Journal* **2020**, *131*, 109701.

20. H. Kweon, M.K. Yoo, I.K. Park, T.H. Kim, H.C. Lee, H.-S. Lee, J.-S. Oh, T. Akaike, C.-S. Cho. A novel degradable polycaprolactone networks for tissue engineering. *Biomaterials* **2003**, *24*, 801-808.

21. L. Ludueña, A. Vázquez, V. Alvarez. Effect of lignocellulosic filler type and content on the behavior of polycaprolactone based eco-composites for packaging applications. *Carbohydrate Polymers* **2012**, *87*, 411-421.

22. K.J. Jem, B. Tan. The development and challenges of poly (lactic acid) and poly (glycolic acid). *Advanced Industrial and Engineering Polymer Research* **2020**, *3*, 60-70.

23. A. Nanni, M. Messori. Thermo-mechanical properties and creep modelling of wine lees filled Polyamide 11 (PA11) and Polybutylene succinate (PBS) bio-composites. *Composites Science and Technology* **2020**, *188*, 107974.

24. S.-H. Lee, S. Wang. Biodegradable polymers/bamboo fiber biocomposite with bio-based coupling agent. *Composites Part A: applied science and manufacturing* **2006**, *37*, 80-91.

25. S.S. Ray, M. Bousmina, K. Okamoto. Structure and properties of nanocomposites based on poly (butylene succinate-co-adipate) and organically modified montmorillonite. *Macromolecular materials and engineering* **2005**, *290*, 759-768.

26. C. Pavon, M. Aldas, H.d.l. Rosa-Ramírez, J. López-Martínez, M.P. Arrieta. Improvement of PBAT processability and mechanical performance by blending with pine resin derivatives for injection moulding rigid packaging with enhanced hydrophobicity. *Polymers* **2020**, *12*, 2891.

27. S.Z. Rogovina, G.A. Vikhoreva. Polysaccharide-based polymer blends: Methods of their production. *Glycoconjugate Journal* **2006**, *23*, 611-618.

28. R. Kumar, V. Choudhary, S. Mishra, I.K. Varma, B. Mattiason. Adhesives and plastics based on soy protein products. *Industrial crops and products* **2002**, *16*, 155-172.

29. H. Wieser. Chemistry of gluten proteins. *Food microbiology* **2007**, *24*, 115-119.

30. R. Tylingo, G. Gorczyca, S. Mania, P. Szweda, S. Milewski. Preparation and characterization of porous scaffolds from chitosan-collagen-gelatin composite. *Reactive and Functional Polymers* **2016**, *103*, 131-140.

31. H. Matsusaki, H. Abe, Y. Doi. Biosynthesis and properties of poly (3-hydroxybutyrate-co-3-hydroxyalkanoates) by recombinant strains of Pseudomonas sp. 61-3. *Biomacromolecules* **2000**, *1*, 17-22.

32. V. Sharma, R. Sehgal, R. Gupta. Polyhydroxyalkanoate (PHA): Properties and modifications. *Polymer* **2021**, *212*, 123161.

33. R.L. Quirino, K. Monroe, C.H. Fleischer III, E. Biswas, M.R. Kessler. Thermosetting polymers from renewable sources. *Polymer International* **2021**, *70*, 167-180.

34. N. Saba, M. Jawaid, O.Y. Alothman, M. Paridah, A. Hassan. Recent advances in epoxy resin, natural fiber-reinforced epoxy composites and their applications. *Journal of Reinforced Plastics and Composites* **2016**, *35*, 447-470.

35. F.-L. Jin, X. Li, S.-J. Park. Synthesis and application of epoxy resins: A review. *Journal of Industrial and Engineering Chemistry* **2015**, *29*, 1-11.

36. S. Kumar, S.K. Samal, S. Mohanty, S.K. Nayak. Study of curing kinetics of anhydride cured petroleum-based (DGEBA) epoxy resin and renewable resource based epoxidized soybean oil (ESO) systems catalyzed by 2-methylimidazole. *Thermochimica Acta* **2017**, *654*, 112-120.

37. G. Sudha, H. Kalita, S. Mohanty, S.K. Nayak. Biobased epoxy blends from epoxidized castor oil: effect on mechanical, thermal, and morphological properties. *Macromolecular Research* **2017**, *25*, 420-430.

38. J. Chen, Z. Liu, K. Wang, J. Huang, K. Li, X. Nie, J. Jiang. Epoxidized castor oil-based diglycidyl-phthalate plasticizer: Synthesis and thermal stabilizing effects on poly (vinyl chloride). *Journal of Applied Polymer Science* **2019**, *136*, 47142.

39. N. Khundamri, C. Aouf, H. Fulcrand, E. Dubreucq, V. Tanrattanakul. Bio-based flexible epoxy foam synthesized from epoxidized soybean oil and epoxidized mangosteen tannin. *Industrial Crops and Products* **2019**, *128*, 556-565.

40. N. Mohd Nurazzi, A. Khalina, S. Sapuan, A. Dayang Laila, M. Rahmah, Z. Hanafee. A review: Fibres, polymer matrices and composites. *Pertanika Journal of Science & Technology* **2017**, *25*, 1085 - 1102.

41. F.R. Jones. Unsaturated polyester resins. In *Brydson's Plastics Materials*, Elsevier: 2017; 743-772.

42. L.B. Mehta, K.K. Wadgaonkar, R.N. Jagtap. Synthesis and characterization of high bio-based content unsaturated polyester resin for wood coating from itaconic acid: Effect of various reactive diluents as an alternative to styrene. *Journal of Dispersion Science and Technology* **2019**, *40*, 756-765.

43. J.M. Sadler, F.R. Toulan, A.-P.T. Nguyen, R.V. Kayea III, S. Ziaee, G.R. Palmese, J.J. La Scala. Isosorbide as the structural component of bio-based unsaturated polyesters for use as thermosetting resins. *Carbohydrate polymers* **2014**, *100*, 97-106.

44. B.Z. Fidanovski, P.M. Spasojevic, V.V. Panic, S.I. Seslija, J.P. Spasojevic, I.G. Popovic. Synthesis and characterization of fully bio-based unsaturated polyester resins. *Journal of materials science* **2018**, *53*, 4635-4644.

45. Z. Dai, Q. Li, Z. Chen, R.K. Shawon, Y. Zhu, H. Lv, F. Fu, Y. Zhu, Y. Fu, X. Liu. Reactive diluent derived from ferulic acid for the preparation of a fully biobased

unsaturated polyester resin. *ACS Sustainable Chemistry & Engineering* **2020**, *8*, 17379-17386.

46. P. Penczek, P. Czub, J. Pielichowski. Unsaturated polyester resins: chemistry and technology. *Crosslinking in materials science* **2005**, 1-95.

47. M.B. Launikitis. Vinyl ester resins. In *Handbook of composites*, Springer: 1982; 38-49.

48. S.K. Yadav, K.M. Schmalbach, E. Kinaci, J.F. Stanzione III, G.R. Palmese. Recent advances in plant-based vinyl ester resins and reactive diluents. *European Polymer Journal* **2018**, *98*, 199-215.

49. E. Akpan, B. Wetzel, K. Friedrich. A fully biobased tribology material based on acrylic resin and short wood fibres. *Tribology International* **2018**, *120*, 381-390.

50. Y. Zhang, V.K. Thakur, Y. Li, T.F. Garrison, Z. Gao, J. Gu, M.R. Kessler. Soybean-oil-based thermosetting resins with methacrylated vanillyl alcohol as bio-based, low-viscosity comonomer. *Macromolecular Materials and Engineering* **2018**, *303*, 1700278.

51. Y. Zhang, Y. Li, V.K. Thakur, L. Wang, J. Gu, Z. Gao, B. Fan, Q. Wu, M.R. Kessler. Bio-based reactive diluents as sustainable replacements for styrene in MAESO resin. *RSC advances* **2018**, *8*, 13780-13788.

52. F. Cardona, A.L. Kin-Tak, J. Fedrigo. Novel phenolic resins with improved mechanical and toughness properties. *Journal of applied polymer science* **2012**, *123*, 2131-2139.

53. J. Shafizadeh, S. Guionnet, M. Tillman, J. Seferis. Synthesis and characterization of phenolic resole resins for composite applications. *Journal of Applied Polymer Science* **1999**, *73*, 505-514.

54. J. Li, W. Wang, S. Zhang, Q. Gao, W. Zhang, J. Li. Preparation and characterization of lignin demethylated at atmospheric pressure and its application in fast curing biobased phenolic resins. *RSC advances* **2016**, *6*, 67435-67443.

55. J. Li, J. Zhang, S. Zhang, Q. Gao, J. Li, W. Zhang. Fast curing bio-based phenolic resins via lignin demethylated under mild reaction condition. *Polymers* **2017**, *9*, 428.

56. P. Jia, F. Song, Q. Li, H. Xia, M. Li, X. Shu, Y. Zhou. Recent development of cardanol based polymer materials-a review. *Journal of Renewable Materials* **2019**, *7*, 601-619.

57. W. Zhang, N. Jiang, T. Zhang, T. Li. Thermal stability and thermal degradation study of phenolic resin modified by cardanol. *Emerging Materials Research* **2020**, *9*, 180-185.

58. K.J. Bruemmer, O. Green, T.A. Su, D. Shabat, C.J. Chang. Chemiluminescent probes for activity-based sensing of formaldehyde released from folate degradation in living mice. *Angewandte Chemie* **2018**, *130*, 7630-7634.

59. G. Sui, Y. Cheng, X. Yang, X. Wang, Z. Wang. Use of sustainable glucose and furfural in the synthesis of formaldehyde-free phenolic resole resins. *Journal of Applied Polymer Science* **2019**, *136*, 47733.

60. M.P. Arrieta, M. Perdiguero, S. Fiori, J.M. Kenny, L. Peponi. Biodegradable electrospun PLA-PHB fibers plasticized with oligomeric lactic acid. *Polymer Degradation and Stability* **2020**, *179*, 109226.

61. H. Tsuji. Poly (lactic acid). *Bio-based plastics: materials and applications* **2013**, 171-239.

62. X. Pang, X. Zhuang, Z. Tang, X. Chen. Polylactic acid (PLA): research, development and industrialization. *Biotechnology Journal* **2010**, *5*, 1125-1136.

63. M. Ajioka, K. Enomoto, K. Suzuki, A. Yamaguchi. Basic properties of polylactic acid produced by the direct condensation polymerization of lactic acid. *Bulletin of the Chemical Society of Japan* **1995**, *68*, 2125-2131.

64. L. Quiles-Carrillo, M. Blanes-Martínez, N. Montanes, O. Fenollar, S. Torres-Giner, R. Balart. Reactive toughening of injection-molded polylactide pieces using maleinized hemp seed oil. *European Polymer Journal* **2018**, *98*, 402-410.

65. K.M. Nampoothiri, N.R. Nair, R.P. John. An overview of the recent developments in polylactide (PLA) research. *Bioresource technology* **2010**, *101*, 8493-8501.

66. W.-x. Zhang, Y.-z. Wang. Synthesis and properties of high molecular weight poly (lactic acid) and its resultant fibers. *Chinese Journal of polymer science* **2008**, *26*, 425-432.

67. Y. Yang, M. Zhang, Z. Ju, P.Y. Tam, T. Hua, M.W. Younas, H. Kamrul, H. Hu. Poly (lactic acid) fibers, yarns and fabrics: Manufacturing, properties and applications. *Textile Research Journal* **2021**, *91*, 1641-1669.

68. L. Suryanegara, A.N. Nakagaito, H. Yano. The effect of crystallization of PLA on the thermal and mechanical properties of microfibrillated cellulose-reinforced PLA composites. *Composites Science and Technology* **2009**, *69*, 1187-1192.

69. E. Castro-Aguirre, F. Iniguez-Franco, H. Samsudin, X. Fang, R. Auras. Poly (lactic acid)—Mass production, processing, industrial applications, and end of life. *Advanced drug delivery reviews* **2016**, *107*, 333-366.

70. R. Auras, B. Harte, S. Selke. An overview of polylactides as packaging materials. *Macromolecular bioscience* **2004**, *4*, 835-864.

71. A. Aguero, L. Quiles-Carrillo, A. Jorda-Vilaplana, O. Fenollar, N. Montanes. Effect of different compatibilizers on environmentally friendly composites from poly (lactic acid) and diatomaceous earth. *Polymer International* **2019**, *68*, 893-903.

72. D. Cava, E. Giménez, R. Gavara, J. Lagaron. Comparative performance and barrier properties of biodegradable thermoplastics and nanobiocomposites versus PET for food packaging applications. *Journal of Plastic Film & Sheeting* **2006**, *22*, 265-274.

73. S. Kalia, L. Avérous. *Biodegradable and biobased polymers for environmental and biomedical applications*; John Wiley & Sons: 2016.

74. Y. Yang, L. Zhang, Z. Xiong, Z. Tang, R. Zhang, J. Zhu. Research progress in the heat resistance, toughening and filling modification of PLA. *Science China Chemistry* **2016**, *59*, 1355-1368.

75. J.J. Koh, X. Zhang, C. He. Fully biodegradable poly (lactic acid)/starch blends: A review of toughening strategies. *International journal of biological macromolecules* **2018**, *109*, 99-113.

76. A. Quitadamo, V. Massardier, C. Santulli, M. Valente. Optimization of thermoplastic blend matrix HDPE/PLA with different types and levels of coupling agents. *Materials* **2018**, *11*, 2527.

77. S. Dhinesh, P.S. Arun, K.K. Senthil, A. Megalingam. Study on flexural and tensile behavior of PLA, ABS and PLA-ABS materials. *Materials Today: Proceedings* **2021**, *45*, 1175-1180.

78. B. Imre, D. Bedő, A. Domján, P. Schön, G.J. Vancso, B. Pukánszky. Structure, properties and interfacial interactions in poly (lactic acid)/polyurethane blends prepared by reactive processing. *European polymer journal* **2013**, *49*, 3104-3113.

79. A. Matta, R.U. Rao, K. Suman, V. Rambabu. Preparation and characterization of biodegradable PLA/PCL polymeric blends. *Procedia materials science* **2014**, *6*, 1266-1270.

80. R. Supthanyakul, N. Kaabbuathong, S. Chirachanchai. Poly (l-lactide-b-butylene succinate-bl-lactide) triblock copolymer: A multi-functional additive for PLA/PBS

blend with a key performance on film clarity. *Polymer Degradation and Stability* **2017**, *142*, 160-168.

81. A. Przybytek, M. Sienkiewicz, J. Kucińska-Lipka, H. Janik. Preparation and characterization of biodegradable and compostable PLA/TPS/ESO compositions. *Industrial Crops and Products* **2018**, *122*, 375-383.

82. J.M. Ferri, D. Garcia-Garcia, E. Rayón, M.D. Samper, R. Balart. Compatibilization and characterization of polylactide and biopolyethylene binary blends by non-reactive and reactive compatibilization approaches. *Polymers* **2020**, *12*, 1344.

83. J. Ferri, D. Garcia-Garcia, L. Sánchez-Nacher, O. Fenollar, R. Balart. The effect of maleinized linseed oil (MLO) on mechanical performance of poly (lactic acid)-thermoplastic starch (PLA-TPS) blends. *Carbohydrate polymers* **2016**, *147*, 60-68.

84. B. Wang, K. Hina, H. Zou, D. Zuo, C. Yi. Thermal, crystallization, mechanical and decomposition properties of poly (lactic acid) plasticized with poly (ethylene glycol). *Journal of Vinyl and Additive Technology* **2018**, *24*, E154-E163.

85. N. Burgos, D. Tolaguera, S. Fiori, A. Jiménez. Synthesis and characterization of lactic acid oligomers: Evaluation of performance as poly (lactic acid) plasticizers. *Journal of Polymers and the Environment* **2014**, *22*, 227-235.

86. M. Bouti, R. Irinislimane, N. Belhaneche-Bensemra. Properties investigation of epoxidized sunflower oil as bioplasticizer for poly (lactic acid). *Journal of Polymers and the Environment* **2021**, 1-14.

87. H. Li, M.A. Huneault. Effect of nucleation and plasticization on the crystallization of poly (lactic acid). *Polymer* **2007**, *48*, 6855-6866.

88. C. Lee, M.M. Pang, S.C. Koay, H.L. Choo, K.Y. Tshai. Talc filled polylactic-acid biobased polymer composites: Tensile, thermal and morphological properties. *SN Applied Sciences* **2020**, *2*, 1-6.

89. K. Piekarska, E. Piorkowska, J. Bojda. The influence of matrix crystallinity, filler grain size and modification on properties of PLA/calcium carbonate composites. *Polymer Testing* **2017**, *62*, 203-209.

90. E.A. Segura González, D. Olmos, M.Á. Lorente, I. Vélaz, J. González-Benito. Preparation and characterization of polymer composite materials based on PLA/TiO2 for antibacterial packaging. *Polymers* **2018**, *10*, 1365.

91. N. Salahuddin, M. Abdelwahab, M. Gaber, S. Elneanaey. Synthesis and design of norfloxacin drug delivery system based on PLA/TiO2 nanocomposites:

Antibacterial and antitumor activities. *Materials Science and Engineering: C* **2020**, *108*, 110337.

92. J. Ferri, J. Jordá, N. Montanes, O. Fenollar, R. Balart. Manufacturing and characterization of poly (lactic acid) composites with hydroxyapatite. *Journal of thermoplastic composite Materials* **2018**, *31*, 865-881.

93. M. Syduzzaman, M.A. Al Faruque, K. Bilisik, M. Naebe. Plant-based natural fibre reinforced composites: A review on fabrication, properties and applications. *Coatings* **2020**, *10*, 973.

94. R. Liu, Y. Peng, J. Cao, Y. Chen. Comparison on properties of lignocellulosic flour/polymer composites by using wood, cellulose, and lignin flours as fillers. *Composites Science and Technology* **2014**, *103*, 1-7.

95. A. Bledzki, J. Gassan. Composites reinforced with cellulose based fibres. *Progress in polymer science* **1999**, *24*, 221-274.

96. S. Rojas-Lema, J. Ivorra-Martinez, D. Lascano, D. Garcia-Garcia, R. Balart. Improved performance of environmentally friendly blends of biobased polyethylene and kraft lignin compatibilized by reactive extrusion with dicumyl peroxide. *Macromolecular Materials and Engineering* **2021**, 2100196.

97. D.J. Gardner, Y. Han, L. Wang. Wood–plastic composite technology. *Current Forestry Reports* **2015**, *1*, 139-150.

98. P. Borysiuk, P. Boruszewski, R. Auriga, L. Danecki, A. Auriga, K. Rybak, M. Nowacka. Influence of a bark-filler on the properties of PLA biocomposites. *Journal of Materials Science* **2021**, *56*, 9196-9208.

99. J. Balart, D. García-Sanoguera, R. Balart, T. Boronat, L. Sánchez-Nacher. Manufacturing and properties of biobased thermoplastic composites from poly (lactid acid) and hazelnut shell wastes. *Polymer composites* **2018**, *39*, 848-857.

100. L. Quiles-Carrillo, N. Montanes, C. Sammon, R. Balart, S. Torres-Giner. Compatibilization of highly sustainable polylactide/almond shell flour composites by reactive extrusion with maleinized linseed oil. *Industrial Crops and Products* **2018**, *111*, 878-888.

101. M. González-López, J. Robledo-Ortíz, R. Manríquez-González, J. Silva-Guzmán, A. Pérez-Fonseca. Polylactic acid functionalization with maleic anhydride and its use as coupling agent in natural fiber biocomposites: a review. *Composite Interfaces* **2018**, *25*, 515-538.

102. D. Garcia-Garcia, L. Quiles-Carrillo, N. Montanes, V. Fombuena, R. Balart. Manufacturing and characterization of composite fibreboards with Posidonia oceanica wastes with an environmentally-friendly binder from epoxy resin. *Materials* **2018**, *11*, 35.

103. M. Islam, K. Pickering, N. Foreman. Influence of alkali treatment on the interfacial and physico-mechanical properties of industrial hemp fibre reinforced polylactic acid composites. *Composites Part A: Applied Science and Manufacturing* **2010**, *41*, 596-603.

104. B. Koohestani, A. Darban, P. Mokhtari, E. Yilmaz, E. Darezereshki. Comparison of different natural fiber treatments: a literature review. *International Journal of Environmental Science and Technology* **2019**, *16*, 629-642.

105. X. Li, L.G. Tabil, S. Panigrahi. Chemical treatments of natural fiber for use in natural fiber-reinforced composites: a review. *Journal of Polymers and the Environment* **2007**, *15*, 25-33.

106. Y. Xie, C.A. Hill, Z. Xiao, H. Militz, C. Mai. Silane coupling agents used for natural fiber/polymer composites: A review. *Composites Part A: Applied Science and Manufacturing* **2010**, *41*, 806-819.

107. S. Qian, K. Sheng, K. Yu, L. Xu, C.A.F. Lopez. Improved properties of PLA biocomposites toughened with bamboo cellulose nanowhiskers through silane modification. *Journal of Materials Science* **2018**, *53*, 10920-10932.

108. S.-Y. Lee, I.-A. Kang, G.-H. Doh, H.-G. Yoon, B.-D. Park, Q. Wu. Thermal and mechanical properties of wood flour/talc-filled polylactic acid composites: Effect of filler content and coupling treatment. *Journal of Thermoplastic Composite Materials* **2008**, *21*, 209-223.

109. Á. Csikós, G. Faludi, A. Domján, K. Renner, J. Móczó, B. Pukánszky. Modification of interfacial adhesion with a functionalized polymer in PLA/wood composites. *European Polymer Journal* **2015**, *68*, 592-600.

110. S.H. Ghaffar, O.A. Madyan, M. Fan, J. Corker. The influence of additives on the interfacial bonding mechanisms between natural fibre and biopolymer composites. *Macromolecular Research* **2018**, *26*, 851-863.

111. G. Faludi, G. Dora, K. Renner, J. Móczó, B. Pukánszky. Improving interfacial adhesion in pla/wood biocomposites. *Composites science and technology* **2013**, *89*, 77-82.

112. L. Kerni, S. Singh, A. Patnaik, N. Kumar. A review on natural fiber reinforced composites. *Materials Today: Proceedings* **2020**, *28*, 1616-1621.

113. A.K. Mohanty, M. Misra, L. Drzal. Sustainable bio-composites from renewable resources: opportunities and challenges in the green materials world. *Journal of Polymers and the Environment* **2002**, *10*, 19-26.

114. M.S. Anbupalani, C.D. Venkatachalam, R. Rathanasamy. Influence of coupling agent on altering the reinforcing efficiency of natural fibre-incorporated polymers–a review. *Journal of Reinforced Plastics and Composites* **2020**, *39*, 520-544.

115. D. Chandramohan, K. Marimuthu. A review on natural fibers. *International Journal of Research and Reviews in Applied Sciences* **2011**, *8*, 194-206.

116. M. Alzeer, K.J. MacKenzie. Synthesis and mechanical properties of new fibre-reinforced composites of inorganic polymers with natural wool fibres. *Journal of Materials Science* **2012**, *47*, 6958-6965.

117. F. Pawlak, M. Aldas, F. Parres, J. López-Martínez, M.P. Arrieta. Silane-functionalized sheep wool fibers from dairy industry waste for the development of plasticized PLA composites with maleinized linseed oil for injection-molded parts. *Polymers* **2020**, *12*, 2523.

118. A. Martínez-Hernández, C. Velasco-Santos, M. De-Icaza, V.M. Castano. Dynamical–mechanical and thermal analysis of polymeric composites reinforced with keratin biofibers from chicken feathers. *Composites Part B: Engineering* **2007**, *38*, 405-410.

119. S. Liu, G. Wu, J. Yu, X. Chen, J. Guo, X. Zhang, P. Wang, X. Yin. Surface modification of basalt fiber (BF) for improving compatibilities between BF and poly lactic acid (PLA) matrix. *Composite Interfaces* **2019**, *26*, 275-290.

120. S. Yu, Y.H. Hwang, J.Y. Hwang, S.H. Hong. Analytical study on the 3D-printed structure and mechanical properties of basalt fiber-reinforced PLA composites using X-ray microscopy. *Composites Science and Technology* **2019**, *175*, 18-27.

121. K. Karvanis, S. Rusnáková, O. Krejčí, M. Žaludek. Preparation, thermal analysis, and mechanical properties of basalt fiber/epoxy composites. *Polymers* **2020**, *12*, 1785.

122. A. Carbonell-Verdú, D. García-García, A. Jordá, M. Samper, R. Balart. Development of slate fiber reinforced high density polyethylene composites for injection molding. *Composites Part B: Engineering* **2015**, *69*, 460-466.

123. H. Awais, Y. Nawab, A. Amjad, A. Anjang, H.M. Akil, M.S.Z. Abidin. Environmental benign natural fibre reinforced thermoplastic composites: A review. *Composites Part C: Open Access* **2021**, *4*, 100082.

124. A. Gholampour, T. Ozbakkaloglu. A review of natural fiber composites: Properties, modification and processing techniques, characterization, applications. *Journal of Materials Science* **2020**, *55*, 829-892.

125. M. Sanjay, S. Siengchin, J. Parameswaranpillai, M. Jawaid, C.I. Pruncu, A. Khan. A comprehensive review of techniques for natural fibers as reinforcement in composites: Preparation, processing and characterization. *Carbohydrate polymers* **2019**, *207*, 108-121.

126. D. Verma, K.L. Goh. Effect of mercerization/alkali surface treatment of natural fibres and their utilization in polymer composites: Mechanical and morphological studies. *Journal of Composites Science* **2021**, *5*, 175.

127. Á. Agüero, D. Garcia-Sanoguera, D. Lascano, S. Rojas-Lema, J. Ivorra-Martinez, O. Fenollar, S. Torres-Giner. Evaluation of different compatibilization strategies to improve the performance of injection-molded green composite pieces made of polylactide reinforced with short flaxseed fibers. *Polymers* **2020**, *12*, 821.

128. L. Zhang, S. Lv, C. Sun, L. Wan, H. Tan, Y. Zhang. Effect of MAH-g-PLA on the properties of wood fiber/polylactic acid composites. *Polymers* **2017**, *9*, 591.

129. K.M. Charlebois, R. Boukhili, O. Zebdi, F. Trochu, A. Gasmi. Evaluation of the physical and mechanical properties of braided fabrics and their composites. *Journal of reinforced plastics and composites* **2005**, *24*, 1539-1554.

130. S.K. Ramamoorthy, M. Skrifvars, A. Persson. A review of natural fibers used in biocomposites: plant, animal and regenerated cellulose fibers. *Polymer reviews* **2015**, *55*, 107-162.

131. T. Katayama, K. Tanaka, T. Murakami, K. Uno. Compression moulding of jute fabric reinforced thermoplastic composites based on PLA non-woven fabric. *WIT transactions on the built environment* **2006**, *85*.

132. G.A. Khan, H. Shaikh, M.S. Alam, M.A. Gafur, S.M. Al-Zahrani. Effect of chemical treatments on the physical properties of non-woven jute/PLA biocomposites. *BioResources* **2015**, *10*, 7386-7404.

133. G.A. Khan, M. Terano, M. Gafur, M.S. Alam. Studies on the mechanical properties of woven jute fabric reinforced poly (l-lactic acid) composites. *Journal of King Saud University-Engineering Sciences* **2016**, *28*, 69-74.

134. U.K. Komal, M.K. Lila, I. Singh. PLA/banana fiber based sustainable biocomposites: a manufacturing perspective. *Composites Part B: Engineering* **2020**, *180*, 107535.

135. J. Luedtke, M. Gaugler, W.J. Grigsby, A. Krause. Understanding the development of interfacial bonding within PLA/wood-based thermoplastic sandwich composites. *Industrial Crops and Products* **2019**, *127*, 129-134.

136. H. Rebelo, D. Lecompte, C. Cismasiu, A. Jonet, B. Belkassem, A. Maazoun. Experimental and numerical investigation on 3D printed PLA sacrificial honeycomb cladding. *International Journal of Impact Engineering* **2019**, *131*, 162-173.

137. E.G. Giakoumis. Analysis of 22 vegetable oils' physico-chemical properties and fatty acid composition on a statistical basis, and correlation with the degree of unsaturation. *Renewable energy* **2018**, *126*, 403-419.

138. A. Kadam, M. Pawar, O. Yemul, V. Thamke, K. Kodam. Biodegradable biobased epoxy resin from karanja oil. *Polymer* **2015**, *72*, 82-92.

139. M. Galià, L.M. de Espinosa, J.C. Ronda, G. Lligadas, V. Cádiz. Vegetable oil-based thermosetting polymers. *European journal of lipid science and technology* **2010**, *112*, 87-96.

140. N. Karak. Overview of epoxies and their thermosets. In *Sustainable Epoxy Thermosets and Nanocomposites*, ACS Publications: 2021; 1-36.

141. E. Budiyati, R. Rochmadi, A. Budiman, B. Budhijanto. Studies on epoxidation of tung oil with hydrogen peroxide catalyzed by sulfuric acid. *Bulletin of Chemical Reaction Engineering & Catalysis* **2020**, *15*, 674-686.

142. R. Turco, R. Tesser, V. Russo, T. Cogliano, M. Di Serio, E. Santacesaria. Epoxidation of linseed oil by performic acid produced in situ. *Industrial & Engineering Chemistry Research* **2021**, *60*, 16607-16618.

143. A. Carbonell-Verdu, L. Bernardi, D. Garcia-Garcia, L. Sanchez-Nacher, R. Balart. Development of environmentally friendly composite matrices from epoxidized cottonseed oil. *European Polymer Journal* **2015**, *63*, 1-10.

144. M.-D. Samper, J.M. Ferri, A. Carbonell-Verdu, R. Balart, O. Fenollar. Properties of biobased epoxy resins from epoxidized linseed oil (ELO) crosslinked with a mixture of cyclic anhydride and maleinized linseed oil. *Express Polymer Letters* **2019**, *13*, 407-418.

145. X.-M. Ding, L. Chen, D.-M. Guo, B.-W. Liu, X. Luo, Y.-F. Lei, H.-Y. Zhong, Y.-Z. Wang. Controlling cross-linking networks with different imidazole accelerators toward high-performance epoxidized soybean oil-based thermosets. *ACS Sustainable Chemistry & Engineering* **2021**, *9*, 3267-3277.

146. M. Qi, Y.-J. Xu, W.-H. Rao, X. Luo, L. Chen, Y.-Z. Wang. Epoxidized soybean oil cured with tannic acid for fully bio-based epoxy resin. *RSC advances* **2018**, *8*, 26948-26958.

147. F.S. Güner, Y. Yağcı, A.T. Erciyes. Polymers from triglyceride oils. *Progress in Polymer Science* **2006**, *31*, 633-670.

148. S.N. Khot, J.J. Lascala, E. Can, S.S. Morye, G.I. Williams, G.R. Palmese, S.H. Kusefoglu, R.P. Wool. Development and application of triglyceride-based polymers and composites. *Journal of applied polymer science* **2001**, *82*, 703-723.

149. P. Zhang, J. Zhang. One-step acrylation of soybean oil (SO) for the preparation of SO-based macromonomers. *Green Chemistry* **2013**, *15*, 641-645.

150. T. Eren, S.H. Kusefoglu. Synthesis and polymerization of the acrylamide derivatives of fatty compounds. *Journal of applied polymer science* **2005**, *97*, 2264-2272.

151. Y. Su, S. Zhang, Y. Chen, T. Yuan, Z. Yang. One-step synthesis of novel renewable multi-functional linseed oil-based acrylate prepolymers and its application in UV-curable coatings. *Progress in Organic Coatings* **2020**, *148*, 105820.

152. Y. Wu, K. Li. Replacement of styrene with acrylated epoxidized soybean oil in an unsaturated polyester resin from propylene glycol, isophthalic acid, and maleic anhydride. *Journal of Applied Polymer Science* **2016**, *133*, 43052.

153. S. Grishchuk, J. Karger-Kocsis. Hybrid thermosets from vinyl ester resin and acrylated epoxidized soybean oil (AESO). *Express Polymer Letters* **2011**, *5*, 2–11.

154. W. Liu, T. Chen, M.-e. Fei, R. Qiu, D. Yu, T. Fu, J. Qiu. Properties of natural fiber-reinforced biobased thermoset biocomposites: Effects of fiber type and resin composition. *Composites Part B: Engineering* **2019**, *171*, 87-95.

155. J. Chen, H. Liu, W. Zhang, L. Lv, Z. Liu. Thermosets resins prepared from soybean oil and lignin derivatives with high biocontent, superior thermal properties, and biodegradability. *Journal of Applied Polymer Science* **2020**, *137*, 48827.

156. R.C. Chikhalonde, M. Bhalerao, V. Karadbhajane. Study on modification processes of vegetable oils and detrimental efects of petroleum products **2019**, 707-709.

157. T. Eren, S.H. Küsefoğlu, R. Wool. Polymerization of maleic anhydride–modified plant oils with polyols. *Journal of applied polymer science* **2003**, *90*, 197-202.

158. V. Fombuena, R. Petrucci, F. Dominici, A. Jordá-Vilaplana, N. Montanes, L. Torre. Maleinized linseed oil as epoxy resin hardener for composites with high bio content obtained from linen byproducts. *Polymers* **2019**, *11*, 301.

159. D.L. Motoc, J.M. Ferri, S. Ferrandiz-Bou, D. Garcia-Garcia, R. Balart. Dynamic–mechanical and decomposition properties of flax/basalt hybrid laminates based on an epoxidized linseed oil polymer. *Polymers* **2021**, *13*, 479.

160. H. Ma, X. Zhang, F. Ju, S.-B. Tsai. A study on curing kinetics of nano-phase modified epoxy resin. *Scientific Reports* **2018**, *8*, 1-15.

161. M. Brown, M. Maciejewski, S. Vyazovkin, R. Nomen, J. Sempere, A.a. Burnham, J. Opfermann, R. Strey, H. Anderson, A. Kemmler. Computational aspects of kinetic analysis: part A: The ICTAC kinetics project-data, methods and results. *Thermochimica Acta* **2000**, *355*, 125-143.

162. S. Vyazovkin, A.K. Burnham, J.M. Criado, L.A. Pérez-Maqueda, C. Popescu, N. Sbirrazzuoli. ICTAC Kinetics Committee recommendations for performing kinetic computations on thermal analysis data. *Thermochimica acta* **2011**, *520*, 1-19.

163. C. Dickinson, G. Heal. A review of the ICTAC Kinetics Project, 2000: Part 1. Isothermal results. *Thermochimica Acta* **2009**, *494*, 1-14.

164. S. Vyazovkin, N. Sbirrazzuoli. Isoconversional kinetic analysis of thermally stimulated processes in polymers. *Macromolecular Rapid Communications* **2006**, *27*, 1515-1532.

165. M. Stanko, M. Stommel. Kinetic prediction of fast curing polyurethane resins by model-free isoconversional methods. *Polymers* **2018**, *10*, 698.

166. H.L. Friedman. Kinetics of thermal degradation of char-forming plastics from thermogravimetry. Application to a phenolic plastic. In Proceedings of Journal of polymer science part C: polymer symposia; 183-195.

167. J.H. Flynn. The 'temperature integral'—its use and abuse. *Thermochimica Acta* **1997**, *300*, 83-92.

168. C.D. Doyle. Kinetic analysis of thermogravimetric data. *Journal of applied polymer science* **1961**, *5*, 285-292.

169. A.W. Coats, J. Redfern. Kinetic parameters from thermogravimetric data. *Nature* **1964**, *201*, 68-69.

170. S. Vyazovkin, D. Dollimore. Linear and nonlinear procedures in isoconversional computations of the activation energy of nonisothermal reactions in solids. *Journal of chemical information and computer sciences* **1996**, *36*, 42-45.

171. G.I. Senum, R. Yang. Rational approximations of the integral of the Arrhenius function. *Journal of thermal analysis* **1977**, *11*, 445-447.

172. L. Pérez-Maqueda, J. Criado. The accuracy of Senum and Yang's approximations to the Arrhenius integral. *Journal of thermal analysis and calorimetry* **2000**, *60*, 909-915.

173. M. Starink. The determination of activation energy from linear heating rate experiments: a comparison of the accuracy of isoconversion methods. *Thermochimica acta* **2003**, *404*, 163-176.

174. J.H. Flynn, L.A. Wall. General treatment of the thermogravimetry of polymers. *Journal of research of the National Bureau of Standards. Section A, Physics and chemistry* **1966**, *70*, 487.

175. T. Ozawa. A new method of analyzing thermogravimetric data. *Bulletin of the chemical society of Japan* **1965**, *38*, 1881-1886.

176. C. Doyle. Estimating isothermal life from thermogravimetric data. *Journal of Applied Polymer Science* **1962**, *6*, 639-642.

177. T. Akahira, T. Sunose. Method of determining activation deterioration constant of electrical insulating materials. *Res Rep Chiba Inst Technol (Sci Technol)* **1971**, *16*, 22-31.

178. P. Murray, J. White. Kinetics of the thermal dehydration of clays. Part IV. Interpretation of the differential thermal analysis of the clay minerals. *Trans Br Ceram Soc* **1955**, *54*, 204-238.

179. H.E. Kissinger. Reaction kinetics in differential thermal analysis. *Analytical chemistry* **1957**, *29*, 1702-1706.

180. J. Farjas, N. Butchosa, P. Roura. A simple kinetic method for the determination of the reaction model from non-isothermal experiments. *Journal of thermal analysis and calorimetry* **2010**, *102*, 615-625.

181. J. Criado, J. Malek, A. Ortega. Applicability of the master plots in kinetic analysis of non-isothermal data. *Thermochimica Acta* **1989**, *147*, 377-385.

182. J. Málek. The kinetic analysis of non-isothermal data. *Thermochimica Acta* **1992**, *200*, 257-269.

183. S. Chandrakar, A. Agrawal, P. Prakash, I.A. Khan, A. Sharma. Physical and mechanical properties of epoxy reinforced with pistachio shell particulates. In Proceedings of AIP Conference Proceedings; 040012.

184. A. Khazaeian, A. Ashori, M.Y. Dizaj. Suitability of sorghum stalk fibers for production of particleboard. *Carbohydrate polymers* **2015**, *120*, 15-21.

185. M. Mandal, P. Begum, R.C. Deka, T.K. Maji. Wood flour thermoset composites using chemically modified epoxidized soybean oil. *European Journal of Wood and Wood Products* **2019**, *77*, 569-580.

186. A. Wechsler, M. Zaharia, A. Crosky, H. Jones, M. Ramírez, A. Ballerini, M. Nuñez, V. Sahajwalla. Macadamia (Macadamia integrifolia) shell and castor (Rícinos communis) oil based sustainable particleboard: A comparison of its properties with conventional wood based particleboard. *Materials & Design* **2013**, *50*, 117-123.

187. T. Czigány, J. Vad, K. Pölöskei. Basalt fiber as a reinforcement of polymer composites. *Periodica Polytechnica Mechanical Engineering* **2005**, *49*, 3-14.

188. M. Samper, R. Petrucci, L. Sánchez-Nacher, R. Balart, J. Kenny. New environmentally friendly composite laminates with epoxidized linseed oil (ELO) and slate fiber fabrics. *Composites Part B: Engineering* **2015**, *71*, 203-209.

II. Objetivos

II.1. Objetivo General

El objetivo principal de esta tesis doctoral se enfoca en la búsqueda de nuevos materiales basados en matrices poliméricas con un alto rendimiento medioambiental, y reforzados por partículas y fibras de origen natural. Para esto se parte de una mejora y optimización de propiedades de las matrices, por un lado, se pretende sobrellevar carencias como la falta de tenacidad que presentan matrices termoplásticas como el PLA. Y por otro lado se pretende comprender y optimizar el proceso de entrecruzado de resinas termoestables parcial y totalmente biobasadas. Además de someter a los refuerzos naturales a varias modificaciones con ansias de mejorar su interacción con las diferentes matrices. Finalmente se busca obtener materiales compuestos con un alto contenido natural con propiedades mejoradas y fabricados por medios que tengan una aplicabilidad a nivel industrial.

II.2. Objetivos Específicos

Para lograr el objetivo general se plantearon una serie de objetivos específicos que se han ido elaborando durante el desarrollo de la tesis doctoral. Estos objetivos específicos se han agrupado en dos bloques dependiendo al tipo de matriz polimérica utilizada, entre las que se encuentran mezclas y compuestos con matrices termoplásticas de alto rendimiento medioambiental y compuestos con matrices termoestables con alto rendimiento medioambiental.

Mezclas y compuestos con matrices termoplásticas con alto rendimiento medioambiental

- Estudio del efecto de la incorporación de diferentes cantidades de poli (butileno succinato-*co*-adipato) (PBSA) en las propiedades mecánicas, morfológicas y de memoria de forma una matriz de PLA.
- Estudio del efecto de la adición de un nuevo tipo de oligómero de ácido láctico (OLA) en las propiedades mecánicas, térmicas, termomecánicas, morfológicas y de memoria de forma en una matriz de PLA.
- Estudio del efecto de la altura en núcleos en forma de panal de abeja compuestos íntegramente de PLA sobre las propiedades a flexión y compresión en la fabricación de nuevas estructuras sándwich, con caras exteriores de PLA y fibras de lino.

- Estudio del efecto de la distribución y cantidad de carga de fibra de yute en las propiedades mecánicas de compuestos basados en una matriz de PLA, fabricados por métodos convencionales

Compuestos con matrices termoestables con alto rendimiento medioambiental

- Análisis cinético del curado de una resina epoxi con un 31 % de contenido de origen natural a través de métodos isoconversionales en condiciones no isotermas por medio de DSC.
- Análisis cinético del curado de una resina epoxi basada en aceite de linaza epoxidado (ELO) entrecruzados con anhídridos a través de métodos isoconversionales en condiciones no isotermas por medio de DSC.
- Optimización de los parámetros de curado a través del estudio de diferentes temperaturas de curado y de poscurado de una resina epoxi con un 31 % de contenido de origen natural.
- Estudio del efecto del tamaño y cantidad de carga de partículas lignocelulosicas obtenidas de la industria del lino en las propiedades mecánicas, térmicas, de color, morfológicas y de resistencia al agua de compuestos basados una matriz epoxi con un 31 % de contenido de origen natural.
- Estudio del efecto de diferentes secuencias de apilamientos de fibras de basalto y de lino tratadas con agentes de acoplamiento, en las propiedades mecánicas, termomecánicas y morfológicas de laminados fabricados con una matriz epoxi con un 31 % de contenido de origen natural.
- Estudio del efecto de diferentes secuencias de apilamientos de fibras de basalto y de lino tratadas con agentes de acoplamiento, en las propiedades mecánicas de estructuras sándwich ligeras con núcleos permeables fabricados con una matriz epoxi con un 31 % de contenido de origen natural.

En la figura II.1. se puede observar la planificación de los objetivos específicos realizados durante la tesis doctoral.

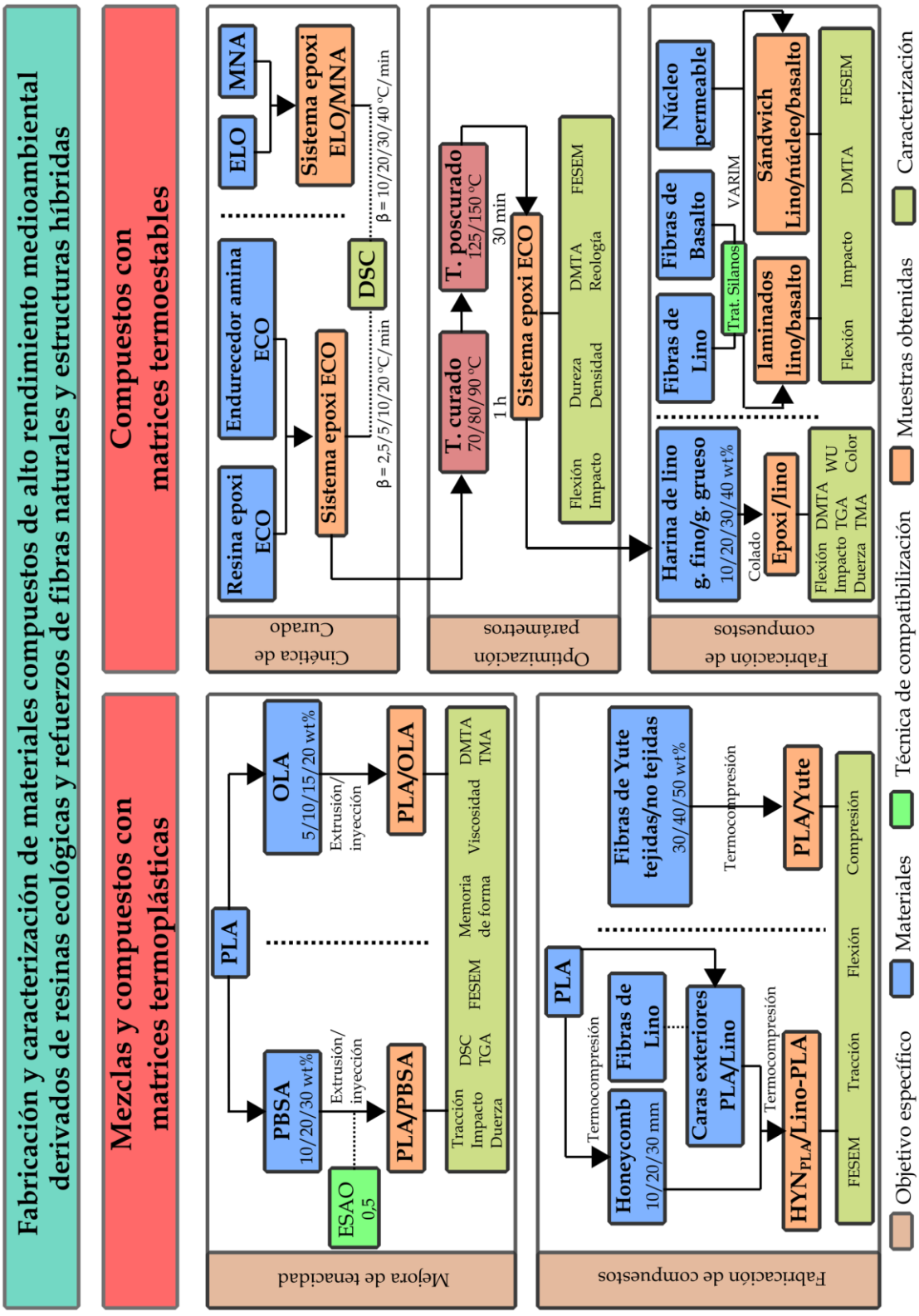

Figura II.1. Esquema de la planificación del trabajo de la tesis doctoral.

III. RESULTS AND DISCUSSION

The following section gathers the most outstanding results regarding developing and optimizing new polymeric materials with low environmental impact and balanced properties. For this purpose, in this work, different polymeric materials were used, e.g., thermoplastic materials such as PLA and thermosetting materials such as epoxy resins with fillers and natural fibers as reinforcing materials.

The results obtained were grouped into two blocks to better understand the document, with ten chapters. The blocks were structured, considering the polymeric matrix used and its application.

Block 1. Blends and composites with thermoplastic matrices of high environmental performance

This block contains the results obtained from the improvement of PLA toughness after several modifications, one of them by binary blends with flexible thermoplastics such as PBSA and the addition of different lactic acid oligomers. Additionally, the document evaluates the use of PLA as the main constituent in the manufacture of honeycomb cores and its use as a matrix in developing composites reinforced with natural fibers.

Chapter III.1.1.

Toughened poly (lactic acid)-PLA formulations by binary blends with poly(butylene succinate-*co*-adipate)-PBSA and their shape memory behavior.

Chapter III.1.2.

Development of injection-molded polylactide pieces with high toughness by the addition of lactic acid oligomer and characterization of their shape memory behavior.

Chapter III.1.3.

Manufacturing and characterization of highly environmentally friendly sandwich composites from polylactide cores and flax-polylactide faces

Chapter III.1.4.

A comparative study of mechanical properties of polylactide bio-composites with woven and non-woven jute reinforcements

Block 2. Composites based on thermosetting matrices with high environmental performance.

This block includes the most relevant results of the kinetic study of the curing process of epoxy resins with a partial and total content of the natural source and the optimization of the curing process parameters. This work evaluates the performance of these optimized matrices in the fabrication of different composite materials reinforced with natural fillers and fibers to produce industrially scalable composite materials with good mechanical properties and minimum environmental impact. For this purpose, this block gathers the manufacture and characterization of WPC, laminates, and sandwich structures with permeable cores.

Chapter III.2.1.

Kinetic analysis of the curing of a partially biobased epoxy resin using dynamic differential scanning calorimetry

Chapter III.2.2.

Kinetic analysis of the curing process of biobased epoxy resin from epoxidized linseed oil by dynamic differential scanning calorimetry

Chapter III.2.3.

Optimization of the curing and post-curing conditions for the manufacturing of partially bio-based epoxy resins with improved toughness

Chapter III.2.4.

Manufacturing and characterization of green composites with partially biobased epoxy resin and flaxseed flour wastes

Chapter III.2.5.

Manufacturing and characterization of hybrid composites with basalt and flax fabrics and a partially bio-based epoxy resin

Chapter III.2.6.

Manufacturing of composite materials with high environmental efficiency using epoxy resin of renewable origin and permeable light cores for vacuum-assisted infusion molding.

III.1. Blends and composites with thermoplastic matrices of high environmental performance

Adaptado del artículo

III.1.1. Toughened poly (lactic acid)-PLA formulations by binary blends with poly(butylene succinate-*co*-Adipate)-PBSA and their shape memory behaviour

Diego Lascano[1], Luis Quiles-Carrillo[2], Rafael Balart[2], Teodomiro Boronat[2] and Nestor Montanes[2]

[1] Escuela Politécnica Nacional, 17-01-2759 Quito, Ecuador

[2] Technological Institute of Materials (ITM), Universitat Politècnica de València (UPV),Plaza Ferrándiz y Carbonell 1, 03801 Alcoy, Spain

Materials **2019**, *12*(4), 622

materials

MDPI

Article

Toughened Poly (Lactic Acid)—PLA Formulations by Binary Blends with Poly(Butylene Succinate-*co*-Adipate)—PBSA and Their Shape Memory Behaviour

Diego Lascano [1], Luis Quiles-Carrillo [2,*], Rafael Balart [2], Teodomiro Boronat [2] and Nestor Montanes [2]

[1] Escuela Politécnica Nacional, 17-01-2759 Quito, Ecuador; dielas@epsa.upv.es
[2] Technological Institute of Materials (ITM), Universitat Politècnica de València (UPV), Plaza Ferrándiz y Carbonell 1, 03801 Alcoy, Spain; rbalart@mcm.upv.es (R.B.); tboronat@dimm.upv.es (T.B.); nesmonmu@upvnet.upv.es (N.M.)
* Correspondence: luiquic1@epsa.upv.es; Tel.: +34-966-528-433

Received: 16 January 2019; Accepted: 16 February 2019; Published: 22 February 2019

Abstract: This study reports the effect of poly(butylene succinate-*co*-adipate) (PBSA) on the mechanical performance and shape memory behavior of poly(lactic acid) (PLA) specimens that were manufactured by injection molding and hot-press molding. The poor miscibility between PLA and PBSA was minimized by the addition of an epoxy styrene-acrylic oligomer (ESAO), which was commercially named Joncryl®. It was incorporated during the extrusion process. Tensile, impact strength, and hardness tests were carried out following international standards. PLA/PBSA blends with improved mechanical properties were obtained, which highlighted the sample that was compatibilized with ESAO, leading to a remarkable enhancement in elongation at break, but showing poor shape memory behaviour. Field Emission Scanning Electron Microscopy (FESEM) images showed how the ductile properties were improved, while PBSA loading increased, thus leading to minimizing the brittleness of neat PLA. The differential scanning calorimetry (DSC) analysis revealed the low miscibility between these two polymers and the improving effect of PBSA in PLA crystallization. The bending test carried out on the sheets of PLA/PBSA blends showed the direct influence that the PBSA has on the reduction of the shape memory that is intrinsically offered by neat PLA.

Keywords: poly (lactic acid) (PLA); poly(butylene succinate-co-adipate) (PBSA); binary blends; shape memory behaviour

1. Introduction

The use of polymers and plastics in our daily life is almost mandatory due to their huge range of properties. For this reason, the demand for these materials has remarkably increased in the last decades. Unlike their production, the treatment of these materials after their end-of-life has been neglected, resulting in the oversaturation of plastic wastes in the environment. Since most of these plastics are synthetic, petroleum-derived materials, they have a high resistance to microbial degradation, so their decomposition is complex and extremely slow [1]. The development of new environmentally friendly polymeric materials has become a leading force in this industry because of this. The environmentally friendly properties of a polymer could be related to their origin (bio-sourced) or to their end-of-life (biodegradable or disintegrable in controlled compost soil). Taking into account their origin, some of the polymers have been fully or partially obtained from renewable resources,

Toughened poly (lactic acid)-pla formulations by binary blends with poly(butylene succinate-co-adipate)-pbsa and their shape memory behaviour

Abstract

This study reports the effect of poly(butylene succinate-co-adipate) (PBSA) on the mechanical performance and shape memory behavior of poly(lactic acid) (PLA) specimens that were manufactured by injection molding and hot-press molding. The poor miscibility between PLA and PBSA was minimized by the addition of an epoxy styrene-acrylic oligomer (ESAO), which was commercially named Joncryl®. It was incorporated during the extrusion process. Tensile, impact strength, and hardness tests were carried out following international standards. PLA/PBSA blends with improved mechanical properties were obtained, which highlighted the sample that was compatibilized with ESAO, leading to a remarkable enhancement in elongation at break, but showing poor shape memory behaviour. Field Emission Scanning Electron Microscopy (FESEM) images showed how the ductile properties were improved, while PBSA loading increased, thus leading to minimizing the brittleness of neat PLA. The differential scanning calorimetry (DSC) analysis revealed the low miscibility between these two polymers and the improving effect of PBSA in PLA crystallization. The bending test carried out on the sheets of PLA/PBSA blends showed the direct influence that the PBSA has on the reduction of the shape memory that is intrinsically offered by neat PLA.

Keywords: poly (lactic acid) (PLA); poly(butylene succinate-co-adipate) (PBSA); binary blends; shape memory behaviour

III.1.1.1. Introduction

The use of polymers and plastics in our daily life is almost mandatory due to their huge range of properties. For this reason, the demand for these materials has remarkably increased in the last decades. Unlike their production, the treatment of these materials after their end-of-life has been neglected, resulting in the oversaturation of plastic wastes in the environment. Since most of these plastics are synthetic, petroleum-derived materials, they have a high resistance to microbial degradation, so their decomposition is complex and extremely slow [1]. The development of new environmentally friendly polymeric materials has become a leading force in this industry because of this. The environmentally friendly properties of a polymer could be related to their origin (bio-sourced) or to their end-of-life (biodegradable or disintegrable in controlled compost soil). Taking into account their origin, some of the polymers have been fully or partially obtained from renewable resources, such as poly(ethylene) (PE) and poly(propylene) (PP) from sugarcane, poly(amides) (PAs) from castor oil, poly(carbonate) (PC) from corn, and so on [2-4]. These biobased polymers are identical to their counterpart petroleum-derived polymers and despite that they are not biodegradable, they have a positive effect on carbon footprint [3]. Another interesting group of environmentally friendly polymers is that which includes some petroleum-derived poly(esters), but, due to the nature of the ester group, they can disintegrate in controlled compost conditions. This groups includes poly(ε-caprolactone) (PCL), poly(butylene succinate) (PBS), poly(butylene succinate-co-adipate) (PBSA), poly(glycolic acid) (PGA), among others [1,5-7]. Finally, the most interesting group of environmentally friendly polymers is that of biobased and biodegradable polymers. Polysaccharides (starch, cellulose, chitin, and so on), protein based polymers (gluten, soybean protein, casein, collagen, among others), and bacterial polymers, such as poly(3-hydroxybutyrate) (PHB) or poly(3-hydroxybutyrate-*co*-3-hydroxyvalerate) (PHBV) are included in this group. Although these polymers are very promising, their properties are still quite far from those of commodities and engineering plastics [8-11].

Nowadays, poly(lactic acid) (PLA) is one of the most studied aliphatic polyesters thanks to its good mechanical properties and it can be either obtained from petroleum or renewable resources. Bio-sourced PLA is produced by anaerobic fermentation of sugars that are derived starch-rich plants, such as corn, sugarcane, beet sugar, potato, and so on [12]. It can also be obtained through the direct condensation of lactic acid and by ring opening polymerization of cyclic lactide dimer (ROP) [6,13]. The excellent tensile strength that PLA presents is the reason why it is used as an alternative to conventional plastics, such as high and low-density poly(ethylenes) (HDPE/LDPE), poly(styrene)

(PS), and poly(ethylene terephthalate) (PET) [6]. It can be manufactured in a wide range of processing methods, such as conventional extrusion, injection molding, blow molding, film forming, three-dimensional (3D)-printed, and so on [14-17]. All of these features make PLA exceptionally useful in the packaging industry, food containers [12,18], and in biomedicine for controlled drug delivery and tissue engineering [19]. Although PLA presents good balanced properties and remarkable environmental benefits, its use has been limited due to its cost [13] and, in addition, it is a quite brittle material. With the aim of improving the ductility and toughness of PLA [20], many research approaches have been used. One is plasticization with conventional plasticizers, such as poly(ethylene glycol) (PEG), poly(propylene glycol) (PPG), lactic acid oligomers (OLAs), modified vegetable oils (MVOs), esters from citric acid or adipic acid, and so on [21-23]. All of these plasticizers contribute to improving ductile properties due to a remarkable decrease in the glass transition temperature, T_g, but the mechanical resistant properties are highly reduced. Another approach to overcome (or minimize) the extremely high brittleness of PLA is by blending with other flexible polymers. Regarding blends, compatibility/miscibility issues must be taken into account [24]. Bhatia, *et al.* [25] have reported the properties of binary blends of PLA with PBS. The addition of 30 wt % PBS to PLA resulted in a clear increase in toughness, but over 50 wt % PBS addition, the clarity of the materials is reduced. As PLA and PBS show restricted miscibility, Harada, *et al.* [26] used an isocyanate as a reactive processing aid to increase the impact strength of PLA/PBS binary blends. PCL is another flexible aliphatic poly(ester) that can provide increased toughness to PLA, as reported by Matta, *et al.* [6]. Poly(butylene adipate-*co*-terephthalate) (PBAT) has great flexibility and it maintains excellent biodegradability properties. As can be shown by Khatsee, *et al.* [27], binary PLA/PBAT blends can be obtained by electrospinning for controlled antibiotic release. Poly(propylene carbonate) (PPC) has been successfully used in PLA blends with good shape memory polymers [28].

Taking advantage of the PLA structure and materials that are based on PLA, a new research field has emerged, which is shape memory. Because of its particular structure, this field is promising for PLA. PLA has crystalline domains that define the permanent shape and switching segments that fix the temporary shape [29]. This particular structure allows for PLA to switch from a temporary shape to its permanent shape. The switching segments are activated by an external stimulus that can be either physical or chemical, but temperature is the most common stimulus leading to a thermal-responsive memory shape by selecting the appropriate temperature cycle regarding the T_g [30-32]. Shape memory behaviour has been used in electronics [29], and one of most

recent applications include pieces that are made by 3D printing with PLA matrix filaments [33]. As these 3D-printed parts can change their shape by heating/cooling above/below the T_g, this technology is known as four-dimensional (4D)-printing. Taking advantage of the PLA biocompatibility with the human body, recent applications of PLA are focused on tissue engineering by making scaffold systems of physical blends, with TPU for support material in cartilage or bone repair [32,34]. The aim of this research is to enhance PLA toughness, through physical blending with poly(butylene succinate-*co*-adipate) (PBSA) to obtain flexible shape memory polymers with improved toughness. Despite that PBSA is based on fossil resources, it can undergo disintegration in controlled compost [35,36]. PBSA could offer high flexibility and great impact strength properties to PLA [37]. As these two poly(esters) show restricted miscibility, an epoxy styrene-acrylic oligomer (ESAO) will be used.

III.1.1.2. Materials and Methods

Materials

PLA was an IngeoTM Biopolymer 6201D that was obtained from NatureWorks (Minnetonka, MN, USA). It is a thermoplastic resin derived from annually renewable resources. Its glass transition temperature, T_g, is comprised between 55-60 °C and the melt peak temperature is located in the 155-170 °C range. Its density is 1.25 g cm^{-3} and it possesses a melt flow index, MFI of 15-30 g/10 min. With regard to the flexible polymer for binary blends, an aliphatic poly(ester) copolymer, PBSA, was used. A commercial Bionolle grade 3002 MD was obtained from Showa Denko Europe GmbH (Munich, Germany). It shows good processability for extrusion and blow molding. The density reported is for this PBSA grade is 1.23 g cm^{-3}. Regarding its thermal properties, its T_g is close to -45 °C and the melt peak temperature is 94 °C.

A multi-functional epoxy-based styrene-acrylic oligomer (ESAO) was used as a compatibilizer. A commercial ESAO grade JONCRYL® ADR-4300 that was distributed by Basf (Barcelona, Spain) was used. This compatibilizer has a glass temperature T_g of 56 °C and an epoxy equivalent weight of 445 g mol^{-1}. figure III.1.1.1 shows the schematic representation of the structures of both PLA and PBS and the ESAO generic structure.

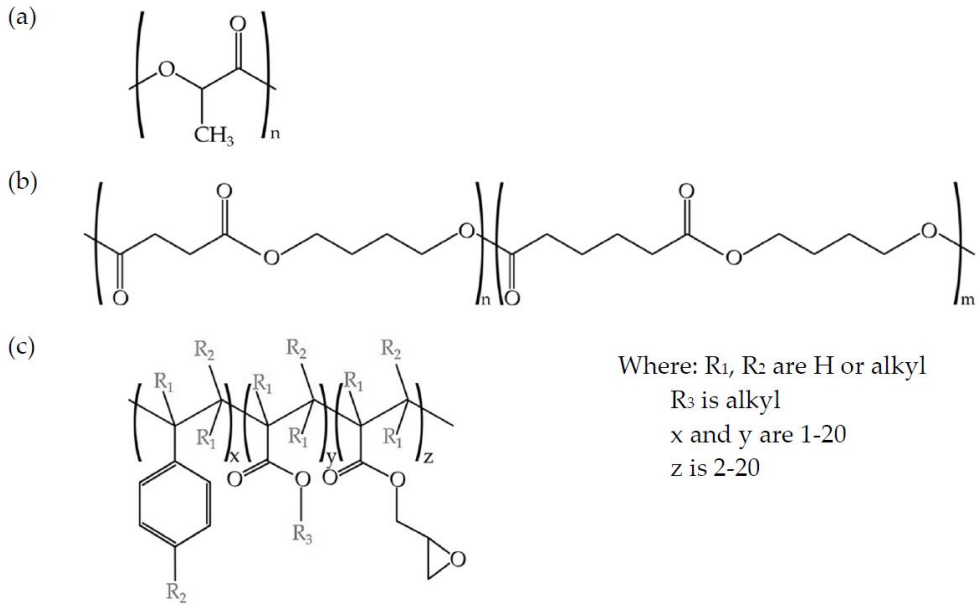

Figure III.1.1.1. Schematic representation of (**a**) poly(lactic acid) (PLA), (**b**) poly(butylene succinate-*co*-adipate) (PBSA), and (**c**) epoxy styrene-acrylic oligomer (ESAO) (Joncryl® ADR-4300).

Manufacturing of PLA/PBSA Binary Blends

Prior to processing, as both of the poly(esters) are highly sensitive to hydrolysis, PLA and PBSA were dried at 50 °C for 48 h. Table III.1.1.1 shows the labelling and the compositions of the developed blends. According to the literature [38], PLA blends with 20 wt % of PBS have a good balance between mechanical properties and shape memory behaviour. Thus, the addition of a compatibilizer to the $PLA_{80}PBSA_{20}$ mixture was decided to determine whether it causes any effect in its properties. To obtain homogeneous mixtures, all of the materials were subjected to a mechanical pre-mixing for 3 min in a zipper bag. These mixtures were extruded using a co-rotating twin-screw extruder ZSK-18 MEGAlab from Coperion (Stuttgart, Germany) that was equipped with a screw diameter of 18 mm with a length to diameter ratio, L/D of 48. The dosage of each component was controlled by a side twin-screw feeder ZS-B 18 from K-Tron (Pitman, NJ, USA). The screw speed was set to 180 rpm using a temperature profile of 145-155-160-180-185-190-190 °C from the feeding to the die. The feed rate was set to 2 kg h^{-1}. Once the different blends were extruded, they were cooled down to 15 °C in a water bath and subsequently pelletized using an air knife unit.

Table III.1.1.1. Composition and labelling of PLA/PBSA binary blends.

Code	PLA (wt %)	PBSA (wt %)	Joncryl® ADR (phr)
PLA	100	-	-
$PLA_{90}PBSA_{10}$	90	10	-
$cPLA_{80}PBSA_{20}$	80	20	0.5
$PLA_{80}PBSA_{20}$	80	20	-
$PLA_{70}PBSA_{30}$	70	30	-
PBSA	-	100	-

* phr denotes the weight parts of Joncryl® per hundred parts by weight of PLA/PBSA blend.

The pelletized compounds were shaped into standard samples for characterization by injection molding in a Meteor 270/75 from Mateu & Solé (Barcelona, Spain). The temperature profile was set at 175-180-185-190 °C for PLA-based blends, while PBSA was programmed with a lower temperature profile of 105 °C for the different heating barrels. A clamping force of 75 tons was applied. The cooling time was set to 10 s.

Mechanical Properties

The tensile test was carried out following the recommendation of the ISO 527 standard while using a mechanical universal testing machine ELIB 50 from S.A.E. Ibertest (Madrid, Spain). It was equipped with a 5 kN load cell and the selected crosshead speed of 10 mm min^{-1} was used. The impact strength test was performed on a Charpy pendulum from Metrotec (San Sebastián, Spain), following the recommendations of ISO 179, using a 6 J pendulum on unnotched samples and a 1 J pendulum on notched samples (“V” type, 2 mm depth and a radio of 0.5 mm). Hardness measurements were obtained in a durometer 676-D from J. Bot Instruments (Barcelona, Spain) using Shore D scale following ISO 868.

All of the tests were carried out at room temperature with at least five samples and the corresponding properties were averaged.

Thermal Characterization

The main thermal transitions were analyzed by differential scanning calorimetry (DSC) in an 821 DSC calorimeter from Mettler-Toledo, Inc. (Schwerzenbach, Switzerland). The samples weight was between 5-10 mg. The samples were placed into standard sealed aluminum pans (40 µL) and then subjected to a thermal cycle consisting of three steps: initial heating from 30 °C to 200 °C, followed by a cooling process to -60

°C and after that, a second heating process up to 350 °C. The heating/cooling rate was set to 10 °C min^{-1}. These tests were carried out under a dry atmosphere with a constant nitrogen flow of 30 mL min^{-1}. The glass temperature (T_g), cold crystallization temperature peak (T_{cc}), the melting temperature (T_m), and the melt enthalpy (ΔH_m) were obtained from second heating step in this analysis.

The thermal degradation (weight loss) and thermal stability were followed by thermogravimetric analysis (TGA) in a TGA/SDTA 851 thermobalance from Mettler-Toledo (Schwerzenbach, Switzerland). The average weight of the samples was between 5-10 mg. These samples were placed on standard alumina crucibles with a total volume capacity of 70 µL and subsequently exposed to a heating program from 30 °C up to 700 °C at a constant heating rate of 20 °C min^{-1} in an air atmosphere.

Morphology Characterization by Field Emission Scanning Electron Microscopy (FESEM)

To analyze the morphology of fractured surfaces from impact tests, field emission scanning electron microscopy (FESEM) was used. A ZEISS ULTRA 55 FESEM microscope from Oxford Instruments (Abingdon, UK) was used working at an accelerating voltage of 2 kV. Prior to the test, the samples' surfaces were coated by an ultrathin gold-palladium layer in a high vacuum sputter coater EM MED20 from Leica Microsystem (Milton Keynes, UK).

Shape Memory Behaviour Characterization

The shape memory behaviour of the materials was evaluated using a conventional bending test on sheets with dimensions of 65 x 10 x 1 mm^3. These sheets were obtained by hot-press molding at 140 °C in a hot press Hoytom M.N.1417 (Bilbao, Spain) from Robima S.A. The switch transition temperature that leads the programming and the recovery cycle was set at 70 °C (PLA glass transition). The cooling temperature was set to 22 °C and the stabilization time was 15 min. The temporary shape was fixed to bending angles of 120° and 90°.

III.1.1.3. Results

Mechanical Properties and Morphology of Binary PLA/PBSA Blends

The tensile behaviour of binary PLA/PBSA blends is shown in table III.1.1.2. The tensile modulus, E_T of neat PLA is relatively high, about 1165 MPa. Regarding its tensile

strength (σ_T), PLA offers a relatively high value of 64.0 MPa, as compared to other commodities. While intrinsic mechanical resistant properties of neat PLA are high, its elongation (ε_b) at break is only of 9.23 %, which is responsible for high brittleness and the fragility of this material. Blending PLA with a flexible PBSA polymer has noticeable effects on overall mechanical performance. So that, the addition of 10 wt % PBSA to PLA leads to an expected decrease on mechanical resistant properties, such as E_T and σ_T, down to values of 1012 MPa and 52.6 MPa, respectively. As the wt % PBSA increases, both tensile modulus and strength decrease, which means that the brittle behaviour is diminished. At room temperature, PBSA is above its corresponding T_g value -41 °C [36], which means a flexible behaviour, as observed in table III.1.1.2. Above its T_g, the PBSA chains can move freely, as reported by Ojijo, *et al.* [39], thus leading to high ε_b value of 432.7 %. This improved chain mobility can exert a positive effect on PLA toughness.

Table III.1.1.2. Summary of mechanical properties of binary PLA/PBSA blends obtained from tensile tests.

Code	Tensile Strength, σ_T (MPa)	Elastic Modulus, E_T (MPa)	Elongation at Break, ε_b (%)
PLA	64.0 ± 1.2	1165 ± 44	9.2 ± 1.5
$PLA_{90}PBSA_{10}$	52.6 ± 0.8	1012 ± 21	12.2 ± 3.8
$cPLA_{80}PBSA_{20}$	41.2 ± 2.0	754 ± 47	121.2 ± 18.7
$PLA_{80}PBSA_{20}$	42.0 ± 3.6	849 ± 75	29.7 ± 6.3
$PLA_{70}PBSA_{30}$	37.7 ± 3.0	625 ± 72	56.5 ± 10.3
PBSA	18.3 ± 1.6	159 ± 61	432.7 ± 57.4

As expected, with PBSA addition, the elongation at break tends to increase. Only the addition of 10 wt % PBSA to PLA gives an increased ε_b value of 12.2 % and this is still more evident for PLA/PBSA blends containing 20 wt % and 30 wt % PBSA with ε_b values of 29.7 % and 56.5 %, respectively, thus leading to a clear increase in mechanical ductile properties.

Although good mechanical properties can be obtained by blending PLA with PBSA, the poor miscibility between these two polymers does not allow good interface interactions, as reported by Nofar, *et al.* [40]. For this reason, a compatibilizer agent, namely Joncryl®, has been added to the binary blend of 80 wt % PLA and 20 wt % PBSA. This compatibilizer agent has been extensively used as chain extender in poly(esters) due to the reaction of epoxy groups with hydroxyl terminal groups in poly(esters) [41,42]. This particular behaviour can be positive in binary blends of poly(esters), as this

compatibilizer can react either with the hydroxyl terminal groups of PLA and PBSA, thus leading to a compatibilization effect. The relatively low compatibilizer loading (0.5 phr) allows for this, since higher loadings could lead to branching, gel formation, and, even, some crosslinking [43,44]. As observed in table III.1.1.2, the uncompatibilized blend containing 20 wt % PBSA gives an ε_b value of 29.7 %, while the compatibilized blend with the same composition offers an ε_b increase up to values of 121.2 %, thus giving clear evidences of chain extension/compatibilization, as reported by Eslami and Kamal [45]. A low percentage of chain extender in blends leads to obtaining an improvement in the interface with both materials, improving some properties. In this particular case, this blend takes advantages of PBSA, improving the elongation at break. The increase in the ductile behaviour observed in PLA/PBSA blends and, specifically in the compatibilized PLA/PBSA blend, suggest an increase in toughness.

Nevertheless, it is worthy to note that toughness is not uniquely linked to ductile properties (i.e. elongation at break), but also to mechanical resistant properties (tensile strength). In this work, toughness has been quantitatively measured through the determination of the impact-absorbed energy in impact test (Charpy). **Table III.1.1.3** shows the impact strength values as a function of the composition of the developed materials. In a very first attempt, a 6 J pendulum was used, it did not provide enough energy to break some specimens, in order to have all the measurements in the same conditions, a "V" notch was done in all samples and then tested with a 1 J pendulum. As one can see, PLA is a brittle material with very low energy absorption (2.48 kJ m^{-2}) when compared to PBSA (26.02 kJ m^{-2}). As expected, the impact strength increases with the PBSA loading on binary blends up to values of 5.75 kJ m^{-2} for the uncompatibilized PLA/PBSA blend containing 30 wt % PBSA. It is worthy to note the good impact strength that was achieved with the blend with 20 wt % PBSA (3.28 kJ m^{-2}) and the clear positive effect of the compatibilizing effect provided by Joncryl®, since the same blend is able to reach an impact strength of about 4.33 kJ m^{-2}. figure III.1.1.2 presents the stress-strain curves of the developed blends. As it was expected, the stress tends to decrease when PBSA is added. On the other hand, the tensile strain or percentage elongation tends to increase, with the case of the compatibilized blend ($cPLA_{80}PBSA_{20}$) being more noticeable, which shows strain values of about 120 %. This results in an increase in the area below the curve, together with the increasing tendency of the impact strength, makes an improvement on toughness when PBSA is added. With regard to hardness, the tendency is similar to other mechanical resistant properties. A clear decreasing tendency in the Shore D hardness values can be observed when PBSA

is added. Nevertheless, the standard deviation does not allow for identifying a clear effect of the compatibilizer on Shore D values.

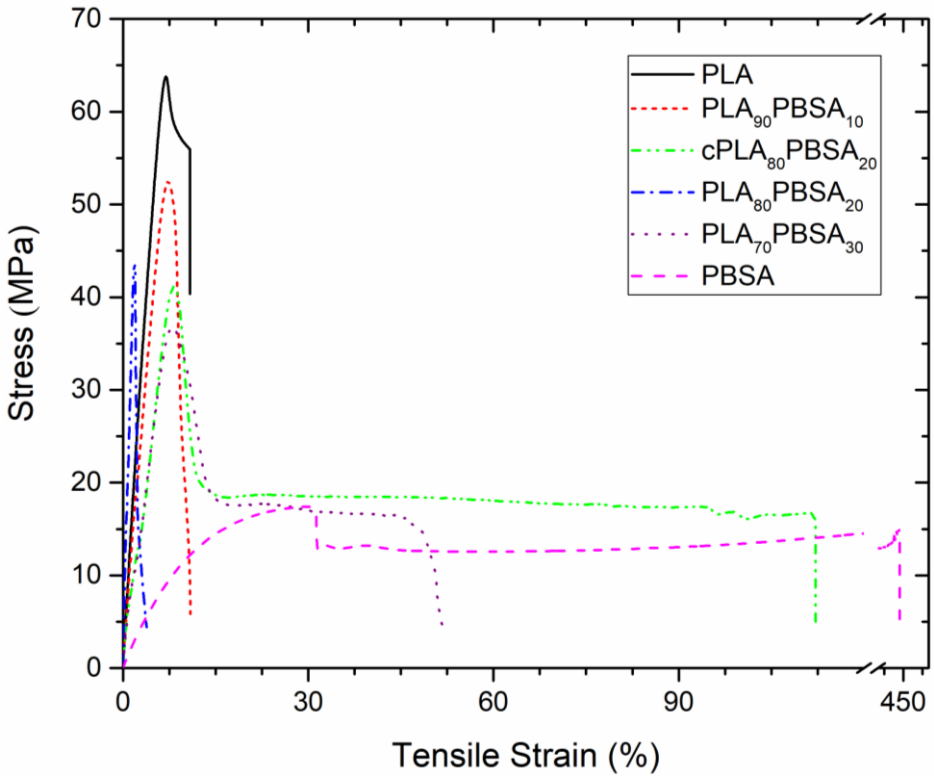

Figure III.1.1.2. Strain–stress curves corresponding to binary PLA/PBSA blends.

Table III.1.1.3. Impact absorbed energy (Charpy test) and Shore D hardness of binary PLA/PBSA blends.

Code	Impact Strength (kJ m^{-2}) ("V" notched)	Impact Strength (kJ m^{-2}) (unnotched)	Shore D Hardness
PLA	2.48 ± 0.22	28.10 ± 2.40	78.80 ± 0.84
$PLA_{90}PBSA_{10}$	2.54 ± 0.34	23.03 ± 2.80	74.00 ± 2.74
$cPLA_{80}PBSA_{20}$	4.33 ± 0.02	28.90 ± 0.85	75.00 ± 1.00
$PLA_{80}PBSA_{20}$	3.28 ± 0.28	27.52 ± 2.13	73.00 ± 1.41
$PLA_{70}PBSA_{30}$	5.75 ± 0.60	N/B	72.20 ± 1.60
PBSA	26.02 ± 0.60	N/B	57.00 ± 0.71

This particular behaviour is directly related to the morphology of the developed materials (figure III.1.1.3). figure III.1.1.3a shows the FESEM images of the fractured surfaces corresponding to unblended PLA. As it can be seen, the surface is uniform and smooth typical of a brittle fracture, with different crack growths [41]. This morphology is in total agreement with previous mechanical results. A remarkable change in the fracture

surface morphology can be observed in figure III.1.1.3e, which corresponds to the binary PLA/PBSA blend with 30 wt % PBSA. The surface is not as smooth, and it shows increased roughness due to increased plastic deformation. Similar morphology can be observed for uncompatibilized PLA/PBSA blends with different PBSA loading. The compatibilized blend with 20 wt % PBSA shows different fracture morphology due to its higher elongation at break, which allows more deformation before fracture (figure III.1.1.3c). It can be seen in figure III.1.1.**3c** that the surface presents a greater tear on it, which suggests increased PLA-PBSA interaction, because the compatibilizer works as a bridge between these two polymers, as reported Eslami and Kamal [45]. Obviously, PBSA shows a typical ductile fracture (figure III.1.1.3f), with a wavy surface topography that is representative for plastic deformation (even in impact conditions).

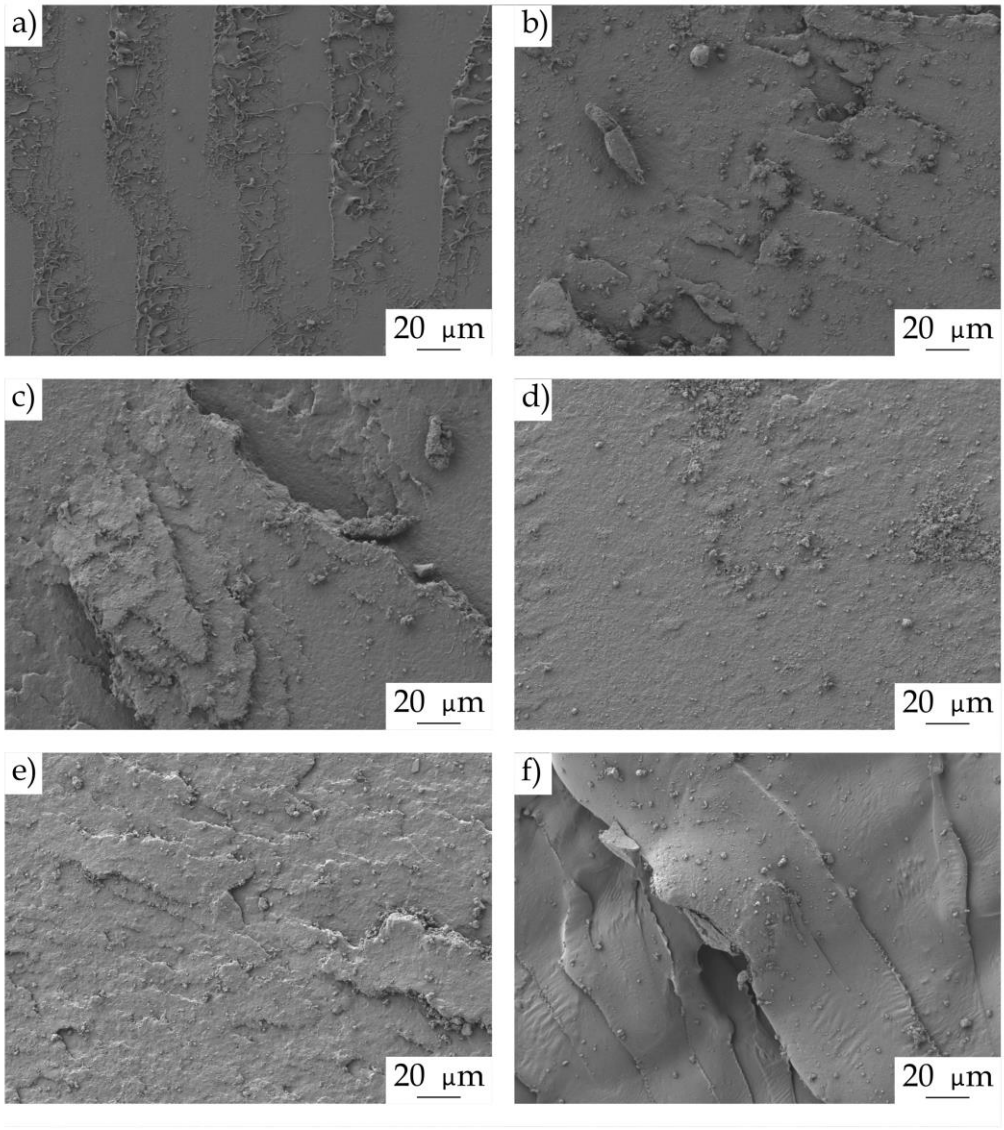

Figure III.1.1.3. Field emission scanning electron microscopy (FESEM) images at x500 corresponding to fractured surfaces from impact tests of (**a**) PLA, (**b**) $PLA_{90}PBSA_{10}$, (**c**) $cPLA_{80}PBSA_{20}$, (**d**) $PLA_{80}PBSA_{20}$, (**e**) $PLA_{70}PBSA_{30}$, and (**f**) PBSA.

Thermal Behaviour of Binary PLA/PBSA Blends

Figure III.1.1.4 shows the DSC thermograms corresponding to the second heating cycles of the developed PLA/PBSA blends, while table III.1.1.4 gathers the main parameters that were obtained by DSC. The first thermal transition that can be observed in figure III.1.1.4 is the glass transition temperature, T_g of the PLA-rich phase. This is located between 60-70 °C. As the temperature rises above the T_g, an exothermal peak appears between 95-110 °C, which corresponds to the cold crystallization process of PLA chains. This cold crystallization process is related to a rearrangement of the PLA chains to an ordered structure that is activated by temperature. At higher temperatures comprised in the 155-170 °C range, an endothermic peak is observed, which is attributable to the melting process of the crystalline domains in PLA [46]. Regarding neat PBSA, it shows a melting process comprised between 70-100 °C that overlaps the cold crystallization process of PLA. Neat PLA shows a T_g of 63.4 °C and this is slightly reduced to 61.1 °C in the blend with 10 wt % PBSA, which suggests slight miscibility between these two polys(esters). Higher PBSA contents of 30 wt % only promote a slight decrease in T_g down to values of 60.6 °C, which corroborates the restricted miscibility between PLA and PBSA. This slight change in the T_g by the addition of PBSA to PLA is a clear indication of restricted miscibility of these two biopolymers, as reported Lee and Lee [5]. Another important finding that can be outlined from DSC thermograms is the cold crystallization process. Although it overlaps with the melting process of PBSA, one important change can be identified. In particular, the cold crystallization process is moved toward lower temperatures, which means that the energy barrier for PLA crystallization is reduced. This could be due to partial miscibility between PLA and PBSA, but the most important mechanism that is responsible for this is the melting of the PBSA-rich phase that contributes to increase chain motion, thus allowing PLA chains to arrange into a packed structure at lower temperatures, due to the lubricant effect of the melted PBSA-rich phase, as reported by Lee and Lee [5] in previous researches. In particular, the cold crystallization peak temperature, T_{cc} is reduced below 100 °C, while the typical T_{cc} for neat PLA is close to 109 °C. As expected, the compatibilization effect that Joncryl® provides leads somewhat to a restriction in chain motion, thus leading to a slightly higher T_{cc} value, as compared to all other blends. This similar behaviour has been reported in PLA-based materials by Quiles-Carrillo, *et al.* [47] in PLA/Almond shell flour composites that were compatibilized with ESAO. The T_{cc} of PLA/ASF composites that were obtained were even higher than neat PLA. This shift of the cold crystallization process indicates that crystallites of PLA can be formed at lower temperatures due to the effect of PBSA, as suggested by Ojijo, *et al.* [39]. With regard to the melt peak

temperature of PLA (T_{m_PLA}), the changes are negligible. Neat PLA shows a T_m of 170.9 °C and the melt peak temperature of the PLA-rich phase in the binary PLA/PBSA blends decreases to 168 °C. Frenz, *et al.* [48] have reported an increase in the melt strength of PLA and other poly(esters) by the addition of chain extenders, such as Joncryl®, but no remarkable changes in the peak temperature can be observed.

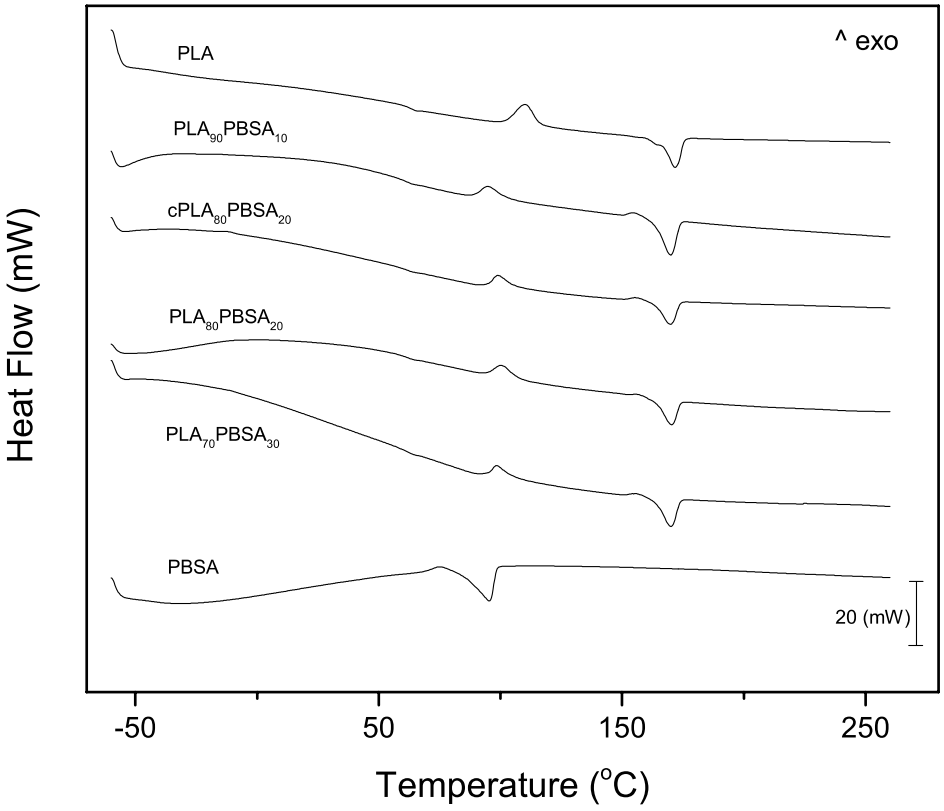

Figure III.1.1.4. Differential scanning calorimetry (DSC) scans (second heating cycle) corresponding to binary PLA/PBSA blends.

Table III.1.1.4. Main thermal parameters obtained by differential scanning calorimetry (DSC) and of binary PLA/PBSA blends.

Code	T_{g_PLA} (°C)	T_{cc_PLA} (°C)	T_{m_PLA} (°C)	T_{m_PBSA} (°C)
PLA	63.4 ± 0.6	109.9 ± 1.1	170.9 ± 3.3	-
$PLA_{90}PBSA_{10}$	61.1 ± 1.2	94.5 ± 1.7	168.9 ± 2.2	-
$cPLA_{80}PBSA_{20}$	61.1 ± 0.9	98.7 ± 1.4	168.8 ± 2.7	-
$PLA_{80}PBSA_{20}$	61.7 ± 0.6	100.3 ± 1.2	169.4 ± 2.6	-
$PLA_{70}PBSA_{30}$	60.6 ± 1.2	97.9 ± 1.0	168.7 ± 2.9	-
PBSA	-	-	-	95.2 ± 1.4

Regarding the thermal stability at high temperatures, figure III.1.1.5 gathers the comparative TGA degradation curves corresponding to the neat PLA, neat PBSA, and

PLA/PBSA blends. The TGA thermograms indicate that neat PLA and PLA/PBSA blends degradation occurs in a single step process. Regarding neat PBSA, its degradation process takes place in two stages. The first one occurs at about 400 °C, with an associated weight loss of around 90 %, and it is in accordance with Renoux, *et al.* [49]. The second stage is about 500 °C and only a 10 % weight loss occurs.

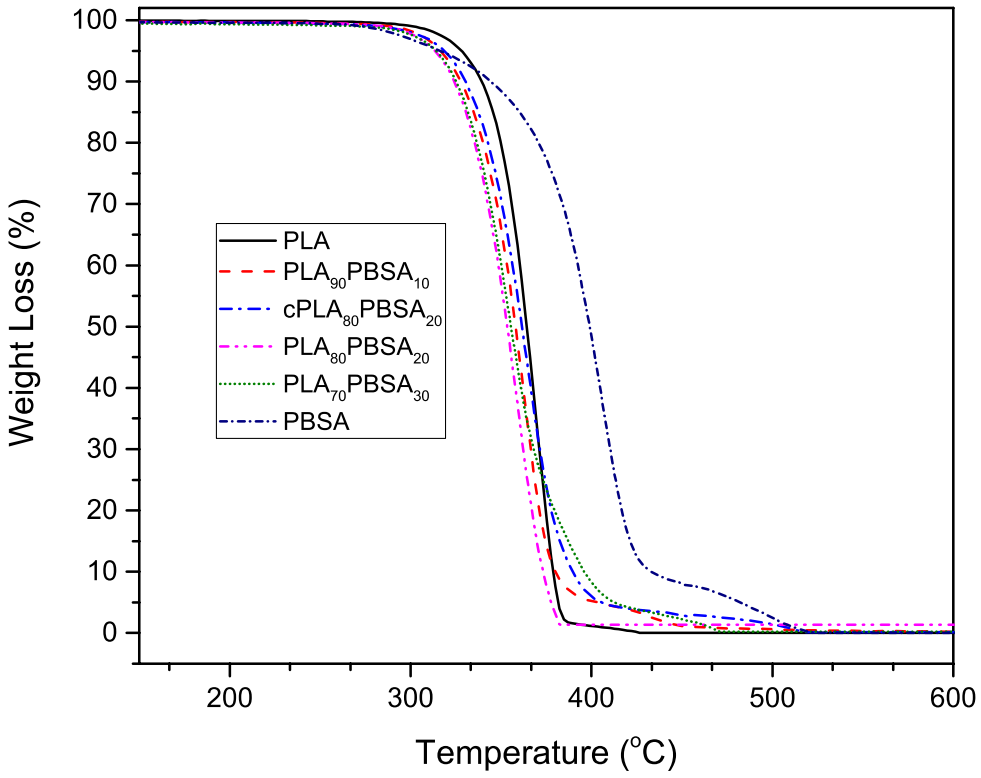

(a)

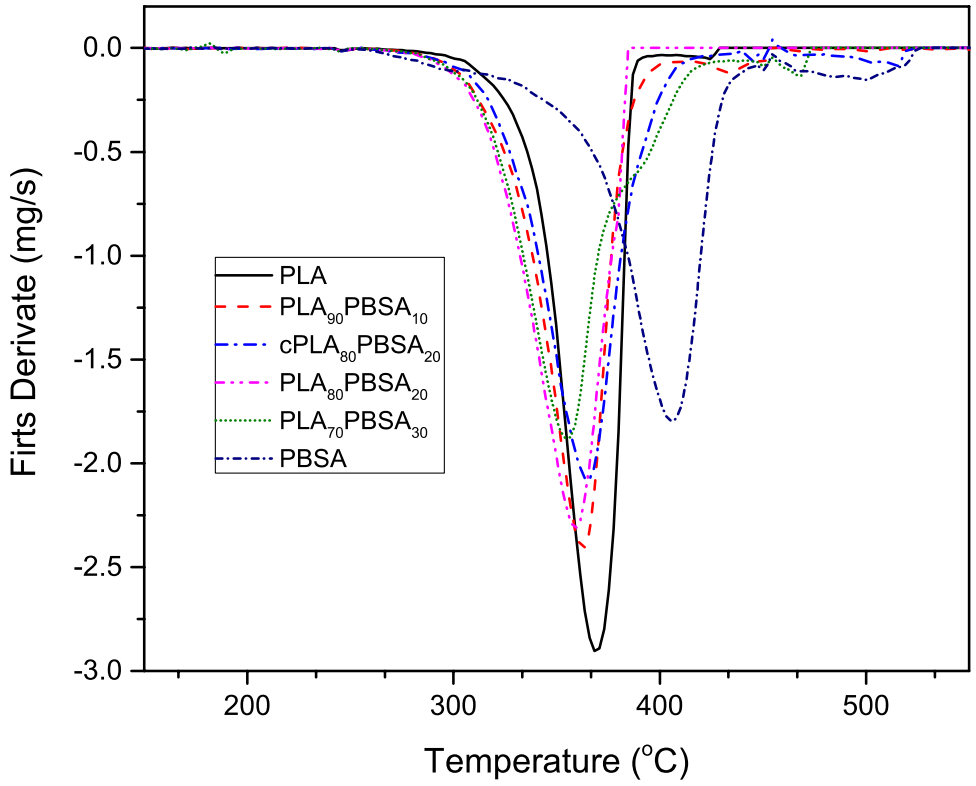

(b)

Figure III.1.1.5. Thermogravimetric (TGA) degradation curves corresponding to binary PLA/PBSA blends, (**a**) thermogravimetry (TG) mass loss and (**b**) differential thermogravimetry (DTG) first derivative.

Table III.1.1.5 shows the thermal parameters that are related to the different materials, specifically the characteristic temperatures at 5 % weight loss ($T_{5\%}$) and the maximum degradation rate temperature (T_{max}). Even though a slight decrease in the thermal stability in $T_{5\%}$ can be detected by the presence of PBSA, in general, it does not cause a noticeable effect in the PLA matrix. In fact, the PLA/PBSA blends show typical PLA behaviour. At high temperatures, a slight increase in thermal stability can be observed, the influence of PBSA on the PLA/PBSA mixtures is evident, since they show a behavior close to the PBSA at a temperature range that is close to its degradation, with neat PBSA being the most thermally stable. The compatibilization effect that Joncryl® provides leads to gaining thermal stability and it can be observed in figure III.1.1.5. The uncompatilized blend containing 20 wt % PBSA degrades at earlier temperature when compared with its compatibilized counterpart, which corroborates what Frenz, *et al.* [48] reported.

Table III.1.1.5. Main thermal parameters obtained by thermogravimetric analysis (TGA) of binary PLA/PBSA blends.

Code	TGA		
	$T_{5\%}$ (°C)	T_{Max} (°C)	$Mass_{Residual}$ (%)
PLA	328.7 ± 5.25	368.1 ± 6.3	0.05 ± 0.01
$PLA_{90}PBSA_{10}$	317.0 ± 4.4	362.5 ± 4.3	0.02 ± 0.02
$cPLA_{80}PBSA_{20}$	319.3 ± 3.5	365.4 ± 5.2	0.12 ± 0.02
$PLA_{80}PBSA_{20}$	312.3 ± 5.2	359.5 ± 5.4	1.37 ± 0.01
$PLA_{70}PBSA_{30}$	314.7 ± 4.7	355.8 ± 5.7	0.20 ± 0.01
PBSA	317.0 ± 5.7	405.3 ± 7.8	0.01 ± 0.01

Shape Memory Behaviour of Binary PLA/PBSA Blends

Several authors have proposed different techniques to characterize the shape memory behaviour in biopolymers, such as tensile and DMA tests [50,51]. These are specifically used to determine the recovery rate after subjecting the sample to a specific thermal cycle. Despite this, the use of a conventional bending test is widely used because of its simplicity and the quality of the information that it can provide. The measurement of the recovery angle is a qualitative/quantitative method to visualize the shape memory behavior and it represents a way to understand the shape memory behaviour of the blends and the effect of the PBSA addition. Table III.1.1.6 shows the recovery percentage of the neat PLA and PLA/PBSA blends after the programming and recovery cycle. As we expected, the neat PLA presents high values of shape memory reaching a recovery of 70 % and 58 % corresponding to the 90° and 120° flexural deformation, respectively. Notice that PLA shape memory effect works better for small deformations.

Table III.1.1.6. Shape memory behaviour parameters corresponding to binary PLA/PBSA blends.

Code	Permanent Shape (º)	Temporal Shape (º)	Final Shape (º)	Recovery (%)	Temporal Shape (º)	Final Shape (º)	Recovery (%)
PLA	180	90	153	70	120	155	58
$PLA_{90}PBSA_{10}$			155	72		158	63
$cPLA_{80}PBSA_{20}$			108	20		141	35
$PLA_{80}PBSA_{20}$			144	60		146	43
$PLA_{70}PBSA_{30}$			109	21		140	33

In fact, with the addition of PBSA, the PLA shape memory capability tends to decrease. It is worthy to note the particular case of $PLA_{90}PBSA_{10}$ shown in figure III.1.1.6b, e, which presents the best recovery behaviour of all of the developed materials, even better than the neat PLA. Tcharkhtchi, *et al.* [38] remarked that, to get an adequate shape memory effect, the PBS percentage must be of about 20 %, which gives consistency to the obtained results

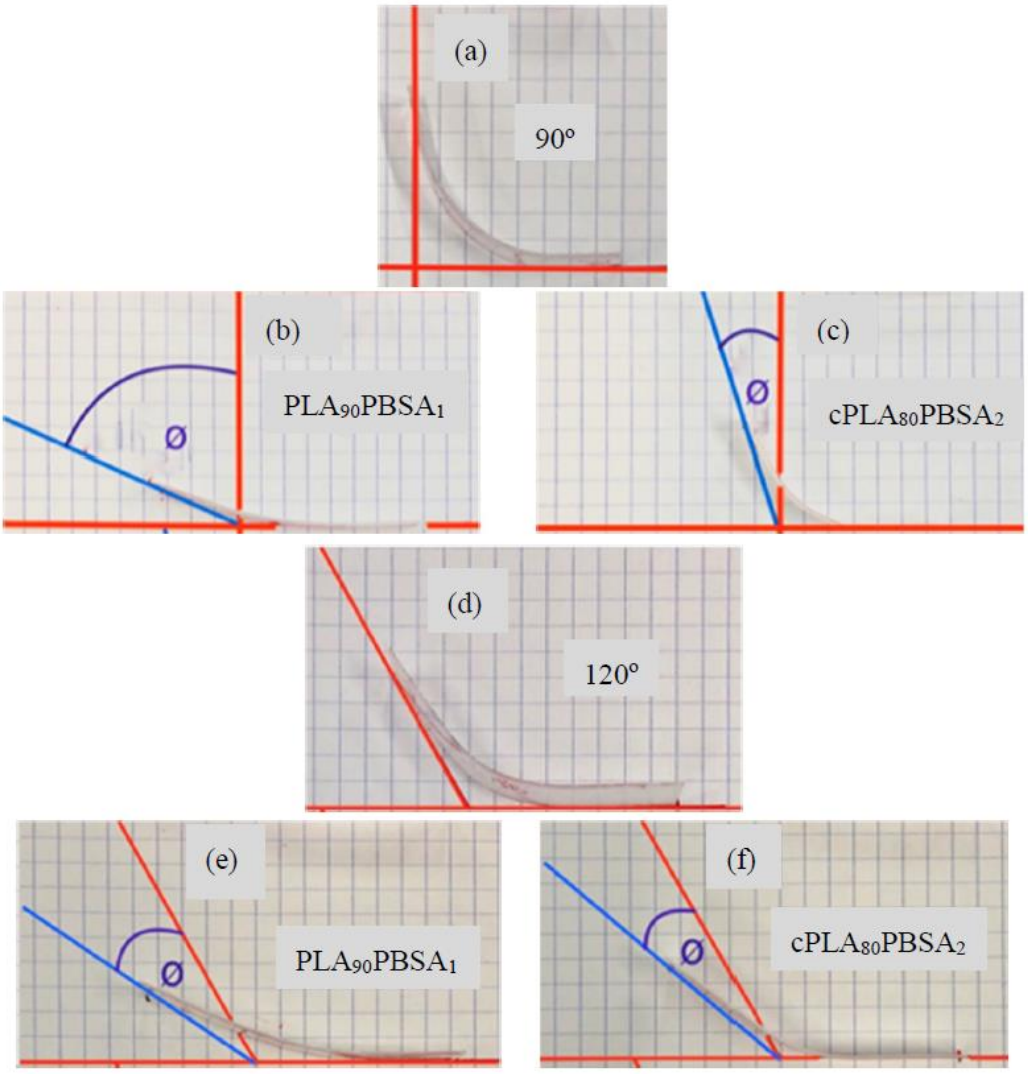

Figure III.1.1.6. Images of the shape memory behaviour of binary PLA/PBSA blends in flexural conditions with a permanent shape after deformation and shape recovery of (**a**) temporary shape (90°), (**b**) shape recovery of PLA90PBSA10 (90°), (**c**) shape recovery of cPLA80PBSA20 (90°), (**d**) temporary shape (120°), (**e**) shape recovery of PLA90PBSA10 (120°), and (**f**) shape recovery of cPLA80PBSA20 (120°).

The clear negative effect that is provided by Joncryl® is noticeable, since almost all of the shape memory capability of the mixtures is lost, reaching values 20 % and 35 %, corresponding to the 90° and 120° deformation, respectively, as can be seen in figure III.1.1.6c, f.

III.1.1.4. Conclusions

Injection molding and the hot-press molding process made binary PLA/PBSA blends. The influence of PBSA has a noticeable effect on mechanical performance, decreasing the tensile modulus and strength, which means that the brittle behaviour of the blends has diminished, thus leading to an increase in mechanical ductile properties. The compatibilized blend shows elongation at break values of 121 %, remarking the evidence of the compatibilization of these two polymers, adding up to the high values that were obtained in the impact test, suggesting the improvement on toughness.

The thermal analysis shows that the presence of PBSA induces a slightly decrease in PLA glass transition temperature (T_g), which corroborates the low miscibility between PLA and PBSA. The PBSA effect is noticeable in the PLA matrix, enhancing the PLA crystallization, and leading to a low cold crystallization temperature (T_{cc}). Although the presence of PBSA induced a decrease in the shape memory behavior on PLA, 10 wt % PBSA in a PLA/PBSA blends shows the best shape memory recovery, reaching values that were even better than PLA.

III.1.1.5. Funding

This research was supported by the Spanish Ministry of Economy and Competitiveness (MINECO) program numbers MAT2017-84909-C2-2-R. L.Q.-C wants to thank GV for his FPI grant (ACIF/2016/182) and the MECD for his FPU grant (FPU15/03812).

III.1.1.6. References

1. I. Vroman, L. Tighzert. Biodegradable polymers. *Materials* **2009**, *2*, 307-344.
2. L. Axelsson, M. Franzén, M. Ostwald, G. Berndes, G. Lakshmi, N. Ravindranath. Jatropha cultivation in southern India: assessing farmers' experiences. *Biofuels, Bioproducts and Biorefining* **2012**, *6*, 246-256.
3. L. Shen, J. Haufe, M.K. Patel. Product overview and market projection of emerging bio-based plastics PRO-BIP 2009. *Report for European polysaccharide network of excellence (EPNOE) and European bioplastics* **2009**, *243*, 1-245.
4. M. Brodin, M. Vallejos, M.T. Opedal, M.C. Area, G. Chinga-Carrasco. Lignocellulosics as sustainable resources for production of bioplastics–A review. *Journal of Cleaner Production* **2017**, *162*, 646-664.
5. S.-M. Lee, J.-W. Lee. Characterization and processing of biodegradable polymer blends of poly (lactic acid) with poly (butylene succinate adipate). *Korea-Australia Rheology Journal* **2005**, *17*, 71-77.
6. A. Matta, R.U. Rao, K. Suman, V. Rambabu. Preparation and characterization of biodegradable PLA/PCL polymeric blends. *Procedia materials science* **2014**, *6*, 1266-1270.
7. B. Geueke. Dossier—bioplastics as food contact materials. In Proceedings of Food Packag. Forum; 1-8.
8. A. Baran, P. Vrábel, D. Olčák, I. Chodák. Solid state 13C-NMR study of a plasticized PLA/PHB polymer blend. *Journal of Applied Polymer Science* **2018**, *135*, 46296.
9. C.P. Pokhrel, S. Ohga. Submerged culture conditions for mycelial yield and polysaccharides production by Lyophyllum decastes. *Food chemistry* **2007**, *105*, 641-646.
10. A. Bledzki, A. Jaszkiewicz. Mechanical performance of biocomposites based on PLA and PHBV reinforced with natural fibres–A comparative study to PP. *Composites science and technology* **2010**, *70*, 1687-1696.
11. D. Duesterhoeft. Congress, Legislation, etc.: About Congress. *Blume Library: LibGuide* **2016**, 10.1002/jbm.a.10416.
12. K. Sudesh, T. Iwata. Sustainability of biobased and biodegradable plastics. *CLEAN–Soil, Air, Water* **2008**, *36*, 433-442.

13. P. Gruber, M. O'Brien. Polylactides “Natureworks® PLA”. *Biopolymers Online: Biology• Chemistry• Biotechnology• Applications* **2005**, *4*.

14. M. Saleem, F. Tanveer, A. Ahmad, S.A. Gilani. Correlation between shoulder pain and functional disability. *Rawal Medical Journal* **2018**, *43*, 483-485.

15. S. Koide, J. Shi. Microbial and quality evaluation of green peppers stored in biodegradable film packaging. *Food Control* **2007**, *18*, 1121-1125.

16. M. Jonoobi, J. Harun, A.P. Mathew, K. Oksman. Mechanical properties of cellulose nanofiber (CNF) reinforced polylactic acid (PLA) prepared by twin screw extrusion. *Composites Science and Technology* **2010**, *70*, 1742-1747.

17. A.M. Harris, E.C. Lee. Improving mechanical performance of injection molded PLA by controlling crystallinity. *Journal of applied polymer science* **2008**, *107*, 2246-2255.

18. L. Serna, F. Albán. Ácido poliláctico (PLA): Propiedades y aplicaciones. *Ingeniería y competitividad* **2003**, *5*, 16-26.

19. S.H. Hyon. Biodegradable poly (lactic acid) microspheres for drug delivery systems. *Yonsei medical journal* **2000**, *41*, 720-734.

20. L. Jiang, M.P. Wolcott, J. Zhang. Study of biodegradable polylactide/poly (butylene adipate-co-terephthalate) blends. *Biomacromolecules* **2006**, *7*, 199-207.

21. E. Piorkowska, Z. Kulinski, A. Galeski, R. Masirek. Plasticization of semicrystalline poly (L-lactide) with poly (propylene glycol). *Polymer* **2006**, *47*, 7178-7188.

22. O. Martin, L. Avérous. Poly (lactic acid): plasticization and properties of biodegradable multiphase systems. *Polymer* **2001**, *42*, 6209-6219.

23. N. Burgos, V.P. Martino, A. Jiménez. Characterization and ageing study of poly (lactic acid) films plasticized with oligomeric lactic acid. *Polymer degradation and stability* **2013**, *98*, 651-658.

24. Y. Li, H. Shimizu. Toughening of polylactide by melt blending with a biodegradable poly (ether) urethane elastomer. *Macromolecular bioscience* **2007**, *7*, 921-928.

25. A. Bhatia, R.K. Gupta, S.N. Bhattacharya, H. Choi. Compatibility of biodegradable poly (lactic acid)(PLA) and poly (butylene succinate)(PBS) blends for packaging application. *Korea-Australia rheology journal* **2007**, *19*, 125-131.

26. M. Harada, T. Ohya, K. Iida, H. Hayashi, K. Hirano, H. Fukuda. Increased impact strength of biodegradable poly (lactic acid)/poly (butylene succinate) blend composites by using isocyanate as a reactive processing agent. *Journal of Applied Polymer Science* **2007**, *106*, 1813-1820.

27. S. Khatsee, D. Daranarong, W. Punyodom, P. Worajittiphon. Electrospinning polymer blend of PLA and PBAT: Electrospinnability–solubility map and effect of polymer solution parameters toward application as antibiotic-carrier mats. *Journal of Applied Polymer Science* **2018**, *135*, 46486.

28. S.-X. Qin, C.-X. Yu, X.-Y. Chen, H.-P. Zhou, L.-F. Zhao. Fully biodegradable poly (lactic acid)/poly (propylene carbonate) shape memory materials with low recovery temperature based on in situ compatibilization by dicumyl peroxide. *Chinese Journal of Polymer Science* **2018**, *36*, 783-790.

29. X. Fan, B.H. Tan, Z. Li, X.J. Loh. Control of PLA stereoisomers-based polyurethane elastomers as highly efficient shape memory materials. *ACS Sustainable Chemistry & Engineering* **2017**, *5*, 1217-1227.

30. T. Mu, L. Liu, X. Lan, Y. Liu, J. Leng. Shape memory polymers for composites. *Composites Science and Technology* **2018**, *160*, 169-198.

31. E.S. Gil, S.M. Hudson. Stimuli-reponsive polymers and their bioconjugates. *Progress in polymer science* **2004**, *29*, 1173-1222.

32. M. Balk, M. Behl, C. Wischke, J. Zotzmann, A. Lendlein. Recent advances in degradable lactide-based shape-memory polymers. *Advanced drug delivery reviews* **2016**, *107*, 136-152.

33. W. Liu, N. Wu, K. Pochiraju. Shape recovery characteristics of SiC/C/PLA composite filaments and 3D printed parts. *Composites Part A: Applied Science and Manufacturing* **2018**, *108*, 1-11.

34. H. Hong, J. Wei, Y. Yuan, F.P. Chen, J. Wang, X. Qu, C.S. Liu. A novel composite coupled hardness with flexibleness—polylactic acid toughen with thermoplastic polyurethane. *Journal of Applied Polymer Science* **2011**, *121*, 855-861.

35. Y. Tokiwa, A. Iwamoto. Enzymatic degradation of polymer blends. Doi, Y., Fukuda, K., Eds. Elsevier: 1994; Vol. 12, 136-149.

36. Y.-A. Chen, G.-S. Tsai, E.-C. Chen, T.-M. Wu. Thermal degradation behaviors and biodegradability of novel nanocomposites based on various poly [(butylene succinate)-co-adipate] and modified layered double hydroxides. *Journal of the Taiwan Institute of Chemical Engineers* **2017**, *77*, 263-270.

37. W. Pivsa-Art, S. Pivsa-Art, K. Fujii, K. Nomura, K. Ishimoto, Y. Aso, H. Yamane, H. Ohara. Compression molding and melt-spinning of the blends of poly (lactic acid) and poly (butylene succinate-co-adipate). *Journal of Applied Polymer Science* **2015**, *132*, 41856.

38. A. Tcharkhtchi, S.A. Elhirisia, K. Ebrahimi, J. Fitoussi, M. Shirinbayan, S. Farzaneh. Partial shape memory effect of polymers. In Proceedings of AIP Conference Proceedings; 278-281.

39. V. Ojijo, S. Sinha Ray, R. Sadiku. Role of specific interfacial area in controlling properties of immiscible blends of biodegradable polylactide and poly [(butylene succinate)-co-adipate]. *ACS applied materials & interfaces* **2012**, *4*, 6690-6701.

40. M. Nofar, A. Tabatabaei, H. Sojoudiasli, C.B. Park, P.J. Carreau, M.C. Heuzey, M.R. Kamal. Mechanical and bead foaming behavior of PLA-PBAT and PLA-PBSA blends with different morphologies. *European Polymer Journal* **2017**, *90*, 231-244.

41. L. Quiles-Carrillo, N. Montanes, C. Sammon, R. Balart, S. Torres-Giner. Compatibilization of highly sustainable polylactide/almond shell flour composites by reactive extrusion with maleinized linseed oil. *Industrial Crops and Products* **2018**, *111*, 878-888.

42. Y. Zhang, X. Yuan, Q. Liu, A. Hrymak. The effect of polymeric chain extenders on physical properties of thermoplastic starch and polylactic acid blends. *Journal of Polymers and the Environment* **2012**, *20*, 315-325.

43. M.J. Garcia-Campo, L. Quiles-Carrillo, J. Masia, M.J. Reig-Pérez, N. Montanes, R. Balart. Environmentally friendly compatibilizers from soybean oil for ternary blends of poly(lactic acid)-PLA, poly(ε-caprolactone)-PCL and poly(3-hydroxybutyrate)-PHB. *Materials* **2017**, *10*, 1339.

44. M. Villalobos, A. Awojulu, T. Greeley, G. Turco, G. Deeter. Oligomeric chain extenders for economic reprocessing and recycling of condensation plastics. *Energy* **2006**, *31*, 3227-3234.

45. H. Eslami, M.R. Kamal. Effect of a chain extender on the rheological and mechanical properties of biodegradable poly (lactic acid)/ poly [(butylene succinate) - co -adipate] blends. **2013**, 2418-2428.

46. L. Quiles-Carrillo, S. Duart, N. Montanes, S. Torres-Giner, R. Balart. Enhancement of the mechanical and thermal properties of injection-molded

polylactide parts by the addition of acrylated epoxidized soybean oil. *Materials and Design* **2018**, *140*, 54-63.

47. L. Quiles-Carrillo, N. Montanes, D. Garcia-Garcia, A. Carbonell-Verdu, R. Balart, S. Torres-Giner. Effect of different compatibilizers on injection-molded green composite pieces based on polylactide filled with almond shell flour. *Composites Part B: Engineering* **2018**, *147*, 76-85.

48. V. Frenz, D. Scherzer, M. Villalobos, A. Awojulu, M. Edison, R. Van Der Meer. Multifunctional polymers as chain extenders and compatibilizers for polycondensates and biopolymers. *Technical Papers, Regional Technical Conference - Society of Plastics Engineers* **2008**, *3*, 1678-1682.

49. J. Renoux, J. Dani, C. Douchain, K. Prashantha, P. Krawczak. Simultaneous plasticization and blending of isolate soy protein with poly[(butylene succinate)-co-adipate] by one-step extrusion process. *Journal of Applied Polymer Science* **2018**, *135*.

50. S. Dogan, S. Boyacioglu, M. Kodal, O. Gokce, G. Ozkoc. Thermally induced shape memory behavior, enzymatic degradation and biocompatibility of PLA/TPU blends:“Effects of compatibilization”. *Journal of the mechanical behavior of biomedical materials* **2017**, *71*, 349-361.

51. L. Peponi, I. Navarro-Baena, A. Sonseca, E. Gimenez, A. Marcos-Fernandez, J.M. Kenny. Synthesis and characterization of PCL–PLLA polyurethane with shape memory behavior. *European Polymer Journal* **2013**, *49*, 893-903.

Adaptado del artículo

III.1.2. Development of injection-molded polylactide pieces with high toughness by the addition of lactic acid oligomer and characterization of their shape memory behavior

Diego Lascano[1,2], Giovanni Moraga[1], Juan Ivorra-Martinez[1], Sandra Rojas-Lema[1,2], Sergio Torres-Giner [3], Rafael Balart[1], Teodomiro Boronat[1] and Luis Quiles-Carrillo[1]

[1] Technological Institute of Materials (ITM), Universitat Politècnica de València (UPV), Plaza Ferrándiz y Carbonell 1, 03801 Alcoy, Spain.

[2] Escuela Politécnica Nacional, 17-01-2759 Quito, Ecuador

[3] Novel Materials and Nanotechnology Group, Institute of Agrochemistry and Food Technology (IATA), Spanish National Research Council (CSIC), Calle Catedrático Agustín Escardino Benlloch 7, 46980 Paterna, Spain

polymers

Polymers **2019**, *11*(12), 2099

polymers

MDPI

Article

Development of Injection-Molded Polylactide Pieces with High Toughness by the Addition of Lactic Acid Oligomer and Characterization of Their Shape Memory Behavior

Diego Lascano [1,2], Giovanni Moraga [1], Juan Ivorra-Martinez [1], Sandra Rojas-Lema [1,2], Sergio Torres-Giner [3,*], Rafael Balart [1], Teodomiro Boronat [1] and Luis Quiles-Carrillo [1]

1 Technological Institute of Materials (ITM), Universitat Politècnica de València (UPV), Plaza Ferrándiz y Carbonell 1, 03801 Alcoy, Spain; dielas@epsa.upv.es (D.L.); giovannimoraga92@gmail.com (G.M.); juaivma@epsa.upv.es (J.I.-M.); sanrole@epsa.upv.es (S.R.-L.); rbalart@mcm.upv.es (R.B.); tboronat@dimm.upv.es (T.B.); luiquic1@epsa.upv.es (L.Q.-C.)

2 Escuela Politécnica Nacional, 17-01-2759 Quito, Ecuador

3 Novel Materials and Nanotechnology Group, Institute of Agrochemistry and Food Technology (IATA), Spanish National Research Council (CSIC), Calle Catedrático Agustín Escardino Benlloch 7, 46980 Paterna, Spain

* Correspondence: storresginer@iata.csic.es; Tel.: +34-963-900-022

Received: 11 November 2019; Accepted: 11 December 2019; Published: 14 December 2019

Abstract: This work reports the effect of the addition of an oligomer of lactic acid (OLA), in the 5–20 wt% range, on the processing and properties of polylactide (PLA) pieces prepared by injection molding. The obtained results suggested that the here-tested OLA mainly performs as an impact modifier for PLA, showing a percentage increase in the impact strength of approximately 171% for the injection-molded pieces containing 15 wt% OLA. A slight plasticization was observed by the decrease of the glass transition temperature (T_g) of PLA of up to 12.5 °C. The OLA addition also promoted a reduction of the cold crystallization temperature (T_{cc}) of more than 10 °C due to an increased motion of the biopolymer chains and the potential nucleating effect of the short oligomer chains. Moreover, the shape memory behavior of the PLA samples was characterized by flexural tests with different deformation angles, that is, 15°, 30°, 60°, and 90°. The obtained results confirmed the extraordinary effect of OLA on the shape memory recovery (R_r) of PLA, which increased linearly as the OLA loading increased. In particular, the OLA-containing PLA samples were able to successfully recover over 95% of their original shape for low deformation angles, while they still reached nearly 70% of recovery for the highest angles. Therefore, the present OLA can be successfully used as a novel additive to improve the toughness and shape memory behavior of compostable packaging articles based on PLA in the new frame of the Circular Economy.

Keywords: PLA; OLA; impact modifier; shape memory; packaging applications

1. Introduction

Polylactide (PLA) is a linear thermoplastic biodegradable polyester that can be obtained from starch-rich materials by fermentation to give lactide, which is polymerized at the industrial scale by ring-opening polymerization (ROP) [1]. PLA is a sound candidate to substitute some plastic commodities such as polypropylene (PP) or polystyrene (PS) in packaging applications [2–6], electronics [7], automotive [8], agriculture [9], textile, consumer goods, 3D printing applications [10–13], biomedical devices [14,15], pharmaceutical carriers [16,17], etc. The main advantage of PLA over

Development of injection-molded polylactide pieces with high toughness by the addition of lactic acid oligomer and characterization of their shape memory behavior

Abstract

This work reports the effect of the addition of an oligomer of lactic acid (OLA), in the 5-20 wt % range, on the processing and properties of polylactide (PLA) pieces prepared by injection molding. The obtained results suggested that the here-tested OLA mainly performs as an impact modifier for PLA, showing a percentage increase in the impact strength of approximately 171 % for the injection-molded pieces containing 15 wt % OLA. A slight plasticization was observed by the decrease of the glass transition temperature (T_g) of PLA of up to 12.5 °C. The OLA addition also promoted a reduction of the cold crystallization temperature (T_{cc}) of more than 10 °C due to an increased motion of the biopolymer chains and the potential nucleating effect of the short oligomer chains. Moreover, the shape memory behavior of the PLA samples was characterized by flexural tests with different deformation angles, that is, 15°, 30°, 60°, and 90°. The obtained results confirmed the extraordinary effect of OLA on the shape memory recovery (R_r) of PLA, which increased linearly as the OLA loading increased. In particular, the OLA-containing PLA samples were able to successfully recover over 95 % of their original shape for low deformation angles, while they still reached nearly 70 % of recovery for the highest angles. Therefore, the present OLA can be successfully used as a novel additive to improve the toughness and shape memory behavior of compostable packaging articles based on PLA in the new frame of the Circular Economy.

Keywords: PLA; OLA; impact modifier; shape memory; packaging applications

III.1.2.1. Introduction

Polylactide (PLA) is a linear thermoplastic biodegradable polyester that can be obtained from starch-rich materials by fermentation to give lactide, which is polymerized at the industrial scale by ring-opening polymerization (ROP) [1]. PLA is a sound candidate to substitute some plastic commodities such as polypropylene (PP) or polystyrene (PS) in packaging applications [2-6], electronics [7], automotive [8], agriculture [9], textile, consumer goods, 3D printing applications [10-13], biomedical devices [14,15], pharmaceutical carriers [16,17], etc. The main advantage of PLA over other biopolymers is its relatively low cost and overall balanced properties and processability [18,19], resulting in compostable articles [20]. In 2018, PLA production represented 10.3 % of the worldwide production capacity of bioplastics, reaching nearly 220,000 tons/year and it is estimated a growth around 60 % by 2023 [21].

Although PLA is a very versatile biopolymer, it results in extremely brittle materials with very low elongation at break and low toughness [22]. Many research works have been focused on overcoming or, at least, minimizing the intrinsic brittleness of PLA materials. One possible strategy is copolymerization with long aliphatic monomers, as suggested by Zhang, *et al.* [23]. This is the case of the new type of polyester amide (PEA) copolymers developed by Zou, *et al.* [24] combining poly(L-lactic acid) (PLLA) and poly(butylene succinate) (PBS) flexible segments. A similar approach was developed by Lan, *et al.* [25] based on PLA-*co*-PBS copolymers. Nevertheless, the most widely used approach is blending with other biopolymers due to its cost effectiveness. For instance, Garcia-Campo, *et al.* [26],[27] reported interesting toughening effects on ternary blends composed of PLA, poly(3-hydroxybutyrate) (PHB), and different rubbery polymers such as PBS, poly(butylene succinate-*co*-adipate) (PBSA) or poly(ε-caprolactone) (PCL). Recently, Sathornluck and Choochottiros [28] developed binary blends of PLA with epoxidized natural rubber (ENR), which can positively contribute to improving toughness due to the effect of the rubber phase finely dispersed in a brittle PLA matrix. Su, *et al.* [29] and Zhang, *et al.* [30] have also reported different approaches to overcome the intrinsic brittleness of PLA by adding different contents of PBS using reactive compatibilizers. Fortelny, *et al.* [31] recently reported, however, that it is possible to obtain “super-toughened” PLA formulations by blending PLA with poly(ε-caprolactone) (PCL) without any compatibilizer but using the appropriate PCL particle size. Addition of modified or unmodified particles is another way to overcome the intrinsic PLA brittleness. For instance, Wang, *et al.* [32] improved the PLA toughness by means of silanized helical carbon nanotubes (CNTs). Similarly, Li, *et al.* [33] reported the positive effect of cellulose nanofibers (CNFs) and a Surlyn® ionomer to improve the interfacial interaction between

CNFs and PLA, leading to a remarkable increase in toughness. The work carried out by Gonzalez-Ausejo, *et al.* [34] reported a clear improvement in toughness by using sepiolite nanoclays as gas barrier and compatibilizer in PLA/poly(butylene adipate-*co*-terephthalate) (PBAT) blends.

Even though copolymerization and blending are some of the most used procedures to overcome the intrinsic brittleness of PLA, plasticization is another interesting approach. Plasticizers have been widely used in PLA formulations to reduce fragility by decreasing the glass transition temperature (T_g). Plasticizers contribute to an increase in ductile properties, such as elongation at break, but mechanical resistant properties are also negatively decreased. Therefore, the use of plasticizers not always provides enhanced toughness since it depends on both ductile and resistant properties. For instance, Tsou, *et al.* [35] improved toughness of PLA by using an adipate ester plasticizer. It has also been reported the positive effect of combining two plasticizers: one solid plasticizer, namely poly(ethylene glycol) (PEG), and a liquid plasticizer derived from soybean oil [36]. Indeed, many research works have been focused on using environmentally friendly plasticizers, which can contribute to improving toughness without compromising the overall biodegradability of PLA. In this regard, Kang, *et al.* [37] described the usefulness of cardanol obtained from cashew nutshell liquid (CNSL) to obtain a 2.6-fold increase in toughness over neat PLA. Carbonell-Verdu, *et al.* [38] developed a new series of dual plasticizer and compatibilizer additives derived from cottonseed oil subjected to epoxidation and/or maleinization as an environmentally friendly solution instead of using conventional epoxy-styrene acrylic oligomers. Other similar multi-functionalized vegetable oils have demonstrated good compatibilizing effects on PLA [39,40] and on its blends with other biopolymers [41]. Ferri, *et al.* [42] recently reported a remarkable increase in toughness of neat PLA by using maleinized linseed oil (MLO) as a bio-based plasticizer, which yielded a slight plasticization that overlapped with chain extension, branching, and some cross-linking. Tributyl citrate (TBC) has also been proposed as an effective plasticizer for PLA by Notta-Cuvier*, et al.* [43], who reported the synergistic effect of TBC in PLA formulations containing halloysite nanotubes (HNTs).

Oligomers of lactic acid (OLAs) can also provide plasticization to PLA and PLA-based materials [44]. As reported by Burgos, *et al.* [45], OLAs can contribute to a significant decrease in T_g, though their role as impact modifiers require further research. Therefore, this study focuses on the effect of the addition of a new type of OLA on PLA pieces prepared by injection molding. In particular, the effect of varying the OLA content on the mechanical, thermal, thermomechanical properties and the morphology of PLA

was reported. Finally, the shape memory behavior of the pieces was analyzed and related to the OLA dispersion within the PLA matrix.

III.1.2.2. Materials and Methods

Materials

PLA was supplied by NatureWorks LLC (Minnetonka, MN, USA) as Ingeo™ Biopolymer 6201D. This PLA grade contains 2 mol % $_D$-lactic acid. It was supplied in pellet form and it had a density of 1.24 g cm^{-3} whereas its melt flow index (MFI) was 20 g/10 min, measured at 210 °C and 2.16 kg. OLA was kindly supplied by Condensia Química S.A. (Barcelona, Spain) as Glyplast OLA 2. It was provided in a liquid form with a viscosity of 90 mPa.s at 40 °C. According to the manufacturer, it has an ester content >99 %, a density of 1.10 g cm^{-3}, a maximum acid index of 2.5 mg KOH g^{-1}, and a maximum water content of 0.1 wt %.

Manufacturing of PLA/PBSA Binary Blends

As PLA is very sensitive to moisture, the biopolyester pellets were dried at 60 °C for 24 h. The OLA content varied in the 0–20 wt % at weight steps of 5 wt %. The terminology used for the formulations was “PLA-OLA x %”, where x represents the weight fraction of OLA in PLA. All the compositions were compounded in a twin-screw co-rotating extruder Coperion ZS-B 18 (Stuttgart, Germany) equipped with a main hopper in which the PLA pellets were fed and a side feeder for liquids to feed OLA. The liquid feeder was heated at 50 °C during compounding to decrease the OLA viscosity and allow efficient mixing. The rotating speed was set to 150 rpm while the temperature profile was modified according to the formulation as shown in table III.1.2.1. These temperatures were selected due to the change in viscosity produced by the OLA addition in order to optimize the processing conditions for each formulation. After extrusion, the different strands were cooled in air and then pelletized using an air-knife unit.

Table III.1.2.1. Temperature profile of the seven barrels in the twin-screw extruder during the compounding of the polylactide (PLA)/oligomer of lactic acid (OLA) formulations

PLA (wt %)	OLA (wt %)	T (°C) Zone 1	T (°C) Zone 2	T (°C) Zone 3	T (°C) Zone 4	T (°C) Zone 5	T (°C) Zone 6	T (°C) Zone 7
100	0	145	150	160	170	175	180	180
95	5	145	150	160	170	175	180	180
90	10	145	150	160	170	170	175	175
85	15	145	150	155	155	160	160	170

80	20	145	150	155	155	160	160	160

The compounded pellets were stored in an air-circulating oven at 60 °C for 24 h to avoid moisture gain. Standard samples for characterization were thereafter obtained in an injection molding machine Meteor 270/75 from Mateu & Solé (Barcelona, Spain). The temperature profile of the four barrels was programmed as indicated in table III.1.2.2. Similar to the extrusion process, it was necessary to optimize the temperature profile for each formulation due to the drop in the melt viscosity after the OLA addition.

Table III.1.2.2. Temperature profile of the four barrels and maximum pressure in the injection-molding machine during the manufacturing of polylactide (PLA)/oligomer of lactic acid (OLA) pieces.

PLA (wt%)	OLA (wt%)	T (°C) Zone 1	T (°C) Zone 2	T (°C) Zone 3	T (°C) Zone 4	Maximum Pressure (Bar)
100	0	175	180	185	190	93
95	5	175	180	185	190	90
90	10	160	165	170	175	118
85	15	150	155	165	170	120
80	20	145	150	155	165	125

Mechanical Properties

Mechanical properties of the OLA-containing PLA pieces were obtained in tensile conditions as indicated by ISO 527-1:1996. A universal testing machine ELIB 30 from S.A.E. Ibertest (Madrid, Spain) was used. At least six different samples were tested at room temperature using a load cell of 50 kN. The cross-head speed rate was set to 10 mm min^{-1}. As recommended by the standard, the tensile modulus (E_t), tensile strength at break (σ_b), and elongation at break ($\%\varepsilon_b$) were determined and averaged. The toughness was estimated using the Charpy method following the guidelines of ISO 179-1:2010 with a 6-J pendulum from Metrotec (San Sebastián, Spain). Unnotched rectangular samples with dimensions 80 x 10 mm^2 and a thickness of 4 mm were tested. The impact strength was obtained from testing five different samples and calculated as the absorbed-energy per unit area (kJ m^{-2}). The Shore D hardness was determined in a 673-D durometer from J. Bot Instruments (Barcelona, Spain) according to ISO 868:2003. Ten different measurements were collected from randomly selected zones and various samples were tested to obtain the average values.

Microscopy

The morphology of the fracture surfaces of the OLA-containing PLA pieces was studied by field emission scanning electron microscopy (FESEM) after the impact tests. A ZEISS Ultra 55 FESEM microscope from Oxford Instruments (Abingdon, UK) operating at 2 kV was used to collect the FESEM images at x1000. To avoid electrical charging during observation, samples were previously coated with an ultrathin gold-palladium alloy in an EMITECH SC7620 sputter-coater from Quorum Technologies Ltd. (East Sussex, UK) in an argon atmosphere.

Thermal Characterization

Thermal properties of the OLA-containing PLA pieces were obtained by differential scanning calorimetry (DSC) and thermogravimetric analysis (TGA). DSC characterization was performed on a Mettler-Toledo DSC calorimeter DSC821e (Schwerzenbach, Switzerland). To carry out the DSC runs, small specimens of each composition with an average weight of 5-7 mg were placed in standard aluminum crucibles with a total volume of 40 mL and sealed with a cap. Then, the samples were subjected to a three-step temperature program. A first heating cycle from 30 °C to 200 °C was followed by a cooling step down to -60 °C and, finally, a second heating cycle from -60 °C to 350 °C was applied. The heating and cooling rates were set to 10 °C min^{-1} whereas the selected atmosphere was nitrogen at a flow-rate of 30 mL min^{-1}. The resultant DSC curves allowed obtaining T_g, the cold crystallization peak temperature (T_{cc}), and the melting peak temperature (T_m). Besides, the cold crystallization (ΔH_{cc}) and melting enthalpies (ΔH_m) were obtained from the integration of the corresponding peaks. The maximum degree of crystallinity ($\%\chi_{cmax}$) was calculated as indicated in Equation (III.1.2.1):

$$\%\chi_{cmax} = \frac{\Delta H_m}{\Delta H_m^0} \cdot \frac{100}{w} \qquad \text{(III.1.2.1)}$$

where w (g) stands for the weight fraction of PLA and ΔH_m^o (J g^{-1}) represents the theoretical melting enthalpy of a fully crystalline PLA polymer, which is close to 93.7 J g^{-1} [46-49].

The effect of the OLA addition on the thermal stability of PLA was studied by TGA in a TGA/SDTA 851 thermobalance from Mettler-Toledo (Schwerzenbach, Switzerland). The temperature sweep was scheduled from 30 °C to 700 °C at a heating rate of 10 °C

min^{-1} in air atmosphere. Samples with an average weight comprised between 5 and 7 mg were placed on standard alumina crucibles and sealed with the corresponding cap. The onset degradation temperature, which was assumed at a weight loss of 5 wt % ($T_{5\%}$), and the maximum degradation rate temperature (T_{deg}) were obtained. All DSC and TGA tests were run in triplicate to obtain reliable results.

Viscosity Characterization

To study the influence of the OLA addition on the viscosity of PLA, cylindrical disks sizing 40 mm diameter and 5 mm thickness were manufactured by hot-press molding in a BUEHLER SimpliMet 1000 (Lake Bluff, IL, USA) at a temperature of 165 °C and a pressure of 7.5 ton. Parallel-plate oscillatory rheometry (OR) was conducted in an AR-G2 rheometer from TA Instruments (New Castle, DE, USA) to obtain the evolution of the complex viscosity (|η*|) as a function of the angular frequency. The selected isothermal temperature was 200 °C and the angular frequency varied in the 100-0.01 rad s^{-1} range. The maximum shear strain (γ) was set to 1 % and the tests were carried out in air atmosphere in triplicate.

Thermomechanical Characterization

The effect of the OLA addition on the thermomechanical behavior of PLA was carried out by dynamic mechanical thermal analysis (DMTA) in a DMA 1 from Mettler-Toledo (Schwerzenbach, Switzerland) working in single cantilever flexural conditions. Rectangular samples with dimensions of 10 x 7 mm^2 and a thickness of 4 mm were subjected to a dynamic heating program from -30 °C to 130 °C at a constant heating rate of 2 °C min^{-1}. The maximum deflection in the free edge was set to 10 μm and the selected frequency was 1 Hz. The storage modulus (*E'*) and the dynamic damping factor (*tan δ*) were collected as a function of increasing temperature.

The dimensional stability of the OLA-containing PLA pieces was studied by thermomechanical analysis (TMA) in a Q400 thermomechanical analyzer from TA Instruments (New Castle, DE, USA). The applied force was set to 0.02 N and the temperature program was scheduled from -30 to 120 °C in air atmosphere (50 mL min^{-1}) at a constant heating rate of 2 °C min^{-1}. The coefficient of linear thermal expansion (CLTE) of the PLA pieces, both below and above T_g, was determined from the change in dimensions versus temperature.

Characterization of the Shape Memory Behavior

The flexural method was used to evaluate the extension of the shape memory behavior. To this end, samples were compression-molded into sheets in the hot-press molding with a thickness of 0.4-0.5 mm. Two different parameters were then calculated to analyze the shape memory behavior in flexural conditions, namely the shape memory recovery (R_r) and stability ratio (R_f) [50,51]. The procedure is described as follows. In the first stage, the sheet specimens were deformed at a particular angle θ_f. For this, the samples were heated at 65 °C and forced to adapt between two aluminum sheets with different angles (15°, 30°, 60°, and 90°) to form a sandwich structure: aluminum/PLA sheet/aluminum. The sandwich was then clamped to allow a permanent deformation to the desired angle. Thereafter, the sandwich was cooled down to 14 °C to achieve its permanent shape after a slight temporary recovery of θ_t. Finally, the specimen was heated above its T_g in an air circulating oven at 65 °C for 3 min. After this, the final angle, that is, θ_f, was measured. At least three different sheets were tested for each composition to obtain reliable values. The same procedure has been used to characterize the shape recovery behavior in several polymer systems [52,53]. The values of R_f and R_r were calculated using the following equations:

$$\%R_f = \frac{(\pi - \theta_t)}{(\pi - \theta_f)} \quad \text{(III.1.2.2)}$$

$$\%R_r = \frac{(\pi - \theta_f)/(\pi - \theta_r)}{(\pi - \theta_f)} \quad \text{(III.1.2.3)}$$

III.1.2.3. Results and Discussion

Effect of OLA on the Mechanical Properties of PLA

Table III.1.2.3 gathers the main results obtained after the mechanical characterization of the PLA pieces with different OLA contents. As expected, the progressive addition of OLA led to lowering σ_b values from 64.6 MPa, for the neat PLA, down to 37.4 MPa, for the PLA pieces containing 20 wt % OLA. This decreasing tendency was almost linear as it can be seen in the table for the other compositions. This tendency on mechanical strength is the typical a plasticizer produces on the base polymer. Some other OLA additives have demonstrated a similar effect on mechanical properties by increasing remarkably ductility, mainly in the film form, as reported by Burgos, *et al.* [45]. In the latter work, it was reported an increase in ε_b from 4 % to 315 % with an OLA content of 25 wt %, but it is worthy to note the OLA previously used was designed for plasticization of PLA films. Such dramatic increase in the ε_b was not observed when

using OLA in this work since the primary use of this type of OLA was to improve impact strength, as indicated by the supplier and it will be discussed further.

Table III.1.2.3. Mechanical properties of the polylactide (PLA) pieces with different weight contents of oligomer of lactic acid (OLA) in terms of: tensile modulus (E_t), strength at break (σ_b), elongation at break (ε_b), impact strength, and Shore D hardness.

Piece	Tensile Tests			Impact Strength (kJ m^{-2})	Shore D Hardness
	E_t (MPa)	σ_b (MPa)	ε_b (%)		
PLA-OLA 0%	2251 ± 45	64.6 ± 1.1	7.9 ± 0.1	25.7 ± 2.7	78.8 ± 0.9
PLA-OLA 5%	2272 ± 94	52.0 ± 2.1	6.8 ± 0.3	30.4 ± 3.6	81.2 ± 1.4
PLA-OLA 10%	2300 ± 82	42.1 ± 1.7	5.6 ±0.2	54.2 ± 4.8	80.9 ± 2.3
PLA-OLA 15%	2400 ± 58	41.4 ± 1.0	5.3 ± 0.3	69.7 ± 5.2	80.9 ± 0.9
PLA-OLA 20%	2101 ± 91	37.4 ± 2.2	5.0 ± 0.2	38.4 ± 5.7	80.5 ± 0.4

Regarding mechanical ductility, the neat PLA piece showed a very low value of 7.9 % and the addition of OLA did not promote an increase in ε_b, but a slight decrease down to values of 5 %. It is not usual that a plasticizer promotes a decrease in ductility since the typical effect of a plasticizer is a decrease in the tensile resistant properties (σ_b and E_t) and an increase in ductile properties (ε_b). Nevertheless, it has been reported that some plasticizers promote a clear plasticization that is detectable by a decrease in T_g while no improvement in ductility occurs. This atypical behavior was reported by Ambrosio-Martin, *et al.* [54] in PLA films blended with different synthesized OLAs. A ε_b value of 5.25 % was reported for neat PLA, while the addition of 25 wt % of a purified OLA yielded a ε_b of 2.52 %. It was also reported a slight increase in E_t and an apparent decrease in σ_b, in a similar way as obtained in this work. It was concluded that, although there is clear evidence of the mechanical plasticization of OLA-containing PLA films, they were not more deformable, which is also in agreement with the work performed by Courgneau, *et al.* [55]. Concerning E_t, the neat PLA piece was characterized by a value of nearly 2.2 GPa and the values remained in the 2.2-2.4 GPa range after the addition of OLA. Thus, the main effect of this type of OLA on the tensile mechanical properties was a remarkable decrease in σ_b, which representative for some plasticization, but also a slight decrease in ε_b. Interestingly, as it can also be seen in table III.1.2.3**,** the addition of OLA successfully increased the impact strength of PLA. Neat PLA showed an impact strength of 25.7 kJ m^{-2}, which indicates a brittle behavior, and the only addition of 5 wt % OLA provided a slight increase in the impact strength to 30.4 kJ m^{-2}. Nevertheless, the most remarkable changes were obtained for OLA additions of 10 wt % and 15 wt %, showing impact strength values of 54.2 kJ m^{-2} and 69.7 kJ m^{-2}, respectively. Therefore,

the PLA piece with 15 wt % OLA presented the maximum impact strength with a percentage increase of approximately 171 % with regard to the neat PLA. It is also worthy to mention that the PLA piece containing 20 wt % OLA showed a decrease in impact strength in comparison with the other OLA-containing PLA pieces, thus suggesting certain OLA saturation in the PLA matrix. In this regard, Fortunati, *et al.* [56] reported the use of isosorbide diester (ISE) as plasticizer for PLA. It was observed plasticizer saturation at 20 wt % ISE and this was attributed to a limitation of T_g decrement. In addition, a noticeable decrease in ε_b was observed once the plasticizer saturation was achieved. Furthermore, Ferri, *et al.* [57] reported the plasticization of PLA by fatty acid esters, observing a remarkable decrease in impact strength above 5 parts per one hundred parts (phr) of PLA. Accordingly, a remarkable decrease in T_g was attained for contents of up to 5 phr whereas, above this, the T_g values did not change in a noticeable way, corroborating the relationship between the impact and thermal properties. Regarding hardness, one can observe that the Shore D values remained nearly constant after the OLA addition, showing values in the 78-82 range. Therefore, the most important feature this OLA can potentially provide to the mechanical properties of PLA is a remarkable improvement in impact strength while the elasticity can be slightly improved and ductility reduced. This particular mechanical behavior could be ascribed to an increase in the sample crystallinity and also to the presence of soft domains of OLA dispersed within the PLA matrix, simultaneously improving impact strength and reducing flexibility.

As previously indicated, one of the most widely used strategies to improve toughness in PLA-based formulations is blending with rubber-like polymers such as PCL [58], PBS [29,59], or PBAT [60,61]. In these immiscible blends, the energy absorption is related to presence of finely dispersed rubber-like small polymer droplets embedded in the brittle PLA matrix. In some cases, a synergistic effect can be found when different reactive or non-reactive compatibilizers are used. In this work, OLA has the same chemical structure than PLA, thus leading to miscibility without the need of compatibilizers. In this regard, Burgos, *et al.* [45] have reported the similarity between the solubility parameters of both PLA and OLA, which plays an essential role in miscibility. According to this, figure III.1.2.1 gathers the FESEM images corresponding to the fracture surfaces from the impact tests of the PLA pieces with the different OLA loadings. figure III.1.2.1a shows the fracture surface of the neat PLA piece. As one can observe in this micrograph, the surface was smooth with multiple microcracks presence, which is an indication of a brittle behavior. As opposite, figure III.1.2.1b shows that the fracture surface morphology of the PLA piece with 5 wt % OLA changed noticeably.

Phase separation could not be detected due to the high chemical affinity between PLA and OLA and the microcracks were not observed but, in contrast, macrocracks were produced. Therefore, the presence of OLA seems to inhibit microcrack formation and growth and, therefore, the cracks could grow to a greater extent thus leading to a rougher surface that is responsible for higher energy absorption during impact. Figure III.1.2.1c,d show the FESEM images corresponding to the fracture surfaces of the PLA pieces with 10 wt % and 15 wt % OLA, respectively. In these images, the above-mentioned effect was more intense then showing rougher surfaces that are related to enhanced energy absorption. Finally, figure III.1.2.1e shows that the PLA piece containing 20 wt % OLA presented a similar fracture surface than the other pieces and, despite there was a clear loss of toughness, its morphology did not allow identifying phase separation.

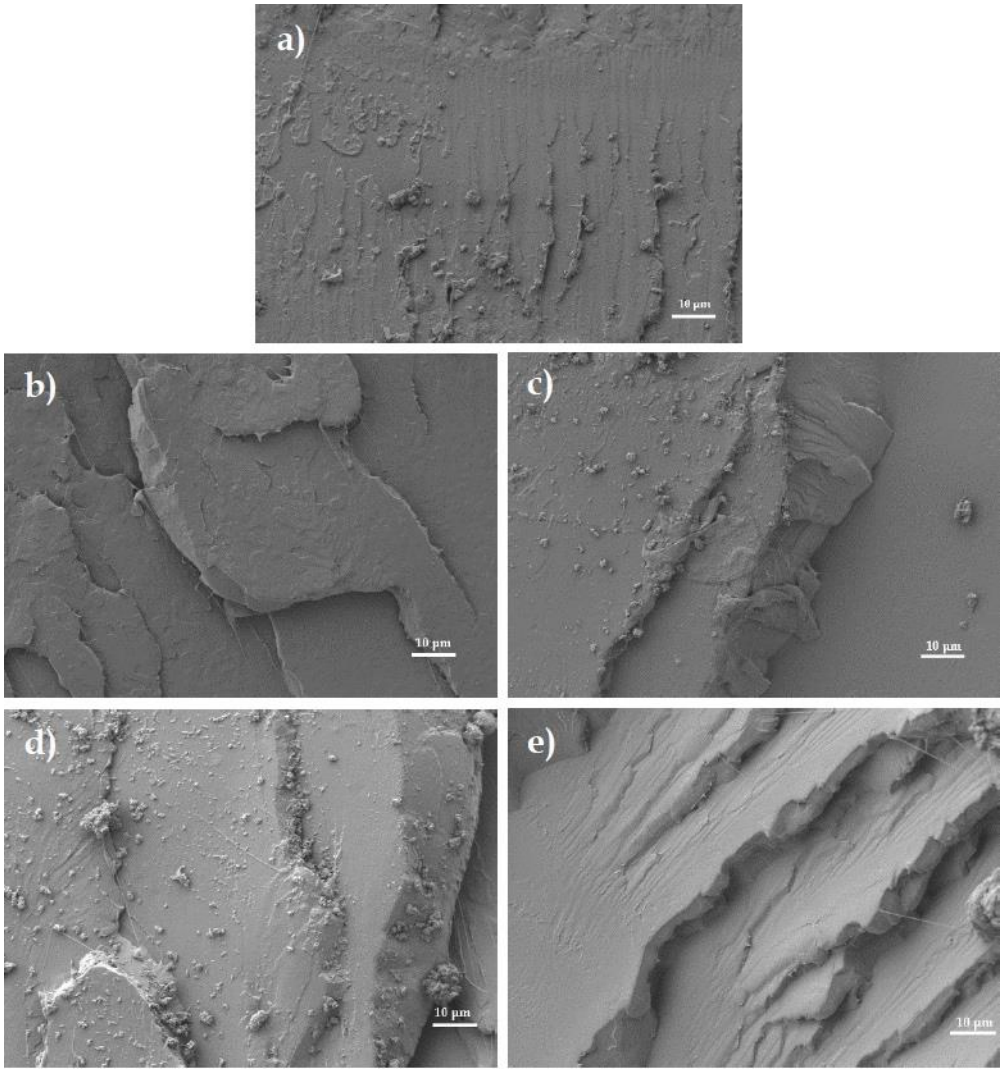

Figure III.1.2.1. Field emission scanning electron microscopy (FESEM) images of the fracture surfaces of the of the polylactide (PLA) pieces with different weight contents of oligomer of lactic acid (OLA): (**a**) 0 wt %; (**b**) 5 wt %; (**c**) 10 wt %; (**d**) 15 wt %; and (**e**) 20 wt %. Images were taken at 1000× and scale markers are of 10 µm.

Effect of OLA on the Thermal and Rheological Properties of PLA

Figure III.1.2.2 shows a comparative graph with the characteristic DSC thermograms during first heating corresponding to the neat PLA piece and the PLA pieces with different OLA loadings. Table III.1.2.4 summarizes the main thermal values obtained from the thermograms. One can observe that T_g of neat PLA was located close to 63 °C. Then, the PLA sample cold crystallized indicating that the biopolyester chains could not crystallize in the injection mold. The process of cold crystallization was characterized by a peak at 109.8 °C. Finally, the melting process was defined by a peak temperature of 170.9 °C in which the whole crystalline fraction melted. The effect of the OLA addition on the thermal properties was remarkable. Concerning T_g, a clear decreasing tendency can be observed. In particular, T_g was reduced after the OLA addition down to 50.8 °C, thus indicating plasticization. Ambrosio-Martin, *et al.* [54] reported a decrease in T_g with addition of OLA to PLA films from 60 °C to 27.7 °C, concluding that this fact is directly related to the mechanical properties of OLA and it depends on the synthesis procedure [62]. In the present work, the T_g value of PLA decreased after the addition of OLA but this reduction was much lower than other reported to other plasticizers. For instance, Ljungberg and Wesslen [63] reported a T_g decrease of 30 °C with 15 wt % addition of different plasticizers such as triacetin, tributyl citrate (TBC), triethyl citrate (TEC), acetyl tributyl citrate (ATBC), and acetyl triethyl citrate (ATEC).

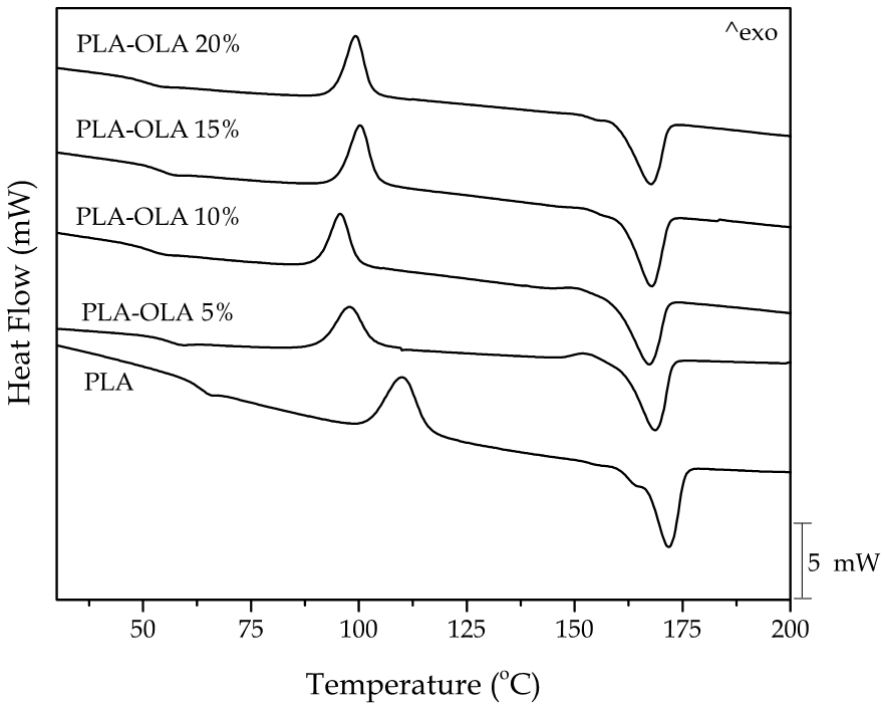

Figure III.1.2.2. Differential scanning calorimetry (DSC) thermograms corresponding to the polylactide (PLA) pieces with different weight contents of oligomer of lactic acid (OLA).

Table III.1.2.4. Thermal properties of the polylactide (PLA) pieces with different weight contents of oligomer of lactic acid (OLA) in terms of: glass transition temperature (T_g), cold crystallization temperature (T_{CC}), cold crystallization enthalpy (ΔH_{cc}), melting temperature (T_m), melting enthalpy (ΔH_m), and degree of crystallinity (χ_{cmax}).

Piece	T_g (°C)	T_{cc} (°C)	ΔH_{cc} (J g^{-1})	T_m (°C)	ΔH_m (J g^{-1})	χ_{cmax} (%)
PLA-OLA 0%	63.3 ± 1.5	109.8 ± 3.8	28.6 ± 0.8	170.9 ± 1.7	33.4 ± 1.6	35.6 ± 1.7
PLA-OLA 5%	55.9 ± 2.4	97.8 ± 2.1	22.5 ± 5.1	168.2 ± 2.4	46.2 ± 4.5	51.9 ± 4.7
PLA-OLA 10%	53.9 ± 1.9	100.1 ± 2.5	21.9 ± 1.7	167.1 ± 3.0	46.3 ± 4.8	54.9 ± 5.3
PLA-OLA 15%	51.3 ± 0.4	96.7 ± 2.1	26.3 ± 3.8	166.5 ± 2.1	42.4 ± 2.1	53.2 ± 2.5
PLA-OLA 20%	50.8 ± 3.2	99.1 ± 2.4	25.0 ± 2.5	166.9 ± 1.8	34.3 ± 3.2	45.8 ± 4.0

Furthermore, the added OLA induced an internal lubricating effect that shifted the cold crystallization of PLA to lower temperatures due to an increase of chain mobility. Then T_{cc} lowered to values in the range of 96-101 °C with the different OLA loadings. Other authors suggested a specific nucleating effect provided by the short length OLA molecules, which are more readily to pack the PLA macromolecular structure thus favoring the cold crystallization process [64]. In addition, a small and broad exothermic peak was seen in the PLA sample processed with OLA, particularly noticeable at the lowest OLA contents. This exothermic peak is related to a pre-melt crystallization just before melting. In this regard, one can consider that the presence of OLA promoted the formation of different crystallites [63]. As reported by Maróti, *et al.* [65] and also Maiza, *et al.* [66], this peak has been observed in neat PLA depending on the heating rate and the applied thermal cycle. One can also observe a slight decrease in the T_m value with the increasing OLA content. Similar findings have been reported by Burgos, *et al.* [62] in PLA films with different OLAs.

In addition to the characteristic values of T_g, T_{cc}, and, T_m, the enthalpies corresponding to the cold crystallization and melting processes, that is, ΔH_{cc} and ΔH_m, respectively, were collected. The maximum degree of crystallinity, that is, χ_{cmax}, which does not consider the amount of crystals formed during cold crystallization, was 35.6 % for the neat PLA. Then, χ_{cmax} increased up to values of around 50 % for the compositions containing 5-15 wt % OLA, while slightly lower values of crystallinity were obtained for

the composition containing 20 wt % OLA, that is, 45.8 %. This increase in crystallinity can be related to the plasticizing effect of OLA, as earlier reported by Burgos, *et al.* [62] in PLA formulations with 15 wt % of different OLAs. This latter study also reported a decrease in the T_m value of approximately 5 °C.

Regarding thermogravimetric characterization, figure III.1.2.3 shows the mass versus temperature (figure III.1.2.3a) and the first derivative (DTG) versus temperature (figure III.1.2.3b) curves for all the PLA pieces. The main results of the thermal decomposition of PLA-OLA blends are summarized in table III.1.2.5. One can observe that the neat PLA was much more thermally stable than the toughened PLA formulations with the different OLA loadings. As the OLA content increased, the characteristic TGA curves in figure III.1.2.3a shifted to lower temperatures, thus indicating a decrease in thermal stability. DTG curves were very useful to determine the maximum degradation rate temperature (T_{deg}), which was seen as peaks in figure III.1.2.3b. It can be seen in the graph that there was a clear decreasing tendency of T_{deg} with increasing OLA content. Furthermore, the residual mass for all PLA formulations with OLA was almost the same, being below 1 wt %.

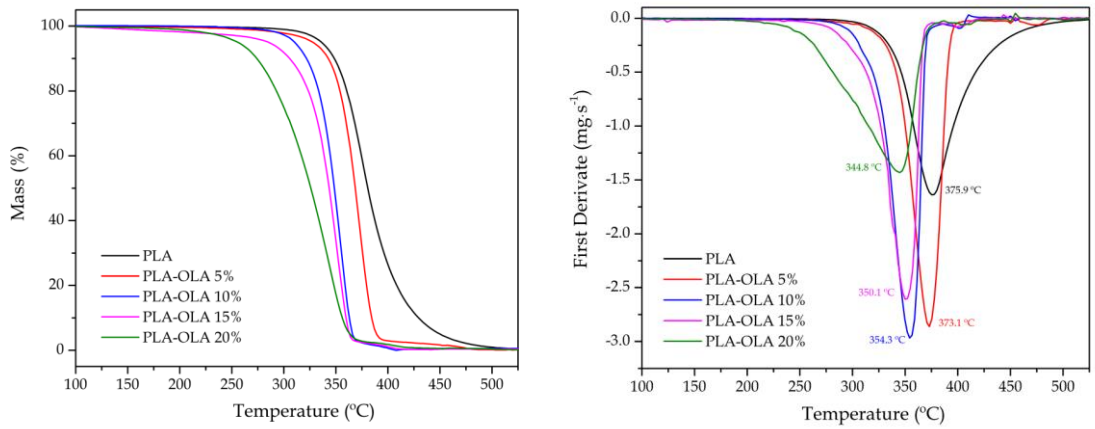

(**a**) (**b**)

Figure III.1.2.3. (**a**) Thermogravimetric analysis (TGA) and (**b**) first derivate thermogravimetric (DTG) curves corresponding to the polylactide (PLA) pieces with different weight contents of oligomer of lactic acid (OLA).

Table III.1.2.5. Main thermal parameters of the polylactide (PLA) pieces with different weight contents of oligomer of lactic acid (OLA) in terms of: onset temperature of degradation ($T_{5\%}$), degradation temperature (T_{deg}), and residual mass at 700 °C.

Piece	$T_{5\%}$ (°C)	T_{deg} (°C)	Residual Mass (%)
PLA-OLA 0%	336.1 ± 2.7	375.9 ± 1.9	0.11 ± 0.02

PLA-OLA 5%	327.2 ± 1.2	373.1 ± 2.3	0.57 ± 0.08
PLA-OLA 10%	310.1 ± 3.2	354.3 ± 3.1	0.65 ± 0.12
PLA-OLA 15%	296.5 ± 3.8	350.1 ± 1.8	0.39 ± 0.08
PLA-OLA 20%	254.8 ± 2.8	344.8 ± 2.6	0.53 ± 0.07

Therefore, OLA induced a remarkable reduction in the thermal stability of PLA, as similarly described by Ambrosio-Martin, *et al.* [54]. In this regard, Burgos, *et al.* [62] also reported individual TGA characterization of different OLAs with their corresponding thermal degradation parameters. A variation in the onset degradation temperature was observed from 179 °C to 214 °C. The lower thermal stability was related to the lower T_g values. Moreover, it was reported a maximum degradation rate temperature ranging from 259 °C to 291 °C. These characteristic degradation temperatures are remarkably lower than those of the neat PLA herein studied. As the OLA content in PLA pieces increased, both the $T_{5\%}$ and the T_{max} values showed a clear decreasing tendency. This decrease was more pronounced in the case of $T_{5\%}$, which varied from 336.1 °C, for the neat PLA piece, to 254.8 °C, for the PLA piece containing 20 wt % OLA.

As indicated previously, OLA provided a lubricating effect, which could potentially lead to a subsequent decrease in the viscosity. Figure III.1.2.4 shows the effect of the different OLA loadings on the $|\eta^*|$ values of the PLA sheets as a function of the angular frequency. As it can be seen, the effect of the angular frequency on the complex viscosity was not highly pronounced but it was possible to detect a decreasing tendency of $|\eta^*|$ with increasing the OLA content. This confirms that OLA lowers the viscosity of the PLA melt during processing and it can therefore potentially act as a processing aid. In fact, as indicated previously, it was necessary to adjust the thermal profile for optimum processing when the OLA content was modified.

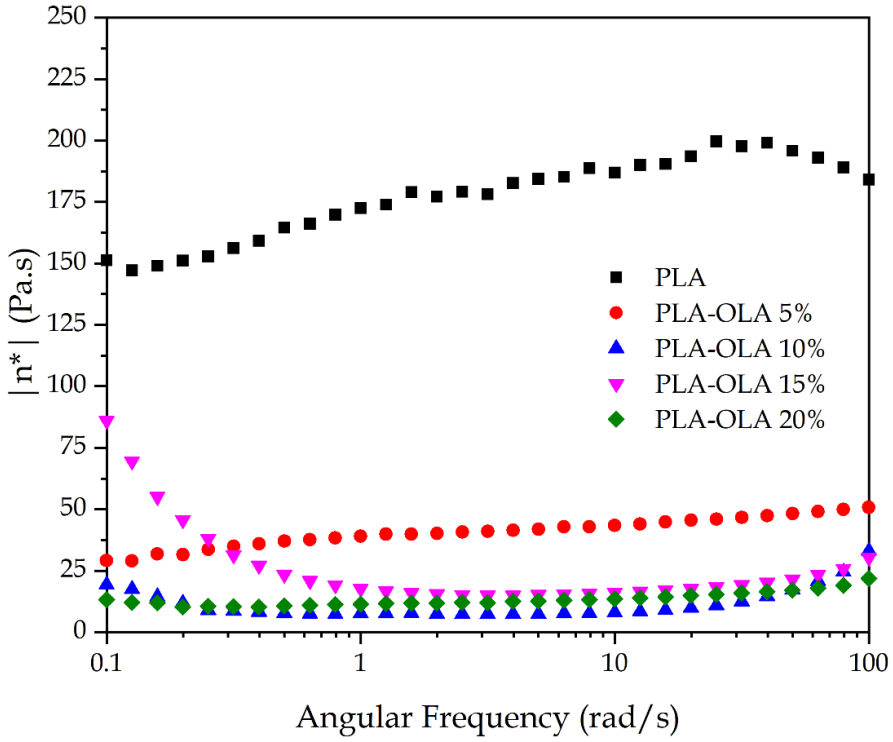

Figure III.1.2.4. A comparative plot of the complex viscosity (|η*|) of the polylactide (PLA) sheets with different weight contents of oligomer of lactic acid (OLA) at a constant temperature of 200 °C as a function of increasing angular frequency.

Effect of OLA on the Thermomechanical Properties of PLA

The results described above indicated a definite improvement in the PLA toughness by using OLA as an impact modifier. Mechanical characterization showed a decrease in mechanical strength while ductility was also slightly reduced. DMTA allows characterization of mechanical properties in dynamic conditions (sinusoidal applied stress) as a function of a heating cycle. Figure III.1.2.5 shows the DMTA curves for the neat PLA piece and the PLA pieces containing different loadings of OLA. The results of the thermomechanical properties obtained by DMTA are summarized in table III.1.2.6. The variation of the *E'* values of the neat PLA (figure III.1.2.5a) showed a dramatic drop between 50 °C and 70 °C, which is representative of the α-relaxation process of the PLA chains as the glass transition region was surpassed. In particular, a three-fold decrease in *E'* was observed. As the OLA loading increased, the *E'* curves shifted to lower temperatures thus indicating a decrease in T_g, as previously observed by DSC analysis. In particular, the *E'* values decreased from 1500 MPa, for the neat PLA piece, to 1197 MPa, for the PLA piece blended with 20 wt % OLA at 30 °C. As reported by other authors, both nucleating agents and plasticizers play a crucial role in the DMTA behavior of PLA [67,68]. Although the characteristic *E'* curves showed a decrease in T_g, more accurate values can be obtained by determining the peak maximum of tan *δ*, as observed in figure

III.1.2.5b. Neat PLA showed a T_g of 68.2 °C and the T_g values decreased progressively as the OLA loading increased, reaching a minimum value of 49.4 °C for the PLA piece containing 20 wt % OLA. These results are in total agreement with the above-described results obtained during the DSC characterization.

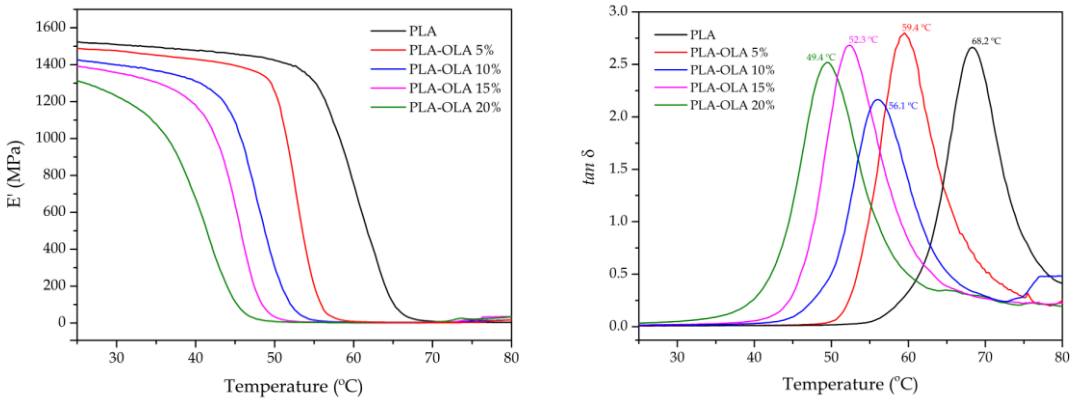

(**a**) (**b**)

Figure III.1.2.5. Evolution as a function of temperature of the (**a**) storage modulus (E') and (**b**) dynamic damping factor (*tan δ*) of the polylactide (PLA) pieces with different weight contents of oligomer of lactic acid (OLA).

Table III.1.2.6. Main thermomechanical parameters of the polylactide (PLA) pieces with different weight contents of oligomer of lactic acid (OLA) in terms of: storage modulus (E') measured at 30 °C and 70 °C, glass transition temperature (T_g), and coefficient of linear thermal expansion (CLTE) below and above T_g.

Piece	**DMTA**			**TMA**	
	E' at 30 °C (MPa)	*E'* at 70 °C (MPa)	T_g * (°C)	CLTE below T_g ($\mu m\ m^{-1}\ K^{-1}$)	CLTE above T_g ($\mu m\ m^{-1}\ K^{-1}$)
PLA-OLA 0%	1500 ± 55	4.9 ± 0.3	68.2 ± 1.2	79.9 ± 3.5	155.4 ± 6.2
PLA-OLA 5%	1467 ± 49	2.4 ± 0.2	59.4 ± 1.4	87.1 ± 4.0	166.4 ± 7.9
PLA-OLA 10%	1389 ± 52	4.6 ± 0.4	56.1 ± 0.7	88.9 ± 3.8	173.8 ± 6.2
PLA-OLA 15%	1343 ± 38	5.2 ± 0.6	52.3 ± 0.9	90.1 ± 1.9	179.9 ± 7.1
PLA-OLA 20%	1197 ± 47	9.9 ± 1.1	49.4 ± 0.8	91.6 ± 3.9	184.5 ± 6.8

Another attractive thermomechanical property is the effect of temperature on the dimensional stability of the PLA-based materials with different OLA loadings. TMA is a

very useful technique to determine the CLTE values, which is a crucial property related to dimensional stability in terms of temperature exposition. Table III.1.2.6 gathers these coefficients for the neat PLA piece and the PLA pieces containing different amount of OLA. As one can observe in the table, two different CLTE values were determined, one corresponding to the slope below T_g and another one corresponding to that above T_g. Plasticization can be observed by seeing the CLTE both below and above T_g. A slight increasing tendency was obtained, thus, indicating more ductility. The CLTE below T_g changed from 79.9 μm m^{-1} K^{-1} to 91.6 μm m^{-1} K^{-1}. The maximum change was therefore 11.7 μm m^{-1} K^{-1}, which is a very narrow range, typical of values below T_g then indicating excellent dimensional stability. Above T_g, the maximum change was 29.1 μm m^{-1} K^{-1}, which is in accordance with the typical plastic thermomechanical behavior above T_g.

Effect of OLA on the Shape Memory Behavior of PLA

Initially, the shape memory behavior was studied qualitatively by introducing the sheet specimens into a glass tube at room temperature, as observed in figure III.1.2.6a, and remained inside for 5 min to retain the shape. Then, the crimped PLA sheets were immersed in a water bath at 70 °C, above the biopolyester's T_g, and allowed to recover their shape. As can it be seen in figure III.1.2.5b, flat sheet shapes were obtained for the PLA materials containing >10 wt % OLA loadings in a short period of 4-10 s, therefore giving support to the significant effect of OLA on the shape memory behavior of PLA. Similar results, under the same conditions, were reported in the development of poly(l-lactide-*co*-ε-caprolactone) (PLACL), which showed recovery times of approximately 20 s [69]. Another study was focused on PLA/thermoplastic polyurethane (TPU) blends in which the recovery times at 70 °C were very similar to those obtained in this work, that is, 7-12 s [50].

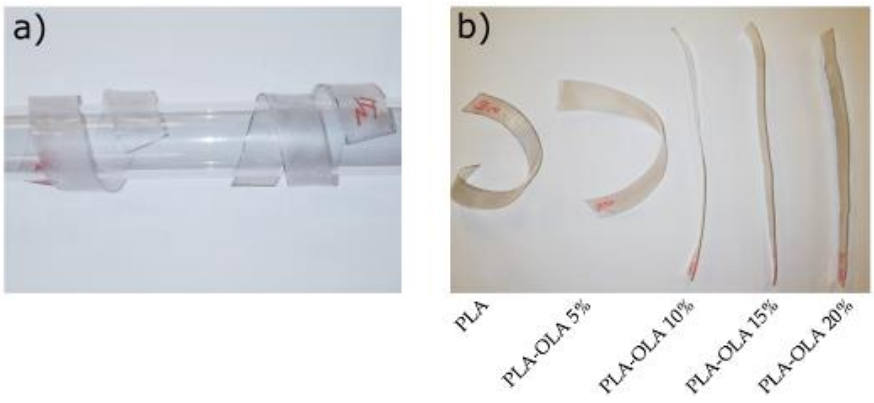

Figure III.1.2.6. Photographs of the qualitative study of the shape memory recovery capacity of the polylactide (PLA) sheets with different weight contents of oligomer of lactic acid (OLA): (**a**) initial deformation of the sheets by introducing them into a glass tube and (**b**) recovered shape of the sheets after heating at 70 °C.

In addition to the qualitative characterization shown above, a quantitative study was carried out to evaluate the influence of the OLA impact modifier on the shape memory behavior of PLA. Figure III.1.2.7 shows the evolution of R_r for different angles as the OLA content was increased. As it can be seen in the plot, the neat PLA sheet showed limited shape recovery properties and, obviously, it highly depended on the deformation angle. This shape memory recovery was close to 77 % for a deformation angle of 90° and it was remarkably lower with more aggressive deformations. For instance, PLA could only recover 55.5 % when the initial deformation angle was 15°. As the OLA loading increased, the ability of PLA to recover its initial flat shape (angle of 180°) increased considerably. It is worthy to note the effect of the addition of 20 wt % OLA, which yielded an almost constant increase in R_r of approximately 20 % for all the tested angles. Therefore, for this OLA loading, the shape recovery ability of PLA remarkably improved thus leading to an exciting shape memory behavior. As reported by Leones, *et al.* [70], a good shape memory behavior can be attained in electrospun PLA-based fibers containing different OLA loadings in the 10-30 wt % range.

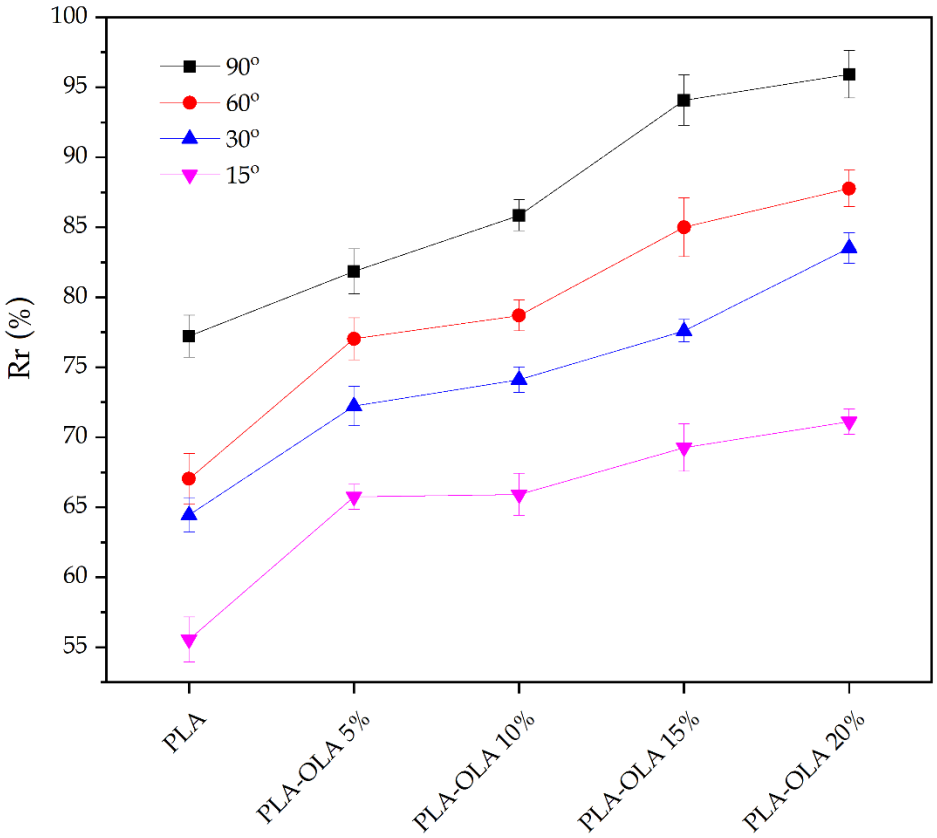

Figure III.1.2.7. Evolution of the percentage of shape memory recovery (%R_r) of polylactide (PLA) sheets with different weight contents of oligomer of lactic acid (OLA) at different initial deformation angles: 15°, 30°, 60°, and 90°.

The R_f value is representative for the dimensional stability below T_g, after an initial deformation. As it can be seen in table III.1.2.7, R_f was very high for all the systems, thus indicating excellent dimensional stability after the first deformation. In general, as the deformation angle was lower, for instance 90º, the stability ratio was higher, showing recovery values over 98 %. Alternatively, if the initial deformation angle was very aggressive, for instance 15°, a slight decrease in the stability ratio can be observed down to values of nearly 85 %. Anyway, these stability ratios can be considered high for all compositions and angles. In this regard, Jing, *et al.* [50] reported lower stability ratios in PLA/TPU blends, which showed less dimensional stability than the materials developed herein. Therefore, one can conclude indicating that this type of OLA is also an exceptional additive for shape memory recovery as shown by the high $\%R_r$ and $\%R_f$ values obtained.

Table III.1.2.7. Variation of the percentage of stability ratio ($\%R_f$) after different initial deformation angles (θ_f) for the polylactide (PLA) sheets with different weight contents of oligomer of lactic acid (OLA).

Piece	***R_f* (%)**			
	θ_f = 90°	θ_f = 60°	θ_f = 30°	θ_f = 15°
PLA	99.6 ± 1.3	98.9 ± 2.1	99.6 ± 1.3	88.2 ± 1.1
PLA-OLA 0%	98.7 ± 1.2	98.1 ± 1.3	88.2 ± 1.3	87.2 ± 2.5
PLA-OLA 5%	98.4 ± 1.5	94.2 ± 2.4	96.8 ± 1.5	86.7 ± 1.3
PLA-OLA 10%	99.3 ± 1.4	98.1 ± 1.8	97.8 ± 2.1	85.2 ± 3.6
PLA-OLA 15%	91.4 ± 2.3	96.5 ± 2.4	98.4 ± 1.4	84.9 ± 1.6

III.1.2.4. Conclusions

The positive effect of OLA to improve PLA toughness was evaluated in this study. The addition of 15 wt % OLA provided an increase in the impact strength from 25.7 kJ m^{-2} to almost 70 kJ m^{-2}, thus showing an extraordinary effect on toughness. Furthermore, the OLA impact modifier also provided a mechanical plasticization as observed by a decrease in the tensile strength though a slight reduction in ductility was also noticed. This plasticizing effect was observable by DSC in which the characteristic T_g of the neat PLA was reduced from 63.3 °C to 50.8 °C for the PLA piece with 20 wt % OLA. Moreover, since OLA was less thermally stable than PLA, a decrease in the onset degradation temperature, reported as $T_{5\%}$, was observed as the OLA loading increased. Nevertheless, the $T_{5\%}$value corresponding to the PLA piece with the highest OLA loading was still high, that is, 254.8 °C, which successfully allows processing these blends without thermal degradation. Another exciting feature that this type of OLA can provide

to PLA is the improvement of its shape memory behavior. In particular, the shape memory recovery parameter, that is, R_r, was very high compared to other PLA-based blends or plasticized PLA systems, thus showing the extraordinary effect of this OLA on the shape memory recovery. As a general conclusion, the here-studied OLA additive represents an interesting technical and environmentally friendly solution to improve the intrinsic brittleness of PLA and it also contributes to somewhat plasticization that allows enhanced shape memory recovery properties. The resultant toughened PLA materials can be of high interest for the development of compostable packaging articles, such as food trays and films, or disposable articles, such as cutlery and straws.

III.1.2.5. Funding

This research work was funded by the Spanish Ministry of Science, Innovation, and Universities (MICIU) project numbers RTI2018-097249-B-C21 and MAT2017-84909-C2-2-R.

III.1.2.6. Acknowledgments

L.Q.-C. wants to thank Generalitat Valenciana (GVA) for his FPI grant (ACIF/2016/182) and the Spanish Ministry of Education, Culture, and Sports (MECD) for his FPU grant (FPU15/03812). D.L. thanks Universitat Politècnica de València (UPV) for the grant received through the PAID-01-18 program. S.T.-G. is recipient of a Juan de la Cierva contract (IJCI-2016-29675) from MICIU. S.R.-L. is recipient of a Santiago Grisolía contract (GRISOLIAP/2019/132) from GVA. J.I.-M. wants to thank UPV for an FPI grant PAID-01-19 (SP2019001). Microscopy services of UPV are acknowledged for their help in collecting and analyzing the microscopy images. Authors also thank Condensia Química S.A. for kindly supplying Glyoplast OLA 2.

III.1.2.7. References

1. P.J. Dijkstra, H. Du, J. Feijen. Single site catalysts for stereoselective ring-opening polymerization of lactides. *Polymer chemistry* **2011**, *2*, 520-527.
2. L. Quiles-Carrillo, N. Montanes, J.M. Lagaron, R. Balart, S. Torres-Giner. Bioactive multilayer polylactide films with controlled release capacity of gallic acid accomplished by incorporating electrospun nanostructured coatings and interlayers. *Applied Sciences* **2019**, *9*, 533.
3. T. Radusin, S. Torres-Giner, A. Stupar, I. Ristic, A. Miletic, A. Novakovic, J.M. Lagaron. Preparation, characterization and antimicrobial properties of electrospun polylactide films containing Allium ursinum L. extract. *Food Packaging and Shelf Life* **2019**, *21*, 100357.
4. P. Scarfato, L. Di Maio, M.R. Milana, S. Giamberardini, M. Denaro, L. Incarnato. Performance properties, lactic acid specific migration and swelling by simulant of biodegradable poly (lactic acid)/nanoclay multilayer films for food packaging. *Food Additives & Contaminants: Part A* **2017**, *34*, 1730-1742.
5. P. Scarfato, L. Di Maio, L. Incarnato. Recent advances and migration issues in biodegradable polymers from renewable sources for food packaging. *Journal of Applied Polymer Science* **2015**, *132*.
6. I.S. Tawakkal, M.J. Cran, J. Miltz, S.W. Bigger. A review of poly (lactic acid)-based materials for antimicrobial packaging. *Journal of food science* **2014**, *79*, R1477-R1490.
7. K.T. Paula, G. Gaál, G. Almeida, M. Andrade, M.H. Facure, D.S. Correa, A. Riul Jr, V. Rodrigues, C.R. Mendonca. Femtosecond laser micromachining of polylactic acid/graphene composites for designing interdigitated microelectrodes for sensor applications. *Optics & Laser Technology* **2018**, *101*, 74-79.
8. S.K. Jeoung, J.U. Ha, Y.K. Ko, B.R. Kim, S.E. Yoo, K.D. Lee, S.N. Lee, P.C. Lee. Aerobic biodegradability of polyester/polylactic acid composites for automotive NVH parts. *International Journal of Precision Engineering and Manufacturing* **2014**, *15*, 1703-1707.
9. V.L. Finkenstadt, B. Tisserat. Poly (lactic acid) and osage orange wood fiber composites for agricultural mulch films. *Industrial crops and products* **2010**, *31*, 316-320.
10. Y.C. Chang, Y. Chen, J.L. Ning, C. Hao, M. Rock, M. Amer, S. Feng, M. Falahati, L.J. Wang, R.K. Chen, J.W. Zhang, J.L. Ding, L. Li. No such thing as trash: A 3D-

printable polymer composite composed of oil-extracted spent coffee grounds and Polylactic acid with enhanced impact toughness. *Acs Sustainable Chemistry & Engineering* **2019**, *7*, 15304-15310.

11. Y. Gao, Y. Li, X.R. Hu, W.D. Wu, Z. Wang, R.G. Wang, L.Q. Zhang. Preparation and properties of novel thermoplastic vulcanizate based on bio-based polyester/polylactic acid, and its application in 3D printing. *Polymers* **2017**, *9*, 15.

12. S. Kumar, R. Singh, T.P. Singh, A. Batish. Investigations of polylactic acid reinforced composite feedstock filaments for multimaterial three-dimensional printing applications. *Proceedings of the Institution of Mechanical Engineers Part C-Journal of Mechanical Engineering Science* **2019**, *233*, 5953-5965.

13. B.D.M. Matos, V. Rocha, E.J. da Silva, F.H. Moro, A.C. Bottene, C.A. Ribeiro, D.D. Dias, S.G. Antonio, A.C. do Amaral, S.A. Cruz, H.G.D. Barud, H.D. Barud. Evaluation of commercially available polylactic acid (PLA) filaments for 3D printing applications. *Journal of Thermal Analysis and Calorimetry* **2019**, *137*, 555-562.

14. I.S. Bayer. Thermomechanical properties of polylactic acid-graphene composites: A state-of-the-art review for biomedical applications. *Materials* **2017**, *10*, 33.

15. M.K. Pierchala, M. Makaremi, H.L. Tan, J. Pushpamalar, S. Muniyandy, A. Solouk, S.M. Lee, P. Pasbakhsh. Nanotubes in nanofibers: Antibacterial multilayered polylactic acid/halloysite/gentamicin membranes for bone regeneration application. *Applied Clay Science* **2018**, *160*, 95-105.

16. Y.F. Chen, J.Y. Xu, Q.G. Tan, Z.L. Zhang, J. Zheng, X.Y. Xu, Y. Li. End-group functionalization of polyethylene glycol-polylactic acid copolymer and its application in the field of pharmaceutical carriers. *Journal of Biobased Materials and Bioenergy* **2019**, *13*, 690-698.

17. S. Torres-Giner, A. Martinez-Abad, J.V. Gimeno-Alcañiz, M.J. Ocio, J.M. Lagaron. Controlled delivery of gentamicin antibiotic from bioactive electrospun polylactide-based ultrathin fibers. *Advanced Engineering Materials* **2012**, *14*, B112-B122.

18. A. Agüero, M.d.C. Morcillo, L. Quiles-Carrillo, R. Balart, T. Boronat, D. Lascano, S. Torres-Giner, O. Fenollar. Study of the influence of the reprocessing cycles on the final properties of polylactide pieces obtained by injection molding. *Polymers* **2019**, *11*, 1908.

19. L. Quiles-Carrillo, N. Montanes, D. Garcia-Garcia, A. Carbonell-Verdu, R. Balart, S. Torres-Giner. Effect of different compatibilizers on injection-molded green composite pieces based on polylactide filled with almond shell flour. *Composites Part B: Engineering* **2018**, *147*, 76-85.

20. L. Quiles-Carrillo, N. Montanes, F. Pineiro, A. Jorda-Vilaplana, S. Torres-Giner. Ductility and toughness improvement of injection-molded compostable pieces of polylactide by melt blending with poly (ε-caprolactone) and thermoplastic starch. *Materials* **2018**, *11*, 2138.

21. E. Bioplastics. *Bioplastics market data 2018. Global production capacities of bioplastics 2018-2023*; 2018; 4.

22. O. Valerio, J.M. Pin, M. Misra, A.K. Mohanty. Synthesis of glycerol-based biopolyesters as toughness enhancers for polylactic acid bioplastic through reactive extrusion. *Acs Omega* **2016**, *1*, 1284-1295.

23. B. Zhang, X.C. Bian, S. Xiang, G. Li, X.S. Chen. Synthesis of PLLA-based block copolymers for improving melt strength and toughness of PLLA by in situ reactive blending. *Polymer Degradation and Stability* **2017**, *136*, 58-70.

24. J. Zou, Y.Z. Qi, L.L. Su, Y. Wei, Z.L. Li, H.Q. Xu. Synthesis and characterization of poly(ester amide)s consisting of poly(L-lactic acid) and poly(butylene succinate) segments with 2,2 '-Bis(2-oxazoline) chain extending. *Macromolecular Research* **2018**, *26*, 1212-1218.

25. X.R. Lan, X. Li, Z.Y. Liu, Z.K. He, W. Yang, M.B. Yang. Composition, morphology and properties of poly(lactic acid) and poly(butylene succinate) copolymer system via Coupling reaction. *Journal of Macromolecular Science Part a-Pure and Applied Chemistry* **2013**, *50*, 861-870.

26. M.J. Garcia-Campo, L. Quiles-Carrillo, J. Masia, M.J. Reig-Perez, N. Montanes, R. Balart. Environmentally friendly compatibilizers from soybean oil for ternary blends of poly(lactic acid)-PLA, poly(epsilon-caprolactone)-PCL and poly(3-hydroxybutyrate)-PHB. *Materials* **2017**, *10*, 19.

27. M.J. Garcia-Campo, L. Quiles-Carrillo, L. Sanchez-Nacher, R. Balart, N. Montanes. High toughness poly(lactic acid) (PLA) formulations obtained by ternary blends with poly(3-hydroxybutyrate) (PHB) and flexible polyesters from succinic acid. *Polymer Bulletin* **2019**, *76*, 1839-1859.

28. S. Sathornluck, C. Choochottiros. Modification of epoxidized natural rubber as a PLA toughening agent. *Journal of Applied Polymer Science* **2019**, *136*, 7.

29. S. Su, R. Kopitzky, S. Tolga, S. Kabasci. Polylactide (PLA) and its blends with poly(butylene succinate) (PBS): A brief review. *Polymers* **2019**, *11*, 21.

30. B. Zhang, B. Sun, X.C. Bian, G. Li, X.S. Chen. High melt strength and high toughness PLLA/PBS blends by copolymerization and in situ reactive compatibilization. *Industrial & Engineering Chemistry Research* **2017**, *56*, 52-62.

31. I. Fortelny, A. Ujcic, L. Fambri, M. Slouf. Phase structure, compatibility, and toughness of PLA/PCL blends: A review. *Frontiers in Materials* **2019**, *6*, 13.

32. Y. Wang, Y. Mei, Q. Wang, W. Wei, F. Huang, Y. Li, J.Y. Li, Z.W. Zhou. Improved fracture toughness and ductility of PLA composites by incorporating a small amount of surface-modified helical carbon nanotubes. *Composites Part B-Engineering* **2019**, *162*, 54-61.

33. J.J. Li, J. Li, D.J. Feng, J.F. Zhao, J.R. Sun, D.G. Li. Excellent rheological performance and impact toughness of cellulose nanofibers/PLA/ionomer composite. *Rsc Advances* **2017**, *7*, 28889-28897.

34. J. Gonzalez-Ausejo, J. Gamez-Perez, R. Balart, J.M. Lagaron, L. Cabedo. Effect of the addition of sepiolite on the morphology and properties of melt compounded PHBV/PLA blends. *Polymer Composites* **2019**, *40*, E156-E168.

35. C.H. Tsou, C. Gao, M. De Guzman, D.Y. Wu, W.S. Hung, L. Yuan, M.C. Suen, J.T. Yeh. Preparation and characterization of poly(lactic acid) with adipate ester added as a plasticizer. *Polymers & Polymer Composites* **2018**, *26*, 446-453.

36. H.C. Huang, L.J. Chen, G.L. Song, G.Y. Tang. An efficient plasticization method for poly(lactic acid) using combination of liquid-state and solid-state plasticizers. *Journal of Applied Polymer Science* **2018**, *135*, 13.

37. H.L. Kang, Y.S. Li, M. Gong, Y.L. Guo, Z. Guo, Q.H. Fang, X. Li. An environmentally sustainable plasticizer toughened polylactide. *Rsc Advances* **2018**, *8*, 11643-11651.

38. A. Carbonell-Verdu, J.M. Ferri, F. Dominici, T. Boronat, L. Sanchez-Nacher, R. Balart, L. Torre. Manufacturing and compatibilization of PLA/PBAT binary blends by cottonseed oil-based derivatives. *Express Polymer Letters* **2018**, *12*, 808-823.

39. L. Quiles-Carrillo, M. Blanes-Martínez, N. Montanes, O. Fenollar, S. Torres-Giner, R. Balart. Reactive toughening of injection-molded polylactide pieces using maleinized hemp seed oil. *European Polymer Journal* **2018**, *98*, 402-410.

40. L. Quiles-Carrillo, S. Duart, N. Montanes, S. Torres-Giner, R. Balart. Enhancement of the mechanical and thermal properties of injection-molded

polylactide parts by the addition of acrylated epoxidized soybean oil. *Materials & Design* **2018**, *140*, 54-63.

41. J.M. Ferri, D. Garcia-Garcia, L. Sanchez-Nacher, O. Fenollar, R. Balart. The effect of maleinized linseed oil (MLO) on mechanical performance of poly(lactic acid)-thermoplastic starch (PLA-TPS) blends. *Carbohydrate Polymers* **2016**, *147*, 60-68.

42. J.M. Ferri, D. Garcia-Garcia, N. Montanes, O. Fenollar, R. Balart. The effect of maleinized linseed oil as biobased plasticizer in poly (lactic acid)-based formulations. *Polymer International* **2017**, *66*, 882-891.

43. D. Notta-Cuvier, M. Murariu, J. Odent, R. Delille, A. Bouzouita, J.M. Raquez, F. Lauro, P. Dubois. Tailoring polylactide properties for automotive applications: Effects of co-Aaddition of halloysite nanotubes and selected plasticizer. *Macromolecular Materials and Engineering* **2015**, *300*, 684-698.

44. F. Luzi, F. Dominici, I. Armentano, E. Fortunati, N. Burgos, S. Fiori, A. Jimenez, J.M. Kenny, L. Torre. Combined effect of cellulose nanocrystals, carvacrol and oligomeric lactic acid in PLA_PHB polymeric films. *Carbohydrate Polymers* **2019**, *223*, 13.

45. N. Burgos, V.P. Martino, A. Jimenez. Characterization and ageing study of poly(lactic acid) films plasticized with oligomeric lactic acid. *Polymer Degradation and Stability* **2013**, *98*, 651-658.

46. D. Battegazzore, S. Bocchini, A. Frache. Crystallization kinetics of poly(lactic acid)-talc composites. *Express Polymer Letters* **2011**, *5*, 849-858.

47. B. Kaygusuz, S. Ozerinc. Improving the ductility of polylactic acid parts produced by fused deposition modeling through polyhydroxyalkanoate additions. *Journal of Applied Polymer Science* **2019**, *136*, 8.

48. Z. Lule, J. Kim. Nonisothermal crystallization of surface-treated alumina and aluminum nitride-filled polylactic acid hybrid composites. *Polymers* **2019**, *11*, 12.

49. L. Quiles-Carrillo, N. Montanes, C. Sammon, R. Balart, S. Torres-Giner. Compatibilization of highly sustainable polylactide/almond shell flour composites by reactive extrusion with maleinized linseed oil. *Industrial Crops and Products* **2018**, *111*, 878-888.

50. X. Jing, H.Y. Mi, X.F. Peng, L.S. Turng. The morphology, properties, and shape memory behavior of polylactic acid/thermoplastic polyurethane blends. *Polymer Engineering and Science* **2015**, *55*, 70-80.

51. T.F. Shen, L.Y. Liang, M.G. Lu. Novel biodegradable shape memory composites based on PLA and PCL crosslinked by polyisocyanate. In *Advances in Biomedical Engineering*, Hu, J., Ed. Information Engineering Research Inst, USA: Newark, 2011; 302-305.

52. Z.X. Zhang, Z.Z. He, J.H. Yang, T. Huang, N. Zhang, Y. Wang. Crystallization controlled shape memory behaviors of dynamically vulcanized poly(L-lactide)/poly(ethylene vinyl acetate) blends. *Polymer Testing* **2016**, *51*, 82-92.

53. L.N. Shao, J. Dai, Z.X. Zhang, J.H. Yang, N. Zhang, T. Huang, Y. Wang. Thermal and electroactive shape memory behaviors of poly(L-lactide)/thermoplastic polyurethane blend induced by carbon nanotubes. *Rsc Advances* **2015**, *5*, 101455-101465.

54. J. Ambrosio-Martin, M.J. Fabra, A. Lopez-Rubio, J.M. Lagaron. An effect of lactic acid oligomers on the barrier properties of polylactide. *Journal of Materials Science* **2014**, *49*, 2975-2986.

55. C. Courgneau, S. Domenek, A. Guinault, L. Averous, V. Ducruet. Analysis of the structure-properties relationships of different multiphase systems based on plasticized poly(lactic acid). *Journal of Polymers and the Environment* **2011**, *19*, 362-371.

56. E. Fortunati, D. Puglia, A. Iannoni, A. Terenzi, J.M. Kenny, L. Torre. Processing conditions, thermal and mechanical responses of stretchable poly (lactic acid)/poly (butylene succinate) films. *Materials* **2017**, *10*, 809.

57. J. Ferri, M. Samper, D. García-Sanoguera, M. Reig, O. Fenollar, R. Balart. Plasticizing effect of biobased epoxidized fatty acid esters on mechanical and thermal properties of poly (lactic acid). *Journal of materials science* **2016**, *51*, 5356-5366.

58. W.K. Chee, N.A. Ibrahim, N. Zainuddin, M.F. Abd Rahman, B.W. Chieng. Impact toughness and ductility enhancement of biodegradable poly(lactic acid)/poly(epsilon-caprolactone) blends via addition of glycidyl methacrylate. *Advances in Materials Science and Engineering* **2013**, 10.1155/2013/976373, 8.

59. B. Xue, H.Z. He, Z.W. Zhu, J.Q. Li, Z.X. Huang, G.Z. Wang, M. Chen, Z.M. Zhan. A facile fabrication of high toughness poly(lactic acid) via reactive extrusion with poly(butylene succinate) and ethylene-methyl acrylate-glycidyl methacrylate. *Polymers* **2018**, *10*, 15.

60. X. Wang, S.X. Peng, H. Chen, X.L. Yu, X.P. Zhao. Mechanical properties, rheological behaviors, and phase morphologies of high-toughness PLA/PBAT blends by in-situ reactive compatibilization. *Composites Part B-Engineering* **2019**, *173*, 10.

61. D. Lascano, L. Quiles-Carrillo, S. Torres-Giner, T. Boronat, N. Montanes. Optimization of the curing and post-curing conditions for the manufacturing of partially bio-based epoxy resins with improved toughness. *Polymers* **2019**, *11*, 1354.

62. N. Burgos, D. Tolaguera, S. Fiori, A. Jimenez. Synthesis and characterization of lactic acid oligomers: evaluation of performance as poly(lactic acid) plasticizers. *Journal of Polymers and the Environment* **2014**, *22*, 227-235.

63. N. Ljungberg, B. Wesslen. The effects of plasticizers on the dynamic mechanical and thermal properties of poly (lactic acid). *Journal of Applied Polymer Science* **2002**, *86*, 1227-1234.

64. Q. Xing, X.Q. Zhang, X. Dong, G.M. Liu, D.J. Wang. Low-molecular weight aliphatic amides as nucleating agents for poly (L-lactic acid): Conformation variation induced crystallization enhancement. *Polymer* **2012**, *53*, 2306-2314.

65. P. Maróti, B. Kocsis, A. Ferencz, M. Nyitrai, D. Lőrinczy. Differential thermal analysis of the antibacterial effect of PLA-based materials planned for 3D printing. *Journal of Thermal Analysis and Calorimetry* **2020**, *139*, 367-374.

66. M. Maiza, M.T. Benaniba, G. Quintard, V. Massardier-Nageotte. Biobased additive plasticizing polylactic acid (PLA). *Polimeros* **2015**, *25*, 581-590.

67. S.K. Jia, D.M. Yu, Y. Zhu, Z. Wang, L.G. Chen, L. Fu. Morphology, crystallization and thermal behaviors of PLA-based composites: wonderful effects of hybrid GO/PEG via dynamic impregnating. *Polymers* **2017**, *9*, 18.

68. X.T. Shi, G.C. Zhang, T.V. Phuong, A. Lazzeri. Synergistic effects of nucleating agents and plasticizers on the crystallization behavior of poly(lactic acid). *Molecules* **2015**, *20*, 1579-1593.

69. X.L. Lu, Z.J. Sun, W. Cai, Z.Y. Gao. Study on the shape memory effects of poly(L-lactide-co-epsilon-caprolactone) biodegradable polymers. *Journal of Materials Science-Materials in Medicine* **2008**, *19*, 395-399.

70. A. Leones, A. Sonseca, D. López, S. Fiori, L. Peponi. Shape memory effect on electrospun PLA-based fibers tailoring their thermal response. *European Polymer Journal* **2019**, *117*, 217-226.

Adaptado del artículo

III.1.3. Manufacturing and characterization of highly environmentally friendly sandwich composites from polylactide cores and flax-polylactide faces

Diego Lascano, Rene Guillen-Pineda, Luis Quiles-Carrillo, Juan Ivorra-Martínez, Rafael Balart, Nestor Montanes and Teodomiro Boronat

Technological Institute of Materials (ITM), Universitat Politècnica de València (UPV), Plaza Ferrándiz y Carbonell 1, 03801 Alcoy, Spain.

Polymers **2021**, *13*(3), 342

polymers

MDPI

Article

Manufacturing and Characterization of Highly Environmentally Friendly Sandwich Composites from Polylactide Cores and Flax-Polylactide Faces

Diego Lascano *, Rene Guillen-Pineda, Luis Quiles-Carrillo, Juan Ivorra-Martínez *, Rafael Balart, Nestor Montanes and Teodomiro Boronat

Technological Institute of Materials (ITM), Universitat Politècnica de València (UPV), Plaza Ferrándiz y Carbonell 1, 03801 Alcoy, Spain; reguipi@upv.es (R.G.-P.); luiquic1@epsa.upv.es (L.Q.-C.); rbalart@mcm.upv.es (R.B.); nesmonmu@upvnet.upv.es (N.M.); tboronat@dimm.upv.es (T.B.)

* Correspondence: dielas@epsa.upv.es (D.L.); juaivmar@doctor.upv.es (J.I.-M.); Tel.: +34-966-528-433 (D.L.)

Abstract: This work focuses on the manufacturing and characterization of highly environmentally friendly lightweight sandwich structures based on polylactide (PLA) honeycomb cores and PLA-flax fabric laminate skins or facings. PLA honeycombs were manufactured using PLA sheets with different thicknesses ranging from 50 to 500 µm. The PLA sheets were shaped into semi-hexagonal profiles by hot-compression molding. After this stage, the different semi-hexagonal sheets were bonded together to give hexagonal panels. The skins were manufactured by hot-compression molding by stacking two Biotex flax/PLA fabrics with 40 wt% PLA fibers. The combined use of temperature (200 °C), pressure, and time (2 min) allowed PLA fibers to melt, flow, and fully embed the flax fabrics, thus leading to thin composite laminates to be used as skins. Sandwich structures were finally obtained by bonding the PLA honeycomb core with the PLA-flax skins using an epoxy adhesive. A thin PLA nonwoven was previously attached to the external hexagonal PLA core, to promote mechanical interlock between the core and the skins. The influence of the honeycomb core thickness on the final flexural and compression properties was analyzed. The obtained results indicate that the core thickness has a great influence on the flexural properties, which increases with core thickness; nevertheless, as expected, the bonding between the PLA honeycomb core and the skins is critical. Excellent results have been obtained with 10 and 20 mm thickness honeycombs with a core shear of about 0.60 and facing bending stresses of 31–33 MPa, which can be considered as candidates for technical applications. The ultimate load to the sample weight ratio reached values of 141.5 $N \cdot g^{-1}$ for composites with 20 mm thick PLA honeycombs, which is comparable to other technical composite sandwich structures. The bonding between the core and the skins is critical as poor adhesion does not allow load transfer and, while the procedure showed in this research gives interesting results, new developments are necessary to obtain standard properties on sandwich structures.

Keywords: PLA honeycomb core; eco-friendly sandwich structures; three-point bending test; hot compression molding

Citation: Lascano, D.; Guillen-Pineda, R.; Quiles-Carrillo, L.; Ivorra-Martínez, J.; Balart, R.; Montanes, N.; Boronat, T. Manufacturing and Characterization of Highly Environmentally Friendly Sandwich Composites from Polylactide Cores and Flax-Polylactide Faces. *Polymers* **2021**, *13*, 342. https://doi.org/10.3390/polym13030342

Received: 10 December 2020
Accepted: 20 January 2021
Published: 21 January 2021

1. Introduction

The demand for low-weight and high-rigidity materials in high-performance sectors has given way to the development of composite materials [1]. Among others, sandwich structures deserve special attention due to their use in a wide variety of sectors, which include conventional packaging with corrugated craft cores [2], and high-performance applications in aerospace [3,4], automotive [5], aeronautics [6], lightweight civil infrastructure [7], and so on. Sandwich panels are composed of a lightweight core and two (top and bottom) skins [8]. The most common cores in sandwich panels are processed woods (i.e., balsa wood), thermoplastic and thermosetting polymer foams, and honeycomb structures. Honeycombs can be obtained from a wide variety of materials such as metals

Manufacturing and characterization of highly environmentally friendly sandwich composites from polylactide cores and flax-polylactide faces

Abstract

This work focuses on the manufacturing and characterization of highly environmentally friendly lightweight sandwich structures based on polylactide (PLA) honeycomb cores and PLA-flax fabric laminate skins or facings. PLA honeycombs were manufactured using PLA sheets with different thicknesses ranging from 50 to 500 μm. The PLA sheets were shaped into semi-hexagonal profiles by hot-compression molding. After this stage, the different semi-hexagonal sheets were bonded together to give hexagonal panels. The skins were manufactured by hot-compression molding by stacking two Biotex flax/PLA fabrics with 40 wt % PLA fibers. The combined use of temperature (200 °C), pressure, and time (2 min) allowed PLA fibers to melt, flow, and fully embed the flax fabrics, thus leading to thin composite laminates to be used as skins. Sandwich structures were finally obtained by bonding the PLA honeycomb core with the PLA-flax skins using an epoxy adhesive. A thin PLA nonwoven was previously attached to the external hexagonal PLA core, to promote mechanical interlock between the core and the skins. The influence of the honeycomb core thickness on the final flexural and compression properties was analyzed. The obtained results indicate that the core thickness has a great influence on the flexural properties, which increases with core thickness; nevertheless, as expected, the bonding between the PLA honeycomb core and the skins is critical. Excellent results have been obtained with 10 and 20 mm thickness honeycombs with a core shear of about 0.60 and facing bending stresses of 31-33 MPa, which can be considered as candidates for technical applications. The ultimate load to the sample weight ratio reached values of 141.5 $N \cdot g^{-1}$ for composites with 20 mm thick PLA honeycombs, which is comparable to other technical composite sandwich structures. The bonding between the core and the skins is critical as poor adhesion does not allow load transfer and, while the procedure showed in this research gives interesting results, new developments are necessary to obtain standard properties on sandwich structures.

Keywords: PLA honeycomb core; eco-friendly sandwich structures; three-point bending test; hot compression molding

III.1.3.1. Introduction

The demand for low-weight and high-rigidity materials in high-performance sectors has given way to the development of composite materials [1]. Among others, sandwich structures deserve special attention due to their use in a wide variety of sectors, which include conventional packaging with corrugated craft cores [2], and high-performance applications in aerospace [3,4], automotive [5], aeronautics [6], lightweight civil infrastructure [7], and so on. Sandwich panels are composed of a lightweight core and two (top and bottom) skins [8]. The most common cores in sandwich panels are processed woods (i.e., balsa wood), thermoplastic and thermosetting polymer foams, and honeycomb structures. Honeycombs can be obtained from a wide variety of materials such as metals (steel, aluminum, titanium) and thermoplastic polymers such as polypropylene or aramid. The skins or faces are usually made of lightweight and stiff materials such as aluminum or fiber-reinforced polymers (FRP) [9,10]. The most critical part in a sandwich structure is the skin-core interface, which plays a key role in load transfer. To enhance this interface, adhesives, fiber mats, or thin sheets are used [11]. The final composition of a sandwich structure depends on the target application. For example, polymer foam cores are generally used in car flooring, boat parts, as well as turbine blades, as they have good rigidity, high strength, and resistance to fatigue and temperature [12-15]. Feng and Aymerich [16] studied the effect of the density of a polyvinyl chloride (PVC) foam core on sandwich panels with carbon/epoxy-laminated facings, resulting in a composite structure with excellent stiffness. They demonstrated an increasing tendency in stiffness with increasing core density. One of the main drawbacks of sandwich-type composites is that they are expensive due to their manufacturing process. On the other hand, sandwich-type composites are difficult to handle with conventional manufacturing processes for composite materials such as vacuum-assisted resin infusion molding (VARIM) or resin transfer molding (RTM). In the last years, important advances have been carried out in the field of composite sandwich structures to overcome or palliate this. Lascano, *et al.* [17] reported the manufacturing of a sandwich-type composite with basalt-flax hybrid laminates skins and a polypropylene-permeating nonwoven core (Lantor Soric© XF) with a hexagonal groove, which allows conventional manufacturing by the resin infusion processes. These new core materials combine lightness, processability, and stiffness.

Sandwich composite structures, particularly with honeycomb cores, are widely used because they offer excellent out-of-plane properties (i.e., bending, compression), compared to conventional composite laminates. This feature, together with their lightness because of the use of a very lightweight core material, have positioned

sandwich structures as high-performance materials for applications in aerospace, automotives, and the sports and marine industry, among others [18]. Initially, sandwich structures with a honeycomb core were only used in aeronautics and aerospace industries due to their extremely positive stiffness-to-weight ratio (ailerons, flaps, rudders, and so on). Nevertheless, their production was laborious and, therefore, expensive, which made them unsuitable for mass production. Aluminum has been, with difference, the most common material for sandwich skins or cores in high-performance composites [9,19]. Nevertheless, with the development of engineering and high-performance polymers, a new series of honeycombs can be found as they also provide high stiffness with lower weight compared to aluminum. Among others, it is worth remarking the increasing use of polypropylene (PP) honeycombs for conventional applications, which provide good rigidity with a considerable decrease in weight, as PP is one of the lightest polymers [20]. For high-performance composites, aramid honeycombs are widely used due to an excellent balance between lightness, stiffness, cost, and temperature resistance [6].

Despite the fact that composite panels usually combine the optimum materials for the core, bonding, and skins, some composite panels are manufactured entirely from one material such as lightweight composite panels consisting of PP skins and PP honeycombs. These composite panels have become very popular in the packaging and construction industries [21,22]. The use of high-performance composite laminates with glass fiber (GF) and carbon fiber (CF) has widened the performance of sandwich structures for applications requiring high strength at low weight, because unlike metallic materials, they offer a better strength-to-weight ratio [23-26].

The increasing awareness of environmental issues has led to the search of new environmentally friendly materials. This situation is more pronounced in the polymers and composites industries, which are highly petroleum-dependent. In the last years, biobased materials are acquiring relevance as they can be obtained from natural resources. Despite there still being a long way to go with biobased polymers and composites, some materials have been positioned as excellent candidates for the replacement of their petrochemical counterparts [27,28]. Companies such as EconCore have developed a revolutionary technology, ‘ThermHex’ [29], which allows the serial production of honeycomb cores in a single sheet of thermoplastics material such as polypropylene (PP), polyethylene terephthalate (PET), and polycarbonate (PC). This process contributes to reduction in both the amount of material used, waste material, and energy consumption, all contributing to reducing the carbon footprint [30]. This technology has given way to the development of fully bio-based honeycomb materials

by using polylactide (PLA), obtained from natural resources [1,26]. PLA is a thermoplastic material obtained from renewable sources through sugar fermentation or from starch-rich products such as potatoes or sugar cane. PLA offers interesting properties such as biodegradability (actually, disintegration in controlled compost soil), biocompatibility, good tensile strength, good stiffness, and shape memory [31]. In addition, it can be manufactured by conventional processing techniques such as injection molding, extrusion, hot compression molding, and 3D printing. For these reasons, the use of PLA has remarkably grown in the last decade, mainly in the packaging industry [32,33], and biomedicine [34,35]. The use of PLA can positively contribute to develop a new series of environmentally friendly composite materials or green composites. In fact, PLA is currently used as matrix in wood plastic composites with natural fibers and/or lignocellulosic fillers [36], and it is increasingly used in several components of composite sandwiches such as 3D-printed honeycombs, adhesion nonwovens, and skins on different composite panel configurations [37].

Furthermore, by replacing the currently used synthetic fibers with natural fibers, materials with balanced properties and environmental efficiency can be obtained. Among different natural fibers such as jute, hemp, sisal, and cotton, flax fibers are increasingly being used in green composites. Flax fibers offer superior properties to other natural fibers [38] and represent a good choice for green composites. Flax fibers are mainly composed of cellulose (60-85 %) and hemicellulose (14-20 %). The use of cellulosic materials as reinforcements provides low density, renewability, and/or biodegradability with a relatively low cost [39]. Flax fibers offer interesting mechanical properties, but there is very high heterogeneity on these properties depending on the flax variety, crop conditions, fiber diameter, position in the plant, and fiber length, among others [40]. The gauge length of the fiber plays a key role in the mechanical properties as described by Amroune, *et al.* [41]. They reported a dramatic change in tensile strength from 1415 MPa for flax fibers with a gauge length of 10 mm down to values of 431 MPa for a gauge length of 500 mm, thus giving clear evidence of the influence of the gauge length on final performance. The same was observed for the tensile modulus, with changes from 54.20 to 31.45 GPa for gauge lengths of 10 and 500 mm, respectively.

Nevertheless, green composites with natural fibers offer an important drawback that is related to the hydrophilic nature of the reinforcement, which leads to an undesirable water uptake process that is responsible for dimensional changes and ageing [42]. This drawback can be minimized by using chemical or physical surface treatment on the fiber or by using coupling agents [43,44]. Despite flax and other bast fibers such as ramie, jute, kenaf, and hemp finding increasing applications as

reinforcements in construction and building, the automotive sector and the sports industry, as reported by Sadrmanesh and Chen [45], the use of flax and other bast fibers must face some challenges related to standardized mechanical properties for natural fibers (highly dependent on the crop conditions and manufacturing stages), water absorption, poor tensile and impact properties, and price fluctuations, compared to conventional glass, carbon, or aramid fibers [46].

Research conducted by Nickels [47] has shown the potential of PLA-derived materials for use in automobile parts, showing the potential of PLA honeycombs to obtain lightweight materials with balanced mechanical properties and, the most important, contributing to sustainable development.

This work aims to develop highly environmentally friendly sandwich structures for technical applications. To achieve this, this research explores the possibilities of PLA-based honeycomb cores with different thicknesses and the use of flax fabric-PLA laminates as sandwich skins or outer faces. The effect of the PLA honeycomb thickness on mechanical properties (flexural and compression) is evaluated.

III.1.3.2. Materials and Methods

Materials

A commercial aluminum block type 6082-T6 supplied by Broncesval SL (Valencia, Spain) was necessary for the manufacture of the mold to be used in the production of the honeycomb cores.

The semi-hexagonal-shape cell sheets were manufactured using a commercial polylactide (PLA) Ingeo™ 6201D grade supplied by NatureWorks LLC (Minnetonka, MN, USA). This PLA grade has a glass transition temperature (T_g) between 55 and 60 °C and a melting point located in the 155-170 °C range. Its melt flow index ranges between 15 and 30 g/10 min at 210 °C. A transparent ethyl cyanoacrylate adhesive, Loctite® 401, supplied by Henkel (Düsseldorf, Germany) was used to bond the two semi-hexagonal-shaped sheets to obtain the honeycomb. This adhesive provides a rapid bonding and it is recommended to use on plastics. It has a Brookfield viscosity of 100-120 mPa s at 25 °C (screw 1; rotating speed = 30 rpm).

The outer sheets (sandwich skins) were manufactured with Biotex Flax/PLA. This fabric is a commingled textile composed of natural flax fiber and polylactide (PLA). It was supplied by SCABRO tooling and composites (Katwijk, Nederland) in the weave style of 2 x 2 twill and a surface density of 400 $g \cdot m^{-2}$. These commingled textiles can be

converted into rigid engineering parts by applying a combination of pressure and temperature to allow PLA to flow and embed the flax reinforcement. The sandwich skins consisted of two stacked Biotex Flax/PLA fabrics. After being subjected to hot compression molding, the thin laminate offered a flexural modulus of 7.8 GPa and a flexural strength of 131 MPa.

A partially biobased epoxy resin based on soybean oil was used to bond the honeycomb and the skins. This resin was an Ecopoxy fast-curing system supplied by ECOEPOXY (Morris, MB, Canada) with an epoxy-to-hardener (amine-based) ratio of 2:1. This partially biobased epoxy system is composed of a liquid epoxy resin obtained as a reaction between bisphenol A diglycidyl ether (BADGE), alkyl glycidyl ether, and soybean oil resin with a viscosity of 600-700 cps. Regarding the hardener, it is a reaction adduct of ethylene amine, bisphenol A, benzyl alcohol, and soybean oil and has a viscosity of 60 cps.

To increase the contact area between the honeycomb core and the outer sheets, a polylactide (PLA) nonwoven mat was used. This was a spun-bonded PLA nonwoven for disposable clothes, supplied by RCfil NON-TEX (Vigo, Spain).

Manufacturing of PLA-Core Sandwich Structures

The development of the PLA-core sandwich structure was carried out in different stages: (a) Manufacturing of the hexagonal mold, (b) manufacture of the PLA-based honeycomb core, (c) manufacture of the PLA-flax outer sheets reinforced, and finally (d) bonding of the honeycomb core to the skins by means of adhesive joints as it is summarized in figure III.1.3.1.

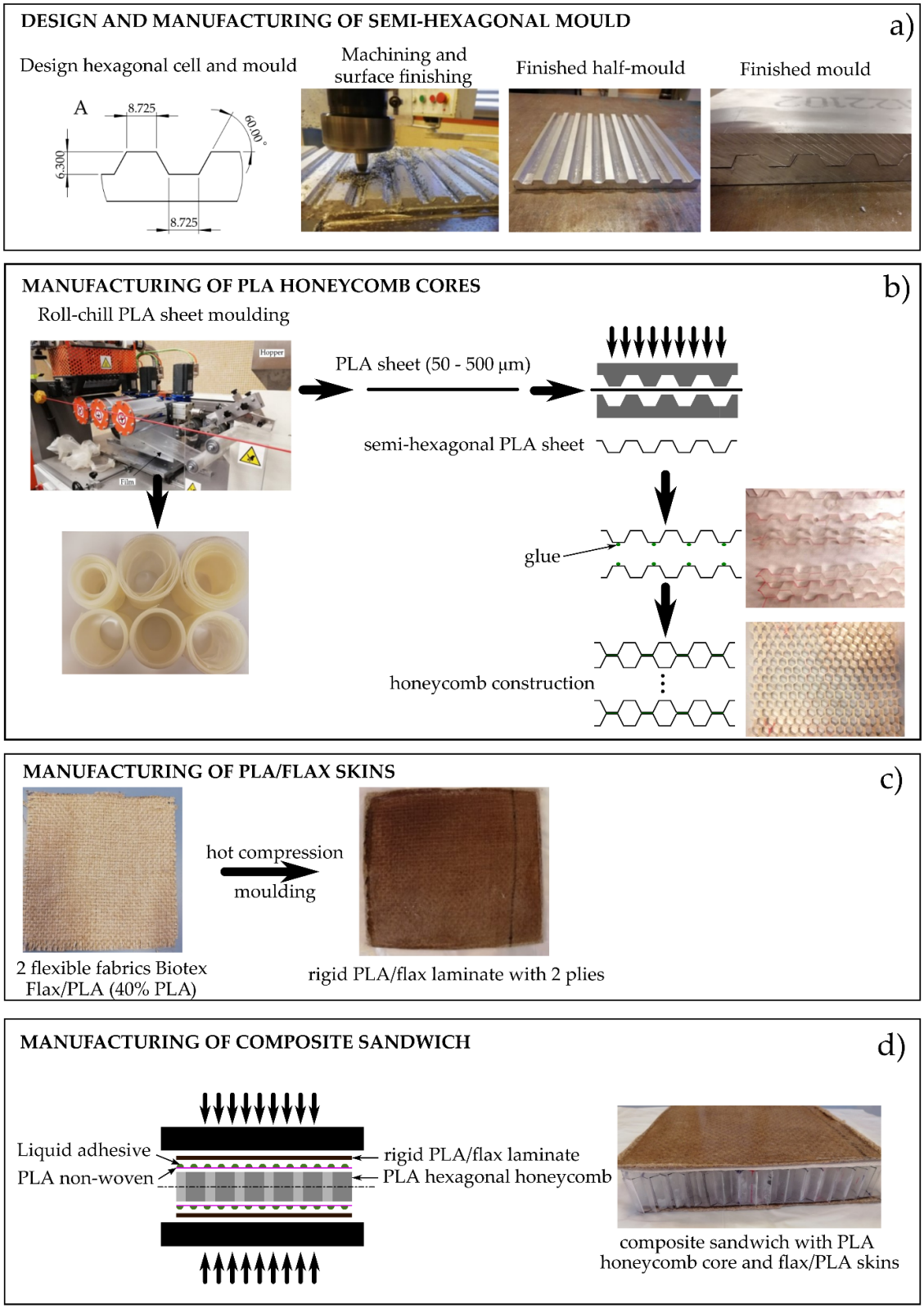

Figure III.1.3.1. Schematic plot showing the different stages of the manufacturing process of (polylactide) PLA-honeycomb core-based sandwich structure.

The design and dimensions of the mold are of great relevance, as this will give the size of the hexagonal cells on honeycomb cores. High precision is required to ensure

reproducibility in obtaining the cores, so that uniform honeycomb cores can be obtained. Figure III.1.3.1a shows the detailed dimensions to obtain hexagonal cells. The aluminum blocks were machined with a WEISS WUM 100 universal rotary head-milling machine from DeTech (Łowicz, Poland) with numerical control. Two different stages were scheduled for the machining process: First, a roughing process with a 5 mm cylindrical milling tool with a spindle speed of 1660 rpm, a longitudinal feed rate of 55 mm min^{-1}, and a plunging depth of 1 mm. After that, the second stage was carried out using a 60° conical milling tool with a spindle speed of 675 rpm, a longitudinal feed rate of 170 mm·min^{-1}, and a plunging depth of 1 mm.

The next stage (figure III.1.3.1b) is the production of the PLA sheets; before further processing, PLA pellets were dried at 60 °C for 24 h due to its sensitivity to hydrolysis. PLA pellets were melted in a chill-roll unit equipped with a single-screw. The unit was a XTR series from Eurotech extrusion machinery SRL (Tradate, Italy). The selected temperature was 200 °C and the screw speed ranged between 43 and 55 rpm, depending on the final thickness: 43, 46, 51, and 55 rpm for 50, 150, 250, and 500 µm, respectively. The calendering rate was set to 0.9 m·min^{-1} for 50 and 100 µm thick sheets, while lower rates were used for thicker sheets, i.e., 0.2 m·min^{-1} for 250 µm and 0.1 m·$min^{-1}$for 250 µm. PLA sheets with a thickness of 50 and 100 µm show very high (50 µm) and high (100 µm) flexibility but (typical film thickness), in contrast, they do not offer handling stability. On the other hand, semi-hexagonal PLA sheets with 500 µm thickness are extremely brittle with very low flexibility. Finally, the semi-hexagonal PLA sheets with a thickness of 250 µm offered the best-balanced properties regarding geometry, flexibility, low brittleness, and good handling.

Additionally, Semi-hexagonal PLA films with thicknesses of 100, 250, and 500 m were subjected to a qualitative evaluation of the shape memory behavior, as shown in figure III.1.3.S1 (available in the Supplementary Information section).

Three different-thickness PLA honeycomb cores of 10, 20, and 30 mm were manufactured. The code used for the different structures was ‘PLA-HYNxx,’ where xx represents the height of each core. The semi-hexagonal sheets were obtained by hot compression molding using a Hoytom M.N 1417 hot compression machine supplied by Robima S.A. (Bilbao, Spain) at a temperature of 135 °C for 2 min with 8 tons of applied load. Finally, different semi-hexagonal sheets were bonded using Loctite®401 glue, to obtain the honeycomb core, as shown in figure III.1.3.1b.

The outer layers (faces or skins) consist of commingled polylactide (PLA) and natural flax fiber fabrics. Each outer skin is composed of two PLA/Flax commingled

fabrics. These flexible fabrics were converted into a rigid laminate by hot compression molding at a temperature of 200 °C and an applied loaf force of 9 tons for 2 min, to allow PLA to melt and fully embed the aligned flax fibers, as shown in figure III.1.3.1c with an image of the flax/PLA commingled fabric before and after hot compression molding.

Finally, the core and the skins were joined by means of an adhesive. For this purpose, a thermosetting adhesive layer was prepared. This adhesive layer consisted of a PLA-based nonwoven mat that was placed between the outer skins and the core, to increase the contact area between them and increase the retention of the EcoPoxy adhesive. The liquid fast-curing epoxy system was spread on the outer skin, and then a nonwoven layer was placed and embedded with a thin layer of the epoxy system using a hand lay-up technique. The same procedure was repeated to bond the outer skin. The final sandwich structure was placed into a press and subjected to slight force to ensure good contact between the honeycomb and the outer faces, while the epoxy adhesive resin crosslinked, leading to final composite sandwich structures with PLA honeycomb cores, as can be seen in figure III.1.3.1d.

Mechanical Characterization of PLA-Based Sandwich Structures

The mechanical properties of sandwich structures with PLA honeycombs were evaluated in flexural and compression conditions. Both were performed on a universal testing machine model ELIB 30 from Ibertest (Madrid, Spain). Flexural tests were carried out using a three-point bending configuration according to ASTM C393-00. The standard size of the samples for flexural tests was 150 mm in length, 50 mm in width, and a variable thickness (10, 20, and 30 mm), depending on the honeycomb thickness. The machine was equipped with a 5 kN load cell and the crosshead rate was set to 10 $mm \cdot min^{-1}$. The corresponding force–displacement graphs were collected, and from the results, it was possible to obtain the maximum load; besides, the core shear stress and the facing bending stress were calculated using equations (III.1.3.1) and (III.1.3.2), respectively.

$$\tau = \frac{P}{(d + c) \cdot b} \quad \text{(III.1.3.1)}$$

$$\sigma_b = \frac{P \cdot L}{2 \cdot t \cdot (d + c) \cdot b} \quad \text{(III.1.3.2)}$$

Where τ is the core shear stress expressed in MPa, *P* is the maximum load expressed in N, *d* and *b* are the thickness and width of the sandwich structure, respectively, and *c* is the honeycomb thickness, all in mm. Regarding Equation (III.1.3.2), σ_b is the facing bending stress expressed in MPa, *t* is the laminate thickness, *d* is the total sandwich thickness, *c* is the thickness of the honeycomb core, and *L* is the span length (constant value of 100 mm), all in mm.

Flatwise compressive tests were done according to ASTM C365/365M-16. This test was carried out on squared samples 50 mm length and width, and a variable thickness (10, 20, and 30 mm). A load cell of 50 kN with a crosshead rate of 10 mm min^{-1} was used. To obtain reliable data, at least 5 different specimens were tested for each sandwich structure.

III.1.3.3. Results

Mechanical Properties of PLA-Based Sandwich Structures

The mechanical behavior of the PLA-based sandwich structures with a PLA honeycomb and PLA/flax outer layers was obtained in flexural and compression conditions. Obviously, as the thickness increases, the density of the panel (including the core and the skins) decreases (table III.1.3.1), mainly due to the PLA-honeycomb core. Some interesting properties of the shape memory behavior of PLA semi-hexagonal shapes are provided as Supplementary Information.

Table III.1.3.1. Equivalent density of the composite sandwiches with PLA honeycomb cores with different thicknesses.

Code	PLA Honeycomb Thickness (mm)	Equivalent Density of Composite Panel (Including Core and Skins) ($kg \cdot m^{-2}$)
PLA-HYN10	10	362
PLA-HYN20	20	279
PLA-HYN30	30	164

Figure III.1.3.2 shows the characteristic force-displacement plots for flexural texts (three-point bending). These show the typical behavior of composite sandwiches in these conditions. An initial elastic stage (almost linear) up to a maximum load value (813.3 N for PLA-HYN10) can be seen. Then, the load decreases to values of 520-530 N. This drop is associated with debonding between the skin and the core as reported by Xu, *et*

al. [48]. A similar pattern can be observed for PLA-HYN20, with a maximum load after the elastic behavior of 1372.3 N, which is reduced to half after the first debonding signs (see figure III.1.3.2).

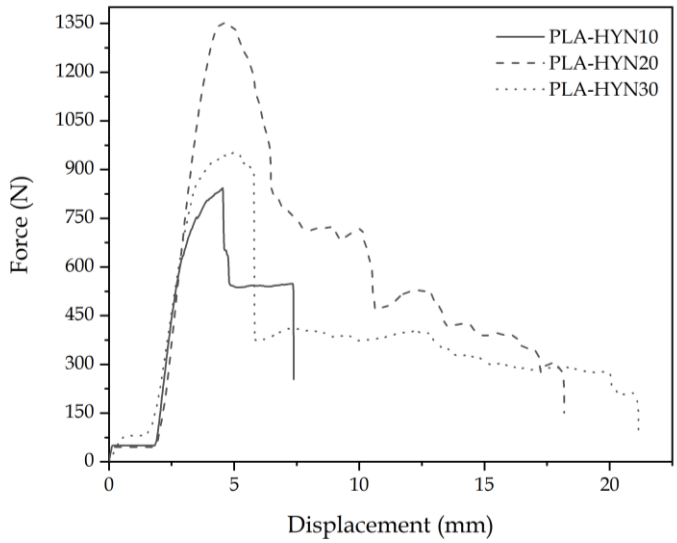

Figure III.1.3.2. Characteristic force–displacement diagrams (three-point bending) for composite sandwiches with PLA honeycomb cores with different thickness.

Figure III.1.3.3 left column pictures show the elastic region for all three composite sandwiches as the corresponding force-displacement curves show. Clear signs of debonding (white ellipse) can be observed for PLA-HYN10 (right column). After this initial debonding, the load is shared by the core and the nondebonded skins until the core or the skin fails. As it can be seen in figure III.1.3.3, PLA-HYN-10 failure occurs by breakage of the core and the bottom face, while in PLA-HYN-20, failure occurs by progressive debonding (white ellipse) as its corresponding force–displacement curve suggests. Regarding the composite with a 30 mm PLA honeycomb, failure occurs in a different way. It seems that the core-skin adhesion is not as good as in other composites, and the core fails by shear at a relatively low force of 912.5 N. The failure image (figure III.1.3.3) shows a clear buckling-shear combined effect on the PLA honeycomb core that promotes early failure (white square). Similar results have been reported by Li, *et al.* [49] in composite sandwiches subjected to out-of-plane loads, while Khan, *et al.* [50] carried out an in-depth experimental study on the damage of honeycomb sandwich panels and compared the experimental results with those obtained by finite element analysis (FEA).

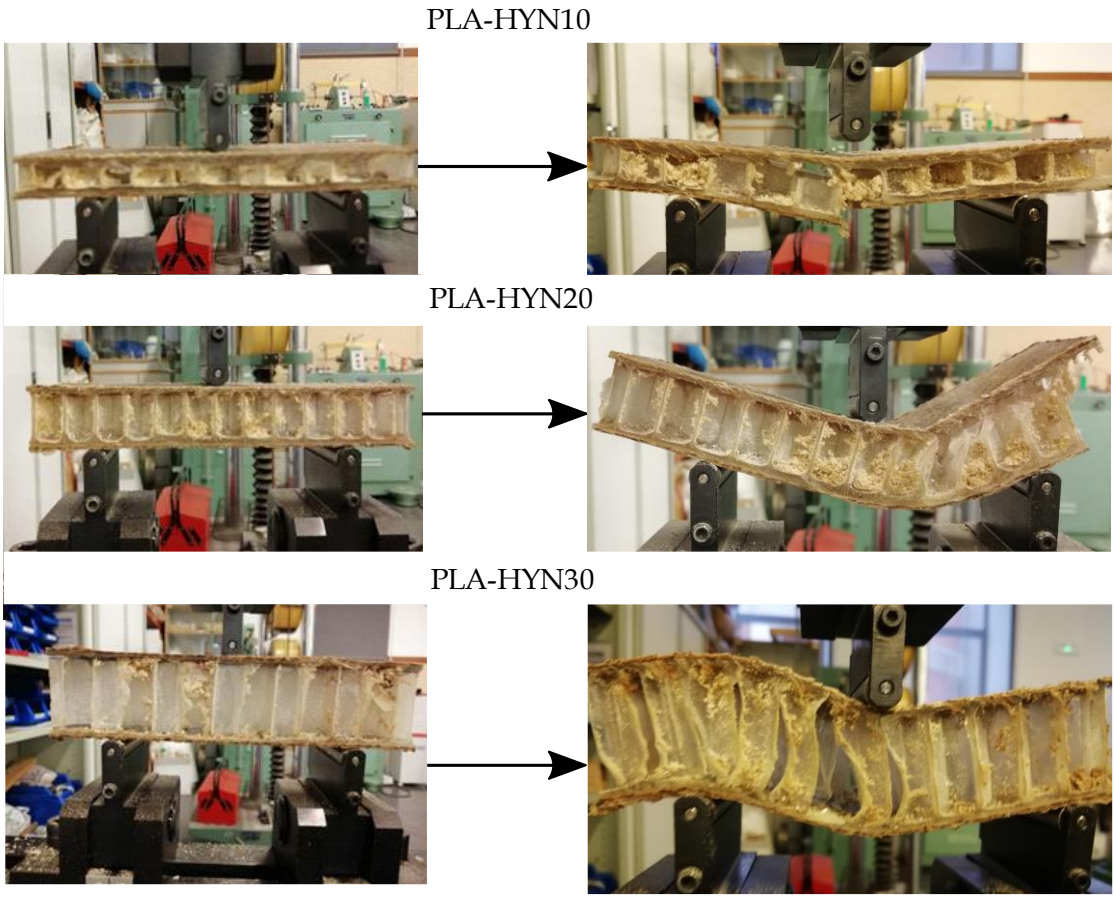

Figure III.1.3.3. Pictures of the three-point bending test of composite sandwiches with PLA honeycomb cores with different thicknesses: The left column shows the initial elastic stage; the right column shows the image after the failure.

Table III.1.3.2 summarizes the main results from both characterizations. It can be observed that the PLA-HYN10 sandwich structure, with a PLA honeycomb core thickness of 10 mm, shows the facing bending stress and the core shear stress with relatively high values of 33.0 and 0.66 MPa, respectively. These values are directly related to the maximum load the sandwich structure can withstand. These good results may be because the structure offers a good stability (no buckling in hexagonal cells) due to its low thickness compared to the 20 and 30 mm thickness honeycombs. In addition, the results suggest that the bonding between the components is good. Good bonding allows stress/load transfer by the shear between the outer faces and the core. The obtained results are comparable to those observed by Farooq, *et al.* [18], with sandwich panels made from carbon fibers with an epoxy matrix (outer faces), Nomex® honeycomb core and an epoxy-based adhesive film. Therefore, the mechanical properties of the PLA-based sandwich structures with PLA-based honeycombs could be considered a potential replacement for medium-to-high-performance structures based on synthetic materials. Cabrera, *et al.* [51] produced polypropylene sandwich panels based on

polypropylene composite laminates combined with a honeycomb polypropylene core, which presented a core shear stress and a face bending stress of 65 % and 38 %, respectively, lower than those obtained in this work for the same core thickness (20 mm).

Table III.1.3.2. Flexural (three-point bending) properties of PLA-based sandwich structures with PLA honeycomb cores.

Code	Flexural Properties				
	Ultimate Load, P (N)	**Sample Weight, W (g)**	**P/W ($N \cdot g^{-1}$)**	**Core Shear Stress, τ (MPa)**	**Facing Bending Stress, σ_b (MPa)**
PLA-HYN10	813.3 ± 31.1	7.3 ± 0.3	111.4	0.66 ± 0.03	33.0 ± 1.7
PLA-HYN20	1372.3 ± 59.8	9.7 ± 0.8	141.5	0.63 ± 0.03	31.4 ± 1.4
PLA-HYN30	912.5 ± 55.6	11.7 ± 0.9	78.0	0.29 ± 0.02	14.7 ± 0.9

The PLA-HYN20, with a 20 mm thick PLA-honeycomb structure, shows similar values of facing bending stress and core shear stress to PLA-HYN10. This means good load transfer from the faces to the core by shear. It should be noted that an increase in the core thickness results in a considerable increase in maximum load the sandwich structure can support, which is approximately 68 % higher compared to the 10 mm thick core structure. Arbaoui, *et al*. [52] and Xie, *et al.* [53] suggested that by increasing the core thickness, the resulting sandwich structures allow better load transfer before they fail. This may be related to the fact that by increasing the core thickness, the final structure increases its stiffness-to-weight ratio. This is because the core structure mainly increases the bending moment of the structure by distancing the outer faces from the neutral axis and resisting shear loads. This also suggests excellent properties of the face-to-core bonding with the partially biobased epoxy resin.

Unlike the other structures, the PLA-HYN30 structure presents the lowest values concerning the core shear stress and facing bending stress, being approximately 53 % lower in both cases, when compared to structures with a lower thickness (10 and 20 mm thick honeycombs). This can be caused by some separation that the outer faces had with the core, due to manufacturing issues decreasing the interface interaction between the core and the outer faces. This results in the stress not being correctly distributed and, subsequently, a decrease in the load that the structure can withstand, thus leading to a premature failure by a combination of shear and buckling [54]. In addition, table III.1.3.2 also includes the sample weight (W) and the ultimate load-to-weight (P/W) ratio, which agrees with the previous discussed results. These P/W ratios are very interesting

and comparable to others reported in the literature with epoxy-carbon fiber (T700) skins (1 mm thick) and different cores (triangular and hexagonal panels, 15 mm thick). Xu, *et al.* [48] reported higher core shear stress values up to 3 MPa as the skin contained carbon fiber and the cores and was also fiber-reinforced. Nevertheless, the P/W ratios were lower than those obtained in this work, thus showing the interesting properties PLA-honeycombs can provide to composite structures in terms of mechanical properties and lightness.

Concerning the flatwise-compressive properties of the sandwich structures, figure III.1.3.4 shows the characteristic force-displacement curves, while the damaged samples after compression are gathered in figure III.1.3.5. The force-displacement curves show an elastic behavior before a maximum compression load is reached. This is close to 5620 N for the PLA-HYN10. Above this, the core collapses and, finally, when both skins are almost in contact, the force increases, as the densification stage is reached, as reported by Feng, *et al.* [55]. Similar behavior can be observed for the other tested composites; nevertheless, the densification stage is delayed as the core thickness increases.

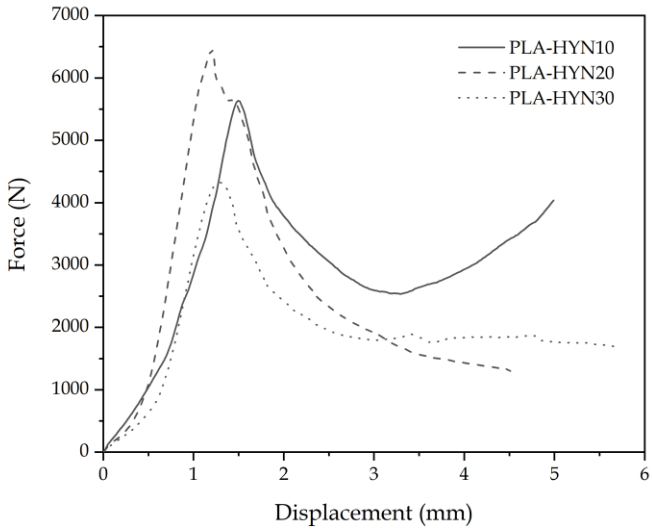

Figure III.1.3.4. Characteristic force–displacement diagrams (flatwise compression test) for composite sandwiches with PLA honeycomb cores with different thicknesses.

Figure III.1.3.5. Pictures of the flatwise compression test of composite sandwiches with PLA honeycomb cores with different thicknesses: The left column shows the initial elastic stage; the right column shows the image after the failure.

The main parameters from this test are summarized in table III.1.3.3; one can see that the PLA-HYN10 panel has a relatively low compressive strength value of 2.3 MPa. As with the flexural properties, it can be seen that when the core thickness is increased to 20 mm, the compressive strength has a slight increase value, reaching 2.6 MPa. Sallih, *et al.* [56] suggested that in honeycomb structures, the core thickness does not have a great influence on its compressive properties and is directly related to the thickness of the cell. This is because the compressive strength of the core is limited by the compressive strength of the original material. On the other hand, the structure with a 30 mm-thick core presents an unexpected drop in its compression properties. The compressive strength decreases by approximately 35 % compared to the structure with a honeycomb PLA core 20 mm thick. This may be due to the lack of synergy between the core and the outer faces, causing the structure to lose stability, resulting in premature material failure, as detected by flexural characterization.

Table III.1.3.3. Flatwise compressive properties of PLA-based sandwich structures with PLA honeycomb cores.

Code	Maximum Load, P (N)	Sample Weight, W (g)	P/W ($N \cdot g^{-1}$)	Compressive Strength, σ_c (MPa)
PLA-HYN10	5620 ± 300	18.0 ± 0.3	312.2	2.3 ± 0.3
PLA-HYN20	6419 ± 254	18.6 ± 0.5	345.1	2.6 ± 0.1
PLA-HYN30	4300 ± 420	21.1 ± 0.8	203.8	1.7 ± 0.1

III.1.3.4. Conclusions

Through this study, it was possible to develop highly environmentally friendly sandwich structures based on the PLA honeycomb core and PLA/flax outer faces. The manufacturing process used in the core and in the outer layers provides good control over the size and shape of the hexagonal cells and the thickness of the layers, which is a first step in the reproducibility of this process. The use of a nonwoven PLA and epoxy resin as a bonding medium gave good adhesion between the core and the outer faces (mainly on PLA-honeycomb cores with 10 and 20 mm thickness), which is a critical issue in sandwich structures. Good control of the pressure exerted on the structure must be necessary to ensure sufficient contact between the PLA honeycomb and the outer PLA/flax faces. If the applied pressure is too high, it can lead the core to failure as observed in composites with 30 mm thick PLA honeycombs.

It was observed that a PLA honeycomb core with a height of 20 mm (wall thickness of 250 μm) offered excellent results in terms of flexural and flatwise compressive properties because the forces to which the structure is subjected can be appropriately transferred.

This work has demonstrated that PLA-based honeycombs can be interesting candidates to obtain environmentally friendly sandwich structures with good balanced mechanical properties for medium-to-high technological applications. These environmentally friendly composite sandwich panels can offer more than 95 wt. % biobased content, with balanced mechanical properties for engineering applications, which would greatly help to reduce the carbon footprint.

III.1.3.5. Supplementary Materials

The following are available online at **https://www.mdpi.com/2073-4360/13/3/342/s1**, figure S1: Visual illustration of the qualitative shape memory evaluation in the recovery cycle of PLA films with different thicknesses: 100 μm (left column), 250 μm (middle column), and 500 μm (right column).

III.1.3.6. Funding

This research work was funded by the Spanish Ministry of Science and Innovation (MICI) project number MAT2017-84909-C2-2-R.

III.1.3.7. Acknowledgments

D.L. wants to thank Universitat Politècnica de València (UPV) for the grant received through the PAID-01-18 program. L.Q.-C. thanks Generalitat Valenciana (GVA) for his FPI grant (ACIF/2016/182) and the Spanish Ministry of Education, Culture, and Sports (MECD) for his FPU grant (FPU15/03812). R.G.-P. is the recipient of a Santiago Grisolía contract (GRISOLIAP/2018/168) from GVA. J.I-M. wants to thank Universitat Politècnica de València for his FPI grant (PAID-2019- SP20190011) and the Spanish Ministry of Science, Innovation and Universities for his FPU grant (FPU19/01759).

III.1.3.8. References

1. R. Stewart. Sandwich composites excel at cost-effective, lightweight structures. *Reinforced Plastics* **2011**, *55*, 27-31.
2. T. Garbowski, T. Gajewski, J.K. Grabski. Role of transverse shear modulus in the performance of corrugated materials. *Materials* **2020**, *13*, 3791.
3. S.D. la Pierre des Ammbrois, I. Corazzari, O. Damiano, L. Cornillon, A. Terenzi, V. Casalegno, M. Ferraris. Adhesive joining of zerodur–CFRP–zerodur sandwich structures for aerospace applications. *Macromolecular Materials and Engineering* **2020**, *305*, 2000464.
4. V.T. Le, N.S. Goo. Thermomechanical performance of bio-inspired corrugated-core sandwich structure for a thermal protection system panel. *Applied Sciences* **2019**, *9*, 5541.
5. A. Pavlović, D. Sintoni, G. Minak, C. Fragassa. On the modal behaviour of ultralight composite sandwich automotive panels. *Composite Structures* **2020**, *248*, 112523.
6. S. Ahmad, J. Zhang, P. Feng, D. Yu, Z. Wu, K. Ma. Processing technologies for nomex honeycomb composites (NHCs): A critical review. *Composite Structures* **2020**, 112545.
7. A. Manalo, T. Aravinthan, A. Fam, B. Benmokrane. State-of-the-art review on FRP sandwich systems for lightweight civil infrastructure. *Journal of Composites for Construction* **2017**, *21*, 04016068.
8. R. Stewart. At the core of lightweight composites. *Reinforced Plastics* **2009**, *53*, 30-35.
9. W. Ashraf, M. Ishak, M. Zuhri, N. Yidris, A. Yaacob, M. Asyraf. Investigation of different facesheet materials on compression properties of honeycomb sandwich composite. *Semin. Enau Kebangs. Bahau, Negeri Sembilan, Malaysia* **2019**, 129-132.
10. O. Sokolova, M. Kühn, H. Palkowski. Deep drawing properties of lightweight steel/polymer/steel sandwich composites. *Archives of civil and mechanical engineering* **2012**, *12*, 105-112.
11. Y. Feng, H. Qiu, Y. Gao, H. Zheng, J. Tan. Creative design for sandwich structures: A review. *International Journal of Advanced Robotic Systems* **2020**, *17*, 1729881420921327.

12. L. CoDyre, K. Mak, A. Fam. Flexural and axial behaviour of sandwich panels with bio-based flax fibre-reinforced polymer skins and various foam core densities. *Journal of Sandwich Structures & Materials* **2018**, *20*, 595-616.

13. J. Liu, J. Tao, F. Li, Z. Zhao. Flexural properties of a novel foam core sandwich structure reinforced by stiffeners. *Construction and Building Materials* **2020**, *235*, 117475.

14. O.R. Shah, M. Tarfaoui. Determination of mode I & II strain energy release rates in composite foam core sandwiches. An experimental study of the composite foam core interfacial fracture resistance. *Composites Part B: Engineering* **2017**, *111*, 134-142.

15. F. Balıkoğlu, N. Arslan, T. Demircioğlu, O. İnal, M. İren, A. Ataş. Improving four-point bending performance of marine composite sandwich beams by core modification. *Journal of Composite Materials* **2020**, *54*, 1049-1066.

16. D. Feng, F. Aymerich. Effect of core density on the low-velocity impact response of foam-based sandwich composites. *Composite Structures* **2020**, *239*, 112040.

17. D. Lascano, J. Valcárcel, R. Balart, L. Quiles-Carrillo, T. Boronat. Manufacturing of composite materials with high environmental efficiency using epoxy resin of renewable origin and permeable light cores for vacuum-assisted infusion molding. *Ingenius* **2020**, 62-73.

18. U. Farooq, M. Ahmad, S. Rakha, N. Ali, A. Khurram, T. Subhani. Interfacial mechanical performance of composite honeycomb sandwich panels for aerospace applications. *Arabian Journal for Science and Engineering* **2017**, *42*, 1775-1782.

19. V. Crupi, E. Kara, G. Epasto, E. Guglielmino, H. Aykul. Theoretical and experimental analysis for the impact response of glass fibre reinforced aluminium honeycomb sandwiches. *Journal of Sandwich Structures & Materials* **2018**, *20*, 42-69.

20. N. Sawal, M.A. Hazizan. Effect of core thicknesses on impact performance of thermoplastic honeycomb core sandwich structure under low-velocity impact loading. In Proceedings of Key Engineering Materials; 461-465.

21. C.O. Burada, C.M. MIRIŢOIU, M.M. STĂNESCU, D. Bolcu. Experimental determinations of some mechanical properties for new types of composite bars with polypropylene honeycomb core. *Proceedings of the Romanian Academy, Series A* **2015**, *16*, 70-79.

22. T. Czarnecki, J. Pflug. Polypropylene honeycomb boards from EconCore provide high performance at minimal costs. *REINFORCED PLASTICS-LONDON*- **2019**, *63*, 90-92.

23. J. Wang, C. Shi, N. Yang, H. Sun, Y. Liu, B. Song. Strength, stiffness, and panel peeling strength of carbon fiber-reinforced composite sandwich structures with aluminum honeycomb cores for vehicle body. *Composite Structures* **2018**, *184*, 1189-1196.

24. A. Khosravi, A. Fereidoon, M.M. Khorasani, G. Naderi, M.R. Ganjali, P. Zarrintaj, M.R. Saeb, T.J. Gutiérrez. Soft and hard sections from cellulose-reinforced poly (lactic acid)-based food packaging films: A critical review. *Food Packaging and Shelf Life* **2020**, *23*, 100429.

25. P. Nagasankar, S.B. Prabu, R. Velmurugan. Role of different fiber orientations and thicknesses of the skins and the core on the transverse shear damping of polypropylene honeycomb sandwich structures. *Mechanics of Materials* **2015**, *91*, 252-261.

26. J. Sewell, T. Czarnecki, J. Pflug. Continuous thermoplastic honeycomb sandwich panel process technology for cost optimal lightweight composites. *Reinforced Plastics* **2016**, *60*, 146-150.

27. V. Fombuena, S. MD. Study of the properties of thermoset materials derived from epoxidized soybean oil and protein fillers. *Journal of the American Oil Chemists' Society* **2013**, *90*, 449-457.

28. A. Carbonell-Verdu, L. Bernardi, D. Garcia-Garcia, L. Sanchez-Nacher, R. Balart. Development of environmentally friendly composite matrices from epoxidized cottonseed oil. *European Polymer Journal* **2015**, *63*, 1-10.

29. J. Pflug, I. Verpoest. Thermoplastic folded honeycomb structure and method for the production thereof. Google Patents: 2004.

30. J.P. Bratfisch, D. Vandepitte, J. Pflug, I. Verpoest. Development and validation of a continuous production concept for thermoplastic honeycomb. In *Sandwich structures 7: advancing with sandwich structures and materials*, Springer: 2005; 763-772.

31. D. Lascano, G. Moraga, J. Ivorra-Martinez, S. Rojas-Lema, S. Torres-Giner, R. Balart, T. Boronat, L. Quiles-Carrillo. Development of injection-molded polylactide pieces with high toughness by the addition of lactic acid oligomer and characterization of their shape memory behavior. *Polymers* **2019**, *11*, 2099.

32. M.P. Arrieta, A. Díez García, D. López, S. Fiori, L. Peponi. Antioxidant bilayers based on PHBV and plasticized electrospun PLA-PHB fibers encapsulating catechin. *Nanomaterials* **2019**, *9*, 346.

33. C. Villegas, M.P. Arrieta, A. Rojas, A. Torres, S. Faba, M. Toledo, M. Gutierrez, E. Zavalla, J. Romero, M. Galotto. PLA/organoclay bionanocomposites impregnated with thymol and cinnamaldehyde by supercritical impregnation for active and sustainable food packaging. *Composites Part B: Engineering* **2019**, *176*, 107336.

34. B.I. Oladapo, I.A. Daniyan, O.M. Ikumapayi, O.B. Malachi, I.O. Malachi. Microanalysis of hybrid characterization of PLA/cHA polymer scaffolds for bone regeneration. *Polymer Testing* **2020**, *83*, 106341.

35. T. Serra, M.A. Mateos-Timoneda, J.A. Planell, M. Navarro. 3D printed PLA-based scaffolds: a versatile tool in regenerative medicine. *Organogenesis* **2013**, *9*, 239-244.

36. L. Quiles-Carrillo, N. Montanes, D. Garcia-Garcia, A. Carbonell-Verdu, R. Balart, S. Torres-Giner. Effect of different compatibilizers on injection-molded green composite pieces based on polylactide filled with almond shell flour. *Composites Part B: Engineering* **2018**, *147*, 76-85.

37. L. Azzouz, Y. Chen, M. Zarrelli, J.M. Pearce, L. Mitchell, G. Ren, M. Grasso. Mechanical properties of 3-D printed truss-like lattice biopolymer non-stochastic structures for sandwich panels with natural fibre composite skins. *Composite structures* **2019**, *213*, 220-230.

38. A. Bourmaud, J. Beaugrand, D.U. Shah, V. Placet, C. Baley. Towards the design of high-performance plant fibre composites. *Progress in Materials Science* **2018**, *97*, 347-408.

39. J. España, M. Samper, E. Fages, L. Sánchez-Nácher, R. Balart. Investigation of the effect of different silane coupling agents on mechanical performance of basalt fiber composite laminates with biobased epoxy matrices. *Polymer composites* **2013**, *34*, 376-381.

40. M. Ramesh. Flax (Linum usitatissimum L.) fibre reinforced polymer composite materials: A review on preparation, properties and prospects. *Progress in Materials Science* **2019**, *102*, 109-166.

41. S. Amroune, A. Belaadi, M. Bourchak, A. Makhlouf, H. Satha. Statistical and experimental analysis of the mechanical properties of flax fibers. *Journal of Natural Fibers* **2020**, 1-15.

42. J.C. dos Santos, L.A. de Oliveira, T.H. Panzera, C.D. Remillat, I. Farrow, V. Placet, F. Scarpa. Ageing of autoclaved epoxy/flax composites: Effects on water absorption, porosity and flexural behaviour. *Composites Part B: Engineering* **2020**, *202*, 108380.

43. B. Enciso, J. Abenojar, M.A. Martínez. Effect of APPT treatment on mechanical properties and durability of green composites with woven flax. *Materials* **2020**, *13*, 4762.

44. A. Wang, G. Xian, H. Li. Effects of fiber surface grafting with nano-clay on the hydrothermal ageing behaviors of flax fiber/epoxy composite plates. *Polymers* **2019**, *11*, 1278.

45. V. Sadrmanesh, Y. Chen. Bast fibres: structure, processing, properties, and applications. *International Materials Reviews* **2019**, *64*, 381-406.

46. M. George, M. Chae, D.C. Bressler. Composite materials with bast fibres: Structural, technical, and environmental properties. *Progress in materials Science* **2016**, *83*, 1-23.

47. L. Nickels. Car with a biodegradable core. *Reinforced Plastics* **2017**, *61*, 332-334.

48. C. Xu, H. Yanjiao, W. Shou, L. Chun, F. Luping. Stress distribution on sandwich structure with triangular grid cores suffered from bending load. *International Journal of Aerospace Engineering* **2015**, *2015*, 8.

49. W. Li, C. Qiu, Z. Li, H. Nie. A failure criterion for honeycomb structures considering the onset of instability under out-of-plane loads. *Journal of Sandwich Structures & Materials* **2021**, *23*, 3519-3539.

50. M.S. Khan, A. Abdul-Latif, S.S.R. Koloor, M. Petrů, M.N. Tamin. Representative cell analysis for damage-based failure model of polymer hexagonal honeycomb structure under the out-of-plane loadings. *Polymers* **2021**, *13*, 52.

51. N. Cabrera, B. Alcock, T. Peijs. Design and manufacture of all-PP sandwich panels based on co-extruded polypropylene tapes. *Composites Part B: Engineering* **2008**, *39*, 1183-1195.

52. J. Arbaoui, H. Moustabchir, C.I. Pruncu, Y. Schmitt. Modeling and experimental analysis of polypropylene honeycomb multi-layer sandwich composites under

four-point bending. *Journal of Sandwich Structures & Materials* **2018**, *20*, 493-511.

53. S. Xie, Z. Feng, H. Zhou, D. Wang. Three-point bending behavior of Nomex honeycomb sandwich panels: Experiment and simulation. *Mechanics of Advanced Materials and Structures* **2020**, 1-15.

54. J. Grünewald, P. Parlevliet, V. Altstädt. Manufacturing of thermoplastic composite sandwich structures: A review of literature. *Journal of Thermoplastic Composite Materials* **2017**, *30*, 437-464.

55. H. Feng, L. Liu, Q. Zhao. Experimental and numerical investigation of the effect of entrapped air on the mechanical response of Nomex honeycomb under flatwise compression. *Composite Structures* **2017**, *182*, 617-627.

56. N. Sallih, P. Lescher, D. Bhattacharyya. Flatwise compressive properties of kenaf/polypropylene honeycomb core. In Proceedings of IOP Conference Series: Materials Science and Engineering; 012031.

Adaptado del artículo

III.1.4. A comparative study of mechanical properties of polylactide bio-composites with woven and non-woven jute reinforcements

Diego Lascano[1], Cristobal Aljaro[2], Eduardo Fages[3], Sandra Rojas-Lema[1], Juan Ivorra-Martinez[1], Nestor Montanes[1]

[1] Technological Institute of Materials (ITM), Universitat Politècnica de València (UPV), Plaza Ferrándiz y Carbonell 1, 03801 Alcoy, Spain.

[2] Hilaturas Ferre S.A., Calle Molines, 2, 03450 Banyeres de Mariola, Spain.

[3] Textile Research Institute (AITEX), Plaza Emilio Sala, 1 03801 Alcoy, Alicante, Spain.

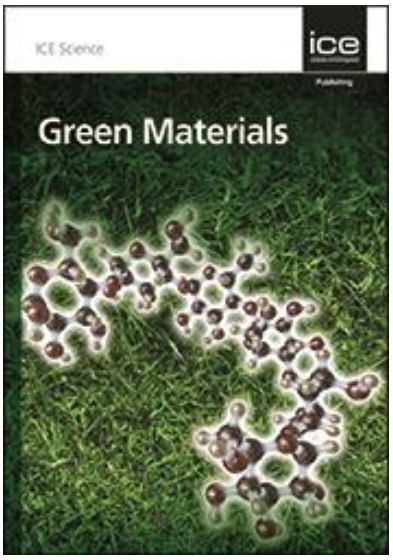

Green Materials. Under review

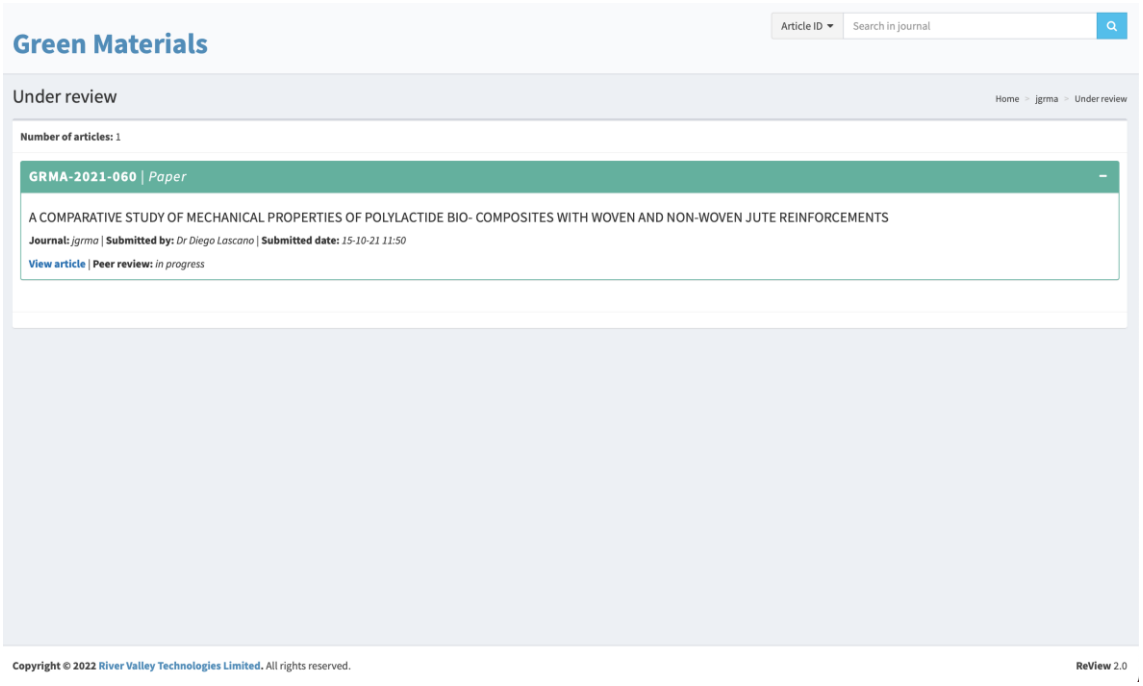
Green Materials
Article ID
Search in journal
Under review
Home > jgrma > Under review
Number of articles: 1
GRMA-2021-060 | Paper
A COMPARATIVE STUDY OF MECHANICAL PROPERTIES OF POLYLACTIDE BIO- COMPOSITES WITH WOVEN AND NON-WOVEN JUTE REINFORCEMENTS
Journal: jgrma | Submitted by: Dr Diego Lascano | Submitted date: 15-10-21 11:50
View article | Peer review: in progress
Copyright © 2022 River Valley Technologies Limited. All rights reserved.
ReView 2.0

A comparative study of mechanical properties of polylactide bio-composites with woven and non-woven jute reinforcements

Abstract

The concern that has arisen in recent years over the excessive use of oil-based materials has made the development of new materials with low environmental impact imminent, in this context. In this study, eco-friendly compounds were produced with a thermoplastic poly (lactic acid) matrix (PLA)and jute fibers (woven and non-woven) as reinforcement. PLA/jute bio- composites were manufactured by hot-press molding. The effect of the amount of jute fibers reinforcement (in the 30-50 wt. % range) on the tensile and bending properties of bio- composites was analyzed, and the fiber-matrix interaction were assessed by scanning electron microscopy (SEM). The results suggest hot compression moulding is a simple technique to obtain high environmental efficiency bio-composites with high reinforcement loading (up to 50 wt. %). As expected, the tensile properties are directly related to the amount of fiber loading, as well as the directionality that the fibers have in the composite. Mechanical performance is also highly dependent on fiber-matrix interactions. These bio- composites could be attractive as substitutes for conventional composites and/or engineering plastics.

Keywords: Biopolymers; mechanical properties; biofiber.

III.1.4.1. Introduction

The search for high mechanical performance materials that can replace conventional metallic materials and their alloys has made the development of new materials imminent. Recently, composite materials have been extensively studied due to the diverse range of final properties that can be obtained, making them invaluable in industrial and highly engineered applications [1]. Fiber-reinforced polymeric materials are among the most common, as materials with unique properties can be tailored by correctly defining the type of matrix and reinforcing fibers, these materials generally have high strength, good stiffness, and low weight [2]. Thermoset matrices such as epoxy resins, polyurethanes, unsaturated polyesters, among others [3-6], and thermoplastic matrices such as polyethylene (PE), polypropylene (PP), and polyvinylchloride (PVC), among others [7-9], have been some of the most widely used materials in composites. This has resulted in a huge production of polymers reaching 368 million tonnes worldwide by 2019, with the largest producers being Asia with 51 %, followed by North America with 19 % and Europe with 16 % [10]. This has led to an increase in the CO_2 emissions to the environment during their production. This phenomenon, together with the low capacity common plastics have to biodegrade, has led to the accumulation of these materials over long periods [11]. Given that the amount of plastic waste has increased from 24.5 Mt in 2006 to 29.1 Mt in 2018 [10].

Due to the relatively good ratio between final properties and production cost has made them one of the most widely used reinforcement fibers, as can be seen in the extensive literature on glass fibers (GF) and their derivatives [12-14]. Despite carbon fibers (CF) are more expensive than GF, they offer unique mechanical properties (strength and stiffness) that, together with a remarkably low density, allow their use in high-performance applications such as aerospace, aeronautics, automotive areas, and so on [15-18]. Nevertheless, manufacturing of CF requires complex processes at high temperatures which contribute to increase the overall carbon footprint. This has led to increased awareness in the last few years of the significant environmental effects associated with the indiscriminate consumption of petroleum-derived materials and high energy consumption manufacturing processes. For this reason, the research and development of new materials with a lower environmental impact for their eventual substitution has emerged in the last decade [19]. The concept of environmentally friendly materials can be related to two opposite stages in their life-cycle. The first concern is directly related to the origin, which can be petroleum or a renewable resource. The second topic considers the end of the life-cycle, thus sorting materials in two main groups, namely biodegradable (disintegrable or compostable), or non-biodegradable

[20,21]. Despite some remarkable advances have been done in the field of bio-based thermosetting materials such as epoxies (EP) from epoxidized vegetable oils [6,22-24], unsaturated polyesters (UP) with fully or partial bio-based content [25,26], phenolics (PF) [27,28], and so on, the most important advances in the field of biopolymers has been observed in the thermoplastic industry.

Thermoplastic biopolymers include both bio-based and/or biodegradable polymers. Some aliphatic/aromatic petroleum-derived polyesters such as poly(□-caprolactone) (PCL), poly(butylene succinate) (PBS), poly(butylene adipate-*co*-terephthalate) (PBAT), poly(glycolic acid) (PGA), among others have gained interest as can disintegrate under controlled composting conditions. Despite these polymers are interesting, biobased and biodegradable polymers offer the best environmental efficiency. Among these, poly(lactide) – PLA and poly(hydroxyalkanoates) – PHAs are being intensively studied [29-33]. Within these biomaterials, PLA is the one that has reached a greater presence in several sectors, with a production and consumption of 200,000 tons per year and an expected increase of more than 1,000,000 tons at present [34]. PLA is an aliphatic polyester produced exclusively from renewable resources, obtained by fermentation of starch-rich materials such as potato starch, sugar beet or sugar cane, among others [35]. Outstanding properties such as rapid degradability under composting conditions, compatibility with the human body, high tensile strength, good clarity, have positioned PLA as a suitable material for sectors such as biomedical, packaging, films, pharmaceuticals, to name the main ones [36-38]. In addition, PLA has driven the development of new composite materials employing renewable raw materials in the form of reinforcing fibers and/or fillers [20,39,40]. The final properties of these new materials will depend on both the nature of the reinforcement and the amount of filler used, although the biodegradability property would not be affected [41].

The choice of natural plant fibers is a solution to conventional fibers used to improve the mechanical behavior of biopolymers, without impairing their ecological characteristics. Furthermore, the employment of natural fibers presents several advantages over conventional fibers, such as low production costs, biodegradability, low weight, among others [42,43]. Among the most commonly used fibers are flax, sisal, hemp, jute, and many others, which have different physical, chemical and mechanical properties depending on their composition [44-47]. Jute, like most natural fibers, is composed of a cellulose structure (59-71.5 %), which is responsible for its mechanical properties, embedded in a hemicellulose matrix (13.6-20.4 %), which generally controls the ability to absorb moisture and lignin (11.8-13 %), which provides greater thermal stability [48,49]. Jute fiber offers interesting balanced properties in terms of insulating

capacity, hygroscopicity, biodegradability, and rather good mechanical properties. Nevertheless, as with other natural fibers, the final properties are influenced by various parameters such as the fiber length, composition, manufacturing process, crop conditions, plant part, and so on. Biswas*, et al.* [50], reported the importance of fiber length on final mechanical properties. They reported tensile strength values between 200 and 600 MPa with an elongation at break from 1.25 % up to 1.9 % for a fiber span length of 25 mm. With regard to the Young's modulus, as it represents the slope of the stress-strain curve, they reported values ranging from 10 to 27 GPa, depending on the fiber span length. These properties are in agreement with other values as those reported by Ramnath*, et al.* [51], with tensile strength values comprised between 393 – 800 MPa and Young's modulus ranging from 13 to 26.5 GPa. In addition it is cost-effective ($0.5 per kilo) compared to synthetic fibers such as GF [52]. India is one of the world's largest producers, with an annual production of 3,450,000 tons [53,54]. This has led several authors to focus their efforts on the study of jute-based composite materials. Du*, et al.* [55] manufactured bio-composites based on jute fabrics pre-treated with an alkaline solution in a PLA matrix by hot compression molding. The pretreatment resulted in better bonding between the fibers and the matrix, as well as improved thermal stability. Khan*, et al.* [56] investigated the influence of fiber orientation on the mechanical properties of bio-composites made from non-woven jute fabrics and woven jute fabrics in PLLA matrices. They reported that woven materials offer superior mechanical properties compared to non-woven materials, giving better warp than weft directions. Burrola-Núñez*, et al.* [57] used short jute fibers pre-treated with alkaline solutions and maleic anhydride in a PLA matrix in the manufacture of injection molded composites. The addition of 10 % pretreated fibers provided a clear reinforcing effect to the matrix, contributing to an improvement of the overall mechanical and thermal properties. Zafar*, et al.* [58] manufactured bio-composites from PLA and jute fibers treated with different solutions such as NaOH and (NaOH+silane) by melting extrusion, which was subsequently foamed by high-pressure injection molding.

The main objective of this study is the development and characterization of highly environmentally friendly biocomposites based on PLA matrix and different jute reinforcement contents in woven and nonwoven fabrics, by using a cost-effective hot compression moulding process. The influence of the weight content load of the jute fiber on the mechanical properties of the bio-composite in terms of flexural and tensile properties is shown. The originality of this work is the use of a simple process based on direct thermocompression with PLA pellets and woven/non-woven jute layers, to adjust

the desired compositions. Furthermore, the quality of the interface between the jute fiber and the matrix is assessed by scanning electron microscopy (SEM).

III.1.4.2. Experimental

Materials

A commercial Ingeo™ 6201D PLA grade biopolymer obtained by NatureWorks LLC (Minnetonka, MN, USA) was used as the thermoplastic matrix. It has a glass transition temperature (T_g), around 60 ºC and a melting peak temperature close to 170 ºC; this grade possesses a melt flow index (MFI) between 15-30 g/10 min measured at 210 ºC. it also has a relative density of 1.24 g/cm^3. Two types of jute fabrics were used as reinforcement fibers; the first one was a biaxial plain wave fabric with a surface density of 380 g/cm^2. The second one, consisted of a non-woven fabric with a surface density of 270 g/cm^2, both of them were kindly supplied by Hilaturas Ferre S.A. (Alicante, Spain).

Manufacturing of the Pla/Jute Bio-Composites

Manufacturing of Pla/Jute bio-composites was carried out by hot compression molding in a Hoytom M.N 1417 hot-press from Robima S.A. (Bilbao, Spain) equipped with a temperature control from Dupra S.A. (Castalla, Spain). Prior to the processing of the bio- composites, PLA pellets were dried at 60 °C for 24 hours to reduce their moisture content and prevent the hydrolysis deterioration [59]. A schematic plot of the hot compression process can be seen in figure III.1.4.1. Despite there have been developed many processes which combine different stacking sequences of polymer film/sheet and fabrics, this work focuses on the potential of a still more easy processing technology. This consists of depositing interleaved layers of PLA pellets and jute fiber in an aluminum mold (figure III.1.4.1a & figure III.1.4.1b) designed to produce squared plates of 200 x 200 mm and different thickness. Different weight percentages of jute fibers were selected for this work, ranging from 30 to 50 wt. % (table III.1.4.1).

Table III.1.4.1. Composition and code designation of the different PLA/jute bio-composites.

Jute Fiber (wt %)	Type fiber					
	Woven			Non-woven		
	Code	Jute layers	PLA layers	Code	Jute layers	PLA layers
0	PLA_0	-	1	PLA_0	-	1
30	PLA_WJF_{30}	3	4	PLA_NWJF_{30}	5	6

40	PLA_WJF$_{40}$	4	5	PLA_NWJF$_{40}$	6	7
50	PLA_WJF$_{50}$	5	6	PLA_NWJF$_{50}$	8	9

The corresponding amounts of PLA pellets were weighed and distributed appropriately between the jute layers, to give the above-mentioned wt. % jute in the bio-composites. To enhance full embedment of jute fabrics with PLA, both the top and the bottom layers consisted of PLA pellets (figure III.1.4.1c). Since the peak melt temperature of PLA is around 165-170 ºC, the mould was closed and subjected to a temperature of 190 ºC with a constant load of 2 Tn for a total time of 20 min. These conditions allow PLA to flow and embed the jute reinforcements. After the heating program, the mould was cooled down to 70 ºC in a water circulating bath; finally, the obtained green composite plates were released from the mould for further characterization.

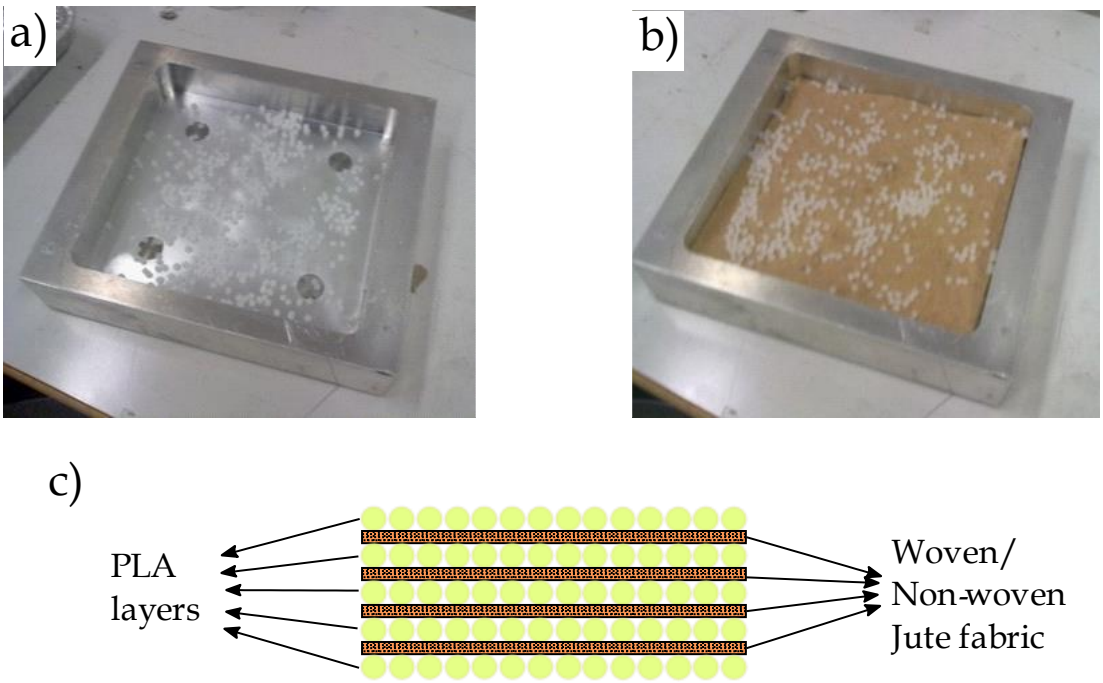

Figure III.1.4.1. Manufacturing process of PLA/jute bio- composites by hot compression moulding. a) placing the first PLA layer on the aluminum mould; b) placing the last PLA layer on top of the jute fiber layer; c) schematic representation of the stacking sequence of PLA pellets and jute fibers.

Figure III.1.4.2 shows the appearance of woven (figure III.1.4.2a) and non-woven (figure III.1.4.2b) jute fiber fabrics supplied by the manufacturer, where the distribution and direction of the fibers in the different fabrics can be seen. Figure III.1.4.2c and figure III.1.4.2d, show the surface appearance obtained after hot compression moulding, where it was possible to observe the good compaction that jute fabrics have with the PLA matrix

since the matrix was able to completely soak the jute fabrics. This results in highly homogeneous composites.

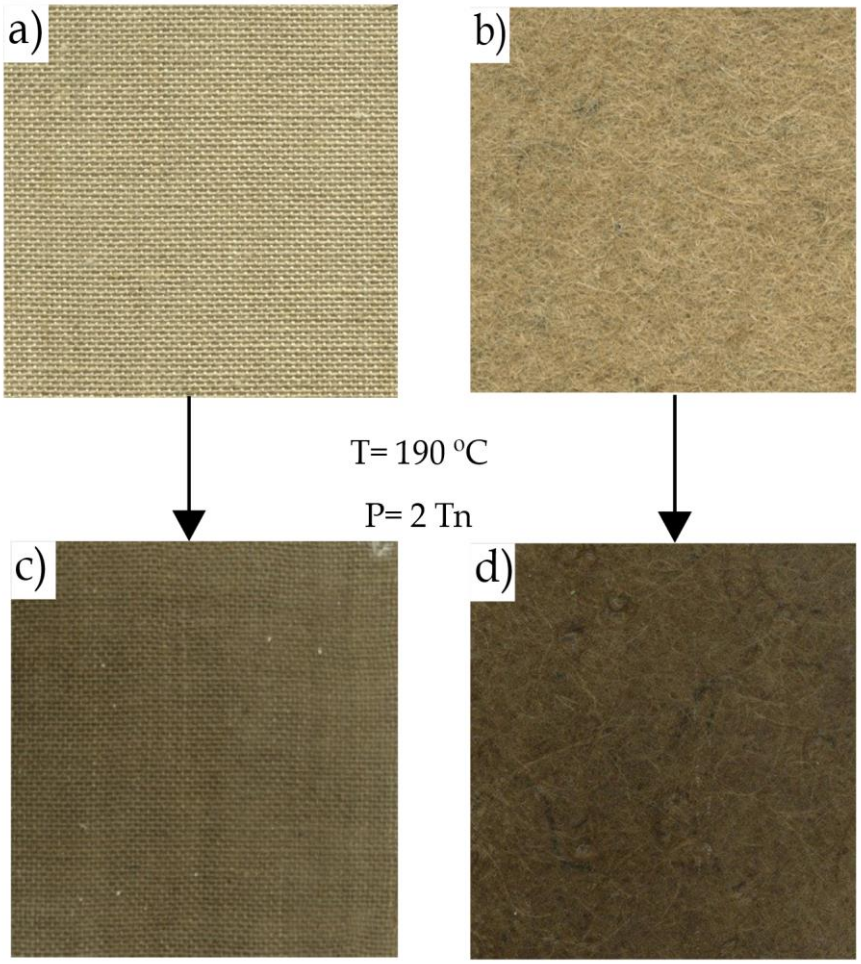

Figure III.1.4.2. Images of the woven jute fabric (left column) and the non-woven jute fabric (right column). a)-b) before hot compression moulding and c)-d) after hot compression moulding.

Mechanical Properties of the Pla/Jute Bio-Composites

The mechanical properties of the Pla/Jute bio- composites were evaluated in tensile and flexural conditions. Both tests were performed in a universal testing machine Instron 3340 (Barcelona, Spain) at room temperature (~25 ºC), the machine was equipped with a load cell of 5 kN. Tensile test was performed following ASTM D3039/D3039M. The standard size of the samples for tensile test was 250 mm length, 25 mm width, and 2.5 mm thick with a crosshead rate of 10 mm/min. By means of this test it was possible to obtain the tensile strength at break (σ_b), the Young's modulus (E_t), and the elongation at break (%ε_b). Flexural test was performed according to the ASTM D790 standard. The specimens for flexural tests had the following dimensions: 100 mm length, 10 mm width, and 2.5 mm thick. The crosshead rate speed was set to 5 mm/min

and the corresponding flexural strength (σ_f) and the flexural modulus (E_f) were obtained. To obtain reliable data, at least five samples were analyzed for each compound.

Morphology Analysis of the Pla/Jute Interface

The interaction between the jute fibers (woven and non-woven fibers) and the PLA matrix was studied by scanning electron microscopy (SEM) in the fractured sections of the specimens after tensile tests. A Phenom scanning electron microscope supplied by FEI (Eindhoven, The Netherlands) operated at 10 kV was used. Prior to the surface analysis, all samples were coated with a thin layer of gold/palladium alloy in an EMITECH Sputter Coater model SC7620 from Quorum Technologies (East Sussex, UK). Furthermore, using a stereomicroscope system model SZX7 supplied by Olympus (Tokyo, Japan) it was possible to observe the morphology of the cross-section of the different bio-composites based on woven and non-woven fibers.

III.1.4.3. Results and Discussion

Mechanical Properties of the Pla/Jute Bio-Composites

The mechanical characterization of neat PLA and the Pla/Jute bio-composites with jute fibers are gathered in table III.1.4.2. It is possible to see that neat PLA has a high Young's modulus (E_t), and a high tensile strength (σ_b) with values of 3430.3 MPa and 56.7 MPa, respectively. This is in line with the literature as PLA is a stiff material that also presents a brittle nature, which is evidenced by its low elongation at break of about 1.7 % [59,60]. The incorporation of 30 % of woven jute fiber promotes a slight decrease in the stiffness of the Pla/Jute bio-composites, which can be seen in a reduction of 7.61 % and 12 % of its Young's modulus and tensile strength, respectively, as well as a notable increase of around 53 % in its elongation at break (2.6 %). It shows that this amount of fiber is not sufficient to reinforce the PLA and in this case would be acting as a filler, similar situation was reported by Burrola-Núñez*, et al.* [57]. In addition, these results also suggest stresses are not transmitted evenly between the matrix and the reinforcing fiber [61], this may be the result of using fibers with polar nature in a non-polar PLA matrix [62,63], without any other treatment or coupling agent. It is worth bearing in mind that the 40 wt % Pla/Jute bio-composites with woven jute fibers presents a slight increase in the Young's modulus and tensile strength with values of 3325.7 MPa and 53.2 MPa, respectively, these values being very close to those of neat PLA, it also has a higher elongation at break than the latter, which makes the properties in general very attractive, since, by integrating natural fibers, the amount of PLA in the material can be reduced, resulting in a material with good properties and reduced costs. These results are in line

with those presented by Singh*, et al.* [64]. By increasing the percentage of jute fibers up to 50 wt. %, a clear increase in the material's stiffness is observed when the bio-composite has Young's modulus of 3779 MPa, and its brittleness also increases. It is necessary to take into account that Young's modulus describes the stress-strain relationship in the linear (elastic) region. Therefore, a decrease in the elongation at break is shown by an increase in the ratio and, subsequently, in the Young's modulus [57,61,65]. The tensile properties of materials reinforced with woven fibers are directly related to the direction of their fabric (weft and warp), so if the applied load is coincident with one of these directions the material will have good properties. Furthermore, the mechanical performance of PLA and jute bio-composites depends to a large extent on the quality of the interface between the reinforcing fiber and the surrounding matrix [66]. As expected, due to the random arrangement of the fibers in the nonwoven jute bio-composites, the resulting tensile properties are lower compared to woven jute fiber bio-composites. Taking this into account, it is remarkable that both Young's modulus and tensile strength show a considerable reduction, reaching values of 1111.7 MPa and 14.7 MPa, respectively, when the composite is reinforced with 30 wt. % non-woven jute fiber. Despite increasing the percentage of jute fiber to 40 or 50 %, the reinforcing effect is not noticeable to any great extent as the modulus remains almost invariable with values around 1300 MPa. This may be because both the fibers and the matrix act as separate phases, i.e. poor load transfer between the matrix and the fiber. This effect can be attributed to several phenomena. On one hand, to the low affinity between the jute fibers and the PLA matrix due to their hydrophilic and hydrophobic nature [67], respectively. On the other hand, Khan*, et al.* [68] claims that in high percentages of fibers the matrix unable to completely wet/embed the fibers, resulting in a lack of bonding between the fibers and the matrix, which causes a decrease in the stiffness of the material due to poor stress distribution. Despite this, it may be observed that the tensile strength is positively influenced by the increase in fiber loading. With a fiber content of 50 wt. %, the σ_b value is 34.5 MPa, 134 % higher than that of the green composite with a 30 wt. % non-woven jute fiber. It should be noted that the amount of non-woven fiber loading does not affect elongation at break, remaining at about 2.6 %. Despite having relatively low tensile properties, when non-woven jute fibers are incorporated, these results are promising as they exhibit mechanical properties similar to those of commodity thermoplastics such as polypropylene (PP) [69], or high-density polyethylene (HDPE) [70], with the advantage that having natural fibers in their structure makes the resulting materials more attractive in environmental terms and production costs.

Table III.1.4.2. Tensile and flexural properties of the Pla/Jute bio-composites.

Code	Tensile Properties			Flexural Properties	
	E_t (MPa)	σ_b (MPa)	ε_b (%)	E_f (MPa)	σ_f (MPa)
PLA_0	3430.3±60.3	56.7±2.8	1.7±0.06	3338.8±102.5	39.8±2.1
PLA_WJF_{30}	3169.2±128.4	49.8±1.9	2.6±0.09	3740.4±152.2	86.0±3.4
PLA_WJF_{40}	3325.7±166.3	53.2±3.1	2.6±0.1	3621.8±144.2	94.0±3.8
PLA_WJF_{50}	3779.0±151.1	44.9±2.8	1.5±0.1	3993.6±115.7	71.7±2.9
PLA_NWJF_{30}	1111.7±65.1	14.7±0.6	2.5±0.02	3489.3±137.2	39.4±2.5
PLA_NWJF_{40}	1078.0±58.7	29.1±1.3	2.6±0.03	3597.1±146.7	42.8±2.6
PLA_NWJF_{50}	1345.3±69.2	34.5±2.1	2.6±0.06	3679.8±128.4	62.2±3.1

Regarding the flexural properties of the PLA-based bio-composites reinforced by jute fiber fabrics, it is possible to see that neat PLA has a flexural modulus and flexural strength of 3338.8 and 39.8 MPa, respectively, which are close to those reported by Dong*, et al.* [71]. It can be clearly noticed that both the flexural modulus and the flexural strength of jute fiber reinforced bio-composites tend to increase with the increase in the wt. % of jute fiber [72]. In composite materials made of fiber fabrics, the flexural strength and stiffness of is generally given by the external layers. In flexural conditions, the upper face is subjected to compressive stress while the bottom face is, mainly subjected to stretching (tension). Therefore, the flexural behaviour of the bio- composites depends on the strength of their external faces [73]. By adding 30 wt. % of the woven jute fiber, an increase of 12 % and 116 % of the flexural modulus and flexural strength, respectively, can be detected, thus showing flexural conditions are less aggressive in terms of stress concentration phenomena as it is the case of tensile tests. By increasing the fiber load by up to 50 wt. %, the flexural modulus rises to 3993.6 MPa, which corresponds to an improvement of about 20 % compared to pure PLA, showing a clear improvement in flexural stiffness. Similarly, there is an increase in flexural strength, reaching values of 71.7 MPa. This is due to the configuration of the jute fibers on the bio-composite structure, i.e. the directionality of the fibers, which makes them capable of withstanding greater loads [74]. As with woven fiber-reinforced composites, the flexural properties of non-woven fiber reinforced bio- composites are related to the amount of fiber loading [75], resulting in increased flexural properties by increasing the wt. % of fiber in the green composite. It can be seen that bio- composites with 50 wt. % non-woven jute, values of 3679.8 and 62.2 MPa with respect to the flexural modulus and flexural strength, respectively, were recorded. The increase in flexural properties achieved by non-woven fibers is slightly less than that achieved by woven fibers. This may be due to several factors, including the low interaction between the jute fibers and the matrix [76], and the

distribution of the fibers in the matrix [68]. Jawaid*, et al.* [77] suggested that the unordered distribution of non-woven fibers in the matrix causes a counterproductive effect on the flexural properties since having a smaller continuous surface makes the composite to have a lower load capacity. This effect that can be clearly seen in woven fibers, which are composed of long, perfectly aligned and continuous fibers, and this, results in better load capacity. Singh*, et al.* [64], have recently reported interesting results in jute/PLA bio-composites by using different processing temperatures ranging from 160 ºC to 180 ºC. The most relevant findings they provide is there is an increasing tendency on mechanical properties up to 30 v/v. % jute fiber and above this, the mechanical properties decrease. They attribute this to the weak fiber-matrix interface interactions as the PLA matrix content is reduced.

Fiber-Matrix Interaction and Morphology Analysis of the Pla/Jute Bio-Composites

In fiber-reinforced bio- composites, factors related to the distribution, fiber-matrix interaction, and directionality of the reinforcement fibers in the matrix, among others, have a significant influence on the mechanical performance of the composite. In general, the reinforcement fiber is stiffer than the matrix and if good fiber-matrix interaction exists (isodeformation conditions), the stress transfer from the lower stiffness (matrix) to the higher stiffness (fiber) component is allowed. In contrast, if the bonding created between the matrix and the fiber is weak, these stresses will be inadequately transmitted from the matrix to the fiber, causing the premature failure of the material due to the lack of cohesion between its components [58]. Distribution and directionality also have a critical role to play in the performance of composite materials, since the directionality of the reinforcement fibers towards the direction of the applied load results in improved strength and stiffness in that direction [74]. Figure III.1.4.3 shows stereomicroscopy images of the cross-section of woven jute fiber reinforced bio- composites (figure III.1.4.3a, figure III.1.4.3c, and figure III.1.4.3e), and non-woven jute fiber-reinforced bio- composites (figure III.1.4.3b, figure III.1.4.3d, and figure III.1.4.3f). The alignment of the fibers in woven jute bio- composites is clearly observed with the typical wave shape. Unlike bio-composites reinforced with woven jute fibers, bio- composites with non-woven fibers show a non-uniform distribution of the fibers characteristic of this type of material (random). Despite this, a good homogeneity impregnation can be observed in both cases between the different jute fibers and the PLA matrix. Similar findings were presented by Gnaba*, et al.* [78].

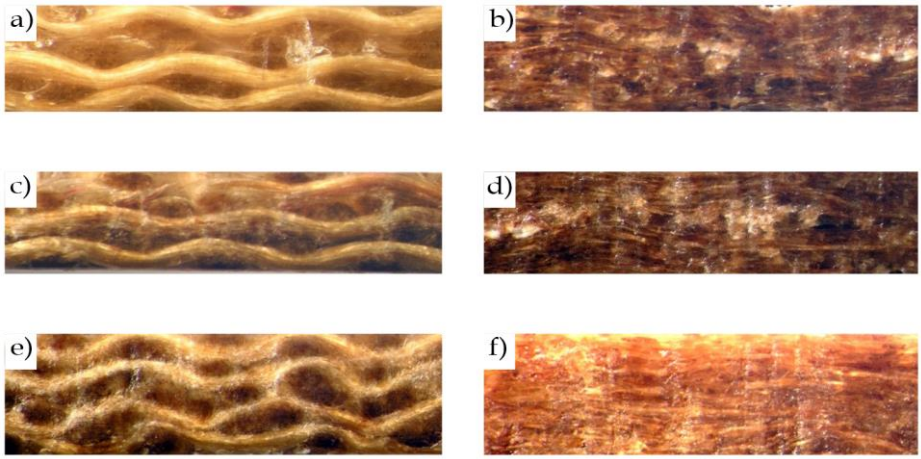

Figure III.1.4.3. Stereomicroscopy images at magnification of 12.5× corresponding to the cross section of the woven jute fiber green composite (left column) and non-woven jute fiber green composite (right column) of a)-b) 30 wt. %, c)-d) 40 wt. %, and e)-f) 50 wt. %.

Jute fiber is composed of aligned tubular cells which are responsible for its moderate mechanical properties and excellent insulation properties according to Fidelis, *et al.* [79]. Figure III.1.4.4 shows images of the jute fiber morphology.

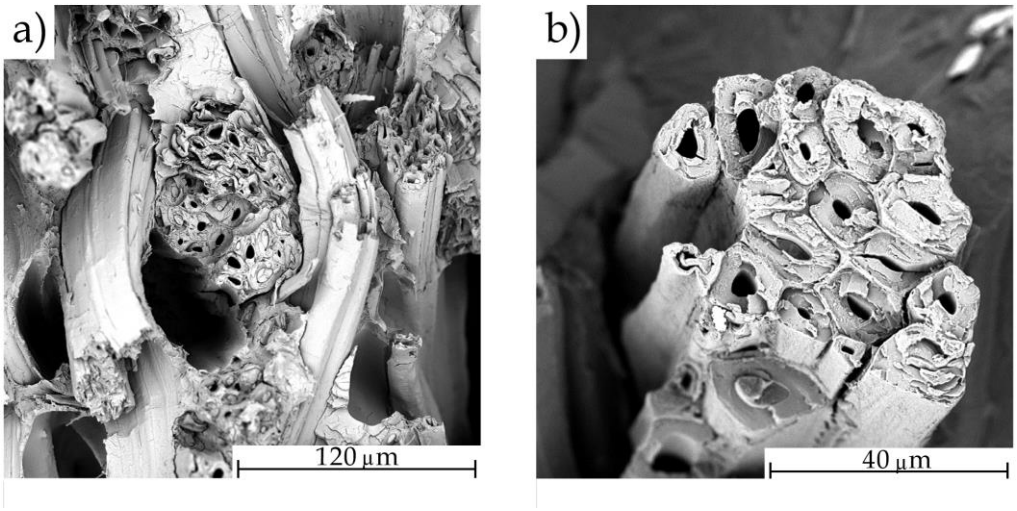

Figure III.1.4.4. SEM images of the jute fiber used: (a) x1000, with a marked scale of 120 µm. (b) x3000, with a marked scale of 40 µm.

To better understand the phenomenon of the interaction between the jute reinforcement fibers and the matrix, the fractured surfaces of the samples subjected to tensile tests of the different bio- composites were observed by SEM. As already mentioned, the good synergy between its components (matrix-fiber) has a direct effect on mechanical performance. The good bond between these elements ensures that the stresses transfer can occur in an appropriate way from the matrix to the fibers, resulting in the desired reinforcing effect by integrating the fibers into the structure of the green

composite [80]. Some SEM images are displayed in figure III.1.4.5. Figures III.1.4.5a and III.1.4.5c refer to the bio-composite reinforced with woven fibers (40 wt. % and 50 wt. %) where the directionality of the fibers can be seen, as well the presence of small gaps in the surrounding fiber and matrix as indicated in the pictures. This is because the wettability of the matrix with the fibers is not good enough, resulting in weak adhesion of the fibers to the matrix identified by the pull-out of the fibers from the matrix [81]. No tear marks are visible on the fiber breakage surface, but a clean break of the fibers. This may be due to the low extensibility of the jute fibers to tensile stress, as suggested by Jawaid*, et al.* [77]. As one can see the small space between the fiber and the supporting matrix might be responsibe for poor load transfer and, subsequently, non-optimum mechanical properties of Pla/Jute bio-composites. The pull-out phenomenon can be clearly observed in figure III.1.4.5a and figure III.1.4.5c since the matrix shows a homogeneous surface that copies the shape of the fiber.

Figure III.1.4.5b and figure III.1.4.5d show the fractured surface of bio-composites reinforced with non-woven fibers. In this type of bio- composites, the random fiber distribution is remarkable. This may be one of the reasons why the gap between the fibers and the matrix is larger compared to woven fiber-reinforced bio-composites as suggested by Khan*, et al.* [56]. The relative random alignment of these fibers can act as stress concentrators when subjected to directional loads, causing premature separation of the fibers from the matrix and causing propagation of matrix cracks, which leads to a reduction in the tensile properties of the bio-composite. This morphology is in accordance with the low values obtained in the tensile tests on bio- composites reinforced with non-woven fibers. Similar results were reported by Alavudeen*, et al.* [81], where the tensile performance of the plain-woven composite was superior to t that of the randomly oriented bio- composites for the same fiber content because the discontinuity of the matrix caused inadequate stress transmission.

The low affinity of the reinforcement fibers and the matrix is largely due to the nature of the PLA matrix and the natural fibers, as jute fibers are mostly composed of cellulose, and lignin, which gives the fiber a hydrophilic character due to the hydroxyl group, and polyesters like PLA have a strong hydrophobic nature. This polarity difference is responsible for the low Pla/jute interactions. [55,82].

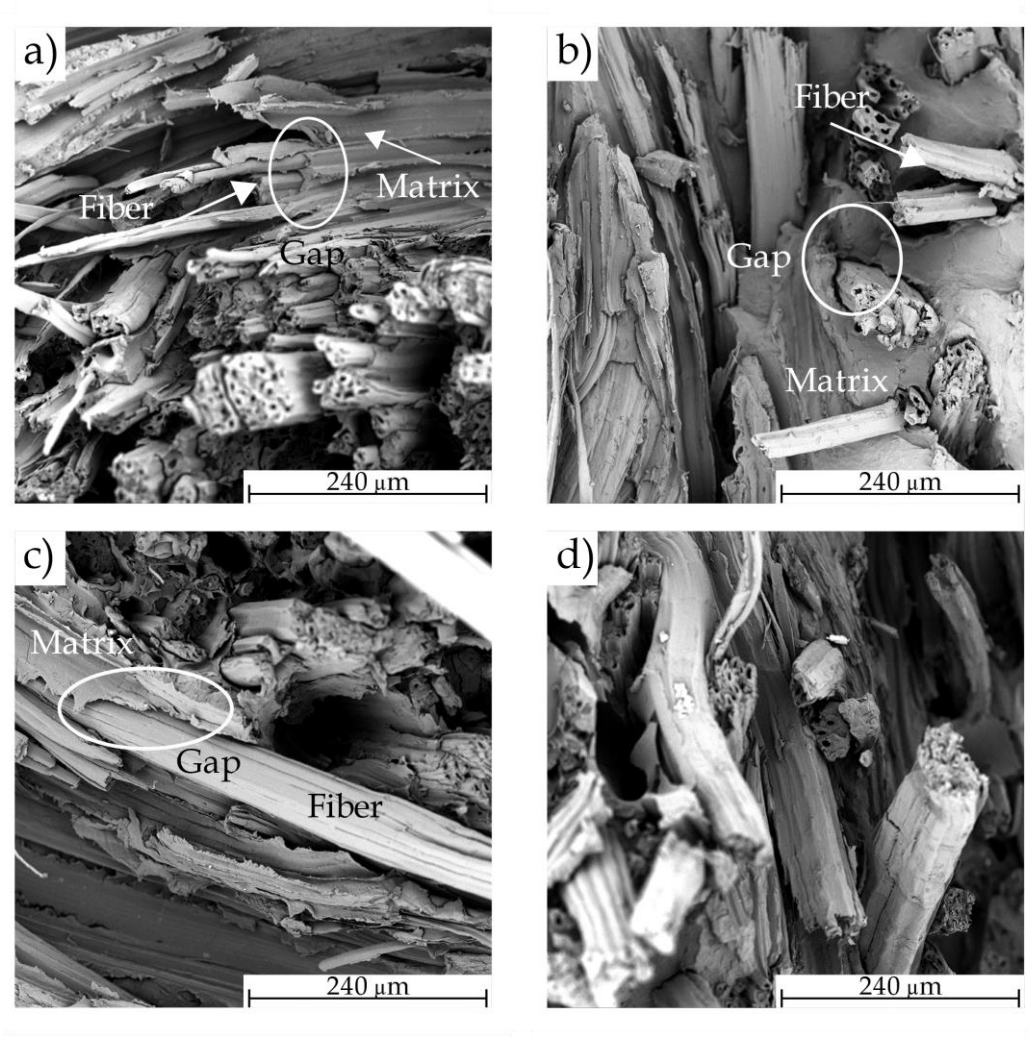

Figure III.1.4.5. Scanning emission microscopy (SEM) images of the fracture surface of PLA-based bio-composites with different percentages of woven jute fiber (left column) and non-woven jute fiber (right column): (a) and (b) 40 wt %; (c) and (d) 50 wt %. The images were taken at 500× with a marked scale of 240 µm.

Figure III.1.4.6 shows an example of the fracture surface of the samples. It may be noted that the fractured surface corresponding to the PLA matrix presents a smooth and homogeneous surface which occurs in a brittle fracture, typical of PLA-based matrices. [38]. In addition, it was possible to observe a pulling out of the fibers with the matrix that, as mentioned above, is due to the little affinity that these two components have.

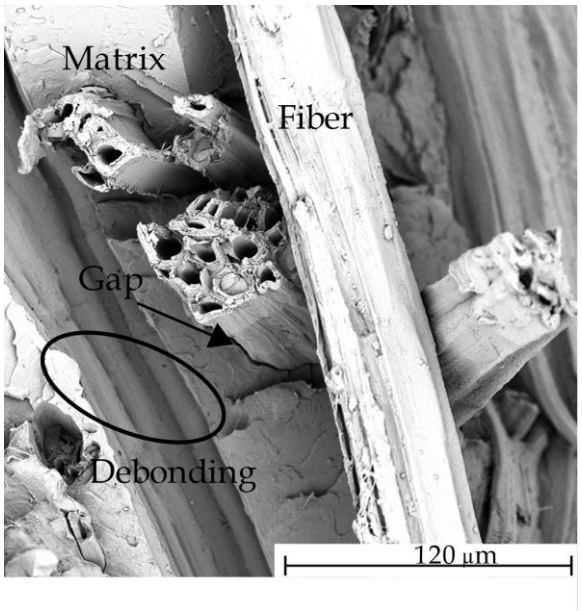

Figure III.1.4.6. Scanning emission microscopy (SEM) image of the fracture surface of PLA-based bio-composites (i.e. 50 wt% woven jute fiber). The image was taken at 1000× with a marked scale of 120 µm.

III.1.4.4. Conclusions

The present work deals with the development of biocomposites of high ecological value based on polylactide (PLA) matrix and jute reinforcement (woven and non-woven jute fiber fabrics). These bio- composites can be easily manufactured by hot compression molding by directly stacking fabrics and PLA pellets. This stacking system provided good wettability of the fibers with the matrix during the hot compression process at 190 ºC, resulting in bio-composites with a high percentage fiber (up to 50 wt. %). The SEM analysis showed that the interaction between the jute fibers and the PLA matrix was relatively low. Despite this, the interaction of the matrix with the woven fibers turned out to be better, since the gap between them is smaller than the one obtained by the non-woven fibers, which allowed a better load distribution. This can be seen in the good mechanical tensile properties obtained, particularly in its high Young's modulus. Furthermore, it was observed that the flexural properties of bio-composites are not directly influenced by the directionality of the reinforcement fibers, tending to increase with increasing fiber content.

These bio-composites obtained entirely from renewable sources have good mechanical performance comparable to conventional petroleum-based polymeric materials available today with the special feature that they are also fully biodegradable. Therefore, the partial or total use of these bio- composites in the different areas of engineering would help to a sustainable development.

III.1.4.5. Acknowledgments

This research work was funded by the Spanish Ministry of Science and Innovation (MICI) project number MAT2017-84909-C2-2-R. D. Lascano wants to thank Universitat Politècnica de València (UPV) for the grant received through the PAID-01-18 program. L. Quiles-Carrillo thanks Universitat Politècnica de València for a postdoctoral position (PAID-10-20)- SP20200073. J. Ivorra-Martinez is the recipient of a FPU grant from the Spanish Ministry of Science, Innovation and Universities, grant number (FPU19/01759).

III.1.4.6. References

1. X. Wei, J. Russell, S. Živanović, J.T. Mottram. Measured dynamic properties for FRP footbridges and their critical comparison against structures made of conventional construction materials. *Composite Structures* **2019**, *223*, 110956.
2. Y. Swolfs, I. Verpoest, L. Gorbatikh. Recent advances in fibre-hybrid composites: materials selection, opportunities and applications. *International Materials Reviews* **2019**, *64*, 181-215.
3. H.-l. Ma, Z. Jia, K.-t. Lau, J. Leng, D. Hui. Impact properties of glass fiber/epoxy composites at cryogenic environment. *Composites Part B: Engineering* **2016**, *92*, 210-217.
4. G.P. Otto, M.P. Moisés, G. Carvalho, A.W. Rinaldi, J.C. Garcia, E. Radovanovic, S.L. Fávaro. Mechanical properties of a polyurethane hybrid composite with natural lignocellulosic fibers. *Composites Part B: Engineering* **2017**, *110*, 459-465.
5. C.M. Vu, D.D. Nguyen, H.J. Choi, T.D. Pham. Micro-fibril cellulose as a filler for glass fiber reinforced unsaturated polyester composites: fabrication and mechanical characteristics. *Macromolecular Research* **2018**, *26*, 54-60.
6. D. Lascano, J. Valcárcel, R. Balart, L. Quiles-Carrillo, T. Boronat. Manufacturing of composite materials with high environmental efficiency using epoxy resin of renewable origin and permeable light cores for vacuum-assisted infusion molding. *Ingenius* **2020**, 62-73.
7. T. Sullins, S. Pillay, A. Komus, H. Ning. Hemp fiber reinforced polypropylene composites: The effects of material treatments. *Composites Part B: Engineering* **2017**, *114*, 15-22.
8. D.R. Mulinari, H.J. Voorwald, M.O. Cioffi, M.L. da Silva. Cellulose fiber-reinforced high-density polyethylene composites—mechanical and thermal properties. *Journal of Composite Materials* **2017**, *51*, 1807-1815.
9. T. Pulngern, T. Chitsamran, S. Chucheepsakul, V. Rosarpitak, S. Patcharaphun, N. Sombatsompop. Effect of temperature on mechanical properties and creep responses for wood/PVC composites. *Construction and Building Materials* **2016**, *111*, 191-198.
10. PlasticsEurope. *Plastics- the Facts 2020: An analysis of European plastics production, demand and waste data*; PlasticsEurope: Belgium, Europe, 2020.

11. S.M. Emadian, T.T. Onay, B. Demirel. Biodegradation of bioplastics in natural environments. *Waste management* **2017**, *59*, 526-536.

12. M. El-Wazery, M. El-Elamy, S. Zoalfakar. Mechanical properties of glass fiber reinforced polyester composites. *International journal of applied science and engineering* **2017**, *14*, 121-131.

13. R. Kaundal. Investigation of mechanical and thermo-mechanical properties of cement-by-pass dust filled short glass fiber reinforced polyester composites. *American Journal of Polymer Science & Engineering* **2018**, *6*, 45-57.

14. S.-Y. Fu, B. Lauke, E. Mäder, C.-Y. Yue, X. Hu. Tensile properties of short-glass-fiber-and short-carbon-fiber-reinforced polypropylene composites. *Composites Part A: Applied Science and Manufacturing* **2000**, *31*, 1117-1125.

15. S. Tang, C. Hu. Design, preparation and properties of carbon fiber reinforced ultra-high temperature ceramic composites for aerospace applications: a review. *Journal of Materials Science & Technology* **2017**, *33*, 117-130.

16. N. Borba, L. Blaga, J. dos Santos, S. Amancio-Filho. Direct-friction riveting of polymer composite laminates for aircraft applications. *Materials Letters* **2018**, *215*, 31-34.

17. F. Meng, J. McKechnie, T. Turner, K.H. Wong, S.J. Pickering. Environmental aspects of use of recycled carbon fiber composites in automotive applications. *Environmental science & technology* **2017**, *51*, 12727-12736.

18. B. Ravishankar, S.K. Nayak, M.A. Kader. Hybrid composites for automotive applications–A review. *Journal of Reinforced Plastics and Composites* **2019**, *38*, 835-845.

19. J.P. Correa, J.M. Montalvo-Navarrete, M.A. Hidalgo-Salazar. Carbon footprint considerations for biocomposite materials for sustainable products: A review. *Journal of cleaner production* **2019**, *208*, 785-794.

20. Á. Agüero, D. Garcia-Sanoguera, D. Lascano, S. Rojas-Lema, J. Ivorra-Martinez, O. Fenollar, S. Torres-Giner. Evaluation of different compatibilization strategies to improve the performance of injection-molded green composite pieces made of polylactide reinforced with short flaxseed fibers. *Polymers* **2020**, *12*, 821.

21. R. Vinayagamoorthy, T. Rajmohan. Machining and its challenges on bio-fibre reinforced plastics: A critical review. *Journal of Reinforced Plastics and Composites* **2018**, *37*, 1037-1050.

22. M.-D. Samper, J.M. Ferri, A. Carbonell-Verdu, R. Balart, O. Fenollar. Properties of biobased epoxy resins from epoxidized linseed oil (ELO) crosslinked with a mixture of cyclic anhydride and maleinized linseed oil. *Express Polymer Letters* **2019**, *13*, 407-418.

23. A. Carbonell-Verdu, L. Bernardi, D. Garcia-Garcia, L. Sanchez-Nacher, R. Balart. Development of environmentally friendly composite matrices from epoxidized cottonseed oil. *European Polymer Journal* **2015**, *63*, 1-10.

24. D. Lascano, D. Garcia-Garcia, S. Rojas-Lema, L. Quiles-Carrillo, R. Balart, T. Boronat. Manufacturing and Characterization of Green Composites with Partially Biobased Epoxy Resin and Flaxseed Flour Wastes. *Applied Sciences* **2020**, *10*, 3688.

25. Z. Dai, Z. Yang, Z. Chen, Z. Zhao, Y. Lou, Y. Zhang, T. Liu, F. Fu, Y. Fu, X. Liu. Fully biobased composites of an itaconic acid derived unsaturated polyester reinforced with cotton fabrics. *ACS Sustainable Chemistry & Engineering* **2018**, *6*, 15056-15063.

26. B.Z. Fidanovski, P.M. Spasojevic, V.V. Panic, S.I. Seslija, J.P. Spasojevic, I.G. Popovic. Synthesis and characterization of fully bio-based unsaturated polyester resins. *Journal of materials science* **2018**, *53*, 4635-4644.

27. E.S. KOKTEN, G. Özbay, N. Ayrilmis. Synthesis of biobased phenolic resins using catalytic pyrolysis oil and its effect on oriented strand board performance. *The Journal of Adhesion* **2018**, 475-489.

28. H.A. Khalil, Y. Davoudpour, C.K. Saurabh, M.S. Hossain, A. Adnan, R. Dungani, M. Paridah, M.Z.I. Sarker, M.N. Fazita, M. Syakir. A review on nanocellulosic fibres as new material for sustainable packaging: Process and applications. *Renewable and Sustainable Energy Reviews* **2016**, *64*, 823-836.

29. E. Malikmammadov, T.E. Tanir, A. Kiziltay, V. Hasirci, N. Hasirci. PCL and PCL-based materials in biomedical applications. *Journal of Biomaterials science, Polymer edition* **2018**, *29*, 863-893.

30. H. Moustafa, C. Guizani, A. Dufresne. Sustainable biodegradable coffee grounds filler and its effect on the hydrophobicity, mechanical and thermal properties of biodegradable PBAT composites. *Journal of Applied Polymer Science* **2017**, *134*, 44498.

31. M. Jorda, S. Montava-Jorda, R. Balart, D. Lascano, N. Montanes, L. Quiles-Carrillo. Functionalization of partially bio-based poly (ethylene terephthalate) by

blending with fully bio-Based poly (amide) 10, 10 and a glycidyl methacrylate-based compatibilizer. *Polymers* **2019**, *11*, 1331.

32. C. Kourmentza, J. Plácido, N. Venetsaneas, A. Burniol-Figols, C. Varrone, H.N. Gavala, M.A. Reis. Recent advances and challenges towards sustainable polyhydroxyalkanoate (PHA) production. *Bioengineering* **2017**, *4*, 55.

33. C. Pavon, M. Aldas, J. López-Martínez, S. Ferrándiz. New materials for 3D-printing based on polycaprolactone with gum rosin and beeswax as additives. *Polymers* **2020**, *12*, 334.

34. Z. Yuan, X. Zhang, Q. Yao, Y. Zhang, Y. Fu. Production of acetonitrile via catalytic fast pyrolysis of biomass derived polylactic acid under ammonia atmosphere. *Journal of Analytical and Applied Pyrolysis* **2019**, *140*, 376-384.

35. J.-R. Riba, R. Cantero, V. García-Masabet, J. Cailloux, T. Canals, M.L. Maspoch. Multivariate identification of extruded PLA samples from the infrared spectrum. *Journal of Materials Science* **2020**, *55*, 1269-1279.

36. S. Rojas-Lema, L. Quiles-Carrillo, D. Garcia-Garcia, B. Melendez-Rodriguez, R. Balart, S. Torres-Giner. tailoring the properties of thermo-compressed polylactide films for food packaging applications by individual and combined additions of lactic acid oligomer and halloysite nanotubes. *Molecules* **2020**, *25*, 1976.

37. B. Tyler, D. Gullotti, A. Mangraviti, T. Utsuki, H. Brem. Polylactic acid (PLA) controlled delivery carriers for biomedical applications. *Advanced Drug Delivery Reviews* **2016**, *107*, 163-175.

38. D. Lascano, L. Quiles-Carrillo, R. Balart, T. Boronat, N. Montanes. Toughened poly (lactic acid)—PLA formulations by binary blends with poly (butylene succinate-co-adipate)—PBSA and their shape memory behaviour. *Materials* **2019**, *12*, 622.

39. J. Balart, D. García-Sanoguera, R. Balart, T. Boronat, L. Sánchez-Nacher. Manufacturing and properties of biobased thermoplastic composites from poly (lactid acid) and hazelnut shell wastes. *Polymer composites* **2018**, *39*, 848-857.

40. L. Quiles-Carrillo, N. Montanes, C. Sammon, R. Balart, S. Torres-Giner. Compatibilization of highly sustainable polylactide/almond shell flour composites by reactive extrusion with maleinized linseed oil. *Industrial Crops and Products* **2018**, *111*, 878-888.

41. A. Bourmaud, J. Beaugrand, D.U. Shah, V. Placet, C. Baley. Towards the design of high-performance plant fibre composites. *Progress in Materials Science* **2018**, *97*, 347-408.

42. C. Chen, Y. Yang, Y. Zhou, C. Xue, X. Chen, H. Wu, L. Sui, X. Li. Comparative analysis of natural fiber reinforced polymer and carbon fiber reinforced polymer in strengthening of reinforced concrete beams. *Journal of Cleaner Production* **2020**, 121572.

43. R. Vinayagamoorthy. A review on the polymeric laminates reinforced with natural fibers. *Journal of Reinforced Plastics and Composites* **2017**, *36*, 1577-1589.

44. M. Ramesh. Flax (Linum usitatissimum L.) fibre reinforced polymer composite materials: A review on preparation, properties and prospects. *Progress in Materials Science* **2019**, *102*, 109-166.

45. J. Naveen, M. Jawaid, P. Amuthakkannan, M. Chandrasekar. Mechanical and physical properties of sisal and hybrid sisal fiber-reinforced polymer composites. In *Mechanical and physical testing of biocomposites, fibre-reinforced composites and hybrid composites*, Elsevier: 2019; 427-440.

46. H. Wang, H. Memon, E. AM Hassan, M. Miah, M. Ali. Effect of jute fiber modification on mechanical properties of jute fiber composite. *Materials* **2019**, *12*, 1226.

47. H. Jariwala, P. Jain. A review on mechanical behavior of natural fiber reinforced polymer composites and its applications. *Journal of Reinforced Plastics and Composites* **2019**, *38*, 441-453.

48. N.L. Feng, S.D. Malingam, R. Jenal, Z. Mustafa, S. Subramonian. A review of the tensile and fatigue responses of cellulosic fibre-reinforced polymer composites. *Mechanics of Advanced Materials and Structures* **2020**, *27*, 645-660.

49. V.K. Thakur, M.K. Thakur, R.K. Gupta. raw natural fiber–based polymer composites. *International Journal of Polymer Analysis and Characterization* **2014**, *19*, 256-271.

50. S. Biswas, Q. Ahsan, A. Cenna, M. Hasan, A. Hassan. Physical and mechanical properties of jute, bamboo and coir natural fiber. *Fibers and polymers* **2013**, *14*, 1762-1767.

51. B.V. Ramnath, V. Manickavasagam, C. Elanchezhian, C.V. Krishna, S. Karthik, K. Saravanan. Determination of mechanical properties of intra-layer abaca–jute–glass fiber reinforced composite. *Materials & Design* **2014**, *60*, 643-652.

52. D.B. Dittenber, H.V. GangaRao. Critical review of recent publications on use of natural composites in infrastructure. *Composites Part A: Applied Science and Manufacturing* **2012**, *43*, 1419-1429.

53. M.A. Alam, J. Ferdous, M.R. Debnath, M.S. Hossain, M.M. Islam. Reduction of production cost of jute (BJRI Tossa Pat 5) as influenced by urea top dressing does and period. *Research Journal of Food and Nutrition* **2019**, *3*, 1-5.

54. A. Gholampour, T. Ozbakkaloglu. A review of natural fiber composites: properties, modification and processing techniques, characterization, applications. *Journal of Materials Science* **2020**, 1-64.

55. S. Du, X. Peng, H. Gu. Experimental investigation on fabrication and thermal-stamping of woven jute/polylactic acid biocomposites. *Journal of Composite Materials* **2019**, *53*, 851-861.

56. G.A. Khan, M. Terano, M. Gafur, M.S. Alam. Studies on the mechanical properties of woven jute fabric reinforced poly (l-lactic acid) composites. *Journal of King Saud University-Engineering Sciences* **2016**, *28*, 69-74.

57. H. Burrola-Núñez, P. Herrera-Franco, H. Soto-Valdez, D.E. Rodríguez-Félix, R. Meléndrez-Amavizca, T.J. Madera-Santana. Production of biocomposites using different pre-treated cut jute fibre and polylactic acid matrix and their properties. *Journal of Natural Fibers* **2019**, 1-14.

58. M.T. Zafar, S. Kumar, R.K. Singla, S.N. Maiti, A.K. Ghosh. Surface treated jute fiber induced foam microstructure development in poly (lactic acid)/jute fiber biocomposites and their biodegradation behavior. *Fibers and Polymers* **2018**, *19*, 648-659.

59. A. Agüero, M.d.C. Morcillo, L. Quiles-Carrillo, R. Balart, T. Boronat, D. Lascano, S. Torres-Giner, O. Fenollar. Study of the influence of the reprocessing cycles on the final properties of polylactide pieces obtained by injection molding. *Polymers* **2019**, *11*, 1908.

60. J. Ferri, D. Garcia-Garcia, L. Sánchez-Nacher, O. Fenollar, R. Balart. The effect of maleinized linseed oil (MLO) on mechanical performance of poly (lactic acid)-thermoplastic starch (PLA-TPS) blends. *Carbohydrate polymers* **2016**, *147*, 60-68.

61. S. Qian, H. Wang, E. Zarei, K. Sheng. Effect of hydrothermal pretreatment on the properties of moso bamboo particles reinforced polyvinyl chloride composites. *Composites Part B: Engineering* **2015**, *82*, 23-29.

62. C. Álvarez-Chávez, D. Sánchez-Acosta, J. Encinas-Encinas, J. Esquer, P. Quintana-Owen, T. Madera-Santana. Characterization of extruded poly (lactic acid)/pecan nutshell biocomposites. *International Journal of Polymer Science* **2017**, *2017*, 12.

63. D. Garcia-Garcia, L. Quiles-Carrillo, N. Montanes, V. Fombuena, R. Balart. Manufacturing and characterization of composite fibreboards with Posidonia oceanica wastes with an environmentally-friendly binder from epoxy resin. *Materials* **2018**, *11*, 35.

64. J.I.P. Singh, S. Singh, V. Dhawan. Influence of fiber volume fraction and curing temperature on mechanical properties of jute/PLA green composites. *Polymers and Polymer Composites* **2020**, *28*, 273-284.

65. L. Luan, W. Wu, M.H. Wagner, M. Mueller. Seaweed as novel biofiller in polypropylene composites. *Journal of applied polymer science* **2010**, *118*, 997-1005.

66. A. Ali, K. Shaker, Y. Nawab, M. Jabbar, T. Hussain, J. Militky, V. Baheti. Hydrophobic treatment of natural fibers and their composites—A review. *Journal of Industrial Textiles* **2018**, *47*, 2153-2183.

67. S.K. Roy, G.A. Khan, M.A. Haque, M.S. Alam, M.I. Haque, M. Gafur. Effect of chemical treatments and coupling agents on the properties of unidirectional jute fiber reinforced polypropylene composite. *Jurnal Kejuruteraan* **2017**, *29*, 63-70.

68. G.A. Khan, H. Shaikh, M.S. Alam, M.A. Gafur, S.M. Al-Zahrani. Effect of chemical treatments on the physical properties of non-woven jute/PLA biocomposites. *BioResources* **2015**, *10*, 7386-7404.

69. O. Das, D. Bhattacharyya, D. Hui, K.-T. Lau. Mechanical and flammability characterisations of biochar/polypropylene biocomposites. *Composites Part B: Engineering* **2016**, *106*, 120-128.

70. H. Essabir, R. Boujmal, M.O. Bensalah, D. Rodrigue, R. Bouhfid, A. el kacem Qaiss. Mechanical and thermal properties of hybrid composites: oil-palm fiber/clay reinforced high density polyethylene. *Mechanics of Materials* **2016**, *98*, 36-43.

71. Y. Dong, A. Ghataura, H. Takagi, H.J. Haroosh, A.N. Nakagaito, K.-T. Lau. Polylactic acid (PLA) biocomposites reinforced with coir fibres: Evaluation of mechanical performance and multifunctional properties. *Composites Part A: Applied Science and Manufacturing* **2014**, *63*, 76-84.

72. W. Jia, R.H. Gong, P.J. Hogg. Poly (lactic acid) fibre reinforced biodegradable composites. *Composites Part B: Engineering* **2014**, *62*, 104-112.

73. K.S. Ahmed, S. Vijayarangan. Experimental characterization of woven jute-fabric-reinforced isothalic polyester composites. *Journal of applied polymer science* **2007**, *104*, 2650-2662.

74. S. Sudha, G. Thilagavathi. Effect of alkali treatment on mechanical properties of woven jute composites. *The Journal of The Textile Institute* **2016**, *107*, 691-701.

75. M. Durante, A. Formisano, L. Boccarusso, A. Langella, L. Carrino. Creep behaviour of polylactic acid reinforced by woven hemp fabric. *Composites Part B: Engineering* **2017**, *124*, 16-22.

76. M. Sood, G. Dwivedi. Effect of fiber treatment on flexural properties of natural fiber reinforced composites: A review. *Egyptian journal of petroleum* **2018**, *27*, 775-783.

77. M. Jawaid, H.A. Khalil, A.A. Bakar. Woven hybrid composites: Tensile and flexural properties of oil palm-woven jute fibres based epoxy composites. *Materials Science and Engineering: A* **2011**, *528*, 5190-5195.

78. I. Gnaba, P. Wang, D. Soulat, F. Omrani, M. Ferreira, P. Vroman. Investigation about the effect of manufacturing parameters on the mechanical behaviour of natural fibre nonwovens reinforced thermoplastic composites. *Materials* **2019**, *12*, 2560.

79. M.E.A. Fidelis, T.V.C. Pereira, O.d.F.M. Gomes, F. de Andrade Silva, R.D. Toledo Filho. The effect of fiber morphology on the tensile strength of natural fibers. *Journal of Materials Research and Technology* **2013**, *2*, 149-157.

80. R. Gunti, A. Ratna Prasad, A. Gupta. Preparation and properties of successive alkali treated completely biodegradable short jute fiber reinforced PLA composites. *Polymer Composites* **2016**, *37*, 2160-2170.

81. A. Alavudeen, N. Rajini, S. Karthikeyan, M. Thiruchitrambalam, N. Venkateshwaren. Mechanical properties of banana/kenaf fiber-reinforced hybrid polyester composites: Effect of woven fabric and random orientation. *Materials & Design (1980-2015)* **2015**, *66*, 246-257.

82. O. Faruk, A.K. Bledzki, H.-P. Fink, M. Sain. Biocomposites reinforced with natural fibers: 2000–2010. *Progress in polymer science* **2012**, *37*, 1552-1596.

III.2. Composites based on thermosetting matrices with high environmental performance.

Adaptado del artículo

III.2.1. Kinetic analysis of the curing of a partially biobased epoxy resin using dynamic differential scanning calorimetry

Diego Lascano[1], Luis Quiles-Carrillo[2], Rafael Balart[2], Teodomiro Boronat[2], and Nestor Montanes[2]

[1] Escuela Politécnica Nacional, Quito 17-01-2759, Ecuador

[2] Technological Institute of Materials (ITM), Universitat Politècnica de València (UPV), Plaza Ferrándiz y Carbonell 1, 03801 Alcoy, Spain

polymers

Polymers **2019**, *11*(3), 391

polymers

MDPI

Article

Kinetic Analysis of the Curing of a Partially Biobased Epoxy Resin Using Dynamic Differential Scanning Calorimetry

Diego Lascano [1], Luis Quiles-Carrillo [2,*], Rafael Balart [2], Teodomiro Boronat [2] and Nestor Montanes [2]

[1] Escuela Politécnica Nacional, Quito 17-01-2759, Ecuador; dielas@epsa.upv.es
[2] Technological Institute of Materials (ITM), Universitat Politècnica de València (UPV), Plaza Ferrándiz y Carbonell 1, 03801 Alcoy, Spain; rbalart@mcm.upv.es (R.B.); tboronat@dimm.upv.es (T.B.); nesmonmu@upvnet.upv.es (N.M.)
* Correspondence: luiquic1@epsa.upv.es; Tel.: +34-966-528-433

Received: 29 January 2019; Accepted: 19 February 2019; Published: 27 February 2019

Abstract: This research presents a cure kinetics study of an epoxy system consisting of a partially bio-sourced resin based on diglycidyl ether of bisphenol A (DGEBA) with amine hardener and a biobased reactive diluent from plants representing 31 wt %. The kinetic study has been carried out using differential scanning calorimetry (DSC) under non-isothermal conditions at different heating rates. Integral and derivative isoconversional methods or model free kinetics (MFK) have been applied to the experimental data in order to evaluate the apparent activation energy, E_a, followed by the application of the appropriate reaction model. The bio-sourced system showed activation energy that is independent of the extent of conversion, with E_a values between 57 and 62 kJ·mol^{-1}, corresponding to typical activation energies of conventional epoxy resins. The reaction model was studied by comparing the calculated $y(\alpha)$ and $z(\alpha)$ functions with standard master plot curves. A two-parameter autocatalytic kinetic model of Šesták–Berggren [SB(m,n)] was assessed as the most suitable reaction model to describe the curing kinetics of the epoxy resins studied since it showed an excellent agreement with the experimental data.

Keywords: cure kinetics; epoxy resin; bio-sourced epoxy resin; differential scanning calorimetry (DSC)

1. Introduction

Epoxy resins are low molecular weight pre-polymers with at least one epoxide group in their structure. These epoxy rings are usually located in terminal positions due to the high reactivity of this position [1]. Currently epoxy resins are the most used thermosetting resins due to the huge range of properties they can cover such as tensile strength, high adhesion strength, low shrinkage, good chemical resistance, and low volatile emission, among others [2–5]. These outstanding properties make these resins suitable for high technological sectors such as the automotive and aerospace industries. In addition, their versatility makes them useful for industrial applications such as adhesives, paints, surface coatings, advanced composite materials, electrical and electronic components, and high-performance membranes for separation and filtration, among others [3,6–14]. The final properties of a structural epoxy system are greatly influenced by several factors, which include the chemical structure of both the epoxy resin and the curing agent and external factors related to the curing procedure.

Despite the huge range of epoxy resins available worldwide, undoubtedly the most used resin is that based on diglycidyl ether of bisphenol A (DGEBA), which is obtained by reacting

Kinetic analysis of the curing of a partially biobased epoxy resin using dynamic differential scanning calorimetry

Abstract

This research presents a cure kinetics study of an epoxy system consisting of a partially bio-sourced resin based on diglycidyl ether of bisphenol A (DGEBA) with amine hardener and a biobased reactive diluent from plants representing 31 wt %. The kinetic study has been carried out using differential scanning calorimetry (DSC) under non-isothermal conditions at different heating rates. Integral and derivative isoconversional methods or model free kinetics (MFK) have been applied to the experimental data in order to evaluate the apparent activation energy, E_a, followed by the application of the appropriate reaction model. The bio-sourced system showed activation energy that is independent of the extent of conversion, with E_a values between 57 and 62 kJ·mol^{-1}, corresponding to typical activation energies of conventional epoxy resins. The reaction model was studied by comparing the calculated $y(\alpha)$ and $z(\alpha)$ functions with standard master plot curves. A two-parameter autocatalytic kinetic model of Šesták–Berggren [SB(*m*,*n*)] was assessed as the most suitable reaction model to describe the curing kinetics of the epoxy resins studied since it showed an excellent agreement with the experimental data.

Keywords: cure kinetics; epoxy resin; bio-sourced epoxy resin; differential scanning calorimetry (DSC)

III.2.1.1. Introduction

Epoxy resins are low molecular weight pre-polymers with at least one epoxide group in their structure. These epoxy rings are usually located in terminal positions due to the high reactivity of this position [1]. Currently epoxy resins are the most used thermosetting resins due to the huge range of properties they can cover such as tensile strength, high adhesion strength, low shrinkage, good chemical resistance, and low volatile emission, among others [2-5]. These outstanding properties make these resins suitable for high technological sectors such as the automotive and aerospace industries. In addition, their versatility makes them useful for industrial applications such as adhesives, paints, surface coatings, advanced composite materials, electrical and electronic components, and high-performance membranes for separation and filtration, among others [3,6-14]. The final properties of a structural epoxy system are greatly influenced by several factors, which include the chemical structure of both the epoxy resin and the curing agent and external factors related to the curing procedure.

Despite the huge range of epoxy resins available worldwide, undoubtedly the most used resin is that based on diglycidyl ether of bisphenol A (DGEBA), which is obtained by reacting bisphenol A (BPA), and epichlorohydrin [15]. Although some epoxy resins can crosslink via homopolymerization [16], the use of hardeners is usually mandatory to crosslink the liquid epoxy resin. There is a wide variety of commercial hardeners for epoxy systems, with amine systems being one of the most employed. Amines can crosslink an epoxy resin by directly cross-linking or by catalytic cross-linking mechanisms [17,18]. These amine hardeners could be both primary and secondary, which act as reactive hardeners, or tertiary amines, which act as catalytic agents. The crosslinking structure are obtained by the reaction between the epoxide group and the hydrogens contained in the amine groups [19]. One of the main features of amine hardeners is that they can provide curing at low temperatures, or even at room temperature [20,21], which is a key factor compared to other hardeners, such as carboxylic acids or anhydrides, that typically need high temperatures to start and complete the cross-linking process [22-25].

Epoxy resins are petroleum-derived materials that have a remarkable impact on the carbon footprint. This fact, in conjunction with the increasing sensitivity of our society about the environment and sustainable development, are the leading forces toward the development of new environmentally friendly resins that are totally or partially bioderived [26-29]. One of the most promising sources for industrial epoxy resins are vegetable oils. These consist of a triglyceride structure in which three different fatty acids are chemically

attached to glycerol by ester bonds. Unsaturated fatty acids, such as oleic, linoleic, and linolenic acids, with one, two, and three unsaturations, respectively, are the most interesting fatty acids as their unsaturations can be easily converted into oxirane rings via epoxidation [30]. In addition, the metathesis of double bonds has been proposed as a process for undergoing epoxidation of unsaturated fatty acids, among others [31,32]. The most common oils used for epoxidation are canola, corn, palm, linseed, soybean, castor, and so on [33]. Nevertheless, from an industrial point of view, epoxidized soybean oil (ESBO) and epoxidized linseed oil (ELO) are, the most used plant-derived epoxy resins due to an excellent combination of properties. Moreover, they offer a competitive cost since they are widely used in the poly(vinyl chloride) (PVC) industry as secondary plasticizers [34-37]. In addition to this industrial use, epoxidized vegetable oils can be considered epoxy resins, and therefore, they can be cross-linked with the appropriate hardener. Samper, *et al.* [38] obtained eutectic mixtures of epoxidized soybean oil (ESBO) and epoxidized linseed oil (ELO) cured with maleic anhydride. Park, *et al.* [39] focused their research on the effect of the epoxidized castor oil (ECO) in blends with DGEBA-based epoxy resins. Pawar, *et al.* [40] formulated a fully bio-based resin, based on blends of epoxidized cottonseed oil (ECO) and epoxidized algae oil (EAO).

As indicated previously, the final properties are highly influenced by the curing conditions in terms of the time-temperature cycle. At the industrial scale, short curing times are preferred and this leads to the need of higher curing temperatures (more aggressive curing cycles). These aggressive conditions also provide internal stresses due to the fastness of the crosslinking process, which in turn, leads to higher T_g values.

During the crosslinking process between a base epoxy resin and the corresponding hardener, an exothermic reaction occurs. Due to the exothermicity, the temperature of the resin increases, and subsequently, the crosslinking rate raises up in an autocatalytic process. In fact, it is important to control the released heat as in sometimes it can degrade (even burn) the resin leading to a counterproductive effect on final properties [41]. In order to obtain a cured thermosetting with optimal properties, the knowledge of the kinetics is essential [42]. The aim of this research is to study the curing kinetics of a partially biobased epoxy resin using dynamic differential scanning calorimetry (DSC). The work is focused on obtaining the kinetic triplet: E_a, A, and $f(\alpha)$. E_a is obtained by isoconversional methods or model free kinetics (MFK), both differential and integral and the reaction model is obtained by comparison of the $y(\alpha)$ and $z(\alpha)$ characteristic curves with standard master plots.

III.2.1.2. Theoretical Background

Most of the thermally activated processes are based on the general kinetic expression, as shown in Equation (III.2.1.1), where the conversion rate $\frac{d\alpha}{dt}$ is a function of *T* and α [43]:

$$\frac{d\alpha}{dt} = K(T)f(\alpha) \quad \text{(III.2.1.1)}$$

where $K(T)$ is the rate coefficient, which depends on temperature *T*, and $f(\alpha)$ represents the reaction model, which takes different forms depending on the mechanism of the process. The temperature dependence of $K(T)$ could be parameterized through the Arrhenius expression shown in Equation (III.2.1.2):

$$K(T) = A\, e^{\frac{-E_a}{RT}} \quad \text{(III.2.1.2)}$$

where *A* is the pre-exponential factor, E_a is the apparent activation energy, *R* refers to the universal gas constant, and *T* is the absolute temperature. By substituting the Arrhenius temperature coefficient, Equation (III.2.1.1) can be written as Equation (III.2.1.3), which represents the general rate equation for the kinetic study. As one can realize, this is a time-dependent equation, and subsequently, it can be applied to any curing cycle.

$$\frac{d\alpha}{dt} = A\, e^{\frac{-E_a}{RT}} f(\alpha) \quad \text{(III.2.1.3)}$$

This time-dependent expression can be converted into a temperature domain by considering Equation (III.2.1.4), which shows the heating rate β definition:

$$\beta = \frac{dT}{dt} \quad \text{(III.2.1.4)}$$

By substituting Equation (III.2.1.4) into Equation (III.2.1.3), we obtain the general equation for kinetic analysis for dynamic heating cycles:

$$\beta \frac{d\alpha}{dT} = Ae^{\frac{-E_a}{RT}} f(\alpha) \quad \text{(III.2.1.5)}$$

Isoconversional Methods: Model-Free Kinetics (MFK)

Isoconversional methods are derived from the basic isoconversional principle that assumes that the reaction rate at a constant conversion (α_c) depends only on temperature. If we take natural logarithms on both sides of Equation (III.2.1.1), we obtain:

$$ln\left(\frac{d\alpha}{dt}\right) = ln\,K(T) + ln\,f(\alpha) \tag{III.2.1.6}$$

Then, taking partial derivatives with respect to the inverse temperature (1/*T*) on Equation (III.2.1.6) at a constant $\alpha = \alpha_i$, Equation (III.2.1.7) is derived:

$$\left[\frac{\partial\, ln\left(\frac{d\alpha}{dt}\right)}{\partial\, T^{-1}}\right]_{\alpha_i} = \left[\frac{\partial\, ln\,K(T)}{\partial\, T^{-1}}\right]_{\alpha_i} + \left[\frac{\partial\, ln\,f(\alpha)}{\partial\, T^{-1}}\right]_{\alpha_i} \tag{III.2.1.7}$$

Isoconversional conditions, meaning that it has a constant α value of α_i such that its corresponding $f(\alpha)$ value is also constant. Hence, the second term on the right-hand side of Equation (III.2.1.7) is zero. The first term on the right-hand side of Equation (III.2.1.7) can be obtained by taking the partial derivative of the logarithmic Arrhenius coefficient in Equation (III.2.1.2) with respect to 1/*T*, as shown in Equation (III.2.1.8):

$$\left[\frac{\partial\, ln\,K(T)}{\partial\, T^{-1}}\right]_{\alpha i} = \left[\frac{\partial\, ln\,A\, e^{\frac{-E_a}{R\,T}}}{\partial\, T^{-1}}\right]_{\alpha i} = \frac{-E_{a,\alpha i}}{R} \tag{III.2.1.8}$$

By combining Equations (III.2.1.7) and (III.2.1.8), the isoconversional methods indicate that it is possible to obtain E_a (at a particular α_i = constant) without assuming any reaction model, as shown in Equation (III.2.1.9). For this reason, sometimes these methods are called model-free kinetic methods (MFK).

$$\left[\frac{\partial\ ln\left(\frac{d\alpha}{dt}\right)}{\partial\, T^{-1}}\right]_{\alpha i} = \frac{-E_{a,\alpha i}}{R} \tag{III.2.1.9}$$

Isoconversional methods can give accurate values of the apparent activation energy E_a. These methods can be classified as differential, such as Friedman's method,

or integral methods, such as the Flynn-Wall-Ozawa (FWO), Kissinger-Akahira-Sunose (KAS), and Starink methods. The Friedman method [44] is one of the most common differential isoconversional methods used to evaluate the apparent activation energy. By assuming that the reaction model $f(\alpha)$ does not change with the conversion α, the basic differential expression (Equation (III.2.1.3)) can be written in a natural logarithm form, as shown in Equation (III.2.1.10):

$$ln\left(\frac{d\alpha}{dt}\right)_{\alpha,i} = ln[A\, f(\alpha)] - \frac{E_a}{R\, T_{\alpha,i}} = ln\left(\beta\, \frac{d\alpha}{dT}\right)_{\alpha,i} \quad \text{(III.2.1.10)}$$

As suggested by Equation (10), by plotting $\ln\left(\beta\, \frac{d\alpha}{dT}\right)_{\alpha,i}$ versus $\frac{1}{T_{\alpha,i}}$, the E_a can be calculated through the slope of the linear fitting. This method must be evaluated for each value of the conversion α. As suggested by Vyazovkin, *et al.* [43], to check its possible variation with the conversion α, it is recommended to start from α_i = 0.05 up to α_i = 0.95 with an increasing step size of 0.05. The Friedman method does not make any other assumption, and in a first approach, it gives a quite accurate value of E_a.

Isoconversional integral methods are based on integration of Equation (III.2.1.3) or Equation (III.2.1.5), as observed in Equation (III.2.1.11):

$$\int_0^{\alpha} \frac{d\alpha}{f(\alpha)} = \frac{A}{\beta}\int_{T_0}^{T} e^{\frac{-E_a}{R\,T}} dT = A\int_0^{t} E^{\frac{-E_a}{R\,T}} dt \quad \text{(III.2.1.11)}$$

The integral of the temperature-dependent expression from the Arrhenius constant is the so-called “temperature integral” and does not have a direct analytical solution. For this reason, different approximations have been proposed and used, leading to different methods, and obviously, to different accuracies on the E_a estimation. The Flynn-Wall-Ozawa (FWO) method shows very low accuracy as it uses a rude approximation of the temperature integral. Despite this, the FWO is one of the most commonly used. It follows Equation (III.2.1.12) [45]. This suggests that a plot of $\ln(\beta_i)$ versus the inverse temperature ($1/T_\alpha$) for a constant conversion α gives a straight line whose slope is -1.052/R.

$$ln(\beta_i) = constant - 1.052\, \frac{E_a}{R\, T_\alpha} \quad \text{(III.2.1.12)}$$

The Kissinger-Akahira-Sunose [46] method gives more accurate E_a values as it uses a more accurate solution of the temperature integral. The basic expression for the KAS method is shown in Equation (III.2.1.13), which suggests a linear correlation between $\ln\left(\frac{\beta_i}{T_{\alpha,i}^2}\right)$ and the inverse temperature ($1/T_\alpha$) for a particular conversion α value.

$$ln\left(\frac{\beta_i}{T_{\alpha,i}^2}\right) = constant - \frac{E_a}{R\,T_\alpha} \quad \text{(III.2.1.13)}$$

A better evaluation of the activation energy (E_a) can be done using the Starink expression, which is similar to that of the KAS method, but the particular parameters are optimized, as observed in Equation (III.2.1.14). In a similar way to the above-mentioned methods, a plot of $\ln\left(\frac{\beta_i}{T_{\alpha,i}^{1.92}}\right)$ against $(1/T_\alpha)$ for a particular conversion α_i value gives a linear correlation whose slope is -1.0008/R [47].

$$ln\left(\frac{\beta_i}{T_{\alpha,i}^{1.92}}\right) = constant - 1.0008\,\frac{E_a}{R\,T_\alpha} \quad \text{(III.2.1.14)}$$

Although it is not considered an isoconversional method, the Kissinger method (not to be confused with the Kissinger-Akahira-Sunose method) is based on the peak temperature (T_p) observed for the conversion rate at different heating rates β_i [48]. This method is widely used because of its simplicity. It assumes that $\frac{d}{dt}\left(\frac{d\alpha}{dt}\right) = 0$ at the temperature for the maximum conversion rate (T_p). The assumptions of the Kissinger method are only applicable if the conversion for this peak temperature α_m is almost constant for a series of heating rates, β_i. The Kissinger method follows Equation (III.2.1.15). One important drawback of the Kissinger method is that it only provides a single E_a value (at α_m) and cannot follow the evolution of E_a with the conversion α. Despite this, it is widely used due to its simplicity.

$$ln\left(\frac{\beta}{T_p^2}\right) = ln\left(\frac{A\,R}{E_a}\right) - \frac{E_a}{R\,T_P} \quad \text{(III.2.1.15)}$$

By plotting $\ln\left(\frac{\beta}{T_p^2}\right)$ versus $\frac{1}{T_p}$, the activation energy can be obtained through the slope of the linear fit. One of the restrictions of the Kissinger method is that it assumes a single-step process. To check the existence of a single-step degradation process,

different methods have been proposed. In particular, it is worthy to note the methodology described by Farjas, *et al*. [49]. This method is not only based on the peak temperature, but also on the peak width measured as the time corresponding to the full width at half maximum (Δt_{FWHM}), which is more sensitive to the existence of multiple processes. If a plot of the Δt_{FWHM} against $1/T_p$ gives a linear correlation, and the obtained E_a by linear fitting is similar to that obtained by the Kissinger method, then it is possible to conclude that the curing process takes place in a single step (despite the complexity of the occurring reactions).

Isoconversional methods are very useful for giving an accurate estimation of the E_a and do not assume any reaction model $f(\alpha)$. Polymerization processes are very complex, as indicated by D'hooge, *et al.* [50]. In particular they use multi-scale modelling to unveil some of these complex processes governed by free radical polymerization (FRP) or by controlled radical polymerization (CRP). They also pay special attention to chain mobility, which is restricted by crosslinking. To obtain the kinetic triplet, it is necessary to determine the reaction model. One of the most suitable methods is the use of the Málek method [51], which allows determining the reaction model by experimentally calculating two functions defined as $y(\alpha)$ and $z(\alpha)$, as indicated in Equations (III.2.1.16) and (III.2.1.17), with $x = E_a/RT$, i.e., the reduced temperature:

$$y(\alpha) = \frac{d\alpha}{dt}\, e^{x} \tag{III.2.1.16}$$

$$z(\alpha) = \pi(x)\, \frac{d\alpha}{dt}\, \frac{T}{\beta} \tag{III.2.1.17}$$

The particularity of these two functions is the following. Regarding $y(\alpha)$, if we substitute Equation (III.2.1.3) into Equation (III.2.1.16), then Equation (III.2.1.18) is obtained. The relevance of this function is that it can be calculated numerically using Equation (III.2.1.16), and as suggested by Equation (III.2.1.18), it provides a plot representation proportional to $f(\alpha)$ by the factor A. Therefore, $y(\alpha)$ gives a clear idea of the reaction model.

$$y(\alpha) = A\, f(\alpha) \tag{III.2.1.18}$$

Regarding the $z(\alpha)$ function, the solution to the integral expression (Equation (III.2.1.11)) can be defined as:

$$g(\alpha) = \frac{A\,E_a}{\beta\,R}\,P(x) \qquad \text{(III.2.1.19)}$$

where $P(x)$ represents a particular approximation of the temperature integral. The relation between $P(x)$ and $\pi(x)$ is shown in Equation (III.2.1.20):

$$P(x) = \frac{e^{-x}}{x}\,\pi(x) \qquad \text{(III.2.1.20)}$$

By combining Equations (III.2.1.3), (III.2.1.19), and (III.2.1.20), Equation (III.2.1.17) results in the following expression:

$$z(\alpha) = f(\alpha)\,g(\alpha) \qquad \text{(III.2.1.21)}$$

which suggests that the calculated $z(\alpha)$ using **Equation (III.2.1.17)**, can be compared with different theoretical $z(\alpha)$ curves with well-known $f(\alpha)$ and $g(\alpha)$ functions as shown in table III.2.1.1.

Table III.2.1.1. Summary of some $f(\alpha)$ and $g(\alpha)$ functions corresponding to crosslinking of polymers.

	Reaction Model	***f*(α)**	***g*(α)**
P2/3	Power law	$2/3\alpha^{-1/2}$	$\alpha^{3/2}$
P2	Power law	$2\alpha^{1/2}$	$\alpha^{1/2}$
A_2	Avrami–Erofeev	$2(1-\alpha)[-\ln(1-\alpha)]^{1/2}$	$[-\ln(1-\alpha)]^{1/2}$
D_1	Diffusion in one dimension	$1/2\alpha^{-1}$	α^2
D_2	Valensi equation	$-[\ln(1-\alpha)]^{-1}$	$(1-\alpha)\ln(1-\alpha)+\alpha$
F_1	Mample first order.	$(1-\alpha)$	$-\ln(1-\alpha)$
F_2	Random nucleation with two nuclei of individual particle	$(1-\alpha)^2$	$(1-\alpha)^{-1}$
F_n	*n*-order reaction	$(1-\alpha)^n$	$[(1-\alpha)^{1-n}-1]/(n-1)$

Senum and Yang have proposed different approximations of $\pi(x)$ in a rational form [52] and Pérez-Maqueda and Criado [53] have indicated that the use of a rational approximation of $\pi(x)$ with a fourth degree polynomial is enough to give good accuracy. Flynn [54] suggested a correction for the fourth rational approximation expression, as we

can see at the Equation (III.2.1.14). These functions $y(\alpha)$ and $z(\alpha)$ can be calculated from experimental data.

$$\pi(x) = \frac{x^3 + 18x^2 + 86x + 96}{x^4 + 20x^3 + 120x^2 + 240x + 120} \qquad \textit{(III.2.1.22)}$$

III.2.1.3. Experimental

Materials

The commercial epoxy resin used was a Resoltech® 1070 ECO and the hardener was an amine-based type Resoltech® 1074 ECO, both of them supplied by Castro Composites (Pontevedra, Spain). This partially bio-sourced epoxy resin is based on a mixture of a diglycidyl ether of bisphenol A (DGEBA) and a plant-based epoxy reactive diluent. As indicated by the supplier, the cured resin contains 31 % biobased content (according to ASTM D6866-12) and maintains good transparency. The eco-epoxy resin and the hardener were mixed under the stoichiometric ratio 100:35 (%wt epoxy:%wt hardener), following the manufacturer's recommendations.

Scheme III.2.1.1 shows the chemical structures of the components of the epoxy resin as well as the hardener.

BASE EPOXY RESIN

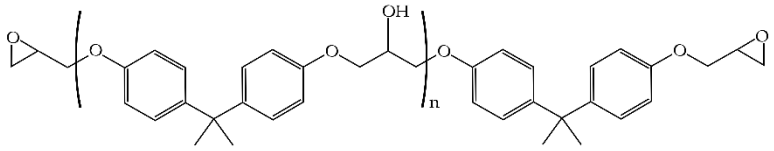

reaction product from bisphenol A and epichlorohydrin (DGEBPA); Av. Mw < 700

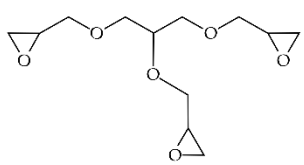

glycerol triglydidyl ether

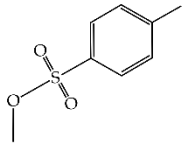

methyl toluene-4-sulphonate

REACTIVE DILUENT

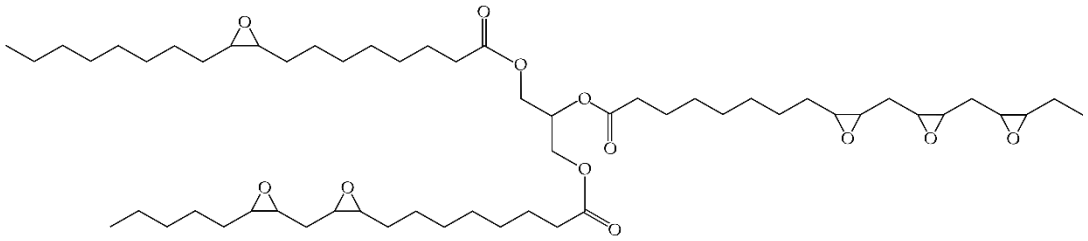

epoxidized vegetable/plant oil (EVO)

HARDENER

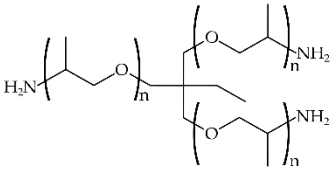

reaction product from propoxylated propylidynetrimethanol and ammonia

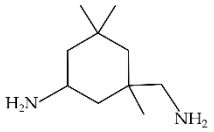

3-aminomethyl-3,5,5-trimethylcyclohexylamine

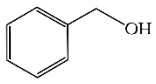

benzyl alcohol

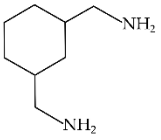

1,3-bis(aminomethyl)cyclohexane

Scheme III.2.1.1. Schematic plot of the main chemical components of the partially bio-based epoxy resin Resoltech® 1070 and its hardener, Resoltech® 1074.

The main component on the epoxy resin is the reaction product of bisphenol A and epichlorohydrin, leading to a typical diglycidyl ether of bisphenol A (DGEBA) resin. With regard to the reactive diluent, it is mainly derived from plant or vegetable oils, in particular, epoxidized vegetable oils. Finally, the hardener is an amine type, mainly

composed of 3-aminomethyl-3,5,5-trimethylcyclohexylamine and the reaction product of propoxylated propylidynetrimethanol and ammonia.

A preliminary FTIR characterization was carried out. The spectra were recorded using a spectrometer Spectrum BX from Perkin-Elmer (Madrid, Spain) together with a special holder for liquid samples. Data were collected from 20 scans between 5500 and 450 cm^{-1} at a spectral resolution of 4 cm^{-1}.

Figure III.2.1.1 shows the FTIR spectra of both the epoxy resin (figure III.2.1.1a) and the hardener (figure III.2.1.1b). The FTIR spectrum of the epoxy base epoxy resin shows the typical peaks and bands of a DGEBPA resin. These peak/band assignments are as follows: O-H stretching at about 3500 cm^{-1}; stretching of the C-H of the oxirane ring at 3057 cm^{-1}; stretching of C-H of CH_2 and CH, both aromatic and aliphatic, at 2965-2873 cm^{-1}; stretching of C=C of aromatic rings at 1608 cm^{-1}; stretching of the C-C of aromatic rings at 1509 cm^{-1}; stretching of the C-O-C of ethers at 1036 cm^{-1}; asymmetric stretching of the C-O in oxirane rings at 1241 cm^{-1}; stretching of the C-O of oxirane ring at 915 cm^{-1}; stretching of the C-O-C of oxirane ring at 831 cm^{-1}; and rocking of CH_2 at 772 cm^{-1}.

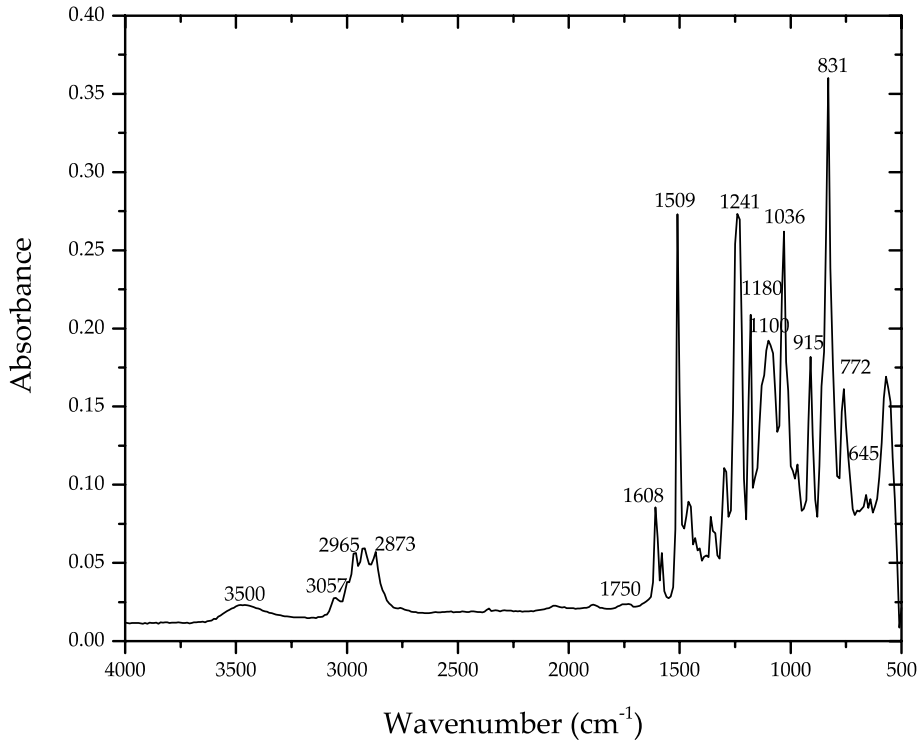

(a)

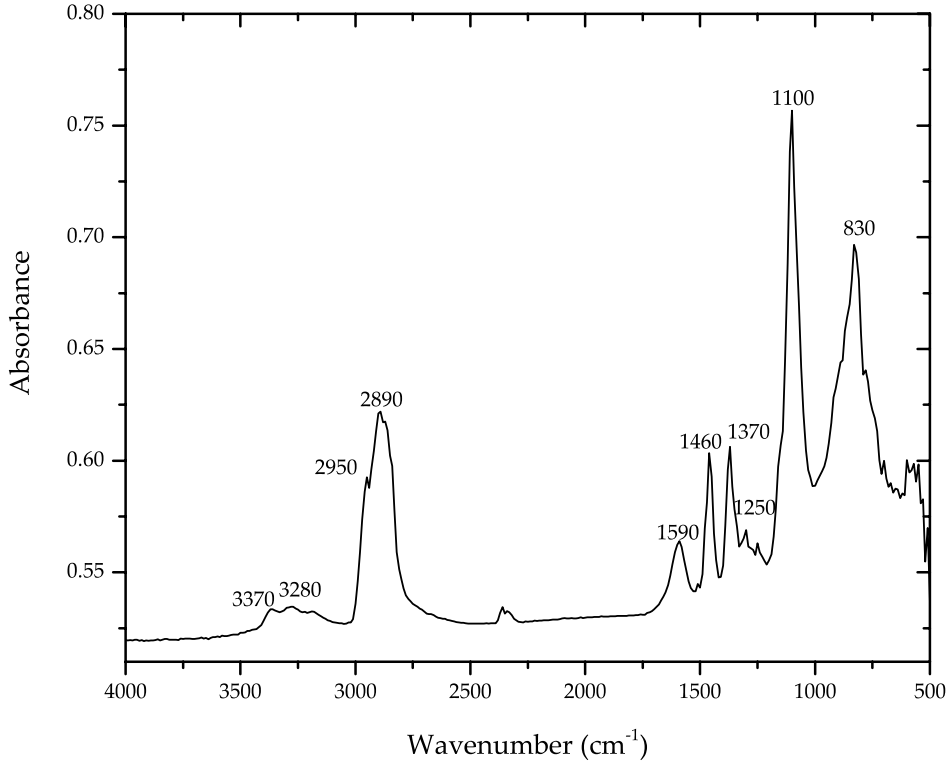

(b)

Figure III.2.1.1. FTIR spectra of (**a**) base epoxy resin Resoltech® 1070 based on DGEBPA, and (**b**) primary amine-based hardener Resoltech® 1074.

With regard to the reactive diluent, an epoxidized vegetable oil contained overlapping peaks and bands of CH_2, CH, and oxirane rings, while the ester groups typical of the triglyceride appeared with a weak signal as it was not the main component. These ester peaks were characterized by a weak signal at 645 cm^{-1} attributable to the O-C=O bending; a peak at 1180 cm^{-1}, which overlaps with ester groups and corresponds to the antisymmetric stretch of C-O-C; and a weak signal at 1765-1720 cm^{-1}, which is characteristic of the C=O stretch. These weak signals typical of the ester groups indicated the presence of triglycerides as reactive diluents.

Regarding the hardener, it was an amine type (figure III.2.1.1b). The peak/band assignment was the following: NH stretching of $-NH_2$ at 3370-3280 cm^{-1}, symmetric and antisymmetric stretching of CH in $-CH_2$ at 2950-2890 cm^{-1}, symmetric and antisymmetric stretching of CH in $-CH_2-$, $-NH_2$ deformation at 1590 cm^{-1}, scissors vibration of $-CH_2-$ at 1370 cm^{-1}, symmetric deformation of $-CH_3$ at 1370 cm^{-1}, stretching of C-O-C ether groups at 1250 cm^{-1}, stretching of -NH in $C-NH_2$ primary amines located at 1100 cm^{-1}, and wagging of -NH in $R-NH_2$ primary amines.

Complementary to this preliminary characterization of the epoxy system, some additional properties are described. Some physical properties of the base epoxy, the hardener, and the uncured mixture are summarized in table III.2.1.2.

Table III.2.1.2. Summary of some physical properties of the epoxy system based on Resoltech® 1070 partially bio-based epoxy resin and Resoltech® 1074 hardener.

Property	**Resoltech® 1070**	**Resoltech® 1074**	**Uncured Mixture (100:35)**
Density at 23 °C (g cm^{-3})	1.18	0.96	1.22
Viscosity at 23 °C (mPa·s)	1750	50	700

With regard to the reactivity of this system, it is worthy to note that the exothermic peak of the epoxy system during curing at 23 °C had a value of 185 °C and occurred at 31 min. It showed a gel time of 28 min when the mixture did not exceed a volume of 70 mL, as indicated by the supplier.

In addition to these properties, the glass transition temperature, T_g, of the cured resin was obtained via dynamic mechanical thermal analysis (DMTA). The curing cycle was 1 h at 90 °C and had a post-curing stage of 30 min at 150 °C. DMTA was carried out in an oscillatory rheometer AR-G2 supplied from TA Instruments (New Castle, DE, USA), using a special clamp system made for solid samples (4 x 10 x 40 mm^3) working in torsion-shear conditions. Cured samples were subjected to a temperature sweep from 30 °C to 140 °C at a heating rate of 2 K min^{-1}, with a maximum deformation (γ) of 0.1 %, and a frequency of 1 Hz. figure II.2.1.2 shows the plot evolution of the storage modulus (*G'*) and the damping factor (tan *δ*). By taking the T_g as the peak maximum of tan *δ*, a value of 95.3 °C was obtained for this cured epoxy system.

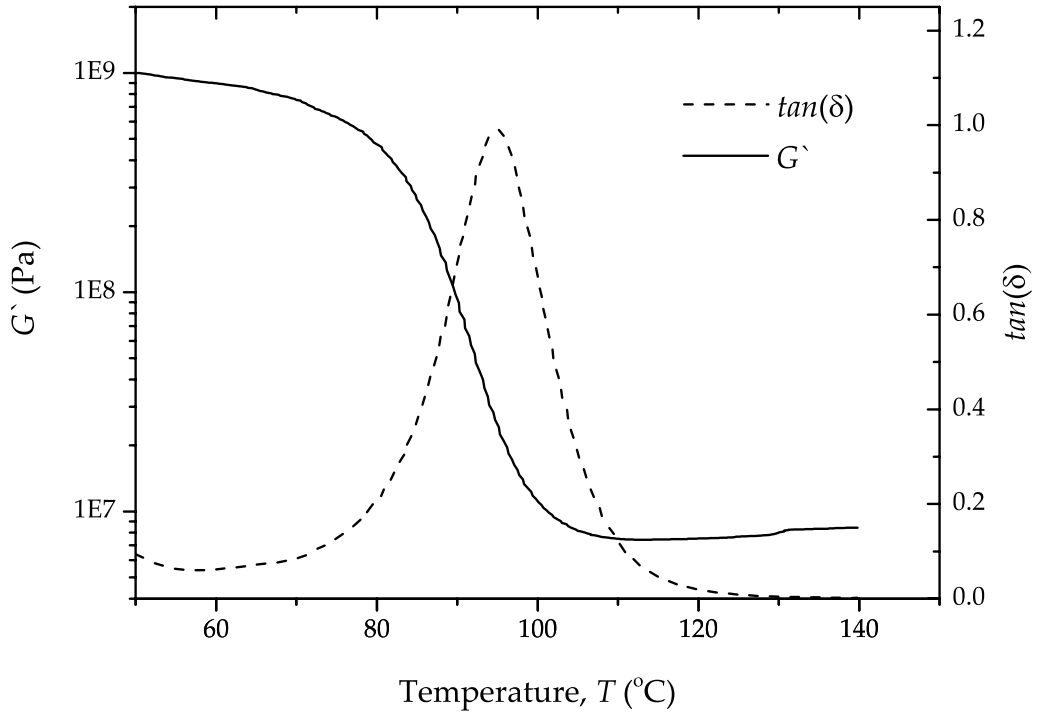

Figure III.2.1.2. Plot evolution of the storage modulus (*G'*) and the damping factor (*tan δ*) of a partially bio-based epoxy resin after curing at 90 °C for 1 h and a post-curing cycle at 150 °C for 0.5 h.

Finally, the Shore D hardness of the cured epoxy material was obtained in a 676-D durometer from J. Bot Instruments (Barcelona, Spain) at room temperature following ISO 868 standard, resulting in a Shore D value of 83.4 ± 1.7.

Differential Scanning Calorimetry (DSC) Kinetic Measurements

The curing kinetics of the eco-epoxy system was analyzed using differential scanning calorimetry (DSC) in a 821 DSC calorimeter from Mettler-Toledo, Inc. (Schwerzenbach, Switzerland). The sample weight was between 10-13 mg, following the recommendations of Vyazovkin, *et al.* [55], suggesting that the sample's mass should be an inverse proportion to the heating rate. The mixtures were prepared at room temperature using the stoichiometric ratio, and then the liquid mixture was stirred until homogenization. Subsequently, the corresponding mass was placed into a standard aluminium pan (40 µL) and sealed with a press. Finally, the samples were subjected to the following thermal program: first, an isothermal stage at 20 °C for 1 min was programmed to stabilize the sample temperature, then a heating process up to (250 °C-280 °C) at different heating rates, β (2.5, 5, 10, and 20 K min^{-1}. This was followed by a cooling step down to 0 °C at a cooling rate of -20 K min^{-1}, and finally, a second heating step up to 180 °C at 10 K min^{-1} was scheduled. All tests were carried out under a dry

atmosphere with a constant nitrogen flow of 30 mL min^{-1}. DSC was used to obtain the heat flow as a function of temperature (from the first heating), and the glass temperature (T_g) (from the second heating).

Processing the thermal data from DSC is necessary to obtain the extent of conversion α. It could be expressed as indicated in Equation (III.2.1.23), where ΔH_t is the released enthalpy or heat at a particular time t, and ΔH_T is the total enthalpy released during the complete reaction. Equation (III.2.1.24) shows how the conversion rate can be obtained from the heat flow of the DSC thermograms.

$$\alpha = \frac{\Delta H_t}{\Delta H_T} \quad \text{(III.2.1.23)}$$

$$\frac{d\alpha}{dt} = \frac{1}{H_T} \cdot \frac{dH(t)}{dt} \quad \text{(III.2.1.24)}$$

III.2.1.4. Results and Discussion

Estimation of the Apparent Activation Energy, E_a

The curing reaction of the partially bio-based epoxy resin at different heating rates was studied using DSC. The first heating cycle was useful for determining the total enthalpy (ΔH_T) and the temperature for the maximum curing rate (T_p), while the second heating cycle was used to study the glass transition temperature (T_g) of the cured resin. These values are gathered in table III.2.1.3 for different heating rates between 2.5 and 20 K min^{-1}. It is important to remark that the T_g decreased with increasing heating rate from 95.8 °C (2.5 K min^{-1}) down to 91.1 °C (for 20 K min^{-1}) which was also in accordance with the curing enthalpy (ΔH_T). Low curing rates allow diffusion and crosslinking reactions to occur more readily. At high curing rates, the overall speed is high and does not allow free diffusion as a crosslinked structure is immediately formed [56].

Table III.2.1.3. Parameters corresponding to DSC characterization of a partially bio-based epoxy system at different heating rates. First heating cycle: DSC characterization of the curing/crosslinking of the liquid resin, and second heating cycle: DSC characterization of the cured resin.

Heating rate β (K min^{-1})	**First heating cycle**			**Second Heating Cycle**
	T_p (K)	**α_p**	**ΔH_T (J g^{-1})**	**T_g (K)**
2.5	351.5	0.401	373.9	368.8
5	361.9	0.425	366.5	367.7

10	373.2	0.408	305.5	365.5
20	388.9	0.417	285.8	364.1

Figure III.2.1.3 shows the conversion α as a function of the absolute temperature *T*. As the heating rate β increased, the characteristic sigmoidal curve moved toward higher values.

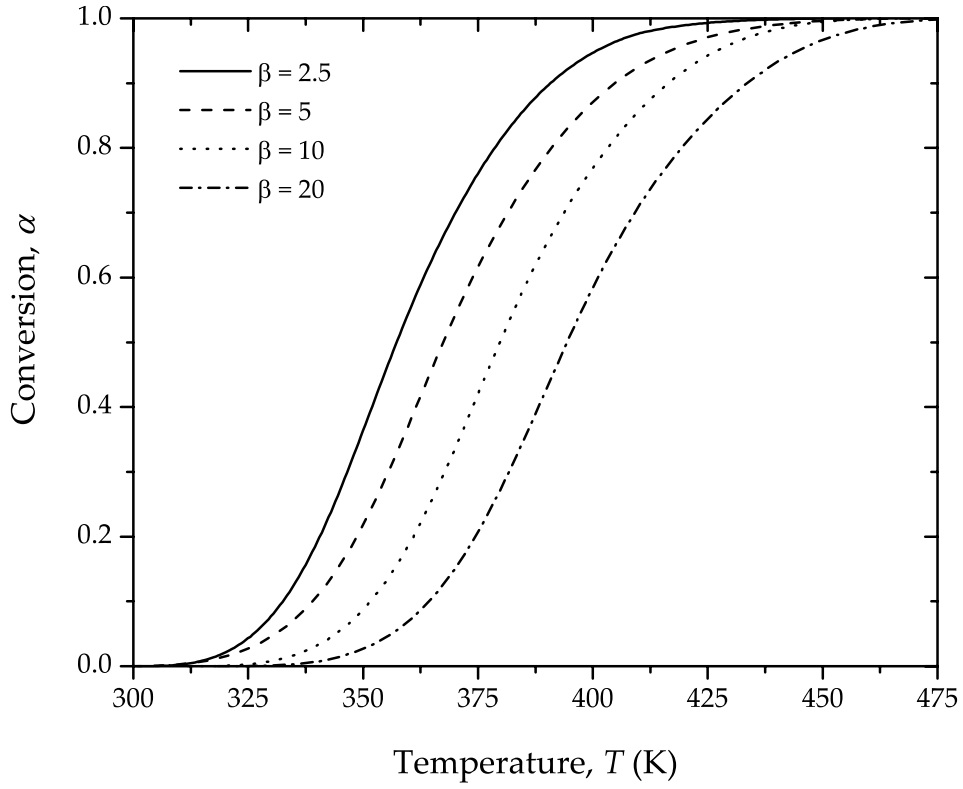

Figure III.2.1.3. Fractional conversion of the curing of a partially bio-based epoxy resin as a function of temperature for different heating rates, β.

Figure III.2.1.4 shows a plot of the curing rate $\left(\frac{d\alpha}{dT}\right)$ as a function of the conversion α obtained using Equation (III.2.1.24). The geometry of these plots is almost the same, thus suggesting there is no change in the reaction model with the heating rate.

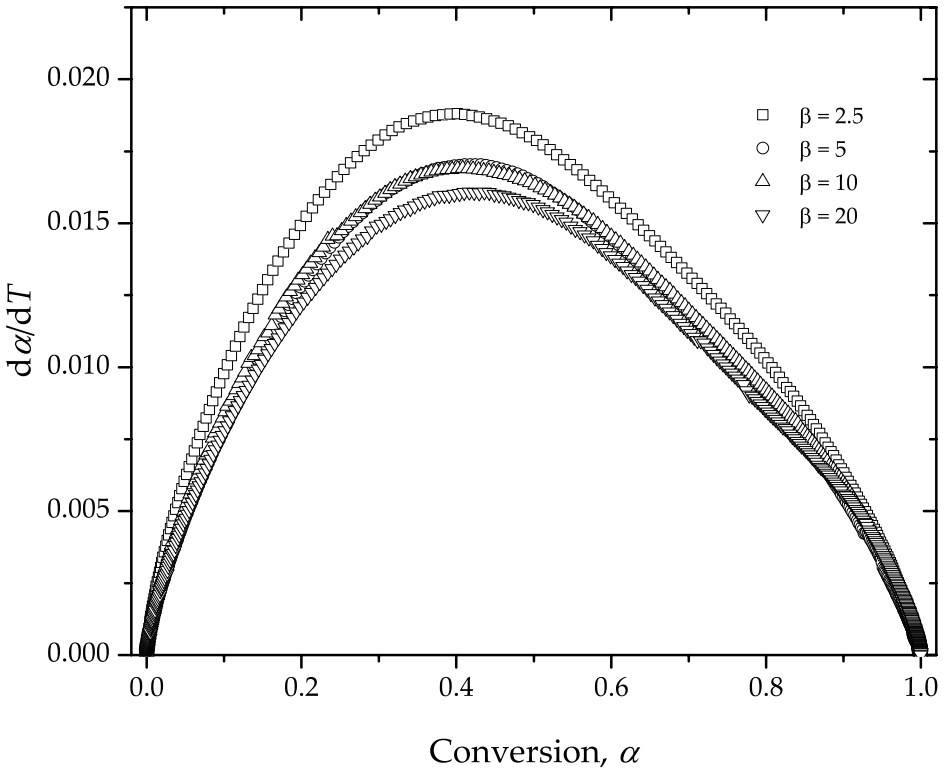

Figure III.2.1.4. The curing rate corresponding to the crosslinking of a partially bio-based epoxy resin as a function of the conversion, *α*, for different heating rates, *β*.

One of the most important parameters of a kinetic study is the apparent activation energy, E_a. As indicated previously, the Kissinger method allows for estimating a single value of E_a for the curing process by using Equation (III.2.1.15). One important condition needed to apply the Kissinger method is that the conversion at the maximum reaction rate, denoted as α_p, must be very similar for all the heating rates. As can be observed in table III.2.1.3, α_p showed an average value of 0.41 ± 0.01, and all the values corresponding to different heating rates are quite similar. Therefore, in a first instance, the Kissinger method could be applied. Figure III.2.1.5 shows the typical plot representation of the Kissinger method, showing good linear fitting. In particular, the E_a obtained from the slope was 57.3 ± 3.1 kJ mol^{-1}. As it has been indicated previously, the peak width of the curing rate is also representative for a single step process. For this reason, a plot of ln Δt_{FWHM} versus $1/T_p$ has been used to check this. The experimental data and the corresponding linear fit can be seen in figure III.2.1.6. The E_a value obtained from the peak width at half maximum was 57.4 ± 3.1 kJ mol^{-1}. This value is in good agreement with that obtained using the Kissinger method, thus suggesting the curing process took place in a single step process. The reactions that take place during a polymerization process could be quite complex due to the polymer chemical structure, diffusion phenomena, crosslinking density, monomer functionality, and chain mobility, among others [50]. Despite this, the overall process for this particular system, analysed

using differential scanning calorimetry, appears to be a single step process (quite homogeneous and symmetric exothermic peak). Therefore, although there could be different activation energies for different processes occurring in the crosslinking, by using DSC, it is possible to obtain a unique “apparent” activation energy, E_a, representative for all the processes that are overlapped.

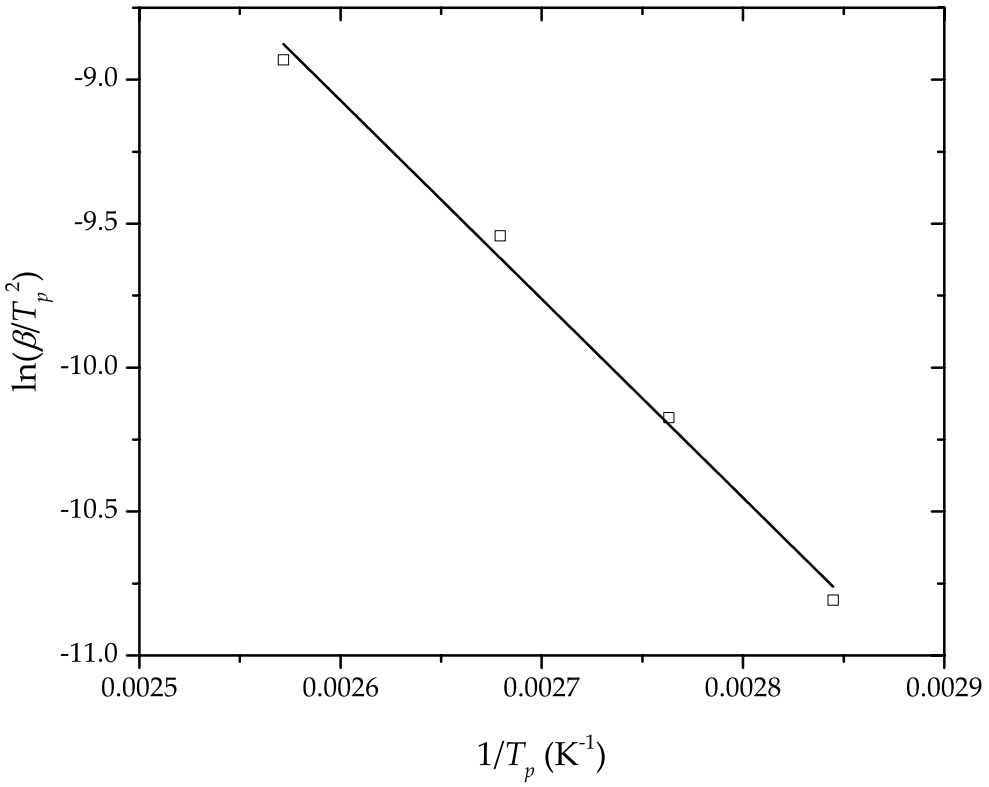

Figure III.2.1.5. Plot of the experimental data according to the Kissinger method and the linear fitting according to Equation (III.2.1.15) corresponding to the crosslinking of a partially bio-based epoxy resin for different heating rates, β.

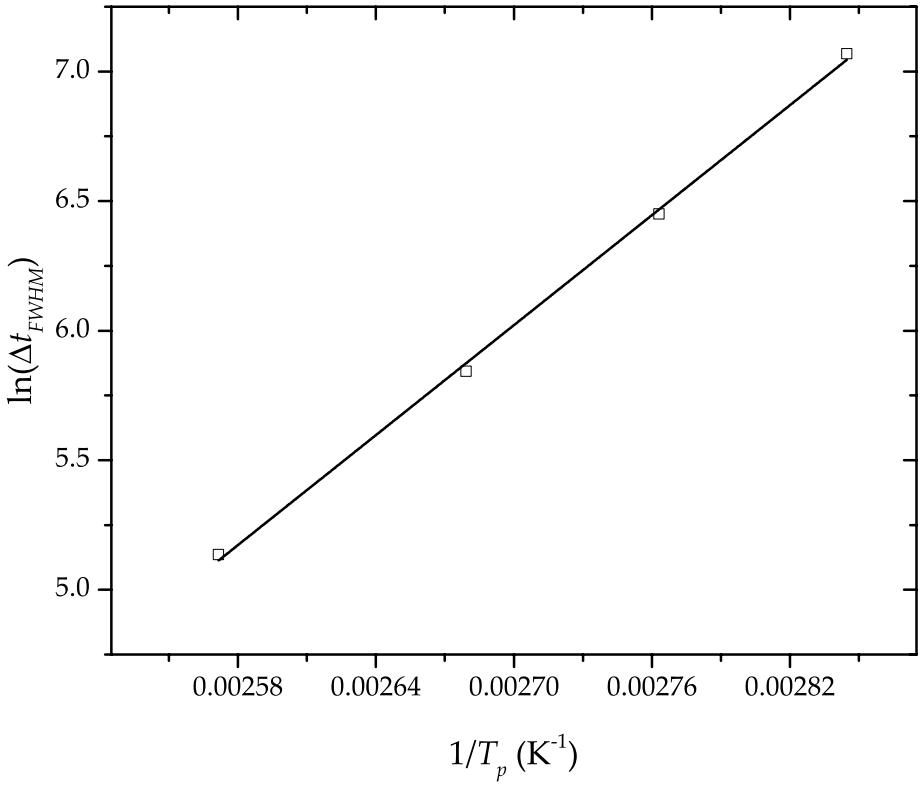

Figure III.2.1.6. Plot of ln Δt_{FWHM} vs $1/T_p$ to check the assumptions of the Kissinger method corresponding to the crosslinking of a partially bio-based epoxy resin for different heating rates, β.

Although the Kissinger method is easy to use and gives an idea of the apparent activation energy of the curing process, it gives a single E_a value. Therefore, the possible change of E_a with the conversion cannot be evaluated using the Kissinger method. To this end, several isoconversional methods have been used. Both differential and integral methods have been used and the corresponding plots are gathered in figure III.2.1.7. The Friedman method (figure III.2.1.7a) shows the calculated data at different conversions and several heating rates. As indicated by Equation (III.2.1.10), the E_a can be obtained through the slope of the linear fits. The Pearson's correlation coefficient *r* for all the linear fits at different conversions was about -0.995. The average E_a obtained with the Friedman method was 61.2 ± 2.6 kJ mol^{-1}. This value is within the same range of the E_a obtained using the Kissinger method. In a first approach, the Friedman method did not use any approximation, so it should be more accurate than integral methods since they use different approximations of the temperature integral. However, due to a noisy signal, errors related to the baseline of DSC curves, and so on, there is no great difference between the Friedman method and other integral methods [43]. The Flynn-Wall-Ozawa (FWO) method is an integral method that uses a quite crude approximation of the temperature integral. Nevertheless, it is widely used and gives quite accurate values of E_a as seen in figure III.2.1.7b. After applying Equation (III.2.1.12), the

average E_a obtained using the FWO method was 62.8 ± 3.1 kJ mol^{-1} with excellent correlation coefficients of $r \approx -0.995$. The low standard deviation was representative of a slight change in E_a with the conversion. A more accurate approximation of the temperature integral is used by the Kissinger-Akahira-Sunose (KAS) method (see figure III.2.1.7c). The correlation factor was also close to -0.995 for all linear fits. The average E_a obtained using the KAS method was 59.8 ± 3.3 kJ mol^{-1}, which is similar to all the previously reported values. The Starink method is an integral method that uses a very accurate approximation of the temperature integral and gave r values of about -0.995 (figure III.2.1.5d). By using the linear fits, the average E_a was 60.0 ± 3.3 kJ mol^{-1}.

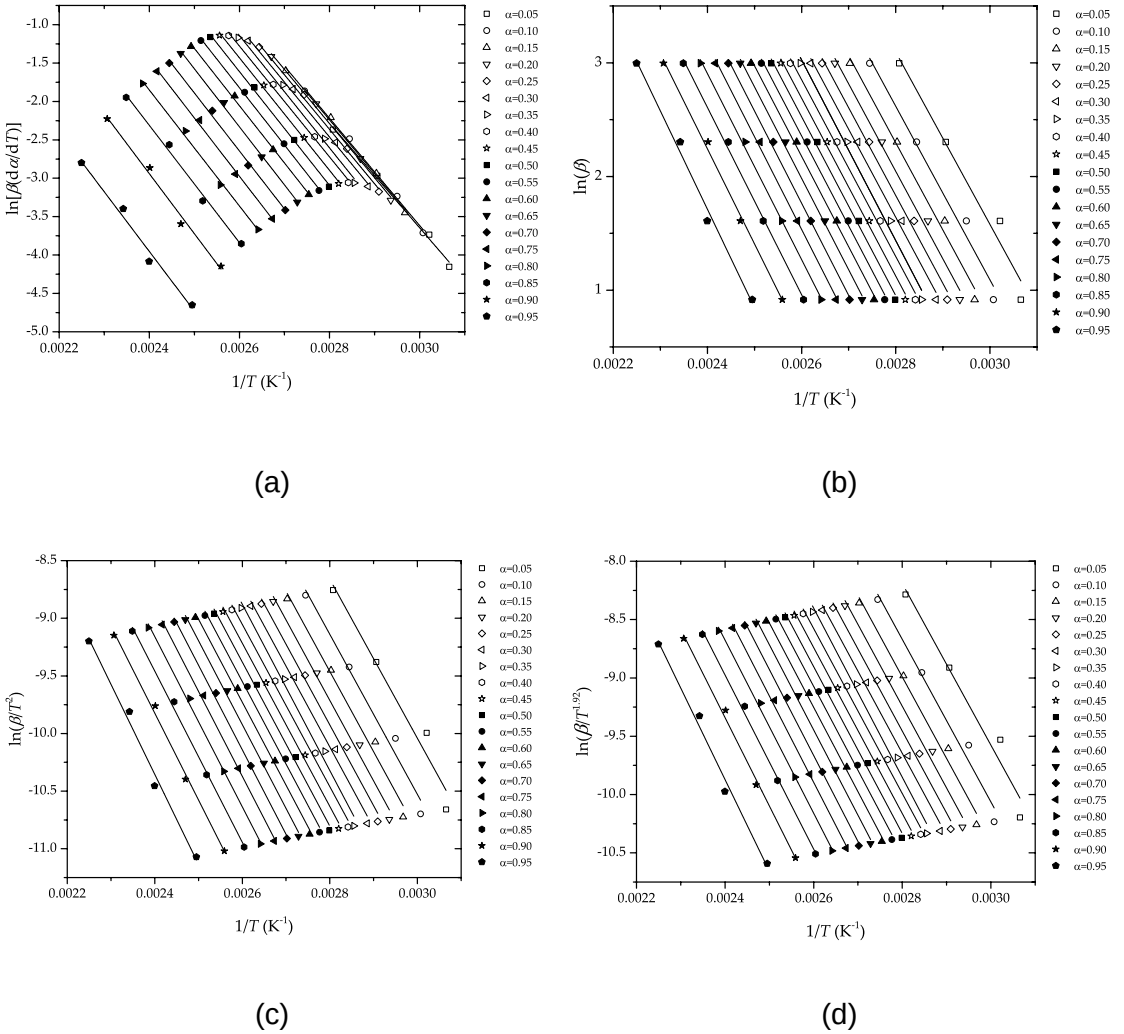

Figure III.2.1.7. Characteristic plots of different isoconversional kinetic methods at different conversions α, corresponding to the crosslinking of a partially bio-based epoxy resin for different heating rates, β: (**a**) Friedman, (**b**) Flynn-Wall-Ozawa (FWO), (**c**) Kissinger-Akahira-Sunose (KAS), and (**d**) Starink.

All the above-mentioned methods give an apparent activation energy between 57 and 62 kJ·mol^{-1}, which is in total accordance with typical E_a values for DGEBA-based

epoxy resins, thus suggesting the plant-derived reactive diluent did not affect in a remarkable way the curing process αof the resin [11]. As suggested by the standard deviation of E_a from different methods, there is very low variation of E_a with α, as can be seen in figure III.2.1.8.

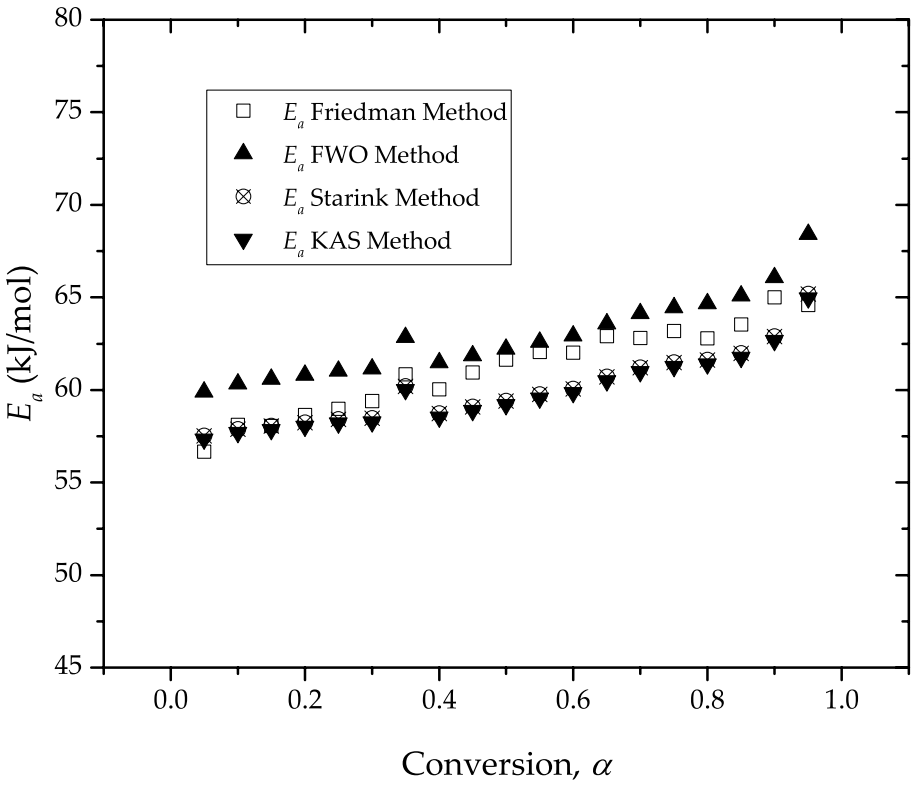

Figure III.2.1.8. Variation of the apparent activation energy, E_a, as a function of function of conversion α, corresponding to the crosslinking of a partially bio-based epoxy resin for different heating rates.

Due to this low variability of E_a, it can be considered that the curing process of this partially bio-based epoxy resin follows a single step process with a global "apparent" activation energy defined by the average for all the conversion range [57]. Once the E_a has been accurately obtained, it is important to obtain the remaining kinetic parameters to complete the kinetic triplet. This means obtaining the reaction model $f(\alpha)$, and the pre-exponential factor, A. As indicated previously, Málek and Criado-Maqueda described a methodology to compare the calculated $y(\alpha)$ and $z(\alpha)$, as indicated by Equation (III.2.1.16) and Equation (III.2.1.17), respectively, with different master plots typical of thermally activated processes, as summarized in table III.2.1.1. Figure III.2.1.9 shows the plot of $y(\alpha)$ as a function of the conversion α for different heating rates. As it can be seen, the maximum of the $y(\alpha)$, denoted as α_M, was not zero (α_M = 0) could be representative for an *n*th order reaction model), thus suggesting another reaction model. In fact, this maximum was located close to 0.1 and the typical geometry

suggested an autocatalytic reaction model as obtained by comparison with different master plots [51,55,58]. The maximum of the calculated $y(\alpha)$ functions for different heating rates are summarized in table III.2.1.4.

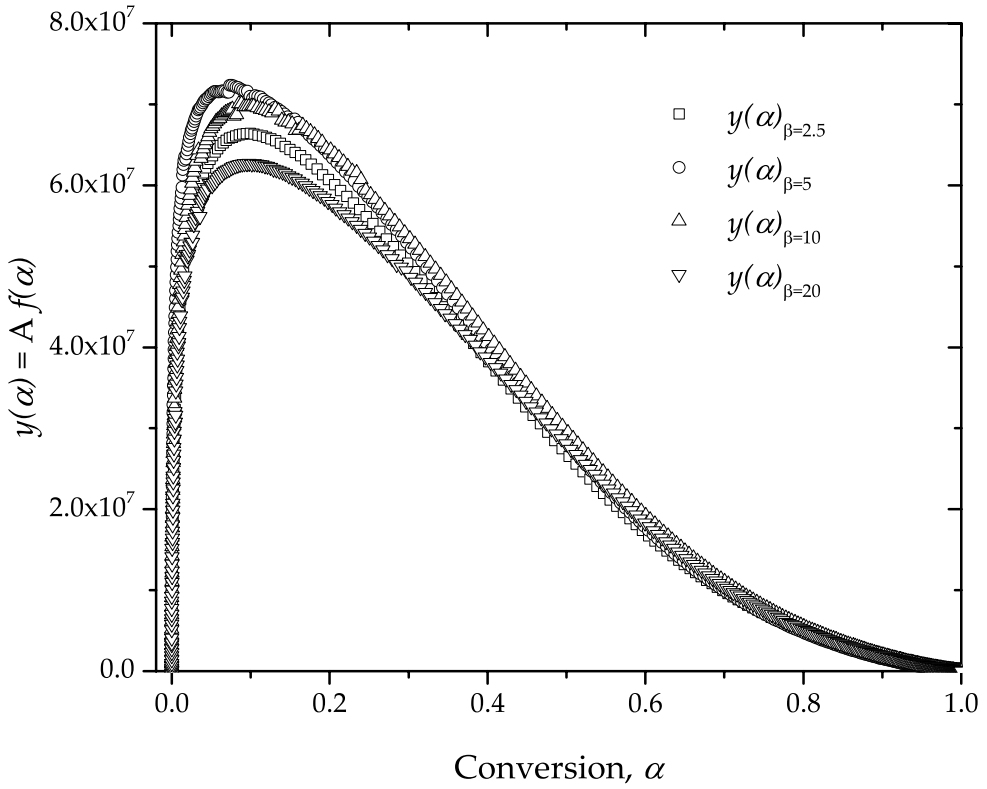

Figure III.2.1.9. Calculated $y(\alpha)$ plots as a function of the conversion α, corresponding to the crosslinking of a partially bio-based epoxy resin for different heating rates.

Table III.2.1.4. Maximum values of the calculated $y(\alpha)$ and $z(\alpha)$ functions corresponding to the crosslinking of a partially bio-based epoxy resin for different heating rates.

Heating Rate β (K min^{-1})	α_M	α_p^∞
2.5	0.099	0.420
5	0.076	0.438
10	0.085	0.442
20	0.098	0.443

Figure III.2.1.10 gathers the $z(\alpha)$plots for different heating rates. As can be seen, the $z(\alpha)$ functions show the same geometry, and some of them are overlapped. In can be clearly seen that the maximum of the $z(\alpha)$ function, denoted as α_p^∞, was between 0.4 and 0.5. The actual values for the different heating rates were obtained from the experimental values of $z(\alpha)$ and are shown in table III.2.1.4. By comparison of the experimental $z(\alpha)$ plots with some generalized master plots [58], this particular geometry

is consistent with an autocatalytic model with a reasonable weight of the autocatalytic effect.

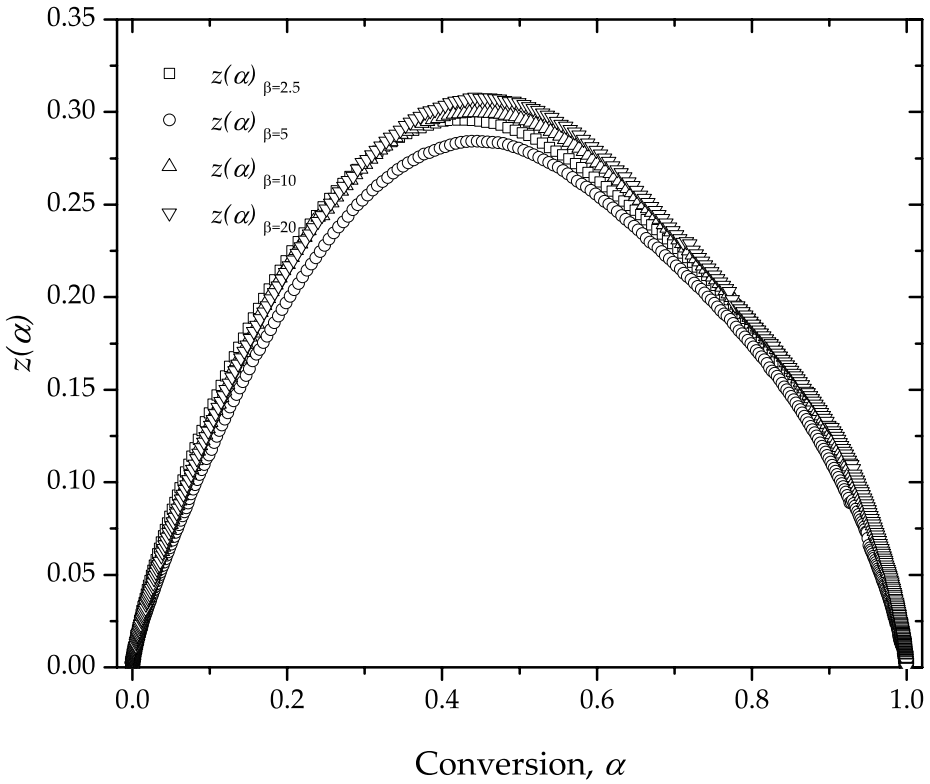

Figure III.2.1.10. Calculated $z(\alpha)$ plots as a function of the conversion **α**, corresponding to the crosslinking of a partially bio-based epoxy resin for different heating rates.

The peak for $y(\alpha)$ functions, α_M, was 0.090 ± 0.011, and this means there was a certain autocatalytic effect on the curing reaction [59,60]. In fact, one of the conditions for an autocatalytic process requires $\alpha_M > 0$. The autocatalytic effect will be more intense with higher $\alpha_M$values. With regard to the maximum of the $z(\alpha)$ plots, the average α_p^∞ was 0.436 ± 0.011. Another condition for an autocatalytic process is that $\alpha_M < \alpha_p^\infty$, and obviously, this is true. Therefore, it is possible to use an autocatalytic reaction model to obtain the remaining parameters for the kinetic triplet. For the curing of epoxies, the two parameters Šesták–Berggren reaction model [SB(*m,n*)] [51] can be used as suggested by both $y(\alpha)$ and $z(\alpha)$functions. The Šesták–Berggren function is shown in Equation (III.2.1.25) and considers two parameters, *n,* and *m*. The *n* parameter represents the typical *n*th order reaction models as it indicates the reaction rate is proportional to the unreacted material $(1-\alpha)$, while the *m* exponent is representing the autocatalytic effect as it indicates, the conversion rate is proportional to the reacted material, α:

$$f(\alpha) = \alpha^m (1-\alpha)^n \qquad \text{(III.2.1.25)}$$

Once the reaction model has been checked, Equation (III.2.1.25) can be substituted into Equation (III.2.1.3), thus leading to Equation (III.2.1.26):

$$\frac{d\alpha}{dt} = A\, e^{\frac{-E_a}{R\,T}}\, \alpha^m\, (1-\alpha)^n \qquad \text{(III.2.1.26)}$$

As the apparent activation energy is known (isoconversional methods), it is possible to write Equation (III.2.1.26) as:

$$\frac{\left(\frac{d\alpha}{dt}\right)}{e^{\frac{-E_a}{R\,T}}} = A\, \alpha^m\, (1-\alpha)^n = \frac{\left(\beta\, \frac{d\alpha}{dT}\right)}{e^{\frac{-E_a}{R\,T}}} \qquad \text{(III.2.1.27)}$$

It is possible to obtain the *n* and *m* exponents using an iterative linear fit, but in this work, a non-linear curve fitting has been used. By applying natural logarithms to both sides of Equation (III.2.1.27), we obtain:

$$ln\left(\beta \frac{d\alpha}{dT}\right) + \frac{E_a}{R\,T} = ln(A) + m\, ln(\alpha) + n\ ln(1-\alpha) \qquad \text{(III.2.1.28)}$$

The term on the left-hand side of Equation (III.2.1.28) is $\ln\big(y(\alpha)\big)$, such that a non-linear curve fitting, as indicated in Equation (III.2.1.29), can be used to obtain the optimum *m* and *n* exponents, as well as the pre-exponential factor, *A*:

$$y = k + m\, ln(x) + n\, ln(1-x) \qquad \text{(III.2.1.29)}$$

The parameters obtained after the non-linear curve fitting are summarized in table III.2.1.5. The average value of ln(*A*) was 18.47 ± 0.05, and regarding the reaction model exponents, *m* = 0.15 ± 0.01 and *n* = 1.76 ± 0.08. The low standard deviation indicates these values did not change in a remarkable way with the heating rate.

Table III.2.1.5. Calculated kinetic parameters for autocatalytic SB(*m,n*) model by using a non-linear curve fitting, corresponding to the crosslinking of a partially bio-based epoxy resin for different heating rates.

Heating Rate β (K min^{-1})	**ln (*A*) (*A* in min^{-1})**	***m***	***n***
2.5	18.464	0.156	1.792
5	18.546	0.143	1.866
10	18.460	0.148	1.677
20	18.415	0.155	1.712

For an autocatalytic reaction model, the maximum of $y(\alpha)$ is related to the *n* and *m* exponents via Equation (III.2.1.30) [51,61]:

$$\alpha_M = \frac{m}{m+n} \tag{III.2.1.30}$$

Substitution of the average *n* and *m* values obtained with the non-linear curve fitting led to a theoretical α_M of about 0.08, which is in total accordance with the calculated value from experimental data.

Once the kinetic triple had been determined, the model was integrated. Figure III.2.1.11 shows a comparison of the experimental data (symbols) and the corresponding theoretical models (lines). As it can be seen, Equation (III.2.1.3), with the obtained kinetic triplet (E_a, *A*, and $f(\alpha)$), gave good accuracy relative to the experimental data for all the heating rates, thus giving consistency to the obtained parameters.

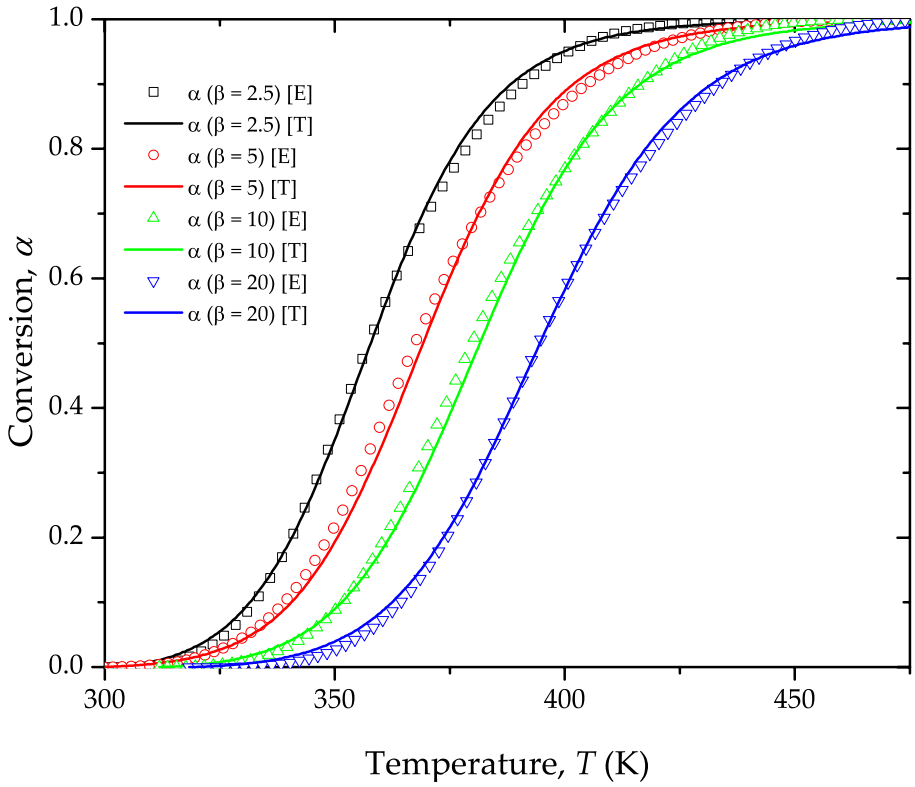

Figure III.2.1.11. Comparison of conversion, α, corresponding to the crosslinking of a partially bio-based epoxy resin for different heating rates. Symbols represent experimental values [E] and lines represent theoretical [T] values.

III.2.1.5. Conclusions

The cure kinetics of a partially bio-based epoxy resin derived from DGEBA and a plant-based reactive diluent (representing 31 % of the cured resin) was analyzed using dynamic DSC at different heating rates. The apparent activation energy, E_a, was determined using different isoconversional methods, and it was found to be between 57 and 62 kJ mol^{-1}. The low dispersion of E_a values for different conversion, α, values suggested a relatively independence of E_a from α.

The reaction model was obtained via comparison of the calculated $y(\alpha)$ and $z(\alpha)$ with some well-established reaction models of thermally activated processes. It was concluded that the two-parameter [SB(m,n)] autocatalytic kinetic model of Šesták–Berggren was the most suitable for the description of the curing process of this partially bio-based epoxy resin. Therefore, this work provides a methodology to obtain the kinetic triplet corresponding to the curing/crosslinking of an epoxy resin. The theoretical curves show a great agreement with the experimental data, thus giving consistency to the obtained kinetic triplet.

III.2.1.6. Funding

This research was supported by the Spanish Ministry of Economy and Competitiveness (MINECO) program number MAT2017-84909-C2-2-R. Quiles-Carrillo wants to thank GV for his FPI grant (ACIF/2016/182) and the MECD for his FPU grant (FPU15/03812).

III.2.1.7. References

1. F.L. Jin, X. Li, S.J. Park. Synthesis and application of epoxy resins: A review. *Journal of Industrial and Engineering Chemistry* **2015**, *29*, 1-11.
2. D. Ratna, M. Patri, B.C. Chakraborty, P.C. Deb. Amine-terminated polysulfone as modifier for epoxy resin. *J Appl Polym Sci* **1997**, *65*, 901-907.
3. R. David, V.S. Raja, S.K. Singh, P. Gore. Development of anti-corrosive paint with improved toughness using carboxyl terminated modified epoxy resin. *Progress in Organic Coatings* **2018**, *120*, 58-70.
4. R.F. Minty, J.L. Thomason, L. Yang, W. Stanley, A. Roy. Development and application of novel technique for characterising the cure shrinkage of epoxy resins. *Polymer Testing* **2019**, *73*, 316-326.
5. C. François, S. Pourchet, G. Boni, S. Rautiainen, J. Samec, L. Fournier, C. Robert, C.M. Thomas, S. Fontaine, Y. Gaillard, V. Placet, L. Plasseraud. Design and synthesis of biobased epoxy thermosets from biorenewable resources. *Comptes Rendus Chimie* **2017**, *20*, 1006-1016.
6. O. Zabihi, M. Ahmadi, S. Nikafshar, K. Chandrakumar Preyeswary, M. Naebe. A technical review on epoxy-clay nanocomposites: Structure, properties, and their applications in fiber reinforced composites. *Composites Part B: Engineering* **2018**, *135*, 1-24.
7. H. Jin, G.M. Miller, N.R. Sottos, S.R. White. Fracture and fatigue response of a self-healing epoxy adhesive. *Polymer* **2011**, *52*, 1628-1634.
8. H. Jin, G.M. Miller, S.J. Pety, A.S. Griffin, D.S. Stradley, D. Roach, N.R. Sottos, S.R. White. Fracture behavior of a self-healing, toughened epoxy adhesive. *International Journal of Adhesion and Adhesives* **2013**, *44*, 157-165.
9. B. Ramezanzadeh, S. Niroumandrad, A. Ahmadi, M. Mahdavian, M.H. Mohamadzadeh Moghadam. Enhancement of barrier and corrosion protection performance of an epoxy coating through wet transfer of amino functionalized graphene oxide. *Corrosion Science* **2016**, *103*, 283-304.
10. S.Y. Zhang, Y.F. Ding, S.J. Li, X.W. Luo, W.F. Zhou. Effect of polymeric structure on the corrosion protection of epoxy coatings. *Corrosion Science* **2002**, *44*, 861-869.
11. C. Yi, P. Rostron, N. Vahdati, E. Gunister, A. Alfantazi. Curing kinetics and mechanical properties of epoxy based coatings: The influence of added solvent. *Progress in Organic Coatings* **2018**, *124*, 165-174.

12. X. Zhao, Y. Li, W. Chen, S. Li, Y. Zhao, S. Du. Improved fracture toughness of epoxy resin reinforced with polyamide 6/graphene oxide nanocomposites prepared via in situ polymerization. *Composites Science and Technology* **2019**, *171*, 180-189.

13. T.H. Ho, C.S. Wang. Modification of epoxy resins with polysiloxane thermoplastic polyurethane for electronic encapsulation: 1. *Polymer* **1996**, *37*, 2733-2742.

14. E. Loccufier, J. Geltmeyer, L. Daelemans, D.R. D'hooge, K. De Buysser, K. De Clerck. Silica nanofibrous membranes for the separation of heterogeneous azeotropes. *Advanced Functional Materials* **2018**, *28*, 1804138.

15. W. Riemenschneider, H.M. Bolt. Esters , Organic. *Ullmann's Encyclopedia of Industrial Chemistry* **2005**, 10.1002/14356007.a09, 8676-8694.

16. I.E. Dell'Erba, R.J.J. Williams. Homopolymerization of epoxy monomers initiated by 4-(dimethylamino) pyridine. *Polymer Engineering & Science* **2006**, *46*, 351-359.

17. B. Francis, V. Lakshmana Rao, S. Jose, B.K. Catherine, R. Ramaswamy, J. Jose, S. Thomas. Poly(ether ether ketone) with pendent methyl groups as a toughening agent for amine cured DGEBA epoxy resin. *Journal of Materials Science* **2006**, *41*, 5467-5479.

18. L. Li, Y. Yu, Q. Wu, G. Zhan, S. Li. Effect of chemical structure on the water sorption of amine-cured epoxy resins. *Corrosion Science* **2009**, *51*, 3000-3006.

19. J.P. Bell. Structure of a typical amine-cured epoxy resin. *Journal of Polymer Science Part A-2: Polymer Physics* **1970**, *8*, 417-436.

20. B. Ellis, W.R. Ashcroft, S.J. Shaw, W.J. Cantwell, H.H. Kausch, G.P. Johari, F.R. Jones, X.M. Chen. *Chemistry and technology of epoxy resins*.

21. D. Bertomeu, D. García-Sanoguera, O. Fenollar, T. Boronat, R. Balart. Use of eco-friendly epoxy resins from renewable resources as potential substitutes of petrochemical epoxy resins for ambient cured composites with flax reinforcements. *Polymer Composites* **2012**, *33*, 683-692.

22. M.D. Samper, R. Petrucci, L. Sánchez-Nacher, R. Balart, J.M. Kenny. New environmentally friendly composite laminates with epoxidized linseed oil (ELO) and slate fiber fabrics. *Composites Part B: Engineering* **2015**, *71*, 203-209.

23. M.D. Samper, R. Petrucci, L. Sanchez-Nacher, R. Balart, J.M. Kenny. Properties of composite laminates based on basalt fibers with epoxidized vegetable oils. *Materials and Design* **2015**, *72*, 9-15.

24. J.M. España, L. Sánchez-Nacher, T. Boronat, V. Fombuena, R. Balart. Properties of biobased epoxy resins from epoxidized soybean oil (ESBO) cured with maleic anhydride (MA). *JAOCS, Journal of the American Oil Chemists' Society* **2012**, *89*, 2067-2075.

25. M. Samper, R. Petrucci, L. Sánchez-Nacher, R. Balart, J. Kenny. Effect of silane coupling agents on basalt fiber–epoxidized vegetable oil matrix composite materials analyzed by the single fiber fragmentation technique. *Polymer Composites* **2015**, *36*, 1205-1212.

26. J.M. Raquez, M. Deléglise, M.F. Lacrampe, P. Krawczak. Thermosetting (bio)materials derived from renewable resources: A critical review. *Progress in Polymer Science (Oxford)* **2010**, *35*, 487-509.

27. M.A.R. Meier, J.O. Metzger, U.S. Schubert. Plant oil renewable resources as green alternatives in polymer science. *Chemical Society Reviews* **2007**, *36*, 1788-1802.

28. M. Stemmelen, F. Pessel, V. Lapinte, S. Caillol, J.P. Habas, J.J. Robin. A fully biobased epoxy resin from vegetable oils: From the synthesis of the precursors by thiol-ene reaction to the study of the final material. *Journal of Polymer Science, Part A: Polymer Chemistry* **2011**, *49*, 2434-2444.

29. J. Michałowicz. Bisphenol A - Sources, toxicity and biotransformation. *Environmental Toxicology and Pharmacology* **2014**, *37*, 738-758.

30. A. Carbonell-Verdu, L. Bernardi, D. Garcia-Garcia, L. Sanchez-Nacher, R. Balart. Development of environmentally friendly composite matrices from epoxidized cottonseed oil. *European Polymer Journal* **2015**, *63*, 1-10.

31. R.A. Ortiz, D.P. López, M.D.L.G. Cisneros, J.C.R. Valverde, J.V. Crivello. A kinetic study of the acceleration effect of substituted benzyl alcohols on the cationic photopolymerization rate of epoxidized natural oils. *Polymer* **2005**, *46*, 1535-1541.

32. U. Biermann, W. Friedt, S. Lang, W. Lühs, G. Machmüller, J.O. Metzger, M. Rüsch gen. Klaas, H.J. Schäfer, M.P. Schneider. New syntheses with oils and fats as renewable raw materials for the chemical industry. *Angewandte Chemie International Edition* **2000**, *39*, 2206-2224.

33. S.N. Khot, J.J. Lascala, E. Can, S.S. Morye, G.I. Williams, G.R. Palmese, S.H. Kusefoglu, R.P. Wool. Development and application of triglyceride-based polymers and composites. *Journal of applied polymer science* **2001**, *82*, 703-723.

34. J.M. Ferri, M.D. Samper, D. García-Sanoguera, M.J. Reig, O. Fenollar, R. Balart. Plasticizing effect of biobased epoxidized fatty acid esters on mechanical and thermal properties of poly(lactic acid). *Journal of Materials Science* **2016**, *51*, 5356-5366.

35. A. Carbonell-Verdu, D. Garcia-Sanoguera, A. Jordá-Vilaplana, L. Sanchez-Nacher, R. Balart. A new biobased plasticizer for poly(vinyl chloride) based on epoxidized cottonseed oil. *Journal of Applied Polymer Science* **2016**, *133*, 1-10.

36. O. Fenollar, D. Garcia-Sanoguera, L. Sanchez-Nacher, J. Lopez, R. Balart. Effect of the epoxidized linseed oil concentration as natural plasticizer in vinyl plastisols. *Journal of Materials Science* **2010**, *45*, 4406-4413.

37. O. Fenollar, D. Garcia-Sanoguera, L. Sánchez-Nácher, J. López, R. Balart. Characterization of the curing process of vinyl plastisols with epoxidized linseed oil as a natural-based plasticizer. *Journal of applied polymer science* **2012**, *124*, 2550-2557.

38. M.D. Samper, V. Fombuena, T. Boronat, D. García-Sanoguera, R. Balart. Thermal and mechanical characterization of epoxy resins (ELO and ESO) cured with anhydrides. *JAOCS, Journal of the American Oil Chemists' Society* **2012**, *89*, 1521-1528.

39. S.J. Park, F.L. Jin, J.R. Lee. Effect of biodegradable epoxidized castor oil on physicochemical and mechanical properties of epoxy resins. *Macromolecular Chemistry and Physics* **2004**, *205*, 2048-2054.

40. M. Pawar, A. Kadam, O. Yemul, V. Thamke, K. Kodam. Biodegradable bioepoxy resins based on epoxidized natural oil (cottonseed & algae) cured with citric and tartaric acids through solution polymerization: A renewable approach. *Industrial Crops and Products* **2016**, *89*, 434-447.

41. D. Incerti, T. Wang, D. Carolan, A. Fergusson. Curing rate effects on the toughness of epoxy polymers. *Polymer* **2018**, *159*, 116-123.

42. M. Javdanitehran, D.C. Berg, E. Duemichen, G. Ziegmann. An iterative approach for isothermal curing kinetics modelling of an epoxy resin system. *Thermochimica Acta* **2016**, *623*, 72-79.

43. S. Vyazovkin, A.K. Burnham, J.M. Criado, L.A. Pérez-Maqueda, C. Popescu, N. Sbirrazzuoli. ICTAC Kinetics Committee recommendations for performing kinetic computations on thermal analysis data. *Thermochimica acta* **2011**, *520*, 1-19.

44. H.L. Friedman. Kinetics of thermal degradation of char-forming plastics from thermogravimetry. Application to a phenolic plastic. *Journal of Polymer Science Part C: Polymer Symposia* **2007**, *6*, 183-195.

45. C.D. Doyle. Estimating isothermal life from thermogravimetric data. *Journal of Applied Polymer Science* **1962**, *6*, 639-642.

46. T. Akahira, T. Sunose. Transactions of joint convention of four electrical institutes. **1969**, 246-246.

47. M.J. Starink. The determination of activation energy from linear heating rate experiments: A comparison of the accuracy of isoconversion methods. *Thermochimica Acta* **2003**, *404*, 163-176.

48. H.E. Kissinger. Variation of peak temperature with heating rate in differential thermal analysis. *Journal of Research of the National Bureau of Standards* **1956**, *57*, 217-217.

49. J. Farjas, N. Butchosa, P. Roura. A simple kinetic method for the determination of the reaction model from non-isothermal experiments. *Journal of thermal analysis and calorimetry* **2010**, *102*, 615-625.

50. D.R. D'hooge, P.H. Van Steenberge, M.-F. Reyniers, G.B. Marin. The strength of multi-scale modeling to unveil the complexity of radical polymerization. *Progress in Polymer Science* **2016**, *58*, 59-89.

51. J. Málek. The kinetic analysis of non-isothermal data. *Thermochimica Acta* **1992**, *200*, 257-269.

52. G.I. Senum, R.T. Yang. Rational approximations of the integral of the Arrhenius function. *Journal of Thermal Analysis* **1977**, *11*, 445-447.

53. L.A. Pérez-Maqueda, J.M. Criado. Accuracy of Senum and Yang's approximations to the Arrhenius integral. *Journal of Thermal Analysis and Calorimetry* **2000**, *60*, 909-915.

54. J.H. Flynn. The "temperature integral" - Its use and abuse. *Thermochimica Acta* **1997**, *300*, 83-92.

55. S. Vyazovkin, K. Chrissafis, M.L. Di Lorenzo, N. Koga, M. Pijolat, B. Roduit, N. Sbirrazzuoli, J.J. Suñol. ICTAC Kinetics Committee recommendations for collecting experimental thermal analysis data for kinetic computations. *Thermochimica Acta* **2014**, *590*, 1-23.

56. A. Hale, C.W. Macosko, H.E. Bair. Glass transition temperature as a function of conversion in thermosetting polymers. *Macromolecules* **1991**, *24*, 2610-2621.

57. S. Vyazovkin, N. Sbirrazzuoli. Isoconversional kinetic analysis of thermally stimulated processes in polymers. *Macromolecular Rapid Communications* **2006**, *27*, 1515-1532.

58. J. Criado, J. Malek, A. Ortega. Applicability of the master plots in kinetic analysis of non-isothermal data. *Thermochimica Acta* **1989**, *147*, 377-385.

59. B. Bilyeu, W. Brostow, K.P.K.P. Menard. Epoxy thermosets and their applications. III. Kinetic equations and models. *J Mater Educ* **2001**, *23*, 189-204.

60. A. Benedetti, P. Fernandes, J.L. Granja, J. Sena-Cruz, M. Azenha. Influence of temperature on the curing of an epoxy adhesive and its influence on bond behaviour of NSM-CFRP systems. *Composites Part B: Engineering* **2016**, *89*, 219-229.

61. J. Málek. A computer program for kinetic analysis of non-isothermal thermoanalytical data. *Thermochimica Acta* **1989**, *138*, 337-346.

Adaptado del artículo

III.2.2. Kinetic analysis of the curing process of biobased epoxy resin from epoxidized linseed oil by dynamic differential scanning calorimetry

Diego Lascano[1,2], Alejandro Lerma-Canto[1], Vicent Fombuena[1], Rafael Balart[1], Nestor Montanes[1] and Luis Quiles-Carrillo[1]

[1] Technological Institute of Materials (ITM), Universitat Politècnica de València (UPV), Plaza Ferrándiz y Carbonell 1, 03801 Alcoy, Spain

[2] Escuela Politécnica Nacional, Quito 17-01-2759, Ecuador

polymers

Polymers **2021**, *13*(8), 1279

polymers

MDPI

Article

Kinetic Analysis of the Curing Process of Biobased Epoxy Resin from Epoxidized Linseed Oil by Dynamic Differential Scanning Calorimetry

Diego Lascano [1,2], Alejandro Lerma-Canto [1], Vicent Fombuena [1,*], Rafael Balart [1], Nestor Montanes [1] and Luis Quiles-Carrillo [1]

[1] Technological Institute of Materials (ITM), Universitat Politècnica de València (UPV), Plaza Ferrándiz y Carbonell 1, 03801 Alcoy, Spain; dielas@epsa.upv.es (D.L.); allercan@epsa.upv.es (A.L.-C.); rbalart@mcm.upv.es (R.B.); nesmonmu@upvnet.upv.es (N.M.); luiquic1@epsa.upv.es (L.Q.-C.)
[2] Escuela Politécnica Nacional, Quito 17-01-2759, Ecuador
* Correspondence: vifombor@upv.es

Abstract: The curing process of epoxy resin based on epoxidized linseed oil (ELO) is studied using dynamic differential scanning calorimetry (DSC) in order to determine the kinetic triplet (E_a, $f(\alpha)$ and A) at different heating rates. The apparent activation energy, E_a, has been calculated by several differential and integral isoconversional methods, namely Kissinger, Friedman, Flynn–Wall–Ozawa (FWO), Kissinger–Akahira–Sunose (KAS) and Starink. All methods provide similar values of E_a (between 66 and 69 kJ/mol), and this shows independence versus the heating rate used. The epoxy resins crosslinking is characterized by a multi-step process. However, for the sake of the simplicity and to facilitate the understanding of the influence of the oxirane location on the curing kinetic, this can be assimilated to a single-step process. The reaction model has a high proportion of autocatalytic process, fulfilling that α_M is between 0 and α_p and $\alpha_M < \alpha_p^\infty$. Using as reference the model proposed by Šesták–Berggren, by obtaining two parameters (n and m) it is possible to obtain, on the one hand, the kinetic parameters and, on the other hand, a graphical comparison of the degree of conversion, α, versus temperature (T) at different heating rates with the average n and m values of this model. The good accuracy of the proposed model with regard to the actual values obtained by DSC gives consistency to the obtained parameters, thus suggesting the crosslinking of the ELO-based epoxy has apparent activation energies similar to other petroleum-derived epoxy resins.

Keywords: epoxidized linseed oil; kinetic analysis; biobased epoxy resin; flax

Citation: Lascano, D.; Lerma-Canto, A.; Fombuena, V.; Balart, R.; Montanes, N.; Quiles-Carrillo, L. Kinetic Analysis of the Curing Process of Biobased Epoxy Resin from Epoxidized Linseed Oil by Dynamic Differential Scanning Calorimetry. *Polymers* **2021**, *13*, 1279. https://doi.org/10.3390/polym13081279

Academic Editor: Nicolas Sbirrazzuoli

Received: 2 March 2021
Accepted: 7 April 2021
Published: 14 April 2021

1. Introduction

Flax is one of the industrial crops that, thanks to its versatility, has been used since ancient times both in food and in clothes manufacturing for approximately 30,000 years [1]. Nowadays, flax derivatives are continuously gaining importance, due to the productive and economic nature of its sowing. For this reason, the largest producers of flax (Russia, China, Kazakhstan, Argentina and Canada) have increased their production capability [2,3]. In addition to the main uses related to flax crops, namely textile fibers and seeds for food industry, while new uses are being developed for other by-products or co-products linked to the flax industry. In the last decade, flax oil, biodiesel and flax flour have found increasing applications in the market [4–6].

One of the most interesting by-product is flax oil (or linseed oil), which represents approximately 45% of the seeds [3,7]. The main fatty acids are linolenic acid (56.6%), oleic acid (19.1%) and linoleic acid (15.3%), with three, one and two unsaturations, respectively [2]. In addition to foods and feeding applications, linseed oil offers very attractive industrial applications due to its high unsaturated fatty acid content. Among other uses, it has been reported the use of linseed oil and derivatives into paints, surface protection, cosmetic products and biodiesel generation [8–10].

Kinetic analysis of the curing process of biobased epoxy resin from epoxidized linseed oil by dynamic differential scanning calorimetry

Abstract

The curing process of epoxy resin based on epoxidized linseed oil (ELO) is studied using dynamic differential scanning calorimetry (DSC) in order to determine the kinetic triplet (E_a, $f(\alpha)$ and A) at different heating rates. The apparent activation energy, E_a, has been calculated by several differential and integral isoconversional methods, namely Kissinger, Friedman, Flynn-Wall-Ozawa (FWO), Kissinger-Akahira-Sunose (KAS) and Starink. All methods provide similar values of E_a (between 66 and 69 kJ/mol), and this shows independence versus the heating rate used. The epoxy resins crosslinking is characterized by a multi-step process. However, for the sake of the simplicity and to facilitate the understanding of the influence of the oxirane location on the curing kinetic, this can be assimilated to a single-step process. The reaction model has a high proportion of autocatalytic process, fulfilling that α_M is between 0 and α_p and $\alpha_M < \alpha_p^{\infty}$. Using as reference the model proposed by Šesták–Berggren, by obtaining two parameters (n and m) it is possible to obtain, on the one hand, the kinetic parameters and, on the other hand, a graphical comparison of the degree of conversion, α, versus temperature (T) at different heating rates with the average n and m values of this model. The good accuracy of the proposed model with regard to the actual values obtained by DSC gives consistency to the obtained parameters, thus suggesting the crosslinking of the ELO-based epoxy has apparent activation energies similar to other petroleum-derived epoxy resins.

Keywords: epoxidized linseed oil; kinetic analysis; biobased epoxy resin; flax

III.2.2.1. Introduction

Flax is one of the industrial crops that, thanks to its versatility, has been used since ancient times both in food and in clothes manufacturing for approximately 30,000 years [1]. Nowadays, flax derivatives are continuously gaining importance, due to the productive and economic nature of its sowing. For this reason, the largest producers of flax (Russia, China, Kazakhstan, Argentina and Canada) have increased their production capability [2,3]. In addition to the main uses related to flax crops, namely textile fibers and seeds for food industry, while new uses are being developed for other by-products or co-products linked to the flax industry. In the last decade, flax oil, biodiesel, and flax flour have found increasing applications in the market [4-6].

One of the most interesting by-product is flax oil (or linseed oil), which represents approximately 45 % of the seeds [3,7]. The main fatty acids are linolenic acid (56.6 %), oleic acid (19.1 %) and linoleic acid (15.3 %), with three, one and two unsaturations, respectively [2]. In addition to foods and feeding applications, linseed oil offers very attractive industrial applications due to its high unsaturated fatty acid content. Among other uses, it has been reported the use of linseed oil and derivatives into paints, surface protection, cosmetic products, and biodiesel generation [8-10].

By taking into account the high degree of unsaturated carbons contained in the main fatty acids, which represents about 73 %, its chemical modifications open a broad potential for industrial applications [11,12]. Some of the simplest and cost-effective modification processes are epoxidation and maleinization. Fombuena, *et al.* [13], reported the development of high renewable content green composites, with more than 78 wt % of flax-derived materials, namely biobased epoxidized linseed oil (ELO) as epoxy resin, maleinized linseed oil (MLO) as hardener and flax fibers as reinforcement. Carbonell-Verdu, *et al*. [14] and Liminana, *et al.* [15] reported the potential of MLO as compatibilizer between a natural reinforcement (almond shell flour) and a thermoplastic polyester such as poly (butylene succinate) (PBS); they showed improved polymer-particle interaction due to presence of MLO and somewhat plasticization effect provided by this maleinized-derivative from linseed oil.

As above-mentioned, one of the most common chemical modifications on unsaturated fatty acids is epoxidation. This increases the reactivity of the linseed oil since the oxirane rings are much more reactive than unmodified unsaturations in fatty acids [16,17]. Epoxidized linseed oil is commercially available and finds industrial applications as secondary plasticizer in poly (vinyl chloride) plastisols and partially biobased epoxy resins [18,19]. ELO-based epoxies can represent a sustainable solution to traditional

epoxy resins, generally derived from petroleum, which has a large impact on increasing the carbon footprint and can also be toxic to humans [20]. The epoxidation process takes advantage of the unsaturations contained in the fatty acids of linseed oil by converting them into oxirane rings [21]. Miyagawa, *et al*. [22] formulated a resin based on bisphenol F with the presence of ELO and an anhydride as hardener. The results showed lower thermomechanical and thermal properties at higher ELO content. Boquillon and Fringant [23] formulated anhydride cured ELO-based resins catalyzed with amines and imidazoles. In this case, the presence of imidazole catalyst improved the obtained results since it improved the crosslinking process with the subsequent improvement on mechanical performance.

This crosslinking process between an epoxy resin and the hardener provides an exothermic reaction, with an important release of heat that can contribute to increase the temperature, and subsequently, the possibility to provide an autocatalytic process. In previous works, the curing kinetics of a bisphenol A-based resin with a content of 31 % by weight of ELO was studied, and it was observed that the mechanical properties obtained were similar to those of a conventional petroleum-derived epoxy resin [24]. In the present work, the curing kinetics of an ELO-based epoxy resin crosslinked with a liquid anhydride is studied by differential scanning calorimetry (DSC) using non-isothermal runs. By means of differential and integral isoconversional models, the apparent activation energy, E_a, the reaction model, $f(\alpha)$ and the pre-exponential factor, A, are determined. The main aim of this work is to compare the kinetic triplet of the ELO-based epoxy resin with other petroleum-derived epoxies to assess the effect of non-terminal oxirane groups in ELO with regard to conventional epoxy resins with epoxy groups located in terminal and more readily available positions. Furthermore, through the comparison of the experimental functions $y(\alpha)$ and $z(\alpha)$, with standard master plots and the determination of the m and n parameters of Šesták-Berggren model ($SB(m,n)$), the influence of autocatalysis process and the accuracy of the kinetic triplet parameters are determined.

III.2.2.2. Experimental

Materials

Commercial epoxidized linseed oil was used as base epoxy resin to carry out a kinetic study. ELO was obtained from Traquisa S.L. (Barberá del Vallés, Barcelona, Spain). This biobased epoxy stands out for having a fatty acid composition of: Stearic acid (3-5 %), palmitic acid (5-7 %), linoleic acid (14-20 %), oleic acid (18-26 %) and

linolenic acid (51-56 %). It also presents an average molecular weight of 1.038 g/mol triglyceride, and a density of 1.05-1.06 g/cm^3 at 20 °C. The epoxy equivalent weight (EEW) of the ELO-based epoxy resin was 178 g/equiv. A liquid at room temperature cyclic anhydride, namely, methyl nadic anhydride (MNA), with an anhydride equivalent weight (AEW) of 178.18 g/equiv was employed. This anhydride-based hardener was employed due to epoxy/anhydride systems have higher glass transition and less shrinkage, interesting properties if the objective is the use of ELO resin in industrial applications [25]. The epoxy to anhydride ratio (EEW:AEW) was set to 1:1. The crosslinking system also consisted of 2 wt % of 1-methyl imidazole which acts as accelerator, and 0.8 wt. % glycerol that plays a key role as a catalyst/initiator. All these products were supplied by Sigma Aldrich (Sigma Aldrich, Madrid, Spain). To carry out the kinetic study, all the components of the crosslinking system were weighed on a balance with an accuracy of 0.01 grams and were mixed at room temperature and stirred vigorously until obtaining a homogeneous mixture [26]. The liquid nature of the MNA anhydride allows good mixing at room temperature thus avoiding precipitation and the starting of the crosslinking process.

Kinetic Study by Differential Scanning Calorimetry (DSC)

The kinetic analysis of the curing process was carried out by following the crosslinking enthalpy which allowed calculating the degree of advance (β). The evolution of the crosslinking enthalpy was obtained in a DSC Mettler-Toledo DSC 821e (Metler-Toledo S.A.E., Barcelona, Spain). After the corresponding mixing of all components and homogenization, a small drop of the liquid mixture containing between 10-12 mg was placed into a standard aluminum crucible (40 µL) following the recommendations of Vyazovkin, *et al.* [27]. Samples were sealed with a press and tested using a non-isothermal heating program from 20 °C up to 300 °C at different heating rates (10, 20, 30, 40 °C/min) and N_2 atmosphere with constant flow rate of 30 mL/min. Parameters such as the degree of curing, and the maximum curing rate (T_p) can be easily obtained applying this methodology [28].

Theoretical Background

Kinetic studies are based on the principle that the degree of conversion, α, can be obtained (using a non-isothermal heating) by the heat produced by the curing process with respect to time, divided by the total heat of curing of the resin as presented in Equation (III.2.2.1) [29]:

$$\alpha = \frac{\Delta H_t}{\Delta H_T} \quad \text{(III.2.2.1)}$$

Taking this into account, the conversion rate $\frac{d\alpha}{dt}$ can be expressed according to Equation (III.2.2.2):

$$\frac{d\alpha}{dt} = k(T) \cdot f(\alpha) \quad \text{(III.2.2.2)}$$

where $k(T)$ is the rate coefficient, depending on the reaction temperature and $f(\alpha)$ represents the reaction model. The Arrhenius equation (Equation (III.2.2.3)) expresses the dependence of the temperature:

$$k(T) = A \cdot e^{\frac{-E_a}{R\,T}} \cdot f(\alpha) \quad \text{(III.2.2.3)}$$

where E_a stands for the apparent activation energy, A represents the pre-exponential factor, R is the universal gas constant (8.314 J mol^{-1} K^{-1}) and T is the absolute temperature. Combining Equations (III.2.2.2) and (III.2.2.3), the general expression in the kinetic analysis of the curing resin is obtained Equation (III.2.2.4):

$$\frac{d\alpha}{dt} = A \cdot e^{\frac{-E_a}{R \cdot T}} \cdot f(\alpha) \quad \text{(III.2.2.4)}$$

The parameters E_a, $f(\alpha)$ and A are known as the kinetic triplet. The determination of this triplet is of huge importance to understand the kinetics of crosslinking process. The apparent activation energy (E_a) can be obtained through different methods, the accuracy of which depends on the fulfilment of approaches such as the type of transformation process being carried out, single or multi-step process. Due to its simplicity, Kissinger method is one of the most used [30]. The apparent activation energy (E_a) is evaluated based on the peak temperature (T_p) measurements at maximum curing rate, taking into account that Kissinger method is only valid for a one-step process [31]. The Kissinger method follows Equation (III.2.2.5):

$$ln\left(\frac{\beta}{T_p^2}\right) = ln\left(\frac{A \cdot R}{E_a}\right) - \frac{E_a}{R \cdot T_p} \quad \text{(III.2.2.5)}$$

By plotting $\ln\left(\frac{\beta}{T_p^2}\right)$ versus $\frac{1}{T_p}$, the apparent activation energy is obtained through the slope of the linear fit. As a main drawback, the Kissinger method only provides a single value of the E_a at the peak temperature and cannot follow the evolution of E_a with the conversion α. Despite this, several authors have tried to overcome this drawback, such as Farjas, *et al.* [32]. This method complements the maximum peak values with additional values such as the time corresponding to the full width at half maximum (Δt_{FWHM}), which is more sensitive to the existence of multiple processes.

An alternative to the Kissinger method is the isoconversional methods, which, together with their simplicity, provide an accurate estimation of the E_a. Vyazovkin, *et al.* [33], proposes different isoconversional methods, evaluating the E_a throughout the conversion process with the advantage of not having to assume a reaction model. Isoconversional methods can be differential or integral. The expressions of these methods, regardless of their type, can be obtained from Equation (III.2.2.4), applying the principle of isoconversion, results in Equation (III.2.2.6):

$$\left[\frac{\partial\ ln\left(\frac{d\alpha}{dt}\right)}{\partial \frac{1}{T}}\right]_{\alpha i} = -\frac{E_{a,\alpha i}}{R} \quad \text{(III.2.2.6)}$$

As above-mentioned, the adequate estimation of apparent activation energy (E_a) determines the accuracy of the kinetic study of the crosslinking process and here is where isoconversional integral methods play an important role. Based on integration of Equation (III.2.2.4), the resulting expression is observed in Equation (III.2.2.7):

$$\int_0^{\alpha} \frac{d\alpha}{f(\alpha)} = A \cdot \int_0^{t} e^{\frac{-E_a}{R \cdot T}}\, dt \quad \text{(III.2.2.7)}$$

As an example of differential isoconversional method, the Friedman method [34], takes natural logarithms. Rearranging terms for Equation (III.2.2.8), this method assumes that the reaction model stays constant throughout the full conversion process. The advantage of this method is that does not make approaches but provides valuable information of the actual crosslinking process [35].

$$ln\left(\beta \cdot \frac{d\alpha}{dT}\right) = ln[A \cdot f(\alpha)] - \frac{E_a}{R \cdot T_\alpha} \quad \text{(III.2.2.8)}$$

Different isoconversional integral methods with different accuracies on the E_a estimation have been developed by some authors. The accuracy of these methods depends on the numerical approximation obtained by solving the temperature-dependent integral term of the Arrhenius constant (temperature integral). Among others, the usefulness of the Flynn-Wall-Ozawa (FWO) Equation (III.2.2.9) [36,37], Kissinger-Akahira-Sunose (KAS) Equation (III.2.2.10) [38] or Starink methods Equation (III.2.2.11) [39] should be noted. This last method (Starink method), playing with the optimization of the mathematical parameters obtain a slope of $-1.008 \cdot \frac{E_a}{R \cdot T_\alpha}$ when $\ln\left(\frac{\beta}{T_\alpha^{1.92}}\right)$ is plotted versus $\frac{1}{T_\alpha}$, while FWO and KAS methods provide a slope of −1.000 and −1.052, respectively. The mathematical approximation done by Starink method has demonstrated higher accuracy than FWO and KAS methods.

$$ln(\beta) = C - 1.052 \cdot \frac{E_a}{R \cdot T_\alpha} \quad \text{(III.2.2.9)}$$

$$ln\left(\frac{\beta}{T_\alpha^2}\right) = C - 1.000 \cdot \frac{E_a}{R \cdot T_\alpha} \quad \text{(III.2.2.10)}$$

$$ln\left(\frac{\beta}{T_\alpha^{1.92}}\right) = C - 1.008 \cdot \frac{E_a}{R \cdot T_\alpha} \quad \text{(III.2.2.11)}$$

On the other hand, Vyazovkin, *et al.* [33], with the aim of reducing, as far as possible, the deviation of E_a, recommends that the values of the conversion degree should be taken from α = 0.05 to α = 0.95 by increasing steps of 0.05. In this way, expanding the analysis range, the accuracy of the estimation of E_a is increased. Malek [40], proposes a method by determining the reaction model calculating two functions $y(\alpha)$ and $z(\alpha)$, defined as shown in Equations (III.2.2.12) and (III.2.2.13):

$$y(\alpha) = \frac{d\alpha}{dt} \cdot e^x = A \cdot f(\alpha) \quad \text{(III.2.2.12)}$$

$$z(\alpha) = \pi(x) \cdot \left(\frac{d\alpha}{dt}\right) \cdot \frac{T}{\beta} \quad \text{(III.2.2.13)}$$

Looking for similarities between the FWO method Equation (III.2.2.9) and the method proposed by Malek, the term *x* is equivalent to $\frac{E_a}{R \cdot T_\alpha}$, and *A* to $f(\alpha)$, that represents the function reaction model, during the crosslinking process. Regarding the $z(\alpha)$, it is determined by the expression of the temperature integral $\pi(x)$, which can be obtained using the 4th rational expression proposed by Senum and Yang [41]. On the other hand, Flynn [42], suggested a correction in the expression as it is shown in Equation (III.2.2.14), that has been obtained from experimental data:

$$\pi(x) = \frac{x^3 + 18x^2 + 86x + 96}{x^4 + 20x^3 + 120x^2 + 240x + 120} \quad \text{(III.2.2.14)}$$

Table III.2.2.1 summarizes several kinetic models with expressions of their characteristic function $f(\alpha)$, whose representation of the selected reaction model determines the accuracy of the linear fit to obtain E_a.

Table III.2.2.1. Summary of algebraic expression for reaction model $f(\alpha)$.

Reaction Model	Code	$f(\alpha)$	
2D-Ractieon	R2	$(\mathbf{1}-\boldsymbol{\alpha})^{1/2}$	(III.2.2.15)
2D-Diffusion	D2	$\frac{\mathbf{1}}{-\mathbf{ln}(\mathbf{1}-\boldsymbol{\alpha})}$	(III.2.2.16)
Johnson-Mehl-Avrami	JMA(n)	$\boldsymbol{n}(\mathbf{1}-\boldsymbol{\alpha})\cdot[-\mathbf{ln}(\mathbf{1}-\boldsymbol{\alpha})]^{1-1/n}$	(III.2.2.17)
Jander	D3	$\frac{\mathbf{3/2}\cdot(\mathbf{1}-\boldsymbol{\alpha})^{2/3}}{[\mathbf{1}-(\mathbf{1}-\boldsymbol{\alpha})]^{2/3}}$	(III.2.2.18)

The success of a correct kinetic model that accurately predicts the complex mechanism of curing of vegetal oil resins derives from several factors, among the main ones the use of appropriate methods for the determination of the kinetic triplet as well as the correct data collection. In the current literature, several articles related to the kinetic study of different vegetable oils can be found. Due to the similarity in the number and position of epoxide groups, the studies carried out on soybean oil are noteworthy [43-46]. Regarding epoxidized linseed oil, studies with the use of photocrosslinkers have been carried out for the use of ELO as a coating for wood [47]. Kinetic studies have been done which carried out by means of crosslinking with acid hardeners, supporting the use of isoconversional methods for the determination of the kinetic parameters [48]. In this

study, catalysts and accelerators are not employed restricting the extrapolation of the results to industrial scale, where these elements are key in process acceleration and scale-up. In another example, Lascano et al. in a previous study, determined the accuracy of different isoconversional methods by comparing different methods, but in this case, applied to a resin based on diglycidyl ether of bisphenol A (DGEBA) cross-linked with amine hardener [24]. On the other hand, in a study by Mahendran et al. different isoconversional methods such as Friedman (FR), KAS and Vyazovkin (VA) were studied on an ELO resin cross-linked with ahnidrides [49], but in contrast to the present article, the study of the possible autocatalytic contribution in the cross-linking process, using the Šesták-Berggren methodology, has not been carried out. In view of the above-mentioned aspects, the present article performs a thorough comparison of the different isoconversional methods in order to determine their adequacy for an ELO-based epoxy resin crosslinked with anhydrides. In addition, the possible autocatalytic contribution in the crosslinking process is studied, as well as the possible influence of the location of the different epoxy groups in the determination of these parameters.

III.2.2.3. Results and Discussion

Dynamic differential scanning calorimetry was employed to analyze the curing kinetics of the epoxy resin based on epoxidized linseed oil. Samples were subjected to a single step heating cycle, obtaining the total enthalpy released (ΔH_T) during the crosslinking process. Figure III.2.2.1 shows the DSC plot representation of the curing process of epoxy resin based on epoxidized linseed oil at different heating rates (10, 20, 30 and 40 °C/min). The temperature for the maximum curing rate or peak temperature (T_p), was determined analyzing the peak during the heating cycle

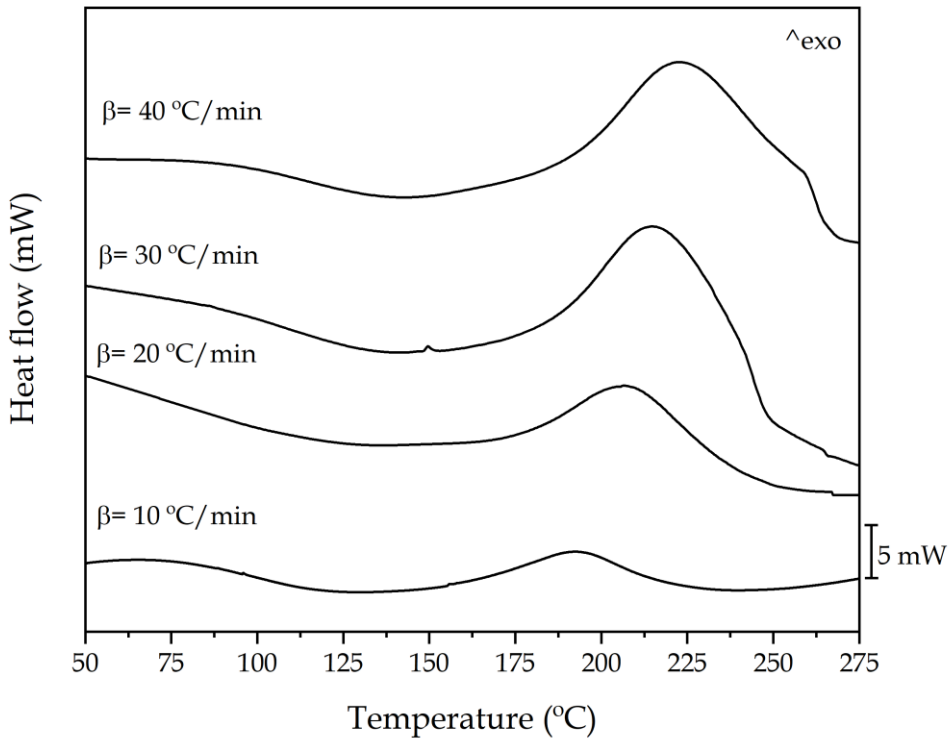

Figure III.2.2.1. Differential scanning calorimetry (DSC) thermal curves of epoxidized linseed oil (ELO)-methyl nadic anhydride (MNA) system at various heating rates, showing the exothermicity of the crosslinking process.

DSC results are summarized in table III.2.2.2. A clear increasing tendency can be observed for the temperature peak for the maximum curing rate (T_p). This changes from 192.8 °C using a heating rate (β) of 10 °C/min, and exceeds 223 °C for the highest heating rate in this study (40 °C/min). The acceleration of the crosslinking reaction, increasing β, gives rise to a three-dimensional crosslinked net structure which is responsible for reducing chain mobility and, subsequently, hindering the free diffusion, this having an effect on both temperature for the maximum rate (T_p) and the total released enthalpy (ΔH_T), as some authors as Carbonell-Verdu, *et al.* [50] and Rocks, *et al.* [51]. On the other hand, the glass transition temperature (T_g) can vary depending on the heating rate and the post-curing process. Using a dynamic-mechanical thermal analysis (DMTA), Samper, *et al.* [52] demonstrated a glass transition temperature (T_g) of the cured ELO-MNA system without post-curing process close to 127 °C, with a heating rate of 5 °C/min. Therefore, knowing that higher heating rates can cause an increase in T_g, it is expected that these values are higher than the 127 °C obtained in the study by Samper et al., and lower than the 148 °C obtained when a post-cure of 2 h at 160 °C is applied.

Table III.2.2.2. Main data obtained from dynamic DSC runs of ELO/MNA epoxy system at different heating rates.

β (°C·min^{-1})	Curing Cycle	
	T_p (°C)	ΔH_T (J·g^{-1})
10	192.80	140.72
20	206.70	146.07
30	216.17	198.51
40	223.32	215.77

Figure III.2.2.2a shows the plot representation of conversion (α) versus absolute temperature (T). It is important to remark that as the heating rate increased, the sigmoidal curves are displaced to higher temperature. As the geometric shape and the distance between curves are almost the same, it is possible to suggest that the heating rate (β) does not affect the reaction model $f(\alpha)$ even though the crosslinking process of an epoxy resin is not a simple process. Figure III.2.2.2b shows the plot representation of the curing rate $\left(\frac{d\alpha}{dT}\right)$ as a function of the conversion (α). Once again, it can be seen how increasing the heating rate (β) from 10 to 40 °C/min, the shape of the curve remains almost invariable, thus suggesting the same reaction model $f(\alpha)$ for the entire range studied. It is worthy to note that the curing or crosslinking process of an epoxy resin is not a typical single-step reaction. It consists of several overlapped processes related with the studies initiated by authors such as Fischer and Tanaka and Kakiuchi in the 1960s [53-55]. Multiple reactions occur at the same time, related with the presence of a proton donor, which can start the reaction with the epoxy groups, and the anhydride-based hardener [56]. Nevertheless, the overall process, as shown in figure III.2.2.1, can be assimilated to a single-step process for the sake of simplicity and comparison with kinetic parameters of other petroleum-derived epoxy resins and assess the effect of the oxirane location on the curing kinetics.

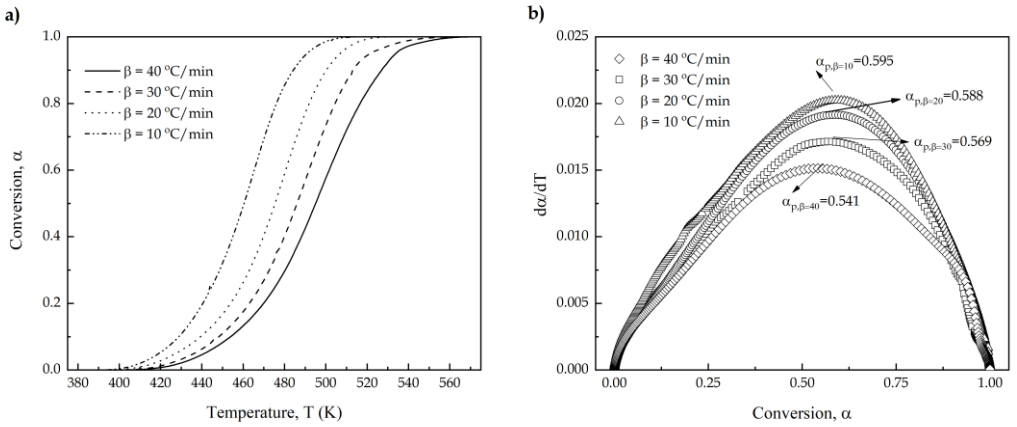

Figure III.2.2.2. (**a**) the extent of conversion (α) and (**b**) the curing rate of an ELO/MNA epoxy system at different heating rates of ELO/MNA epoxy system.

Within the goal to determinate the kinetic triplet (E_a, $f(\alpha)$ and A), the apparent activation energy is one of the most important parameters. Kissinger method is one of the simplest methods Equation (III.2.2.5**)**, since it can be used independently of the transformation process, in this case, a curing process. Despite this, this method assumes a single-step process and, as above-mentioned, the crosslinking process of an epoxy resin is a multi-step process, as such the Kissinger method gives an initial approximation of the kinetic parameters. As above-mentioned, the accuracy of these methods depends on the type of reaction that is taking place, being the accuracy enhanced if the reaction occurs in a single step for the different heating rates (β). For this reason, the conversion at the maximum reaction rate α_p, must be very similar, independently of the heating rate (β) used. In the previous figure III.2.2.2b α_p is shown in the highest point of the plot representation. These values are giving as average value of α_p, 0.5733 ± 0.02 with values very similar to the different heating rates used and values reported by literature [24,57].

Using the Kissinger method, figure III.2.2.3a represents the linear fitting, whose slope correspond to the E_a. In this case the value obtained is 70.07 ± 0.066 kJ/mol, which is a typical value consistent with the literature data of epoxy resin (E_a = 70 kJ/mol) [57]. As above-mentioned, one of the main drawbacks of the Kissinger method is the analysis of one-step reaction model using only one point equivalent to maximum reaction temperature [58]. For this reason, following the approach suggested by Farjas, *et al.* [32], the variation of ln Δt_{FWHM} versus $1/(T_p)$ has been plotted in figure III.2.2.3b. In the case to obtain values of E_a very similar to Kissinger method it would indicate that the reaction is indeed carried out in one-step. The slope obtained after linear fitting is 69.12 ± 0.039

kJ/mol being practically the same, which corroborates the correct approximation done with the use of Kissinger method.

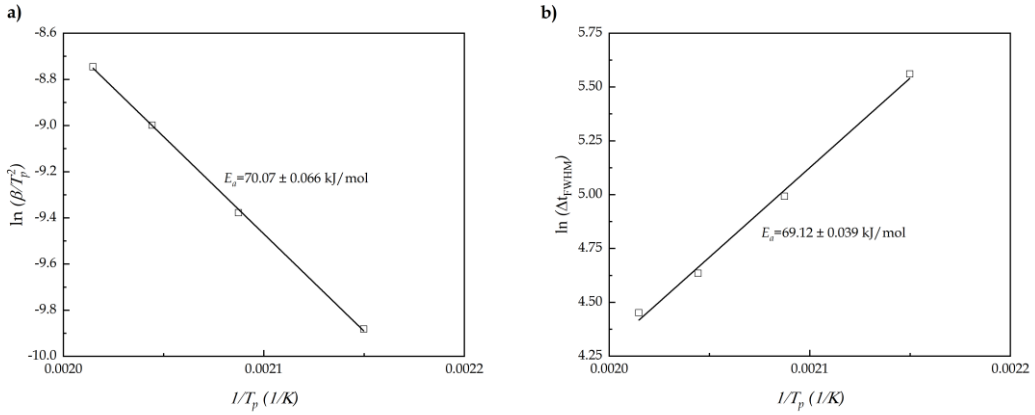

Figure III.2.2.3. Experimental plot corresponding to (**a**) the Kissinger method and (**b**) Δt_{FWHM} against $1/(T_p)$ of an ELO/MNA epoxy system at different heating rates.

Notwithstanding the ease of application of the Kissinger method, it does not fail to give a single value for E_a. Thus, to evaluate possible change of E_a with the conversion, the use of isoconversional methods (both differential and integral methods) is needed. Results obtained by Friedman, FWO, KAS and Starink methods are gathered in table III.2.2.3. In The first approach done by Friedman method (differential method), the apparent energy is determined from the slope of the plot $\ln\left(\frac{d\alpha}{dT}\right)$ vs T^{-1} for various degree of conversion. Taking into account the use of a linear heating rate ($\beta = dT/dt$) and solving the resulting integration, the temperature integral does not provide an exact analytical solution. For this reason, the value of E_a obtained (66.83 ± 2.7 kJ/mol) it is considered to be less accurate than other isoconversional methods differing in their approximations. For example, FWO method, by Doyle's approximation [37,59] and KAS method through the approximation done by Murray and White leads accurate approximation [60,61]. Finally, the Starink method uses a more accurate approximation of the temperature integral (figure III.2.2.4) and, consequently, E_a obtained is 68.57 ± 4.38 kJ/mol with r values of -0.992. For all the aforementioned methods, E_a ranges from 66 to 69 kJ/mol, which is in total accordance with most epoxy systems reported by the literature and showing how the use of epoxidized linseed oil as biobased epoxy resin does not affect the conversion (α) of the curing process and a single-step analysis is a valid approximation.

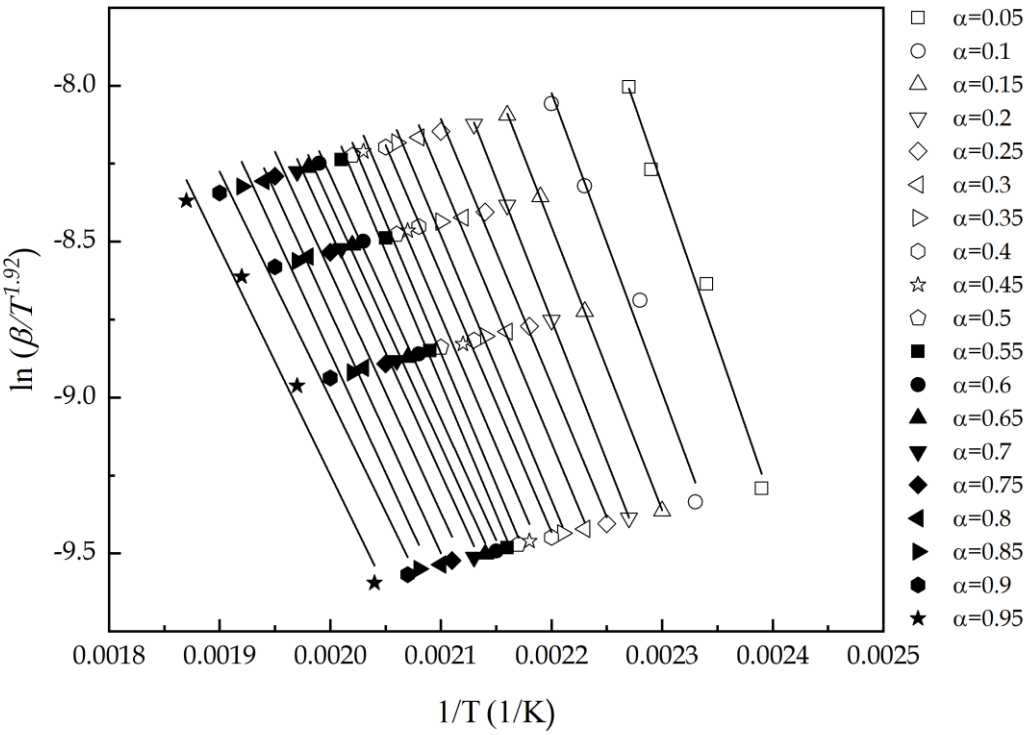

Figure III.2.2.4. Plot corresponding to Starink method during all the extent of conversion of an ELO/MNA epoxy system at different heating rates.

Table III.2.2.3. Apparent activation energy values obtained by isoconversional methods of an ELO/MNA epoxy system at different heating rates

Isoconversional Method	**Apparent Activation Energy, E_a (kJ/mol)**
Friedman	66.83 ± 2.70
Flynn–Wall–Ozawa (FWO)	66.27 ± 3.56
Kissinger–Akahira–Sunose (KAS)	66.22 ± 2.62
Starink	68.57 ± 4.38

The wide evaluation range (α = 0.05 – α = 0.95) of E_a, provides a high accuracy, although this is only the first approach, since the accuracy of the kinetic analysis depends on other parameters of the kinetic triplet, such as reaction model $f(\alpha)$ and pre-exponential factor, A. As summarized in Equations (III.2.2.12) and (III.2.2.13), Malek proposed a method to determine these two parameters by calculating the functions $y(\alpha)$ and $z(\alpha)$ by graphical methods related to the thermally activated process [62]. Figure

III.2.2.5 shows the plot of $y(\alpha)$ versus the conversion $f(\alpha)$ at different heating rates. The maximum value of $y(\alpha)$, denoted as α_M, has been highlighted in the graphic representation. In this case, regardless of the analyzed heating rate, all values obtained are higher than 0 (values listed in table III.2.2.4). Due to the values obtained between 0.04 and 0.1 and the geometry of the curves, an autocatalytic reaction model with a high proportion of the autocatalytic process is suggested [63,64]. To fulfil this premise, one of the conditions is that value of α_M is between 0 and α_p (condition clearly fulfilled) and that the maximum of the $z(\alpha)$ function obtained at different heating rates, denoted as α_p^{∞} is higher than α_M. Figure III.2.2.6 shows $z(\alpha)$ plot of experimental data as a function of the degree of conversion by Equation (III.2.2.13), and values of α_p^{∞} are summarized in table III.2.2.4.

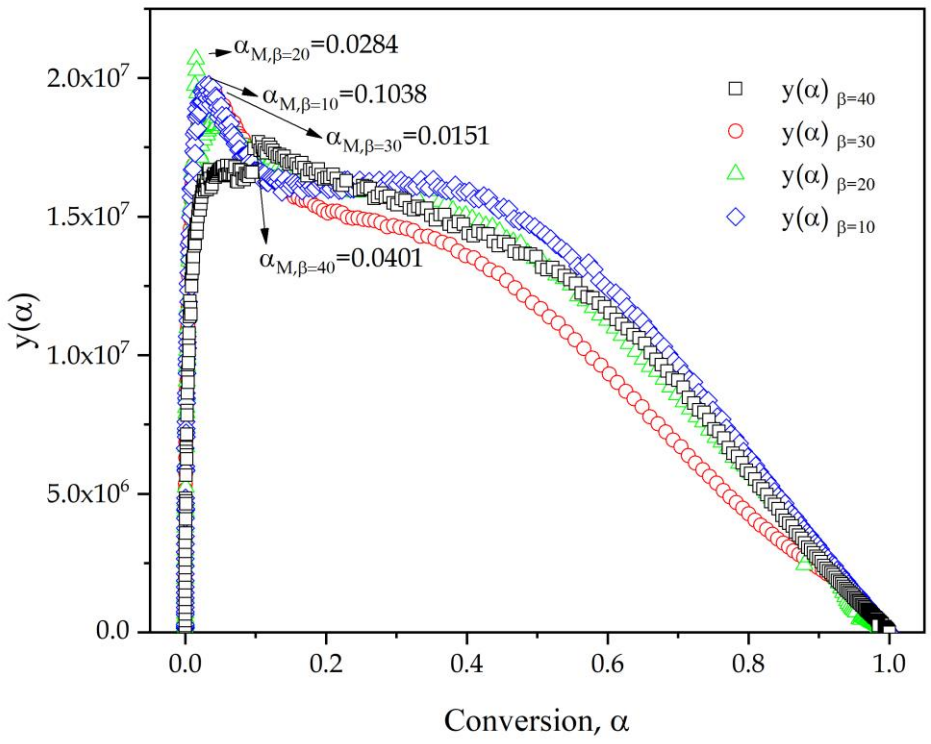

Figure III.2.2.5. $y(\alpha)$ plot of experimental data as a function of the extent of conversion of an ELO/MNA epoxy system at different heating rates.

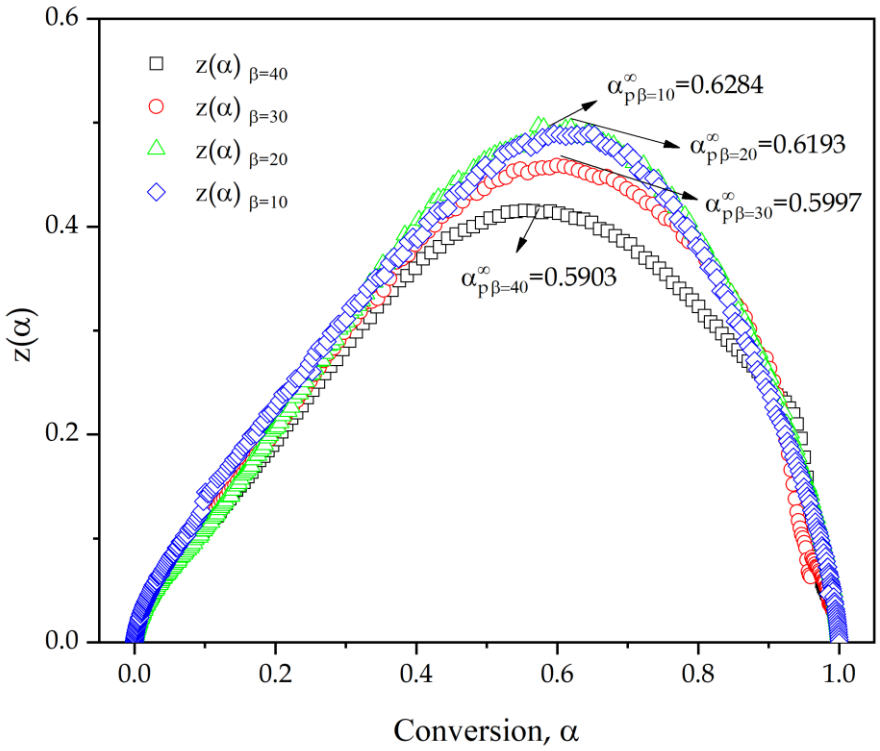

Figure III.2.2.6. $z(\alpha)$ plot of experimental data as a function of the extent of conversion of an ELO/MNA epoxy system at different heating rates.

Table III.2.2.4. Maximum values obtained from $d(\alpha)/dT$, $y(\alpha)$ and $z(\alpha)$ function of an ELO/MNA epoxy system at different heating rates.

β (°C/min)	α_p	α_M	α_p^{∞}
10	0.595	0.1038	0.6284
20	0.588	0.0284	0.6193
30	0.569	0.0151	0.5997
40	0.541	0.0401	0.5903

Once again, regardless of the heating rate used, $\alpha_M < \alpha_p^{\infty}$; therefore, the second condition is accomplished to determine that the kinetic process is autocatalytic. Analyzing the evolution of α_M as a function of the heating rate, it is possible to observe a decreasing relationship, with higher values of α_M (0.1038) for a lower heating rate (10 °C/min), indicating that the autocatalytic effect is greater at lower heating rates. This statement agrees with what was found by Lascano, *et al.* [24] in previous studies, where it is stated that the autocatalytic effect is more intense with higher α_M values. Furthermore, as can be seen in figure III.2.2.6, the experimental comparison of $z(\alpha)$ with

some generalized master plots [65], shows, according to the particular geometry, a consistent model with a large contribution of the autocatalytic effect.

Thereupon, it is possible to use an autocatalytic reaction model by determining the parameters (*n* and *m*) characteristic of the Šesták–Berggren model (*SB*(*m*,*n*)) as recommended by Malek in the case, accomplished in the actual ELO/MNA system cured at different heating rates, which $\alpha_p^\infty \neq 0.632$ and $\alpha_M \in (0, \alpha_p)$ [40]. This reaction model is governed by Equation (III.2.2.19), when *n* is the *n*th reaction order and the exponent *m* represents the autocatalytic effect, indicating that the conversion rates are directly related to the reacted (crosslinked) material α:

$$f(\alpha) = \alpha^m \cdot (1-\alpha)^n \tag{III.2.2.19}$$

Replacing the function in Equation (III.2.2.4), the following expression is obtained Equation (III.2.2.20):

$$\frac{d\alpha}{dt} = A \cdot e^{\frac{-E_a}{R \cdot T}} \cdot \alpha^m \cdot (1-\alpha)^n \tag{III.2.2.20}$$

Some authors, like Criado, *et al.* [66] and Málek [40] describe linear iterations to obtain the mentioned *m* and *n* parameters. While other authors like Krishnaswamy, *et al.* [67] and El-Thaher, *et al.* [68] use non-linear curve fitting to obtain *m* and *n* parameters and the pre-exponential factor, *A* by applying natural logarithms, Equation (III.2.2.21):

$$ln\left(\beta \cdot \frac{d\alpha}{dT}\right) + \frac{E_a}{R \cdot T} = ln(A) + m \cdot ln(\alpha) + n \cdot ln(1-\alpha) \tag{III.2.2.21}$$

The values of ln(*A*), *n* and *m* parameters obtained after non-linear curve fitting are summarized in table 5. Average value of ln(*A*) is 16.924 ± 0.087, and *m* and *n* 0.107 ± 0.065 and 0.973 ± 0.041, respectively, so determination of the kinetic triplet has been carried out. Finally, in order to corroborate the fit of the theoretical model, figure III.2.2.7 shows the comparison between the values obtained using the proposed model and the experimental data, represented by symbols. Due to the overlap concordance in both representations, it is possible to state that the kinetic triplet obtained has a good accuracy compared with the experimental data, regardless of the heating rate used.

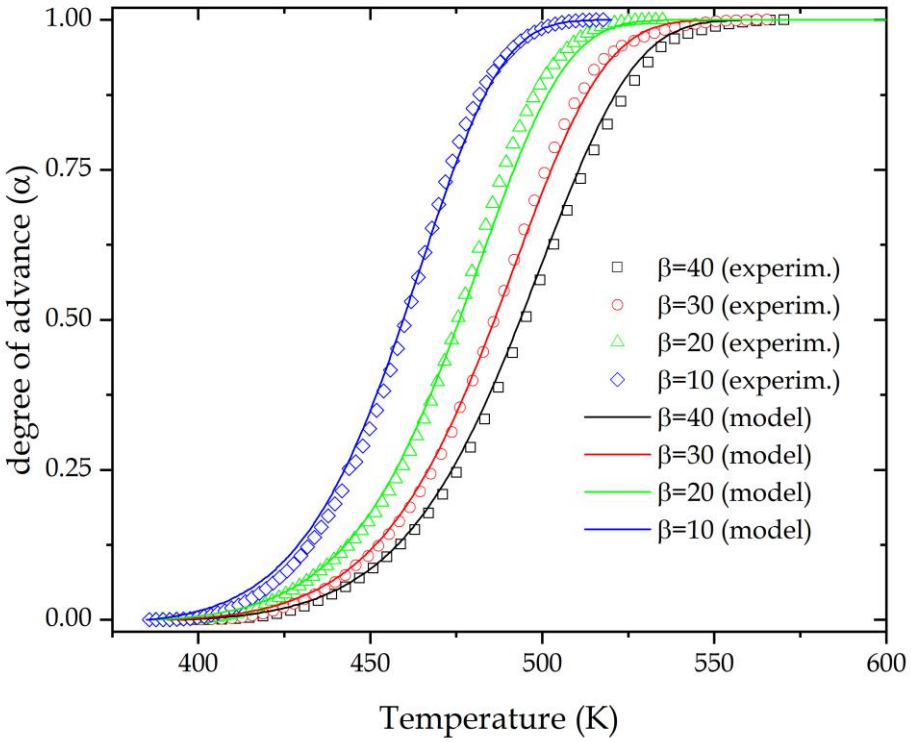

Figure III.2.2.7. Theoretical and experimental comparison of the extent of conversion of an ELO/MNA epoxy system at different heating rates.

Table III.2.2.5. Calculated *SB*(*m*,*n*) parameters by nonlinear fit of a ELO/MNA epoxy system at different heating rates.

β (°C/min)	ln(*A*)	*m*	*n*
10	17.015 ± 0.011	0.185 ± 0.041	1.011 ± 0.007
20	16.939 ± 0.018	0.127 ± 0.006	0.916 ± 0.011
30	16.939 ± 0.019	0.0283 ± 0.006	0.975 ± 0.013
40	16.805 ± 0.019	0.089 ± 0.006	0.993 ± 0.013
Average Value	16.924 ± 0.087	0.107 ± 0.065	0.973 ± 0.041

III.2.2.4. Conclusions

The curing kinetics of bio-based epoxy resin from epoxidized linseed oil has been broadly analyzed using dynamic DSC at four different heating rates (10, 20, 30 and 40 °C/min). The apparent activation energy (E_a), one of the main kinetic parameters, was determined using differential and integral isoconversional models, giving results with low dispersion [66-69 kJ/mol] and independently of the conversion rate α.

The analysis of the highest point in the graphical representation of parameters $y(\alpha)$ and $z(\alpha)$ versus conversion, α, allowed obtaining the parameters

denoted α_M and α_p^∞, which fulfill two conditions (1: α_M is between 0 and α_p and 2: $\alpha_M < \alpha_p^\infty$). The higher value of α_M (0.1038), indicates that the autocatalytic effect is greater at low heating rates (10 °C/min). The reaction model, $f(\alpha)$ and the pre-exponential factor, *A*, were obtained through the Šesták-Berggren parameters (*SB*(*m,n*)). Theoretical curves plotted applying the values of kinetic triplet obtained show a great concordance with the experimental data, confirming the accuracy of the parameters obtained for an epoxy resin based on ELO. This widens the use of flax crops as linseed oil can be converted into a biobased epoxy resin with similar curing/crosslinking parameters to those of petroleum-derived epoxy resins.

III.2.2.5. Acknowledgments

D.L. thanks UPV for the grant received through the PAID-01-18 program.

III.2.2.6. References

1. K. Charlet, J. Jernot, S. Eve, M. Gomina, J. Bréard. Multi-scale morphological characterisation of flax: From the stem to the fibrils. *Carbohydrate Polymers* **2010**, *82*, 54-61.
2. S. Cloutier. Linseed. *Reference Module in Food Sciences* **2016**, 6.
3. A. Gruia, D.-G. Dumbravă, C. Moldovan, D.-M. Bordean. Fatty acids composition and oil characteristics of linseed (Linum Usitatissimum L.) from Romania. *Journal of Agroalimentary Processes and Technologies* **2012**, *18*, 136-140.
4. S. Dixit, S. kanakraj, A. Rehman. Linseed oil as a potential resource for bio-diesel: A review. *Renewable and Sustainable Energy Reviews* **2012**, *16*, 4415-4421.
5. F.I.G.d.R. Concenço, R.N.d.L. Gonzales, M. Vizzotto, L. Nora. Manufacturing and sensorial acceptance of cereal bars enriched with flaxseed (Linum usitatissimum) flour. *Journal of Food Research* **2019**, *8*, 1-11.
6. A. Uyumaz. Experimental evaluation of linseed oil biodiesel/diesel fuel blends on combustion, performance and emission characteristics in a DI diesel engine. *Fuel* **2020**, *267*, 117150.
7. Y. Wang, D. Li, L.-J. Wang, Y.L. Chiu, X.D. Chen, Z.-H. Mao, C.-F. Song. Optimization of extrusion of flaxseeds for in vitro protein digestibility analysis using response surface methodology. *Journal of Food Engineering* **2008**, *85*, 59-64.
8. N. Sanyaolu, A. Awosanya, O. Sonde, F. Kareem, S. Yussuf, F. Akinwunmi, A. Ibikunle. Comparative evaluation of the alkyd resins of the composite oils of soybean (Ricinus communis) and castor (Glycine max) seed oils with castor seed oil for alkyd paint formulation. *Journal of Chemical Society of Nigeria* **2019**, *44*.
9. S. Copaci, Ş. Jurcoane. Researches conserning the use of camelina oil in the composition of cosmetic products. 173-177.
10. N.I. Guzman Barrera. Eco-compatible syntheses of bio-based solvents for the paint and coating industry. 2018.
11. X. Pan, P. Sengupta, D.C. Webster. High biobased content epoxy-anhydride thermosets from epoxidized sucrose esters of Fatty acids. *Biomacromolecules* **2011**, *12*, 2416-2428.
12. A. Vereshchagin, G.V. Novitskaya. The triglyceride composition of linseed oil. *Journal of the American Oil Chemists Society* **1965**, *42*, 970-974.

13. V. Fombuena, R. Petrucci, F. Dominici, A. Jorda-Vilaplana, N. Montanes, L. Torre. Maleinized linseed oil as epoxy resin hardener for composites with high bio content obtained from linen byproducts. *Polymers (Basel)* **2019**, *11*, 301.

14. A. Carbonell-Verdu, D. Garcia-Garcia, F. Dominici, L. Torre, L. Sanchez-Nacher, R. Balart. PLA films with improved flexibility properties by using maleinized cottonseed oil. *European Polymer Journal* **2017**, *91*, 248-259.

15. P. Liminana, D. Garcia-Sanoguera, L. Quiles-Carrillo, R. Balart, N. Montanes. Optimization of maleinized linseed oil loading as a biobased compatibilizer in poly(butylene succinate) composites with almond shell flour. *Materials (Basel)* **2019**, *12*, 685.

16. V. Fombuena, S. MD. Study of the properties of thermoset materials derived from epoxidized soybean oil and protein fillers. *Journal of the American Oil Chemists' Society* **2013**, *90*, 449-457.

17. L. Quiles-Carrillo, S. Duart, N. Montanes, S. Torres-Giner, R. Balart. Enhancement of the mechanical and thermal properties of injection-molded polylactide parts by the addition of acrylated epoxidized soybean oil. *Materials & Design* **2018**, *140*, 54-63.

18. C. Musa, A. Kervoëlen, P.-E. Danjou, A. Bourmaud, F. Delattre. Bio-based unidirectional composite made of flax fibre and isosorbide-based epoxy resin. *Materials Letters* **2020**, *258*, 126818.

19. J.P. Espinosa, V. Hanazumi, P.M. Stefani, R.A. Ruseckaite. Curing behavior and properties of high biosourced epoxy resin blends based on a triepoxy monomer and a tricarboxylic acid hardener from 10-undecenoic acid. *Polymer Testing* **2020**, *81*, 106208.

20. V.G.O. Falcão, D. de Carvalho Carneiro, S.A. Pereira, M.R.D. da Silva, A.A. Candé, S.T. da Cunha Lima. Analyzing the toxicity of bisphenol-A to microalgae for ecotoxicological applications. *Environmental Monitoring and Assessment* **2020**, *192*, 8.

21. M.R. Janković, O.M. Govedarica, S.V. Sinadinović-Fišer. The epoxidation of linseed oil with in situ formed peracetic acid: A model with included influence of the oil fatty acid composition. *Industrial Crops and Products* **2020**, *143*, 111881.

22. H. Miyagawa, A.K. Mohanty, M. Misra, L.T. Drzal. Thermo-physical and impact properties of epoxy containing epoxidized linseed oil, 1. *Macromolecular Materials and Engineering* **2004**, *289*, 629-635.

23. N. Boquillon, C. Fringant. Polymer networks derived from curing of epoxidised linseed oil: influence of different catalysts and anhydride hardeners. *Polymer* **2000**, *41*, 8603-8613.

24. D. Lascano, L. Quiles-Carrillo, R. Balart, T. Boronat, N. Montanes. Kinetic analysis of the curing of a partially biobased epoxy resin using dynamic differential scanning calorimetry. *Polymers* **2019**, *11*, 391.

25. J.M. Pin, N. Sbirrazzuoli, A. Mija. From epoxidized linseed oil to bioresin: an overall approach of epoxy/anhydride cross-linking. *ChemSusChem* **2015**, *8*, 1232-1243.

26. D. Roşu, C. Caşcaval, F. Mustată, C. Ciobanu. Cure kinetics of epoxy resins studied by non-isothermal DSC data. *Thermochimica Acta* **2002**, *383*, 119-127.

27. S. Vyazovkin, K. Chrissafis, M.L. Di Lorenzo, N. Koga, M. Pijolat, B. Roduit, N. Sbirrazzuoli, J.J. Suñol. ICTAC Kinetics Committee recommendations for collecting experimental thermal analysis data for kinetic computations. *Thermochimica Acta* **2014**, *590*, 1-23.

28. C. Yi, P. Rostron, N. Vahdati, E. Gunister, A. Alfantazi. Curing kinetics and mechanical properties of epoxy based coatings: The influence of added solvent. *Progress in Organic Coatings* **2018**, *124*, 165-174.

29. J. Wan, C. Li, Z.-Y. Bu, C.-J. Xu, B.-G. Li, H. Fan. A comparative study of epoxy resin cured with a linear diamine and a branched polyamine. *Chemical engineering journal* **2012**, *188*, 160-172.

30. H.E. Kissinger. Variation of peak temperature with hedting rote in differentidl thermal analysis. *Journal of research of the National Bureau of Standards* **1956**, *57*, 217.

31. P. Budrugeac, E. Segal. Applicability of the Kissinger equation in thermal analysis. *Journal of thermal analysis and calorimetry* **2007**, *88*, 703-707.

32. J. Farjas, N. Butchosa, P. Roura. A simple kinetic method for the determination of the reaction model from non-isothermal experiments. *Journal of thermal analysis and calorimetry* **2010**, *102*, 615-625.

33. S. Vyazovkin, A.K. Burnham, J.M. Criado, L.A. Pérez-Maqueda, C. Popescu, N. Sbirrazzuoli. ICTAC Kinetics Committee recommendations for performing kinetic computations on thermal analysis data. *Thermochimica Acta* **2011**, *520*, 1-19.

34. H.L. Friedman. Kinetics of thermal degradation of char-forming plastics from thermogravimetry. Application to a phenolic plastic. In Proceedings of Journal of polymer science part C: polymer symposia; 183-195.

35. N. Sbirrazzuoli. Advanced isoconversional kinetic analysis for the elucidation of complex reaction mechanisms: A new method for the identification of rate-limiting steps. *Molecules* **2019**, *24*, 1683.

36. C. Doyle. Estimating isothermal life from thermogravimetric data. *Journal of Applied Polymer Science* **1962**, *6*, 639-642.

37. T. Ozawa. A new method of analyzing thermogravimetric data. *Bulletin of the chemical society of Japan* **1965**, *38*, 1881-1886.

38. T. Akahira, T. Sunose. Transactions of joint convention of four electrical institutes. **1969**, 246-246.

39. M. Starink. Analysis of hydrogen desorption from linear heating experiments: Accuracy of activation energy determinations. *International Journal of Hydrogen Energy* **2018**, *43*, 6632-6641.

40. J. Málek. The kinetic analysis of non-isothermal data. *Thermochimica acta* **1992**, *200*, 257-269.

41. G.I. Senum, R.T. Yang. Rational approximations of the integral of the Arrhenius function. *Journal of Thermal Analysis* **1977**, *11*, 445-447.

42. J.H. Flynn. The 'temperature integral'—its use and abuse. *Thermochimica Acta* **1997**, *300*, 83-92.

43. A. Ručigaj, B. Alič, M. Krajnc, U. Šebenik. Investigation of cure kinetics in a system with reactant evaporation: Epoxidized soybean oil and maleic anhydride case study. *European polymer journal* **2014**, *52*, 105-116.

44. E. Santacesaria, R. Turco, V. Russo, M. Di Serio, R. Tesser. Kinetics of soybean oil epoxidation in a semibatch reactor. *Industrial & Engineering Chemistry Research* **2020**, *59*, 21700-21711.

45. E. Santacesaria, R. Turco, V. Russo, R. Tesser, M. Di Serio. Soybean oil epoxidation: Kinetics of the epoxide ring opening reactions. *Processes* **2020**, *8*, 1134.

46. S. Tan, Z. Ahmad, W. Chow. Relationships of cure kinetics and processing for epoxidized soybean oil bio-thermoset. *Industrial Crops and Products* **2013**, *43*, 378-385.

47. G. Wuzella, A.R. Mahendran, U. Müller, A. Kandelbauer, A. Teischinger. Photocrosslinking of an acrylated epoxidized linseed oil: kinetics and its application for optimized wood coatings. *Journal of Polymers and the Environment* **2012**, *20*, 1063-1074.

48. C. Menager, N. Guigo, L. Vincent, N. Sbirrazzuoli. Polymerization kinetic pathways of epoxidized linseed oil with aliphatic bio-based dicarboxylic acids. *Journal of Polymer Science* **2020**, *58*, 1717-1727.

49. A.R. Mahendran, G. Wuzella, A. Kandelbauer, N. Aust. Thermal cure kinetics of epoxidized linseed oil with anhydride hardener. *Journal of thermal analysis and calorimetry* **2012**, *107*, 989-998.

50. A. Carbonell-Verdu, L. Bernardi, D. Garcia-Garcia, L. Sanchez-Nacher, R. Balart. Development of environmentally friendly composite matrices from epoxidized cottonseed oil. *European Polymer Journal* **2015**, *63*, 1-10.

51. J. Rocks, G.A. George, F. Vohwinkel. Curing kinetics and thermomechanical behaviour of co-anhydride cured aminoglycidyl epoxy resins. *Polymer International* **2003**, *52*, 1758-1766.

52. M.-D. Samper, J.M. Ferri, A. Carbonell-Verdu, R. Balart, O. Fenollar. Properties of biobased epoxy resins from epoxidized linseed oil (ELO) crosslinked with a mixture of cyclic anhydride and maleinized linseed oil. *Express Polymer Letters* **2019**, *13*, 407-418.

53. R. Fischer. Polyesters from expoxides and anhydrides. *Journal of Polymer Science* **1960**, *44*, 155-172.

54. Y. Tanaka, H. Kakiuchi. Study of epoxy compounds. Part I. Curing reactions of epoxy resin and acid anhydride with amine and alcohol as catalyst. *Journal of Applied Polymer Science* **1963**, *7*, 1063-1081.

55. Y. Tanaka, H. Kakiuchi. Study of epoxy compounds. Part VI. Curing reactions of epoxy resin and acid anhydride with amine, acid, alcohol, and phenol as catalysts. *Journal of Polymer Science Part A: General Papers* **1964**, *2*, 3405-3430.

56. H.F. Mark, J.I. Kroschwitz. *Encyclopedia of polymer science and engineering*; 1985.

57. M.D. Samper, R. Petrucci, L. Sánchez-Nacher, R. Balart, J.M. Kenny. New environmentally friendly composite laminates with epoxidized linseed oil (ELO) and slate fiber fabrics. *Composites Part B: Engineering* **2015**, *71*, 203-209.

58. N. Sbirrazzuoli, D. Brunel, L. Elegant. Neural networks for kinetic parameters determination, signal filtering and deconvolution in thermal analysis. *Journal of thermal analysis* **1997**, *49*, 1553-1564.

59. J.H. Flynn, L.A. Wall. General treatment of the thermogravimetry of polymers. *Journal of research of the National Bureau of Standards. Section A, Physics and chemistry* **1966**, *70*, 487.

60. H.E. Kissinger. Reaction kinetics in differential thermal analysis. *Analytical chemistry* **1957**, *29*, 1702-1706.

61. T. Akahira, T. Sunose. Research report Chiba Institute. *Technology* **1971**, *16*, 22.

62. M. Jouyandeh, S.M.R. Paran, S.S.M. Khadem, M.R. Ganjali, V. Akbari, H. Vahabi, M.R. Saeb. Nonisothermal cure kinetics of epoxy/MnxFe3-xO4 nanocomposites. *Progress in Organic Coatings* **2020**, *140*, 105505.

63. J. Lv, J. Hong, B. Liang, E. Zhao, K. Zeng, M. Chen, J. Hu, G. Yang. Study of the curing kinetics of melamine/phthalonitrile resin system. *Thermochimica Acta* **2020**, *683*, 178442.

64. J.M. Morancho, X. Fernández-Francos, C. Acebo, X. Ramis, J.M. Salla, À. Serra. Thermal curing of an epoxy-anhydride system modified with hyperbranched poly(ethylene imine)s with different terminal groups. *Journal of Thermal Analysis and Calorimetry* **2016**, *127*, 645-654.

65. J. Criado, J. Malek, A. Ortega. Applicability of the master plots in kinetic analysis of non-isothermal data. *Thermochimica Acta* **1989**, *147*, 377-385.

66. J. Criado, J. Málek, F. Gotor. The applicability of the Šesták-Berggren kinetic equation in constant rate thermal analysis (CRTA). *Thermochimica acta* **1990**, *158*, 205-213.

67. S. Krishnaswamy, V. Marchante, H. Abhyankar, Z. Huang, J. Brighton. Non-isothermal cure kinetics of aerogel/epoxy composites using differential scanning calorimetry. *Polymer-Plastics Technology and Materials* **2019**, *58*, 1757-1765.

68. N. El-Thaher, T. Mekonnen, P. Mussone, D. Bressler, P. Choi. Nonisothermal DSC Study of Epoxy Resins Cured with Hydrolyzed Specified Risk Material. *Industrial & Engineering Chemistry Research* **2013**, *52*, 8189-8199.

Adaptado del artículo

III.2.3. Optimization of the curing and post-curing conditions for the manufacturing of partially bio-based epoxy resins with improved toughness

Diego Lascano[1,2], Luis Quiles-Carrillo[2], Sergio Torres-Giner[3], Teodomiro Boronat[2] and Nestor Montanes[2]

[1] Escuela Politécnica Nacional, Ladrón de Guevara E11-253, Quito 17-01-2759, Ecuador

[2] Technological Institute of Materials (ITM), Universitat Politècnica de València (UPV), Plaza Ferrándiz y Carbonell 1, 03801 Alcoy, Spain

[3] Novel Materials and Nanotechnology Group, Institute of Agrochemistry and Food Technology (IATA), Spanish National Research Council (CSIC), Calle Catedrático Agustín Escardino Benlloch 7, 46980 Paterna, Spain

Polymers **2019**, *11*(8), 1354

polymers

MDPI

Article

Optimization of the Curing and Post-Curing Conditions for the Manufacturing of Partially Bio-Based Epoxy Resins with Improved Toughness

Diego Lascano [1,2], Luis Quiles-Carrillo [2], Sergio Torres-Giner [3,*], Teodomiro Boronat [2] and Nestor Montanes [2]

1 Escuela Politécnica Nacional, Ladrón de Guevara E11-253, Quito 17-01-2759, Ecuador
2 Technological Institute of Materials (ITM), Universitat Politècnica de València (UPV), Plaza Ferrándiz y Carbonell 1, 03801 Alcoy, Spain
3 Novel Materials and Nanotechnology Group, Institute of Agrochemistry and Food Technology (IATA), Spanish National Research Council (CSIC), Calle Catedrático Agustín Escardino Benlloch 7, 46980 Paterna, Spain
* Correspondence: storresginer@iata.csic.es; Tel.: +34-963-900-022

Received: 22 July 2019; Accepted: 13 August 2019; Published: 15 August 2019

Abstract: This research deals with the influence of different curing and post-curing temperatures on the mechanical and thermomechanical properties as well as the gel time of an epoxy resin prepared by the reaction of diglycidyl ether of bisphenol A (DGEBA) with an amine hardener and a reactive diluent derived from plants at 31 wt %. The highest performance was obtained for the resins cured at moderate-to-high temperatures, that is, 80 °C and 90 °C, which additionally showed a significant reduction in the gel time. This effect was ascribed to the formation of a stronger polymer network by an extended cross-linking process of the polymer chains during the resin manufacturing. Furthermore, post-curing at either 125 °C or 150 °C yielded thermosets with higher mechanical strength and, more interestingly, improved toughness, particularly for the samples previously cured at moderate temperatures. In particular, the partially bio-based epoxy resin cured at 80 °C and post-cured at 150 °C for 1 h and 30 min, respectively, showed the most balanced performance due to the formation of a more homogeneous cross-linked structure.

Keywords: bio-based thermosets; post-curing; gel time; mechanical properties

1. Introduction

Since their early introduction in the 1930s, epoxy resins have been the most used thermosetting polymers available. Epoxy resins show a great range of inherent properties, resulting from their highly reactive epoxy groups located in the terminal chains [1,2]. The resultant outstanding properties make these thermosets suitable for high-performance applications, for instance in aircraft and automotive industries [3,4]. Currently, epoxy systems based on diglycidyl ether of bisphenol A (DGEBA) are widely used in the plastic industry since they present remarkable structural properties including low shrinkage, coating properties, and high chemical resistance [5,6]. Despite this, thermosetting polymer materials are typically known by their intrinsic brittleness due to the high cross-linking density formed during curing [7,8]. Thus, the final properties of a structural epoxy system are not only highly influenced by the type and chemical structure of the monomers and the curing agent, which is the cross-linking precursor, but also by the curing conditions and external factors, such as the curing temperature, pressure, and so forth [9,10].

A potential advantage of epoxy systems is their capability to tailor their final properties on the basis of the selection of the processing conditions and parameters. In this context, choosing the type

Optimization of the curing and post-curing conditions for the manufacturing of partially bio-based epoxy resins with improved toughness

Abstract

This research deals with the influence of different curing and post-curing temperatures on the mechanical and thermomechanical properties as well as the gel time of an epoxy resin prepared by the reaction of diglycidyl ether of bisphenol A (DGEBA) with an amine hardener and a reactive diluent derived from plants at 31 wt %. The highest performance was obtained for the resins cured at moderate-to-high temperatures, that is, 80 ºC and 90 ºC, which additionally showed a significant reduction in the gel time. This effect was ascribed to the formation of a stronger polymer network by an extended cross-linking process of the polymer chains during the resin manufacturing. Furthermore, post-curing at either 125 ºC or 150 ºC yielded thermosets with higher mechanical strength and, more interestingly, improved toughness, particularly for the samples previously cured at moderate temperatures. In particular, the partially bio-based epoxy resin cured at 80 ºC and post-cured at 150 ºC for 1 h and 30 min, respectively, showed the most balanced performance due to the formation of a more homogeneous cross-linked structure.

Keywords: bio-based thermosets; post-curing; gel time; mechanical properties

III.2.3.1. Introduction

Since their early introduction in the 1930s, epoxy resins have been the most used thermosetting polymers available. Epoxy resins show a great range of inherent properties, resulting from their highly reactive epoxy groups located in the terminal chains [1,2]. The resultant outstanding properties make these thermosets suitable for high-performance applications, for instance in aircraft and automotive industries [3,4]. Currently, epoxy systems based on diglycidyl ether of bisphenol A (DGEBA) are widely used in the plastic industry since they present remarkable structural properties including low shrinkage, coating properties, and high chemical resistance [5,6]. Despite this, thermosetting polymer materials are typically known by their intrinsic brittleness due to the high cross-linking density formed during curing [7,8]. Thus, the final properties of a structural epoxy system are not only highly influenced by the type and chemical structure of the monomers and the curing agent, which is the cross-linking precursor, but also by the curing conditions and external factors, such as the curing temperature, pressure, and so forth [9,10].

A potential advantage of epoxy systems is their capability to tailor their final properties on the basis of the selection of the processing conditions and parameters. In this context, choosing the type of cross-linking agent is one of the most effective methods. Different amine hardeners, anhydride hardeners, and acid hardeners have been tested to develop epoxy-type thermosetting polymers [11-14]. Among them, amine hardeners are the most employed as they can provide cross-linking at relatively low temperatures [15,16]. The stoichiometric ratio between the epoxy resin components and the hardener should be carefully chosen. Any variation on this ratio may cause an excess or lack of either epoxide or amine groups, modifying, in a direct way, the epoxy system properties [17]. This effect is particularly relevant for the glass transition temperature (T_g) of the resultant epoxy resins [18,19]. In this regard, many research studies have found that the optimal properties are achieved at the stoichiometric point [17,20]. Another strategy to modify their properties is based on the addition of some diluents or “flexibilizers” [21,22]. Besides changing viscosity and toughness, these additives are also added for manufacturing purposes, since epoxy resins may present an excessively short pot-life that can lead to an earlier gelation process, making the systems difficult to handle [23].

In recent years, a wide range of several renewable building blocks and green composites [24] have been pursued in the polymer industry, with the aim to reduce the dependence on petrochemical feedstocks. Industry can take advantage of the long

chains of vegetable oils, which are made of three fatty acids, that is, triglycerides structures linked to a glycerol base molecule [25]. Vegetable oils present interesting features due to their carbon-carbon double bonds and the high reactivity provided by the multiple functional groups [26]. The addition of vegetable oils to conventional resins can successfully reduce the fossil content of synthetic resins and thus, partially decouple them to petroleum. Then, several research works have been recently devoted to exploring substitutes obtained from renewable resources to produce epoxy systems. For instance, Jaillet, *et al.* [27] successfully synthesized a polyacid hardener from soybean of higher reactivation, which could potentially replace amine hardeners. In another study, Stemmelen*, et al.* [28] synthesized aminated fatty acid (AFA) hardeners for curing epoxidized linseed oil (ELO), observing a beneficial effect on the thermochemical properties due to the improved oxidation profile of the epoxy resin.

The improvement of the final properties of a given epoxy system can also be obtained by optimizing the curing process [29]. In particular, the application of low temperatures during curing can yield a thermosetting resin with a low T_g, since some reactive groups, either from the epoxy resins or hardeners, do not react completely [30]. Thereafter, post-curing is habitually needed in order to maximize the final T_g value [31]. Post-curing is habitually set at a higher temperature than that applied during curing in order to reach the optimal state of cross-linking of the thermoset [32,33]. This process results in a resin with improved mechanical properties that, in combination to the low shrinkage attained, offers the highest stability. Furthermore, it can also provide greater resistance in coating surfaces and higher adhesion strength, making the resultant resins suitable for several industrial applications such as paints, adhesives, high-performance membranes, and so on [34-36].

The objective of this work is to study and optimize the temperature applied during curing and post-curing of a partially bio-based epoxy resin. The newly produced thermoset was evaluated in terms of its mechanical, morphological, rheological, and thermomechanical properties.

III.2.3.2. Experimental

Materials

The commercial partially bio-based epoxy system was composed of an epoxy resin and an amine-based type hardener supplied as Resoltech® 1070 ECO and Resoltech® 1074 ECO, respectively, by Castro Composites (Pontevedra, Spain). The epoxy resin is particularly made of a mixture of petroleum-derived DGEBA and a plant-

based reactive diluent from vegetable oil epoxidation. As indicated by the supplier, the bio-based content of the cured resin is 31 wt %, as determined by ASTM D6866-12. The chemical structure of the main reactive components of the epoxy resin and the cross-linking/hardening system are shown in figure III.2.3.1.

Main components of the petroleum derived epoxy resin:

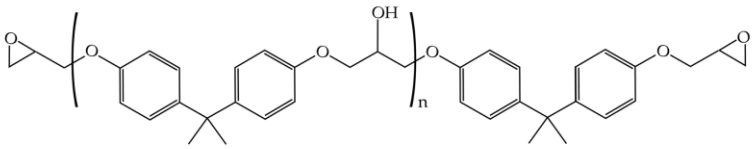

Reaction product from bisphenol A and epichlorohydrin (Av. Mw < 700 Da)

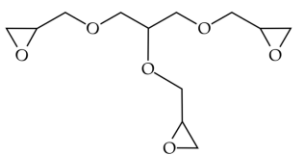

Glycerol triglycidyl ether

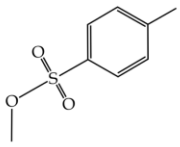

Methyl toluene-4-sulfonate

Plant-based reactive diluent from vegetable oil epoxidation:

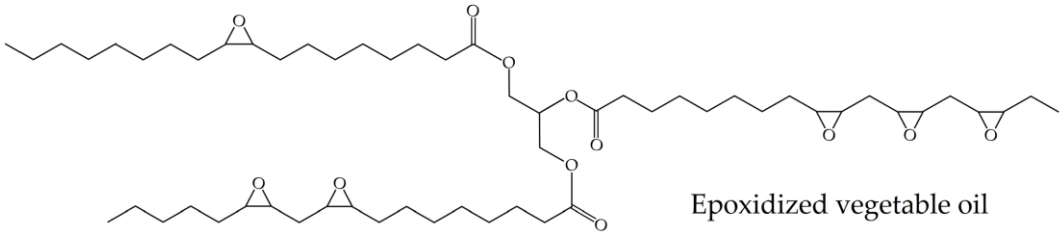

Epoxidized vegetable oil

Main components of the cross-linking/hardening system:

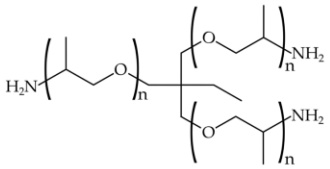

Reaction product from propoxylated propylidynetrimethanol and ammonia

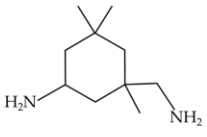

3-aminomethyl-3,5,5-trimethylcyclohexylamine

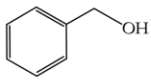

Benzyl alcohol

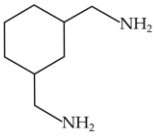

1,3-bis(aminomethyl)cyclohexane

Figure III.2.3.1. Main reactive components of the partially bio-based epoxy system.

Resin Manufacturing

The bio-based epoxy resin and the hardener were added under the stoichiometric ratio 100:35 (*wt/wt*) in a glass vessel, following the manufacturer recommendations. To this end, the bio-based epoxy resin and the curing agent were thoroughly mixed manually for 5 min and then casted into a silicon mold. The resultant mixture has a density of 1.22 $g \cdot cm^{-3}$ and viscosity of 700 mPa·s and also, according to the manufacturer, its T_g can reach values of up to 73 ºC. Further details about the uncured mixture can be found in our previous research [37]. All samples were cured for 1 h and subsequently post-cured for 30 min. The different curing and post-curing temperatures are summarized in table III.2.3.1.

Table III.2.3.1. Composition and labelling of the partially bio-based epoxy resins according to the selected curing and post-curing temperatures. The standard curing (SC) and the post-curing (PC) treatments were applied for 1 h and 30 min, respectively.

Resin	**T_{curing} (ºC)**	**$T_{post\text{-}curing}$ (ºC)**
SC_{70}		-
$SC_{70}PC_{125}$	70	125
$SC_{70}PC_{150}$		150
SC_{80}		-
$SC_{80}PC_{125}$	80	125
$SC_{80}PC_{150}$		150
SC_{90}		-
$SC_{90}PC_{125}$	90	125
$SC_{90}PC_{150}$		150

Mechanical Tests

Flexural tests were performed according to ISO 178 on rectangular pieces with dimensions of 4 x 10 x 80 mm^3 in a mechanical universal testing machine ELIB 50 from S.A.E. Ibertest (Madrid, Spain) with a 5 kN load cell. The cross-head speed was set at 10 $mm \cdot min^{-1}$. The impact strength was determined by the Charpy test, following the recommendations of ISO 179, in a Charpy pendulum from Metrotec (San Sebastián, Spain) using a 1-J pendulum. Hardness was obtained following ISO 868 in a durometer 676-D from J. Bot Instruments (Barcelona, Spain). Tests were carried out at room temperature using, at least, six specimens of each sample.

Microscopy

The morphology of the fracture surfaces of the bio-based epoxy resins obtained from the impact tests was analyzed by using field-emission scanning electron microscopy (FESEM) in a ZEISS ULTRA 55 FESEM microscope from Oxford Instruments (Abingdon, UK). An acceleration voltage of 2 kV was used. All samples' surfaces were previously coated with an ultrathin gold-palladium layer in a high-vacuum sputter coater EM MED20 from Leica Microsystem (Milton Keynes, UK).

Thermomechanical and Rheological Tests

The thermomechanical properties of the bio-based epoxy resins were evaluated by dynamic mechanical thermal analysis (DMTA) in an oscillatory rheometer AR-G2 from TA Instruments (New Castle, DE, USA). Tests were carried out in torsion–shear conditions, with a special clamp system made for solid samples. The samples, sizing 4 x 10 x 40 mm^3, were subjected to a heating program from 30 ºC to 140 ºC at a heating rate of 2 $ºC \cdot min^{-1}$. The curing behavior was studied by means of a system of parallel plates of 25 mm diameter made for liquid samples, with a constant gap of 0.2 mm. These samples were extended over the preheated plates and subjected to an isothermal heating program at 70 ºC, 80 ºC, and 90 ºC for 1 h. In both cases, a maximum deformation (γ) of 0.1 % and a constant frequency of 1 Hz were set. The gel time was obtained from the crossover point between the storage modulus (G') and the loss modulus (G''), in $G' = G''$ conditions, according to Equation (III.2.3.1):

$$t_{gel} = C\frac{1}{k} \tag{III.2.3.1}$$

where t_{gel} is the gel time, C is a constant, and k is the reaction rate constant that can be parameterized through the Arrhenius expression, shown in Equation (III.2.3.2):

$$k = A\, e^{-\frac{E_a}{R\,T}} \tag{III.2.3.2}$$

where A is the frequency factor, E_a is the apparent activation energy, R refers to the universal gas constant, and T is the absolute temperature. By substituting Equation (III.2.3.2) in Equation (III.2.3.1), the following Equation (III.2.3.3) was obtained:

$$t_{gel} = C' \frac{1}{e^{-\frac{E_a}{RT}}} \quad \text{(III.2.3.3)}$$

Then, Equation (III.2.3.4) resulted by taking natural logarithms on both sides of Equation (III.2.3.3):

$$ln(t_{gel}) = C'' + \frac{E_a}{RT} \quad \text{(III.2.3.4)}$$

Finally, by plotting $\ln(t_{gel})$ versus $\frac{1}{T}$ the value of E_a was calculated through the slope of the linear fitting.

III.2.3.3. Results and Discussion

Mechanical Properties of Partially Bio-Based Epoxy Resins

The flexural properties of the partially bio-based epoxy resins after curing and post-curing are gathered in table III.2.3.2. The value of the flexural modulus (E_f) of the bio-based epoxy resin cured at 70 ºC was 977 ± 127 MPa, whereas its flexural strength (σ_f) was 77.4 ± 13.4 MPa, thus both values were relatively high. One can observe that the curing temperature increase led to an increase of the flexural strength properties of the thermosetting system. In particular, E_f increased to values of 1260 ± 192 MPa and 2403 ± 210 MPa when the samples were cured at 80 ºC and 90 ºC, respectively, representing an increase of 191 % and 245 % when compared with the specimen cured at 70 ºC. This effect can be ascribed to the fact that the application of high curing temperatures promotes cross-linking of the thermosetting resin and then yields a stronger polymer network, in which the density of the cross-linked chains increases, and the chain mobility is reduced [38]. In relation to post-curing, all the samples showed a further mechanical strength improvement by the application of the thermal post-treatment at both 125 ºC and 150 ºC. However, one notices that the highest improvement in the flexural properties was attained by subjecting the samples to, first, a curing at 80 ºC and, subsequently, a post-curing at 150 ºC. This bio-based epoxy resin reached E_f and σ_f values of 3237 ± 377 MPa and 123.9 ± 7.6 MPa, respectively, which represents an increase of approximately 231 % and 60.1 % compared with the specimen cured at 70 ºC without any thermal post-treatment. Unexpectedly, the partially bio-based epoxy resins cured at 90 ºC and then post-cured at either 125 ºC or 150 ºC showed lower mechanical values than those obtained for the samples previously cured at 80 ºC and

subjected to the same post-curing conditions. The decrease observed in the mechanical resistance for the sample cured at the highest temperature can be ascribed to an excessive increase of the cross-linking degree that potentially yields a polymer structure with a heterogeneous load distribution and also a wide distribution of gaps between the cross-linked regions. In this regard, Gupta, *et al.* [31] and also Bueche [39] reported that, although the mechanical performance of epoxy-type thermosetting resins habitually tends to increase with the cross-linking degree, excessively cross-linked structures can also promote a decrease of the average number of cross-linking points. Therefore, the use of excessive high temperatures can potentially restrict the formation of homogeneously cross-linked structures by limiting the molecular diffusion during the resin manufacturing. The resultant phenomenon increases the chance that polymer chains achieve a tension large enough to break, thus reaching a final value of stress at break below the one initially expected to occur.

Table III.2.3.2. Flexural modulus (E_f), and flexural strength (σ_f), Shore D hardness, and impact strength of the partially bio-based epoxy resins subjected to standard curing (SC) and post-curing (PC) treatments.

Resin	Flexural test		Shore D hardness	Impact strength ($kJ \cdot m^{-2}$)
	E_f (MPa)	σ_f (MPa)		
SC_{70}	977 ± 127	77.4 ± 13.4	77.4 ± 2.9	11.9 ± 2.1
$SC_{70}PC_{125}$	1766 ± 391	89.2 ± 13.1	81.3 ± 1.2	12.2 ± 1.9
$SC_{70}PC_{150}$	1854 ± 256	93.2 ± 22.2	80.0 ± 1.2	12.8 ± 1.3
SC_{80}	1260 ± 192	81.1 ± 15.9	82.2 ± 1.8	11.5 ± 1.6
$SC_{80}PC_{125}$	2379 ± 185	114.4 ± 22.0	85.3 ± 1.0	13.3 ± 1.7
$SC_{80}PC_{150}$	3237 ± 377	123.9 ± 7.6	85.3 ± 0.5	16.8 ± 2.5
SC_{90}	2403 ± 210	105.6 ± 10.3	85.0 ± 1.5	12.0 ± 0.9
$SC_{90}PC_{125}$	2520 ± 298	110.6 ± 6.3	84.3 ± 0.6	15.9 ± 3.7
$SC_{90}PC_{150}$	2207 ± 164	101.1 ± 12.3	83.4 ± 1.7	12.4 ± 1.2

The hardness at the Shore D scale and the impact-absorbed energy values, obtained by the Charpy test, are also gathered in table III.2.2.2. In relation to hardness, the values followed the same tendency as observed above for E_f and σ_f since this property is related to the mechanical resistance properties. Similarly, the Shore D hardness value increased from 77.4 ± 2.9, for the partially bio-based epoxy resin cured at 70 ºC without any thermal post-treatment, up to 85.3 ± 0.5, for the specimens cured at 80 ºC and post-cured at 125 ºC or 150 ºC. In the case of the impact strength, it can be observed that all the partially bio-based epoxy resins showed no dependency on the

curing temperature, that is, the samples absorbed nearly the same quantity of energy, of about 12 kJ·m^{-2}, after being cured at 70 ºC, 80 ºC, and 90 ºC. Interestingly, the partially bio-based epoxy resins developed improved toughness when subjected to the different post-curing treatments. Thus, the samples cured at 70 ºC, 80 ºC, and 90 ºC and thereafter post-cured at 125 ºC showed values of 12.2 ± 1.9 kJ·m^{-2}, 13.3 ± 1.7 kJ·m^{-2}, and 15.9 ± 3.7 kJ·m^{-2}, respectively. The maximum energy absorption was also observed for the resin cured at 80 ºC and post-cured at 150 ºC, which showed an impact-strength value 16.8 ± 2.5 kJ·m^{-2}. Although fracture resistance tends to decrease when the cross-linking density increases [40], this property can be additionally dependent on other structural parameters. For instance, Min, *et al.* [41] reported that toughness is also affected by the free volume, chain flexibility, and degree of the intermolecular packing of the thermoset. Therefore, it can increase at temperatures below T_g. This effect is explained by the fact that the conformation configuration of the individual bonds is modified and, thus, the resultant free volume varies due to the rotation of the benzene rings in the epoxy resin.

Morphology and Density of Partially Bio-Based Epoxy Resins

The FESEM images of the surface fractures from the impact tests are shown in figure III.2.3.2. Left and right images gather the FESEM micrographs taken at high and low magnification, respectively. The images corresponding to the specimen cured at 80 ºC without being post-cured are presented in figure III.2.3.2a,b. As it can be seen, the surface fractures were uniform, showing many crack growths. The surfaces are typical of a brittle fracture caused by the absence of plastic deformation [42], which is in accordance to the mechanical properties reported above. One can observe a morphological change in the fracture surface of the partially bio-based epoxy resin that was subjected to post-curing at 125 ºC, shown in figure III.2.3.2c,d. These images revealed the existence of a ductile fracture, presenting some rough and tearing zones. A similar morphology can be observed in the sample post-cured at 150 ºC, included in figure III.2.3.2e,f. Alternatively, one can observe in figure III.2.3.2g,h that the surface fracture corresponding to the sample subjected to curing and post-curing at 70 ºC and 125 ºC, respectively, was relatively smooth and uniform. This surface is typical of a brittle fracture, and it was relatively similar to that observed for the sample cured at 80 ºC without any post-curing treatment. In this regard, Min, *et al.* [41] indicated that epoxy systems can unexpectedly present a more ductile fracture behavior at higher curing temperatures. This observation is in agreement with the above-reported mechanical properties, since both samples showed similar values of impact strength. A

rougher surface can be observed in figure III.2.2.2i,j, which correspond to the partially bio-based epoxy resin subjected to curing at 90 ºC and post-curing at 125 ºC. The morphology attained indicates that the fracture surface was relatively ductile, as supported by the mechanical analysis, due to the fact that both the use of high curing temperatures and the application of a post-curing treatment leads to an increase in mechanical ductility.

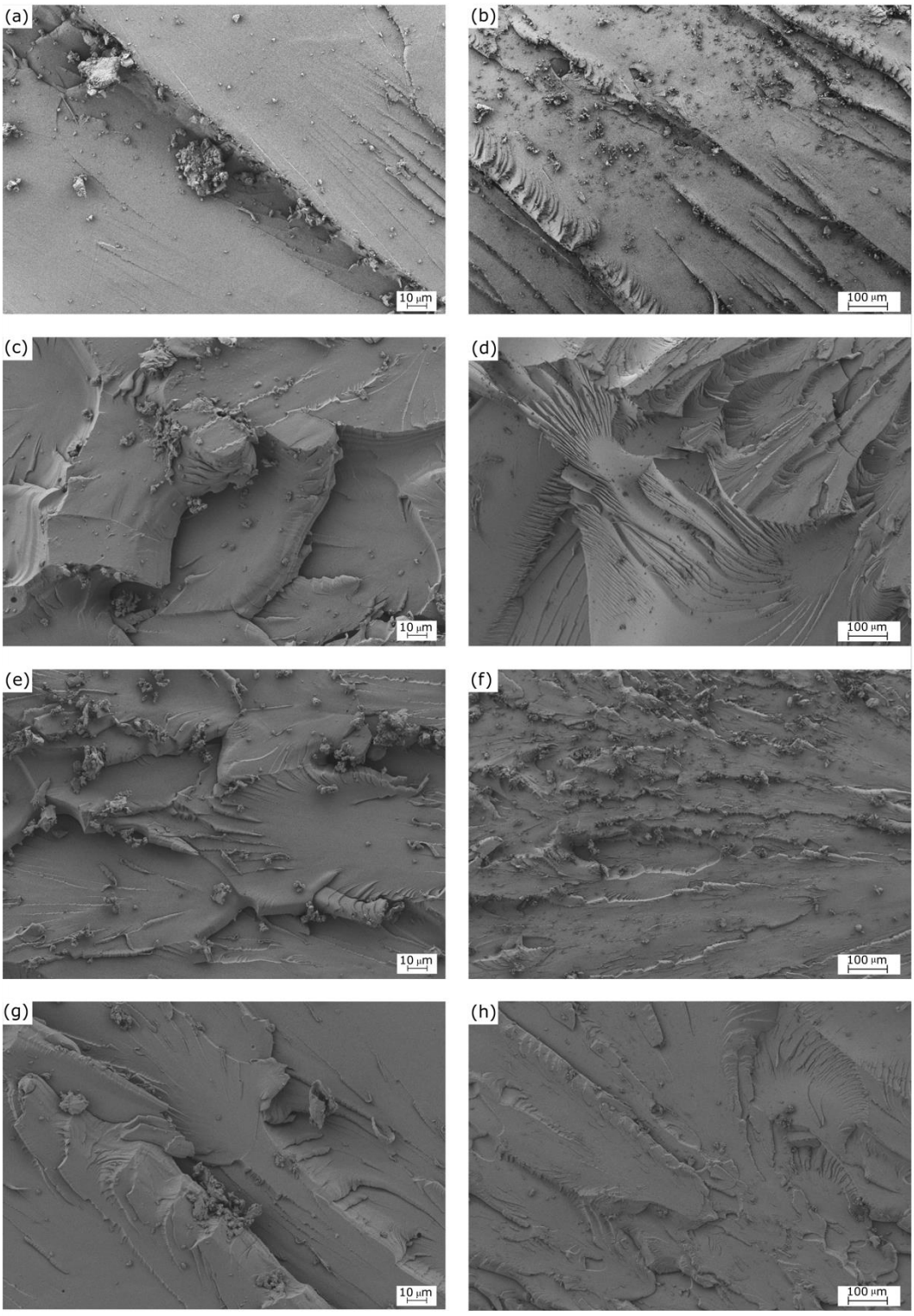
(a)
10 µm
(b)
100 µm
(c)
10 µm
(d)
100 µm
(e)
10 µm
(f)
100 µm
(g)
10 µm
(h)
100 µm

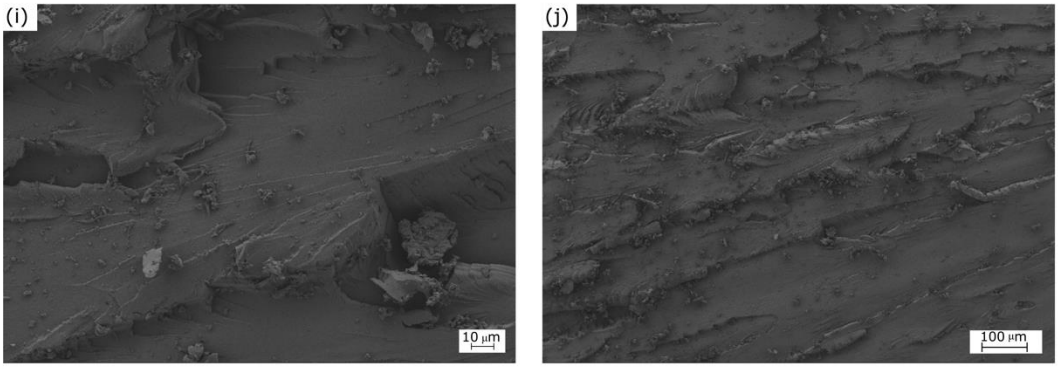

Figure III.2.3.2. Field-emission scanning electron microscopy (FESEM) corresponding to the fracture surfaces from impact tests of the partially bio-based epoxy resins subjected to standard curing (SC) and post-curing (PC) treatments: (**a**,**b**) SC_{80}; (**c**,**d**) $SC_{80}PC_{125}$; (**e**,**f**) $SC_{80}PC_{150}$; (**g**,**h**) $SC_{70}PC_{125;}$ (**i**,**j**) $SC_{90}PC_{125}$. Images were taken at x500 (left column) and x100 (right column), with scales of 10 µm and 100 µm, respectively.

The densities of the partially bio-based epoxy resins after the different curing and post-curing processes were also evaluated in order to ascertain the effect of the thermal treatments on the resin free volume. The values of density are summarized in table III.2.3.3. One notices that the density values of the samples significantly increased from 1.15 ± 0.02 $g \cdot cm^{-3}$, for a curing temperature of 70 ºC, to 1.60 ± 0.26 $g \cdot cm^{-3}$, for 80 ºC. This effect is in accordance with the literature, where it is proposed that by increasing the curing temperature, the cross-linking density increases, thus obtaining stiffer materials [38]. However, the sample cured at 90 ºC showed a density of only 1.19 ± 0.01 $g \cdot cm^{-3}$, which can be ascribed to the formation of the aforementioned excessive cross-linked structure with a higher free volume. In this regard, Gupta and Brahatheeswaran [43] proposed that, although increasing the curing temperature generally yields cross-linking density increases, an opposite effect can be attained at excessive high temperatures, in which high degrees of cross-linking results in an increase in the resin free volume due to the formation of an heterogeneously cross-linked structure. Therefore, as described above, the use of excessive high temperatures can not only increase the curing speed but also limits the molecular diffusion process during the resin formation, resulting in cross-linked structures with lower mechanical performance and also lower densities [39]. Moreover, one can observe that the post-curing treatment also induced a noticeable effect on the density of all the partially bio-based thermosetting resins. It can be observed that, in all cases, the specimens subjected to post-curing at 125 ºC showed an unexpected decrease of density, which are in agreement to the increase of the sample free volume due to a low intermolecular packing of the thermoset. Interestingly, a more extended cross-linking between the resin molecules and the hardener molecules was attained in the specimens that were cured at 70 ºC and 80 ºC and subsequently post-cured at 150 ºC, since their density presented an increase of 21

% and 9 %, respectively, compared with the samples thermally post-treated at 125 ºC. Otherwise, the samples cured at 90 ºC and post-cured at 150 ºC presented a lower density value. Therefore, for samples cured at moderate temperatures, that is, 70 ºC and 80 ºC, the use of high temperatures during post-curing can result advantageous to obtain thermosets with a cross-linked structure that is more homogenous. This observation suggests that, on the basis of the toughness improvement reported above, in addition to cross-linking, other phenomena affecting the intermolecular packing occurred in the thermoset.

Table III.2.3.3. Density of the partially bio-based epoxy resins subjected to standard curing (SC) and post-curing (PC) treatments.

Resin	Density ($g \cdot cm^{-3}$)
SC_{70}	1.15 ± 0.02
$SC_{70}PC_{125}$	1.11 ± 0.05
$SC_{70}PC_{150}$	1.35 ± 0.17
SC_{80}	1.60 ± 0.26
$SC_{80}PC_{125}$	1.32 ± 0.07
$SC_{80}PC_{150}$	1.45 ± 0.19
SC_{90}	1.19 ± 0.01
$SC_{90}PC_{125}$	1.07 ± 0.04
$SC_{90}PC_{150}$	0.97 ± 0.17

Rheological Properties of Partially Bio-Based Epoxy Resins

The curing processes of the partially bio-based epoxy resin carried out at 70 ºC, 80 ºC, and 90 ºC were studied by oscillatory rheometry, and the results are gathered in figure III.2.3.3. In the evolution of G' with time, shown in figure III.2.3.3a, low values can be observed at the early stages of the curing process. However, as cross-linking occurred, the M_W of the bio-based epoxy resin increased and, thus, the values of G' increased, improving the material elastic behavior. Figure III.2.3.3b shows the phase angle (δ) between the obtained deformation (γ) and the applied stress (σ). At the first step of the curing process, the δ value was close to 90°, which is characteristic of a liquid behavior. The curing process was identified by the decrease of δ with time, being reduced to approximately 0°. Therefore, for an elastic solid material, this rheological behavior confirms that the curing process fully ended.

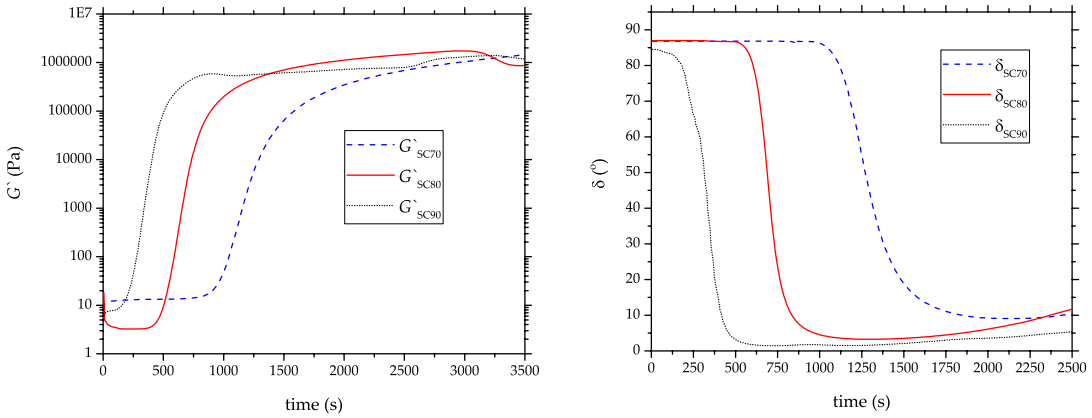

(a) (b)

Figure III.2.3.3. Evolution of (**a**) storage modulus (*G′*) and (**b**) phase angle (*δ*) with time of the partially bio-based epoxy resins subjected to standard curing (SC) treatment, obtained by rheometry.

The gel time is one of the most important parameters from a manufacturing point of view since it delimits the change from the liquid to the solid state and it is noticed by an increase in the mixture viscosity. The gel point of these polymer networks occurred in a conversion around 0.7. This parameter can be estimated either when *δ* is 45° or by the crossover point between *G′* and *G″*. Table III.2.3.4 summarizes the gel time values at different curing temperatures. As mentioned above, the cross-linking process ended when the *δ* value was 0°. One can observe that the gel time decreased from 1426.1 s, at the curing temperature of 70 ºC, to 445.2 s, when the curing temperature was set at 90 ºC. Then, as expected, the gel time decreased markedly with the curing temperature increase, since high temperatures can significantly speed up the cross-linking process. This observation represents a valuable indicator of the cross-linking reaction course. In particular, for a curing temperature of 70 ºC, the curing time was 2250.3 s, whereas it decreased significantly to 750.2 s when the curing temperature increased to 90 ºC. Alternatively, the maximum storage modulus (G'_{max}) values were achieved when the samples were completely cured. These values are also gathered in table III.2.3.4, in which one can observe that the highest value was attained for the sample cured at 80 ºC, which is in accordance with the mechanical properties reported above.

Table III.2.3.4. Gel time (t_{gel}), curing time (t_{curing}), and maximum storage modulus (G'_{max}) of the partially bio-based epoxy resins after the different curing temperatures.

T_{curing} (℃)	t_{gel} (s)	t_{curing} (s)	G'_{max} (GPa)
70	1426.1 ± 28.5	2250.3 ± 56.1	1.042 ± 0.02
80	760.6 ± 15.2	1250.0 ± 18.8	1.738 ± 0.03
90	445.2 ± 8.9	750.2 ± 18.7	1.311 ± 0.03

E_a was obtained through the slope of the linear fitting of the plot of $\ln(t_{gel})$ versus $\frac{1}{T}$, shown in figure III.2.3.4. It resulted in a value of 60.28 kJ·mol^{-1}, having an excellent correlation coefficient ($R^2 \approx 0.999$). This is in agreement with our previous work dealing with the kinetic analysis of the curing process of DGEBA-based epoxy resins using bio-based diluents, in which the E_a values ranged between 50 kJ·mol^{-1} and 70 kJ·mol^{-1} [37]. The E_a value of the here-prepared partially bio-based epoxy resin is similar, for instance, to the values reported for conventional epoxy–amine systems, that is, 58-59 kJ·mol^{-1} [44], but higher than those of epoxy-anhydride systems, that is, 46-48 kJ·mol^{-1} [45]. In this regard, Karger-Kocsis, *et al*. [46] indicated that E_a increased from 53 kJ·mol^{-1} to 72 kJ·mol^{-1} by increasing the vegetable oil content in the epoxy system.

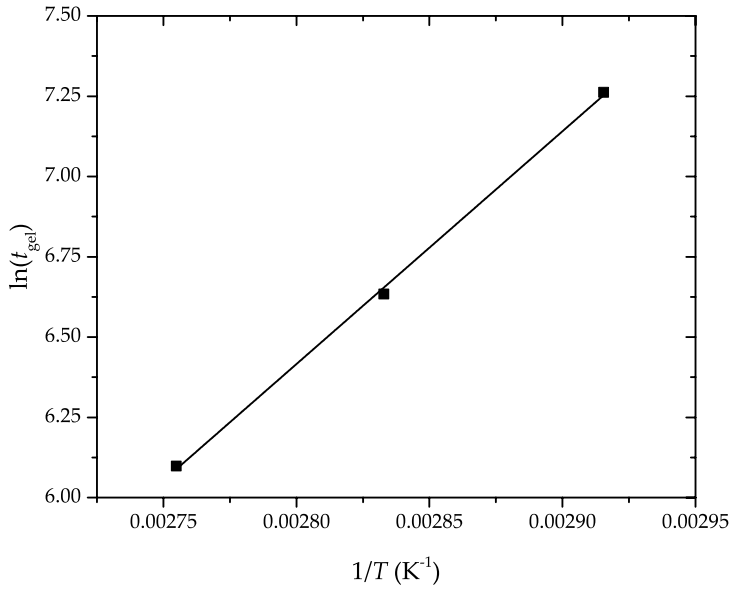

Figure III.2.3.4. Determination of the apparent activation energy (E_a) of the partially bio-based epoxy resins by the linear fitting of the gel time versus the inverse temperature, according to Equation (III.2.3.4).

Thermomechanical Properties of Partially Bio-Based Epoxy Resins

Figure III.2.3.5 shows the thermomechanical behavior of the bio-based epoxy resins after the different curing and post-curing treatments. Table III.2.3.5 summarizes the values of *G′* at 40 ºC and 110 ºC and also of T_g, obtained from the DMTA curves. Figure III.2.3.5a–c depict the evolution of *G′* with temperature for the samples that were subjected to curing at 70 ºC, 80 ºC, 90 ºC and post-curing at 125 ºC and 150 ºC. At 40 ºC, the values of *G′* were 1.029 ± 0.021 GPa, 1.039 ± 0.025 GPa, and 1.037 ± 0.024 GPa for the resins cured at 70 ºC, 80 ºC, and 90 ºC, respectively. As the temperature increased, a sharp drop in the *G′* values of two orders of magnitude were observed, indicating that the partially bio-based epoxy resins underwent glass transition. At a higher temperature, that is, 110 ºC, the samples showed similar *G′* values, that is, 4.29 ± 0.09 MPa, 4.99 ± 0.15 MPa, and 4.68 ± 0.09 MPa, for each respective curing temperature. It is also worthy to mention that higher *G′* values were attained with the curing temperature increase. This result can be explained by the fact that the increase in the cross-linking density results in a material's stiffness [47].

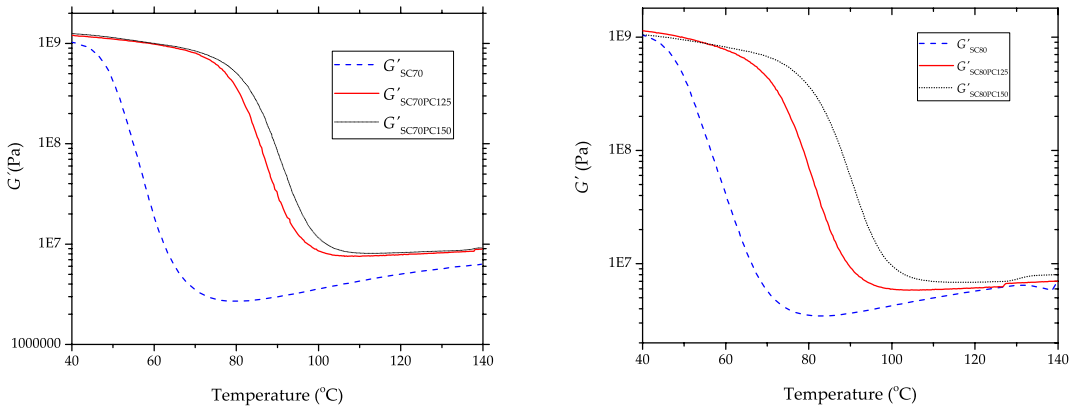

(a) (b)

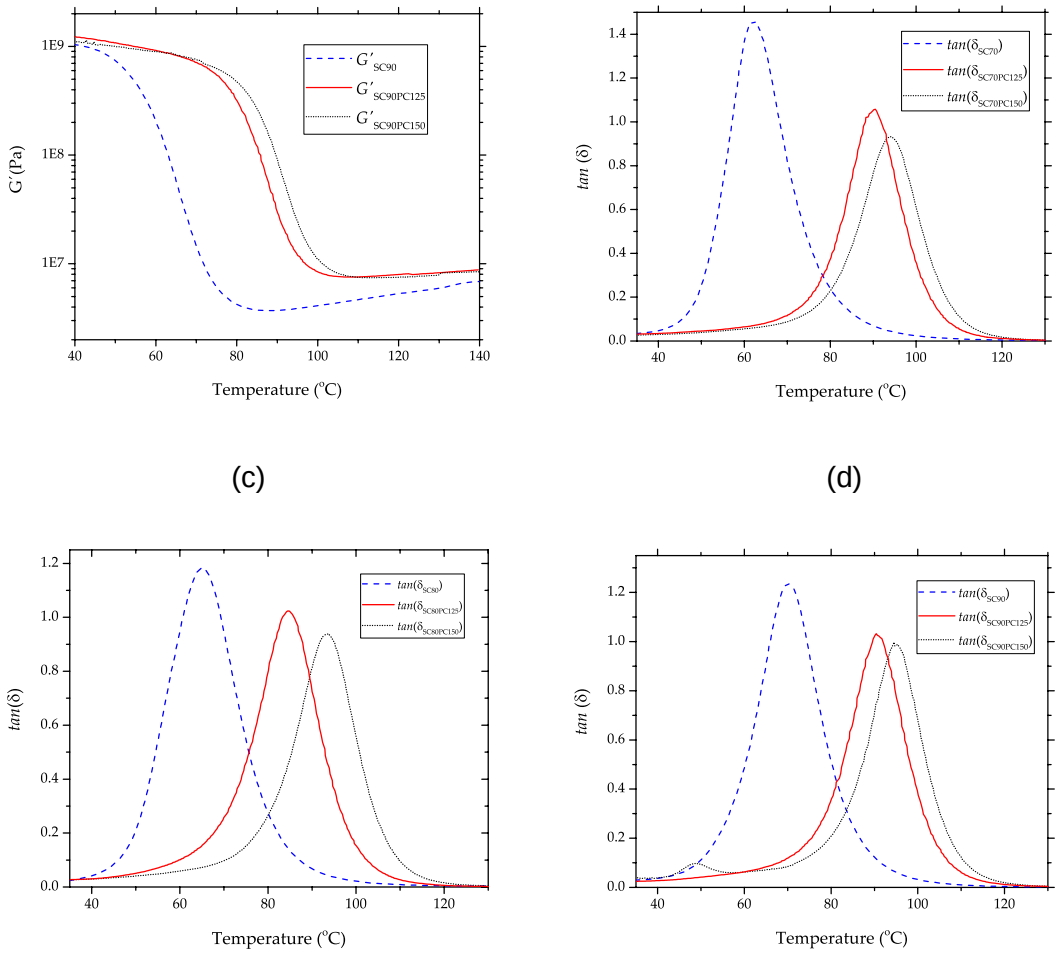

Figure III.2.3.5. Thermomechanical behavior of the partially bio-based epoxy resins subjected to standard curing (SC) and post-curing (PC) treatments: (**a**-**c**) storage modulus (*G'*); (**d**-**f**) damping factor (*tan δ)*.

Table III.2.3.5. Storage modulus (*G'*) at 40 °C and 110 °C and glass transition temperature (T_g) of the partially bio-based epoxy resins subjected to standard curing (SC) and post-curing (PC) treatments.

Resin	*G'* at 40 °C (GPa)	*G'* at 110 °C (MPa)	T_g (°C)
SC_{70}	1.029 ± 0.021	4.29 ± 0.09	62.5 ± 1.25
$SC_{70}PC_{125}$	1.203 ± 0.024	7.56 ± 0.15	90.5 ± 1.71
$SC_{70}PC_{150}$	1.255 ± 0.027	8.15 ± 0.16	94.1 ± 1.97
SC_{80}	1.039 ± 0.025	4.99 ± 0.09	65.1 ± 1.63
$SC_{80}PC_{125}$	1.132 ± 0.019	5.89 ± 0.11	84.9 ± 1.95
$SC_{80}PC_{150}$	1.048 ± 0.022	6.96 ± 0.17	93.4 ± 1.87
SC_{90}	1.037 ± 0.024	4.68 ± 0.09	70.4 ± 1.47
$SC_{90}PC_{125}$	1.230 ± 0.025	7.57 ± 0.15	90.7 ± 2.35
$SC_{90}PC_{150}$	1.121 ± 0.02	7.47 ± 0.14	95.3 ± 3.01

Furthermore, the effect of the post-curing treatment was noticeable, especially for the partially bio-based epoxy resins that were thermally post-treated at 150 ºC. These samples showed a significant improvement in elasticity, reaching values of 1.255 ± 0.027 GPa, 1.048 ± 0.022 GPa, and 1.221 ± 0.02 GPa at a temperature of 40 ºC, and values of 8.15 ± 0.16 GPa, 6.96 ± 0.17 GPa, and 7.47 ± 0.14 GPa at 110 ºC, for curing temperatures of 70 ºC, 80 ºC, and 90 ºC, respectively. Therefore, the partially bio-based epoxy resin cured and post-cured at 70 ºC and 150 ºC, respectively, showed the highest *G′* values. However, it is worth emphasizing that, despite the fact that the post-curing treatment tended to increase *G′*, the samples cured at 80 ºC and 90 ºC and then subjected to post-curing at 150 ºC presented lower *G′* values at 40 ºC than those post-cured at 125 ºC. In particular, unexpected low *G′* values were attained for the resins cured at 80 ºC and then post-cured at either 125 ºC or 150 ºC, even though they presented a highly cross-linked structure. In this regard, Dyakonov, *et al.* [48] indicated that elasticity in epoxy resins is not only related to an increase in the cross-linking density but also to a phenomenon of resin vitrification. Therefore, it is proposed that resin vitrification was successfully prevented for the samples cured at moderate temperatures and then post-cured at high temperature, that is, 150 ºC, due to a more efficient molecular diffusion. This result supports the improved toughness of the partially bio-based epoxy resin observed during the mechanical analysis, and it offers a new technological advantage from a mechanical point of view.

The evolution of the damping factor (*tan δ*) with temperature is shown in figure III.2.3.5d–f. The *tan δ* peak relates to the T_g of the biopolymer. The resins cured at 70 ºC, 80 ºC, 90 ºC presented T_g values of approximately 62.5 ± 1.25 ºC, 65.1 ± 1.63 ºC, 70.4 ± 1.47 ºC, respectively. It is noteworthy that by increasing the curing temperature, the cross-linking degree was extended, and it resulted in an increase of T_g [49]. The effect of post-curing on the thermomechanical behavior of the samples was noticeable since it favored the functional groups to react after the curing process. Higher temperatures promoted the cross-linking process to continue and led to a further increase in the T_g values. For instance, the partially bio-based epoxy resins that were subjected to curing at 70 ºC or 80 ºC and subsequent post-curing at 125 ºC had an increase of 28 % and 45 %, respectively, in the T_g values when compared with their counterpart resin without post-curing. In particular, the latter samples reached values of 90.5 ± 1.71 ºC and 84.9 ± 1.95 ºC. In the case of the partially bio-based epoxy resins subjected to post-curing at 150 °C, the increase in T_g was even more significant. In particular, the values obtained after post-curing at 150 ºC were 94.1 ± 1.97 °C, 93.4 ± 1.87 ºC, and 95.3 ± 3.01 ºC for the samples previously cured at 70 ºC, 80 ºC, and 90 ºC, respectively. Wu [50] suggested

that T_g stabilization relates to a restriction of the mobility degree of the polymer chains. Therefore, the T_g values attained correlate with the previous density measurements, confirming the reduction of the sample free volume due to the successful extension of the cross-linking process by the formation of a more homogeneous structure. In addition, the partially bio-based epoxy resins subjected to post-curing at 125 ºC presented lower T_g values than those post-cured at 150 ºC, even though the latter samples showed higher toughness.

III.2.3.4. Conclusions

The effect of the curing and post-curing conditions on epoxy resins prepared by the reaction of DGEBA with amine hardener and a bio-based reactive diluent at 31 wt % was analyzed by flexural tests, FESEM, and oscillatory rheometry at different isothermal heating rates. It was observed that the partially bio-based thermosetting resins cured and post-cured at higher temperatures tended to present higher mechanical and thermomechanical performance due to the formation of a highly cross-linked structure of lower free volume. However, interestingly, the samples cured at moderate temperatures and then post-cured at high temperatures unexpectedly developed improved toughness performance. In particular, it was observed that curing at 80 ºC for 1 h and subsequent post-curing at 150 ºC for 30 min yielded the partially bio-based epoxy resin with the most balanced mechanical and thermomechanical properties. This result was ascribed to the formation of a more homogeneous cross-linked structure based on a strong polymer network but with also improved chain mobility. Based on the above, it can be concluded that the final properties of these epoxy resin systems can be effectively controlled by the selection of the curing and post-curing temperatures. The application of the optimal conditions can then yield partially bio-based epoxy resins with improved toughness that represent an environmentally friendly solution for the thermosetting industry. Moreover, they can be manufactured in a shorter production time since the gel time is also reduced.

III.2.3.5. Funding

This research was supported by the Spanish Ministry of Science, Innovation, and Universities (MICIU) through the MAT2017-84909-C2-2-R program number

III.2.3.6. Acknowledgments

D.L. acknowledges Universitat Politècnica de València (UPV) for the grant received through the PAID-01-18 program. L.Q.-C. wants to thank the Generalitat Valenciana (GVA) for his FPI grant (ACIF/2016/182) and the Spanish Ministry of

Education, Culture, and Sports (MECD) for his FPU grant (FPU15/03812). S.T.-G. is a recipient of a Juan de la Cierva–Incorporación contract (IJCI-2016-29675) from MICIU.

III.2.3.7. References

1. F.L. Jin, X. Li, S.J. Park. Synthesis and application of epoxy resins: A review. *Journal of Industrial and Engineering Chemistry* **2015**, *29*, 1-11.
2. S. Yu, X. Li, X. Guo, Z. Li, M. Zou. Curing and characteristics of N, N, N′, N′-tetraepoxypropyl-4, 4′-diaminodiphenylmethane epoxy resin-based buoyancy material. *Polymers* **2019**, *11*, 1137.
3. J. Njuguna, K. Pielichowski, J.R. Alcock. Epoxy-based fibre reinforced nanocomposites. *Advanced Engineering Materials* **2007**, *9*, 835-847.
4. J. Holbery, D. Houston. Natural-fiber-reinforced polymer composites in automotive applications. *JOM* **2006**, *58*, 80-86.
5. N.J. Jin, I. Seung, Y.S. Choi, J. Yeon. Prediction of early-age compressive strength of epoxy resin concrete using the maturity method. *Construction and Building Materials* **2017**, *152*, 990-998.
6. Y.B. Yin, Q.S. Yang, S.L. Wang, H.D. Gao, Y.W. He, X.L. Li. Formation of CO2 bubbles in epoxy resin coatings: A DFT study. *Journal of Molecular Graphics and Modelling* **2019**, *86*, 192-198.
7. F.L. Jin, S.J. Park. Thermomechanical behavior of epoxy resins modified with epoxidized vegetable oils. *Polymer International* **2008**, *57*, 577-583.
8. B. Ellis, W.R. Ashcroft, S.J. Shaw, W.J. Cantwell, H.H. Kausch, G.P. Johari, F.R. Jones, X.M. Chen. *Chemistry and technology of epoxy resins*; 1993; 10.1007/978-94-011-2932-9.
9. R.-W. Kim, C.-M. Kim, K.-H. Hwang, S.-R. Kim. Embedded based real-time monitoring in the high-pressure resin transfer molding process for CFRP. *Applied Sciences* **2019**, *9*, 1795.
10. A. Rudawska. The impact of the seasoning conditions on mechanical properties of modified and unmodified epoxy adhesive compounds. *Polymers* **2019**, *11*, 804.
11. J.B. Enns, J.K. Gillham. Effect of the extent of cure on the modulus, glass transition, water absorptio, and density of an amine-cured epoxy. *Journal of Applied Polymer Science* **1983**, *28*, 2831-2846.
12. M. Ivankovic, L. Incarnato, J.M. Kenny, L. Nicolais. Curing kinetics and chemorheology of epoxy/anhydride system. *Journal of Applied Polymer Science* **2003**, *90*, 3012-3019.

13. C. Zilg, R. Mülhaupt, J. Finter. Morphology and toughness/stiffness balance of nanocomposites based upon anhydride-cured epoxy resins and layered silicates. *Macromolecular Chemistry and Physics* **1999**, *200*, 661-670.

14. T. Zheng, X. Wang, C. Lu, X. Zhang, Y. Ji, C. Bai, Y. Chen, Y. Qiao. Studies on curing kinetics and tensile properties of silica-filled phenolic amine/epoxy resin nanocomposite. *Polymers* **2019**, *11*, 680.

15. N. Guermazi, N. Haddar, K. Elleuch, H.F. Ayedi. Investigations on the fabrication and the characterization of glass/epoxy, carbon/epoxy and hybrid composites used in the reinforcement and the repair of aeronautic structures. *Materials and Design* **2014**, *56*, 714-724.

16. S.J. Park, M.K. Seo, J.R. Lee. Isothermal cure kinetics of epoxy/phenol-novolac resin blend system initiated by cationic latent thermal catalyst. *Journal of Polymer Science, Part A: Polymer Chemistry* **2000**, *38*, 2945-2956.

17. S. Mostovoy, E. Ripling. Fracture toughness of an epoxy system. *Journal of Applied Polymer Science* **1966**, *10*, 1351-1371.

18. B. Mohammadi, M.R. Nokken. Influence of moisture content on water absorption in concrete. *Proceedings, Annual Conference - Canadian Society for Civil Engineering* **2013**, *5*, 4092-4100.

19. K. Fu, Q. Xie, F. Lü, Q. Duan, X. Wang, Q. Zhu, Z. Huang. Molecular dynamics simulation and experimental studies on the thermomechanical properties of epoxy resin with different anhydride curing agents. *Polymers* **2019**, *11*, 975.

20. A. Kenyon, L. Nielsen. Characterization of network structure of epoxy resins by dynamic mechanical and liquid swelling tests. *Journal of Macromolecular Science—Chemistry* **1969**, *3*, 275-295.

21. P. Czub. Application of modified natural oils as reactive diluents for epoxy resins. *Macromolecular Symposia* **2006**, *242*, 60-64.

22. Y.T. Park, Y. Qian, C. Chan, T. Suh, M.G. Nejhad, C.W. Macosko, A. Stein. Epoxy toughening with low graphene loading. *Advanced Functional Materials* **2015**, *25*, 575-585.

23. H. Okabe, H. Nishimura, K. Hara, S. Kai. Gelation and glass transition in thermosetting process of epoxy resin. *Progress of Theoretical Physics Supplement* **1997**, *126*, 119-122.

24. L. Quiles-Carrillo, N. Montanes, J.M. Lagaron, R. Balart, S. Torres-Giner. On the use of acrylated epoxidized soybean oil as a reactive compatibilizer in injection-

molded compostable pieces consisting of polylactide filled with orange peel flour. *Polymer International* **2018**, *67*, 1341-1351.

25. S. Torres-Giner, N. Montanes, O. Fenollar, D. García-Sanoguera, R. Balart. Development and optimization of renewable vinyl plastisol/wood flour composites exposed to ultraviolet radiation. *Materials & Design* **2016**, *108*, 648-658.

26. S.N. Khot, J.J. Lascala, E. Can, S.S. Morye, G.I. Williams, G.R. Palmese, S.H. Kusefoglu, R.P. Wool. Development and application of triglyceride-based polymers and composites. *Journal of Applied Polymer Science* **2001**, *82*, 703-723.

27. F. Jaillet, M. Desroches, R. Auvergne, B. Boutevin, S. Caillol. New biobased carboxylic acid hardeners for epoxy resins. *European Journal of Lipid Science and Technology* **2013**, *115*, 698-708.

28. M. Stemmelen, V. Lapinte, J.P. Habas, J.J. Robin. Plant oil-based epoxy resins from fatty diamines and epoxidized vegetable oil. *European Polymer Journal* **2015**, *68*, 536-545.

29. R.A. Pethrick, E.A. Hollins, I. McEwan, E.A. Pollock, D. Hayward, P. Johncock. Effect of cure temperature on the structure and water absorption of epoxy/amine thermosets. *Polymer International* **1996**, *39*, 275-288.

30. S.J. Tucker, B. Fu, S. Kar, S. Heinz, J.S. Wiggins. Ambient cure POSS-epoxy matrices for marine composites. *Composites Part A: Applied Science and Manufacturing* **2010**, *41*, 1441-1446.

31. V.B. Gupta, J. Rich, L.T. Drazal, C.Y.C. Lee. The temperature-dependence of some mechanical properties of a cured epoxy resin system. **1985**, *25*, 812-823.

32. J.M. Barton, I. Hamerton, B.J. Howlin, J.R. Jones, S. Liu. Studies of cure schedule and final property relationships of a commercial epoxy resin using modified imidazole curing agents. *Polymer* **1998**, *39*, 1929-1937.

33. C. Russo, X. Fernández-Francos, S. De la Flor. Rheological and mechanical characterization of dual-curing thiol-acrylate-epoxy thermosets for advanced applications. *Polymers* **2019**, *11*, 997.

34. D. Kotnarowska. Influence of ultraviolet radiation and aggressive media on epoxy coating degradation. *Progress in Organic Coatings* **1999**, *37*, 149-159.

35. M. Imanaka, X. Liu, M. Kimoto. Comparison of fracture behavior between acrylic and epoxy adhesives. *International Journal of Adhesion and Adhesives* **2017**, *75*, 31-39.

36. R. Rahman, S.Z.F.S. Putra. Tensile properties of natural and synthetic fiber-reinforced polymer composites. *Mechanical and physical testing of biocomposites, fibre-reinforced composites and hybrid composites* **2019**, 81-102.

37. D. Lascano, L. Quiles-Carrillo, R. Balart, T. Boronat, N. Montanes. Kinetic analysis of the curing of a partially biobased epoxy resin using dynamic differential scanning calorimetry. *Polymers* **2019**, *11*, 391.

38. C. Lambert, M. Larroque, J.T. Subirats, J.F. Gérard. Food-contact epoxy resin: Co-variation between migration and degree of cross-linking. Part II. *Food Additives & Contaminants* **1998**, *15*, 318-328.

39. F. Bueche. Tensile strength of rubbers. *Journal of Polymer Science* **1957**, *24*, 189-200.

40. G. Levita, S. De Petris, A. Marchetti, A. Lazzeri. Crosslink density and fracture toughness of epoxy resins. *Journal of materials science* **1991**, *26*, 2348-2352.

41. B.G. Min, J. Hodgkin, Z. Stachurski. The dependence of fracture properties on cure temperature in a DGEBA/DDS epoxy system. *Journal of applied polymer science* **1993**, *48*, 1303-1312.

42. M. Turk, I. Hamerton, D.S. Ivanov. Ductility potential of brittle epoxies: Thermomechanical behaviour of plastically-deformed fully-cured composite resins. *Polymer* **2017**, *120*, 43-51.

43. V. Gupta, C. Brahatheeswaran. Molecular packing and free volume in crosslinked epoxy networks. *Polymer* **1991**, *32*, 1875-1884.

44. P.I. Karkanas, I.K. Partridge. Cure modeling and monitoring of epoxy/amine resin systems. I. Cure kinetics modeling. *Journal of applied polymer science* **2000**, *77*, 1419-1431.

45. E. Woo, J. Seferis. Cure kinetics of epoxy/anhydride thermosetting matrix systems. *Journal of applied polymer science* **1990**, *40*, 1237-1256.

46. J. Karger-Kocsis, S. Grishchuk, L. Sorochynska, M. Rong. Curing, gelling, thermomechanical, and thermal decomposition behaviors of anhydride-cured epoxy (DGEBA)/epoxidized soybean oil compositions. *Polymer Engineering & Science* **2014**, *54*, 747-755.

47. C. Li, A. Strachan. Evolution of network topology of bifunctional epoxy thermosets during cure and its relationship to thermo-mechanical properties: A molecular dynamics study. *Polymer* **2015**, *75*, 151-160.

48. T. Dyakonov, Y. Chen, K. Holland, J. Drbohlav, D. Burns, D. Vander Velde, L. Seib, E.J. Soloski, J. Kuhn, P.J. Mann. Thermal analysis of some aromatic amine cured model epoxy resin systems—I: Materials synthesis and characterization, cure and post-cure. *Polymer degradation and stability* **1996**, *53*, 217-242.

49. T. Chang, S.H. Carr, J. Brittain. Studies of epoxy resin systems: Part B: Effect of crosslinking on the physical properties of an epoxy resin. *Polymer Engineering & Science* **1982**, *22*, 1213-1220.

50. C.-S. Wu. Influence of post-curing and temperature effects on bulk density, glass transition and stress-strain behaviour of imidazole-cured epoxy network. *Journal of materials science* **1992**, *27*, 2952-2959.

Adaptado del artículo

III.2.4. Manufacturing and characterization of green composites with partially biobased epoxy resin and flaxseed flour wastes

Diego Lascano[1,2], Daniel Garcia-Garcia[1], Sandra Rojas-Lema[1,2], Luis Quiles-Carrillo[1], Rafael Balart[1] and Teodomiro Boronat[1]

[1] Technological Institute of Materials (ITM), Universitat Politècnica de València (UPV), Plaza Ferrándiz y Carbonell 1, 03801 Alcoy, Spain

[2] Escuela Politécnica Nacional, Ladrón de Guevara E11-253, Quito 17-01-2759, Ecuador

Appl. Sci. **2020**, *10*(11), 3688

applied sciences

MDPI

Article

Manufacturing and Characterization of Green Composites with Partially Biobased Epoxy Resin and Flaxseed Flour Wastes

Diego Lascano [1,2], Daniel Garcia-Garcia [1,*], Sandra Rojas-Lema [1,2], Luis Quiles-Carrillo [1], Rafael Balart [1] and Teodomiro Boronat [1]

[1] Technological Institute of Materials (ITM), Universitat Politècnica de València (UPV), Plaza Ferrándiz y Carbonell 1, 03801 Alcoy, Spain; dielas@epsa.upv.es (D.L.); sanrole@epsa.upv.es (S.R.-L.); luiquic1@epsa.upv.es (L.Q.-C.); rbalart@mcm.upv.es (R.B.); tboronat@dimm.upv.es (T.B.)

[2] Escuela Politécnica Nacional, Quito 17-01-2759, Ecuador

* Correspondence: dagarga4@epsa.upv.es; Tel.: +(34)96-652-84-34

Received: 29 April 2020; Accepted: 25 May 2020; Published: 26 May 2020

check for updates

Featured Application: In the present work, green-composites have been developed from a partially biobased epoxy resin reinforced with flaxseed flour wastes. The attractive aesthetic appearance, similar to wood, and the balanced overall properties of the obtained composites may be interesting for use in sectors such as decoration, furniture or automotive industry.

Abstract: In the present work, green-composites from a partially biobased epoxy resin (BioEP) reinforced with lignocellulosic particles, obtained from flax industry by-products or wastes, have been manufactured by casting. In this study, the flaxseed has been crushed by two different mechanical milling processes to achieve different particle sizes, namely coarse size (CFF), and fine size (FFF) particle flaxseed flour, with a particle size ranging between 100–220 μm and 40–140 μm respectively. Subsequently, different loadings of each particle size (10, 20, 30, and 40 wt%) were mixed with the BioEP resin and poured into a mold and subjected to a curing cycle to obtain solid samples for mechanical, thermal, water absorption, and morphological characterization. The main aim of this research was to study the effect of the particle size and its content on the overall properties of composites with BioEP. The results show that the best mechanical properties were obtained for composites with a low reinforcement content (10 wt%) and with the finest particle size (FFF) due to a better dispersion into the matrix, and a better polymer-particle interaction too. This also resulted in a lower water absorption capacity due to the presence of fewer voids in the developed composites. Therefore, this study shows the feasibility of using flax wastes from the seeds as a filler in highly environmentally friendly composites with a wood-like appearance with potential use in furniture or automotive sectors.

Keywords: Flax seed; biobased epoxy; green-composite; waste valorization; size particle

1. Introduction

During the last years, there has been a significant increase in social concern for the environmental problem generated by petrochemical polymeric materials [1–3]. For this reason, one of the main objectives of the scientific community is the research and development of new highly environmentally friendly materials which could be suitable to replace petroleum-based polymers to reduce their carbon footprint [4]. Many of these researches focus on the field of polymer composites reinforced with lignocellulosic particles giving rise to the so-called wood plastic composites (WPC). A series of advantages make the use of lignocellulosic reinforcements very attractive for their use as reinforcement,

Manufacturing and characterization of green composites with partially biobased epoxy resin and flaxseed flour wastes

Abstract

In the present work, green-composites from a partially biobased epoxy resin (BioEP) reinforced with lignocellulosic particles, obtained from flax industry by-products or wastes, have been manufactured by casting. In this study, the flaxseed has been crushed by two different mechanical milling processes to achieve different particle sizes, namely coarse size (CFF), and fine size (FFF) particle flaxseed flour, with a particle size ranging between 100-220 µm and 40-140 µm respectively. Subsequently, different loadings of each particle size (10, 20, 30, and 40 wt %) were mixed with the BioEP resin and poured into a mold and subjected to a curing cycle to obtain solid samples for mechanical, thermal, water absorption, and morphological characterization. The main aim of this research was to study the effect of the particle size and its content on the overall properties of composites with BioEP. The results show that the best mechanical properties were obtained for composites with a low reinforcement content (10 wt %) and with the finest particle size (FFF) due to a better dispersion into the matrix, and a better polymer-particle interaction too. This also resulted in a lower water absorption capacity due to the presence of fewer voids in the developed composites. Therefore, this study shows the feasibility of using flax wastes from the seeds as a filler in highly environmentally friendly composites with a wood-like appearance with potential use in furniture or automotive sectors.

Keywords: Flax seed; biobased epoxy; green-composite; waste valorization; size particle

III.2.4.1. Introduction

During the last years, there has been a significant increase in social concern for the environmental problem generated by petrochemical polymeric materials [1-3]. For this reason, one of the main objectives of the scientific community is the research and development of new highly environmentally friendly materials which could be suitable to replace petroleum-based polymers to reduce their carbon footprint [4]. Many of these research focus on the field of polymer composites reinforced with lignocellulosic particles giving rise to the so-called wood plastic composites (WPC). A series of advantages make the use of lignocellulosic reinforcements very attractive for their use as reinforcement, such as their low cost, low density, non-abrasive properties, non-toxic, biodegradable, and their environmentally friendly nature [5,6]. Besides, the lignocellulosic particles usually provide an aesthetic wood-like surface finish, which makes them very interesting for use in sectors where aesthetics is an essential factor, such as the furniture or automotive sectors. Furthermore, WPCs have several advantages over wood, such as low maintenance, high dimensional stability, and high resistance to biological attack [7,8]. There are many research works that have focused on the effect of different types of lignocellulosic particles on the properties of both thermoplastic and thermoset matrices. For example, interesting works have been developed with rice husks [9-11], peanut shells [7,12,13], almond shells [14-16], hazelnut shells [17,18], date palm seeds [19], lemon peel [20], *Posidonia oceanica* [21,22], olive stones [23], among others. Most of these lignocellulosic particles come from agricultural by-products or wastes that are currently used for animal feeding and just left on controlled landfills. Therefore, the use of these wastes, widely available as a source of fillers for composite materials, can be a new economic opportunity for the agricultural sector and thereby contributing to generate sustainable circular economies [24-26].

Flax (*Linum usitatissimum L*.) is a worldwide cultivated plant, mainly for obtaining fibers and oil-rich seeds [27]. It is estimated that the world production of flaxseed, also known as linseed, was approximately 3.2 million tons during 2018 [28]. Traditionally flaxseeds have been used as an oil source, due to its high triglyceride content (between 30 and 41 wt %), for use in paints and coatings, linoleum, inks, varnishes, cosmetics, soap production, among others [29,30]. However, over the past few years, the flaxseed oil has also gained popularity as a nutritional supplement due to its high content of α-linolenic acid (ALA), an omega-3 fatty acid beneficial in preventing cardiovascular disease or hypertension [31]. In addition, many studies have shown that flaxseed oil has a positive effect on diseases such as hyperlipidaemia, colon and breast cancer, or atherosclerosis [32]. The main by-product generated during oil extraction is flaxseed

cake, which is the solid mass left after the seeds are pressed during the oil extraction process. For this reason, flaxseed cake is widely available and, a cost-effective and environmentally friendly material to be used in composites [33]. The flaxseed cake is rich in cyanogenic glycosides, which may be degraded to toxic hydrogen cyanide (HCN) upon ingestion and may represent a risk to human health if used in food applications without prior detoxification treatment [31]. For this reason, currently, a part of this by-product is spray-dried to obtain flour (flaxseed flour), which is used as a low-value by-product for obtaining livestock feed or fertilizers [34,35]. In other cases, this waste is used for composting or simply incinerated [36]. Therefore, the flaxseed flour can potentially be a candidate for use in composites.

Furthermore, a significant part of the plastic matrices used in WPCs is thermoplastic petroleum-derived polymers such as polypropylene (PP), polyethylene (PE), polystyrene (PS), polyvinylchloride (PVC), among others. However, there has been a tendency in recent years to replace these matrices by biobased and biodegradable (actually soil compostable) polymers such as polylactic acid (PLA) or polyhydroxyalkanoates (PHA) [37], to achieve fully biodegradable WPCs. Natural fiber reinforced plastics (NFRP) represent a wider group that includes WPCs and thermosetting-based composites, as well. For thermosetting resins, this trend is focused on the use of fully or partially biobased resins [38-42]. With this, it is possible to reduce the dependence on fossil fuels. Besides this, these fully/partially thermosetting resins, positively contribute to reducing the carbon footprint generated by their petrochemical counterparts such as phenolics (PF), epoxies (EP), or unsaturated polyesters (UP). A promising source for biobased epoxy resins and plasticizers are epoxidized vegetable oils, which are obtained by epoxidizing the C-C double bonds of unsaturated fatty acids contained in triglycerides, the main component of vegetable oils [43-45]. However, due to the long aliphatic chains in the triglycerides and their low cross-linking density, epoxy resins obtained from vegetable oils tend to have low glass transition temperatures (T_g) and lower mechanical properties than traditional epoxy resins [46]. Therefore, to obtain environmentally friendly materials with balanced mechanical and thermal properties, one of the most efficient approaches is copolymerization of epoxidized vegetable oils with petroleum-derived epoxy resins, thus giving rise to a partially biobased epoxy resin with high mechanical properties [47]. Niedermann, *et al*. [48] investigated the effect of the epoxidized soybean oil (ESO) content (0, 25, 50, 75, and 100 wt %) on bisphenol-A based aromatic epoxy resin (DGEBA). The results showed a decrease in T_g as the ESO content increased but indicated that T_g of the DGEBA/ESO system (75/25) was very similar (138 °C) to the base DGEBA resin (140 °C). Obviously, this was remarkably

higher than the T_g of neat crosslinked ESO (75 °C). Similar trends were also observed for mechanical properties such as tensile strength and impact energy, where the addition of 25 wt % ESO decreased the mechanical properties of DGEBA resin but made them more resistant than ESO resin. Regarding the manufacturing of materials with these cast resins, Wu, *et al.* [49] reported impregnation bamboo with epoxy with previous delignification processes to obtain almost transparent bamboo goods. Salasinska, *et al*. [50], reported new environmentally friendly composites with epoxy resins and *Pinus sibirica* lignocellulosic fillers at a constant wt % of 20 %. These composites were manufactured at a laboratory scale by mixing the components and finally, a conventional cast method was used to pour the liquid mixture into a mold. Casting is the most widely used method to manufacture composites with thermosetting resins and lignocellulosic particles. Kumar, *et al.* [51] reported manufacturing by casting and characterization of epoxy composites with up to 12.5 wt % wood particles. Centrifugal casting is a way to obtain gradation of the filler due to centrifugal forces as reported by Stabik and Chomiak [52]. They report that as well as the particle gradation occurs, gradation of properties occurs too which could be interesting from different standpoints (decorative, percolation thresholds in some parts, and so on.

The main objective of the present work was to obtain green composites from a partially biobased epoxy resin reinforced with flaxseed flour waste using the casting method. Specifically, the effect of particle size and the content of flaxseed flour on the mechanical, morphological, thermal, and water absorption properties of the bioepoxy/flaxseed flour composites, has been investigated. In the present work, four compositions (10, 20, 30, and 40 wt %) and two-particle sizes (CFF and FFF) were investigated.

III.2.4.2. Experimental

Materials

The matrix material used in this study was a commercial epoxy resin Resoltech® 1070 ECO (viscosity of 1750 mPa s and a density of 1.18 g cm^{-3} at 23 °C). The hardener was an amine-based system Resoltech® 1074 ECO (viscosity of 50 mPa s and density of 0.96 g cm^{-3} at 23 °C). Both were supplied by Castro Composites (Pontevedra, Spain). The epoxy resin was based on a mixture of a diglycidyl ether of bisphenol A (DGEBA) and a plant-based epoxy reactive diluent from vegetable oil epoxidation. The resin to hardener weight ratio was 100:35 (parts by weight), and as

indicated by the supplier the cured resin contained 31 wt % biobased content (according to ASTM D6866-12).

Flaxseed (FS) used in this work was supplied by Sorribas S.A. (Polinyà, Spain). The raw FS was crushed in a grinder (Moulinex, Allençon, France) to obtain flaxseed flour (FF) with an average particle size of 157 µm (CFF-coarse flaxseed flour). Then, a part of the obtained CFF was ground using an ultra-centrifugal mill from Retsch Gmbh model Mill ZM 1000 (Haan, Germany) with a sieve of 250 µm and a rotating speed of 10,000 rpm, obtaining FF with an average particle size of 91 µm (FFF-fine flaxseed flour). Figure III.2.4.1 shows an image of the raw FS and the obtained FF after each of the grinding processes.

Figure III.2.4.1. Images corresponding to (**a**) raw flaxseeds (FS); (**b**) flaxseed flour (FF) obtained by grinder (CFF); (**c**) flaxseed flour (FF) obtained by ultracentrifuge (FFF).

BioEP/FF Composites' Manufacturing

Different contents (10, 20, 30, and 40 wt %) of CFF and FFF were added to the liquid epoxy resin Resoltech® 1070 ECO and were mixed at room temperature in a planetary mixer KAPL 5KPM5 from KitchenAid (Benton Harbor, MI, USA) with a total volume of 4.8 L. First, the FF was added to the mixer with the biobased resin and was subjected to initial homogenization at 40 rpm for 5 min. Then, Resoltech® 1074 ECO hardener was added in the stoichiometric ratio (100:35 wt/wt) to the BioEP/FF mixture and subjected to a second mixing cycle at 60 rpm for 2.5 min. After this two-stage mixing cycle, the resin was subjected to vacuum to remove air bubbles in a vacuum chamber MCP 00ILC from HEK-GmbH (Lubeck, Germany) for 5 min. A maximum vacuum of -1 bar was applied. The resulting resin-filler mixture was poured into a silicone mold designed with standardized cavities for mechanical characterization and then subjected to a curing cycle in an oven at 80 °C for 1 h. Cured samples were post-cured at 150 °C for 30 min. The optimal curing and post-curing conditions of the partially biobased epoxy resin were selected according to a previous study [53]. Finally, cured samples were demolded from the silicone molds and used for different characterizations.

The nomenclature of the samples is denoted with the acronym BioEP_iCFF for samples with FF obtained by a simple grinding process, and BioEP_iFFF for samples reinforced with FF obtained by using an ultra-centrifugal mill, where *i* represents the filler content (10, 20, 30 and 40 wt %).

BioEP/FF Composites' Characterization

Mechanical Properties

Flexural properties of BioEP resin and BioEP/FF composites were obtained at room temperature in a universal test machine Ibertest ELIB 30 (S.A.E. Ibertest, Madrid, Spain) equipped with a 5 kN load cell following the guidelines of the ISO 178. Rectangular samples with dimensions 80 x 40 x 4 mm^3 were subjected to a three-point bending flexural test with a crosshead speed of 5 mm min^{-1}. At least five specimens of each composition were tested, and characteristic average values were calculated.

Impact-absorbed energy of different samples was obtained in a 1-J Charpy's impact pendulum from Metrotec S.A. (San Sebastián, Spain) as indicated in ISO 179:1993. The values of the impact-absorbed energy of each sample were calculated as the average of the energies obtained for five different specimens.

Shore D hardness values of BioEP resin and BioEP/FF composites were obtained with a Shore D hardness durometer model 676-D from J. Bot Instruments S.A. (Barcelona, Spain) according to ISO 868. At least five different measurements were taken at room temperature, and average values were calculated.

Thermal Properties

Thermal stability at elevated temperatures of BioEP and BioEP/FF composites was studied by thermogravimetric analysis (TGA) using a TGA/SDT 851 thermobalance from Mettler-Toledo Inc. (Schwerzenbach, Switzerland). Samples with an average weight ranging from 7 to 9 mg were heated from 30 to 700 °C at a constant heating rate of 10 °C min^{-1}. All samples were tested in triplicate in a nitrogen atmosphere with a constant nitrogen flow rate of 66 mL min^{-1}. The onset degradation temperature (T_0) was assumed at a weight loss of 5 wt %, and the maximum degradation rate temperature (T_{max}) was obtained as the corresponding peak in the first derivative from TGA curves (DTG).

Thermo-Mechanical Properties

Dynamic mechanical thermal analysis (DMTA) of BioEP and BioEP/FF composites was carried out in torsion mode in an oscillatory rheometer AR G2 by TA Instruments (New Castle, DE, USA) equipped with a special clamp system for solid samples working in a combination of torsion and shear. Rectangular samples (40 x 10 x 4 mm^3) were subjected to a temperature sweep program from 30 °C to 140 °C at a constant heating rate of 2 °C min^{-1}. The frequency of the dynamic stress was set to 1 Hz, and a maximum shear strain (γ) of 0.1 % was used in all tests. The evolution of the storage modulus (*G'*) and the dynamic damping factor (*tan δ*) were recorded as a function of increasing temperature.

The effect of temperature on the dimensional stability of BioEP/FF composites was studied by thermomechanical analysis (TMA) using a Q400 TMA analyzer from TA Instruments (New Castle, DE, USA). Samples with dimensions of 4 x 10 x 10 mm^3 were subjected to a heating ramp from 0 °C to 140 °C, at a constant heating rate of 2 °C min^{-1}, with an applied load of 20 mN. The coefficient of linear thermal expansion (CLTE) was calculated as the slope of the linear relationship between the expansion and temperature, both below and above T_g. All measurements were done in triplicate to obtain reliable values.

Morphological Properties

The morphology of fractured surfaces from an impact test of BioEP resin, different BioEP/FF composites, and flaxseed flour particles was observed using a field emission scanning electron microscope (FESEM) ZEISS model ULTRA55 (Eindhoven, The Netherlands) working at an acceleration voltage of 2 kV. Before the morphological characterization, all samples were surface coated with a thin layer of platinum in a high vacuum sputter coater EM MED20 from Leica Microsystems (Milton Keynes, UK) to provide electrical conductivity to samples.

Water Uptake

Water absorption of samples was carried out in triplicate by immersion of samples (80 x 10 x 4 mm^3) in distilled water at room temperature following ISO 62:2008. Samples were extracted at different times and appropriately weighed using an analytical balance with an accuracy of ± 0.001 g, after removing the residual water with a dry cloth. Before the initial water immersion, samples were dried at 60 °C for 24 h to remove residual

moisture. Water absorption percentage was calculated by using the following expression:

Water absorption of samples was carried out in triplicate by immersion of samples (80 x 10 x 4 mm^3) in distilled water at room temperature following ISO 62:2008. Samples were extracted at different times and appropriately weighed using an analytical balance with an accuracy of ± 0.001 g, after removing the residual water with a dry cloth. Before the initial water immersion, samples were dried at 60 °C for 24 h to remove residual moisture. Water absorption percentage was calculated by using the following expression:

$$Water\ uptake\ (\%) = \left[\frac{(W_t - W_0)}{W_0}\right] 100 \quad \text{(III.2.4.1)}$$

where W_t is the dry weight of the sample after the corresponding time *t*, and W_0 is the initial weight of the sample before water immersion. The evolution of water uptake was followed in a total period of 12 weeks.

The diffusion coefficient (*D*) for all samples was calculated by the application of the first Fick's law using the following equation [54]:

$$D = \pi \left[\frac{m\ h}{4}\right]^2 \quad \text{(III.2.4.2)}$$

where *m* is a slope value, that can be calculated from the plot of W_t/W_s (dry weight after the corresponding time/saturation weight of the sample) versus $t^{1/2}$, and *h* stands for the initial thickness of the sample.

The previous equation for the calculation of *D* is only valid for a one-dimensional shape. To obtain the accurately corrected diffusion coefficient (D_c) for three-dimensional shapes, the Stefan approximation was applied, which assumes that the diffusion rates are the same for all directions [18]:

$$D_c = D\left[1 + \frac{h}{L} + \frac{h}{w}\right]^{-2} \quad \text{(III.2.4.3)}$$

where *L* and *w* are the length and width of each sample, respectively.

Color Properties

The influence of the FF content and size in the color of BioEP/FF composites were studied in a colorimeter model KONICA CM-3600d Colorflex-DIFF2 from Hunter Associates Laboratory (Virginia, EEUU). The CIELab color scale was used to measure the degree of *L** (lightness), *a** (color coordinate from red to green) and *b** (color coordinate from yellow to blue). The total color difference (*ΔE*) was calculated using the following equation:

$$\Delta E = \sqrt{(\Delta L^*)^2 + (\Delta a^*)^2 + (\Delta b^*)^2} \quad \text{(III.2.4.4)}$$

where Δ*L**, Δ*a**, and Δ*b** are the differences between the corresponding color parameter of the composites and the color parameter values of the reference material, i.e., BioEP matrix. Measurements were done in triplicate.

III.2.4.3. Results and Discussion

Morphology of FF Particles

Figure III.2.4.2 shows the FESEM images of the flax flour powder, as well as the particle size distribution after each grinding process. Figure III.2.4.2 includes representative images of each particle size at different magnifications while the particle size distribution plots were obtained by taking at least 50 measurements on different FESEM images corresponding to each particle size, namely fine (F) or coarse (C), using the software analysis included in the FESEM microscope. The following parameters were obtained (area, angle, and length), and the histogram plots included the length.

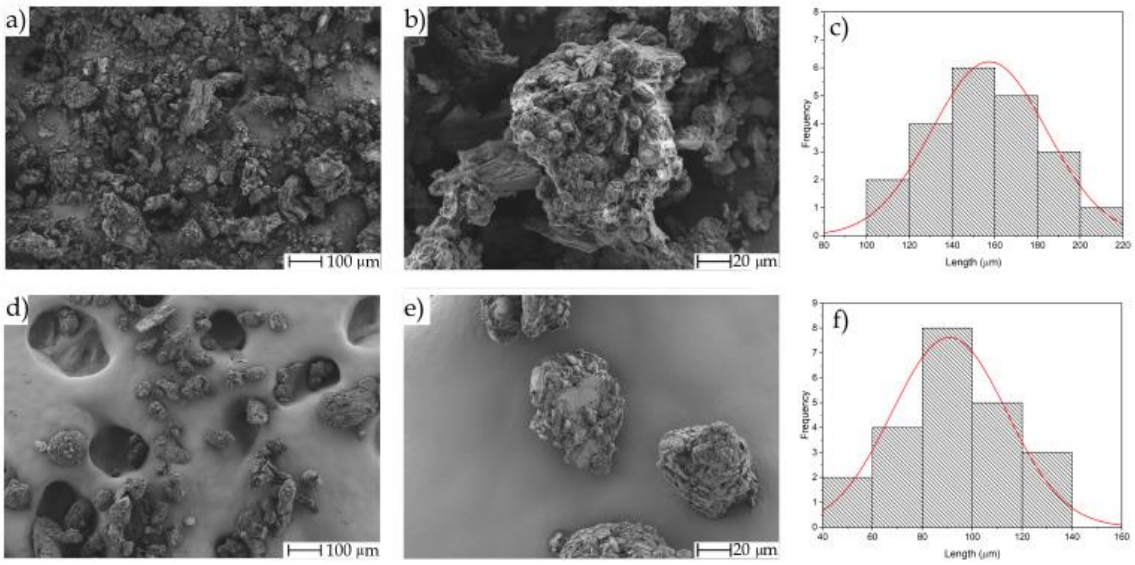

Figure III.2.4.2. Field emission scanning electron microscope (FESEM) images corresponding to (**a**) CFF at x100 with a scale marker of 100 µm; (**b**) CFF at x500 with a scale marker of 20 µm; (**c**) particle size histogram of CFF; (**d**) FFF at x100 with a scale marker of 100 µm; (**e**) FFF at x500 with a scale marker of 20 µm; (**f**) particle size histogram of FFF.

As can be seen in the FESEM images at lower magnifications (figure III.2.4.2a,d), coarse particles obtained by simple grinding (CFF) as well as fine flax flour particles with smaller dimensions (FFF), tend to form aggregates due to their high hydrophilicity. Quantitatively we can see from the size distribution made by measuring randomly chosen particles (figure III.2.4.2c,f), that CFF offers a particle size of 100-220 µm with an average particle size around 157 µm and remarkably higher particle content in the 140-160 µm range. On the other hand, FFF particle distribution shows that their size changes in the 40-140 µm range with smaller average particle size, of about 91 µm, and the most abundant content of particles is in the range of 80-100 µm. Therefore, it is evident that with the grinding of FF by ultra-centrifugation, finer particle sizes were obtained, which resulted in a better filler dispersion in the matrix, as well as improved polymer-filler interactions, with a positive effect on the general properties of the developed composites.

The grinding process has a relevant effect on both particle aggregate and geometry. Despite this, these differences can be seen in figure III.2.4.2 since in general, both CFF and FFF particles had an irregular morphology with a rough surface and the presence of granular fractures (typical morphology of hard lignocellulosic particles after being subjected to crushing processes [54-56]). Figure III.2.4.3 shows in a more detailed way the above-mentioned effects. Figure III.2.4.3a shows the morphology of directly ground flax particles after the cold press process. One can see these particles show very irregular shapes. Moreover, it is possible to find particles with high size and very small particles. This is because no particle size separation has been carried out after this

grinding process which led to coarse flax flour (CFF). In addition, aggregate formation is evident (in fact, the adhesive carbon tape cannot be seen).

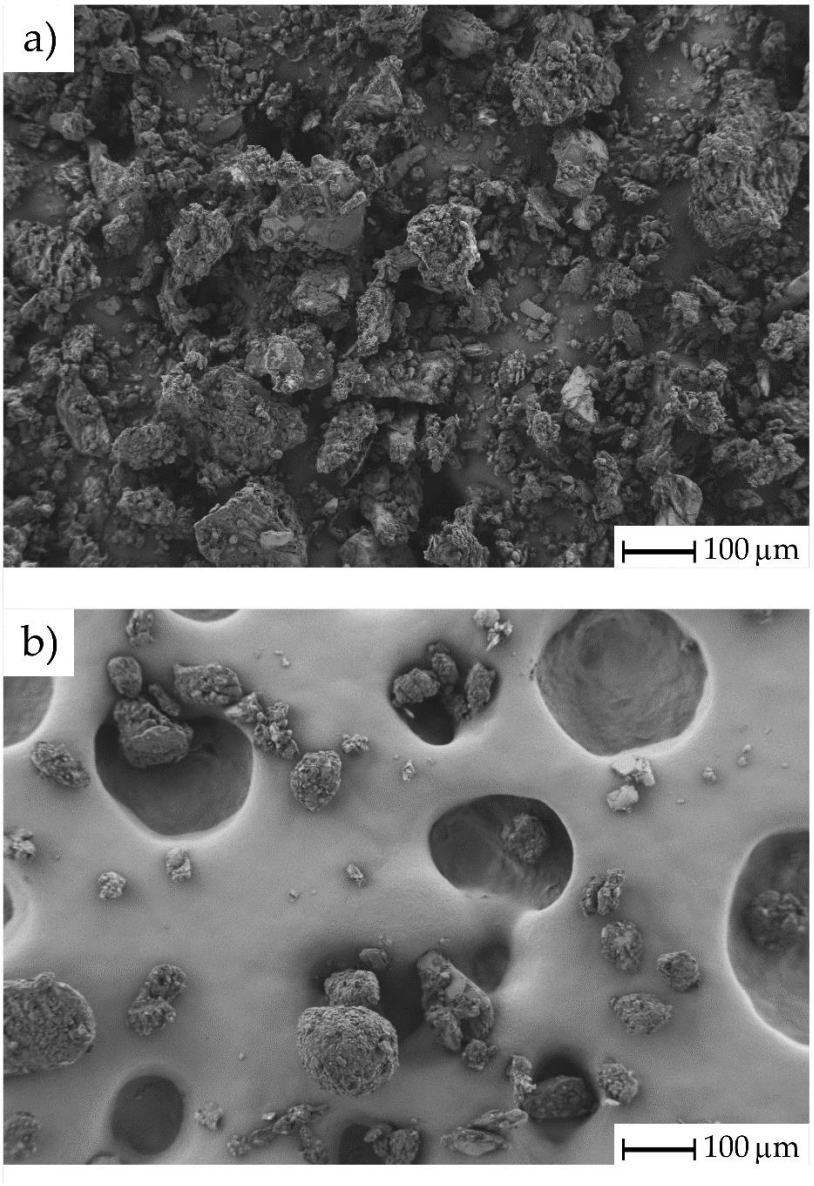

Figure III.2.4.3. FESEM images corresponding to (**a**) CFF at x100 with a scale marker of 100 µm; (**b**) FFF at x100 with a scale marker of 100 µm.

Regarding fine flax flour (FFF), as shown in figure III.2.4.3b, it is evident that the shape is more likely spherical, the particle size range is narrower, and the aggregation phenomenon is less pronounced. The sieving process after ultra-centrifugation gives more homogeneity on the obtained morphologies and less aggregation.

Mechanical Properties

Table III.2.4.1 shows the mechanical behavior of unfilled BioEP resin and BioEP/FF composites reinforced with different contents of CFF and FFF. Regarding the flexural properties, it can be seen that FF addition to the BioEP matrix results in a significant decrease in flexural strength compared to the unfilled BioEP resin. This decrease is much more pronounced as the FF content (both CFF and FFF) increases. As expected, the lowest flexural strength is obtained in composites reinforced with 40 wt % of CFF and FFF, obtaining a flexural strength of 22.5 and 22.9 MPa, respectively, which represents a decrease of 76.4 % and 75.9 % in comparison to the flexural strength of the unfilled BioEP resin (95.2 MPa). This decrease in flexural strength is due to the lack of adhesion between the lignocellulosic filler and the surrounding matrix, which causes stress concentration phenomena that promote breakage [20]. Another issue with a high influence on the mechanical properties of composites is the filler aspect ratio. High filler aspect ratios (above 6) result in a better stress transfer from the matrix to the filler/reinforcement, thus improving their mechanical properties. However, this stresses transfer is poorer in the case of low aspect ratio filler, such as the FF used, with an aspect ratio comprised between 1-2 [57]. If the two types FF, i.e., coarse and fine FF (CFF and FFF, respectively) are compared, it can be seen that the flexural strength is always lower for all composites containing CFF. This is because the bigger particle size causes a larger weak interfacial area between the BioEP resin and the reinforcement, i.e., it decreases the adhesion between the hydrophobic matrix and the hydrophilic reinforcement which generates an increase in the stress concentration phenomena that negatively affect the mechanical properties of composites [58]. The biggest difference in flexural strength between composites with CFF and FFF is obtained for samples with 10 wt % of FF. For this composition, the flexural strength was 24.2 % higher for FFF-reinforced composite compared to CFF-reinforced composite.

Table III.2.4.1. Summary of the main mechanical properties of BioEP and BioEP/FF composites reinforced with different content of coarse (CFF) and fine (FFF) flaxseed flour particles obtained by flexural, impact, and hardness tests.

Code	Flexural Properties		Impact Energy ($kJ\ m^{-2}$)	Hardness (Shore D)
	FS (MPa)	E_f (MPa)		
BioEP	95.2 ± 3.4	2985 ± 115	21.8 ± 3.4	83.2 ± 1.0
BioEP_10CFF	40.4 ± 1.3	2840 ± 242	2.7 ± 0.9	83.3 ± 0.6
BioEP_20CFF	31.5 ± 0.5	2878 ± 86	2.6 ± 0.6	82.3 ± 1.0
BioEP_30CFF	28.0 ± 2.0	2930 ± 93	2.4 ± 0.2	82.2 ± 1.0
BioEP_40CFF	22.5 ± 0.8	2290 ± 127	2.2 ± 0.3	81.0 ± 1.0

BioEP_10FFF	50.2 ± 1.4	3579 ± 53	3.6 ± 0.5	83.3 ± 1.0
BioEP_20FFF	38.7 ± 7.0	2975 ± 84	3.4 ± 0.1	83.7 ± 0.5
BioEP_30FFF	31.8 ± 1.5	2696 ± 20	2.7 ± 0.4	83.0 ± 1.1
BioEP_40FFF	22.9 ± 2.4	2108 ± 204	2.4 ± 0.2	81.6 ± 0.8

Regarding the flexural modulus, different trends can be observed for each of the fillers. The flexural modulus of CFF-reinforced composites is hardly affected by 10, 20, and 30 wt % filler and the modulus values are similar to those obtained for BioEP resin (2840–2985 MPa). However, the flexural modulus of the composite reinforced with 40 wt % CFF decreases significantly to 2290 MPa, representing a decrease of 23.3 % compared to the unfilled BioEP resin. This is directly related to an embrittlement process which is much more evident at higher filler loadings. It is important to bear in mind that the flexural modulus is directly related to the supported stress and inversely related to the flexural deformation. BioEP is intrinsically brittle, therefore, the change in the flexural deflection before fracture is very low. This is even reduced in BioEP/FF composites, but the most important parameter is a clear decrease of the flexural strength from 95.2 MPa down to 22.9 MPa. For this reason, at 40 wt % CFF, the modulus decreases in a remarkable way since the flexural stress is remarkably reduced while the elongation is almost identical to neat BioEP, which is an intrinsically brittle material.

In the case of FFF-reinforced composites, the addition of 10 wt % FFF to the BioEP matrix significantly increases the flexural modulus from 2985 MPa (unreinforced BioEP) resin up to 3579 MPa, which is an increase of nearly 20 %. This increase in the flexural modulus compared to the 10 wt % CFF reinforced composite may be due to the better dispersion of fine particles into the matrix and improved polymer-particle interaction due to its smaller size, which results in comparatively higher flexural strength values, and consequently higher modulus and stiffness. It should be noted that the sample reinforced with 10 wt % FFF has similar and even higher flexural mechanical properties than those obtained in commercial WPCs currently used in furniture applications [59,60]. For higher FFF contents, it is observed that the flexural modulus decreases as the reinforcement content increases, obtaining the lowest modulus for the sample reinforced with 40 wt % FFF, 2108 MPa, which shows the same behavior above-mentioned.

Regarding the impact energy (Charpy test), it can be seen in table III.2.4.1, that the incorporation of both CFF and FFF in the BioEP resin results in a remarkable decrease in impact-absorbed energy from 21.8 kJ m^{-2} corresponding to the unfilled

BioEP resin to values around 3 kJ m^{-2} for FF reinforced composites. This behavior is typical of polymeric composites filled with lignocellulosic particles due to the lack of (or very poor) interfacial adhesion between the reinforcement and the matrix, which gives rise to stress concentration points, promoting the formation of microcracks at the interface when impact conditions are applied that easily induce crack propagation, thus decreasing their impact resistance [61,62]. Impact energy absorption is also influenced by the filler content in the matrix. As can be seen, the impact energy absorption becomes lower as the reinforcement content increases, obtaining the lowest impact-absorbed energy for composites reinforced with 40 wt % CFF and FFF, with an impact energy of 2.2 and 2.4 kJ m^{-2} respectively, which represents a decrease of nearly 90 % in both cases with respect to the BioEP resin. This decrease in impact energy with the higher filler content is due to the greater lack of interaction between the filler and the matrix, which results in a higher void content, thus increasing the stress concentration phenomena. Particle size is another factor affecting the impact of energy absorption. When comparing the composites, the energy absorption values for the different percentages of reinforcement are slightly lower in the case of CFF-reinforced composites. This is because the coarse particles have less dispersion in the matrix as well as a larger surface area that leaves a greater amount of surface-exposed between the filler and the matrix, negatively affecting the mechanical properties [63]. It is worthy to note that the better results regarding mechanical properties, obtained with FFF were expected as the morphology of FFF is rounded (almost spherical in most cases) while CFF show very irregular shapes with angular geometries that contribute to micro crack formation and subsequent growth.

Regarding the Shore D hardness, it can be seen in Table III.2.4.1 that the incorporation of the FF filler into the BioEP matrix hardly affects hardness. Only a slight decrease is seen in samples reinforced with 40 wt % CFF and FFF, in which a hardness of 81.0 and 81.6 Shore D, respectively, was obtained, which means a decrease of 2.6 % and 1.9 %, respectively, in comparison to the BioEP resin hardness (83.2 Shore D). The slight decrease in hardness in composites reinforced with a high amount of FF may be due to the lower lignocellulosic reinforcement hardness compared to the thermosetting matrix used [58]. By considering these mechanical properties, it seems that composites with 10 wt % FFF offer the best-balanced properties. Despite this, other compositions must not be discarded as they offer a higher biobased content and wood-like surface finish. Obviously, these high wt % FF composites would not be suitable for technical applications since there brittle and with low tensile strength, but they can find interesting applications in the decorative sector and leather goods (buckles, buttons, among others).

Thermal Properties

The thermal stability at high temperatures of FF, BioEP resin, and different BioEP/FF composites was obtained by thermogravimetric analysis (TGA). The temperature effect on the mass of each sample is shown in table III.2.4.2, while figure III.2.4.**4** shows the corresponding TGA and DTG curves for FF, BioEP resin and BioEP/FF with varying CFF and FFF content from 10 to 40 wt %.

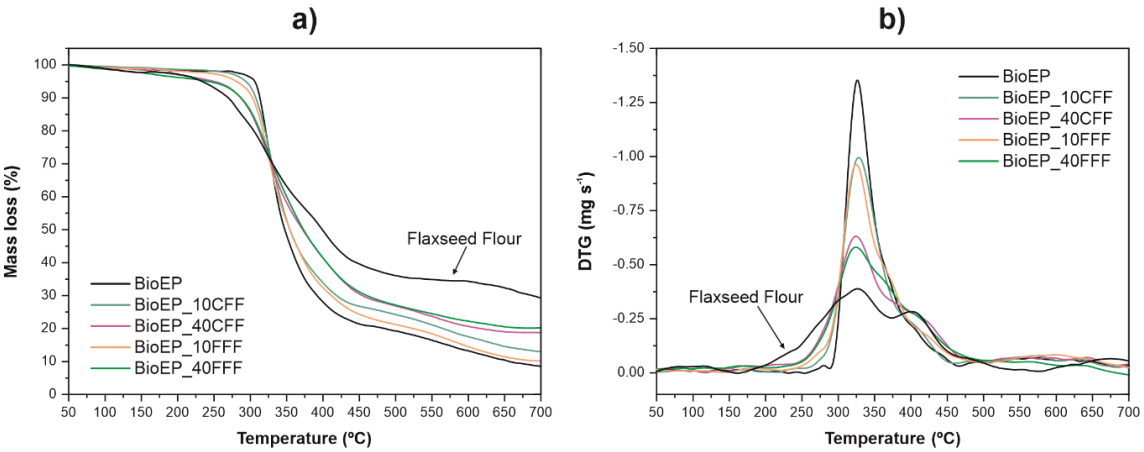

Figure III.2.4.4. Thermal degradation of BioEP, FF, and BioEP/FF composites reinforced with a different content of coarse (CFF) and fine (FFF) flaxseed flour (**a**) thermogravimetry (TG) weight loss and (**b**) differential thermogravimetry (DTG) first derivative curves.

Table III.2.4.2. Thermal parameters of BioEP and BioEP/FF composites reinforced with different contents of coarse (CFF) and fine (FFF) flaxseed flour, obtained by thermogravimetry (TGA).

Code	T_0[1] (ºC)	T_{max} (°C)	Wt % residual mass
BioEP	306.0 ± 2.1	327.5 ± 1.7	8.5 ± 0.3
BioEP_10CFF	292.7 ± 2.8	322.2 ± 2.5	12.9 ± 0.4
BioEP_20CFF	273.7 ± 1.9	322.2 ± 1.9	13.5 ± 0.5
BioEP_30CFF	268.0 ± 3.1	322.0 ± 2.5	15.0 ± 0.6
BioEP_40CFF	249.2 ± 2.0	323.2 ± 1.4	18.7 ± 0.6
BioEP_10FFF	279.2 ± 1.0	322.2 ± 1.8	10.1 ± 0.5
BioEP_20FFF	270.1 ± 2.4	323.0 ± 3.2	12.7 ± 0.4
BioEP_30FFF	264.0 ± 1.6	321.1 ± 1.8	15.7 ± 0.3
BioEP_40FFF	244.2 ± 2.2	319.0 ± 2.1	20.3 ± 0.4

[1] T_0, calculated at 5 % mass loss.

As shown in figure III.2.4.4a, the FF showed four typical degradation stages of lignocellulosic materials. In the first stage, produced at 50-150 °C, the moisture contained in the material evaporated, which was reflected by a mass loss of around 2.3 wt % [64]. In the second stage thermal depolymerization of hemicelluloses took place in the

temperature range from 150 to 375 °C with a weight loss of about 41.4 % [65]. In the third stage, which was located at 375-450 °C, cellulose degradation occurred, this stage being observed by a weight loss of 18.9 % [61]. Finally, the lignin degradation was detected, which begins at around 250 °C, but due to its complex structure, it degraded more slowly, producing a progressive weight loss up to 500 °C. Its decomposition being overlapped with that of other compounds [14]. As shown in the TGA graph, the residual mass of FF was high, which can be due to its high mineral content [66]. On the other hand, as can be seen in table III.2.4.2, the thermal degradation of the BioEP resin occurred in a single step, starting its degradation (T_0) around 306 °C and with a maximum degradation temperature (T_{max}) of 327.5 °C. Regarding BioEP/FF composites degradation, it can be seen that the FF filler addition to the matrix results in a slight decrease of the composites' thermal stability, which is reflected by a T_0 decrease.

This is due to the low thermal stability of the lignocellulosic reinforcement, whose degradation onset temperature begins around 234 °C, which affects the overall thermal stability of composites negatively. Besides, the increased filler content in composites results in a reduced weight fraction of the BioEP resin, causing a more significant decrease in T_0 as the filler content increases [20]. Comparing the two types of composites obtained according to the filler size, it can be seen that the thermal stability was slightly lower, i.e., lower T_0, for composites with different FFF contents. This lower thermal stability was more evident for composites with 10 wt % FFF, where a decrease in T_0 of 27 °C compared to the T_0 of the BioEP resin can be observed, while this decrease is only 13 °C for the same composite containing 10 wt % CFF. By observing the DTG curves (figure III.2.4.4b) it can be seen that the thermal degradation of BioEP/FF composites takes place in two stages. These stages were more evident in the reinforced samples with high filler contents (40 wt %). In the first stage, BioEP resin was thermally degraded along with the low molecular weight components of FF such as hemicelluloses, while in the second stage the thermal degradation of cellulose and lignin occurred. For this reason, this stage was more evident in composites with high filler content. Regarding the maximum degradation temperature (T_{max}), obtained from the peak of the first degradation stage of the DTG curves, it can be seen that the incorporation of the reinforcement into the BioEP matrix slightly decreases this temperature (it almost remains constant). In this case, the T_{max} of composites did not vary significantly with the particle size or content, obtaining a T_{max} of around 322 °C for all developed composites, except for the composite reinforced with 40 wt % of FFF, which has a T_{max} slightly lower of about 319 °C. Therefore, after thermogravimetric analysis, the results suggest that as the lignocellulosic reinforcement content increases, the thermal stability of the

composites decreases, while the residual mass at high temperatures (700 °C) increases. Nevertheless, the overall thermal stability of these composites is not compromised by incorporating FF in both coarse and fine particle size.

Morphological Properties

The particle dispersion and its interaction with the matrix are two of the main aspects that influence the composite's mechanical properties. To study these phenomena, a morphological study was carried out using FESEM on impact fractured surfaces of BioEP resin and BioEP/FF composites filled with 10 wt % and 40 wt % CFF and FFF. Figure III.2.4.5a shows the BioEP resin fracture surface, which is characterized by a smooth surface with the presence of cleavage planes characteristic of a brittle fracture.

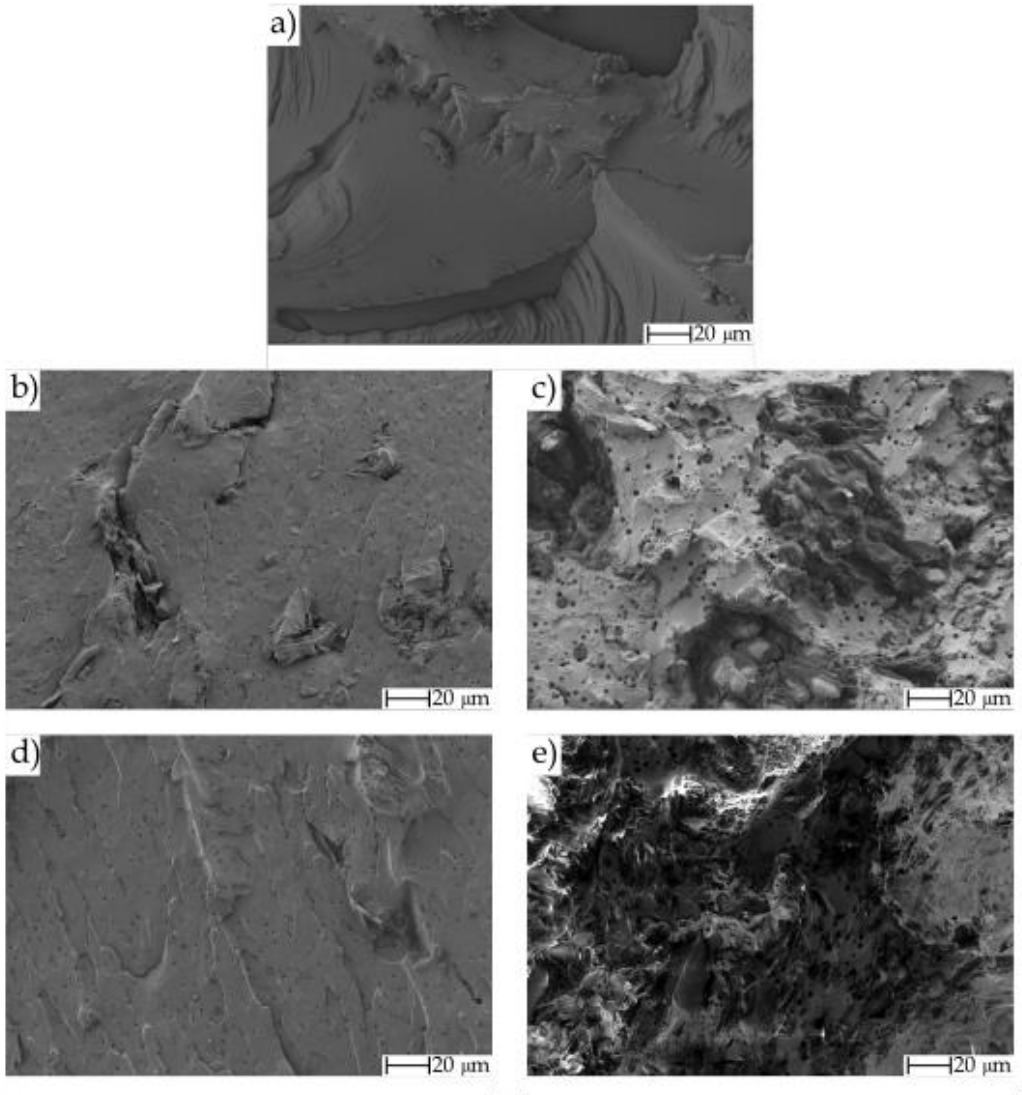

Figure III.2.4.5. FESEM images at x500 of impact-fracture surface of: (**a**) BioEP; (**b**) BioEP_10CFF; (**c**) BioEP_40CFF; (**d**) BioEP_10FFF and (**e**) BioEP_40FFF.

After the addition of 10 wt % of both CFF and FFF filler (figure III.2.4.5b,d), it can be seen that the fracture surface acquires a noticeable roughness, and small holes appear randomly located on the surface, which corresponds to the particles pulled out after the impact test. These voids/holes are representative of poor adhesion between the polymeric matrix and the lignocellulosic filler, which results, as above-mentioned, in low stresses transfer from the matrix to the filler, thus negatively affecting the overall mechanical properties of the obtained composites. Comparing the two types of composites reinforced with 10 wt % FF, it can be seen that fine particles (FFF) reinforced composites, a better particle dispersion in the matrix is achieved due to the smaller particle size, which is reflected in the absence of aggregates in the fracture surface. Such aggregates are observed on the fracture surface of the coarse particles (CFF) reinforced composites, as the larger particle size promotes their aggregation. The higher lack of adhesion between these aggregates and the matrix due to the increase of the exposed surface area intensifies the stress concentration phenomena that negatively affects the mechanical properties, as it has been evidenced by a lower impact energy absorption and lower flexural strength than the composite reinforced with 10 wt % FFF. Higher filler contents (figure III.2.4.5c,e) lead to an increase in the fracture surface roughness with the presence of particles embedded in the matrix. An increase in the size of the voids/holes was also observed, possibly because the higher filler content promoted aggregate formation. This increase in the void size results in reduced interfacial adhesion between the reinforcement and the matrix for composites reinforced with high FF contents, which is reflected in poor mechanical properties. Comparing both composites reinforced with 40 wt % of FF, the presence of large aggregates in the CFF reinforced sample can be seen more clearly, while in the FFF reinforced sample, the dispersion of particles was more homogeneous. Therefore, the increase of the filler content in the matrix results in a significant decrease in ductile and resistant mechanical properties, as shown by the evolution of impact energy absorption and flexural strength, due to a reduction in interfacial adhesion between filler and matrix by a decrease in the resin's ability to fully embed the particles. This also occurs with coarse particles (CFF), which have a higher surface area, exposing more surface area to weak bonding with the matrix, resulting in lower flexural strength and higher water absorption capacity.

Thermo-Mechanical Properties

Figure III.2.4.6 shows the evolution of the storage modulus (*G'*) and the dynamic damping factor (*tan δ*) as a function of the temperature of BioEP resin and BioEP composites reinforced with 10 wt % and 40 wt % of CFF and FFF. On the other

hand, Table III.2.4.3 shows the storage modulus at 40 °C and 110 °C, as well as the glass transition temperature (T_g), obtained from the peak maximum of the *tan δ* curve for all considered composites.

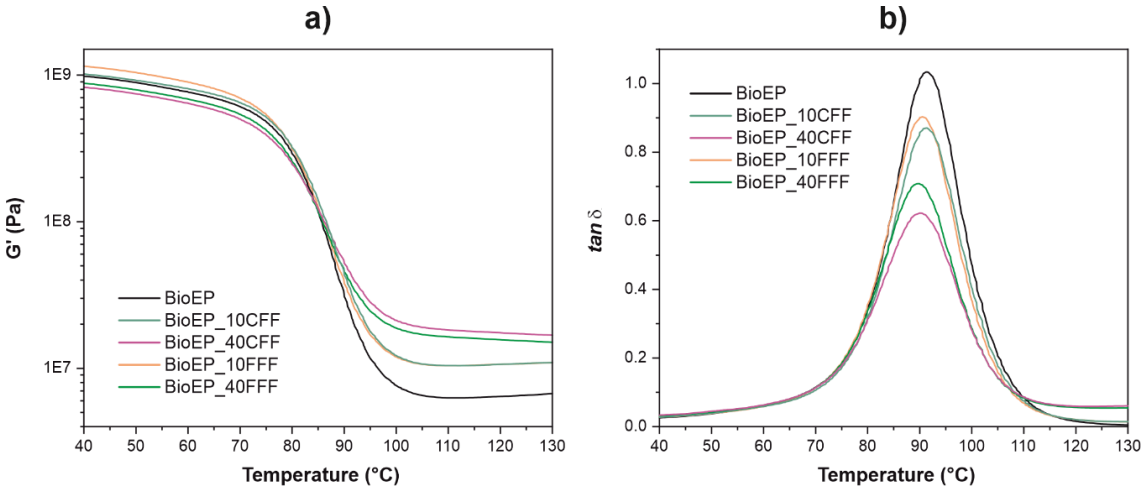

Figure III.2.4.6. A comparative plot of the dynamic mechanical thermal analysis (DMTA) behavior of BioEP and BioEP/FF composites reinforced with CFF (10 and 40 wt %) and FFF (10 and 40 wt %): (**a**) storage modulus (*G'*), and (**b**) dynamic damping factor (*tan δ*).

Table III.2.4.3. Values of dynamic mechanical, thermal analysis (DMTA), and thermomechanical analysis (TMA) of BioEP and BioEP composites reinforced with different CFF and FFF content.

Code	DMTA			TMA	
	***G'* at 40 ºC (MPa)**	***G'* at 110 ºC (MPa)**	**T_g (ºC)**	***CLTE* below T_g (μm m^{-1} K^{-1})**	***CLTE* above T_g (μm m^{-1} K^{-1})**
BioEP	981 ± 25	6.3 ± 0.3	91.8 ± 2.1	0.356 ± 0.008	0.565 ± 0.005
BioEP_10CFF	1015 ±36	10.4 ± 0.2	90.8 ± 2.7	0.395 ± 0.015	0.938 ± 0.005
BioEP_20CFF	1041 ± 58	12.5 ± 0.3	90.7 ± 1.7	0.385 ± 0.002	0.621 ± 0.005
BioEP_30CFF	1091 ± 49	18.4 ± 0.9	89.8 ± 2.5	0.570 ± 0.006	0.813 ± 0.005
BioEP_40CFF	826 ± 30	18.5 ± 0.8	90.2 ± 2.5	0.404 ± 0.010	0.727 ± 0.007
BioEP_10FFF	1147 ± 13	10.4 ± 0.2	89.8 ± 2.1	0.529 ± 0.013	0.824 ± 0.003
BioEP_20FFF	1064 ± 52	11.5 ± 0.3	89.1 ± 1.8	0.380 ± 0.009	0.687 ± 0.006
BioEP_30FFF	935 ± 40	14.1 ± 0.4	89.2 ± 1.6	0.436 ± 0.007	0.635 ± 0.002
BioEP_40FFF	878 ± 24	16.3 ± 0.4	89.9 ± 2.2	0.554 ± 0.002	0.770 ± 0.001

The storage modulus (*G'*) (figure III.2.4.6a) shows different behavior depending on the filler content. As shown in table III.2.4.3, the addition of a lignocellulosic filler into the BioEP resin hardly affects the storage modulus at low temperatures (40 °C), resulting in very similar *G'* values to the unfilled BioEP resin. However, at high temperatures (110 °C), it can be seen more clearly how the filler content leads to an increase in *G'*. As observed in figure III.2.4.6a, *G'* increases as the filler content increases, resulting in more rigid materials as the FF content increases. This is because the particles give rise to a high degree of mechanical restriction since they act as interlock points that reduce the mobility of the polymeric 3D-thermosetting net and their deformation ability. This phenomenon is much more pronounced at high temperatures when the chain motion or vibration is greater [22,61]. Comparing the composites according to the type of reinforcement, it can be seen that the reinforced composites with coarse particles (CFF) have a higher modulus at high temperatures, thus showing their higher capacity to maintain the mechanical load with recoverable viscoelastic deformation at high temperatures compared to the FFF-reinforced composites [56]. Figure III.2.4.6b shows the dynamic damping factor (*tan δ*) evolution regarding temperature. As can be seen, the BioEP resin curve has the highest value of *tan δ*; however, this value decreases as the FF content in the matrix increases.

This decrease is due to the attenuation that the addition of the filler stiff domains causes in the resin since filler particles act as a steric hindrance [56]. As shown in table III.2.4.3, the T_g of the BioEP resin, obtained from the peak maximum of the dynamic damping factor, is around 92 °C. After the addition of the lignocellulosic filler, the T_g remains almost constant, with slight changes due to the restriction that the rigid particles randomly dispersed in the epoxy matrix cause [51]. Comparing both composites, it can be seen that the T_g decrease is slightly higher for FFF-reinforced composites, with a T_g of around 89 °C for all of them, on the other hand, it can be seen that T_g obtained for CFF-reinforced composites is about 90 °C. This slight difference in T_g between the two composites may be because the smaller size of the particles and the greater dispersion of them in the matrix results in greater interaction between the filler and the matrix and, therefore, the mobility of the polymer chains in these regions are more restricted [67]. Despite this hypothesis, the changes in T_g are so slight that it is not possible to hypothesize a remarkable effect of the filler on T_g. In addition, it is worthy to note that FF has been obtained after cold-pressing flaxseed and some residual oil could be present in the flour, thus explaining this slight decrease in T_g [68].

To analyze the dimensional stability of the obtained composites, the coefficient of linear thermal expansion (CLTE) was determined by thermomechanical analysis

(TMA). Table III.2.4.3 shows the CLTE of BioEP resin and FF-reinforced BioEP composites obtained from the slope of the thermal expansion curves in the rubbery (above T_g) and glassy (below T_g) regions. As shown in table III.2.4.3, the BioEP resin shows a low CLTE, both below and above the T_g, characteristic of thermosetting resins, which usually exhibit excellent dimensional stability [69]. As can be seen, the CLTE is lower for all the samples obtained at temperatures below T_g. This is due to the lower mobility of the polymeric chains in the glassy state, which results in low values of linear expansion [70]. Concerning CLTE below T_g, it was observed that the addition of FF filler to BioEP resin increased its value, which evidenced lower dimensional stability of composites with respect to BioEP resin; nevertheless, the dimensional stability of these composites was not compromised since the CLTE values obtained for all composites were still very low. In table III.2.4.3, it can be seen how the CLTE values below T_g in the developed composites did not show any clear trend regarding the filler content. This was also observed for CLTE above T_g, where there was an increase in this value after the addition of FF filler into the BioEP resin, but there was no trend with respect to the filler content used in the matrix. In this case, it can be seen how the lowest dimensional stability of the developed composites was obtained for composites filled with 10 wt % for both types of filler size, CFF and FFF, with CLTE values of 0.938 and 0.824 μm $m^{-1}K^{-1}$ respectively. Despite this slight increase, the dimensional stability of the developed composites was very high compared to conventional WPCs with CLTE values higher than 50 μm m^{-1} K^{-1} [71-73].

Water Uptake Properties

Figure III.2.4.7 shows the evolution of the water absorption over time for BioEP resin and BioEP/FF composites filled with 10 wt % and 40 wt % of CFF and FFF. The water diffusion in the wood plastic composites is based on three different mechanisms, the first one involves the water molecules diffusion inside the micro-voids of the polymeric chains, the second mechanism is based on the water absorption by capillarity inside the voids and defects present at the matrix-filler interface, finally, the third mechanism involves the transport through the micro cracks that appear from the swelling of the fillers, namely, the swelling of the reinforcement produced by the contact with the water gives rise to the appearance of microcracks in the fragile thermosetting resin, which facilitates its penetration in the interface between the filler and the matrix [74]. As can be seen in figure III.2.4.7, the addition of FF into the BioEP resin significantly increased its water absorption capacity, which rose as the reinforcement content in the matrix increased. This could be due to two possible reasons, one of them is to the

hydrophilic nature of the lignocellulosic filler, since cellulose and hemicellulose contain hydroxyl (-OH) groups in their structure that can easily interact with water molecules through hydrogen bonding, thus allowing a path for water entering [61,75]. The other reason is the presence of small voids, pores and microcracks in the internal structure due to the lack of interfacial interaction between the filler and matrix and to the filler swelling. that facilitates the water accumulation in the composite by capillarity [24,76]. By observing the water absorption curves of BioEP/FF composites, two stages can be clearly differentiated. We can see an initial stage with rapid water absorption, followed by a second stage where the curve stabilized into an asymptotic value, thus indicating saturation. Therefore, the water absorption of BioEP/FF composites followed Fickian's diffusion behavior. However, at low immersion times, figure III.2.4.7a, it can be seen how the weight gain in the curves of the composites stops being gradual and a rapid increase in weight appears between 10 and 12 h of immersion in all of them. This can be due to the appearance of deformations or damage to the matrix for that immersion time, such as the appearance of microcracks due to the swelling of the filler or the fiber/matrix debonding [77]. As shown in table III.2.4.4, the water saturation of composites increases as the filler content does. In this case, it can be seen how the water saturation of composites reinforced with 10 wt % of FF (both CFF and FFF) reaches values of 4.8 wt %. Obviously, composites with 40 wt % of FF water saturation are located at about 12.5 wt %, which means an increase in water absorption compared to neat BioEP resin of 114.3 % and 458 % respectively. A comparison of the two types of composites obtained shows that CFF-reinforced composites have a slightly higher water absorption compared to their FFF counterparts. This may be due to the larger particle size of the CFF filler, which results in less interaction with the matrix, producing a higher number of voids within the structure of composites. These voids allow the accumulation of water at the interface between the particle and the matrix thus increasing the absorption capacity of the composites [78]. In addition, the increased contact between FF particles as their size and content in the matrix increases contributes to water absorption by capillarity due to the creation of a percolating path through the filler network [79]. It should be noted that the water absorption of FF waste is lower than that obtained from other agroforestry waste that has been used in similar amounts as reinforcements in thermosetting polymeric matrices, such as peanut shells [63] or palm kernel shell [80]. As can be seen in figure III.2.4.7, there are some slight differences between the sort-term behavior (first 24 h, figure III.2.4.7a) and the long-term behavior (90 days immersion, figure III.2.4.7b). Despite this visual difference, it is worthy to note the scale. For the short-term graph, some specimens do not follow the expected behavior (e.g., BioEP/CFF 10 wt %), but the changes in the water absorption are very low, of about 0.2-0.3 wt %, which could be even

included in the measurement error. In addition, this initial stage (24 h), is very sensitive to the surface, i.e., the presence of particles not fully embedded and directly exposed to water, which could cause these slight changes. The stationary water absorption after 90 days, represents the actual water uptake behavior as all these initial phenomena disappear, and this agrees with the expected behavior in terms of particle size and loading.

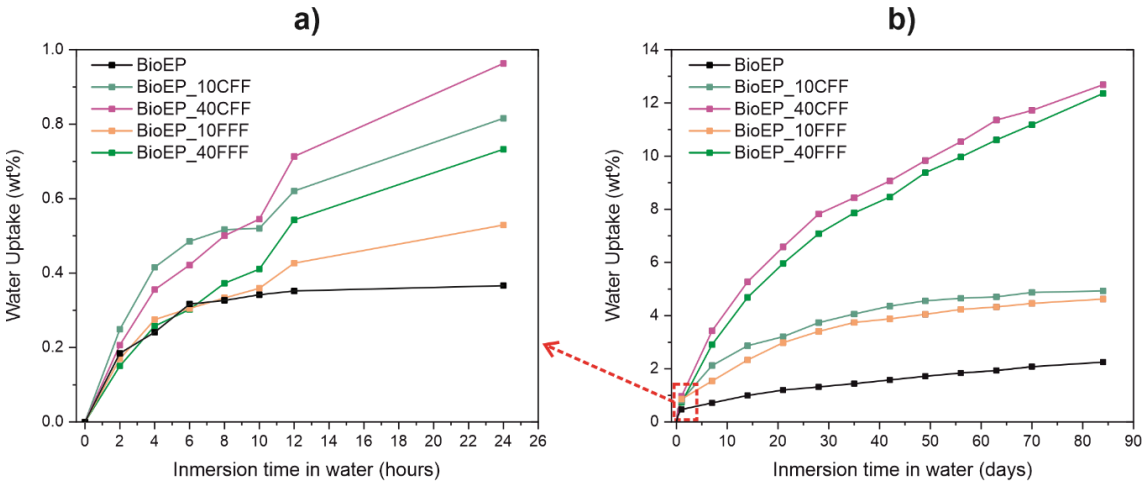

Figure III.2.4.7. Evolution of water absorption over time of BioEP resin and BioEP composites filled with CFF (10 and 40 wt %) and FFF (10 and 40 wt %): (**a**) water absorption during the first 24 h; (**b**) water absorption during a period of 12 weeks.

Table III.2.4.4. Values of water saturation (W_s), diffusion coefficient (D) and the corrected diffusion coefficient (D_c) for BioEP resin and BioEP composites reinforced with different CFF and FFF content.

Code	W_s (*wt %*)	D x 10^{-9} ($cm^2\ s^{-1}$)	D_c x 10^{-9} ($cm^2\ s^{-1}$)
BioEP	2.2 ± 0.0	0.72 ± 0.90	0.36 ± 0.42
BioEP_10CFF	4.9 ± 0.1	1.51 ± 0.40	4.99 ± 2.03
BioEP_20CFF	7.5 ± 0.1	2.07 ± 0.06	6.84 ± 2.9
BioEP_30CFF	8.4 ± 0.2	3.35 ± 0.10	11.1 ± 2.5
BioEP_40CFF	12.7 ± 0.1	4.27 ± 0.05	14.2 ± 0.9
BioEP_10FFF	4.6 ± 0.1	1.38 ± 0.01	4.56 ± 0.2
BioEP_20FFF	6.5 ± 0.1	2.23 ± 0.05	7.37 ± 0.6
BioEP_30FFF	7.7 ± 0.1	2.39 ± 0.04	7.9 ± 0.8
BioEP_40FFF	12.4 ± 0.1	3.39 ± 0.05	11.2 ± 0.9

Table III.2.4.4 shows the values of the saturation by weight (W_s), as well as the diffusion coefficient (D) and the corrected diffusion coefficient (D_c) of BioEP resin and the obtained BioEP/FF composites. The diffusion coefficient is one of the most important parameters of the Fick's model, which is related to the initial diffusion of water molecules

into the matrix surface by entering through external micro-voids towards the internal structure of the composites [81]. As can be seen, the BioEP resin is characterized by a W_s of 2.2 wt %, a D of 0.72 × 10^{-9} cm^2 $s^{-1,}$ and a D_c of 0.36 × 10^{-9} cm^2 s^{-1}. After the incorporation of the highly hydrophilic lignocellulosic residue, it is observed, as expected, that D and D_c increase as the CFF and FFF content does, following the behavior shown by other composites reinforced with natural fillers [18,82,83]. Therefore, it can be concluded that the increase in the amount of lignocellulosic filler increases the ability of water molecules to enter through the composite. Comparing both composites (with CFF and FFF), it can be seen how CFF-filled materials tend to have a higher diffusion coefficient than FFF-filled composites, mainly due to the larger particle size and the more significant presence of voids in the internal structure of the composite due to the lack of matrix-filler interaction [84].

Color Properties

Figure III.2.4.8 shows the resulting visual aspect of BioEP resin and BioEP/FF composites filled with coarse particles-CFF (figure III.2.4,8a) and fine particles-FFF (figure III.2.4.8b) after the curing/post-curing cycle.

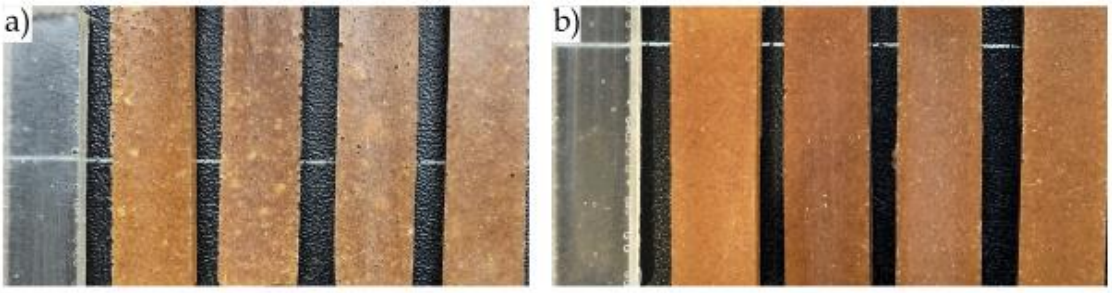

Figure III.2.4.8. Visual aspect of BioEP and BioEP composites reinforced with different FF content; (**a**) (left to right) BioEP resin and BioEP composites reinforced with 10, 20, 30 and 40 wt% of CFF; (**b**) (left to right) BioEP resin and BioEP composites reinforced with 10, 20, 30 and 40 wt % of FFF.

Table III.2.4.5 gathers the color parameters for the BioEP resin and BioEP/FF composites. As can be seen in figure III.2.4.8, BioEP/FF composites obtained by casting show dimensional uniformity as well as a uniform and defect-free surface appearance. This situation is even more evident in composites with FFF. As can be seen, the unfilled BioEP resin sample has some degree of transparency, which is reflected by the low a^* and b^* values. After the addition of the FF filler, composites become brown due to the natural color of the lignocellulosic filler (see figure III.2.4.1), which produces an increase in the values in the a^* and b^* coordinates (table III.2.4.5). As it can be seen

in figure III.2.4.8, and quantitatively analyzed by the CIElab coordinates, the color of composites filled with FF is very similar in all of them except that with 10 wt % of FFF, which presents a lighter brown color, obtaining a lower *ΔE* with respect to the BioEP than the rest of the composites. Comparing both types of composites according to the filler size (CFF or FFF), it can be seen how the surface appearance of FFF-filled composites is much more homogeneous than CFF-filled composites. In the case of CFF-reinforced composites, random whitish spots are present on the surface, which may be due to the formation of large filler aggregates, which negatively affect both aesthetics and mechanical properties. The brown wood color acquired by the samples after the filler incorporation, and the excellent surface appearance acquired mainly in the samples reinforced with FFF can be attractive from the aesthetic point of view for applications in sectors such as furniture, construction, or automotive [85,86].

Table III.2.4.5. Color parameters from the CIELab space of BioEP resin and BioEP composites reinforced with different CFF and FFF content.

Code	*L**	*a**	*b**	*ΔE*
BioEP	39.50	−0.48	1.60	-
BioEP_10CFF	39.51	8.97	19.02	19.82
BioEP_20CFF	40.77	9.51	19.36	20.42
BioEP_30CFF	40.93	9.59	19.54	20.62
BioEP_40CFF	41.48	9.68	19.83	20.97
BioEP_10FFF	35.82	9.61	15.80	17.80
BioEP_20FFF	36.27	9.52	16.83	18.50
BioEP_30FFF	37.77	9.44	17.11	18.49
BioEP_40FFF	39.55	9.63	18.42	19.62

III.2.4.4. Conclusions

The main objective of the present work was to evaluate the influence of FF particle size, i.e., coarse (CFF) and fine (FFF), and the filler content (10, 20, 30 and 40 wt%) on the mechanical, thermal, water uptake and morphological properties of composites of a partially biobased epoxy (BioEP) resin processed by casting. The addition of this lignocellulosic filler into the BioEP matrix resulted in a decrease in flexural strength and impact absorption energy with increasing filler content. This is because of the lack of (or very poor) polymer matrix-particle filler interactions. However, this decrease is lower for composites with finer particles, due to their better dispersion and better interaction with the matrix. In this work, it has been observed that the composite

filled with 10 wt % of FFF presents a flexural strength and impact energy absorption 24.2 % and 33.3 % higher than its counterpart with CFF. Particle size has also a high influence on water absorption. It has been observed that composites with fine particles (FFF) filler offer less water absorption due to the presence of fewer voids in their structure as a result of better dispersion and fewer aggregates. In the case of CFF-filled composites, the larger size increases the lack of adhesion with the matrix generating voids and aggregates that allow the water entering, thus leading to a higher water absorption and diffusion coefficient.

Therefore, the present work has revealed that the finer filler particle size results in better mechanical and water absorption properties in these natural fiber reinforced plastics (NFRPs). Besides, a partially biobased, high environmentally friendly material can be obtained. On one hand, the partial biobased epoxy content (31 wt %) can be increased up to almost 70 wt % renewable origin in composites with 40 wt % FF (both CFF or FFF). In addition, this work has revealed an alternative to upgrading wastes from the flaxseed industry. The developed BioEP/FF composites offer an attractive wood-like aesthetic appearance, and therefore, they can be used in sectors such as decoration, furniture, or the automotive industry.

Once the particle size and the amount of FF have been optimized to obtain more balanced mechanical, thermal and water absorption properties in the BioEP/FF composite, further studies will focus on the use of highly reactive coupling agents, i.e., silanes such as (3-glycidyloxypropyl) trimethoxy silane and (3-aminopropyl) trimethoxy silane, to provide increased interaction between the epoxy matrix and the embedded FF particles. All these steps, including an industrial scalation and cost study will assess the viability of these materials to contribute to the circular economy in the flax industry.

III.2.4.5. Funding

This research was funded by Spanish Ministry of Science, Innovation, and Universities (MICIU), project numbers MAT2017-84909-C2-2-R. This work was supported by the POLISABIO program grant number (2019-A02).

III.2.4.6. Acknowledgments

D. Lascano thanks Universitat Politècnica de València (UPV) for the grant received through the PAID-01-18 program. D. Garcia-Garcia wants to thank Generalitat Valenciana (GVA) for their financial support through a post-doctoral grant (APOSTD/2019/201). S. Rojas-Lema is a recipient of a Santiago Grisolía contract

(GRISOLIAP/2019/132) from GVA. L. Quiles-Carrillo wants to thank GV for his FPI grant (ACIF/2016/182) and MECD for his FPU grant (FPU15/03812). Microscopy services at UPV are acknowledged for their help in collecting and analyzing FESEM images.

III.2.4.7. References

1. A. Capezza, W. Newson, R. Olsson, M. Hedenqvist, E. Johansson. Advances in the use of protein-based materials: toward sustainable naturally sourced absorbent materials. *ACS Sustainable Chemistry & Engineering* **2019**, *7*, 4532-4547.
2. R.P. Babu, K. O'connor, R. Seeram. Current progress on bio-based polymers and their future trends. *Progress in biomaterials* **2013**, *2*, 1-16.
3. J.-Y. Kim, H.W. Lee, S.M. Lee, J. Jae, Y.-K. Park. Overview of the recent advances in lignocellulose liquefaction for producing biofuels, bio-based materials and chemicals. *Bioresource technology* **2019**, *279*, 373-384.
4. T. Boronat, V. Fombuena, D. Garcia-Sanoguera, L. Sanchez-Nacher, R. Balart. Development of a biocomposite based on green polyethylene biopolymer and eggshell. *Materials & Design* **2015**, *68*, 177-185.
5. I. Naghmouchi, P. Mutjé, S. Boufi. Olive stones flour as reinforcement in polypropylene composites: A step forward in the valorization of the solid waste from the olive oil industry. *Industrial Crops and Products* **2015**, *72*, 183-191.
6. N.F. Zaaba, H. Ismail. Thermoplastic/natural filler composites: A short review. *Journal of Physical Science* **2019**, *30*, 81–99.
7. D. Garcia-Garcia, A. Carbonell-Verdu, A. Jordá-Vilaplana, R. Balart, D. Garcia-Sanoguera. Development and characterization of green composites from bio-based polyethylene and peanut shell. *Journal of Applied Polymer Science* **2016**, *133*, 43940.
8. S. Torres-Giner, N. Montanes, O. Fenollar, D. García-Sanoguera, R. Balart. Development and optimization of renewable vinyl plastisol/wood flour composites exposed to ultraviolet radiation. *Materials & Design* **2016**, *108*, 648-658.
9. M. Ghofrani, S. Pishan, M.R. Mohammadi, H. Omidi. A study on rice-husk/recycled high density polyethylene composites–their physical and mechanical properties. *Enviromental Sciences* **2011**, *9*, 99-112.
10. B. Dimzoski, G. Bogoeva-Gaceva, G. Gentile, M. Avella, A. Grozdanov. Polypropylene-based eco-composites filled with agricultural rice hulls waste. *Chemical and Biochemical Engineering Quarterly* **2009**, *23*, 225-230.
11. V.A. Prabu, R.D.J. Johnson, P. Amuthakkannan, V. Manikandan. Usage of industrial wastes as particulate composite for environment management:

hardness, tensile and impact studies. *Journal of environmental chemical engineering* **2017**, *5*, 1289-1301.

12. M. Prabhakar, A.U.R. Shah, K.C. Rao, J.-I. Song. Mechanical and thermal properties of epoxy composites reinforced with waste peanut shell powder as a bio-filler. *Fibers and Polymers* **2015**, *16*, 1119-1124.

13. N. Ikladious, N. Shukry, S. El-Kalyoubi, J. Asaad, S. Mansour, S. Tawfik, R. Abou-Zeid. Eco-friendly composites based on peanut shell powder/unsaturated polyester resin. *Proceedings of the Institution of Mechanical Engineers, Part L: Journal of Materials: Design and Applications* **2019**, *233*, 955-964.

14. L. Quiles-Carrillo, N. Montanes, D. Garcia-Garcia, A. Carbonell-Verdu, R. Balart, S. Torres-Giner. Effect of different compatibilizers on injection-molded green composite pieces based on polylactide filled with almond shell flour. *Composites Part B: Engineering* **2018**, *147*, 76-85.

15. V. Singh, G. Bansal, M. Agarwal, P. Negi. Experimental determination of mechanical and physical properties of almond shell particles filled biocomposite in modified epoxy resin. *Journal of Material Science andEngineering* **2016**, *5*, 2169-0022.

16. P. Liminana, D. Garcia-Sanoguera, L. Quiles-Carrillo, R. Balart, N. Montanes. Development and characterization of environmentally friendly composites from poly (butylene succinate)(PBS) and almond shell flour with different compatibilizers. *Composites Part B: Engineering* **2018**, *144*, 153-162.

17. M. Barczewski, K. Sałasińska, J. Szulc. Application of sunflower husk, hazelnut shell and walnut shell as waste agricultural fillers for epoxy-based composites: A study into mechanical behavior related to structural and rheological properties. *Polymer Testing* **2019**, *75*, 1-11.

18. J. Balart, N. Montanes, V. Fombuena, T. Boronat, L. Sánchez-Nacher. Disintegration in compost conditions and water uptake of green composites from poly (lactic acid) and hazelnut shell flour. *Journal of Polymers and the Environment* **2018**, *26*, 701-715.

19. A.O. Ameh, M.T. Isa, I. Sanusi. Effect of particle size and concentration on the mechanical properties of polyester/date palm seed particulate composites. *Leonardo Electronic Journal of Practices and Technologies* **2015**, *26*, 65-78.

20. H. Sharma, I. Singh, J.P. Misra. Mechanical and thermal behaviour of food waste (Citrus limetta peel) fillers–based novel epoxy composites. *Polymers and Polymer Composites* **2019**, *27*, 527-535.

21. D. Garcia-Garcia, L. Quiles-Carrillo, N. Montanes, V. Fombuena, R. Balart. Manufacturing and characterization of composite fibreboards with Posidonia oceanica wastes with an environmentally-friendly binder from epoxy resin. *Materials* **2018**, *11*, 35.

22. B. Ferrero, V. Fombuena, O. Fenollar, T. Boronat, R. Balart. Development of natural fiber-reinforced plastics (NFRP) based on biobased polyethylene and waste fibers from Posidonia oceanica seaweed. *Polymer Composites* **2015**, *36*, 1378-1385.

23. A. Koutsomitopoulou, J. Bénézet, A. Bergeret, G. Papanicolaou. Preparation and characterization of olive pit powder as a filler to PLA-matrix bio-composites. *Powder technology* **2014**, *255*, 10-16.

24. I. Naghmouchi, F.X. Espinach, P. Mutjé, S. Boufi. Polypropylene composites based on lignocellulosic fillers: how the filler morphology affects the composite properties. *Materials & Design (1980-2015)* **2015**, *65*, 454-461.

25. D. D'Amato, S. Veijonaho, A. Toppinen. Towards sustainability? Forest-based circular bioeconomy business models in Finnish SMEs. *Forest policy and economics* **2020**, *110*, 101848.

26. A.J. Capezza, M. Lundman, R.T. Olsson, W.R. Newson, M.S. Hedenqvist, E. Johansson. Carboxylated wheat gluten proteins: a green solution for production of sustainable superabsorbent materials. *Biomacromolecules* **2020**, *21*, 1709-1719.

27. M. Barczewski, O. Mysiukiewicz, A. Kloziński. Complex modification effect of linseed cake as an agricultural waste filler used in high density polyethylene composites. *Iranian Polymer Journal* **2018**, *27*, 677-688.

28. F.a.A. Organization. Availabe online: https://www.fao.org/home/en/ (accessed on 28/05/2020).

29. Z.-S. Zhang, L.-J. Wang, D. Li, S.-S. Jiao, X.D. Chen, Z.-H. Mao. Ultrasound-assisted extraction of oil from flaxseed. *Separation and Purification Technology* **2008**, *62*, 192-198.

30. M. Yasmeen, S. Nisar, V. Tavallali, T. Khalid. A review of phytochemicals and uses of flaxseed. *Int. J. Chem. Biochem. Sci* **2018**, *13*, 70-75.

31. A.E.-D.A. Bekhit, A. Shavandi, T. Jodjaja, J. Birch, S. Teh, I.A.M. Ahmed, F.Y. Al-Juhaimi, P. Saeedi, A.A. Bekhit. Flaxseed: Composition, detoxification, utilization, and opportunities. *Biocatalysis and agricultural biotechnology* **2018**, *13*, 129-152.

32. Z.-S. Zhang, L.-J. Wang, D. Li, S.-J. Li, N. Özkan. Characteristics of flaxseed oil from two different flax plants. *International Journal of Food Properties* **2011**, *14*, 1286-1296.

33. A. Mannucci, A. Castagna, M. Santin, A. Serra, M. Mele, A. Ranieri. Quality of flaxseed oil cake under different storage conditions. *LWT* **2019**, *104*, 84-90.

34. L. Brison, P. Bertin, Y. Larondelle. Evaluation of the effect of nitrogen fertilization and tillage on the yield and the nutritional profile of flaxseed. *Master's Thesis, Universite catholique de Louvain, Ottignies-Louvain-la-Neuve, Belgium* **2019**.

35. A. Wirkijowska, P. Zarzycki, A. Sobota, A. Nawrocka, A. Blicharz-Kania, D. Andrejko. The possibility of using by-products from the flaxseed industry for functional bread production. *LWT* **2020**, *118*, 108860.

36. P. Kolodziejczyk, L. Ozimek, J. Kozłowska. The application of flax and hemp seeds in food, animal feed and cosmetics production. In *Handbook of natural fibres*, Elsevier: 2012; 329-366.

37. C.M. Chan, L.-J. Vandi, S. Pratt, P. Halley, D. Richardson, A. Werker, B. Laycock. Composites of wood and biodegradable thermoplastics: A review. *Polymer reviews* **2018**, *58*, 444-494.

38. J. España, M. Samper, E. Fages, L. Sánchez-Nácher, R. Balart. Investigation of the effect of different silane coupling agents on mechanical performance of basalt fiber composite laminates with biobased epoxy matrices. *Polymer composites* **2013**, *34*, 376-381.

39. D. Bertomeu, D. García-Sanoguera, O. Fenollar, T. Boronat, R. Balart. Use of eco-friendly epoxy resins from renewable resources as potential substitutes of petrochemical epoxy resins for ambient cured composites with flax reinforcements. *Polymer Composites* **2012**, *33*, 683-692.

40. M. Samper, V. Fombuena, T. Boronat, D. García-Sanoguera, R. Balart. Thermal and mechanical characterization of epoxy resins (ELO and ESO) cured with anhydrides. *Journal of the American Oil Chemists' Society* **2012**, *89*, 1521-1528.

41. V. Fombuena, S. MD. Study of the properties of thermoset materials derived from epoxidized soybean oil and protein fillers. *Journal of the American Oil Chemists' Society* **2013**, *90*, 449-457.

42. A. Carbonell-Verdu, L. Bernardi, D. Garcia-Garcia, L. Sanchez-Nacher, R. Balart. Development of environmentally friendly composite matrices from epoxidized cottonseed oil. *European Polymer Journal* **2015**, *63*, 1-10.

43. A. Anusic, K. Resch-Fauster, A.R. Mahendran, G. Wuzella. Anhydride cured bio-based epoxy resin: Effect of moisture on thermal and mechanical properties. *Macromolecular Materials and Engineering* **2019**, *304*, 1900031.

44. L. Quiles-Carrillo, S. Duart, N. Montanes, S. Torres-Giner, R. Balart. Enhancement of the mechanical and thermal properties of injection-molded polylactide parts by the addition of acrylated epoxidized soybean oil. *Materials & Design* **2018**, *140*, 54-63.

45. O. Fenollar, L. Sanchez-Nacher, D. Garcia-Sanoguera, J. López, R. Balart. The effect of the curing time and temperature on final properties of flexible PVC with an epoxidized fatty acid ester as natural-based plasticizer. *Journal of materials science* **2009**, *44*, 3702-3711.

46. X. Liu, W. Huang, Y. Jiang, J. Zhu, C. Zhang. Preparation of a bio-based epoxy with comparable properties to those of petroleum-based counterparts. *Express Polymer Letters* **2012**, *6*, 293–298.

47. P. Niedermann, G. Szebényi, A. Toldy. Characterization of high glass transition temperature sugar-based epoxy resin composites with jute and carbon fibre reinforcement. *Composites Science and Technology* **2015**, *117*, 62-68.

48. P. Niedermann, G. Szebényi, A. Toldy. Effect of epoxidized soybean oil on curing, rheological, mechanical and thermal properties of aromatic and aliphatic epoxy resins. *Journal of Polymers and the Environment* **2014**, *22*, 525-536.

49. Y. Wu, Y. Wang, F. Yang, J. Wang, X. Wang. Study on the properties of transparent bamboo prepared by epoxy resin impregnation. *Polymers* **2020**, *12*, 863.

50. K. Salasinska, K. Mizera, M. Barczewski, M. Borucka, M. Gloc, M. Celiński, A. Gajek. The influence of degree of fragmentation of Pinus sibirica on flammability, thermal and thermomechanical behavior of the epoxy-composites. *Polymer Testing* **2019**, *79*, 106036.

51. R. Kumar, K. Kumar, S. Bhowmik. Mechanical characterization and quantification of tensile, fracture and viscoelastic characteristics of wood filler reinforced epoxy composite. *Wood Science and Technology* **2018**, *52*, 677-699.

52. J. Stabik, M. Chomiak. Graded epoxy-hard coal composites: Analysis of filler particle distribution in the epoxy matrix. *Journal of Composite Materials* **2016**, *50*, 3663-3677.

53. D. Lascano, L. Quiles-Carrillo, S. Torres-Giner, T. Boronat, N. Montanes. Optimization of the curing and post-curing conditions for the manufacturing of partially bio-based epoxy resins with improved toughness. *Polymers* **2019**, *11*, 1354.

54. Á. Agüero, D. Lascano, D. Garcia-Sanoguera, O. Fenollar, S. Torres-Giner. Valorization of linen processing by-products for the development of injection-molded green composite pieces of polylactide with improved performance. *Sustainability* **2020**, *12*, 652.

55. A.K. Bledzki, A.A. Mamun, J. Volk. Barley husk and coconut shell reinforced polypropylene composites: the effect of fibre physical, chemical and surface properties. *Composites Science and Technology* **2010**, *70*, 840-846.

56. K. Salasinska, M. Barczewski, R. Górny, A. Kloziński. Evaluation of highly filled epoxy composites modified with walnut shell waste filler. *Polymer Bulletin* **2018**, *75*, 2511-2528.

57. H.-J. Kwon, J. Sunthornvarabhas, J.-W. Park, J.-H. Lee, H.-J. Kim, K. Piyachomkwan, K. Sriroth, D. Cho. Tensile properties of kenaf fiber and corn husk flour reinforced poly (lactic acid) hybrid bio-composites: Role of aspect ratio of natural fibers. *Composites Part B: Engineering* **2014**, *56*, 232-237.

58. N. Bisht, P.C. Gope. Mechanical properties of rice husk flour reinforced epoxy bio-composite. *Int Journal of Engineering Research and Applications* **2015**, *5*, 123128.

59. Novowood. Availabe online: https://www.novowood.it/en/download-technical-sheet-wpc_39c7.html (accessed on 18/05/2020).

60. Jeluplast. Availabe online: https://www.jeluplast.com/wp-content/uploads/2013/09/WPC-PE-H70-800-03.pdf (accessed on 18/05/2020).

61. D. García-García, A. Carbonell, M. Samper, D. García-Sanoguera, R. Balart. Green composites based on polypropylene matrix and hydrophobized spend coffee ground (SCG) powder. *Composites part B: engineering* **2015**, *78*, 256-265.

62. A. Yussuf, I. Massoumi, A. Hassan. Comparison of polylactic acid/kenaf and polylactic acid/rise husk composites: the influence of the natural fibers on the

mechanical, thermal and biodegradability properties. *Journal of Polymers and the Environment* **2010**, *18*, 422-429.

63. G. Raju, S. Kumarappa. Experimental study on mechanical and thermal properties of epoxy composites filled with agricultural residue. *Polymers from renewable resources* **2012**, *3*, 117-138.

64. W.-H. Chen, P.-C. Kuo. A study on torrefaction of various biomass materials and its impact on lignocellulosic structure simulated by a thermogravimetry. *Energy* **2010**, *35*, 2580-2586.

65. R. Moriana, F. Vilaplana, M. Ek. Forest residues as renewable resources for bio-based polymeric materials and bioenergy: chemical composition, structure and thermal properties. *Cellulose* **2015**, *22*, 3409-3423.

66. S. Hussain, F. Anjum, M. Butt, M. Sheikh. Chemical composition and functional properties of flaxseed (Linum usitatissimum) flour. *Sarhad J. Agric* **2008**, *24*, 649-653.

67. S. Sengupta, P. Maity, D. Ray, A. Mukhopadhyay. Stearic acid as coupling agent in fly ash reinforced recycled polypropylene matrix composites: Structural, mechanical, and thermal characterizations. *Journal of Applied Polymer Science* **2013**, *130*, 1996-2004.

68. O. Mysiukiewicz, M. Barczewski. Utilization of linseed cake as a postagricultural functional filler for poly (lactic acid) green composites. *Journal of Applied Polymer Science* **2019**, *136*, 47152.

69. R. Liu, J. Wang, Q. He, L. Zong, X. Jian. Interaction and properties of epoxy-amine system modified with poly (phthalazinone ether nitrile ketone). *Journal of Applied Polymer Science* **2016**, *133*, 42938.

70. J. Balart, D. García-Sanoguera, R. Balart, T. Boronat, L. Sánchez-Nacher. Manufacturing and properties of biobased thermoplastic composites from poly (lactid acid) and hazelnut shell wastes. *Polymer composites* **2018**, *39*, 848-857.

71. J. Balart, V. Fombuena, O. Fenollar, T. Boronat, L. Sánchez-Nacher. Processing and characterization of high environmental efficiency composites based on PLA and hazelnut shell flour (HSF) with biobased plasticizers derived from epoxidized linseed oil (ELO). *Composites Part B: Engineering* **2016**, *86*, 168-177.

72. P. Liminana, L. Quiles-Carrillo, T. Boronat, R. Balart, N. Montanes. The effect of varying almond shell flour (ASF) loading in composites with poly (butylene

succinate (PBS) matrix compatibilized with maleinized linseed oil (MLO). *Materials* **2018**, *11*, 2179.

73. R. Reixach, J. Puig, J.A. Méndez, J. Gironès, F.X. Espinach, G. Arbat, P. Mutjé. Orange wood fiber reinforced polypropylene composites: Thermal properties. *BioResources* **2015**, *10*, 2156-2166.

74. H.M. Akil, L.W. Cheng, Z.M. Ishak, A.A. Bakar, M. Abd Rahman. Water absorption study on pultruded jute fibre reinforced unsaturated polyester composites. *Composites Science and Technology* **2009**, *69*, 1942-1948.

75. B. Ferrero, T. Boronat, R. Moriana, O. Fenollar, R. Balart. Green composites based on wheat gluten matrix and posidonia oceanica waste fibers as reinforcements. *Polymer composites* **2013**, *34*, 1663-1669.

76. B. Alander, A. Capezza, Q. Wu, E. Johansson, R.T. Olsson, M. Hedenqvist. A facile way of making inexpensive rigid and soft protein biofoams with rapid liquid absorption. *Industrial Crops and Products* **2018**, *119*, 41-48.

77. H. Ben Daly, H. Ben Brahim, N. Hfaied, M. Harchay, R. Boukhili. Investigation of water absorption in pultruded composites containing fillers and low profile additives. *Polymer Composites* **2007**, *28*, 355-364.

78. R. Udhayasankar, B. Kathikeyan. Preparation and properties of cashew nut shell liquid-Based composite reinforced by coconut shell particles. *Surface Review and Letters* **2019**, *26*, 1850174.

79. I. Naghmouchi, P. Mutjé, S. Boufi. Polyvinyl chloride composites filled with olive stone flour: Mechanical, thermal, and water absorption properties. *Journal of Applied Polymer Science* **2014**, *131*, 41083.

80. U. Shehu, O. Aponbiede, T. Ause, E. Obiodunukwe. Effect of particle size on the properties of polyester/palm kernel shell (PKS) particulate composites. *J. Mater. Environ. Sci* **2014**, *5*, 366-373.

81. M.A. Thirmizir, Z.M. Ishak, R.M. Taib, R. Sudin, Y. Leong. Mechanical, water absorption and dimensional stability studies of kenaf bast fibre-filled poly (butylene succinate) composites. *Polymer-Plastics Technology and Engineering* **2011**, *50*, 339-348.

82. S.M. Zabihzadeh, A. Omidvar, M.A.B. Marandi, F. Dastoorian, S.M. Mirmehdi. Effect of filler loading on physical and flexural properties of rapeseed stem/PP composites. *BioResources* **2011**, *6*, 1475-1483.

83. Z.M. Ishak, B. Yow, B. Ng, H.A. Khalil, H. Rozman. Hygrothermal aging and tensile behavior of injection-molded rice husk-filled polypropylene composites. *Journal of Applied Polymer Science* **2001**, *81*, 742-753.

84. A. Najafi, H. Khademi-Eslam. Lignocellulosic filler/recycled HDPE composites: Effect of filler type on physical and flexural properties. *BioResources* **2011**, *6*, 2411-2424.

85. S. Sapuan, N. Harun, K. Abbas. Design and fabrication of a multipurpose table using a composite of epoxy and banana pseudostem fibres. *Journal of Tropical Agriculture* **2008**, *45*, 66-68.

86. S. Sapuan, M. Maleque. Design and fabrication of natural woven fabric reinforced epoxy composite for household telephone stand. *Materials & design* **2005**, *26*, 65-71.

Adaptado del artículo

III.2.5. Manufacturing and characterization of hybrid composites with basalt and flax fabrics and a partially bio-based epoxy resin

Diego Lascano[1,2], Rafael Balart[2], David Garcia-Sanoguera[2], Angel Agüero[2], Teodomiro Boronat[2], and Nestor Montanes[2]

[1] Escuela Politécnica Nacional, Ladrón de Guevara E11-253, Quito 17-01-2759, Ecuador

[2] Technological Institute of Materials (ITM), Universitat Politècnica de València (UPV), Plaza Ferrándiz y Carbonell 1, 03801 Alcoy, Spain

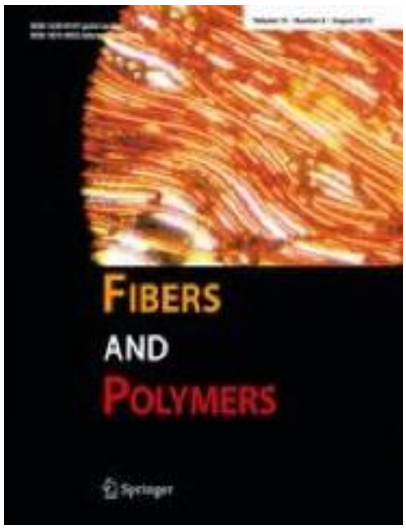

Fibers and Polymers 22, 751-763 (2021)

Fibers and Polymers 2021, Vol.22, No.3, 751-763
DOI 10.1007/s12221-021-0209-5

ISSN 1229-9197 (print version)
ISSN 1875-0052 (electronic version)

Manufacturing and Characterization of Hybrid Composites with Basalt and Flax Fabrics and a Partially Bio-based Epoxy Resin

Diego Lascano[1,2]*, Rafael Balart[2], David Garcia-Sanoguera[2], Angel Agüero[2], Teodomiro Boronat[2], and Nestor Montanes[2]

[1]*National Polytechnic School, Quito 17-01-2759, Ecuador*
[2]*Technological Institute of Materials, Polytechnic University of Valencia, Alcoy 03801, Spain*
(Received February 25, 2020; Revised June 3, 2020; Accepted June 4, 2020)

Abstract: This research is focused on manufacturing and characterization of hybrid composite laminates obtained different stacking sequences of basalt and flax fabrics with silane treatments embedded in a partially bio-sourced epoxy resin as matrix. They were manufactured by the vacuum-assisted resin infusion molding and mechanical properties were tested in tensile, flexural and impact conditions. The effect of the coupling agent on the fiber/matrix interface was studied by FESEM. The effect of temperature on mechanical properties was evaluated by DMTA and TMA. FESEM images revealed improved fiber/matrix interactions with silane treatment, having a more satisfactory effect on basalt fibers than on flax fibers because of its silica-based structure, leading to improved mechanical properties. It is worthy to note that the hybrid stacking sequence has no remarkable influence on the elongation at break. On the contrary, the hybrid stacking sequence offered a great influence on both the elastic modulus and the tensile strength.

Keywords: Bio-based epoxy resin, Hybrid composites laminates, VARIM

Introduction

Composite materials are one of the most promising areas of thermosetting polymers. Conventional fibers such as carbon, aramids, and glass, offer superior mechanical properties to most materials and this has led composite materials into advanced materials sectors and high-performance applications. Some of their outstanding properties are lightness, high Young's modulus, high tensile strength and good thermal stability, among others [1-3]. When these fibers are used as reinforcements embedded into a polymeric matrix (usually a thermosetting polymer), the obtained composite materials offer a synergistic improvement in both manufacturing and final properties. These composites are lightweight technical materials with growing uses in advanced industrial sectors such as aerospace, aeronautics, automotive, medical devices and equipment, or construction sector [4-6]. The excellent performance of these materials allows them to substitute other conventional materials such as steel in civil applications [7]. Despite these notorious qualities, the overall cost of these fibers, mainly carbon and aramids is still high due to complex manufacturing processes [8]. To overcome the cost-related problem, some efforts have been done to totally or partially replace the content of these fibers in composite materials or laminates, aiming a good balance between performance and cost. In the last decade, most research works have focused on the potential of hybrid composite materials laminates with different fibers/fabrics in a particular stacking sequence. Artemenko *et al*. [9], reported a hybrid composite with carbon and glass fibers, with the subsequent cost reduction. Nevertheless, the decrease in mechanical properties was noticeable. In particular, these hybrid carbon/glass composites showed a flexural strength 40 % lower than carbon fiber composites. Marom *et al*. [10], manufactured hybrid composite laminates with aramid (Kevlar®) and carbon fiber, achieving hybrid materials with good impact absorption properties when Kevlar plies were located in the outer layers of the composite material.

In addition to the cost reduction, in the last decade the increasing concern about environment is leading the change to the use of environmentally friendly materials and processes. In accordance to this tendency, the use of natural fibers has emerged as an interesting alternative to give high environmental efficiency materials. Natural fibers are obtained from renewable resources which represents a notorious advantage from a production standpoint [11], and a positive effect on reducing greenhouse gases emissions. The most used fibers in the manufacture of composite materials are jute, hemp, cotton and flax, among others [12, 13]. One of the most interesting fibers for the composite's industry is flax. Due to its composition, which is mostly made up of helical structures (microfibrils) of cellulose, flax fibers can provide high tensile strength and modulus. The microfibril orientation in flax fibers is 10 º, and the cellulose content is around 71 %, which can lead to values of the tensile strength of up to 1129 MPa [14]. Several authors have focused their research works on hybrid structures between synthetic and natural fibers. Zhang *et al.* [15], reported interesting properties on hybrid composite materials with flax and glass fibers. The showed good interaction between the fibers since fracture toughness and interlaminar shear strength turned out to be higher compared with composite laminates with glass fibers. Morye *et al.* [16],

*Corresponding author: dielas@epsa.upv.es

Manufacturing and characterization of hybrid composites with basalt and flax fabrics and a partially bio-based epoxy resin

Abstract

This research is focused on manufacturing and characterization of hybrid composite laminates obtained different stacking sequences of basalt and flax fabrics with silane treatments embedded in a partially bio-sourced epoxy resin as matrix. They were manufactured by the vacuum-assisted resin infusion molding and mechanical properties were tested in tensile, flexural and impact conditions. The effect of the coupling agent on the fiber/matrix interface was studied by FESEM. The effect of temperature on mechanical properties was evaluated by DMTA and TMA. FESEM images revealed improved fiber/matrix interactions with silane treatment, having a more satisfactory effect on basalt fibers than on flax fibers because of its silica-based structure, leading to improved mechanical properties. It is worthy to note that the hybrid stacking sequence has no remarkable influence on the elongation at break. On the contrary, the hybrid stacking sequence offered a great influence on both the elastic modulus and the tensile strength.

Keywords: Bio-based epoxy resin, Hybrid composites laminates, VARIM

III.2.5.1. Introduction

Composite materials are one of the most promising areas of thermosetting polymers. Conventional fibers such as carbon, aramids, and glass, offer superior mechanical properties to most materials and this has led composite materials into advanced materials sectors and high- performance applications. Some of their outstanding properties are lightness, high Young's modulus, high tensile strength and good thermal stability, among others [1-3]. When these fibers are used as reinforcements embedded into a polymeric matrix (usually a thermosetting polymer), the obtained composite materials offer a synergistic improvement in both manufacturing and final properties. These composites are lightweight technical materials with growing uses in advanced industrial sectors such as aerospace, aeronautics, automotive, medical devices and equipment, or construction sector [4-6]. The excellent performance of these materials allows them to substitute other conventional materials such as steel in civil applications [7]. Despite these notorious qualities, the overall cost of these fibers, mainly carbon and aramids is still high due to complex manufacturing processes [8]. To overcome the cost-related problem, some efforts have been done to totally or partially replace the content of these fibers in composite materials or laminates, aiming a good balance between performance and cost. In the last decade, most research works have focused on the potential of hybrid composite materials laminates with different fibers/fabrics in a particular stacking sequence. Artemenko and Kadykova [9], reported a hybrid composite with carbon and glass fibers, with the subsequent cost reduction. Nevertheless, the decrease in mechanical properties was noticeable. In particular, these hybrid carbon/glass composites showed a flexural strength 40 % lower than carbon fiber composites. Marom, *et al.* [10], manufactured hybrid composite laminates with aramid (Kevlar®) and carbon fiber, achieving hybrid materials with good impact absorption properties when Kevlar plies were located in the outer layers of the composite material.

In addition to the cost reduction, in the last decade the increasing concern about environment is leading the change to the use of environmentally friendly materials and processes. In accordance to this tendency, the use of natural fibers has emerged as an interesting alternative to give high environmental efficiency materials. Natural fibers are obtained from renewable resources which represents a notorious advantage from a production standpoint [11], and a positive effect on reducing greenhouse gases emissions. The most used fibers in the manufacture of composite materials are jute, hemp, cotton and flax, among others [12,13]. One of the most interesting fibers for the composite's industry is flax. Due to its composition, which is mostly made up of helical structures (microfibrils) of cellulose, flax fibers can provide high tensile strength and

modulus. The microfibril orientation in flax fibers is 10°, and the cellulose content is around 71 %, which can lead to values of the tensile strength of up to 1129 MPa [14]. Several authors have focused their research works on hybrid structures between synthetic and natural fibers. Zhang, *et al*. [15], reported interesting properties on hybrid composite materials with flax and glass fibers. The showed good interaction between the fibers since fracture toughness and interlaminar shear strength turned out to be higher compared with composite laminates with glass fibers. Morye and Wool [16], reported an increase in the flexural an impact strength properties on hybrid composites of flax and glass fibers. Ramesh, *et al.* [17] studied the hybrid effect of synthetic fibers such as carbon and natural fibers such as hemp. Natural fibers were pre-treated with alkaline solutions, which determined that the pre-treatment increased the mechanical properties compared to untreated fibers, and caused water absorption to decrease too. Bajpai, *et al*. [18] developed safety helmets based on hybrid fiberglass and jute fiber materials embedded in an epoxy resin matrix. It was determined that the flexural properties were superior when the fiberglass content was lower, thus allowing these materials with a high percentage of natural fibers to replace conventional materials such as ABS. Palanikumar, *et al*. [19] developed hybrid composites based on sisal and glass fibers, where the incorporation of 20 % sisal fibers resulted in increased mechanical properties in tensile and bending. Therefore, these hybrid composites were confirmed as an alternative to all-glass fiber composite.

As an alternative to glass fibers, it is possible to find some different siliceous fibers with interesting properties from a technical point of view. These fibers are obtained from mineral products such as rocks, therefore, these fibers are known commercially as rock wool, depending on the type of rock [20]. Among the rocks used for this purpose, basalt is the most promising. This rock is the result of the cooling of magma on the earth's surface [21]. Due to its particular structure, processing of basalt rocks is much simpler, cheaper and with less environmental impact than production of glass fibers, which generates too much waste [22]. Properties such as low or no chemical reactivity, good thermal behavior, good mechanical properties, high modulus, are some of the features of basalt fibers [23,24]. Tehrani Dehkordi, *et al*. [25] reported improved buckling strength when subjected to high impact energies on hybrid composites of basalt-nylon intraply fabrics. Matykiewicz, *et al*. [26] reported the thermomechanical properties of hybrid composites of basalt fibers and basalt powder. The hybrid composition achieved a synergistic effect by improving the thermal resistance and the stiffness of the composite. Several authors have studied the hybrid effect with natural fibers, Matykiewicz and Barczewski [27], prepared a hybrid composite with basalt and flax fibers pre-treated with

silanes. These hybrid fibers were embedded in an epoxy resin filled with basalt powder. They determined that the mechanical properties of the composites were not affected by the incorporation of the flax fibers. Moreover, they reported a clear coupling effect by using silanes, resulting in a better fiber-matrix interaction and, subsequently, the stiffness was increased. Sergi, *et al*. [28] investigated the effect of water aging and UV radiation on hybrid composites based on basalt and hemp fibers, embedded into a thermoplastic matrix of high-density polyethylene modified with maleic anhydride. They also reported the positive effect of an accelerated aging on improving mechanical properties. In addition, water absorption decreased due the compatibilizing effect of the aging process with UV. Despite the good properties of these fibers, the interaction between them and the surrounding thermosetting matrix is usually deficient, resulting in a marked decrease in mechanical properties, since the loads are not transmitted correctly to the fibers [29,30]. To improve this interaction, different types of treatments are usually performed to selectively modify the fiber surface. Different physical and chemical processes have been proposed to overcome this drawback. Among all these treatments, silanization seems to be the most effective from both technical and economic considerations [31]. The dual functionality of silanes allows formation of bridges between the fiber surface and the thermosetting polymer matrix [32].

Typical thermosetting resins for composites include unsaturated polyesters (UP), epoxies (EP), phenolics (PF), vinyl ester (VE), among others. Epoxies are widely used in engineering due to excellent properties they can provide [33,34]. conventional epoxies for composites are based on diglycidyl ether of bisphenol A, DGEBA [35,36]. DGEBPA epoxies are petroleum-based materials and substantially contribute to increase the carbon footprint. With the aim of reducing this, different bio-based materials have been proposed [37,38], mainly derived from non-edible vegetable oils (VO) [39]. The particular structure of vegetable oils, based on a triglyceride with three different fatty acids allows some chemical modifications, especially on unsaturated fatty acids such as oleic, linoleic and linolenic acids [40].

The purpose of this research is to assess the potential of hybrid composite laminates of flax and basalt fibers embedded into a partially bio-based epoxy resin, obtained by vacuum assisted resin infusion molding (VARIM). This work also covers the study of the interaction between basalt and flax fibers subjected to a silanization process. In addition, the stacking sequence of flax and basalt fabrics on composite laminates is evaluated in terms of mechanical performance.

III.2.5.2. Experimental

Materials

The matrix was a partially bio-based epoxy resin, commercial grade Resoltech® 1070 ECO and an amine- based hardener type Resoltech® 1074 ECO, both of them supplied by Castro Composites (Pontevedra, Spain). The epoxy resin is based on diglycidyl ether of bisphenol A (DGEBA) with 31 % of plant-based reactive diluent. It provides good UV stability and high mechanical properties. The ratio between the epoxy resin and the hardener was 100:35 respectively (parts by weight), as recommend the manufacturer. Two types of fabrics were used to manufacture hybrid composite laminates. Basalt fabric BAS 940.1270.T supplied by Basaltex (Wevelgem, Belgium) with a specific surface weight of 940 g cm^{-2} and Biotex Flax fibers supplied by Composites evolution (Chesterfield, United Kingdom) with a specific surface weight of 400 g cm^{-2}. Some properties of flax fiber and basalt fiber fabrics are summarized in table III.2.5.1, all fabrics present a compensated setup on weft and warp directions. The glycidyl-functional silane (3-glycidyloxypropyl) trimethoxysilane was used as a coupling agent and was obtained from Sigma-Aldrich (Madrid, Spain).

Table III.2.5.1. Physical properties of flax and basalt fibers, and their corresponding fabrics used for composite manufacturing.

Properties	Basalt fibers	Flax fiber
Density od unsized filament (kg dm^{-3})	2.67	1.5
Moisture content (%)	0.1	-
Melting point (ºC)	1350	-
Weave type	Twill 2/2	Twill 2/2
Fiber diameter (µm)	17	20
Young Modulus (GPa)	85	50
Yarn density: warp (ends cm^{-1})	3.8	7
Yarn density: weft (ends cm^{-1})	3.8	7
Ply thickness (mm)	0.53	0.6-0.8

Pre-treatment of Fibers

In order to remove any external agents (sizings), which can interfere with the manufacturing process of basalt/flax composite laminates, basalt fabrics were initially washed in a distilled water bath and then subjected to a thermal program at 300 ºC for 3 h to remove any organic sizing.

In order to improve the surface interaction between the reinforcing fibers and the thermosetting matrix, both basalt and flax fabrics were subjected to a silanization treatment. The aqueous solution for this treatment contained 1 wt % silane. Then the solution was magnetically stirred for 2 hours at room temperature until homogenization. Then, the corresponding fabrics were immersed in this solution for 2 hours at room temperature. After this stage, the fabrics were removed from the bath and were dried at 80 ºC for 12 hours.

Manufacturing of Hybrid Basalt/flax Composite Laminates

Manufacturing process of basalt/flax/epoxy composites was carried out by the VARIM process. This method consists on a conventional infusion process assisted by vacuum. VARIM process follows different stages. First, basalt and flax fabrics with different stacking sequences as summarized in table III.2.5.2, were placed on a board coated with a thin layer of a release agent (polyvinyl alcohol) as it is shown in Scheme III.2.5.1a, all layers are biaxial fabrics $(0/90)_{2S}$. Then, a peel-ply sheet was placed above the stacked fabrics followed by the bleeding fabric, to ensure good resin flow and spreading (scheme III.2.5.1b). Then, the system was sealed with a plastic bag with double-side sealing tape. Finally, the resin inlet and the vacuum outlet were placed appropriately (scheme III.2.5.1c). Then the vacuum was tested to ensure no leaking. Once this stage was checked and it was confirmed there was no leaking, the resin was infused thus embedding all fabrics (Scheme III.2.5.1d). After the infusion, the hybrid composites were subjected to a curing cycle of 1 h at 80 ºC and a subsequent post curing cycle at 125 ºC for 30 min.

Table III.2.5.2. Composition and stacking sequence of hybrid composite laminates with different basalt/flax plies.

Code	Ply number ratio (basalt/flax)	Stacking Sequence	Image view of the cross section
B8F0	8/0		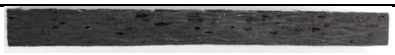
B6F2	6/2		
B4F4	4/4		
B2F6	2/6		
B4F4alt	4/4		
B0F8	0/8		

Basalt fabric ply Flax fabric ply

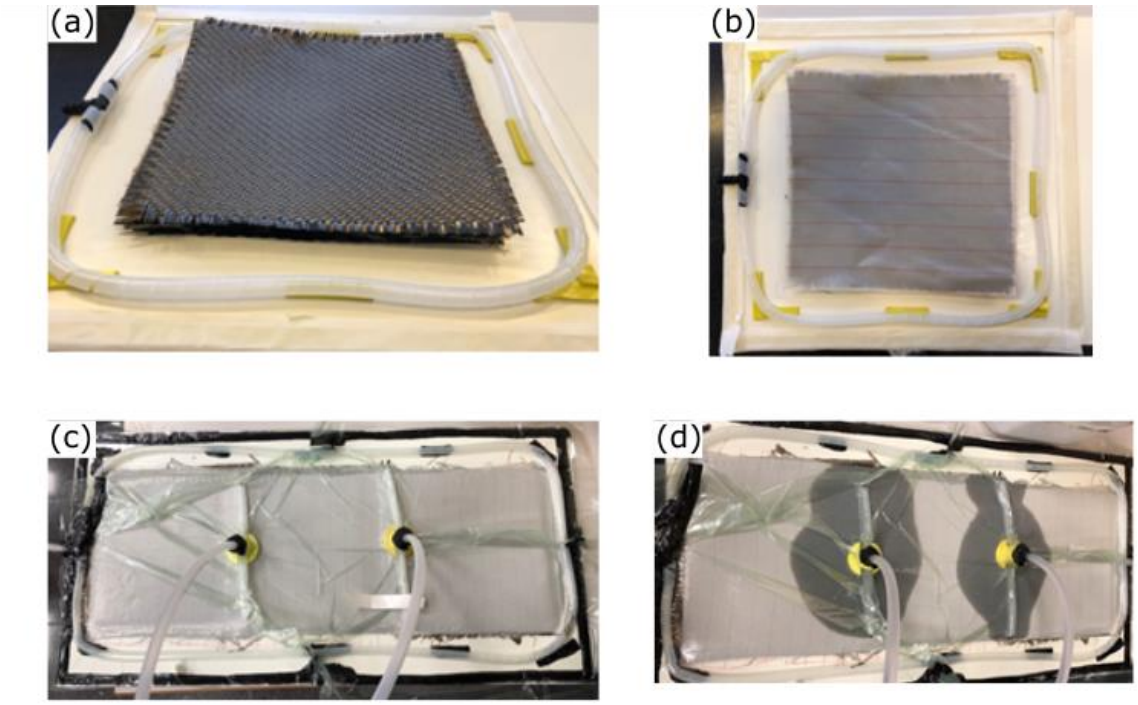

Scheme III.2.5.1. Stages of the VARIM of hybrid composite laminates with different basalt/flax plies with a partially bio-based epoxy resin; (a) defining the stacking sequence, (b) adding the peel-ply and bleeding fabric, (c) testing the vacuum level to check no leakage, and (d) resin infusion assisted by vacuum.

Mechanical Properties of Laminate Composites

Mechanical properties of hybrid basalt/flax epoxy composite laminates with bio-based epoxy resin were evaluated in flexural and impact conditions. The flexural test was performed following the guidelines of ISO 178 standard; the crosshead rate was set at 5 mm min^{-1}. Flexural test was performed on an electromechanical universal testing machine ELIB 50 from S. A. E. Iberest (Madrid, Spain), with a 50 kN load cell. Impact strength was evaluated by the Charpy test, following the guidelines of ISO 179 standard in a Charpy pendulum from Metrotec (San Sebastián, Spain), using a 6 J pendulum on notched samples (U type, 2 mm depth and a radio of 0.5 mm) as it is shown in figure III.2.5.1. All tests were conducted at room temperature with at least five samples of each laminate. The average values of the corresponding parameters of each test were calculated.

Figure III.2.5.1. Detail of U type notched samples for Charpy test to evaluate the impact strength of hybrid composite laminates with different basalt/flax plies with a partially bio-based epoxy resin.

In order to have a better understanding of the effect of the hybrid structure of composite laminates on toughness, a conventional tensile test with the same notched samples (figure III.2.5.1) used for impact tests was carried out. This tensile test was carried out in a ELIB 50 from S. A. E. Iberest (Madrid, Spain), with a 50 kN load cell and the crosshead rate was set to 3 mm min^{-1}. This test allows calculating the area below its characteristic tensile diagram, which is directly related to overall toughness. The main parameters obtained from this test were the maximum tensile strength and the area below the tensile curve. Five different samples were tested, and the corresponding values were averaged, in addition, longitudinal and cross-sectional data have been considered.

Thermomechanical Characterization

Thermomechanical properties of hybrid basalt/flax composite laminates with bio-based epoxy resin were evaluated by dynamic mechanical thermal analysis (DMTA). An oscillatory rheometer AR-G2 from TA Instruments (New Castle, USA) equipped with a clamp system for solid samples working in torsion-shear conditions was used. The samples had a rectangular shape size of 40x10x4 mm^3. The heating program was a temperature sweep from 30 ºC up to 200 ºC at a constant heating rate of 2 ºC min^{-1}. The maximum shear/torsion deformation (γ) was defined as a percentage of 0.1 % and the selected frequency for the oscillations was 1 Hz.

Additionally, to the dynamic characterization of basalt/ flax hybrid composites by DMTA, their dimensional stability was analyzed by obtaining the coefficient of linear thermal expansion (CLTE) in a thermomechanical analyzer (TMA) Q400 from TA Instruments, using square samples (10x10 mm^2) with a variable thickness from 7 to 11 mm, with parallel faces. The dynamic heating program was scheduled from 30 ºC up to 170 ºC to cover the range in which the T_g of the epoxy is expected. A constant heating rate of 2 ºC min^{-1} was used with a constant load of 20 mN.

Fiber/matrix Interaction and Morphology Analysis

The interaction between basalt fibers and flax fibers with the epoxy resin matrix in hybrid basalt/flax composite laminates was analyzed by field emission scanning electron microscopy (FESEM), in a ZEISS ULTRA 55 FESEM microscope from Oxford Instruments (Abingdon, United Kingdom) working at an acceleration voltage of 2 kV. Prior to observation by FESEM, all samples were coated with an ultrathin gold-palladium layer in a high vacuum sputter coater EM MED20 from Leica Microsystem (Milton Keynes, United Kingdom), to provide electrical-conducting properties to samples. In addition, the morphology of the fractured surfaces from fractured specimens from impact test was observed using a stereomicroscope system SZX7 model from Olympus (Tokyo, Japan). It was equipped with a KL 1500-LCD light source.

Statistical Analysis

The data obtained when analyzing the different properties of epoxy basalt/flax composite laminates were evaluated with a $p < 0.05$ (95 %) confidence interval using an analysis of variance (ANOVA). The OriginPro8 software from OriginLab Corporation (Northampton, MA, USA) was used to perform the Tukey multiple comparison tests.

III.2.5.3. Results and Discussion

Morphology of Untreated and Silanized Basalt and Flax Fibers

Mechanical properties of composites are directly related to fiber/matrix interactions. Strong fiber/matrix interactions allow load transfer from the matrix to the reinforcing fiber and this has a positive effect on overall mechanical performance. On the contrary, poor fiber/matrix interactions are responsible for poor mechanical properties due to poor material's cohesion. The surfaces of the reinforcing fibers after the silane treatment were analyzed by FESEM; these images are displayed in figure III.2.5.2. Both figure III.2.5.2(a) and figure III.2.5.2(b), show basalt fiber surface as-received, without any treatment. It can be noticed that the surface has some impurities, which appear in the form of roughness on these surfaces. This roughness is no more than the protective sizing of basalt fibers. This sizing is usually added to facilitate their handling during manufacturing due to its brittleness. Flax fibers, unlike basalt fibers, do not have a uniform surface, they have a fluted structure, generally having between 5 and 7 lateral sides as indicated in figure III.2.5.2(c) and figure III.2.5.2(d), which is quite typical of natural fibers, as this particular shape allows packing fibers [16]. Figure III.2.5.2(e) and

figure III.2.5.2(f) show the surfaces of basalt fibers subjected to cleaning and subsequent heat treatment at 300 ºC to remove organic sizings. The results obtained after this process is notorious as the initial roughness of untreated basalt fibers has almost disappeared, resulting in completely smooth surfaces, meaning that the initial sizing of the basalt fibers has been removed. This is necessary due to the presence of undesired elements such as binders, sizings dirt, and others, which are usually present in the surface of basalt fibers. Some of these chemicals are needed to appropriately manufacture the highly brittle basalt fibers. If these chemicals and/or dirt are not removed, the silanization process lose its effectiveness because these elements prevent anchoring between the hydroxyl groups of the fibers on their surface and the hydrolyzed silanol groups contained in the glycidyl-functional silane (3-glycidyloxypropyl), as observed in previous studies [41], so that it does not cause subsequent failures while manufacturing composite laminates and, moreover, allows good anchorage of silane after silanization. The effect of silanization on both fibers can be seen in figure III.2.5.2(g) and figure III.2.5.2(h) for basalt and in figure III.2.5.2(i) and figure III.2.5.2(j) for flax fibers. As it can be seen for both fibers, the surface roughness has increased which is due to formation of a thin layer of silane that has been strongly adhered to the fibers in a similar way as reported by Park, *et al*. [42] and Samper, *et al.* [29].

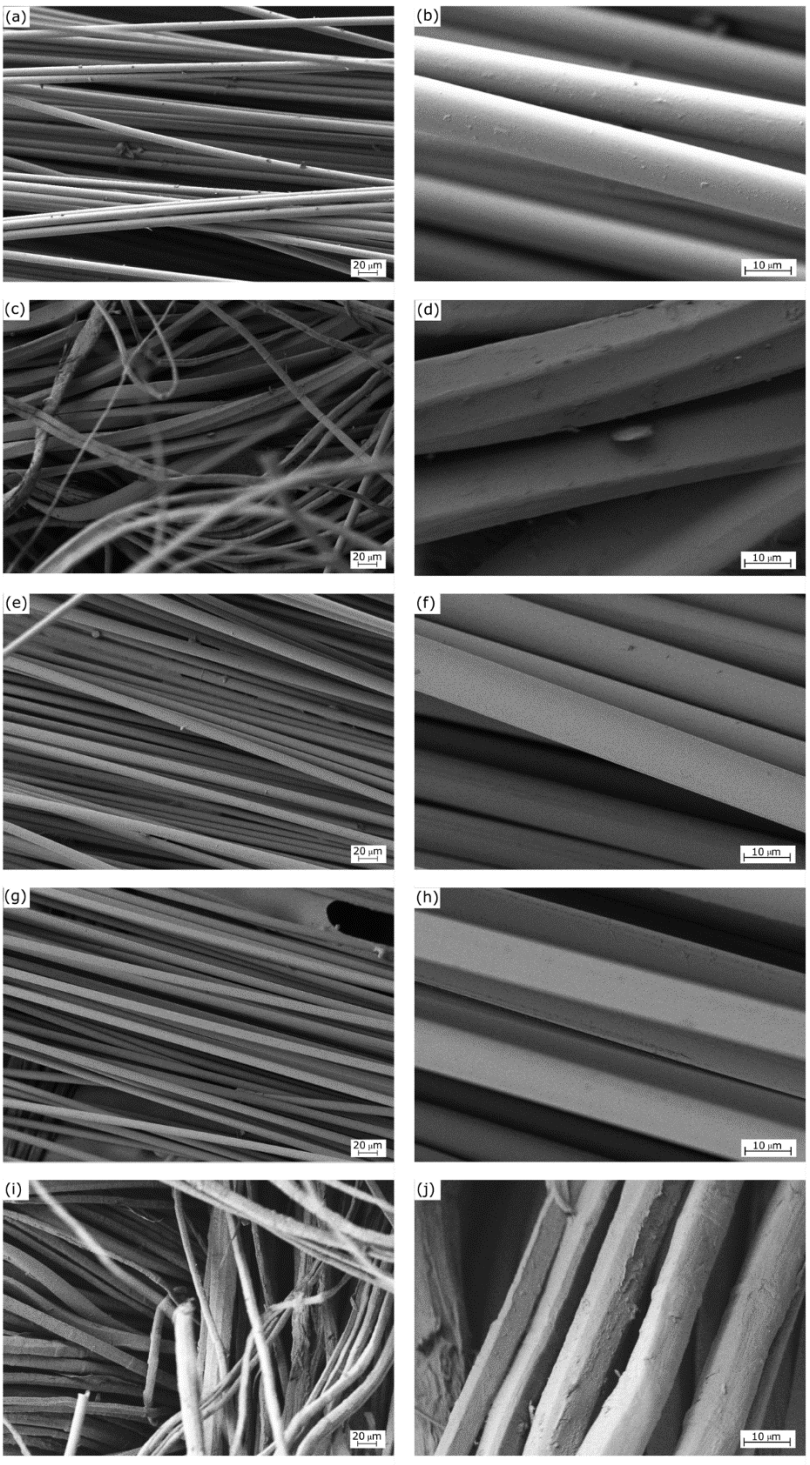

Figure III.2.5.2. FESEM images at different magnifications (x200 left column, x1000 right column) corresponding to surface morphology of (a), (b) as-received basalt fibers, (c), (d) untreated flax fibers, (e), (f) basalt fibers subjected to cleaning + heat treatment, (g), (h) silanized basalt fibers and (i), (j) silanized flax fibers.

Mechanical Properties and Morphology of Basalt/flax Hybrid Composite Laminates

The mechanical behaviour of basalt/flax hybrid laminates was studied through flexural and Charpy tests (as an estimation of the toughness). The values obtained by the different mechanical tests are summarize in table III.2.5.3. It is noteworthy that the high values obtained for flexural strength and impact strength are mainly due to the effect provided by the coupling agent as observed in other similar composite laminates [43-45]. It can be seen that the flexural strength (σ_f) and flexural modulus (E_f) for B8F0 laminate are 467.9 MPa and 14.7 GPa respectively, which are relatively high due to the stiff properties of basalt fiber which are comparable to those of glass fibers and slate fibers as reported by Samper, *et al*. [46]. In addition, this is due to the great affinity that these types of fibers have with a polymeric matrix after silanization process, in this case, with a glycidyl silane which can readily react with the epoxy resin. On the contrary, as flax fiber is characterized by remarkably lower mechanical properties, the B0F8 composite laminate offers a flexural strength of 51.5 MPa and a flexural modulus of 2.2 GPa which are close to some engineering plastics. It is evident that this composite laminate with all-basalt fabrics (B8F0) is the one with the highest flexural strength and modulus but it is possible to substitute some basalt fabrics with flax fabrics, which leads to increased environmental efficiency and balanced mechanical properties. For example, the B6F2 composite laminate, with two flax plies offers high flexural properties of 307.7 MPa (flexural strength) and 12.2 GPa (flexural modulus) which can compete with some conventional glass fiber composites. Even the composite with 4 flax plies and 4 basalt plies (B4F4) shows interesting mechanical performance, with a flexural strength of 241.9 MPa and a flexural modulus close to 10 GPa (9.5 GPa). This increase in flexural properties can be attributed to the good synergy that the reinforcement fibers have with the matrix because of the treatment with coupling agents carried out before their manufacture, as above-mentioned. Usually, polymer-matrix interactions are not good enough to guaranty load transfer, and this results in poor or decreased mechanical properties. Nevertheless, coupling agents such as silanes, as they possess dual functionality, they can react/interact with both the thermosetting matrix and the reinforcing fiber and, positively contribute to load transfer, with a subsequent positive effect on mechanical properties. The literature presents hybrid materials in which the incorporation of glass fiber resulted in flexural properties similar to those obtained in this work [47,48], making this a potential environmentally friendly alternative for some glass-fiber composites in many applications. It is important to remark that even with the same number of flax and basalt pies, B4F4 and B4F4alt composite laminates offer remarkably

different flexural properties. In B4F4 composites, basalt fabrics are located in the external plies of the symmetric laminates (see table III.2.5.2) This stacking sequence provides increased stiffness and strength. On the contrary, the B4F4alt composite laminate, contains one external basalt ply and two internal (in the middle) basalt plies; so that, flax fiber acts as the principal reinforcement material thus leading to decreased mechanical properties. In particular, the flexural strength and modulus for the B4F4alt laminate are 156.5 MPa and 4.0 GPa which are almost half the values of the B4F4 stacking sequence. As reported by Park and Jang [49], in hybrid carbon/polyethylene composites, the stacking sequence and the relative position of the carbon plies play a key role on final performance. As the flax ply number increases, it is detectable a decrease in flexural performance but even for the B2F6 composite laminate, the flexural strength is interesting (129.7 MPa) with a flexural modulus of 6.4 GPa. These properties are typical of engineering plastics reinforced with short glass and/or carbon fibers [50,51], thus giving an alternative to the high cost of these engineering plastics and, what is more interesting, providing increased environmental efficiency.

With respect to the impact strength obtained by the Charpy test, table III.2.5.3 shows the effect of hybridization on toughness, measured as the impact strength. In a similar way to flexural properties, the highest impact strength is obtained for the all-basalt composite (B8F0) with and absorbed energy of 116.9 kJ m^{-2}. This impact energy is relatively high compared to other composite laminates. For example, Samper, *et al*. [46] reported an impact strength of almost 80 kJ m^{-2} in composites with slate 4 plies embedded into an epoxy resin, using a glycidyl silane as coupling agent. Basalt laminates offer superior impact strength properties. As some basalt plies are exchanged by flax plies, the impact strength decreases down to values of 9.0 kJ m^{-2} for the all-flax composite laminate (B0F8) which indicates very low energy absorption, even lower than some engineering plastics, such as PBSA injected samples (26 kJ m^{-2}), PCL/PHB binary blends with 75 % of PCL and 25 % of PHB (11 kJm^{-2}), and LDPE injected specimens (53 kJ m^{-2}) [52-54]. It should be noted that composite laminates made by four basalt plies and four flax plies show relatively high values for the impact strength (B4F4alt), of 77.8 kJ m^{-2}. Once again, composite laminates with the same number of basalt and flax plies but with different stacking sequences show different behaviour. As indicated previously, flax plies are not good energy absorbers; for this reason, the B4F4 shows slightly lower energy absorption than the B4F4alt, with values of 64.0 kJ m^{-2} and 77.8 kJ m^{-2} respectively. In B4F4 composite, the outer plies are basalt fabrics and they can absorb some energy in the initial stages of the impact process. Once the basalt fabrics are broken, flax plies do not offer high resistance to deformation thus leading to slightly

reduced impact strength values compared to B4F4alt. In this last case, an outer basalt ply receives the impact and breaks and then, immediately, flax fibers are exposed to impact with very low energy absorption but this stacking sequence contains two basalt plies in the middle which are able to absorb energy once the pendulum has lost some of its initial impact energy and this gives slightly higher impact strength. In addition, when the strongest fibers are located at the skin region (outer plies), they can withstand high tensile and compression stresses during the impact and this positively contributes improved toughness as reported by Ary Subagia, *et al.* [55]. It is possible to observe similar results in different hybrid composite structures in which, the stacking sequence is a key parameter on final performance of composite plates; in general when the stiffer and strongest plies are located in the skins (outer plies), flexural and impact properties are remarkably improved [56].

Table III.2.5.3. Mechanical properties of basalt/flax hybrid composite laminates with different stacking sequences obtained from flexural and Charpy tests

Code	Flexural properties		Impact strength (kJ m^{-2})
	σ_f (MPa)	E_f (GPa)	
B8F0	467.9 ± 83.3^{a}	14.7 ± 1.0^{a}	116.9 ± 2.1^{a}
B6F2	307.7 ± 53.9^{a}	12.2 ± 0.7^{b,a}	88.0 ± 5.7^{b}
B4F4	241.9 ± 39.6^{b}	9.5 ± 0.4^{c}	64.0 ± 4.8^{d,e}
B2F6	129.7 ± 24.7^{c,d}	6.4 ± 0.4^{d}	58.1 ± 1.2^{e,d}
B4F4alt	156.5 ± 28.6^{d,c}	4.0 ± 0.2^{e}	77.8 ± 5.0^{c}
B0F8	51.5 ± 10.2^{e}	2.2 ± 0.1^{f}	9.0 ± 0.8^{f}

$^{a-f}$ different letters in the same column indicate a significant difference among the samples $p<0.05$

Energy absorption and subsequently, toughness, is key parameter on selecting materials for engineering applications. For this reason, an additional estimation of the toughness has been carried out by tensile tests with the same samples used for impact tests. Figure III.2.5.3 gathers a comparative plot of the stress-strain diagrams obtained for basalt/flax hybrid composite plates. The area below the characteristic stress-strain curve is representative for the overall toughness or the absorbed energy during the deformation and fracture of composite plates. All composites show a linear behaviour until fracture occurs. The most relevant information obtained from this test is summarized in table III.2.5.4. As one can see, a simple observation of figure III.2.5.3 indicates that the all-basalt composite plate is, with difference, the one with the highest toughness, measured as the area below the stress-strain curve. In particular, this area is 25.06 MN m m^{-3}which is remarkably higher than the area below the stress-strain curve for all-flax

composite plate (B0F8), which is 1.77 MN m m^{-3}. These units, i.e. MN m m^{-3}, suggest energy or work (MN m) units per volume fraction (m^{-3}), so that, it is possible to use this value as an estimation of the energy absorbed until failure. As expected, when some basalt plies are exchanged by flax plies, the area below the σ - ε diagram decreases as basalt is much tougher than flax. These results are in total agreement with those obtained by the conventional Charpy test. Nevertheless, with regard to composites with the same number of basalt and flax plies with different stacking sequences (B4F4 and B4F4 alt), it is possible to observe some differences with the results obtained by the Charpy test. Although there is a correlation between these two tests, the conditions are, obviously, different since the Charpy considers energy absorption in a very short period of time (impact) while the tensile test offers the energy absorption in a larger period of time. Therefore, it is possible to conclude that the way the load is applied can influence the final energy absorption as in this case. With regard to the maximum stress before failure occurs, table III.2.5.4 shows the same tendency observed by flexural tests. The maximum stress value for the notched sample in this tensile test corresponds to the B8F0 laminate with a value of 211.9 MPa. On the contrary, the lowest value can be detected for the all- flax composite (B0F8) with a maximum tensile stress of 21.7 MPa. As the basalt plies are exchanged by flax plies, the maximum tensile stress decreases.

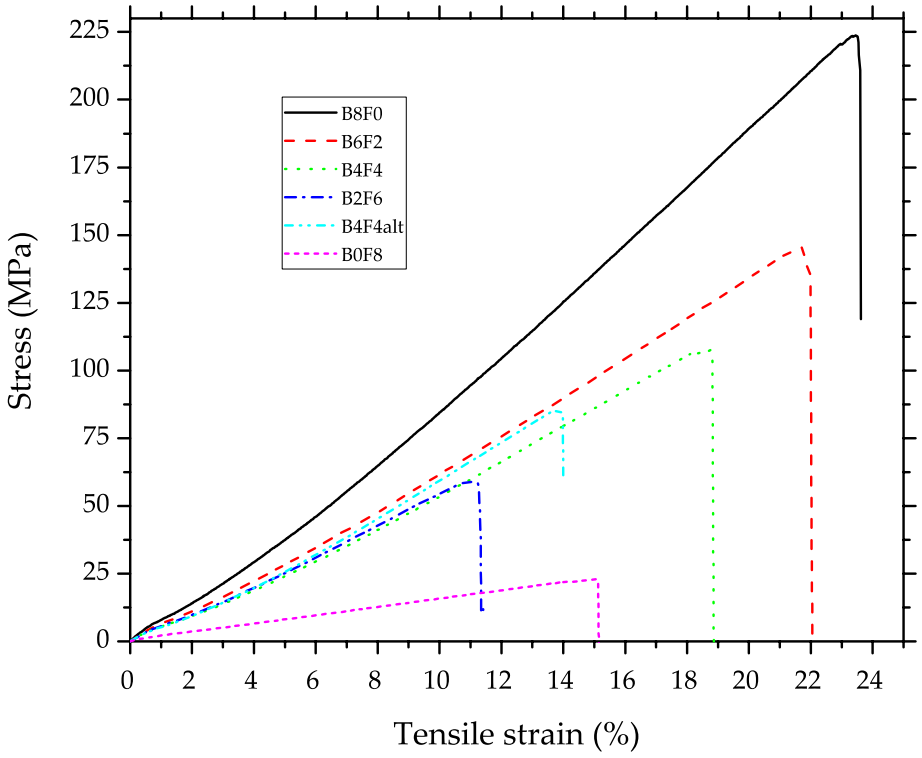

Figure III.2.5.3. Stress-strain curve plots of notched samples (U type) of basalt/flax hybrid composite laminates with different stacking sequences obtained from tensile tests.

Table III.2.5.4. Mechanical properties of basalt/flax hybrid composite laminates with different stacking sequences obtained tensile tests on notched samples (U type)

Code	σ_t (MPa)	ε_b (%)	Area (MN m m^{-3})
B8F0	211.9 ± 13.8^{a}	23.0 ± 0.8^{a}	25.06 ± 2.03^{a}
B6F2	146.8 ± 18.1^{b}	21.1 ± 2.8^{a,c}	15.41 ± 1.24^{b}
B4F4	104.8 ± 12.9^{c}	19.7 ± 0.5^{b,c,a}	9.69 ± 1.02^{c}
B2F6	54.9 ± 12.8^{e}	11.4 ± 3.0^{d}	3.39 ± 0.31^{d}
B4F4alt	85.9 ± 5.4^{d}	18.3 ± 1.0 ^{c,b,a}	5.65 ± 0.49^{e}
B0F8	21.7 ± 6.8^{f}	16.2 ± 3.5^{c,b,a}	1.77 ± 0.15^{f}

$^{a-f}$ different letters in the same column indicate a significant difference among the samples $p<0.05$

The fractured surfaces of the hybrid composite plates from impact tests were observed by FESEM in order to assess the effectiveness of the coupling agent in terms of the interface phenomena of the reinforcing fibers and the polymer matrix. The polymer-fiber interface gives an idea of the effect of the coupling agent treatment on mechanical properties. Figure III.2.5.4a and III.2.5.4b correspond to the fracture of the all basalt (B8F0) composite laminate. It can be observed that there are no discontinuities between the matrix and the surrounding fibers, that is, which indicates good wettability of the fiber resin with the resin. This is because the coupling agent (glycidyl silane) has an epoxy functionality that can react with both basalt fiber and epoxy matrix. The coupling between the glycidyl silane and the basalt fiber takes place by the condensation reaction of the hydrolyzed silane and the hydroxyl groups in the outmost layers of basalt fiber. This chemical anchorage of the silane onto the basalt fiber is achieved during the pre-treatment stage, and there is still a glycidyl group which can be able to react with the epoxy resin during the crosslinking. For this reasons, coupling agents act as a physical bridges between the fibers and the matrix and this allows good material's cohesion and continuity which has a positive effect on mechanical performance as described by España, *et al*. [57]. As one can see, the individual fibers show a very rough surface which corresponds to the failure of the epoxy matrix instead of fiber debonding or pull-out, which is indicating good interface interactions as reported by Samper, *et al.* [46]. The fracture surface corresponding to all-flax composite plate (B0F8) is shown in figure III.2.5.4c and III.2.5.4d. As it can be seen, there are some small gaps around the flax fibers, which leads to poor interaction between the fiber and the epoxy resin. This is indicating that the fiber is not well embedded into the epoxy resin, even with the previous silanization process. As reported by Bertomeu, *et al.* [58], in flax/epoxy composites, the gap around the fiber and the surrounding matrix can be reduced by using conventional

silanization treatment on flax fabrics; nevertheless, this gap does not disappear. The presence of these gaps does not allow right load transfer from the epoxy matrix to the flax fiber, and this has a negative effect on final properties. In addition, it is important to bear in mind that the mechanical properties of flax fibers are remarkably lower than those of basalt fibers, and all this has an effect on final performance of all-flax composites [59,60].

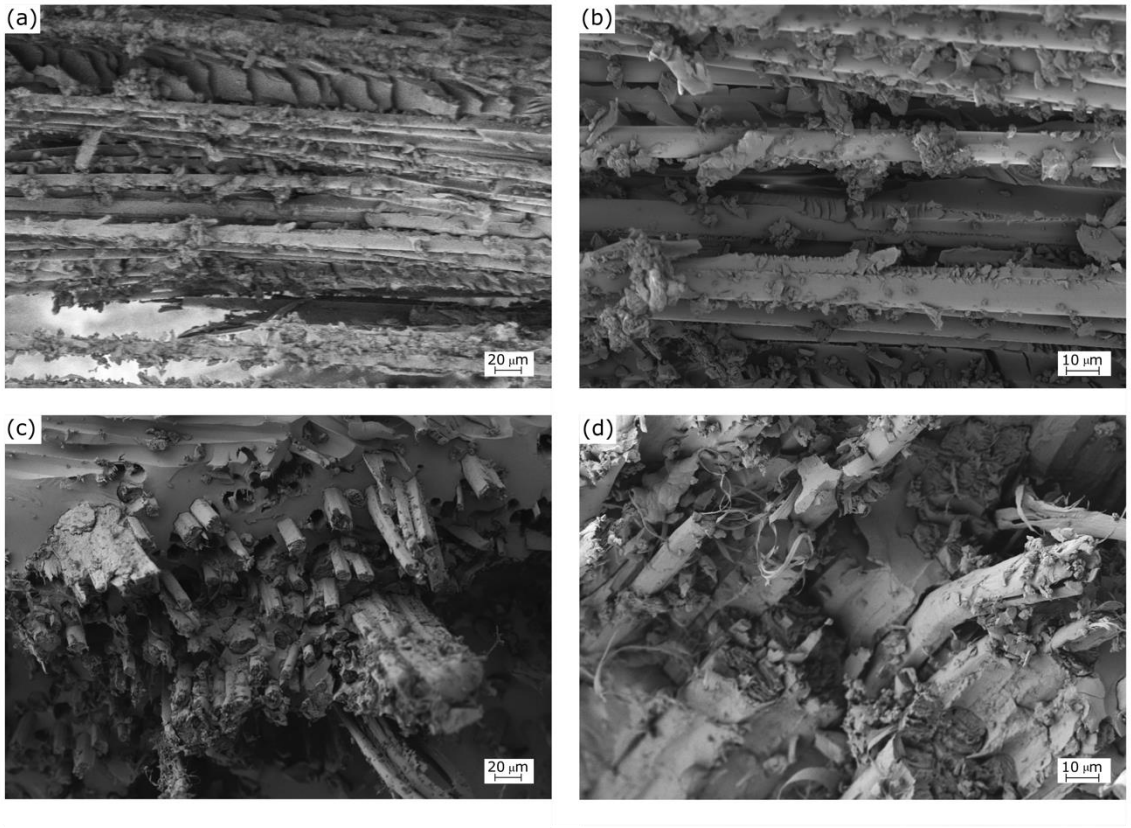

Figure III.2.5.4. FESEM images at different magnifications (x200 left column, x500 right column) corresponding to fractured surfaces from impact tests of composites with different fibers embedded into an epoxy resin matrix, (a), (b) all-basalt B8 F0 composite plate, (c), (d) all- flax B0F8 composite plate.

In order to better ascertain the characteristics of the fractured surfaces of the hybrid composite laminates from impact test, fractured surfaces were also observed by optical stereomicroscopy with different ocular magnifying glasses. Figure III.2.5.5 gathers the cross-section and the fracture surfaces from impact tests corresponding to the different hybrid composite laminates. The fractured surface of the all-basalt B8F0 composite plate is displayed in figures III.2.5.5b and III.2.5.5c which shows the fracture surface is the result of a low matrix resistance (rigid epoxy matrix) compared to the strong basalt fiber. It is possible to see that the fibers exhibit small tearing areas at their fracture points, which is representative for a brittle behaviour of basalt fibers [42]. This is an indication of the strength these fibers provide to composites and this agrees with the

above-mentioned impact-absorbed energy values which were the highest for B8F0 composite plate, due mostly to the excellent mechanical properties of the basalt fiber and the good fiber/matrix interface achieved after the silanization, as observed in the FESEM analysis. For hybrid composites, the fractured surface always shows the same morphology. As it can be seen in figures III.2.5.5e and III.2.5.5f, corresponding to the hybrid B6F2 composite plate, the fracture is caused by the premature failure of the flax fibers, since these present a lower pull-out length compared to the basalt fibers. This is due to their lower strength compared to basalt fiber as reported in literature [61,62]. Although the interface between the flax fiber and the epoxy matrix is good enough, there is poor interaction with basalt plies and, therefore, these laminates show small gaps between the flax and basalt plies, causing delamination failure at the interface. On one hand, this poor interlaminar interaction can be caused by the manufacturing process since, the behaviour of both fibers with the epoxy resin is completely different. On the other hand, the silanized basalt fibers stablish strong interactions with the epoxy resin while the highly porous flax fiber absorbs more epoxy resin and this leads to a heterogeneous epoxy distribution in the plies. The same comments can be done for hybrid composite plates with different stacking sequences as shown in figure III.2.5.5 with increasing the number of flax plies: Figures III.2.5.5h and III.2.5.5i (B4F4), figures III.2.5.5k and III.2.5.5l (B2F6). In all these composites, flax fabrics fails before basalt fabrics. Figures III.2.5.5q and III.2.5.**5r** show the fractured surface all-flax B0F8 composite laminate. Despite the fiber/matrix interface interaction was relatively good, the presence of interlaminar gaps was greater, which resulted in a decrease in its mechanical properties as described previously. Jusoh, *et al.* [63] suggested that the different nature of natural and basalt fibers resulted in poor interfacial bonding. Possible premature delamination of the layers may be caused by an internal failure of the interlayer as occurred in laminates made with glass and flax fibers, and with glass and jute laminates, that presented a high degree of stretching causing the fibers to pull out during fracture.

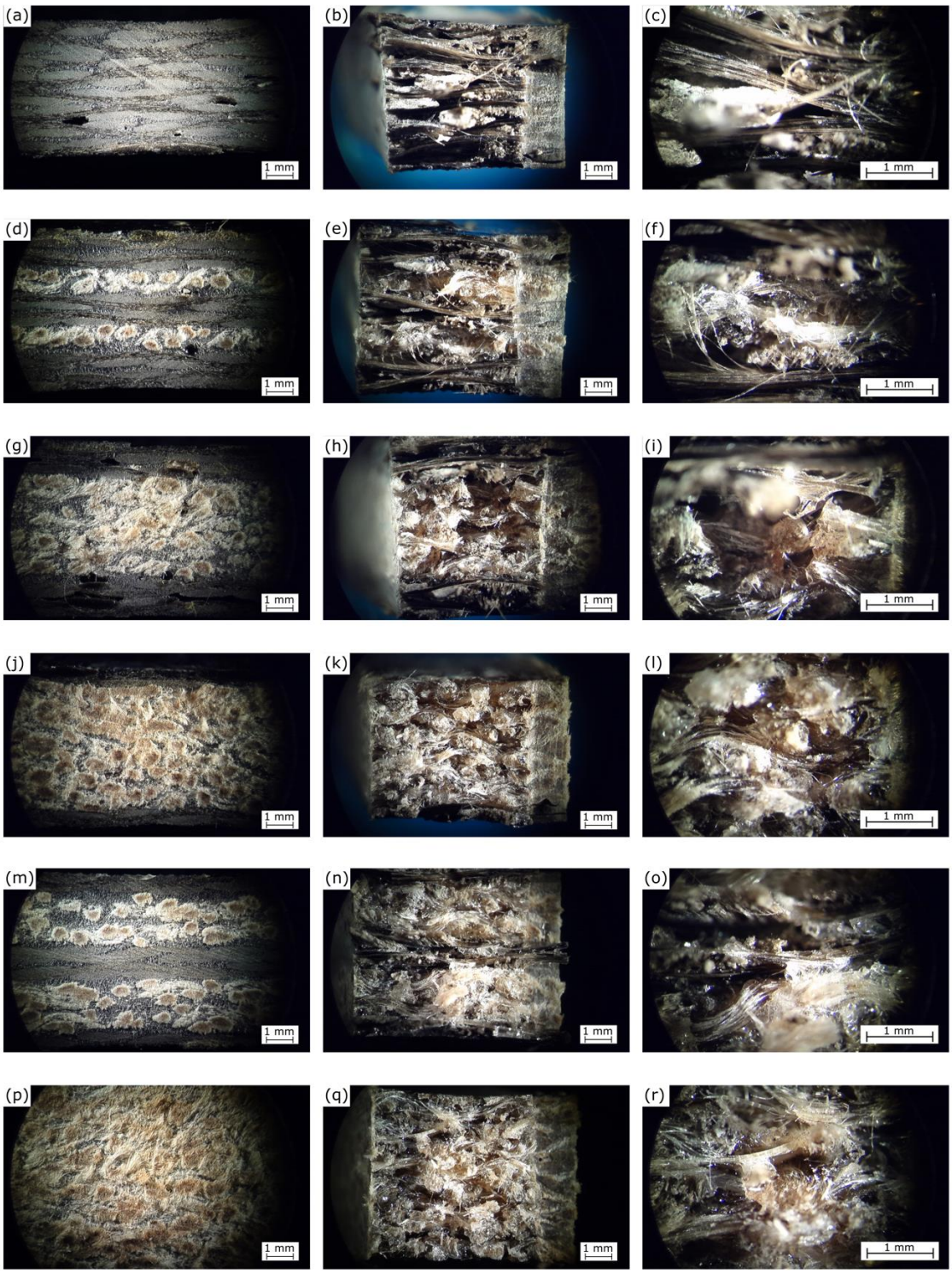

Figure III.2.5.5. Stereomicroscopy images at different magnifications (x16, left and central column; x40 right column) corresponding to the cross section and the fracture surfaces from impact tests of (a), (b), (c) B8F0, (d), (e), (f) B6F2, (g), (h), (i) B4F4, (j), (k), (l) B2F6, (m), (n), (o) B4F4alt, (p), (q), (r) B0F8.

Thermal and Thermomechanical Properties of Basalt/ flax Hybrid Composite Laminates

Regarding to the dynamic mechanical thermal behaviour (DMTA) of hybrid basalt/flax composite laminates, figure III.2.5.6 gathers the comparative plots of the storage modulus (*G'*) and the dynamic damping factor (*tan δ*) with respect to temperature. Table III.2.5.5 includes some characteristic values of *G'* at 60 ºC and 125 ºC as to compare the dynamic performance of the hybrid composites. Figure III.2.5.6a shows the evolution of the storage modulus (*G'*) as a function of the increasing temperature. It is important to bear in mind that the storage modulus is directly related to the stiffness of the material and its elastic behaviour (ability to storage energy when dynamically loaded). It can be seen that all-basalt B8F0 composite plate has a *G'* value of 1.78 GPa at a temperature of 60 ºC. Above this temperature, between 70 ºC and 110 ºC a remarkable decrease in *G'* (about two- fold decrease) can be observed, which is attributable to the α-relaxation of the epoxy resin or its glass transition temperature (T_g). The α-relaxation in crosslinked thermosetting resins is directly related chain mobility. Below the α-relaxation, the chain mobility into the 3D crosslinked epoxy resin is highly restricted. Nevertheless, above the α-relaxation, the material behaves as a rubber like material and this is a clear evidence of the structure relaxation. Although the crosslinked structure is not lost, some segments can move, vibrate, and so on, leading to this rubbery behaviour. The internal structural stresses due to the fully crosslinked epoxy resin, is relaxed at moderate-to-high temperatures, thus indicating a transition from a rigid state to a rubbery state, which is representative for the glass transition temperature (T_g) this movement is made between the crosslinking points in the glass-to-rubber transition, and this is related to the *tan δ* peak [64]. As one can see, a clear decrease in *G'* takes place during the α-relaxation or T_g. For example, for the B8F0 composite plate, the *G'* value below T_g (at 60 ºC) is 1.78 GPa and this is reduced down to values of 98.4 MPa above the T_g (at 125 ºC). This indicates that below T_g the material behaves as a stiff and rigid material while above the T_g, the material has become soft. The hybrid stacking sequence has a clear effect on *G'*. The *G'* curve for the all-basalt B8F0 composite laminate corresponds to the highest values of the developed materials. As the flax content increases in hybrid basalt/flax composites, these plates become less stiff and, subsequently, the *G'* characteristic curves are shifted to lower values. The shape of the curve is the same but all the curves are moved down which indicate softer composites [16]. This corroborates the data obtained by flexural tests; by increasing the number of flax fibers layers the material's stiffness decreases. The lowest storage modulus corresponds, as expected, to the all-flax B0F8 composite plate with a value of *G'* of 0.57

GPa at 60 ºC. Figure III.2.5.6b shows the evolution of the dynamic damping factor which is a measure of the lost energy to the stored energy ratio, *tan δ* with increasing temperature. The glass transition temperature (T_g) is gathered in table III.2.5.5. Despite there are several criteria to obtain the T_g, one of the most recognized methods is that based on the peak maximum for the dynamic damping factor. The glass transition temperature corresponds to the matrix (epoxy resin), and, as it can be observed, there is not a remarkable change for all hybrid basalt/flax composites ($p<0.05$). The T_g is highly dependent on several factors such as the type of epoxy resin, the functionality, the hardener, the curing cycle, the use of a post-curing cycle, the use of accelerators, among others [65-67]. Varley, *et al.* [68] have reported a T_g value of a partially bio-based epoxy resin of about 90 ºC after a curing and a post-curing cycle. They reported that reinforcing fibers (with or without a previous surface treatment) do not affect in a remarkable way the T_g.

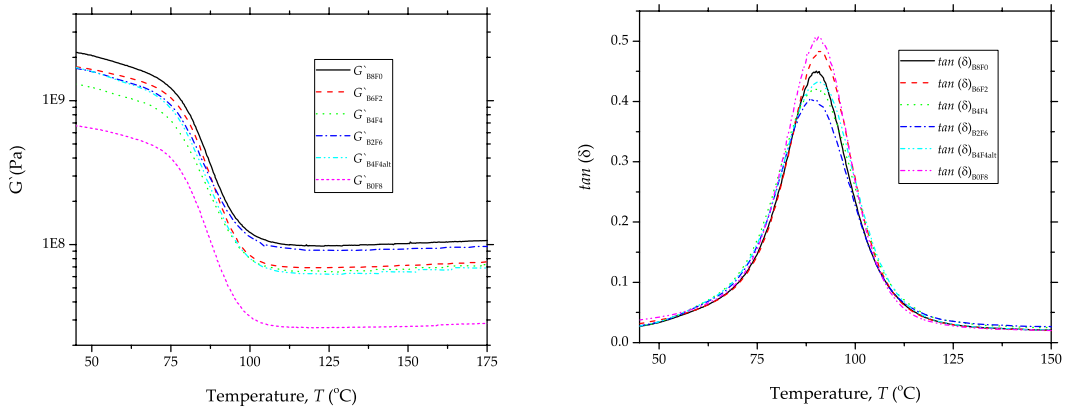

(a) (b)

Figure III.2.5.6. DMTA behaviour of hybrid basalt/flax composite laminates with different stacking sequences; (a) storage modulus, *G'* and (b) dynamic damping factor, *tan (δ).*

The dimensional stability has been determined through the estimation of the coefficient of linear thermal expansion (CLTE) below and above T_g of all composite laminates in this study. As it can be seen in table III.2.5.5, the CLTE of all laminates below T_g is comprised between 250 μm m^{-1} $K^{-1}$and 260 μm m^{-1} K^{-1}, and although small changes can be observed, they are comprised within the standard deviation (lower than 10 %). These values are typical of a glassy state as the CLTE is directly related to the deformation ability [58]. Above the T_g it is possible to see some differences; both all-basalt and all-flax composite laminates show a CLTE of 296.0 μm m^{-1} $K^{-1}$and 273.2 μm m^{-1} K^{-1}, respectively, while all hybrid composites show slightly higher CLTE comprised between 320-370 μm m^{-1} K^{-1}. This phenomenon above T_g has been observed by Gupta

and Brahatheeswaran [69] that suggested an additional expansion of the rubber state compared to the glassy state.

Table III.2.5.5. Thermomechanical properties basalt/flax hybrid laminate composites obtained by DMTA and TMA

Code	DMTA results			CLTE ($\mu m\ m^{-1}\ K^{-1}$) by TMA	
	T_g (ºC)	*G'* at 60 ºC (GPa)	*G'* at 125 ºC (MPa)	Below T_g	Above T_g
B8F0	90.1 ± 1.8[a]	1.78 ± 0.04[a]	98.4 ± 2.0[a]	260.9 ± 17.2[a,b]	296.0 ± 17.0[a,b]
B6F2	91.1 ± 2.0[a]	1.47 ± 0.03[b]	69.3 ± 1.7[b]	256.1 ± 21.0[a,b]	323.6 ± 18.8[a]
B4F4	91.8 ± 2.1[a]	1.07 ± 0.03[d]	64.9 ± 1.1[c]	245.7 ± 19.2[b,a]	367.8 ± 19.2[c]
B2F6	90.4 ± 2.3[a]	1.37 ± 0.05[c]	91.3 ± 2.2[a]	254.2 ± 21.8[a,b]	320.6 ± 17.1[a]
B4F4alt	90.4 ± 1.3[a]	1.35 ± 0.04[c]	62.3 ± 1.6[c]	260.3 ± 22.8[a,b]	376.9 ± 22.1[c]
B0F8	90.9 ± 1.5[a]	0.57 ± 0.01[e]	26.6 ± 0.5[d]	250.9 ± 20.3[a,b]	273.2 ± 20.7[b,a]

[a-e] different letters in the same column indicate a significant difference among the samples $p<0.05$

III.2.5.4. Conclusions

This work has assessed the potential of hybrid basalt/flax composite laminates with a partially bio-based epoxy resin for applications in engineering. These composite laminates can be manufactured by the vacuum assisted resin infusion moulding (VARIM) with excellent reproducibility. A previous treatment of both basalt and flax fabrics gives enhanced mechanical properties on composites. Obviously, the all-basalt composite laminate (8 basalt plies) shows the maximum flexural strength and modulus of 467.9 MPa and 14.7 GPa respectively. But the most important findings of this work is that hybrid composite laminates containing different flax plies can give interesting properties from a technical point of view. It is worthy to remark the high flexural strength and modulus of hybrid composites containing 2 flax plies and 6 basalt plies (307.7 MPa and 12.2 GPa respectively) and the composite with 4 flax plies and 4 basalt plies with a flexural strength of 241.9 MPa and a flexural modulus of almost 10 GPa. These properties allow the use of these composites as potential substitutes of glass and basalt composites in technical applications. In addition, hybrid basalt/flax composites give improved environmental efficiency that can positively contribute to a sustainable development in the field of composite materials. It is important to bear in mind that flax fibers and the partially bio-based resin offer decreased footprint compared to conventional petroleum-derived matrices, i.e. epoxies, unsaturated polyesters, vinyl esters, phenol-formaldehyde resins, among other, and the typical reinforcing fibers in composites, i.e. carbon, aramid and glass fibers.

III.2.5.5. Acknowledgments

This research was funded by the Ministerio de Economía, Industria y Competitividad (MICINN) project number MAT2017-84909-C2-2-R. D. Lascano wants to thank UPV for the grant received though the PAID-01-18 program. Microscopy services at UPV are acknowledged for their help in collecting and analyzing FESEM images.

III.2.5.6. References

1. S. Yang, V.B. Chalivendra, Y.K. Kim. Fracture and impact characterization of novel auxetic Kevlar®/Epoxy laminated composites. *Composite Structures* **2017**, *168*, 120-129.
2. R. Rahman, S.Z.F.S. Putra. Tensile properties of natural and synthetic fiber-reinforced polymer composites. *Mechanical and physical testing of biocomposites, fibre-reinforced composites and hybrid composites* **2019**, 81-102.
3. B. Song, T. Wang, L. Wang, H. Liu, X. Mai, X. Wang, N. Wang, Y. Huang, Y. Ma, Y. Lu. Interfacially reinforced carbon fiber/epoxy composite laminates via in-situ synthesized graphitic carbon nitride (g-C3N4). *Composites Part B: Engineering* **2019**, *158*, 259-268.
4. C. Soutis. Fibre reinforced composites in aircraft construction. *Progress in Aerospace Sciences* **2005**, *41*, 143-151.
5. R.A. Sullivan. Automotive carbon fiber: Opportunities and challenges. *Jom* **2006**, *58*, 77-79.
6. E. Monaldo, F. Nerilli, G. Vairo. Basalt-based fiber-reinforced materials and structural applications in civil engineering. *Composite Structures* **2019**, *214*, 246-263.
7. Z.S.W. J. Yin. Structural performances of short steel-fiber reinforced concrete beams with externally bonded FRP sheets. *Construction and Building Materials* **2003**, *17*, 463-470.
8. D. Church. A revolution in low-cost carbon fiber production. *Reinforced Plastics* **2018**, *62*, 35-37.
9. S.E. Artemenko, Y.A. Kadykova. Polymer composite materials based on carbon, basalt, and glass fibres. *Fibre Chemistry* **2008**, *40*, 37-39.
10. G. Marom, E. Drukker, A. Weinberg, J. Banbaji. Impact behaviour of carbon/Kevlar hybrid composites. *Composites* **1986**, *17*, 150-153.
11. A.-C. Corbin, D. Soulat, M. Ferreira, A.-R. Labanieh, X. Gabrion, P. Malécot, V. Placet. Towards hemp fabrics for high-performance composites: Influence of weave pattern and features. *Composites Part B: Engineering* **2020**, *181*, 107582.
12. O. Faruk, A.K. Bledzki, H.P. Fink, M. Sain. Biocomposites reinforced with natural fibers: 2000-2010. *Progress in Polymer Science* **2012**, *37*, 1552-1596.

13. S. Shahinur, M. Hasan. Natural fiber and synthetic fiber composites: Comparison of properties, performance, cost and environmental benefits. *Elsevier* **2020**, 794-802.

14. M. Ramesh. Flax (Linum usitatissimum L.) fibre reinforced polymer composite materials: A review on preparation, properties and prospects. *Progress in Materials Science* **2019**, *102*, 109-166.

15. Y. Zhang, Y. Li, H. Ma, T. Yu. Tensile and interfacial properties of unidirectional flax/glass fiber reinforced hybrid composites. *Composites Science and Technology* **2013**, *88*, 172-177.

16. S.S. Morye, R.P. Wool. Mechanical properties of glass/flax hybrid composites based on a novel modified soybean oil matrix material. *Polymer Composites* **2005**, *26*, 407-416.

17. M. Ramesh, C. Deepa, G. Arpitha, V. Gopinath. Effect of hybridization on properties of hemp-carbon fibre-reinforced hybrid polymer composites using experimental and finite element analysis. *World Journal of Engineering* **2019**, *16*.

18. P.K. Bajpai, K. Ram, L.K. Gahlot, V.K. Jha. Fabrication of glass/jute/epoxy composite based industrial safety helmet. *Materials Today: Proceedings* **2018**, *5*, 8699-8706.

19. K. Palanikumar, M. Ramesh, K. Hemachandra Reddy. Experimental investigation on the mechanical properties of green hybrid sisal and glass fiber reinforced polymer composites. *Journal of Natural Fibers* **2016**, *13*, 321-331.

20. V. Fiore, T. Scalici, G. Di Bella, A. Valenza. A review on basalt fibre and its composites. *Composites Part B: Engineering* **2015**, *74*, 74-94.

21. T. Czigány, J. Vad, K. Pölöskei. Basalt fiber as a reinforcement of polymer composites. *Periodica Polytechnica Mechanical Engineering* **2005**, *49*, 3-14.

22. T. Deák, T. Czigány. Chemical composition and mechanical properties of basalt and glass fibers: A comparison. *Textile Research Journal* **2009**, *79*, 645-651.

23. M. Birkner, S. Spange, K. Koschek. Basalt fiber reinforced polymers with improved thermal and mechanical properties by combination of twin polymerization with epoxide chemistry. *Polymer Composites* **2019**, *40*, 3115-3121.

24. J.J. Lee, J. Song, H. Kim. Chemical stability of basalt fiber in alkaline solution. *Fibers and Polymers* **2014**, *15*, 2329-2334.

25. M. Tehrani Dehkordi, H. Nosraty, M.M. Shokrieh, G. Minak, D. Ghelli. The influence of hybridization on impact damage behavior and residual compression strength of intraply basalt/nylon hybrid composites. *Materials and Design* **2013**, *43*, 283-290.

26. D. Matykiewicz, M. Barczewski, D. Knapski, K. Skórczewska. Hybrid effects of basalt fibers and basalt powder on thermomechanical properties of epoxy composites. *Composites Part B: Engineering* **2017**, *125*, 157-164.

27. D. Matykiewicz, M. Barczewski. On the impact of flax fibers as an internal layer on the properties of basalt-epoxy composites modified with silanized basalt powder. *Composites Communications* **2020**, *20*, 100360.

28. C. Sergi, J. Tirillò, M.C. Seghini, F. Sarasini, V. Fiore, T. Scalici. Durability of basalt/hemp hybrid thermoplastic composites. *Polymers* **2019**, *11*, 603.

29. M.D. Samper, R. Petrucci, L. Sánchez-Nacher, R. Balart, J.M. Kenny. Effect of silane coupling agents on basalt fiber-epoxidized vegetable oil matrix composite materials analyzed by the single fiber fragmentation technique. *Polymer Composites* **2015**, *36*, 1205-1212.

30. B.V. Ramnath, C. Elanchezhian, P.V. Nirmal, G.P. Kumar, V.S. Kumar, S. Karthick, S. Rajesh, K. Suresh. Experimental investigation of mechanical behavior of jute-flax based glass fiber reinforced composite. *Fibers and Polymers* **2014**, *15*, 1251-1262.

31. J. Yang, J. Xiao, J. Zeng, L. Bian, C. Peng, F. Yang. Matrix modification with silane coupling agent for carbon fiber reinforced epoxy composites. *Fibers and Polymers* **2013**, *14*, 759-766.

32. Y. Xie, C.A.S. Hill, Z. Xiao, H. Militz, C. Mai. Silane coupling agents used for natural fiber/polymer composites: A review. *Composites Part A: Applied Science and Manufacturing* **2010**, *41*, 806-819.

33. H.A. Al-Qureshi. Automobile leaf springs from composite materials. *Journal of Materials Processing Technology* **2001**, *118*, 58-61.

34. H. Kishi, A. Fujita, H. Miyazaki, S. Matsuda, A. Murakami. Synthesis of wood-based epoxy resins and their mechanical and adhesive properties. *Journal of Applied Polymer Science* **2006**, *102*, 2285-2292.

35. W. Riemenschneider, H.M. Bolt. Esters , Organic. *Ullmann's Encyclopedia of Industrial Chemistry* **2005**, *12*, 8676-8694.

36. F.L. Jin, X. Li, S.J. Park. Synthesis and application of epoxy resins: A review. *Journal of Industrial and Engineering Chemistry* **2015**, *29*, 1-11.

37. B. Ferrero, V. Fombuena, O. Fenollar, T. Boronat, R. Balart. Development of natural fiber-reinforced plastics (NFRP) based on biobased polyethylene and waste fibers fromPosidonia oceanicaseaweed. *Polymer Composites* **2015**, *36*, 1378-1385.

38. T. Boronat, V. Fombuena, D. Garcia-Sanoguera, L. Sanchez-Nacher, R. Balart. Development of a biocomposite based on green polyethylene biopolymer and eggshell. *Mater. Des.* **2015**, *68*, 177-185.

39. A. Carbonell-Verdu, L. Bernardi, D. Garcia-Garcia, L. Sanchez-Nacher, R. Balart. Development of environmentally friendly composite matrices from epoxidized cottonseed oil. *European Polymer Journal* **2015**, *63*, 1-10.

40. S. Torres-Giner, N. Montanes, O. Fenollar, D. García-Sanoguera, R. Balart. Development and optimization of renewable vinyl plastisol/wood flour composites exposed to ultraviolet radiation. *Mater. Des.* **2016**, *108*, 648-658.

41. D. Lascano, J. Valcárcel, R. Balart, L. Quiles-Carrillo, T. Boronat. Manufacturing of composite materials with high environmental efficiency using epoxy resin of renewable origin and permeable light cores for vacuum-assisted infusion molding. *Ingenius* **2020**, 62-73.

42. J.M. Park, W.G. Shin, D.J. Yoon. A study of interfacial aspects of epoxy-based composites reinforced with dual basalt and SiC fibres by means of the fragmentation and acoustic emission techniques. *Composites Science and Technology* **1999**, *59*, 355-370.

43. J. Cruz, R. Fangueiro. Surface modification of natural fibers: A review. *Procedia Engineering* **2016**, *155*, 285-288.

44. H. Luo, G. Xiong, C. Ma, P. Chang, F. Yao, Y. Zhu, C. Zhang, Y. Wan. Mechanical and thermo-mechanical behaviors of sizing-treated corn fiber/polylactide composites. *Polymer Testing* **2014**, *39*, 45-52.

45. M. Sood, G. Dwivedi. Effect of fiber treatment on flexural properties of natural fiber reinforced composites: A review. *Egyptian Journal of Petroleum* **2018**, *27*, 775-783.

46. M.D. Samper, R. Petrucci, L. Sánchez-Nacher, R. Balart, J.M. Kenny. New environmentally friendly composite laminates with epoxidized linseed oil (ELO) and slate fiber fabrics. *Composites Part B: Engineering* **2015**, *71*, 203-209.

47. R. Petrucci, C. Santulli, D. Puglia, E. Nisini, F. Sarasini, J. Tirillò, L. Torre, G. Minak, J.M. Kenny. Impact and post-impact damage characterisation of hybrid composite laminates based on basalt fibres in combination with flax, hemp and glass fibres manufactured by vacuum infusion. *Composites Part B: Engineering* **2015**, *69*, 507-515.

48. R. Petrucci, C. Santulli, D. Puglia, F. Sarasini, L. Torre, J.M. Kenny. Mechanical characterisation of hybrid composite laminates based on basalt fibres in combination with flax, hemp and glass fibres manufactured by vacuum infusion. *Materials and Design* **2013**, *49*, 728-735.

49. R. Park, J. Jang. Performance improvement of carbon fiber/polyethylene fiber hybrid composites. *Journal of Materials Science* **1999**, *34*, 2903-2910.

50. L.V.J. Lassila, T. Nohrström, P.K. Vallittu. The influence of short-term water storage on the flexural properties of unidirectional glass fiber-reinforced composites. *Biomaterials* **2002**, *23*, 2221-2229.

51. F. Rezaei, R. Yunus, N.A. Ibrahim, E.S. Mahdi. Development of short-carbon-fiber-reinforced polypropylene composite for car bonnet. *Polymer - Plastics Technology and Engineering* **2008**, *47*, 351-357.

52. D. Lascano, L. Quiles-Carrillo, R. Balart, T. Boronat, N. Montanes. Toughened poly(lactic acid)—PLA formulations by binary blends with poly(butylene succinate-co-adipate)—PBSA and their shape memory behaviour. *Materials* **2019**, *12*, 622-622.

53. D. Garcia-Garcia, J.M. Ferri, T. Boronat, J. Lopez-Martinez, R. Balart. Processing and characterization of binary poly(hydroxybutyrate) (PHB) and poly(caprolactone) (PCL) blends with improved impact properties. *Polymer Bulletin* **2016**, *73*, 3333-3350.

54. M. Evstatiev, S. Fakirov, B. Krasteva, K. Friedrich, J.A. Covas, A.M. Cunha. Recycling of poly(ethylene terephthalate) as polymer-polymer composites. *Polymer Engineering and Science* **2002**, *42*, 826-835.

55. I.D.G. Ary Subagia, Y. Kim, L.D. Tijing, C.S. Kim, H.K. Shon. Effect of stacking sequence on the flexural properties of hybrid composites reinforced with carbon and basalt fibers. *Composites Part B: Engineering* **2014**, *58*, 251-258.

56. J. Zhang, K. Chaisombat, S. He, C.H. Wang. Hybrid composite laminates reinforced with glass/carbon woven fabrics for lightweight load bearing structures. *Materials and Design* **2012**, *36*, 75-80.

57. J.M. España, M.D. Samper, E. Fages, L. Sánchez-Nácher, R. Balart. Investigation of the effect of different silane coupling agents on mechanical performance of basalt fiber composite laminates with biobased epoxy matrices. *Polymer Composites* **2013**, *34*, 376-381.

58. D. Bertomeu, D. García-Sanoguera, O. Fenollar, T. Boronat, R. Balart. Use of eco-friendly epoxy resins from renewable resources as potential substitutes of petrochemical epoxy resins for ambient cured composites with flax reinforcements. *Polymer Composites* **2012**, *33*, 683-692.

59. J. Militký, V. Kovačič, J. Rubnerová. Influence of thermal treatment on tensile failure of basalt fibers. *Engineering Fracture Mechanics* **2002**, *69*, 1025-1033.

60. P. Wambua, J. Ivens, I. Verpoest. Natural fibres: Can they replace glass in fibre reinforced plastics? *Composites Science and Technology* **2003**, *63*, 1259-1264.

61. V. Fiore, G. Di Bella, A. Valenza. Glass-basalt/epoxy hybrid composites for marine applications. *Materials and Design* **2011**, *32*, 2091-2099.

62. G. Romhány, J. Karger-Kocsis, T. Czigány. Tensile fracture and failure behavior of technical flax fibers. *Journal of Applied Polymer Science* **2003**, *90*, 3638-3645.

63. M.S.M. Jusoh, C. Santulli, M.Y.M. Yahya, N. Hussein, H.A.I. Ahmad. Effect of stacking sequence on the tensile and flexural properties of glass fibre epoxy composites hybridized with basalt, flax or jute fibres. *Mater. Sci. Eng. Adv. Res* **2016**, *1*, 19-25.

64. B.H. Jones, D.R. Wheeler, H.T. Black, M.E. Stavig, P.S. Sawyer, N.H. Giron, M.C. Celina, T.N. Lambert, T.M. Alam. Stress relaxation in epoxy thermosets via a ferrocene-based amine curing agent. *Macromolecules* **2017**, *50*, 5014-5024.

65. R.A. Pethrick, E.A. Hollins, I. McEwan, E.A. Pollock, D. Hayward, P. Johncock. Effect of cure temperature on the structure and water absorption of epoxy/amine thermosets. *Polymer International* **1996**, *39*, 275-288.

66. V.B. Gupta, J. Rich, L.T. Drazal, C.Y.C. Lee. The temperature-dependence of some mechanical properties of a cured Epoxy resin system. **1985**, *25*, 812-823.

67. P. Czub. Application of modified natural oils as reactive diluents for epoxy resins. *Macromolecular Symposia* **2006**, *242*, 60-64.

68. R.J. Varley, W. Tian, K.H. Leong, A.Y. Leong, F. Fredo, M. Quaresimin. The effect of surface treatments on the mechanical properties of basalt-reinforced epoxy composites. *Polymer Composites* **2013**, *34*, 320-329.

69. V.B. Gupta, C. Brahatheeswaran. Molecular packing and free volume in crosslinked epoxy networks. *Polymer* **1991**, *32*, 1875-1884.

Adaptado del artículo

III.2.6. Manufacturing of composite materials with high environmental efficiency using epoxy resin of renewable origin and permeable light cores for vacuum-assisted infusion molding

Diego Lascano[1,2], Jorge Valcácel[1], Rafael Balart[1], Luis Quiles-Carrillo[1] and Teodomiro Boronat[1]

[1] Instituto Tecnológico de Materiales (ITM), Universitat Politècnica de València (UPV), Plaza Ferrándiz y Carbonell 1, 03801 Alcoy, Spain

[2] Escuela Politécnica Nacional, Ladrón de Guevara E11-253, Quito 17-01-2759, Ecuador

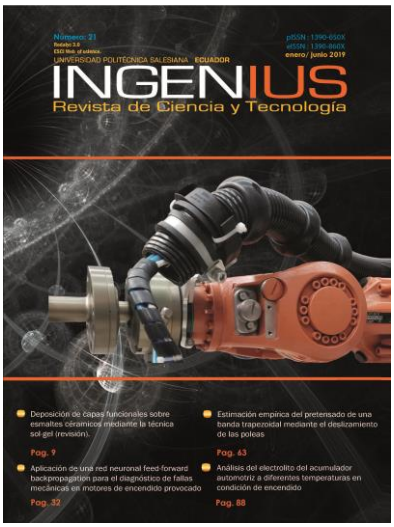

INGENIUS N. 23, january-june of 2020

Scientific Paper / Artículo Científico

UNIVERSIDAD POLITÉCNICA SALESIANA ECUADOR
INGENIUS
Revista de Ciencia y Tecnología
https://doi.org/10.17163/ings.n23.2020.06
pISSN: 1390-650X / eISSN: 1390-860X

Manufacturing of composite materials with high environmental efficiency using epoxy resin of renewable origin and permeable light cores for vacuum-assisted infusion molding

Fabricación de materiales compuestos de alto rendimiento medioambiental con resina epoxi de origen renovable y núcleos ligeros permeables para infusión asistida por vacío

Diego Lascano[1,2], Jorge Valcárcel[1], Rafael Balart[1], Luís Quiles-Carrillo[1], Teodomiro Boronat[1]

Abstract

This work focuses on the manufacturing and characterization of novel and lightweight hybrid sandwich-type structures, using different stacking sequences of flax and basalt fabrics as reinforcement fibers, both of them previously silanized. To reduce the overall weight and facilitate the manufacturing process, a polyester non-woven core, was used which, besides reducing the weight of the composite it also acts as a media to spread the resin. These composites were manufactured with a partially bio-based epoxy resin with a reactive diluent derived from epoxidized vegetable oils that contributes to a 31 % of biobased content. The hybrid composites were obtained by vacuum-assisted resin infusion moulding (VARIM), where the core was used as a media to spread the resin. The mechanical properties were evaluated in flexural and impact conditions.

Resumen

Este trabajo se centra en la fabricación y caracterización de nuevos materiales tipo sándwich híbridos de bajo peso, con diferentes configuraciones de apilamiento de refuerzo de basalto y lino tratadas previamente con silanos. Para aligerar el peso y facilitar la fabricación, se empleó un núcleo de poliéster no tejido que, además de aligerar el peso del compuesto también actuó como medio de difusión de la resina. Se empleó una resina epoxi de origen parcialmente renovable con un diluyente reactivo derivado de aceites vegetales epoxidados que contribuye a un 31 % de origen renovable. Los compuestos híbridos se fabricaron mediante moldeado por infusión de resina asistida por vacío (VARIM), donde el núcleo se utilizó como medio de infusión de la resina. Las propiedades mecánicas se evaluaron en condiciones de impacto y de flexión.

[1,*]Technological Institute of Materials (ITM), Universitat Politècnica de València (UPV), Plaza Ferrándiz y Carbonell 1, 03801 Alcoy, España. Corresponding author ✉: dielas@epsa.upv.es http://orcid.org/0000-0002-0996-1946 https://orcid.org/0000-0001-9053-4425, http://orcid.org/0000-0001-5670-7126 http://orcid.org/0000-0001-8037-2215, http://orcid.org/0000-0002-2144-2874
[2]Escuela Politécnica Nacional, 17-01-2759, Quito, Ecuador

Received: 07-11-2019, accepted after review: 09-12-2019

Suggested citation: Lascano, D.; Valcácer, J.; Balart, R.; Quiles-Carrillo, L. and Boronat, T. (2020). «Manufacturing of composite materials with high environmental efficiency using epoxy resin of renewable origin and permeable light cores for vacuum-assisted infusion molding». Ingenius. N.° 23, (january-june). pp. 62-73. DOI: https://doi.org/10.17163/ings.n23.2020.06.

Manufacturing of composite materials with high environmental efficiency using epoxy resin of renewable origin and permeable light cores for vacuum-assisted infusion molding

Abstract

This work focuses on the manufacturing and characterization of novel and lightweight hybrid sandwich-type structures, using different stacking sequences of flax and basalt fabrics as reinforcement fibers, both of them previously silanized. To reduce the overall weight and facilitate the manufacturing process, a polyester non-woven core, was used which, besides reducing the weight of the composite it also acts as a media to spread the resin. These composites were manufactured with a partially bio-based epoxy resin with a reactive diluent derived from epoxidized vegetable oils that contributes to a 31 % of biobased content. The hybrid composites were obtained by vacuum-assisted resin infusion moulding (VARIM), where the core was used as a media to spread the resin. The mechanical properties were evaluated in flexural and impact conditions. The interactions in the fiber-matrix interface were studied through field emission scanning electron microscopy (FESEM). The obtained data revealed that the silane (coupling agent) treatment works better on basalt fibers than on flax fibers, resulting in superior flexural properties on structures where these fibers are present. It is noteworthy to mention that the stacking sequence of plies directly influences the flexural properties, but it does not significantly affect the energy absorbed when these composites work on impact conditions.

Keywords: Hybrid composite materials, non-woven cores, silane coupling agents, VARIM process, basalt fibers, flax fibers

III.2.6.1. Introduction

The use of composite polymeric materials has increased considerably in our lives not only in technical applications but in everyday applications. This is due to their ability to tailor the desired properties [1]. Thermosetting matrices such as unsaturated polyester resins (UP), epoxies (EP), phenolics (PF) [2-4], among others, and reinforcing fibers such as carbon (CF), aramid (AF), and glass (GF) are the most used due to the high mechanical properties they can provide together with very low weights that make them suitable for automotive, sports, ballistic, civil construction applicatiozns among others [5-9]. Despite this, the conventional highperformance fibers offer some disadvantages. Among others, a critical drawback of these fibers is related to the production costs and conditions as, for example, CF requires extremely high temperatures to obtain highly purified fibers. On the other hand, these conventional reinforcing fibers have a substantial environmental impact, related to the production stages and the problematics after their useful life; this means thattheir mass production is practically unfeasible [10,11].

Matrices based on epoxy resins are the most used, due to excellent mechanical, thermal, and coating properties that provide to composite materials. This is generally achieved by the functional groups that are found in its structure, namely epoxy/oxirane rings which can polymerize to form 3D net structures. Most of the currently available epoxy resins are based on diglycidyl ether of bisphenol A (DGEBA), which comes from the reaction of epichlorohydrin and bisphenol A (BPA) [12]. These components are petroleum-derived materials and, like synthetic fibers have a considerable impact on the increase in the carbon footprint. In order to develop composite materials with low or restricted environmental impact, research studies have been carried out in both components, i.e. the thermosetting matrix and the reinforcing fibers [13]. Traditional epoxies are bioderived as above-mentioned, but in the last decades, new epoxies have been industrially manufactured from renewable resources thus contributing to lowering the overall carbon footprint.

This type of resins is characterized by the fact that part of its content is obtained from renewable resources, unlike conventional resins obtained from petroleum derivatives. Vegetable oils (VOs) have gained high relevance due to their potential in manufacturing biobased materials [14,15]. The basic structure of these vegetable oils is based on a triglyceride structure composed of three different fatty acids chemically attached to a glycerol skeleton. Some of these fatty acids, such as oleic, linoleic, and linolenic acids, contain one, two and three unsaturated carbons, respectively, and this

allows selective modification of VOs with different chemical functionalities. VO's can be epoxidized, maleinized, hydroxylated, acrylated, and so on to give partially bio-based resins. These "eco-friendly" resins have been developed in such a way that their mechanical and thermal properties are similar to their petrochemical counterparts so that they can compete with petroleumderived thermosetting resins with the additional feature of the renewable origin [13].

An alternative to the use of synthetic and rock-wool fibers in the manufacturing of high-performance composite materials is to replace fully or partially some of these fibers and/or fabrics with natural fibers. Several researchers have focused their research on developing hybrid composite materials with conventional and natural fibers. Natural fibers such as hemp, flax, palm leaf are the most used and offer interesting, balanced properties [16,17]. One fiber that stands out for its excellent mechanical properties, due to its composition and structure is flax [9]. Nevertheless, all-flax composites cannot compete with high-performance composite materials. That is why the manufacturing of hybrid composite structures has become an interesting alternative to find a balance between environmental concerns and technical properties.

As natural fibers cannot compete with high-tech fibers such as carbon or aramids, it is quite common to combine natural fibers with mineral fibers, which are cost-effective compared to high tech fibers. Basalt fibers have been used in thermoplastics and thermosetting composite materials as an alternative to glass fiber. These fibers are obtained from basalt rocks, which is one of the most abundant on the earth's surface. Its structure is quite similar to glass fiber but with different silica and alumina content. Unlike glass fiber, the production process of basalt fiber is simpler, more efficient and does not generate waste due to the simple structure. Barouni and Dhakal [18] have developed flax/glass hybrid composites with improvement in the impact damage characteristics due to the capability to absorb the impact energy of flax fibers. On the other hand, Mazur, *et al*. [19] studied the hybrid effect of composites based on basalt and carbon fibers, where an increase in the strength and tensile modulus was reported when the shared mass of the fibers was about 7 wt %.

Among the hybrid composite materials, it is worthy to note the interest on sandwich panels. These have been used in areas where larger thicknesses, lightweights, high rigidity, and insulation capacity are required. They are generally used in the construction, automotive, aircraft areas, and so on, due to their extraordinary ability to support flexural (out-of-the plane) forces [20]. Sandwich panels are composed of two

outer sheets (face sheets) and a core that generally has lower properties than the face sheets but it contributes to support the out-of-plane forces by shear with the outer sheets.

The face sheets are usually composite laminates with several layers with fabrics oriented in different directions to improve the isotropy behaviour [21]. These face sheets often consist of unsaturated polyester (UP) sheets with glass fibers (GF) for applications with moderate mechanical performance, or epoxy (EP) plies with carbon fibers (CF) and/or aramid (AF) for applications with high mechanical responsibility [22,23]. The core is usually made of materials with low density and relatively poor mechanical characteristics, since their purpose is not to support mechanical resistance. Core materials offer high lightness and a very good capacity of shear stresses absorption. Some of the widely used cores include balsa wood, polyurethane, or honeycomb structures [24-26]. Manufacturing of composite sandwich panels usually is carried out by hand layup and vacuum bagging.

In the recent years some research has been focused on the development of cores which are not only a part of the sandwich panel but also, can contribute to improve manufacturing processes. Vacuum assisted resin infusion moulding (VARIM) is a very widely used technique alternative to the industrial resin transfer moulding (RTM) to obtain composite materials with excellent balanced properties in a simple way. Nevertheless, the VARIM process requires different consumables (infusion nozzle, bleeding web, spiral tube, and so on), and it is not the best manufacturing process for sandwich panels since the typical cores do not transfer the infused resin. Recently, new cores have been developed with multifunctional features.

On the one hand, they can act as core materials in sandwich structures, but on the other hand, they offer enough porosity to enhance resin infusion through it. Some of these cores are composed of a cell structure separated by channels with synthetic microspheres, which do not absorb resin; this channel helps the resin flow through the composite material [27]. Chatys, *et al.* [28] have used Lantor Soric® in carbon fiber sandwich composites to manufacture car safety bumpers due to its flexibility and the ability to absorb impact energy compared to conventional metal parts. Eum, *et al.* [29] have reported that using the core as an infusion media in a conventional VARTM process, it is possible to provide similar properties to similar composites since this does not catch resin and helps to the correct its flow.

Hybrid composite materials, due to the diverse nature of their components, do not usually have the required synergy, since the stresses are not correctly transferred to the reinforcement fibers, which are generally the most resistant material. In general, to

improve the interface interaction between fibers and the resin, several methods have been developed. The most used method is chemical treatment with tailored silanes. Silanes offer dual functionality, thus allowing them to react firstly with the fiber surface, and during the crosslinking, they can react with the resin, thus leading to real chemical bridges between the thermosetting matrix and the reinforcement fibers [30,31].

The objective of this work is the development of novel, highly lightweight sandwich structures, using basalt and flax fibers as reinforcement fibers. As a core material, a polyester non-woven with hexagonal cells has been used to assess the potential of manufacturing high-performance composite sandwich panels by using a conventional vacuum assisted resin infusion moulding (VARIM) using the core as infusion media. The obtained sandwich panels have been characterized in flexural and impact conditions to understand the strength properties and the effect of silane treatment. FESEM has been carried out to analyze the interface interaction between the reinforcement fibers and the partially bio-based epoxy resin.

III.2.6.2. Experimental

Materials

A partially bio-based (31 % renewable content according to with ASTM D6866-12) commercial-grade epoxy resin was used as the thermosetting matrix. This consisted on a base epoxy resin Resoltech® 1070 ECO and an amine-based hardener grade Resoltech® 1074 ECO from Castro Composites (Pontevedra, Spain). The resin to hardener ratio was 100/35 parts by weight as recommended by the manufacturer. The system was deeply mixed by manual methods until a uniform mix was obtained.

Two different reinforcement fabrics were used. Basalt fabric BAS 940.1270 from Basaltex® (Wevelgem, Belgium) made of 100 % continuous basalt filaments. This fabric shows a specific surface weight of 940 g/cm^2 and a thickness of 0.54 mm. Flax fabrics Biotex® Flax were obtained from Composites evolution (Chesterfield, United Kingdom) with a specific surface weight of 400 g/cm^2 with a thickness of 0.7 mm.

The core material was a nonwoven Lantor Soric® XF supplied by LANTOR® (Veenendaal, The Netherlands) with a specific surface weight of 250 g/cm^2. This was used as core material and infusion media. To improve the interface interaction between the selected fibers/fabrics and the epoxy matrix, a glycidylfunctional silane (3-glycidyloxypropyl) trimethoxysilane was used as a coupling agent. This was supplied by Sigma- Aldrich (Madrid, Spain).

Pre-Treatment of Fabrics

Generally, basalt fibers are coated by a silane-based sizing to impart strands that can interfere with the panels production process. To remove it and any external impurities, basalt fibers were initially subjected to a thermal treatment at 300 ºC for 3 h.

The interface interaction between the fabrics and the matrix was enhanced by a silanization treatment. Both basalt and flax fibers were immersed in an aqueous solution with 1 wt % silane for 2 h at room temperature; then the solution was stirred with a magnetic stirrer to obtain a uniform solution. During this stage, hydrolysis of silane occurs and the subsequent hudroxyl groups move to the surface of the fabrics.

To complete the silanization process of chemical anchoring of the silanes through condensation with the hydroxyls on the surface of both fibers, an air circulating oven was used to dry the functionalized fabrics for 12 h at 80 ºC. This stage provides strong links between the hydrolyzed silane groups and the hydroxyl goupd in both basalt and flax fabrics, through a condensation process with the release of water that is removed by evaporation.

Manufacturing of Hybrid Basalt/Flax Composite Laminates

The process used to manufacture the hybrid sandwich laminates was the vacuum assisted resin infusion moulding (VARIM), instead of using the usual process with bleeding fabric, absorption mesh, and so on, which are not the best selection to manufacture composite sandwich panels.

Sandwich panels were obtained with Soric® core that acted as porous media for infusion. As in other infusion methods, the vacuum is responsible for spreading the resin throughout the geometry of the composite sandwich and avoids agglomeration of resin in fabrics.

Different stacking sequences were manufactured, as can be seen in table III.2.6.1. The procedure was the following. First, a flat surface was cleaned beforehand, then coated by a thin layer of a release agent, poly(vinyl alcohol) - PVA. Second, a peel-ply sheet was placed on the PVA thin layer to make more accessible the unmolding process. Then the fabrics and the core were stacked as indicated in table III.2.6.1 and figure III.2.6.1a). From this step, the process is slightly different from a conventional resin infusion (VARIM). As can be seen in figure III.2.6.1b), the bleeding mesh instead of covering the whole stacking, it is only placed on one side where the resin inlet will be placed. This is responsible for ensuring the flow of the resin from the resin inlet to the

core. The resin distribution tube was placed over the mesh meanwhile, the vacuum tube was coated with a felt sheet that allowed the vacuum but restricted the resin flow. Finally, all the elements were sealed with a plastic bag and a double side sealing tape (figure III.2.6.1c). To ensure no leaking resin, the vacuum was tested beforehand. Then, the resin was allowed to flow until all the sheets were completely soaked. After this, the resin supply was cut off, but the vacuum was maintained for 8 h until the resin was completely cured at room temperature. With these curing conditions, no additional post curing process is needed. As can be seen in figure III.2.6.1d) the core helps the resin to flow through the sandwich panel. Flax fibers, due to their porous structure, were the ones that better absorb the resin, followed by the basalt fiber. The Soric® Lantor core helps the resin to be spread homogeneously through the face sheets, thus leading to a complete wetting of the composite panel.

The obtained panels were machined by a computer numerical control milling machine to obtain specimens following international standards guidelines.

Table III.2.6.1. Composition and coding of basalt/flax/sandwich composite panels.

Code	Ply number ratio (basalt/flax)	Sandwich upper face	Core	Sandwich bottom base	Volume fraction resin/material
BBSBB	4/0	basalt - basalt	Soric® XF	basalt - basalt	52.20/47.80
BLSLB	2/2	basalt - flax	Soric® XF	flax - basalt	62.62/37.38
LBSBL	2/2	flax - basalt	Soric® XF	basalt - flax	63.10/36.90
LLSLL	0/4	flax - flax	Soric® XF	flax - flax	74.76/25.24
BSB	2/0	basalt	Soric® XF	basalt	58.86/41.14
LSL	0/2	flax	Soric® XF	flax	77.64/22.36

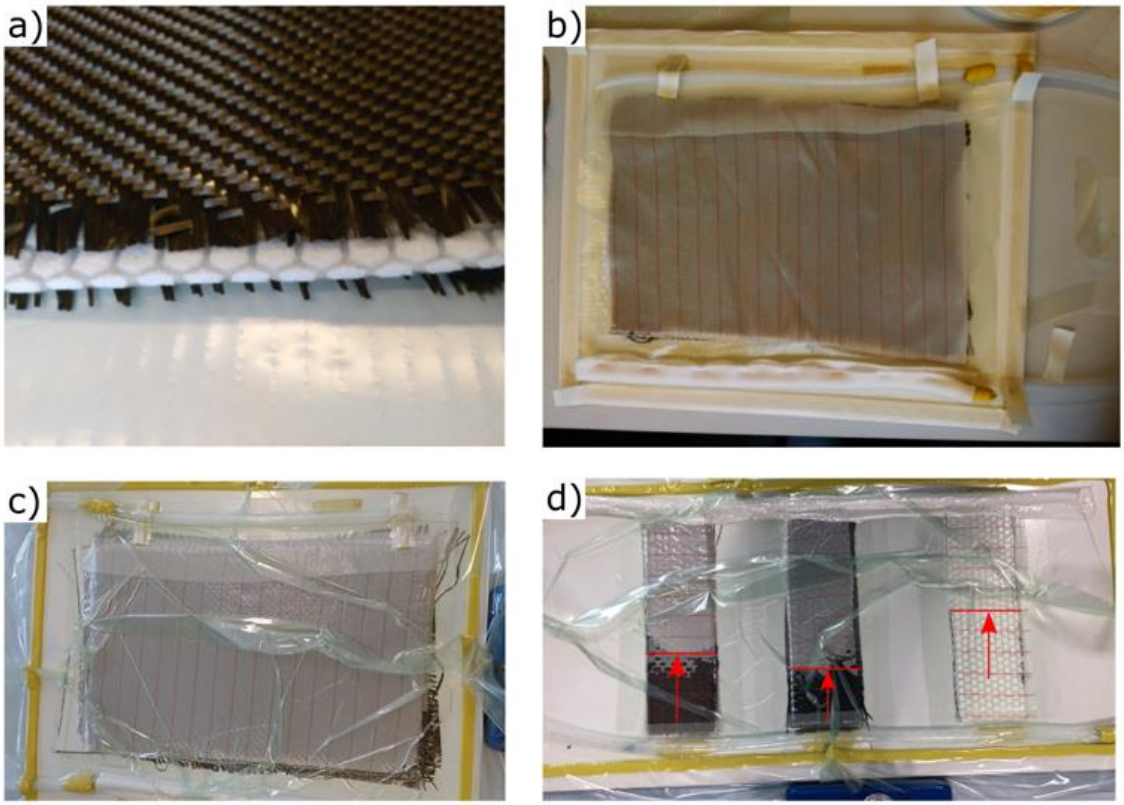

Figure III.2.6.1. Scheme of the manufacturing process of basalt/flax/sandwich composites by vacuum-assisted resin infusion moulding (VARIM) with the nonwoven core as infusion media. a) stacking configuration, b) placement of resin inlet and outlet tubes, c) sealing process and vacuum test procedure, d) resin infusion process with different stacking sequences.

Mechanical Properties

The mechanical properties of sandwich panels were determined in flexural and impact conditions. Flexural tests were carried out on a universal testing machine ELIB 30 form S.A. E. Ibertest (Madrid, Spain). The flexural test was performed following the ISO 14125:1998 standard. In this test, the specimen is supported on two points separated from each other, and the increasing load applied in the center with a crosshead rate of 1 mm/min. The machine was equipped with a cell load of 5 kN.

To evaluate the impact strength of the sandwich panels the Charpy test was carried out in a Charpy pendulum supplied by Metrotec (San Sebastián, Spain), using a 6-J pendulum on “U” type notched samples (radius of 0.5 mm and 2 mm depth) following the guidelines of ISO 179 standard. At least five samples of every material were tested at room temperature; the results of all tests were collected and averaged. In addition, the standard deviation was obtained to estimate the error.

Interface Interaction Analysis by Field Emission Scanning Electron Microscopy (Fesem)

To evaluate the interface interaction between the reinforcing fibers and the epoxy matrix, samples were cryofractured and then, observed by field emission scanning electron microscopy (FESEM), in a ZEISS ULTRA 55 FESEM microscope supplied by Oxford Instruments (Abingdon, United Kingdom) working at an acceleration voltage of 2 kV. To provide electrical conducting properties to the sandwich panels, they were precoated with a gold-palladium layer using a high vacuum sputter coater EM MED20 supplied by Leica Microsystem (Milton Keynes, United Kingdom).

III.2.6.3. Results and Discussion

Mechanical Properties of Sandwich Panels Based on Basalt and Flax Fibers

Subjecting basalt/flax sandwich panels to flexural and impact conditions (Charpy test) gives interesting data about resistant properties as well as the ability to absorb energy in impact conditions. Figure III.2.6.2 shows the values obtained from the two described tests. In sandwich materials, the core does not provide any mechanical strength to the material (in tensile conditions), so final properties are strictly based on the reinforcing fibers. Nevertheless, core materials contribute to support out-of-plane stresses by shear with the face sheets.

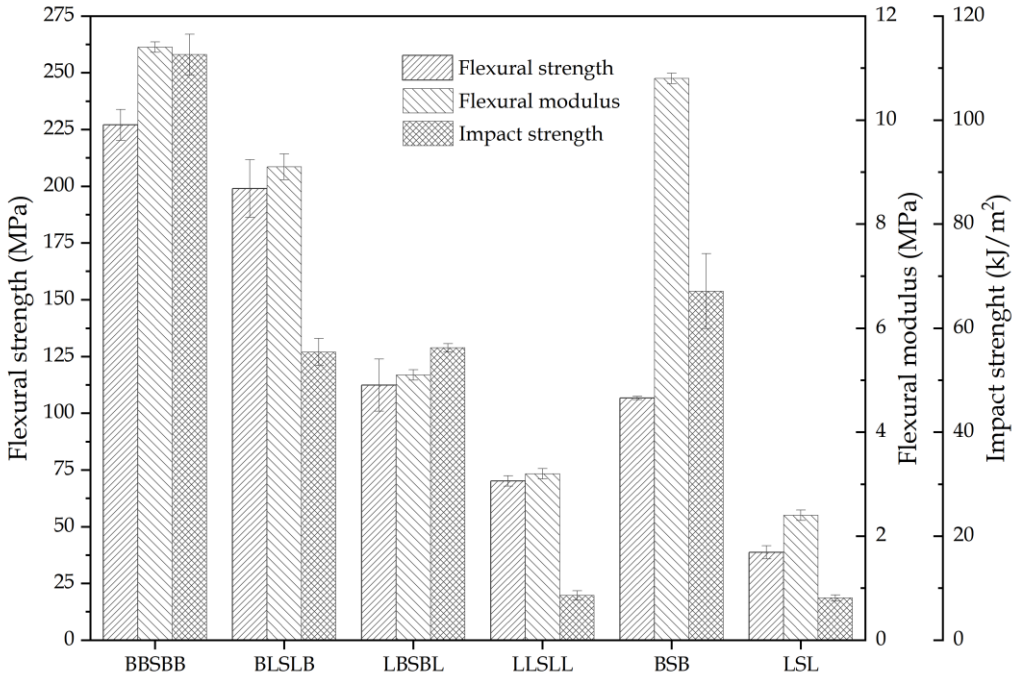

Figure III.2.6.2. Mechanical properties of basalt/flax sandwich hybrid composite with different stacking sequences obtained from flexural and impact tests.

As expected, the BBSBB material with the highest number of basalt plies in its structure (4 basalt sheets, two at the top of the core and two at the bottom), shows a flexural strength, σ_f, and flexural modulus, E_f of 227 ± 6.79 MPa and 11.35 ± 0.04 GPa, respectively. These values as similar to other glass-fiber composite materials. The obtained values are relatively high, which means that besides the fact that basalt fibers have high resistance, the interaction of these fibers and the epoxy matrix is quite good, allowing excellent load transfer between the matrix to the fibers. These results are in accordance with the literature about basalt/epoxy systems [32].

Analyzing materials such as BLSLB and LBSBL, which have the same number of basalt and flax fibers in the face sheets (one basalt ply and one flax ply on each face sheet), but with different stacking configuration, gives impressive results. The panel with the basalt sheets in the outer side of the face sheets offers higher values of flexural strength and modulus being only 12 % and 19 % less, respectively, compared with the material with four basalt plies. BLSLB stacking sequence leads to interesting mechanical properties of 199 ± 12.7 MPa and 9.14 ± 0.25 GPa for the flexural strength and modulus, respectively.

Concerning the LBSBL material, it is worthy to remark a notorious decrease in its flexural properties both in strength and stiffness, having a decrease of 43 % and 44 % in the flexural strength and the flexural modulus, respectively, compared with the BBSBB composite panel. This is clearly due to the nature of the fibers that are supporting the tensile and compression stresses. In the LBSBL composite panel, flax fibers are located at the outer face. As flax fibers are less resistant than basalt fibers, the result is a noticeable decrease in its properties. Similar results were obtained by Dhakal, *et al.* [33] in hybrid reinforced composites based on basalt/hemp fibers, the presence of basalt fibers in the outside of the face sheets improved the flexural strength and modulus. As expected, panels composed entirely by flax fibers are those with the more inferior flexural properties.

Figure III.2.6.3 shows an example of the type of failure suffered by the panels. figure III.2.6.3a) shows the BSB material that is composed only of a basalt ply in each of the faces, as mentioned before the core used, does not provide any extra strength to the final material. It can be seen that the failure of the material is caused by the core and not by the reinforcing fibers. On the other hand, the failure of the LSL material in figure III.2.6.3b) indicates this failure is due to the low resistance that the flax fibers in the bottom face sheet, which are working in tensile conditions.

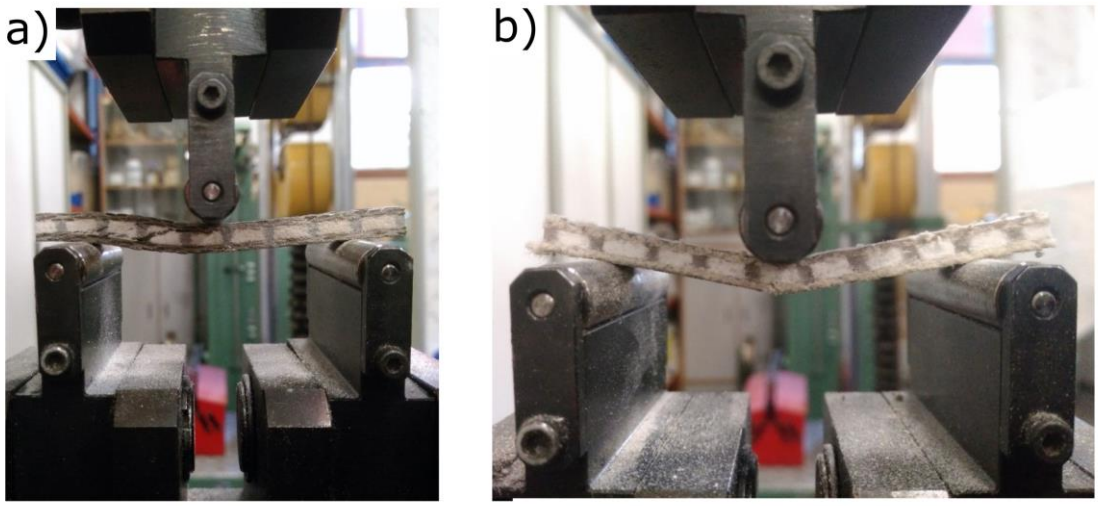

Figure III.2.6.3. Forms of failure in flexion tests of a) BSB sandwich panel and b) LSL sandwich panel.

By using the Charpy impact test, one can estimate the energy that such materials can withstand under impact conditions, thus giving an estimation of the toughness.

As expected just as it happened in flexural characterization, the material composed entirely of basalt fibers (and a Soric® Lantor core), i.e. BBSBB is the one that

absorbs the highest energy, obtaining values of 112.6 ± 3.9 kJ/m^2, which is indicating good stress transfer between the matrix to the reinforcing fabrics.

Basalt fibers, due to their composition, provide high stiffness to the composite but, in contrast, basalt composites cannot support large deformations [34]. By analyzing the composite panels with the same number of basalt and flax fibers (BLSLB and LBSBL), it can be seen that the distribution of the fibers does not affect the impact energy (see figure III.2.6.2), with absorbed energy values of 55-56 kJ/m^2, that are in accordance with the results reported by Fiore, *et al.* [35]. They observed very slight changes in the impact strength by placing basalt or flax fibers in the outer face sheet.

As expected, just by replacing one-ply from basalt to flax, it leads to a decrease in the impact strength of about 50 %. This is consistent because if one observes the BSB material made up by only one basalt layer in the face sheets, it has higher impact strength than materials that have flax fiber in their stacking sequence. It can be concluded that the impact stress is absorbed almost entirely by basalt fibers, since analyzing materials that are made entirely of flax fibers, either by four layers (LLSLL) or two layers (LSL) they have very low values and practically the same, around 8 kJ/m^2. As mentioned above, the core does not improve the final properties of composite materials.

Matrix/Reinforcement Fiber Interface Interaction

The final properties of the hybrid composite materials are related by the strength of the fibers; therefore, a good synergy between them and the matrix is necessary since a functional interaction between the fibers and the matrix will result in superior mechanical properties. This is because good fiber-matrix interactions allow stresses transfer from the matrix (with no reinforcing properties) to the reinforcing fiber [36]. So, a poor synergy between these components would result in composite materials with low mechanical properties.

For an accurate analysis of the interaction between the reinforcement fibers and the surrounding matrix, cryofractured surfaces from the face sheets were observed by FESEM (see figure III.2.6.4). Figure III.2.6.4a**)** shows the interaction of the basalt fibers after the coupling agent treatment based on silane and the surrounding matrix. As can be seen, there is a lack of the gap between the fiber and the surrounding resin, therefore indicating that the silane treatment was successful. Similar findings were reported by Gao, *et al.* [37], in silica-based fibers (glass fiber) and an epoxy matrix. They show the effectiveness of a silanization treatment on fibers which is directly related to improved mechanical properties. Figure III.2.6.4b) shows the flax fibers after being subjected to

the same chemical treatment with the silane coupling agent. In this case, it is shown that the interaction of the fibers was improved since the gap is very small. This improvement has also been reported by Kushwaha and Kumar [38], with hemp fibers subjected to a silanization process with (3 glycidyloxypropyl) trimethoxysilane as a coupling agent.

This coupling agent also decreases the hydrophilic behaviour that natural fibers intrinsically have, and this enhances the compatibility with hydrophobic polymeric matrices. Despite this, the presence of the gap does not allow a perfect stress transfer so that the final mechanical properties of panels will decline. Because the basalt fibers structure is based on silica, the effectiveness of the silanization with hydrolyzed silane, works better. The coupling agent with glycidyl-silane functionality has epoxy functional groups that can readily react with both the epoxy resin during the curing process (cross-linking) and with the hydroxyl functional groups of the basalt fibers, leading to a strong bridge between these two components.

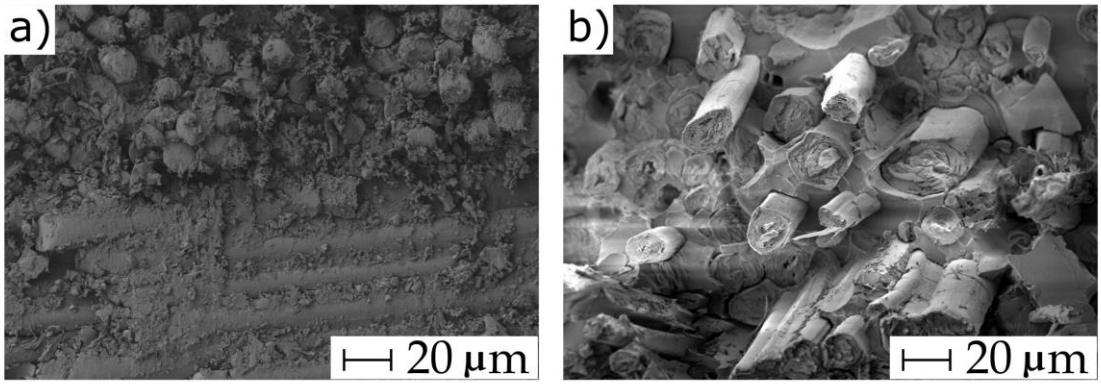

Figure III.2.6.4. Field emission scanning electron microscopy (FESEM) images at x500 magnifications corresponding to cryofracture surfaces from impact tests of a) BSB sandwich panel and b) LSL sandwich panel.

This corroborates the results obtained in the mechanical tests since the improvements of the flexural properties of the panels reinforced by basalt fibers is the result of the good synergy between these fibers and the polymeric matrix, which allows an excellent distribution of stress.

III.2.6.4. Conclusions

Through this research, it has been confirmed that the use of a porous core as a diffusion media in a conventional vacuum assisted resin infusion moulding (VARIM) is a successful alternative process to manufacture sandwich-type lightweight composite structures using a partially biobased epoxy resin (with 31 wt % biobased content derived

from epoxidized vegetable oils). The use of an infusion core material allows reducing weight and costs of manufacturing high-tech composite parts as the typical consumable materials in a VARIM process can be reduced.

Silanes play a key role in improving mechanical performance as the provide strong links between the epoxy resin (through the glycidyl functional group) and the fiber (through a condensation process of the hydrolyzed silane).

Regarding the mechanical properties of sandwich panels, the best performance is obtained in composite panels with the stacking sequence BBSBB. However, the substitution of one of the basalt fabrics in the face sheets by a flax fabric has an essential effect on overall properties, mainly on flexural strength and modulus, while impact strength remains almost invariable. Although these flax-based composite panels offer inferior properties than all-basalt composites, they represent an interesting alternative from both technical and environmental points of view.

III.2.6.5. References

1. P. Cousin, M. Hassan, P. Vijay, M. Robert, B. Benmokrane. Chemical resistance of carbon, basalt, and glass fibers used in frp reinforcing bars. Journal of Composite materials 2019, 53, 3651-3670.
2. B. Wang, Q. Fu, H. Li, L. Qi, Q. Song, Y. Fu. In situ growth of graphene on carbon fabrics with enhanced mechanical and thermal properties for tribological applications of carbon fabric–phenolic composites. Tribology Transactions 2019, 62, 850-858.
3. K. Liu, S. He, Y. Qian, Q. An, A. Stein, C.W. Macosko. Nanoparticles in glass fiber-reinforced polyester composites: comparing toughening effects of modified graphene oxide and core-shell rubber. Polymer Composites 2019, 40, E1512-E1524.
4. M.S.Z. Abidin, T. Herceg, E.S. Greenhalgh, M. Shaffer, A. Bismarck. Enhanced fracture toughness of hierarchical carbon nanotube reinforced carbon fibre epoxy composites with engineered matrix microstructure. Composites Science and Technology 2019, 170, 85-92.
5. M. Flanagan, A. Doyle, K. Doyle, M. Ward, M. Bizeul, R. Canavan, B. Weafer, C. Ó Brádaigh, N.M. Harrison, J. Goggins. Comparative manufacture and testing of induction-welded and adhesively bonded carbon fibre PEEK stiffened panels. Journal of Thermoplastic Composite Materials 2019, 32, 1622-1649.
6. M. Ricciardi, I. Papa, V. Antonucci, V. Lopresto, A. Langella. Impact behavior of polyester gfrp for naval applications: Influence of the clamping device and fluid–material interaction. Journal of Materials Engineering and Performance 2019, 28, 3196-3202.
7. J. Naveen, M. Jawaid, E. Zainudin, M.T. Sultan, R. Yahaya. Effect of graphene nanoplatelets on the ballistic performance of hybrid kevlar/cocos nucifera sheath-reinforced epoxy composites. Textile Research Journal 2019, 89, 4349-4362.
8. J.P. Arenas, J.L. Castaño, L. Troncoso, M.L. Auad. Thermoplastic polyurethane/laponite nanocomposite for reducing impact sound in a floating floor. Applied Acoustics 2019, 155, 401-406.
9. M. Zhang, O. Bareille, M. Salvia. Cure and damage monitoring of flax fiber-reinforced epoxy composite repairs for civil engineering structures using embedded piezo micro-patches. Construction and Building Materials 2019, 225, 196-203.

10. M. Mudhukrishnan, P. Hariharan, K. Palanikumar, B. Latha. Optimization and sensitivity analysis of drilling parameters for sustainable machining of carbon fiber–reinforced polypropylene composites. Journal of Thermoplastic Composite Materials 2019, 32, 1485-1508.

11. R.M. Gandia, F.C. Gomes, A.A.R. Corrêa, M.C. Rodrigues, R.F. Mendes. Physical, mechanical and thermal behavior of adobe stabilized with glass fiber reinforced polymer waste. Construction and Building Materials 2019, 222, 168-182.

12. A.-S. Mora, R. Tayouo, B. Boutevin, G. David, S. Caillol. Synthesis of biobased reactive hydroxyl amines by amination reaction of cardanol-based epoxy monomers. European Polymer Journal 2019, 118, 429-436.

13. C. François, S. Pourchet, G. Boni, S. Rautiainen, J. Samec, L. Fournier, C. Robert, C.M. Thomas, S. Fontaine, Y. Gaillard. Design and synthesis of biobased epoxy thermosets from biorenewable resources. Comptes Rendus Chimie 2017, 20, 1006-1016.

14. S. Torron, S. Semlitsch, M. Martinelle, M. Johansson. Biocatalytic synthesis of epoxy resins from fatty acids as a versatile route for the formation of polymer thermosets with tunable properties. Biomacromolecules 2016, 17, 4003-4010.

15. M. Jebrane, S. Cai, C. Sandström, N. Terziev. The reactivity of linseed and soybean oil with different epoxidation degree towards vinyl acetate and impact of the resulting copolymer on the wood durability. Express Polymer Letters 2017, 11, 383.

16. R. Singh, B. Singh, H. Tarannum. Mechanical properties of jute fiber–reinforced UP/PU hybrid network composites. Polymers and Polymer Composites 2019, 27, 546-556.

17. E. Mahdi, D. Ochoa, A. Vaziri, E. Eltai. Energy absorption capability of date palm leaf fiber reinforced epoxy composites rectangular tubes. Composite Structures 2019, 224, 111004.

18. A.K. Barouni, H.N. Dhakal. Damage investigation and assessment due to low-velocity impact on flax/glass hybrid composite plates. Composite Structures 2019, 226, 111224.

19. K. Mazur, S. Kuciel, K. Salasinska. Mechanical, fire, and smoke behaviour of hybrid composites based on polyamide 6 with basalt/carbon fibres. Journal of Composite Materials 2019, 53, 3979-3991.

20. J.R. Vinson. Sandwich structures: past, present, and future. In Sandwich structures 7: advancing with sandwich structures and materials, Springer: 2005; 3-12.

21. A.S. Herrmann, P.C. Zahlen, I. Zuardy. Sandwich structures technology in commercial aviation. Dordrecht; 13-26.

22. A. Atiqah, M. T Mastura, B. A Ahmed Ali, M. Jawaid, S. M Sapuan. A review on polyurethane and its polymer composites. Current Organic Synthesis 2017, 14, 233-248.

23. M. Yaqoob. Fabrication and structural equivalency analysis of CFRP nomex core sandwiched panels for FSAE race car. The UNSW Canberra at ADFA Journal of Undergraduate Engineering Research 2018, 10.

24. C. Atas, C. Sevim. On the impact response of sandwich composites with cores of balsa wood and PVC foam. Composite Structures 2010, 93, 40-48.

25. G. Zhang, B. Wang, L. Ma, L. Wu, S. Pan, J. Yang. Energy absorption and low velocity impact response of polyurethane foam filled pyramidal lattice core sandwich panels. Composite Structures 2014, 108, 304-310.

26. L. He, Y.-S. Cheng, J. Liu. Precise bending stress analysis of corrugated-core, honeycomb-core and X-core sandwich panels. Composite Structures 2012, 94, 1656-1668.

27. R. Stewart. Sandwich composites excel at cost-effective, lightweight structures. Reinforced Plastics 2011, 55, 27-31.

28. R. Chatys, A. Panich, R.S. Jurecki, M. Kleinhofs. Composite materials having a layer structure of “sandwich” construction as above used in car safety bumpers. In Proceedings of 2018 XI International Science-Technical Conference Automotive Safety; 1-8.

29. S.H. Eum, Y.H. Kim, J.W. Han, K.J. Kim, D.H. Shin, C. Yim, R. Murakami. A study on the mechanical properties of the honeycomb sandwich composites made by VARTM. In Proceedings of Key Engineering Materials; 2746-2751.

30. J. España, M. Samper, E. Fages, L. Sánchez-Nácher, R. Balart. Investigation of the effect of different silane coupling agents on mechanical performance of basalt fiber composite laminates with biobased epoxy matrices. Polymer composites 2013, 34, 376-381.

31. M. Samper, R. Petrucci, L. Sánchez-Nacher, R. Balart, J. Kenny. New environmentally friendly composite laminates with epoxidized linseed oil (ELO) and slate fiber fabrics. Composites Part B: Engineering 2015, 71, 203-209.

32. R. Petrucci, C. Santulli, D. Puglia, F. Sarasini, L. Torre, J. Kenny. Mechanical characterisation of hybrid composite laminates based on basalt fibres in combination with flax, hemp and glass fibres manufactured by vacuum infusion. Materials & Design 2013, 49, 728-735.

33. H.N. Dhakal, F. Sarasini, C. Santulli, J. Tirillò, Z. Zhang, V. Arumugam. Effect of basalt fibre hybridisation on post-impact mechanical behaviour of hemp fibre reinforced composites. Composites Part A: Applied Science and Manufacturing 2015, 75, 54-67.

34. S. Boccardi, N. Boffa, G. Carlomagno, G. Del Core, C. Meola, P. Russo, G. Simeoli. Inline monitoring of basalt-based composites under impact tests. Composite Structures 2019, 210, 152-158.

35. V. Fiore, T. Scalici, L. Calabrese, A. Valenza, E. Proverbio. Effect of external basalt layers on durability behaviour of flax reinforced composites. Composites Part B: Engineering 2016, 84, 258-265.

36. D. Lascano, L. Quiles-Carrillo, S. Torres-Giner, T. Boronat, N. Montanes. Optimization of the curing and post-curing conditions for the manufacturing of partially bio-based epoxy resins with improved toughness. Polymers 2019, 11, 1354.

37. X. Gao, R. Jensen, W. Li, J. Deitzel, S. McKnight, J. Gillespie Jr. Effect of fiber surface texture created from silane blends on the strength and energy absorption of the glass fiber/epoxy interphase. Journal of Composite Materials 2008, 42, 513-534.

38. P.K. Kushwaha, R. Kumar. Effect of silanes on mechanical properties of bamboo fiber-epoxy composites. Journal of Reinforced Plastics and Composites 2010, 29, 718-724.

IV. CONCLUSIONES

IV.1. Conclusiones Parciales

Del análisis de los resultados obtenidos y en virtud de los objetivos específicos planteados, se exponen a continuación las principales conclusiones correspondientes a cada uno de los bloques que forman parte de esta tesis doctoral:

IV.1.1. Mezclas y compuestos con matrices termoplásticas con alto rendimiento medioambiental

Mediante la adición del poli(butileno succinato-*co*-adipato) PBSA se logró modificar las propiedades mecánicas del poli (ácido láctico) PLA, obteniendo un aumento en las propiedades dúctiles, resultando así en una disminución en el comportamiento frágil. La incorporación de algún agente de acoplamiento mejoró la interacción entre los dos polímeros viéndose reflejado en un aumento en su desempeño, siendo más notorio con lo respecta a la resistencia al impacto. Sin embargo, la adición del PBSA disminuyó la capacidad de memoria de forma del PLA, aumentando este efecto cuando se incrementa el porcentaje de PBSA.

La incorporación de un oligómero de ácido láctico (OLA) en la matriz de PLA produjo un aumento en su capacidad de absorber energía de impacto, así como un ligero efecto plastificante notándose en la disminución de la temperatura de transición vítrea. Se observó además una mejora notable en la capacidad de memoria de forma, teniendo una mejor respuesta de recuperación con el aumento en la cantidad de OLA. Sin embargo, la estabilidad térmica de los compuestos se vió disminuida, debido en gran manera a la naturaleza del OLA.

Se determinó que el PLA es un material viable para la fabricación de núcleos en forma de panal de abeja, obteniendo celdas hexagonales con buena estabilidad dimensional a diferentes alturas. Además, se determinó que es una excelente matriz para las fibras de lino en la formación de las caras exteriores. Al incrementar la altura del núcleo se pudo obtener materiales con una alta ligereza con buena respuesta a esfuerzos de flexión y compresión, dando mejores resultados aquellos núcleos con una altura de 20 mm. Sin embargo, debido a la fragilidad inherente que presenta el PLA, los núcleos pueden colapsar si la presión aplicada en el proceso de unión núcleo-caras exteriores es muy alta.

Se estableció que el uso de métodos convencionales como la compresión por temperatura, puede ser una técnica sencilla de fabricación de materiales compuestos

con una alta carga de fibras de refuerzo. La direccionalidad de las mantas formadas por fibras tejidas ayudó a obtener un mejor efecto de refuerzo donde los materiales resultantes presentaron mejores propiedades a tracción. Además, se observó que las propiedades a flexión de los materiales no dependen del direccionamiento de las fibras sino de la cantidad de carga de esta, siendo mayor con el aumento de la carga.

IV.1.2. Compuestos con matrices termoestables con alto rendimiento medioambiental

Se desarrolló y validó el modelo de reacción correspondiente al curado de una resina epoxi con un 31 % de contenido de origen orgánico, se obtuvo que el modelo cinético que más se adecua es el modelo de cinético auto catalítico de dos parámetros. Por medio de métodos isoconversionales se calcularon valores de la energía de activación aparente con una alta precisión, donde se observó que el porcentaje de origen orgánico no afecta a el proceso de curado, siendo similar al de una resina epoxi convencional.

Se desarrolló y validó el modelo de reacción del curado de una resina epoxi derivada de un aceite epoxidado de lino (ELO) entrecruzados por anhídridos. Aplicando diferentes métodos isconversionales se determinó la energía de activación aparente, se observó que el uso de ELO como percusor de una resina epoxi no afecta al proceso de reacción del sistema, comportándose de una forma similar a sistemas epoxi convencionales. Además, se determinó que el modelo cinético que más se ajusta a la reacción es el modelo cinético auto catalítico de dos parámetros.

Se determinó como influye la variación de las temperaturas de curado y de poscurado en el proceso de entrecruzado de una resina epoxi con un 31 % de contenido de origen orgánico y un endurecedor amina. Se estableció que al someter al sistema a un proceso de curado a temperaturas moderadas y posteriormente a un poscurado a altas temperaturas se obtienen materiales con una reticulación más homogénea resultado en materiales con una alta tenacidad. Además de disminuir su tiempo de curado.

La incorporación de partículas de lino en una matriz de resina epoxi con un contenido parcial de origen orgánico produjo una disminución en sus propiedades mecánicas, así como un aumento en la capacidad de absorción de agua, siendo este efecto más pronunciado al incrementar el contenido de carga y el tamaño de la partícula. Sin embargo, el uso de partículas con un tamaño fino promovió una mejor dispersión en la matriz, evitando la formación de agregados lo que permitió que se incremente

ligeramente su interacción, esto se ve reflejado en una mejora en las propiedades mecánicas y en la disminución de la capacidad de absorción de agua. Se obtuvo materiales con apariencia de madera y propiedades balanceadas que pueden ser utilizados en sectores del mueble o decoración.

Se determinó que el pretratamiento con agentes de acoplamiento basado en silanos a los que fueron sometidos las fibras de lino y de basalto funcionó correctamente, teniendo mejores resultados en las fibras de basalto. Esto aumentó la interacción que tienen entre estas fibras y la matriz de resina epoxi con un contenido parcial de origen orgánico. Los resultados demostraron que la buena interacción fibra-matriz llevo a un mejor comportamiento mecánico de los materiales. Donde Se obtuvo materiales híbridos (lino-basalto) con buenas propiedades a flexión, incluso cuando la cantidad de fibras de lino llega al 50 % de su constitución.

El uso de un núcleo permeable en la fabricación de estructuras sándwich permitió obtener compuestos ligeros, además ayudó a la correcta adhesión entre este y las capas de refuerzo. El pretratamiento a base de silanos realizados a las fibras de lino y basalto ayudó a mejorar la interacción fibras/núcleo/resina. De los resultados se obtuvo que la incorporación de fibras de lino en el compuesto disminuye las propiedades a flexión, siendo más notorio este efecto cuando se encuentran en las capas exteriores. A pesar de esto, se observó que la disposición de las fibras de lino en el compuesto no tiene un efecto relevante en la capacidad de absorción de impacto.

IV.2. Conclusiones generales

Como conclusión general de la presente tesis doctoral, se puede afirmar que, mediante la correcta modificación y optimización de diferentes materiales poliméricos con un contenido parcial o total de origen natural, se puede obtener materiales idóneos para ser utilizados como matrices en la formación de compuestos con buenas propiedades y un bajo impacto medioambiental. Así mismo se tiene que el tratamiento adecuado a cargas y fibras de origen natural pueden convertirlos en materiales con propiedades equiparables a refuerzos convencionales. Finalmente se tiene que la obtención de materiales compuestos con alto rendimiento medioambiental y con buenas propiedades fabricados a través de técnicas convencionales es más que factible, lo que demuestra su potencial uso en el área industrial.